Geological and Geochemical Constraints on the Early Evolution of the Panama Arc

Joanna Claire Brims

School of Earth and Environmental Sciences

Cardiff University

Submitted in partial fulfilment of the requirements for the degree of *Doctor of Philosophy*

June 2021

ABSTRACT

The Panama Arc formed following subduction initiation along the southwestern margin of the Caribbean Oceanic Plateau in the Late Cretaceous. Evidence for the arc initiation upon the oceanic plateau basement is preserved in uplifted segments of the forearc basement across southern Central America. Despite subduction initiation being one of the most significant processes of the plate tectonic cycle, it remains the most poorly understood, and the unique geological record of Panama and nearby Costa Rica and Colombia provides a valuable opportunity to investigate magmatic and tectonic processes in a nascent subduction zone. This study uses field observations, biostratigraphic dating, whole-rock geochemistry and Nd isotope geochemistry to investigate the nature of the plateau basement and the first magmatic products of subduction initiation across a ca. 650 km transect from western Panama to northwest Colombia.

New results reveal that the oceanic plateau across this region is lithostratigraphically and geochemically heterogeneous. Similar to the bulk of the Caribbean Oceanic Plateau, the studied plateau sequences were sourced from a heterogeneous mantle plume likely associated with the initiation of the Galapagos hotspot in the Late Cretaceous. Earlier magmatic phases of the oceanic plateau in Panama and nearby Colombia are possible, but remain poorly documented in the studied area. In addition, this study provides a new insight into subduction initiation along the oceanic plateau with the recognition of two compositionally distinct ‘proto-arc’ groups. An early proto-arc magmatic phase includes sequences of pillow basalts, basaltic dykes and gabbroic intrusions that were formed from a plume-like source and are geochemically transitional between plateau and mature arc sequences. The second proto-arc phase is represented by basaltic dykes, locally crosscutting plateau and early proto-arc sequences, which have more depleted geochemical signature, and were produced from a MORB-like source with variable slab input. These proto-arc groups are separated from the plateau by a regional limestone formation that indicates cessation of plateau magmatism ca. 5-10 Myr prior to subduction initiation in the Campanian (ca. 72-73 Ma). Existing geochronological data and new results indicate that the establishment of a mature arc from the onset of supra-subduction magmatism took less than ca. 4 Myr.

Overall, this study shows that igneous complexes of Panama and Colombia represent a novel record of subduction initiation which does not follow previous models of plume-induced subduction initiation in Central America or spontaneous subduction initiation along the Izu-Bonin-Mariana Arc system. New and previous regional constraints suggest instead

that subduction initiation in Panama most likely occurred due to propagation of an east- to north-facing subduction zone along the southern margin of the oceanic plateau during its collision with the South American continent.

ACKNOWLEDGEMENTS

It has only been possible for me to write this thesis due to the immense amount of help and support I have received over the past 4 years from a number of incredible people.

Firstly, I wish to thank my primary supervisor, David Buchs. Over the past 4 years, David has a great source of knowledge and guidance, and has been always encouraging and reassuring when something went a bit wrong along the way. I feel incredibly lucky to have spent time in the field with David – he has an incredible ability to put hundreds of tiny observations into one coherent idea in a matter of seconds, and to understand which specific outcrop I am referring to years later without me even describing it. I also wish to thank Andrew for his many words of wisdom and guidance throughout the project. More importantly, I wish to thank Andrew for teaching me where to find a delicious and reasonably priced curry in Cardiff.

I am indebted to colleagues from the Instituto de Geociencias at the University of Panama who provided support during fieldwork, and without whom this work would not have been possible. In particular, thanks must go to Arkin Tapia for his unwavering enthusiasm and for always making sure I didn't get swept away in a river or eaten alive. I must also thank Iain McDonald, Marc-Alban Millet, Dan Barfod Riana Rossouw and Mareli Grobbelaar-Moolman with all their help and advice in preparing and analysing my samples throughout the PhD. Special thanks to Tony Oldroyd, for not only preparing beautiful thin sections (sometimes at great speed!) but for always being up for a chat which has helped to keep me sane over the years.

To really thank everyone who has helped me to get to this point, I feel I need to go back a bit further in time. Although Dyce Academy may not have been the most inspiring place at the best of times, I feel so lucky to have been taught by some wonderful teachers during my time there. Due to some teachers going above and beyond their duties I was able to have some incredible experiences which taught me the value of curiosity and adventure. When I then went on to decide where to go to university, I was a bit baffled as they all seemed very good. In the end I picked the University of Glasgow as I heard it had the best nightlife…On reflection, this may not have been the soundest way to make a decision about my education, but I am so glad that I found my way to GES. I wish to thank the lecturers and course mates for making my time there so wonderful. I never would have believed that I could pursue a PhD had I not had so much encouragement and support from my lecturers in Glasgow.

I feel so lucky to have joined Cardiff EARTH when I did. I could not have imagined a better cohort begin this PhD journey with and I am so glad that we have stayed in touch throughout, even as we have all gone in slightly different directions. An extra thank you goes to Jamie Price and Jian Wang, who I have shared an office with throughout and who have continued to be so encouraging throughout lockdown. I also wish to thank members of the tea club from though the years, including Michael Hodge, Bob Gooday, Kate Abernethy, Matt Price, Liam Hoare and James Panton who have taught me that there is nothing a good cup of tea cannot solve.

My Glasgow girls Helen, Brogan and Katy have also been hugely supportive and encouraging throughout. I know that they most definitely do not care about rocks, but sometimes they pretend to, and that has meant a lot. I would also like to thank the ISSOS family; I feel so lucky to have been a part of ISSOS and to have worked with such wonderful staff and students who have reminded me of the importance of having a life outside of the PhD. I hope that I can see you all soon at a future Chilli night!

I am so grateful for my family who have supported me throughout my PhD. I especially thank my sister Karin for her unwavering support over the past 4 years, and for taking care of our parents Christmas presents while I have been in the final stages of writing this thesis.

Finally, to Josh. We met on the first day of my PhD and you have been there every step of the way since. I could not have done this without your endless support. Thank you.

TABLE OF CONTENTS

LIST OF FIGURES

LIST OF TABLES

1. INTRODUCTION

1.1 Rationale

The Panama Isthmus lies within the Central American land bridge between Costa Rica and northern Colombia, connecting South America to North America. The isthmus has undergone a complex tectonomagmatic history, culminating in the closure of the inter-American seaway between the Pacific and Atlantic Oceans as recently as 3 Ma (Keigwin Jr., 1978). The Panama Isthmus formed through several stages of volcanism. This began with the development of the Caribbean Oceanic Plateau, followed by the initiation of a subduction zone along the southwestern margin of the plateau, forming the Panama Arc at around 75 - 73 Ma (Buchs et al., 2010). Arc magmatism has continued in Panama from 73 Ma to present, through the evolution of subsequent volcanic fronts across Panama (Lissinna, 2005; Buchs et al., 2010; Wegner et al., 2011; Buchs et al., 2019b; Buchs et al., 2019a).

The project is important with respect to understanding of subduction initiation and arc evolution. Subduction remains to be one of the least understood parts of the plate tectonic process (Ishizuka et al., 2011) as much of the evidence from past subduction zones can be destroyed or is not visible (Gurnis et al., 2004). It is important to understand the mechanics of subduction – and how it initiates – to fully understand the global tectonic cycle. It is difficult to study subduction initiation in modern subduction zones, as much of the evidence of subduction initiation can be destroyed, and products are not visible on land. This is especially prevalent for intra-oceanic convergent margin subduction zones, as opposed to Andean style, as the process is submarine. Much of the study of this subduction style is based on the Izu-Bonin-Mariana system, which has been heavily studied (Niu et al., 2003; Reagan et al., 2010; Ishizuka et al., 2011; Whattam and Stern, 2011). The IBM system has been described as a “spontaneous” style of subduction initiation, in that it formed without the requirement for plate tectonics, as opposed to an “induced” mechanism which requires plate tectonic movement (Stern, 2004). However, multiple zones of subduction initiation need be studied in such detail to allow for stronger characterisation of the subduction process. Furthermore, the initiation of subduction in Panama is distinctive in that this initiation likely occurred along an oceanic plateau boundary. This allows for the investigation how the presence of an oceanic plateau and associated plume head may influence subduction initiation, including if the buoyancy of the plateau or plume head could prompt the initiation of a subduction zone, and how the plume head could contaminate the products of early subduction initiation.

The specific mechanisms and timing of formation of the Panama Arc remain poorly constrained due to the difficulty of geological exploration and study in relevant areas of Panama and Colombia. Prior to this investigation, no comprehensive large-scale study including fieldwork, geochemistry and dating had been undertaken to characterise the timing and mode of subduction initiation in the region. This study provides new geological and geochemical constraints on the earliest subduction related magmas from western Panama to north western Colombia. This will allow for the spatial and temporal evolution of magmas during subduction initiation to be constrained, leading to a model of subduction initiation along the southwest margin of the Caribbean Plateau. To fully understand the early development of the Panama Arc and ongoing tectonics in the Caribbean during the Late Cretaceous, it is also important to understand the nature of the arc basement. In western Panama, an oceanic plateau basement to the arc has been described (Buchs et al., 2010) but these plateau sequences have not been studied in detail. This study will also provide new geological and geochemical constraints on the oceanic plateau basement from western Panama to north western Colombia.

The formation of the Caribbean Plateau and the Panama Arc are further important as they were the first stage of formation of the Panama Isthmus. Although the formation of the isthmus is thought to have closed the inter-American Seaway as recently as 3 Ma (Keigwin Jr., 1978) there is evidence which suggest that the isthmus may have closed the seaway earlier (Montes et al., 2015). This closure has primarily been documented and dated indirectly, and not by using direct geological constraints. Understanding the early evolution of the Caribbean Plateau and the Panama Arc is important in understanding the early closure of the inter-American seaway and how this may have affected the global climate regime at this time.

1.2 Project Objectives

This study provides new field, geochemical and geochronological constraints from Western Panama to Northwest Colombia to reconstruct the mode and timing of subduction initiation along the Caribbean Oceanic Plateau, with a particular focus on spatial and temporal evolution of magmas in the nascent subduction zone. Six main objectives were addressed to develop the new model of subduction initiation, as described below:

- To produce coherent and comprehensive geochemical data sets to characterise the geochemical evolution of the early Panama Arc
- To characterise the spatial and temporal evolution of the Panama Arc from the Late Cretaceous to the Palaeogene, focussing on subduction initiation and the early

development of the arc, specifically the nature of the earliest subduction related magmas

- To investigate further the nature of the plateau arc basement, the extent of this plateau basement and the geochemical heterogeneity from western Panama to northwest Colombia
- To investigate the role of the oceanic plateau in subduction initiation, including understanding if subduction initiation was induced or spontaneous
- To produce a model of subduction initiation along the boundary of the Caribbean plateau, contributing to the understanding of regional tectonics at the beginning of subduction initiation

1.3 Thesis Structure

This thesis contains 7 chapters. Following this introduction, Chapter 2 contains an overview of subduction initiation processes and associated magmatism, followed by a geological overview of the regions of study from western Panama to north western Colombia. Next are the results chapters. Chapter 3 describes the geology and stratigraphy of these regions, based on the results of fieldwork, and also includes details on the petrography of the rock assemblages identified in the field. Chapter 4 describes the outcomes of $^{40}Ar/^{39}Ar$ geochronological analyses along with biostratigraphic ages provided for sedimentary units. The final results chapter, Chapter 5, then presents the major and trace element and Nd isotope results for the rock assemblages described in the previous chapters. Chapter 6 is a discussion chapter. This chapter first summarises the results, before further addressing potential issues with $^{40}Ar/^{39}Ar$ dating in altered tholeiitic basalts, discussing the origins of subduction initiation magmas, and finally discussing the development and origins of the oceanic plateau basement. Finally, Chapter 7 summarises the key findings from this project. The appendices include all methods and geochemical data utilised in this study.

2. GEOLOGICAL OVERVIEW

2.1 Subduction initiation

Subduction initiation is the process by which the oceanic lithosphere first descends into the upper mantle (Gurnis et al., 2004). Subduction is an integral part of plate tectonic cycle, and has large consequences for global tectonics, in that Earth's mantle primarily convects due to the down going cold lithosphere at subduction zones (Hager and O'Connell, 1981). In particular, understanding the initiation of subduction may be relevant to understanding the start of plate tectonics, and the understanding of the forces which both drive and resist plate motions (Gurnis et al., 2004). It is also relevant to the understanding of magma production rates (Ishizuka et al., 2011) and the formation of continental crust (Stern, 2004; Nair and Chacko, 2008; Gazel et al., 2015). Despite this, the process of subduction initiation remains largely unknown. It is now widely accepted that the negative buoyancy of sufficiently old lithosphere provides the main driving force for subduction (Vlaar and Wortel, 1976; Davies, 1999), but that bending and shear resistance of the lithosphere work against subduction initiation, and is some cases can halt it completely (Mckenzie, 1977b). Despite the difficulties in initiating a new subduction zone, current global plate tectonics dictate that certain conditions must lead to subduction initiation which leads to self-sustaining subduction zones. There is also a requirement for subduction to initiate prior to the start of plate tectonics, which led Stern (2004) to classify subduction initiation in two mechanisms: induced (which require the existence of ongoing plate motions) and spontaneous (which form due to causes other than plate tectonics). Nearly half of all currently active subduction zones have formed within the last 65 Ma, with most being intra-oceanic and in the Western Pacific (Gurnis et al., 2004). This suggests that that subduction initiation must have occurred fairly regularly, potentially episodically, and that in recent Earth history circumstances have allowed many subduction zones to initiate, meaning there are active subduction zones to investigate.

The lack of understanding of subduction, and subduction initiation specifically, is partially due to the difficulty surrounding access and study of the subduction system, as subduction zones are often consumed at margins and can be overprinted by thermal and structural processes along with volcanic and sedimentary cover (Gurnis et al., 2004). In addition, subduction initiation as a research topic is still relatively young, with subduction only recognised as a concept 50 years ago by Oliver and Isacks (1967)(1970). Early work on subduction initiation was based on modelling and assumed a compressive tectonic regime (McKenzie, 1977b; Mueller and Phillips, 1991; Toth and Gurnis, 1998). Thinking evolved in 1980s with geodynamicists studying potential fractures between old and young oceanic

lithosphere (Matsumoto and Tomoda, 1983) forming a subduction zone due to lateral density contrasts. Advances in drilling technology allowed for deep sea exploration, which greatly improved subduction initiation understanding. Early work documented the earliest arc lavas as largely tholeiitic and boninitic with lesser calc-alkaline lavas, which formed entirely underwater with no remnant of normal arc crust (Natland, 1981). It was noted then that it had many features of an ophiolite, produced in situ by early arc volcanism, with the necessary upper pillows overlying plutonic rocks (Natland, 1981). Boninites are highly unusual rocks high in SiO_2 and MgO, now known to form in the fore-arcs of intra-oceanic arcs, through partial melting of a depleted mantle harzburgite metasomatized by fluid-mobile elements. Stern and Bloomer (1992) realised that subduction initiation could involve extension, suggesting that the IBM forearc formed by seafloor spreading above a sinking Pacific pate, along an existing transform zone which separated old, dense Pacific lithosphere from young, thin and buoyant lithosphere from the Central Philippine Basin spreading ridge. This created a buoyancy contrast across the transform zone, prompting the Pacific lithosphere to sink. This sinking prompted upwelling of the asthenosphere, leading to decompression melting and formation of the depleted (tholeiitic) and ultra-depleted (boninitic) magmas, from a depleted mantle source with extensive melting. It was key that the early arc magmatism was recognised as extensional and formed at a spreading centre, with similar processes to those at slow spreading ridges (Stern and Bloomer, 1992). This changed the thinking that compressional tectonics were required for subduction initiation, as had been assumed in earlier work (e.g., McKenzie 1977a).

2.1.1 Mechanisms of subduction initiation

The first classification of subduction initiation (SI) mechanisms was outlined by Stern (2004), with the main subdivisions of induced or spontaneous subduction initiation (Figure 2.1). They defined induced subduction initiation as subduction caused by either some ongoing plate motion, or by changes to the plate motion due to changes in force balance away from the SI site. Spontaneous subduction is defined as being caused by forces originating from the SI site and not elsewhere. Under these definitions, spontaneous subduction initiation does not

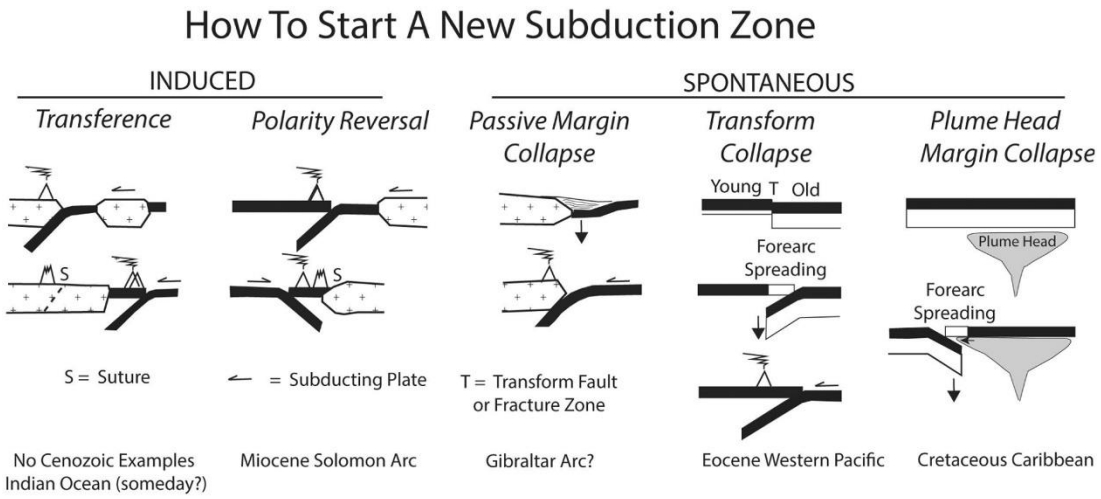

Figure 2.1: Subduction initiation mechanisms from Stern and Gerya (2018), showing both induced and spontaneous mechanisms for subduction initiation

require the existence of ongoing plate tectonics and could therefore be a process though which subduction first began. However, the terms of induced and spontaneous subduction have the potential to be misleading, as spontaneous subduction could in fact be induced by an external cause which originates in the SI location (e.g., plume (Figure 2.1)). It has also been noted that due to current global plate tectonics, some external plate forces will always be present, which may contribute to the current "spontaneous" SI mechanisms (Hall et al., 2003). True spontaneous subduction occurs only where subduction occurs solely due to aging leading to a density contrast (probably along pre-existing fault or weakness) and one slab sinking. In induced scenarios, subduction is forced by ongoing plate motion or a change in plate motion as stated above, along with plume activity. In the remainder of this thesis, the terms spontaneous and induced will refer to these definitions, with plume activity classed as induced subduction initiation. Since Stern (2004), these two main mechanisms have been further divided into different categories of subduction initiation, as summarized in Figure 2.1.

These mechanisms have been proposed through different disciplines, some though modelling only and some with field-based study. Early modelling work on lateral density contrasts continued and was shown to be a factor in initiating new subduction zones, both induced and spontaneous, along passive margins or oceanic plateau boundaries (Niu et al., 2003). Oceanic plateaus can also initiate new induced subduction zones by polarity-reversal of an existing subduction zone due to attempted subduction of buoyant lithosphere. This was suggested for the Solomon Islands arc, where polarity of the subduction zone reversed due to the collision of the Ontong Java Plateau with the northern Solomon Trench (Cooper and Taylor, 1985). It is proposed that as the thickened crust could not be subducted, it blocked the subduction zone and prevented subduction continuing towards the south, thus the arc polarity reversed to be north-directed (Petterson et al., 1999). Polarity reversal of a

subduction zone has also been suggested for the Great Arc of the Caribbean, along the eastern margin of the Caribbean plateau, where the plateau collided with a south-westerly dipping subduction zone causing a new subduction zone to form in a northeast direction (Kerr et al., 2003). Transference is another mechanism of subduction initiation which could be caused by the collision of a fragment of oceanic plateau with a subduction zone. In this case, the plateau is accreted, and a new subduction zone is formed outboard of the accreted fragment and failed subduction zone. This is suggested to be ongoing in the formation of the Massau Trench in the western Pacific, thought to be due to the collision of the thickened Caroline Ridge with the Yap Trench (Lee, 2004), but has also been suggested to occur previously with the accretion of the Siletzia terrane in North America (Gao et al., 2011). It is also important to note that subduction can initiate by propagation of an existing subduction zone along a boundary such as an existing fault or density contrast. This has been documented along multiple subduction zones, such as the Philippine Trench (Lewis and Hayes, 1983; Ozawa et al., 2004).

2.1.2 Spontaneous subduction initiation along a pre-existing fracture: The Izu-Bonin Mariana subduction system

The IBM arc system is an optimal place to study subduction initiation due to submarine evidence of the magmatic sequences produced during subduction initiation, with a lack of overprinting from more recent volcanics or recent tectonic movements (Ishizuka et al., 2018). However, as much of the exposure is submarine, drilling is required. Recent drilling has been undertaken through JAMSTEC (Japan Agency for Marine-Earth Science and Technology) Shinkai 6500 in the Mariana forearc (Reagan et al., 2010), followed by IODP Expeditions 350-352 (Figure 2.2) (Arculus et al., 2015; Busby et al., 2017; Reagan et al., 2017; Hickey-Vargas et al., 2018; Shervais et al., 2019), which covered the rear-arc to forearc regions, and allowed for a development of the initial extension model. This has led to the development of the most complete record of subduction initiation forearc

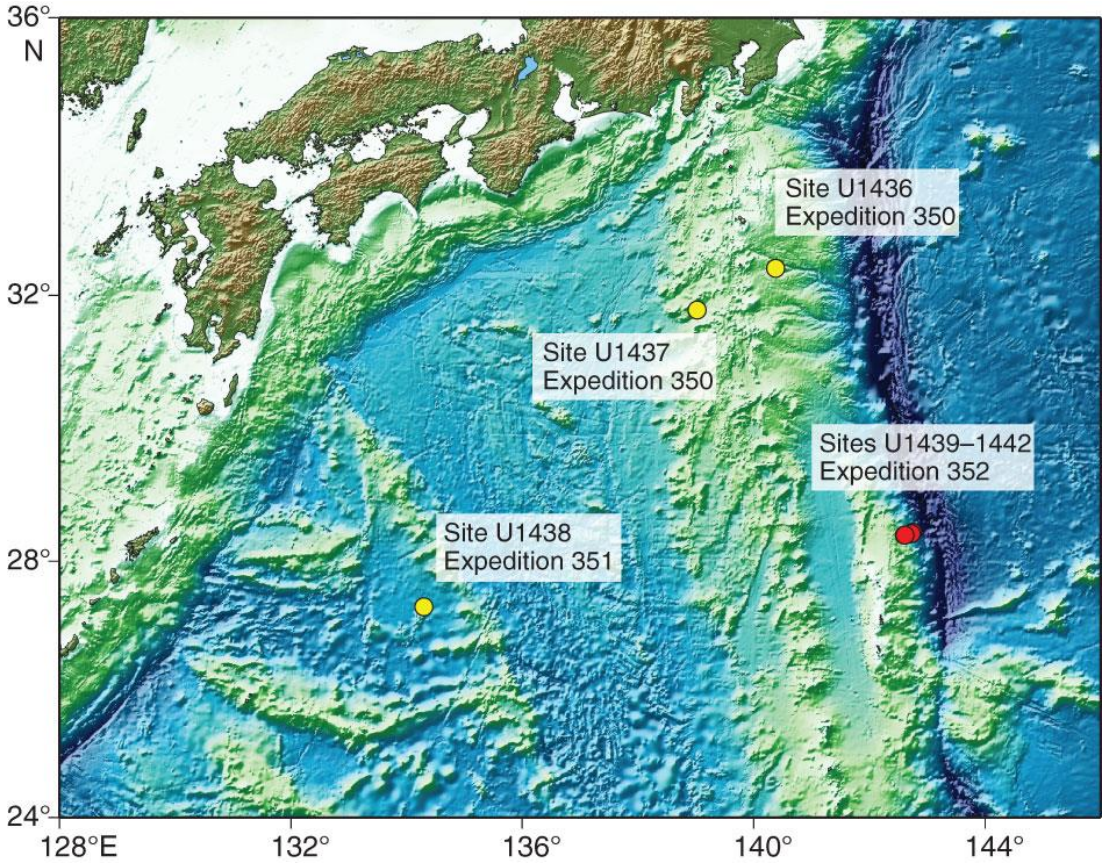

Figure 2.2: Regional map of the Izu-Bonin-Mariana (IBM) system showing the location of sites from Expeditions 350, 351, and 352, from Pearce et al. (2015).

stratigraphy, largely thought to represent a spontaneous subduction zone which formed along a pre-existing fracture due to the sinking Pacific Plate (Figure 2.1) (Stern and Bloomer, 1992; Reagan et al., 2010; Arculus et al., 2015).

After diving and dredging with JAMSTEC south of Japan, Reagan et al. (2010) expanded on the work of Stern and Bloomer (1992), who had identified the occurrence of boninitic and tholeiitic lavas in the forearc. They further investigated the tholeiitic basalts and named them fore-arc basalts (FAB), noting they are MORB-like tholeiites, with lower Ti/V and Yb/V ratios and highly variable concentration of fluid soluble elements such as K, Rb and U. This indicates a source more depleted than that of MORB. The FAB consist mainly of aphyric pillow lavas and diabasic intrusions, with rare euhedral to skeletal olivine (Reagan et al., 2010). FAB locally underly boninites and are interpreted to be the first lavas to erupt following SI, formed due to mantle decompression when the Pacific plate began to sink beneath the Philippine Plate. The boninites were thought to form later when the residual mantle began to melt due to input of water-rich fluid from the sinking plate. Crucially FAB lavas show negligible slab-derived fluid input, indicating that the lavas formed prior to the introduction of fluids. Some lavas were found to be geochemically intermediate between

FAB and boninites, indicating that the relationship is geochemically continuous and the two groups are related (Reagan et al., 2010; Reagan et al., 2017). Through available dates the transition from FAB to boninitic volcanism was constrained to take 2-4 Myr, with development to normal arc magmatism taking 7-8 Myr, occurring simultaneously along the arc (Ishizuka et al., 2011). This stratigraphy was used in the basis for Whattam and Stern (2011)'s "subduction initiation rule" - a diagnostic stratigraphy for the recognition of subduction related ophiolites. Within this stratigraphy, there is an evolution from rocks with a tholeiitic composition, from a lherzolitic source, with no fluid input and higher REE (Rare Earth Elements), to calc-alkaline rocks from a harzburgitic mantle source, with fluid input and lower REE concentrations (Whattam and Stern, 2011).

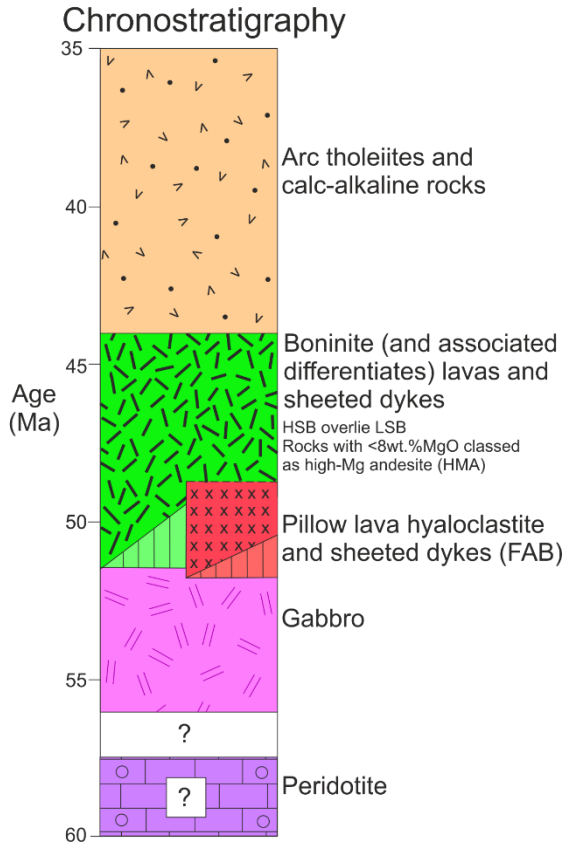

Figure 2.3: Chronostratigraphic chart of the IBM forearc, modelled after Ishizuka et al. (2011) and Reagan et al. (2019). Does not include lithostratigraphic constraints.

This initial classification of FAB to boninite has been built upon, with more in-depth studies of the stratigraphy helping to constrain processes ongoing during spontaneous subduction along a pre-existing fracture. FAB lavas are more depleted than N-MORB, forming at higher degrees of melting at shallower depths (Shervais et al., 2019) and are also differentiated (~7

wt. % MgO) indicating the formation of a pervasive melt lens during spreading (Reagan et al., 2017). Melt modelling of FAB formation found that the system must be 3 stage – melting of an initial source to form the source to FAB (more depleted than DMM), followed by limited melting in a garnet source region then more extensive secondary melting in a spinel source (Shervais et al., 2019). To extract a high melt fraction at a shallow depth from previously depleted mantle, an anomalously hot source region would be required. It was suggested the Manus plume could be involved, which would change the mechanism of subduction initiation from purely spontaneous to having some tectono-magmatic plume-lithosphere interaction (Shervais et al., 2019). However, it is known that the oldest lavas associated with the Manus plume formed after FAB lavas, which makes this suggestion unlikely (Reagan et al., 2019).

The boninites contrast FAB in that they have a higher depletion of HREE (heavy REE) (indicating a more depleted source) and a higher LREE (light REE) (from an enriching subduction component) (Li et al., 2019). Using the classification of Kanayama et al., (2013) the boninites were split in to 2 groups – of low-Si boninites (LSB) and high-Si boninites (HSB) (Reagan et al., 2017). Within the boninite section, it appears that the lowermost lavas (LSB) have uniformly low Cr and MgO concentrations, suggesting that, like FAB, they are fractionated magmas formed during sea-floor spreading (Reagan et al., 2017). However, in the HSB, primitive lavas become more common, with further HREE depletion and LREE enrichment suggesting the system has changed to ephemeral fractionating magma bodies and may have formed off axis (Li et al., 2019). The formation of HSB could also represent the transition between the end seafloor spreading and the beginning of focussed arc magmatism, as declining spreading rates could inhibit the formation of an axial melt lens which led to the formation of the earlier FAB and LSB (Reagan et al., 2017). Observations from Reagan et al. (2010) on the relationship between FAB and boninite were confirmed with drill core from Exp. 352, which showed a continuous transition from FAB to boninite (Reagan et al., 2017). FAB was also found to form closer to the trench than boninites, with increasing subduction input away from the trench, showing that volcanism moves away from the trench with time (Reagan et al., 2017; Ishizuka et al., 2018).

As boninite formed from a continuous transition from FAB, the boninite source may be a residue from the formation of FAB, and so the melting to generate boninites probably occurred at lower temperatures than for the formation of FAB (Reagan et al., 2017). Hf-Nd-Sr-Pb isotopic studies support the idea that the LSB formed by a mixture of mantle and slab component (Li et al., 2019). Li et al. (2019) used a 2 end mixing curve to trace the development of the mantle source from FAB to arc. They found that FAB has no slab detectable component and an “Indian” source, whereas LSB follow simple mixing trends between residual mantle source and shallow amphibolite facies melting of oceanic crust of a

Pacific origin. HSB follow a mixing trend of a hybrid mantle wedge (with both residual mantle and slab melt) combined with an additional subduction component, requiring a contribution from pelagic sediment (Li et al., 2019). In order for FAB to have no subduction input, rapid upwelling is required during subduction initiation (Li et al., 2019), followed by rapid slab melting to produce boninites in quick succession. The addition of pelagic sediments to form HSB also denotes a change from initially accretionary to non-accretionary style of subduction (Li et al., 2019), which could occur as the seafloor spreading declines.

New ages of the rocks sampled during Expedition 352 have introduced constraints on the timing of subduction initiation and lithologies formed (Reagan et al., 2019). The timing for evolution of FAB to boninite was previously estimated to be 2-4 Myr (Ishizuka et al., 2011), however, new high-precision dating revealed that FAB and boninite are almost coeval, indicating that they formed in quick succession (Figure 2.3) (Reagan et al., 2019). FAB lavas were dated to form at 51.34 ± 0.78 Ma, whilst the most reliable boninite date was 51.2 7± 0.09 Ma, from HSB. Several HSB samples were dated and were shown to be older down core, constraining that they formed over at least 0.5 Myr, but up to 1 Myr (Reagan et al., 2019). The age of initiation of spreading was calculated to be ca. 52.5 Ma, using the age of a gabbro dated to be 51.9 Ma and extrapolated to the edge of known spreading distance. They also estimated the spreading time by using the calculated spreading rate and distance, calculated to be between 0.6 Myr and 2 Myr. Importantly, FAB gabbros linked to the start of spreading sampled almost 1700km apart were found to be of the same age, showing that this occurred almost simultaneously along the IBM arc (Reagan et al., 2019).

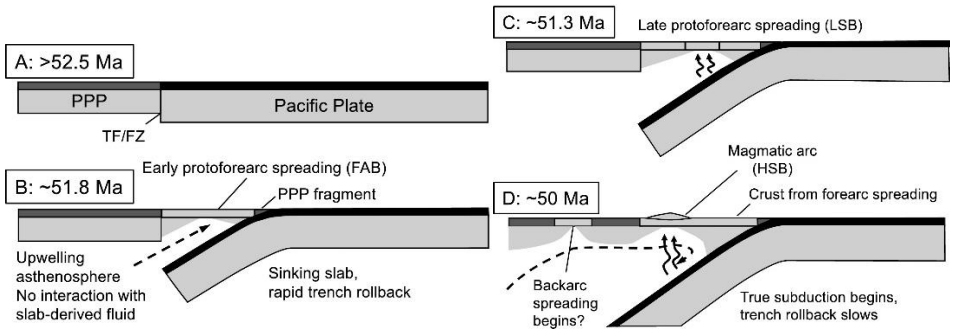

Figure 2.4: Model of subduction initiation in IBM system from Reagan et al. (2019).

Prior to IODP Exp. 352 to the forearc, IODP Exp. 351 aimed to investigate the origins of the IBM arc system in the Amami Sankaku Basin (Figure 2.2). Here there were there were lavas that appeared to be “FAB-like”, dated to be 49.3-46.8Ma, meaning they are younger than FAB by approximately 2-5 m.yr. (Ishizuka et al., 2018). They were interpreted to be lavas formed in a rear-arc spreading centre, indicating that magmatism started later in the rear-arc. It is possible that there was a migration of the spreading centre during subduction

initiation, and that are fore-arc spreading ceased and arc magmatism began, spreading switched to the rear-arc forming these FAB-like lavas. However, it is is possible that this study did not sample the oldest rear-arc lavas along the margins of the basin. Importantly, there is no transition to boninite in the Amami Sankaku Basin, as is seen in the forearc (Ishizuka et al., 2018). The surrounding basement of the Amami Sankaku Basin was also investigated and was found to be remnant crust for an old arc (Ishizuka et al., 2018). This enhances the model of subduction initiation along the IBM due to buoyancy contrasts, as if the overriding crusts has some buoyant, arc like, new crust, as opposed to only oceanic, it will create an even greater buoyancy contrast with the old crust of the Pacific (Ishizuka et al., 2018).

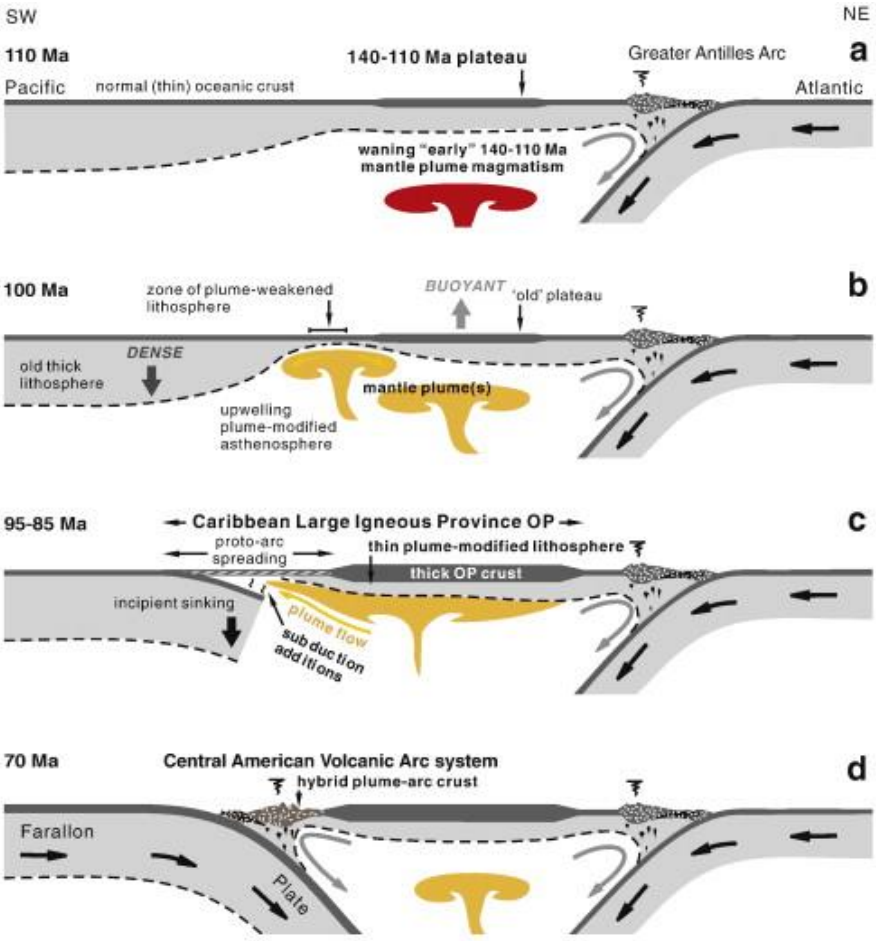

Figure 2.5: Diagram of the PISI model of subduction initiation in the Caribbean from Whattam and Stern (2015), depicting (a) the formation of the early oceanic plateau followed by the subsequent evolution of PISI between (b) 100 Ma, (c) 95–85 Ma and (d) 70 Ma.

This work on the IBM arc has developed an almost complete stratigraphy documenting subduction initiation along a pre-existing fracture (Figure 2.4). Alongside this, modelling has displayed that it is possible to spontaneously initiate intra-oceanic subduction (Dymkova and

Gerya, 2013). However, although this is the best documented cause of subduction initiation, it represents only one of the suggested mechanisms.

2.1.3 Plume-induced subduction initiation (PISI): the Caribbean

The Plume-induced subduction initiation model dictates that subduction initiation could occur around the edge of a plume head as it impinges on cold oceanic lithosphere. The heat and extension from the plume head could potentially weaken the surrounding lithosphere enough for it to rupture and create self-sufficient subduction zones (Ueda et al., 2008; Burov and Cloetingh, 2010). It is thought that this model could explain the initiation of global plate-tectonics, as it does not require an existing plate-tectonic force.

It has been suggested that the PISI model could be applied to the Caribbean, to explain the formation of subduction zones surrounding the Caribbean Plateau in the Cretaceous (Whattam and Stern, 2015). This argument is based on a few key criteria: (1) the existence of arcs around the Caribbean plateau within a similar time period, (2) the apparent lack of known hiatus between the formation of arc and plateau sequences, and (3) the occurrence of sequences of the Caribbean plateau and arc which overlap in time, space, chemical and isotopic compositions , indicating that arc lavas are derived from a Galapagos plume-like mantle which has become increasingly subduction modified (Whattam and Stern, 2015). This model has also been tested geodynamically, which indicates that for PISI to occur, there must be a large hot and long lived mantle plume head impinging on old oceanic lithosphere, which could cause self-sustaining subduction zones around the plume head (Figure 2.5) (Gerya et al., 2015). However, even if verified geodynamically, more study of the associated sequences surrounding the Caribbean is needed to know if this model is feasible. The model of Whattam and Stern (2015) indicates that as the plume head impinges on the base of the oceanic crust and causes it to weaken, there will be extensional “proto-arc spreading” (Figure 2.5). This is similar to the seafloor spreading during spontaneous subduction initiation along the IBM arc (Reagan et al., 2010). Therefore, it could be expected that if the PISI model occured, the forearc stratigraphy of Caribbean arcs could be similar to that of the IBM, with an initial plateau related “FAB” unit, followed by boninites. These first subduction related “FAB” lavas are MORB-like and have little subduction input (Reagan et al., 2010; Shervais et al., 2019). Based on current work in in Panama, this does not seem to be the case, as initial arc lavas appear to be transitional between plateau and arc, and no boninites have been detected (Buchs et al., 2010).

2.2 The Caribbean Oceanic Plateau

2.2.1 Oceanic Plateaus

Oceanic plateaus are a type of Large Igneous Province (LIP) (Coffin and Eldholm, 1992), considered to form by volcanism due to decompression melting of upwelling hotter mantle, known as mantle plumes (Hill, 1993; Kerr, 2003; Kerr and Mahoney, 2007). LIPs are exceptional eruption events, defined as magmatic provinces which cover an area of > 10^5 km^2, with rapidly erupted high Fe-Mg magmatism in an intraplate setting (Tuzo Wilson, 1968; Coffin and Eldholm, 1992). They have intraplate geochemical signatures and active ages of < 50 Myr (Bryan and Ernst, 2008), including a main pulse of magmatism of 1-5 Myr, over which most of the volume of the province is erupted (Bryan and Ernst, 2008). As well as oceanic plateaus, LIPs can be flood basalts, dyke swarms, submarine ridges, seamount chains and volcanic rifted margins. Typically, they are followed by a volcanic chain which becomes younger away from the initial plume head (Morgan, 1971; Hill et al., 1992).

It is thought that most LIPs have formed over several phases of magmatism, but that the majority of eruption and emplacement occurs over one main initial episode, which could last a relatively short time, such as 2–3 Myr (Kerr, 2003). This has been observed for the Ontong Java Plateau with a large percentage erupted between 122 and 120 Ma (Mahoney et al., 1993; Tejada et al., 1996; Tejada et al., 2002; Chambers et al., 2004), and for the southern Kerguelen plateau where the majority erupted in pulses from 120-110 Ma and 105-100 Ma (Coffin et al., 2002; Duncan, 2002). This production of large volumes of melt in such a short time period implies magma production rates up to 25% higher than those observed at present-day mid ocean ridges (Eldholm and Coffin, 2000) with a high flux of asthenospheric mantle with an above ambient temperature (Fitton and Godard, 2004; Herzberg, 2004; Campbell, 2007; Putirka, 2008). This hotter mantle has been modelled to take the form of a mantle plume, ascending through the overlying mantle by thermal buoyancy (McKenzie and Bickle, 1988; Campbell et al., 1989; Loper, 1991; Farnetani and Richards, 1995). Mantle plumes ascend from a boundary at depth and undergo decompression melting as they reach the base of the lithosphere (Campbell and Griffiths, 1990; Hill et al., 1992; Farnetani and Richards, 1995; Fitton and Godard, 2004). They ascend through the mantle with a large “head” and narrower plume tail, and spread out as the reach the base of the lithosphere, to cover as much as 1000km (Kerr, 2003). Adiabatic decompression melting of mantle plumes at the base of the lithosphere remains the most widely accepted mechanism for the formation of LIPs and the eruption of large volumes over short time periods. However, the mantle plume theory does not fit for all LIPs. The Ontong Java Plateau did have a short-lived period in which a large proportion of the overall

magmatism occurred, but the plateau experienced long lived magmatism with no evidence of the expected hotspot track. This indicates that is likely that there is some variability in plume styles, which leads to different characteristics of LIPs. This variability comes in many forms – chemistry, source depth and temperature. There are two boundaries at which the plume could originate from – most are thought to form in the deep mantle at the core-mantle boundary ("D" layer) but it has also been proposed that they could form in the middle mantle at the 670km discontinuity. As well at thermal buoyancy driving plume movement, compositional and density differences can also lead to ascent of several thermochemical plume types (Davaille et al., 2002; Kerr, 2003; Davaille and Vatteville, 2005; Farnetani and Samuel, 2005; Lin and van Keken, 2006b; Lin and van Keken, 2006a). It is thought that plumes with a high proportion of a chemical density anomaly may be anchored to produce a long-lived hotspot (Davaille et al., 2002), whilst plumes with a greater thermal anomaly are domed, and have little to no plume tail (Davaille and Vatteville, 2005; Kerr and Mahoney, 2007). Melt produced is also a variable factor, which is dependent on the thickness of the pre-existing lithosphere and the temperature of the plume, with a higher temperature producing more melt (Kerr, 2003).

Oceanic plateaus are LIPs formed on oceanic crust, with the term oceanic plateau first used by Kroenke (1974) after the recognition of the Ontong Java Plateau. Oceanic plateaus form crust significantly thicker than normal oceanic crust (~7 km) with thicknesses up to 40 km, with erupted volumes of over 4×10^6 km^3 (Kerr et al., 1997b). They represent the ideal setting to understanding the formation and source of LIPs, as they are not contaminated in the way that continental flood basalts are, as they only erupt through thin oceanic crust and avoid continental crust melts. However, oceanic plateaus can be difficult to study as large proportions may be submerged by deep water, restricting the area of study. They may be sampled by drilling (Kerr et al., 1997b) but this can be highly expensive, and will only allow for localised observations. In addition, there is no complete history of oceanic plateau formation, due to subduction and the recycling of oceanic crust older 200 Myr. The oldest in situ oceanic crust is Jurassic in age, and the preservation potential of older oceanic plateaus and crust is very low. However, as oceanic plateaus have elevated topography with a greater crustal thickness and buoyancy than oceanic crust, they are more likely to be accreted to an adjacent upper plate margin if they collide with an island arc or continental margin in a subduction zone shortly after formation (<5 Myr) (Ben-Avraham et al., 1981; Cloos, 1993; Kimura and Ludden, 1995; Kerr et al., 1996c). These accreted fragments allow for the study of the structure and composition of oceanic plateaus through both fieldwork and seismic surveys, greatly contributing to our understanding of their formation and sources. These studies have led to a generalised stratigraphy and structure of oceanic plateaus: basal olivine cumulates, overlain

by isotropic gabbros, followed by geochemically heterogeneous picrites and komatiites and finally thick sequences of homogeneous basaltic lavas and dolerites with very little geochemical variation. The heterogeneous picrites and komatiites have MgO contents > 12 wt. % and wide ranges of both isotopic and incompatible trace element ratios, whilst the homogeneous basalts and dolerite sheets tend to have relatively flat Rare Earth Element (REE) primitive mantle-normalised patterns, with little variation in major, trace element and radiogenic isotope composition (Kerr and Mahoney, 2007). These can also be slightly light REE enriched, and there may be patterns more like MORB or Ocean-Island Basalts (OIB) (Kerr and Mahoney, 2007). However, whilst some plateaus do show this heterogeneity (e.g,. Ontong Java Plateau (Fitton and Godard, 2004)), studies of some plateaus, including the Caribbean plateau, have shown that the basalts are much more heterogeneous (Hauff et al., 2000b; Hoernle et al., 2000; Hoernle et al., 2002; Kerr and Mahoney, 2007).

2.2.2 Origin and Formation of the Caribbean Oceanic Plateau

The Caribbean Plate lies between the North and South American Plates (Figure 2.6) and based on early seismic refraction studies and drillings from DSDP leg 15 and ODP leg 165, is estimated to largely be covered by Cretaceous oceanic plateau crust (Edgar et al., 1971; Donnelly et al., 1973; Donnelly, 1973; Bence et al., 1975; Sigurdsson et al., 1997; Sinton et al., 1998; Sinton et al., 2000; Kerr et al., 2002a; Giunta and Oliveri, 2009). The plateau is thought to be largely underlain by oceanic crust, which was thickened by subsequent magmatism to form the Caribbean Oceanic Plateau. The plateau has a thickness of around 10 to 20km – as indicated by bathymetric and seismic data (Edgar et al., 1971; Kerr et al., 1997b; Wright and Wyld, 2011) and is therefore thicker than standard oceanic crust (Kerr et al., 1997b). The formation of the Caribbean Plateau has long been debated, mainly due to the location in which it formed - with arguments for both an in situ or Pacific origin - and the source of magmatism (Meschede and Frisch, 1998; Pindell and Kennan, 2009; Serrano et al., 2011).

The Caribbean Plateau ages range from 139-69 Ma although the main magmatic pulse is thought to have occurred between 93-89 Ma, based on $^{40}Ar/^{39}Ar$ ages from across the plateau (Walker et al., 1991; Kerr et al., 1997a; Sinton et al., 1998; Lapierre et al., 1999; Walker et al., 1999; Hauff et al., 2000a; Sinton et al., 2000; Kerr et al., 2003; Hoernle et al., 2004). Today, it occurs as thickened crust of the Caribbean Plate, as well as obducted and accreted fragments around the Caribbean and along the northern continental margin of South America, collectively called the Caribbean Large Igneous Province (Figure 2.6) (CLIP) (Hauff et al., 2000b) or Caribbean-Colombian Oceanic Plateau (CCOP) (Kerr et al., 1997b). The idea that the plateau formed in situ is generally an older theory (Meyerhoff and

Meyerhoff, 1972; Kerr et al., 1997a; Meschede and Frisch, 1998; James, 2006). It is now widely accepted by most that the plateau formed in the Pacific Ocean on the Farallon Plate in the Late Cretaceous, due to activity from the Galapagos hotspot (Duncan and Hargraves, 1984; Kerr et al., 1997b; Pindell et al., 2005; Mann, 2007; Pindell and Kennan, 2009; Hastie et al., 2013) and migrated between the North American and South American plates after they opened in the Jurassic (Kerr et al., 1997b; Hastie and Kerr, 2010). As the plateau migrated into this space – due to eastward movement of the Farallon plate – Caribbean terranes were accreted in Colombia and Ecuador as they were too buoyant to subduct (Kerr et al., 1997a; Kennan and Pindell, 2009; Pindell and Kennan, 2009), largely contributing to it being one of the best exposed examples of a oceanic plateau derived from a plume (Kerr et al., 1997b). Plate kinematics indicate that NW-SE divergence between the Americas occurred in the Jurassic, and therefore the opening of the Colombian marginal seaway and production of Proto-Caribbean crust began to occur at this time (Pindell and Kennan, 2009). At this time, the Great Arc of the Caribbean was located at the western side of the Proto-Caribbean, and the Caribbean plateau collided with this arc, initiating subduction polarity reversal. This led to the westerly subduction of the Proto-Caribbean crust beneath the oceanic plateau, and subsequently, the plateau and Great Arc were then emplaced between the Americas to form the Caribbean Plate (Duncan and Hargraves, 1984; Burke, 1988; Hauff et al., 2000b; Kerr et al., 2003; Mann, 2007). Accreted remnants of the Great Arc form much of the Greater Antilles (Duncan and Hargraves, 1984; Burke, 1988; Hastie and Kerr, 2010; Hastie et al., 2013). It has also been suggested that the subduction polarity reversal occurred earlier, at 125-99.6 Ma (Lebrón and Perfit, 1994; Kesler et al., 2005; Pindell et al., 2005; Escuder-Viruete et al., 2007; Marchesi et al., 2011), and that this means the Caribbean plateau may have been formed by magmatism associated with a slab window which formed when an active spreading centre of the Proto-Caribbean subducted below the Great Arc (Pindell and Kennan, 2001; Pindell et al., 2006). However, Hastie and Kerr (2010) showed that the slab gap model would not produce enough melt to form the CCOP, and that

island arc volcanism diagnostic of the slab window are not present in Caribbean plateau assemblages.

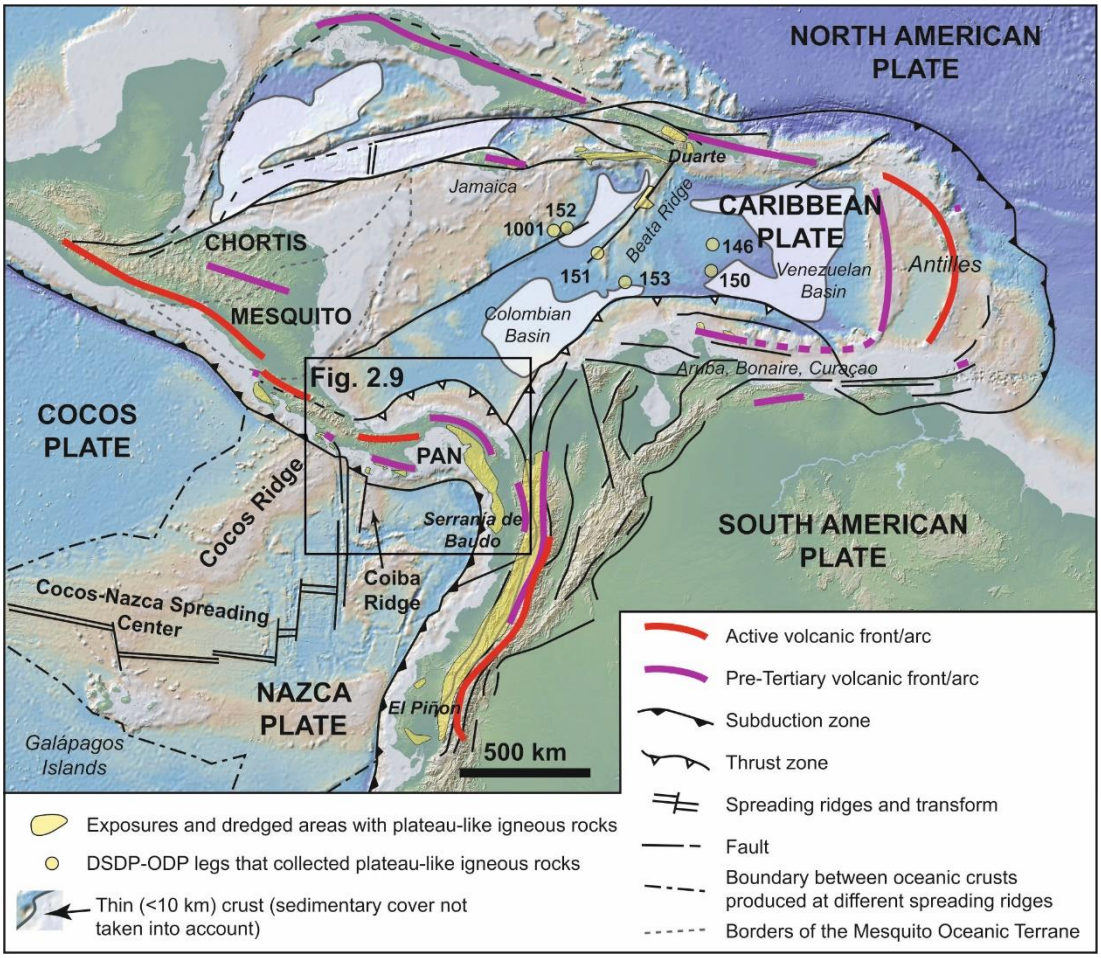

Figure 2.6: Tectonic setting of the Panama Microplate (PAN), modelled after Buchs et al. (2010).

2.2.3 Structure and Geochemistry of the Caribbean Oceanic Plateau

The CCOP has been drilled by DSDP Leg 15 and ODP leg 165, which has allowed for further study of the structure and geochemistry alongside accreted fragments from around the Caribbean. A cross section through the plateau consists of basal dunitic and pyroxenitic cumulates overlain by layered gabbros and more massive gabbros (Kerr et al., 1997b). This is overlain by eruptive heterogeneous picrites (and komatiites on Gorgona) and followed by homogeneous pillow basalts (Kerr et al., 1997b). Geochemically, the lavas of the plateau fall into 3 groups - basalts (along with picrites and komatiites) with light REE depleted chondrite-normalised patterns, basalts with LREE enriched patterns, and the most dominant type, basalts with essentially flat REE patterns – showing the variability and heterogeneity of the plateau magmatism, and therefore source of the magmatism (Kerr et al., 1997b).

The majority of the basalts are tholeiitic and fairly homogeneous in terms of incompatible trace element concentrations, and most samples containing between 6 and 10 wt.% MgO. They have geochemical trends following initial fractional crystallisation and fairly uniform radiogenic isotope values, with ƐNd ranging between +6 and +9 for almost all lavas from the plateau (Kerr, 2003). The high MgO lavas are much more geochemically heterogeneous, as shown on primitive mantle normalized multielement plots where some are more depleted and some more enriched than the basalts in incompatible trace elements. This is also reflected in the radiogenic isotopes, where the high MgO lavas are highly variable, with ƐNd values ranging from < +4.1 to > +8.0. It has been interpreted from this that the high-MgO lavas formed by magmas moving quickly through the lithosphere, whereas the low MgO lavas reflect mixing and fractional crystallisation of the high-MgO lavas trapped in magma chambers (Kerr et al., 1998). The heterogeneity of the high-MgO lavas suggests that they did not form by simply variable melting of a homogeneous source, but that there was likely a heterogeneous source region with depleted and enriched components (Kerr et al., 1996c; Hauff et al., 2000b; Kerr et al., 2002a). It has also been shown that the depleted component is not a part of depleted MORB mantle but is an intrinsic part of the plume (Kerr et al., 2002a). Modelling has suggested that most CCOP lavas were produced by a pervasively heterogeneous mantle plume with enriched blobs, and shallow, extensive melting resulted in the depleted lavas (Kerr et al., 2002a).

Gorgona Island is a significant location with respect to the high-MgO lavas. It is located in the Pacific, off the coast of Colombia and is thought to be a fragment of oceanic plateau (Kerr et al., 1996c) (Figure 2.7). It is highly heterogeneous with both enriched and depleted high MgO lavas, including the only post-Archean spinifex-textured komatiite (Arndt et al., 1997). The depleted lavas, picrites and komatiites of Gorgona are the most geochemically depleted plateau lavas found around the Caribbean and are chemically distinct in Nd-Os isotopes (Kerr and Tarney, 2005). Gorgona rocks have been dated as 86.0 to 88.3 Ma by $^{40}Ar/^{39}Ar$ (Kerr et al., 1997a). Initially the island was thought to represent an extension of the accreted fragments of the Caribbean plateau, as seen in western Colombia. However, it is possible that Gorgona may represent a separate plateau – the Gorgona Plateau. Along with the variations in geochemistry, this is evidenced by a large difference in formation palaeolatitudes, with the Caribbean Plateau shown to come from equatorial latitudes, consistent with forming from the Galapagos hotspot, whilst results from Gorgona Island indicate a latitude of origin of 26-30 Degrees south (Acton et al., 2000; Kerr and Tarney, 2005). It has also been suggested that the CCOP actually represents multiple different plume events, as basalts from Ecuador have different large ion lithophile element concentrations, as well as different Nd and Pb isotopic ratios (Lapierre et al., 2000).

2.2.4 Accretion of Caribbean Plateau fragments in Colombia

Western Colombia is comprised of three north-south trending Cordilleras – the Western, Central and Eastern Cordilleras, which are separated by river basins and fault zones (Figure 2.7). The Eastern Cordillera and the eastern Central Cordillera are composed allochtononous to authochthonous basement rocks, whereas the Western Cordillera and western Central Cordillera are thought to be composed of accreted oceanic terranes (Maya and González 1995). These two units are separated by the Romeral Fault Zone, which extends into Ecuador (Maya and González, 1995). To the east of the fault there are strongly negative Bouguer anomalies, indicating that the basement is buoyant and therefore likely of continental origin, and to the west, Bouguer anomalies are positive, indicating high density material which is consistent with an oceanic origin (Case et al., 1971; Case et al., 1973). The cordilleras young from east to west, with the Central Cordillera thought to be older than

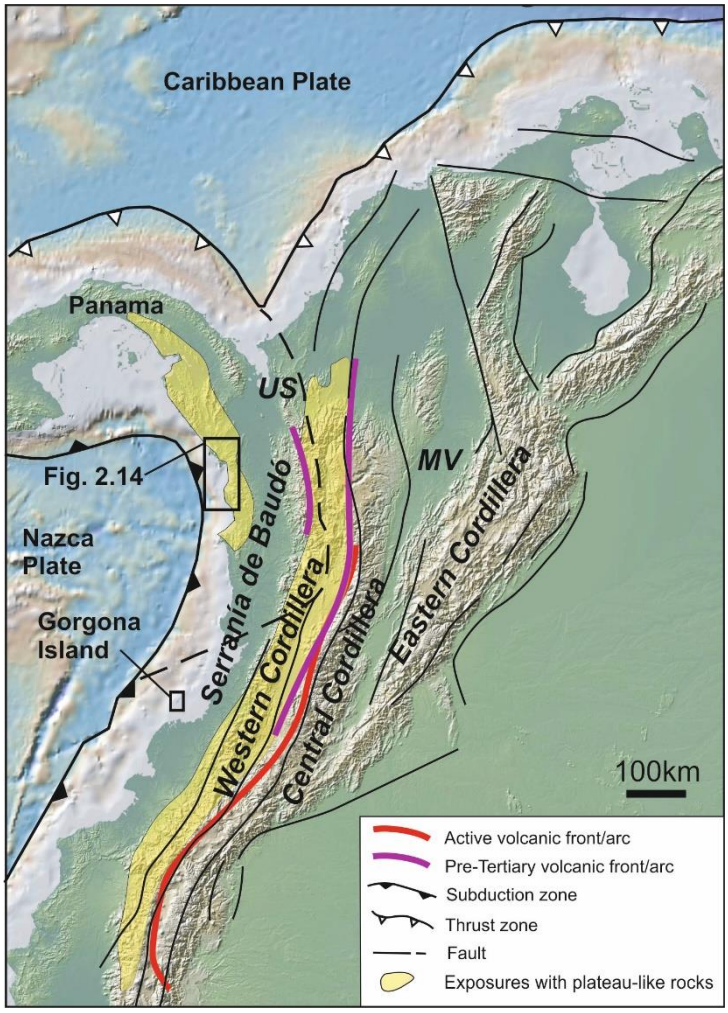

Figure 2.7: Map showing the locations of the Eastern, Central, and Western Cordilleras and the Serranía de Baudó, adapted from Buchs et al. (2010). MV = Magdalena Valley, US = Uramita Suture

100 Ma, the Western Cordillera dated at ~90 Ma, and the youngest in the Serranía de Baudó dated by $^{40}Ar/^{39}Ar$ at 73-38 Ma (Kerr et al., 1997a).

The Central Cordillera is formed largely of a Proterozoic metamorphic basement with Palaeozoic sediments and Jurassic magmatism. The western margin of the Central Cordillera is the Quebradagrande complex, which represents a fringing arc which formed on an extensional continental margin in the Late Cretaceous (Figure 2.8) (Nivia et al., 2006; Villagómez and Spikings, 2013; Spikings et al., 2015; Jaramillo et al., 2017). The Western Cordillera and Serranía de Baudó are largely formed of igneous rocks of the Caribbean Plateau and associated sediments (Nivia, 1996; Kerr et al., 1997a; Villagómez et al., 2011). Basalts and dolerites are tholeiitic with flat primitive mantle-normalised patterns, and some depletion of light REE (Kerr et al., 1997a; Villagómez et al., 2011), consistent with accreted fragments of an oceanic plateau (Kerr et al. 1997a). These plateau fragments were accreted when the Caribbean Plateau impinged against the continental margin of South America (Figure 2.8). The plateau could not be subducted, leading to progressive back-stepping of the subduction zone, with accreted plateau fragments (Kerr et al. 1997a). In the northern Western Cordillera there are also Mesozoic supra-subduction sequences, such as the Buga Tonalites and Santa Fe batholith, which represent a primitive island arc formed due to subduction along the eastern Margin of the Caribbean plateau, prior to its accretion to the South American continent (Weber et al. 2015). These rocks have negative Nb-Ta and Ti anomalies on primitive mantle-normalised multi-element diagrams, typical of subduction zones (Villagómez et al., 2011; Weber et al., 2015). Similar sequences are also thought to be exposed in Aruba (Wright and Wyld, 2011). This origin of the Buga tonalites and Santa Fe batholith is supported by the occurrence of a supra-subduction tuff found within oceanic plateau sequences in the northern Western Cordillera, indicating that there was subaerial volcanic activity along the margin of the plateau in the Late Cretaceous (Figure 2.8) (Buchs et al., 2018). Variable Th enrichments relative to Nb have also been detected within some plateau gabbros of the Western Cordillera, indicating a potential slab component in plateau magmas, potentially also related to this western facing subduction zone along the margin of the Caribbean Plateau (Buchs et al., 2018). If this western-facing subduction zone along the eastern margin of the Caribbean plateau also extended south to south eastern margin of the

Caribbean Plateau, this could explain the formation of the Panama Arc (Figure 2.8).

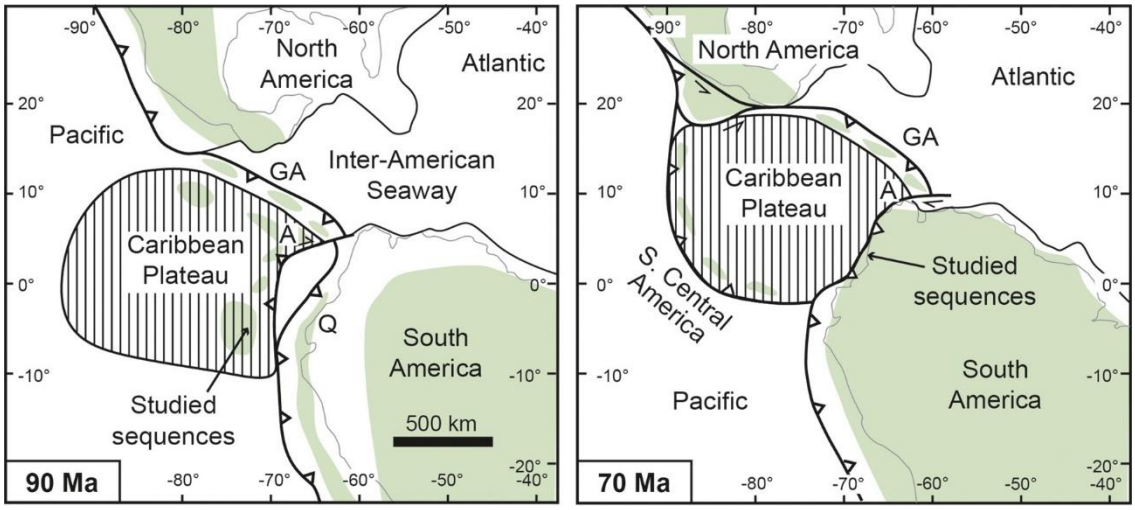

Figure 2.8: Tectonic model of the inter-American seaway in the Late Cretaceous from Buchs et al. (2018). Possible land exposures are shown in green. GA: Greater Antilles arc; A: Aruba Island part of the Colombian-Leeward Antilles arc (Wright and Wyld, 2011); Q: Quebradagrande complex

These findings aid in the understanding of the migration of the Caribbean Plateau between the Americas during the Cretaceous and Paleogene. It is thought that to facilitate this movement, subduction zones formed close to or along the southern and eastern rims of the plateau, forming Cretaceous volcanic arcs, such as those represented by the Santa Fe batholith and Buga Tonalites and in the eastern Caribbean (Figure 2.8) (Villagómez et al., 2011; Weber et al., 2015; Buchs et al., 2018). As the plateau impinged on the South American continent, fragments of both plateau and arc were accreted to the margin of the continent, forming the Western Cordillera. Subsequently, further oceanic plateau fragments were accreted to the margin, forming the Serranía de Baudó (Kerr et al., 1997a).

2.3 The Panama Isthmus

The Panama Isthmus lies on the Panama Microplate, bound to the NW with the continental Chortis block of Costa Rica by the Mesquito terrane, and to the south by the Uramita fault zone in NW Colombia (Figure 2.7) (Montes et al., 2012b). It is bound to the NE (with the current Caribbean plate) by the North Panama Deformed Belt (a diffuse thrust belt) and to the SW by a NE dipping subduction zone with the down going Nazca and Cocos Plates. It is composed of two blocks - Chocos and Chortega (Buchs et al., 2010) - which are composed entirely of magmatic products and sedimentary basins (Montes et al., 2012a). These magmatic products are related to arc volcanism, plateau volcanism and the accretion of oceanic islands (Montes et al., 2012a).

The Uramita fault zone is thought to have previously allowed the subduction of the Farallon plate under South America, prior to the Collision of the arc, with the North Panama Deformed Belt thought to have formed later, potentially during the collision of the arc with South America (Mann and Kolarsky, 1995). The main fault zones in Panama – the Azuero-Soná, Central Coiba, South Coiba and Joaquin – all have a NW-SE strike, with high angle dips (Buchs et al., 2011b). There are major offshore structures in the Gulf of Chiriqui, in the form of the Cebaco basin complex, composed of northeast-striking Plio-Pleistocene half grabens, and the Montuosa basin, an asymmetric Plio-Pleistocene sag basin (Mann and Kolarsky, 1995). The isthmus has a curvilinear shape, due to oroclinal bending of the isthmus, potentially due to the collision of the early isthmus with Colombia (Montes et al., 2012a). This bending has caused associated offset of the older volcanic fronts. The Panama Late Cretaceous –Eocene arc outcrops in the northeast of Panama as the San Blas-Darién Massif (Barat et al., 2014) and Chagres-Bayano Arc (Wegner et al., 2011). It also outcrops from southern Costa Rica through to the Soná and Azuero Peninsulas in western Panama (Figure 2.9) (Buchs, 2008; Buchs et al., 2010). The younger, post-Eocene volcanic arc outcrops across western Panama in the Central Cordillera up to the Panama Canal Fault zone, and is also found in eastern Panama in the Majé (Whattam et al., 2012). In the west of Panama, the young volcanic arc and its associated sediments largely cover the evidence for a Cretaceous-Eocene volcanic arc (Barat et al., 2014).

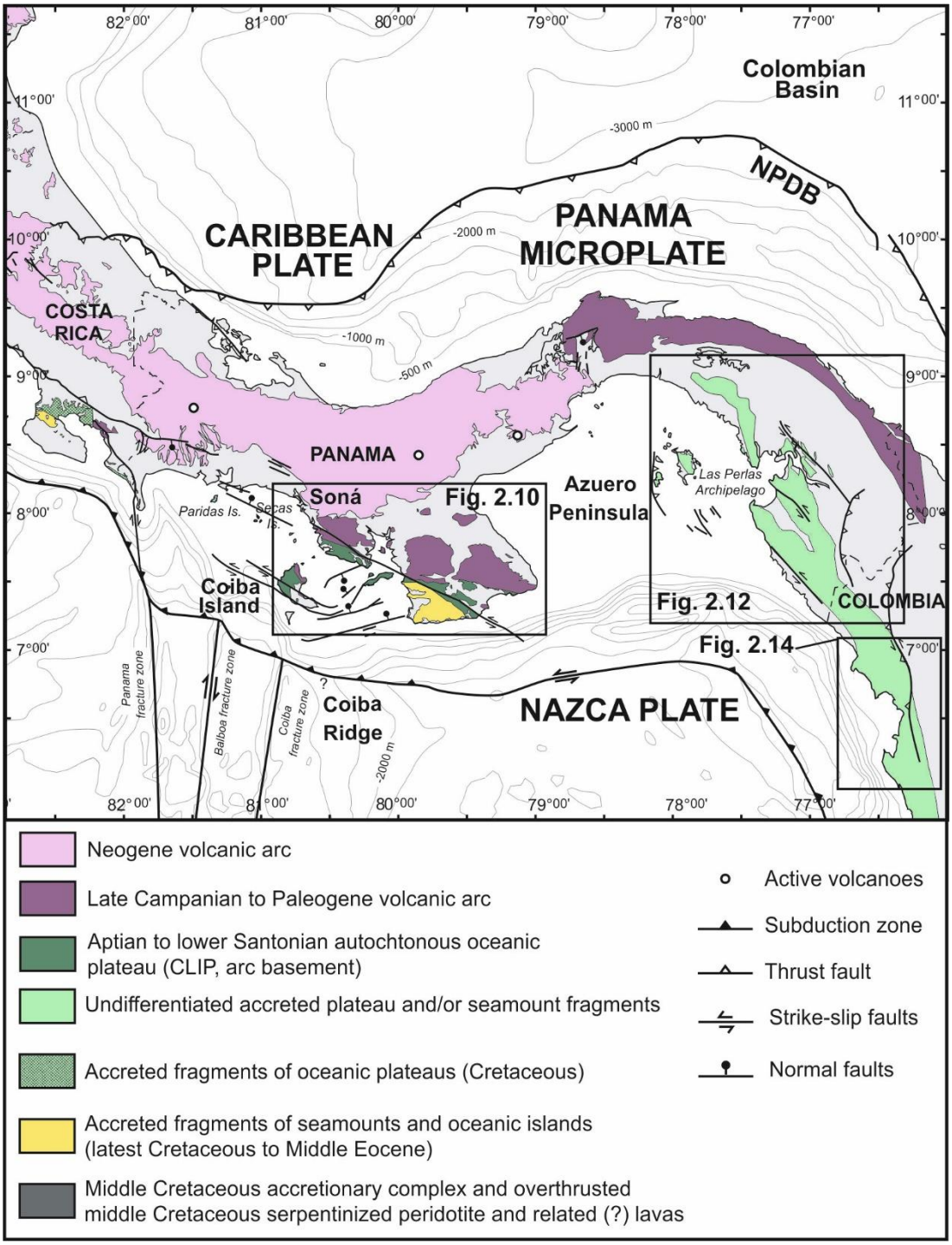

Figure 2.9: Simplified geological map of southern Central America modified after Buchs et al. (2011).

2.3.1 Azuero and Soná

The earliest initiation and development of the Panama Late Cretaceous-Eocene arc is best exposed in the southern coast of eastern Costa Rica and western Panama, where the fore arc has been uplifted due to the subduction of ridges and seamounts of the Cocos and Nazca plates (Gardner et al., 2001; MacMillan et al., 2004; Sak et al., 2009; Buchs et al., 2010). The forearc in these areas is formed of uplifted igneous and accretionary complexes of Early Cretaceous to Miocene age, including seamounts, the oceanic plateau and associated forearc sedimentary deposits (Figure 2.10) (Corral et al., 2013). The Golfito Complex is composed of (1) an igneous basement, formed of Campanian lava flows, overlain by (2) the Golfito Formation, formed of interlayered lava flow and late Campanian to middle Maastrichtian tuffaceous hemipelagic limestones and (3) a Maastrichtian to Paleocene volcaniclastic-tuffittic sequence (Di Marco et al., 1995; Buchs et al., 2010). Although it had previously been interpreted as a sequence of the oceanic plateau, the stratigraphy and geochemistry indicates that the Golfito lavas may have formed above a nascent subduction zone (Buchs et al., 2010). In Panama, the Azuero area, the area including Azuero Peninsula, Soná Peninsula and Coiba Island, can also be described as an igneous basement, overlain by forearc sediments (Buchs et al., 2010). The geology of the Azuero Area is formed of 4 main units: (1) The Azuero Marginal Complex, (2) the Azuero Melange, (3) the Azuero Accretionary Complex and (4) younger overlap sequences, partially overlying 1, 2, and 3 (Figure 2.10). The Azuero Melange lies between the Azuero Marginal Complex and the Azuero Accretionary Complex, and is a tectonic melange which occurs along the Azuero-Soná Fault Zone (Figure 2.10). The Azuero Accretionary Complex occurs in the southwest corner of the Azuero Peninsula, and is composed of large accreted pieces of oceanic islands (Figure 2.10) (Buchs et al., 2011a).

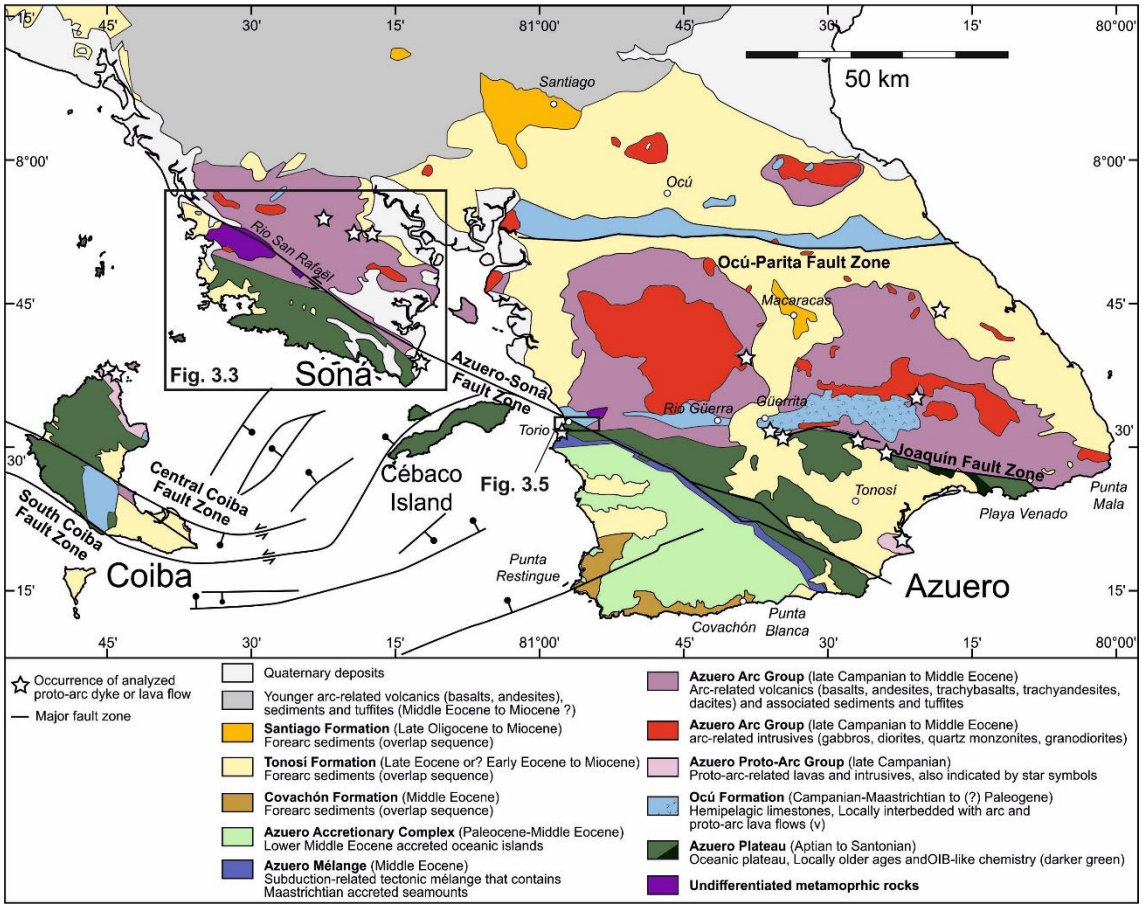

Figure 2.10: Geological Map of the Azuero area modified after Buchs et al. (2011).

The Azuero Marginal Complex is found on Coiba Island, Soná and Azuero Peninsulas, and is composed of plateau sequences and arc related sequences (Figure 2.10). Based on field observations, geochemical data, $^{40}Ar/^{39}Ar$ radiometric ages and biostratigraphic ages, the Azuero Marginal Complex is divided into 5 tectono-stratigraphic units: (1) The Azuero Plateau, (2) the Ocu Formation, (3) the Azuero Protoarc Group, (4) the Azuero Arc Group and (5) undifferentiated metamorphic rocks (Figure 2.11). The Azuero Plateau is part of an oceanic plateau forming the basement to the arc (Buchs et al., 2010). It occurs in the southern part of the Azuero Marginal Complex, and is composed of massive, columnar or pillow basalts, with rare interbeds of red chert. The plateau is locally interbedded with radiolarites which has been dated as Coniacian-early Santonian (~89-85 Ma) (Mann and Kolarsky, 1995). This age is within the range of existing $^{40}Ar/^{39}Ar$ and K/Ar ages from Azuero and Soná, which range from 114.5 ± 2.0 to 71.3 ± 2.1 Ma (Hoernle et al., 2002; Lissinna, 2005). Geochemically, the plateau consists of two groups, which both have tholeiitic differentiation trends. Group I is found across Soná and Azuero Peninsulas and trace elements show typical plateau like affinities, with Group II found only on Azuero Peninsula at Playa Venado and are more enriched in light rare earth elements. The plateau is thought to form the basement to the arc, and be the lowermost unit of the Azuero Marginal Complex

due to dykes and sills of the arc and protoarc intruding into plateau sequences, along with stratigraphic relationships with the Ocu Formation.

The Ocu Formation lies stratigraphically above the plateau and is locally interbedded with lavas of the proto-arc and arc (Kolarsky et al., 1995; Buchs et al., 2010). It is composed of pelagic to hemipelagic limestones, which are located mainly along the Ocu-Parita Fault Zone, the western Azuero Peninsula and Coiba Island (Figure 2.10). The limestone ranges in composition from grey and micritic, with little detrital or tuffaceous input, to a bioturbated and tuffaceous limestone, with a detrital component. Kolarsky et al. (1995) recognised two distinct groups of the Ocu Formation – the first represented by limestone, and the second dominated by fine grained calcareous siltstone and sandstone. The detrital component indicates an intermediate to differentiated volcanic source, and included quartz, amphibole, pumice and zoned feldspars. The Ocu Formation was also divided by Buchs (2008). In this case, the Ocu Formation represented the older, pelagic limestones with little to no detrital component, while the Torio Lithostratigraphic Unit represented hemipelagic limestones, interbedded with the lavas of the proto-arc and arc, with a more significant detrital and tuffaceous component (Buchs, 2008; Buchs et al., 2011b). The limestones from north Azuero were previously been assigned Campanian-Maastrichian age (Del Giudice and Recchi, 1969) but more recently, limestones from north Azuero and Coiba have been assigned a late Campanian age as dated by pelagic foraminifera (Buchs et al., 2010) . The formation is thought to have formed before and during arc development, on top of the Azuero Plateau (Buchs et al., 2011b). Sediments with characteristics similar to those of the Ocu Formation have also been described in central Azuero, in the Rio Quema Formation (Corral et al., 2011). Buchs et al. (2010) named this formation as part of the Ocu Formation, due to the similar lithologies and stratigraphic constraints.

The Azuero Protoarc Group occurs as mafic dykes crosscutting both the Azuero Plateau and Ocu Formation, as well as massive and pillowed lava flows which can be interbedded with limestones of the Ocu Formation. Typically, these rocks have abundant plagioclase phenocrysts, which are generally absent in rocks of the Azuero Plateau. The Azuero Protoarc also has a tholeiitic differentiation trend and has a geochemical composition intermediate between plateau and arc, and is thought to represent a primitive island arc (Buchs et al., 2010). On Coiba Island, a protoarc dyke crosscuts a hemipelagic limestone of the Ocu Formation which displays synvolcanic soft deformation. Foraminifera from this limestone have been dated as late Campanian (~75-73 Ma) which represents only age constraint on the the age of emplacement of the Azuero Protoarc Group (Del Guidice and Recchi, 1969; Buchs et al., 2010). It represents a primitive island arc sequence, which intrudes and overlies the Azuero Plateau and Ocu Formation. The Azuero Arc Group is

exposed across central and northern Azuero and Soná Peninsulas as mainly intermediate to silicic lavas and related intrusives, with tuffites and volcaniclastic sediments (Mann and Kolarsky, 1995; Lissinna, 2005; Wörner et al., 2009; Wegner et al., 2011). The Azuero Arc shows low-Fe differentiation trends and trace element contents are typical of island arcs, with progressive enrichment in incompatible elements, with negative Nb-Ti anomalies on primitive mantle normalised multielementary diagrams. Existing $^{40}Ar/^{39}Ar$ ages of the Azuero Arc rocks range from ~71 to 40 Ma, with a general age trend, with the youngest found towards the south of arc exposures on the peninsulas, and the youngest found in the north into the western isthmus (Lissinna, 2005; Wegner et al., 2011).

The presence of the Ocu Formation, overlying the Azuero Plateau and forming prior to the eruption of the Azuero Protoarc Group suggests that there was a cessation in magmatic activity between the formation of these two groups. This, combined with the apparent gap in ages of formation between plateau and proto-arc, indicates that the the plateau ceased forming before subduction lavas were erupted (Buchs et al., 2010). However, this age gap may only be due to limited dates for the protoarc, and further ages need to be obtained for this to be confirmed. Using currently available dates, it appears that the transition from proto-arc to the mature Azuero Arc could have taken place within ~5 Ma (Buchs et al., 2010; Buchs et al., 2011b). The presence of a porphyritic texture mineral accumulation within the Azuero Protoarc Group indicates that magma chambers developed rapidly after the onset of subduction initiation (Buchs et al., 2010).

Undifferentiated metamorphic rocks have previously been recognised along the Rio Torio on Azuero Peninsula, and Rio San Rafael on Soná Peninsula, and have been described as greenschists (Del Guidice and Recchi, 1969; Recchi, 1976) and as schistose amphibolites, with minor amounts of metasediments and metatuffs (Tournon et al., 1989; Buchs et al., 2011b). They outcrop in association with sequences of the Azuero Plateau, often along faulted zones (Buchs et al., 2011b). Along the Rio Torio, it was noted that sediments interbedded with the amphibolites had relic cross-stratification, and recrystallised shells of mico-organisms (Tournon et al., 1989). Some amphibolites had evidence of amagmatic tecture, with relics of magmatic clinopyroxenes and plagioclase, whereas other samples contained no remnant of magmatic texture (Tournon et al., 1989). In Azuero, rocks which had reached an amphibolite facies conditions, had been partly retromorphosed to greenschist facies (Buchs et al., 2011b). Geochemically, these rocks are ultramafic, with

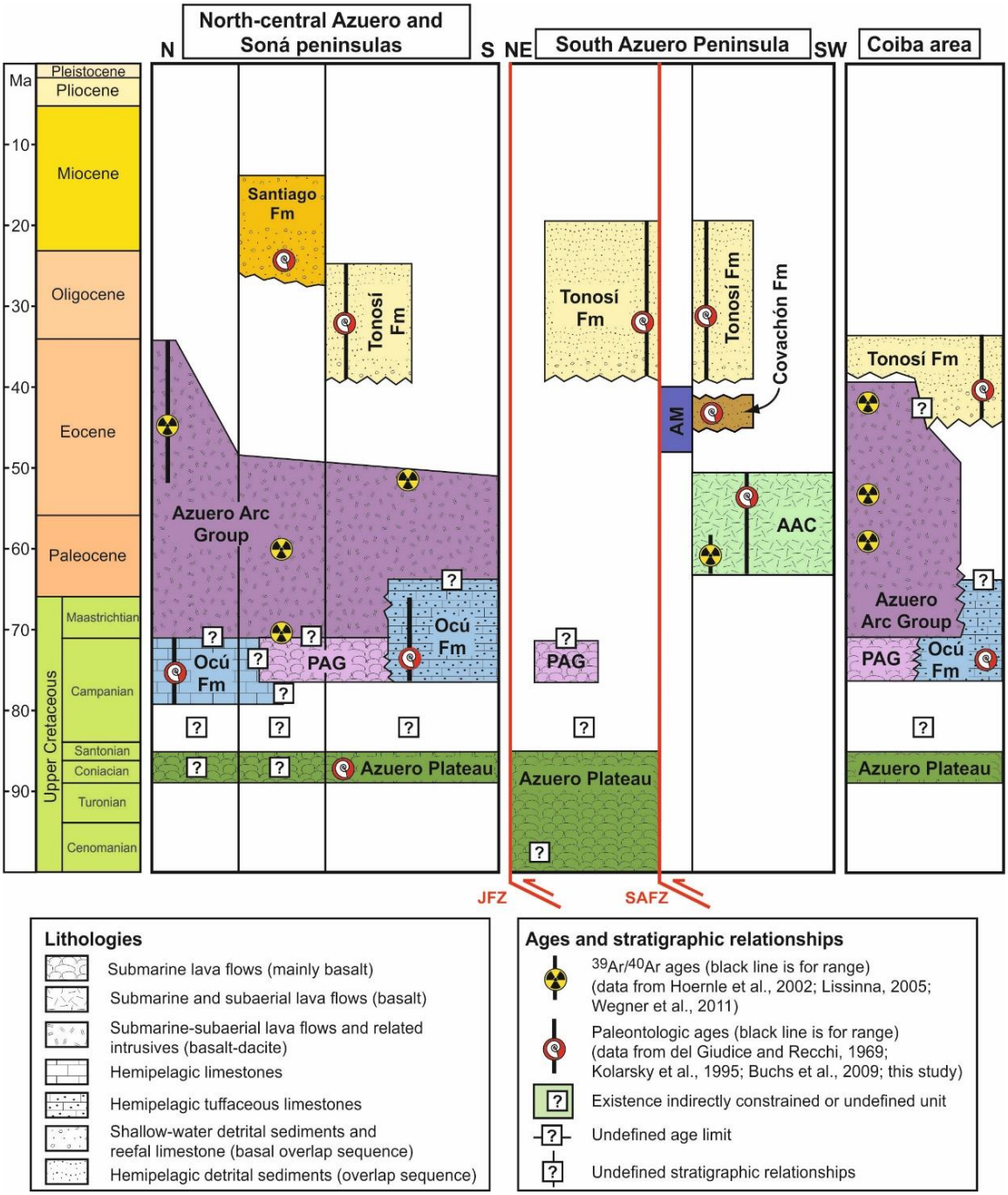

Figure 2.11: Chronostratigraphic chart of Cretaceous to Miocene units and formations of the Azuero area from Buchs et al. (2011). PAG = Proto-arc Group, AM = Azuero Mélange and AAC = Azuero Accretionary Complex.

MgO wt. % =10.87 -21.82 (Tournon et al., 1989). Along both rivers, the greenschists were intruded by unmetamorphosed dykes (Tournon et al., 1989; Buchs et al., 2011b). The age and stratigraphic position of these sequences are not known. It has been suggested that they formed from local recrystallisation of picritic basalts in fracture zones, or that they could be metamorphic remnants of an older volcanic complex (Tournon et al., 1989).

Younger sequences overly the Azuero Marginal Complex, the Azuero Accretionary Complex and the Azuero Melange, and have been described in detail as the Tonosi and Santiago Formations (Recchi and Miranda, 1977; Kolarsky et al., 1995; Buchs et al., 2010), with the Covachon recognised more recently by Buchs et al. (2011b). The Covachon Formation is exposed on the southwest Azuero Peninsula, and unconformably overlies the Azuero Accretionary Complex (Figure 2.10, 2.11). It is separated from the overlying Tonosi formation by another unconformity. The Covachon Formation is over 300m thick, formed of folded and faulted sediments with three main facies (Buchs et al., 2011b). Facies 1 is composed of interbeds of volcaniclastic calcareous mudstone, siltstone and sandstone which exhibit parallel- and cross-bedding and grading. The sediments contain a detrital component, which is composed of feldspar, basaltic fragments, sediment fragments and biogenic debris (Buchs et al., 2011b). Facies 2 is composed of thick chaotic deposits, which vary in thickness from 50cm to potentially 50m, and are interbedded between Facies 1 and 3. These deposits are matrix supported, and are poorly sorted, with clasts that are subangular to well rounded and range in size from a few mm to m. Rarely they reach 30m in size (Buchs et al., 2011b). Clasts are composed of basalt, shallow marine limestone and soft-deformed sediments. Facies 3 is composed of sandstones with pebbles of basalt and shallow marine limestone. The clasts composition for all 3 facies indicate that the source is the Azuero Accretionary Complex (Buchs et al., 2011b). The Covachon Formation is interpreted to be a shallowing up sequence deposited on top of the Azuero Accretionary Complex, synchronously to the emplacement of the Complex. Facies 1 interpreted as turbidites, Facies 2 as a mass-flow deposit, and Facies 3 as slope, near-shore deposits (Buchs et al., 2011b). The Covachon is dated as Early Miocene to Middle Miocene - with an Early-Middle Eocene age from larger benthic formainifera near the base of the section, but a Middle Eocene age from large benthic formaminifera from the chaotic deposits (Buchs et al., 2011b).

The Tonosi formation is exposed across the Azuero area, overlying the Covachon Formation in southwest Azuero Peninsula (Figure 2.10). It has been described as having ~40-400m basal transgressive unit with coarse clastic rocks and interbedded shallow marine limestone, followed by a ~500-800m thick deepening upward section of turbiditic sequences (Kolarsky et al., 1995). Kolarsky et al. (1995) described these as the lower and upper unit of the Tonosi formation of Azuero Peninsula. The lower unit overlies the Azuero Marginal Complex and Azuero Accretionary Complex and is composed of conglomerate, coarse sandstone and shallow marine limestone (Figure 2.11) (Buchs et al., 2011b). The upper unit is composed of deeper marine interbedded graded sandstone, siltstone, shale and calcarenite (Buchs et al., 2011b). The Tonosi formation contains a detrital component, which is composed of

fragments of basalt, plagioclase (some with zonations), larger benthic foraminifera, organic debris, chert, alkali feldspar, clinopyroxene, hornblende, quartz and opaque oxide minerals (Krawinkel et al., 1999; Buchs et al., 2011b). This suggests that the uplifted Azuero Arc Group and the Azuero Accretionary Complex were the sources of the Tonosi formation (Buchs et al., 2011b). The lower Tonosi formation has been dated as Mid Eocene to Late Oligocene (Recchi and Miranda, 1977). However, based on the revised tectonostratigraphic subdivision of Buchs et al. (2011b), three samples from the base of the formation provided Late Eocene to Early Oligocene ages, based on larger bethic foraminiferal biozones. The upper Tonosi formation was dated as late Oligocene to early Miocene, based on nannofossils from four shale samples (Kolarsky et al., 1995). The Tonosi Formation was not observed on Soná Peninsula, but it was noted by Kolarsky et al. (1995) that there were reportedly similar rocks along the southwestern coast (Metti et al., 1972; Metti, 1976).

The Santiago formation is exposed in northern Azuero Peninsula, and in central Panama within the Macaracas Basin in central Azuero (Figure 2.10) (Kolarsky et al., 1995). The sediments of the Maracaras Basin have also previously been described as the “Macaracas Formation” by Krawinkel et al. (1999) and are composed of sandstone, siltstone, shale and coal in a neritic to terrestrial environment. It was postulated by (Buchs et al., 2011b) that this Macaracas sediments may have been deposited at the same time as the upper Tonosi Formation, during the Late Oligocene and Miocene (Kolarsky et al., 1995).

2.3.2 Darién Pacific Coast

In comparison to western and central Panama, eastern Panama has undergone little geological study. Early work in the Darién was undertaken in relation to exploration for canal building, gold mining or oil exploration. Bandy (1970) and Bandy and Casey (1973) were the result of exploration of possible new canal routes, and Esso (Esso Exploration and Production Panama, 1970; Esso Exploration and Production Panama, 1971) produced geological maps for parts of the Darién. These works have been complied and built upon by more recent publications, to develop a new stratigraphic framework for the Darién (Coates et al., 2004; Barat et al., 2014). This stratigraphic framework has been based on the Darién, Bagre and Sapo Massifs, and the Chucunaque-Tuira Basin. The Chucunaque-Tuira basin is a massive basin which forms central lowland parallel to the Darién and San Blas Massifs (Figure 2.12). It continues into Colombia as the Atrato Basin (Duque-Caro, 1990d; Duque-Caro, 1990c). The stratigraphic framework has 3 main sections: (1) Upper Cretaceous to

Eocene basement rocks (San Blas Complex), (2) Eocene to lower Miocene arc-related rocks (The Darién Formation, The Porcona Formation and the Clarita Formation, with intrusive igneous rocks) , and (3) Mid to Late Miocene sedimentary cover (Figure 2.12, 2.13) (Coates et al., 2004; Barat et al., 2014).

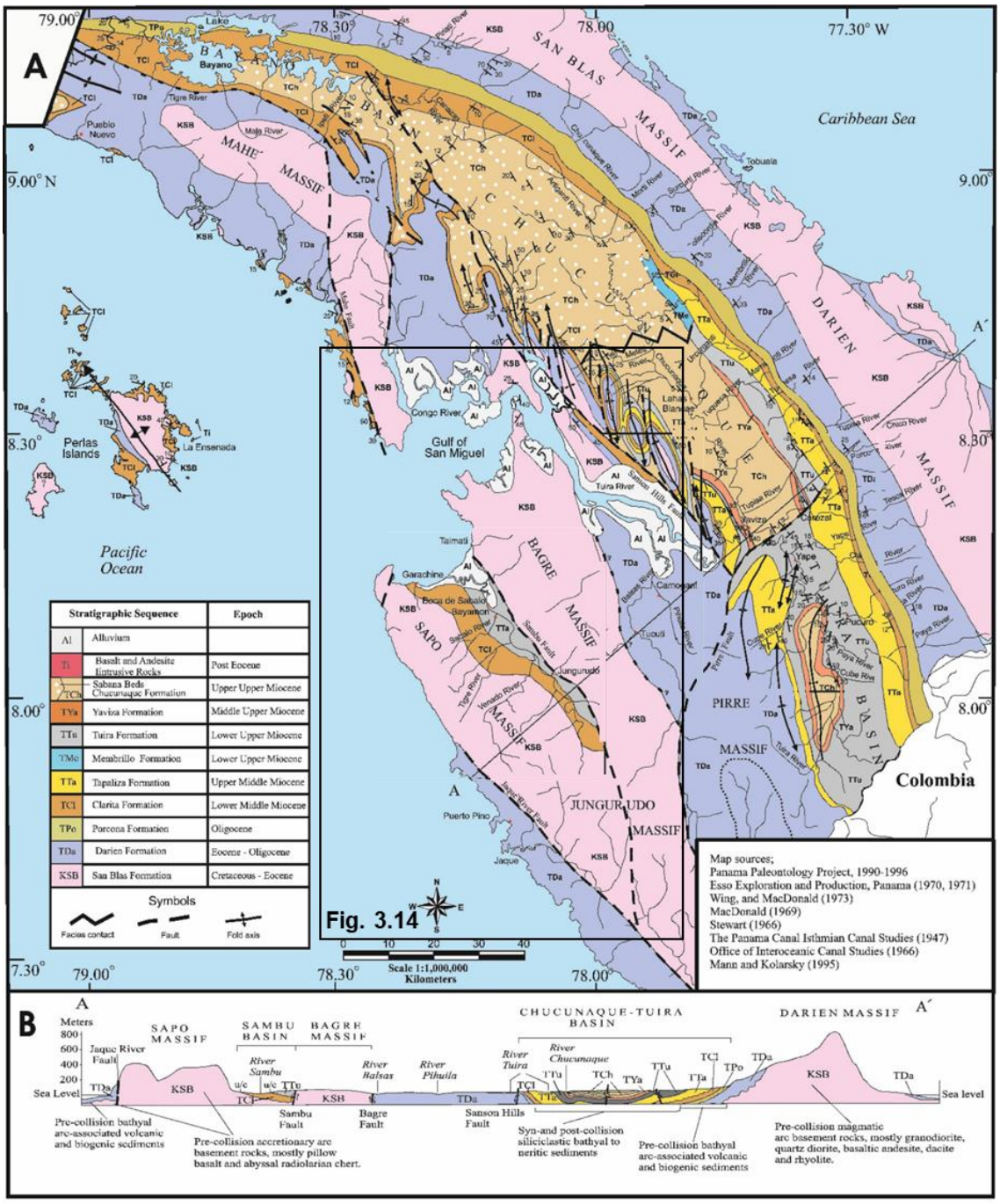

Figure 2.12: Geological map (A) and cross section (B) of the Darién region modified from Coates et al. (2004).

The San Blas Complex is exposed in the San Blas-Darién Massif (in the Chagres-Bayano arc of Wegner et al. (2011)), on the Caribbean Coast of Panama, and though the Maje, Bagre and Sapo Massifs (Figure 2.12) (Barat et al., 2014). It is composed of a pre-Mid Eocene magmatic basement, along with volcanoclastic rocks and sedimentary formations (Esso Exploration and Production Panama, 1970; Esso Exploration and Production Panama, 1971; Bandy and Casey, 1973), thought to represent both plateau and arc related sequences (Lissinna, 2005; Wegner et al., 2011; Barat et al., 2014). Around the North of the Chucunaque-Tuira Basin, in the San Blas-Darién Massif, the complex is largely composed of arc rocks, which are thought to form part of the same arc front as the Azuero Arc (Wegner et al., 2011). It is composed of quartz diorites, granodiorites and dacites, along with basaltic andesites, rhyolites and volcanic breccia interbedded with layers of chert, volcanic sandstone and tuff (Barat et al., 2014). This rock assemblage reflects the composition of a volcanic arc, with the geochemistry of samples showing a typical arc signature, including depletions in Nb and Ta (Wegner et al., 2011). Samples from the Chagres-Bayano arc, dated by $^{40}Ar/^{39}Ar$ geochronology gave ages of between 66 to 42 Ma (Wegner et al., 2011). A stratigraphy similar to that of the Azuero Marginal Complex has also been recognised in Chagres. At the base of this sequence are basalts interpreted to be part of a plateau basement, with moderately depleted patterns on primitive mantle-normalised diagram. These plateau rocks are overlain by proto-arc basaltic sequences, which have trace element contents broadly intermediate between plateau and arc, with variable Th and LREE enrichment and depletion and small Nb and Ti negative anomalies on primitive mantle normalized multielement diagrams (Montes et al., 2012a). The arc rocks overlie these protoarc and plateau sequences, and have depleted to enriched patterns on primitive mantle normalized multielement diagrams, with strong Nb-Ti negative anomalies (Montes et al., 2012a). The compositional and stratigraphic similarity of arc rocks in Azuero (Buchs et al., 2010) and those in Chagres (Wegner et al., 2011; Montes et al., 2012a) suggests that they are part of the same volcanic belt which has now been laterally offset.

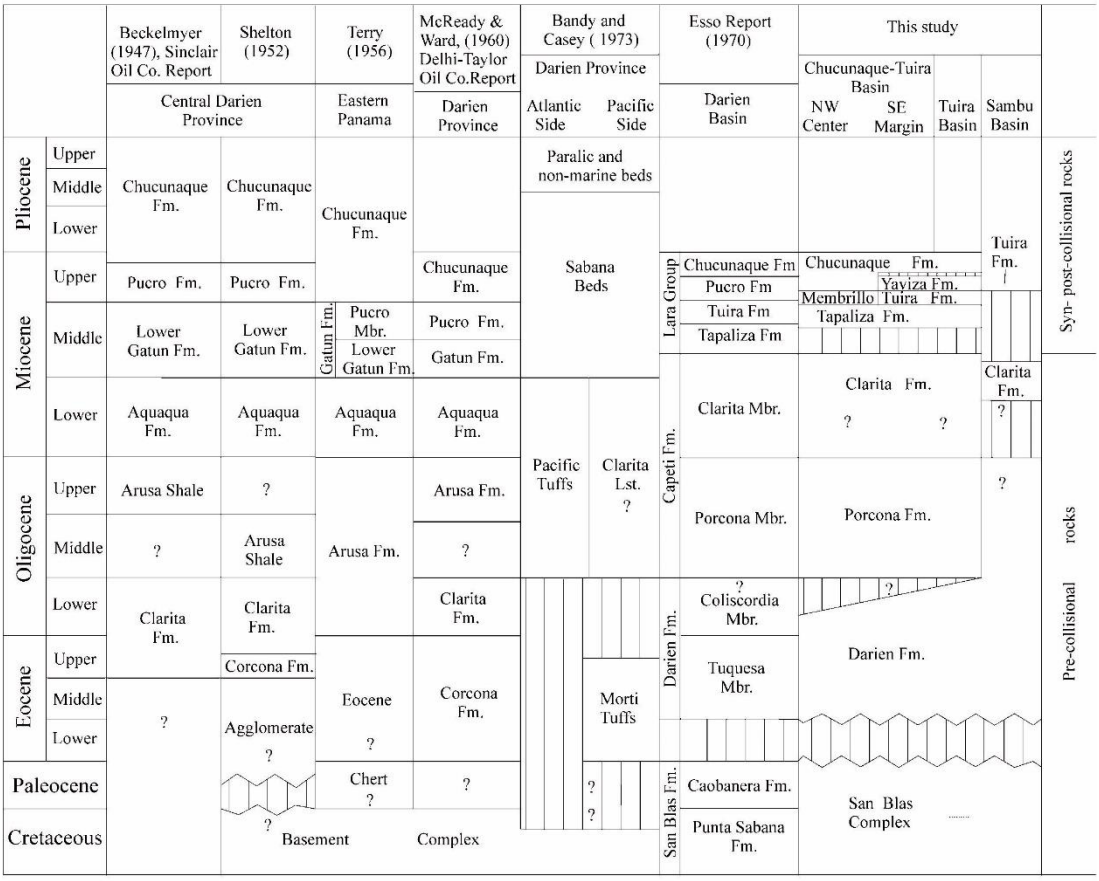

Figure 2.13*:* Summary of previous Darién region lithostratigraphic nomenclature from published and unpublished reports from Coates et al. (2004).

However, to the south, around the San Miguel Gulf, the San Blas Complex is composed of dolerites, pillow basalts and radiolarian chert (Coates et al., 2004). The cherts here are faulted and folded, interbedded with the pillowed and massive basalts (Barat et al., 2014). This southern group has been previously referred to as the Punta Sabana volcanics (Bandy and Casey, 1973). These rocks are also exposed further south along the coast, towards Jaqué (Barat et al., 2014). Cherts from the San Miguel Gulf were estimated to be Late Campanian, based on radiolarian ages (Bandy and Casey, 1973). These lavas and chert have been interpreted to form the plateau basement to the Isthmus, which could be related to the Caribbean Oceanic Plateau (Lissinna, 2005; Barat et al., 2014). These basalts have a plateau geochemistry, with variable enrichment and depletion in incompatible elements (Lissinna, 2005). The age of the San Blas Complex is thought to be Late Cretaceous-mid Eocene (Maury et al., 1995; Lissinna, 2005; Wörner et al., 2009; Wegner et al., 2011). Basalts from from Bahia Piña gave $^{40}Ar/^{39}Ar$ ages of 84.1 ± 1.0 Ma and 71.3 ± 4.4 Ma (Lissinna, 2005). These ages are consistent with ages of the Azuero Plateau (~89-85 Ma) (Kolarsky and Mann, 1995; Buchs et al., 2010) and plateau ages from the Serranía del Baudó (78-72 Ma) (Kerr et al., 1996c). This is supported by early studies found that throughout the east of the Panama Isthmus, Bouguer anomalies were around +120mgal,

indicating a dense basement such as a raised block of oceanic crust (Case, 1974). Similar positive Bouguer anomalies were found over Azuero Peninsula, where there is a plateau basement (Case, 1974).

The Darién formation has been included in recent stratigraphic sections by Coates et al. (2004) and Barat et al. (2014). It is mainly defined by ages of lithologies between Middle Eocene to Late Oligocene and remains poorly constrained in the field. It has an estimated thickness of between 500m and 1500m and is thought to have formed of two sections, with fine to medium grained tuff, volcanic breccia, volcaniclastic sandstone, conglomerate, radiolarian chert and basalt in the lower section (Coates et al., 2004; Barat et al., 2014). The upper Darién Formation unconformably overlies the lower section, and is formed of calcareous and siliceous mudstone, with micritic calcarenite, black sandstone and medium grained tuff (Coates et al., 2004; Barat et al., 2014). Detrital fragments indicate that the source of the upper unit is the San-Blas complex, with fossil assemblages indicating a hemipelagic environment of deposition (Barat et al., 2014). Within the upper unit, nannofossil ages indicate a Late Oligocene to Early Miocene age (Barat et al. 2014). This unit may correlate to the Middle Oligocene to Early Miocene Pacific Tuff described in Bandy (Figure 2.13) (1970). It is thought that the lower section may correlate to the previously described Morti Tuffs (Bandy, 1970), which were described as a deep water facies with agglomerates, basalts, tuffaceous limestone, sandstone and shale, which overly a basaltic basement (Bandy, 1970; Bandy and Casey, 1973). This unit was assigned an Eocene age, although the origin of this age is not clear.

The Porcona Formation is mainly exposed to the north of the Chucunaque-Tuira Basin, with some along the southern flank (Figure 2.12) (Coates et al., 2004; Barat et al., 2014). It has a thickness of between 200m and 700m, and includes foraminiferal shale, glassy tuff with radioalaria and bioclastic limestone (Coates et al., 2004; Barat et al., 2014). The presence of larger benthic foraminifera and red algae in the limestone indicates a shallow marine depositional environment (Coates et al., 2004; Barat et al., 2014). The formation is Late Middle Eocene to Late Oligocene in age, dated by large benthic foraminifera and nannofossil biozones (Barat et al., 2014). The Porcona Formation overlies the San Blas Complex (Figure 2.13) (Coates et al., 2004).

The Clarita Formation is exposed across the Chucanaque-Tuira and Sambu Basins, the Maje Massif and the Sapo Massif, with a thickness ranging between 200m and 2000m (Figure 2.12) (Coates et al., 2004; Barat et al., 2014). It is composed of clastic sediments, containing a high proportion of carbonate fossiliferous clasts. The base of the formation

contains conglomerates, and reworked andesitic volcanic clasts. The sequence then largely alternates between conglomerates, breccias, sandstone, thick calcarenite and fossiliferous sandstone (Barat et al., 2014). On the western flank of the Chucunaque-Tuira Basin, the unit is composed of a fine micritic bioclastic limestone, with a detrial component which is composed of glauconite, feldspar and lithic fragments However, the tlimestone is formed of up to 60% foraminifera (Coates et al., 2004). These sequences contain a detrital component, with glauconite, feldspar and lithic fragments. The top of the formation is composed of siliceous to calcarareous fine tuff and limestone (Barat et al., 2014). The formation unconformably overlies the sequences of the Darién Formation in the Maje but overlies the San Blas Complex in the Sapo Massif (Barat et al., 2014). It is estimated to be deposited at lower to mid bathyal depths during the lower Middle Miocene, dated using calcareous nannoplankton and planktic foraminifera biozones (Coates et al., 2004).

In the Maje, the San Blas Complex and Darién Formations are crosscut by intrusions, composed of mesocratic to leucocratic dykes and andesites to dacites (Barat et al., 2014). These dykes have been reworked in areas, such as the reworked andesite at the base of the Clarita Formation. These rocks are thought to be part of an Oligocene to Late Miocene volcanic arc. A basaltic andesite from Bahia Piña gave an $^{40}Ar/^{39}Ar$ age of 21.7 ± 0.3 Ma, a basalt from Isla del Rey gave a similar age of 21.9 ± 0.7 Ma and a dacite from the Pearl Islands gave a younger age of 18.4 ± 0.3 Ma (Lissinna, 2005) (Figure 2.12). Geochemically the samples have typical arc like characteristics on primitive mantle-normalised multi-element diagram, with negative anomalies of high field strength elements such as Nb, Ta, Zr and Ti. However, this is based on limited trace element data from the Darién, and more investigation is needed to characterise the basement and overlying arc (Lissinna, 2005). There are potentially associated intrusive rocks also found in western Panama at Cerro Petaquilla, and in central Panama in the Panama Canal Basin (Whattam et al., 2012). It is thought that this younger arc assemblage represents the migration of arc volcanism that arc volcanism migrated from the Chagres-Bayano arc and San Blas Cordillera to the Maje range in the Eocene, due to oroclinal bending of the isthmus associated with the collision with Colombia. It is possible that this volcanic arc extends further east into the Darién but this has not yet been documented (Buchs et al., 2019b).

The young overlap sedimentary deposits are of an upper Middle Miocene to Late Miocene age, separated from the older sequences by a regional unconformity from between 14.8-12.8 Ma (Coates et al., 2004). They have a 3000m thickness in the Chucunaque-Tuira Basin, formed of upper Middle Miocene Tapaliza Formation, lower Upper Tuira and Membrillo Formations, middle Upper Miocene Yaviza Formation, Middle to Upper Miocene

Chucunaque Fm (Coates et al., 2004). The Tapaliza Formation is exposed along the Tapaliza River, a tributary of the Tuira River. It is composed of foraminiferal mudstone and siltstone, volcanic sandstone, and alternating sandstone and clayey siltstone. It is thought to be formed at a middle bathyal to upper bathyal depths (Coates et al., 2004). The Tuira Formation is formed of alternating greywacke and arkosic sandstone silty claystone and siltstone, with minor volcanic sandstone and pebble conglomerate. It is thought to have formed at mid bathyal to inner neritic depths (Coates et al., 2004). The Membrillo Formation is exposed along the Membrillo river, within the Bayano Basin, and is the lateral equivalent of the Tuira Formation. It is formed of grey shelly mudstone, forming in middle bathyal, oxygen deficient conditions (Coates et al., 2004). The Yaviza Formation is composed of a massive bedded bioturbated, shelly, lithic sandstone, and was deposited in a middle neritic environment (Coates et al., 2004). The Chucunaque Formation is formed of blocky to massive silty claystone to siltstone with minor volcanic sandstone, formed in an inner neritic to upper bathyal depositional depth (Coates et al., 2004).

This stratigraphy has been interpreted to represent the closure of the Panama Isthmus by Coates et al. (2004), with the San Blas Complex basement rocks, and Eocene to lower Miocene arc-related rocks representing pre-collisional assemblages, and the sedimentary cover being post-collisional assemblages (Figure 2.13). The closure is therefore represented by the unconformity between the Clarita Formation and the overlap sediments, between 14.2 to 12.2 Ma. The precollisional assemblages are formed in open ocean environment, with submarine, volcanic, siliceous and calcareous biogenic sedimentary facies, whereas the younger overlap assemblages are formed of coarsening and shallowing upwards silicilastic facies, indicating a proximal continental landmass (Coates et al., 2004).

2.3.3 Serranía de Baudó

The Serranía de Baudó is located within the Choco Region of Colombia along the Pacific coast (Figure 2.9). It is thought to represent the youngest accreted oceanic plateau fragments in Colombia (Kerr et al., 1997a), and is part of the Panama-Choco block, thought to have accreted to the South American continent along the Uramita suture (Early work on the Serranía de Baudó was undertaken by Bandy (1970), Case et al. (1971), Gansser (1973) and Goossens et al. (1977). More recently, there has been more work on the geochemistry of the basalts of the area (Kerr et al., 1997a), and the stratigraphy ((Duque-Caro, 1990c). INGEOMINAS (Instituto Nacional de Investigaciones Geologico-Mineras – now part of the Servicio Geologico Colombiano) produced maps and stratigraphic sections,

with associated bulletins (Parra and Gonzalez 2002, Cossio, 2003). The stratigraphy as described by the Geological Survey is as follows: (1) Baudó,Basalts (2) Clavo Formation, (3) Uva Formation, (4) Sediments of the Rio Apartado, (5) Napipi Formation and (6) Sierra Formation (Figure 2.14, 2.15) (Parra and Gonzalez 2002, Cossio, 2003).

The Baudó Basalts are the oldest rocks within the Serranía de Baudó, and outcrop along the Baudó coast thought to be exposed from Cape Corrientes to the south, to Panama in the north (Figure 2.6). The unit consists of pillowed and massive basalt, along with some basaltic breccias, dolerites and gabbros, with intercalations of tuff, sandstone, chert and limestones (Kerr et al. 1997a, Parra and Gonzalez 2002, Cossio, 2003).

The basalts form a large proportion of the unit, with it being estimated that the basalts and dolerites form more than 90% (Cossio, 2003). The basalts are generally grey-green, fine grained and aphanitic with rare vesicles. Rare pyroxene phenocrysts are altered to chlorite, tremolite and calcite, and it is common to find veins composed of quartz, epidote, chlorite and zeolites (Cossio, 2003). They can be sheared when proximal to regional fault zones and are occasionally vesicular. The unit is formed of both massive and pillow basalts, with pillow size varying from tens of centimetres to locally over a metre in diameter (Cossio, 2003). The dolerites are massive with a green to grey colour, and are also found along the coast of the Serranía de Baudó (Cossio, 2003). They are medium grained with visible pyroxene and plagioclase between 1 and 2mm. They can also contain a glassy component (up to 15%), which is altered to palagonite and chlorite (Cossio, 2003). The gabbros are again massive and green to grey in colour, and are found in bodies of around 100m long, intruding into the basalt and diabase sequences. Grain size of tabular plagioclase is 4 to 5mm, and the gabbros also contain augite, ilmenite, and opaque oxides (Cossio, 2003).

The Basalto de Baudó group also contains tuffs, sandstone, conglomerate, chert and limestones. These sediments have been observed as interbedded with basaltic sequences, in layers of less than 100m thick. The tuffs are greenish grey, with beds of 10 to 50cm thick. They generally show parallel bedding, with local graded beds. The tuffs have a detrital component, and contain fragments of basalt, glass, plagioclase and pyroxene. The volcanic breccias have beds of over 50cm thick, with rounded basalt clasts forming 60-70 % of the rock, embedded in an grey fine grained matrix. The chert was observed as thin interbeds with the volcanic breccia and tuffs. They are finely laminated with parallel bedding, and are generally black, with rare red and green hues. Numerous recrystallised radiolarians were also found. Rare mudstones were also observed in this sedimentary sequence, and could be calcareous, and dark grey in colour.

Geochemically, the igneous rocks of the Basaltos de Baudó are tholeiitic, with relatively flat primitive mantle-normalised patterns with slight light REE depletions (Kerr et al., 1997a). Three of the southernmost samples from Cabo Corriente are slightly alkaline with more enriched incompatible trace elements (Kerr et al., 1997a). Although it is thought that the Serranía de Baudó may be a continuation of arc from eastern Panama, no arc-like samples have been recognised in the region (Kerr et al., 1997a). Three basalts of the Serranía de Baudó have been dated with $^{40}Ar/^{39}Ar$ as 72.5 ± 0.4Ma, 73.6 ± 0.8 Ma and 77.9 ± 1.0 Ma (Kerr et al., 1997a). These ages largely agree with biostratigraphic ages – ammonites from mudstones interbedded with volcanic rocks on the Uva River have been dated as Turonian (Haffer, 1967). Planktic microfossils from sedimentary rocks interbedded with the volcanic rocks in Nerqua gave an age of Coniacian to Maastrichtian (Bandy, 1970).

The Clavo Formation is exposed within the Atrato Basin, and within the Rio Partado Sediments close to Cupica, and has faulted contacts with the oldest Basaltos de Baudó and the younger Uva Formation (Figure 2.14, 2.15) (Parra and Gonzalez 2002, Cossio, 2003). It is composed of dark grey mudstones, and is finely laminated, with a bed thickness of 0.1-0.4mm. There are rare interbeds of grey limestone, less than 3cm thick, within the mudstone sequences. The unit has been dated as Paleocene to early Eocene, based on foraminiferal biozones (Haffer, 1967).

The Uva Formation is exposed in the western side of the Atrato Basin, along the Uva and Napipi Rivers. It is also exposed within the Rio Partado Sediments close to Cupica (Figure 2.14). The total thickness of the unit is estimated to be 1250m (Parra and Gonzalez 2002; Cossio, 2003). In the lower section of the Uva Formation is it composed of interbedded layers of limestone, calcareous mudstone and calcareous sandstone (Parra and Gonzalez 2002; Cossio, 2003). The limestones are dark grey and range from finely laminated to massive. The mudstones are light grey and can display a strong fabric (Cossio 2003). The sandstones and yellow to grey and medium to coarse grained. Towards the middle and upper Uva Formation, the proportion of sandstone increases, and the sequence is composed of calcareous sandstones with rare thin layers of dark grey mudstone. Towards the top of the formation, there are layers of conglomerate, up to 1m thick (Cossio 2003). The conglomerate contains pebbles of limestone, calcareous sandstone, calcareous mudstone and calcareous claystones, embedded in a white clay-rich matrix (Cossio 2003). The Uva Formation is seen in faulted contact with the Clavo Formation, but it is also seen to rest unconformably on the Basaltos de Baudó along the Napipi River (Cossio, 2003). The Uva Formation is then overlain by the Napipi Formation. The Uva Formation is dated between Oligocene to Early Miocene, based on planktic foraminiferal biozones (Harland et al. 1989).

The Napipi Formation is exposed along the Uva and Napipi River within the Atrato Basin, and within the Rio Partado Sediments (Figure 2.14) (Parra and Gonzalez, 2002; Cossio, 2003). It is estimated to be 1150 m thick (Haffer, 1967). It is composed of grey calcareous mudstones, with interbedded limestones and rare beds of fine grained sandstone. The mudstones have thick beds of between 1 and 2m, with parallel bedding (Cossio, 2003). The sandstone beds are between 0.1 to 0.6m, and exhibit parallel bedding. The Napipi Formation overlies the Uva Formation, and unconformably underlies the Sierra formation (Cossio, 2003). It has been dated between the late Early Miocene and Middle Miocene, by planktic foraminifera biozones (Harland et al., 1989).

The Sierra Formation is exposed along the Atrato Basin, and in the Sediments of the Rio Partado (Figure 2.14) (Parra and Gonzalez, 2002; Cossio, 2003). This formation has also been described as the Bete formation by Barlow (1981) and the top section has been named the Munguido Formation (Duque-Caro, 1990b). The sequence is formed of 3 sections- the lowest section is formed of very fine to fine grained sandstones, with thick graded beds and parallel bedding. They also contain limestone concretions (Cossio, 2003). Interbedded with sandstones are layered siltstone and claystone, with shelly beds containing fish bones and teeth. The middle section is composed of minor mudstone and sandstone with conglomerates. The conglomerates have clasts of sandstone, clays, limestone, chert, quartz and other volcanic and sedimentary rocks (Cossio, 2003). The sandstones are grey and fine grained, with parallel and undulating bedding. The mudstones are dark grey and interbedded with the sandstones (Cossio, 2003). The upper part is formed of black and grey siltstones which are yellow and white, weathered to brown. They have thick parallel bedding with lenses of very fine grained sandstone. These lenses contain abundant fossils fragments of fish, along with shells. Within the siltstones there are lenses of claystone, quartz-rich sandstone and muddy sandstone. The lenses display parallel bedding, which is frequently disturbed by bioturbation (Cossio, 2003). Towards the top of the sequence there are interbedded mudstones, black, grey and brown in colour, with rare sandy mudstone layers. This Sierra Formation is interpreted to represent oscillations in deposition environment, from shallow platform to beach (Duque-Caro, 1990a; Duque-Caro, 1990b). The Formation has been dated as early Middle to Late Miocene, due to planktic foraminifera biozones (Harland et al., 1989).

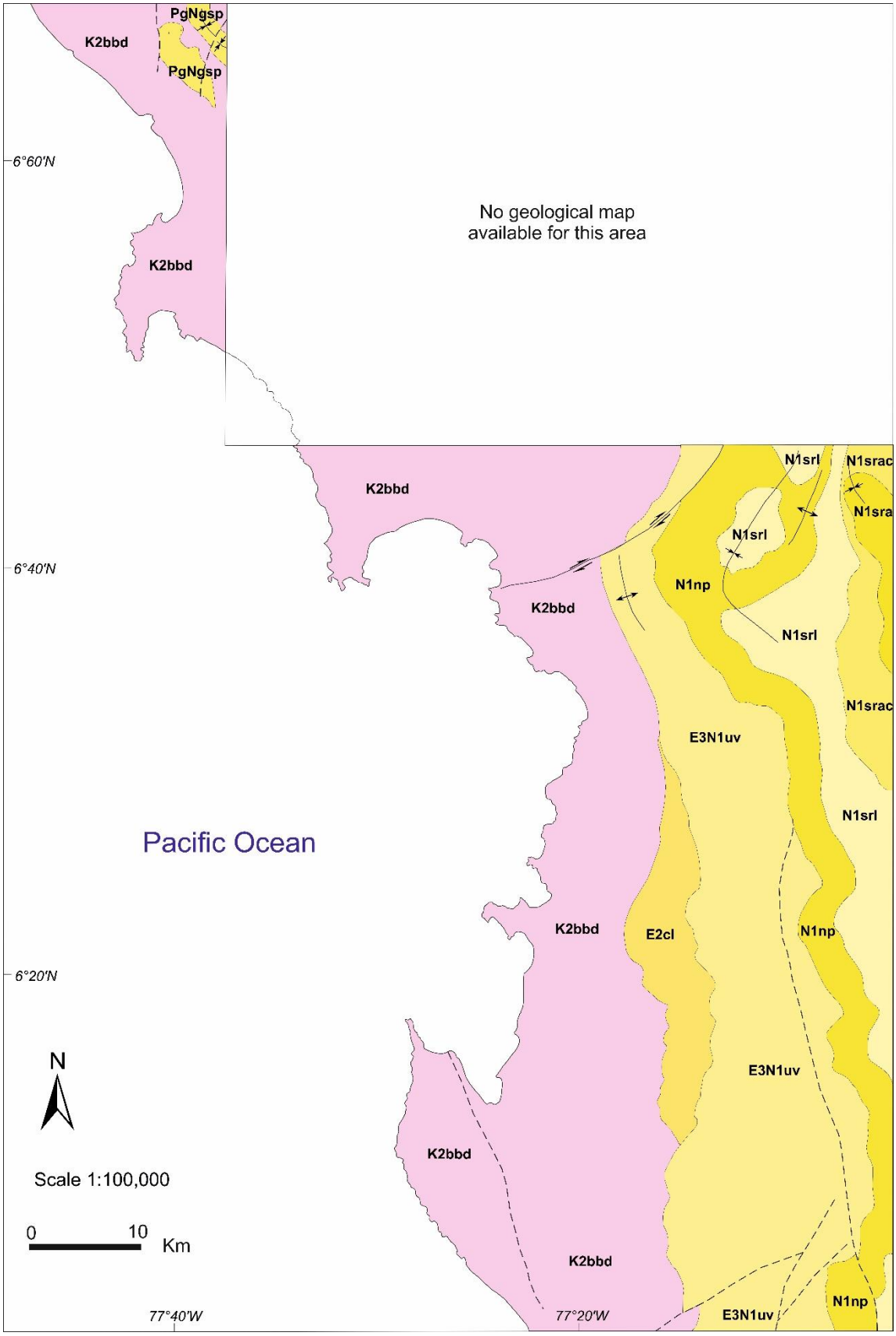

Figure 2.14: Map of the Bahia Solano Coast modified from Parra and Gonzalez (2002) and Cossio (2003).

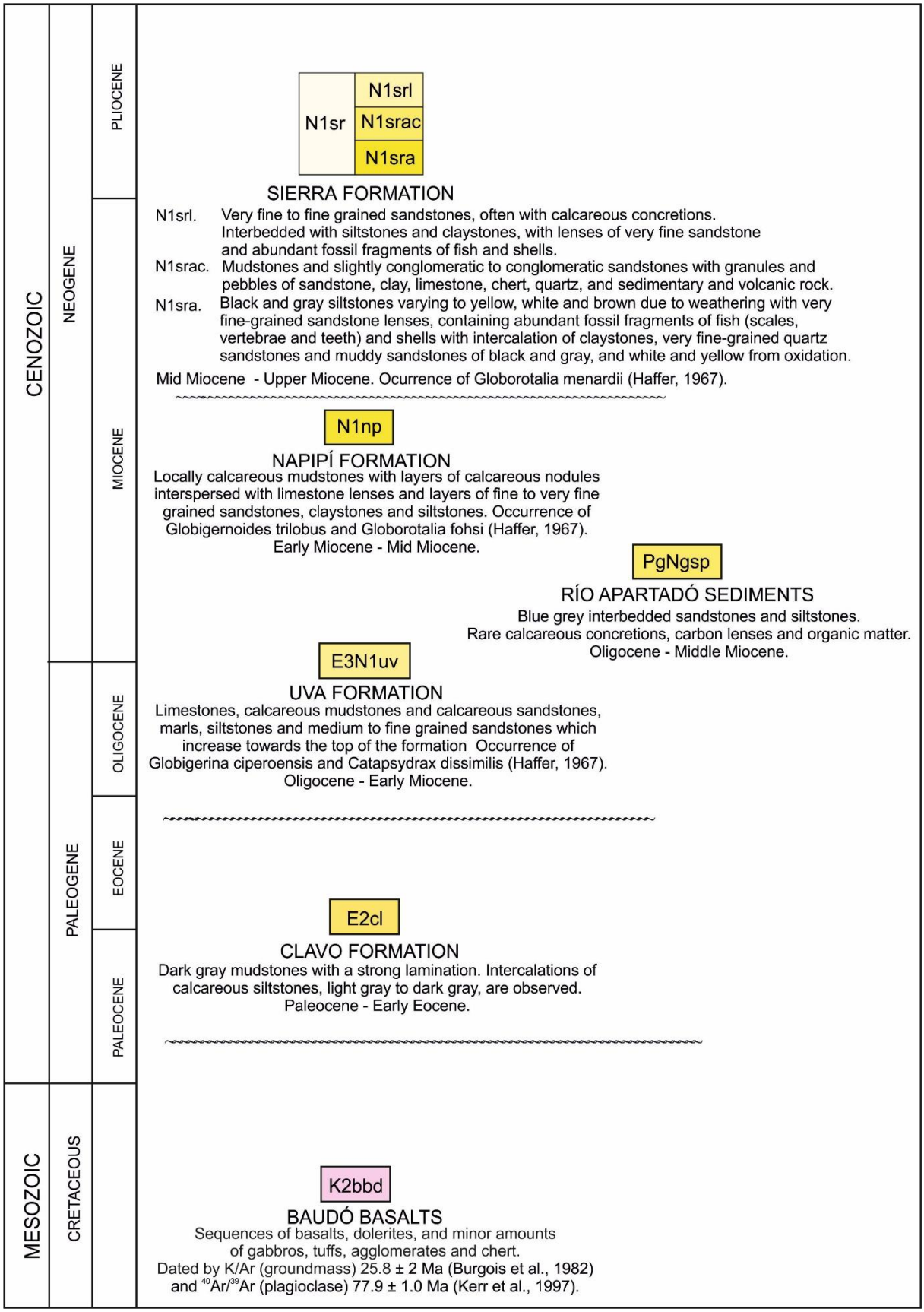

Figure 2.15: Stratigraphy of the Bahia Solano region modified from Parra and Gonzalez (2002) and Cossio (2003).

3. FIELD GEOLOGY AND PETROGRAPHY

3.1 Introduction

This chapter will describe a revised stratigraphic framework for areas in which explorative fieldwork was undertaken. This will include field lithological and petrographic descriptions of units and their stratigraphic relationships. This fieldwork was undertaken in 3 regions (Soná-Torio, Darién Pacific Coast and Serranía de Baudó) (Figure 3.1) and each region will be addressed separately. The area of study largely extends over densely vegetated jungle, with little rock exposure, and none, to limited, previous geological mapping. Rocks can be badly weathered and are mainly exposed in remote locations along rivers and coasts, with rare road cuts. Along rivers, coasts and roads, stratigraphic sequences are discontinuously exposed, making it difficult to understand and reconstruct stratigraphic relationships. Additionally, sequences can be extensively faulted. In some places, blocks were taken from river drainages to assist with regional constraints, due to lack of exposure and difficulty of access. The majority of the fieldwork and sample collection in this study was undertaken by the author in 2017 and 2018, with assistance from Dr David Buchs and collaborators from the Geoscience Department of the University of Panama (Arkin Tapia and Ariadna Flores). This study also utilised minor field observations and sampling undertaken by Dr David Buchs and assistants in 2010, 2015 and 2016. Here, field observations and petrography have been integrated with geochemistry and both biostratigraphic and $^{40}Ar/^{39}Ar$ ages to produce a revised stratigraphic framework.

3.2 Soná-Torio

Fieldwork was undertaken across Soná Peninsula, along the Hicaco Coast (Figure 3.3), the Pixvae Coast (Figure 3.4) and road cuts, rivers and quebradas (small streams) including the Rio San Rafael and El Chorillo. Fieldwork was also undertaken on the Azuero Peninsula along the Rio Torio (Figure 3.5). Work in this region was carried out with the aim of recognising proto-arc units and improving existing basement stratigraphy (Kolarsky et al., 1995; Buchs et al., 2010; Buchs et al., 2011b; Corral et al., 2011; Corral et al., 2012; Corral et al., 2013), which was largely based on work focussed on the Azuero Peninsula and Coiba Island. The area is heavily faulted, with the NW-SE striking Azuero-Soná Fault Zone and Joaquin Fault Zone crossing the Azuero and Soná Peninsula (Figure 3.3). In the

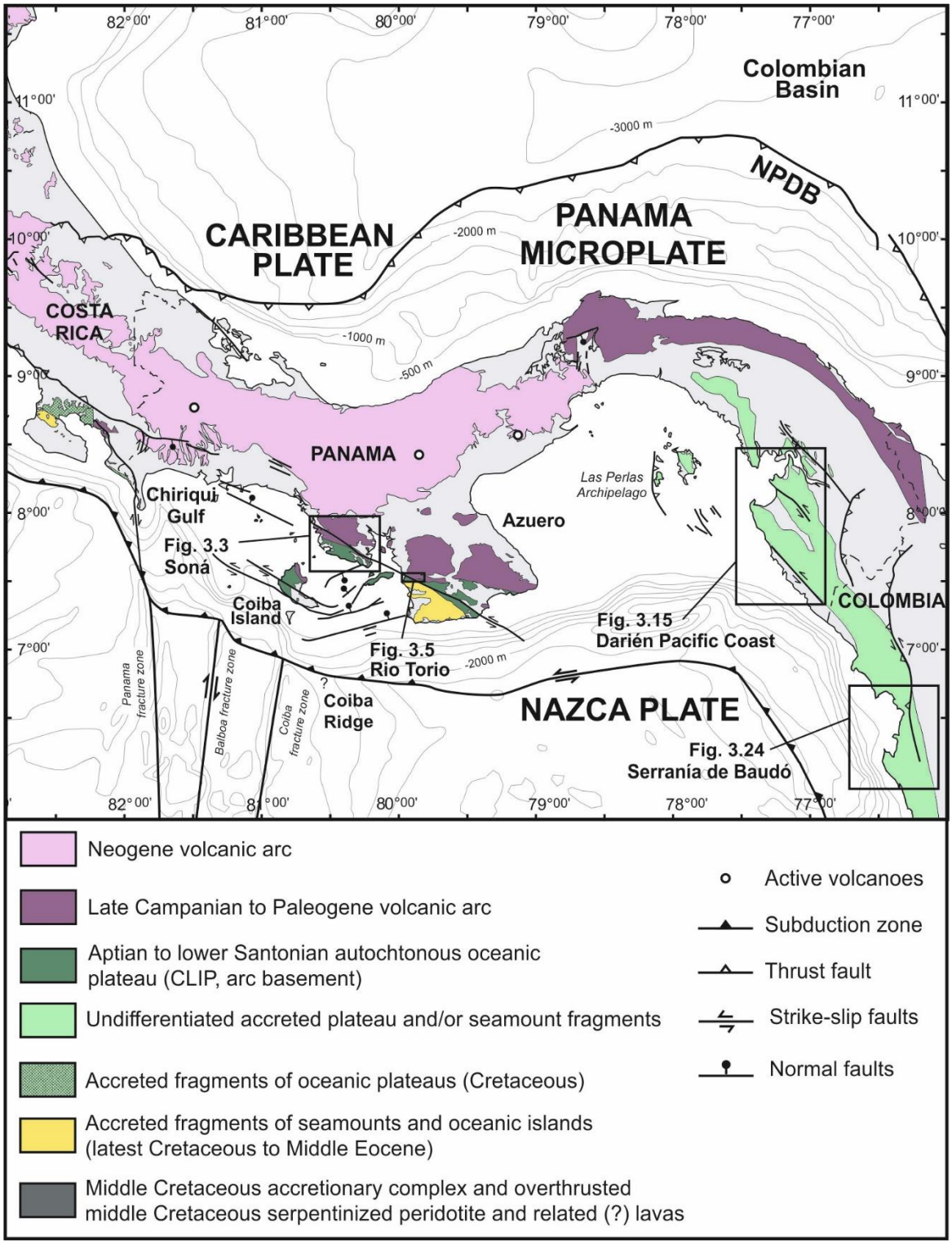

Figure 3.1: Map of the Panama Isthmus, modified after Buchs et al. (2010), showing the sampling and mapping locations described in this chapter: Soná Peninsula (Figure 3.3), Rio Torio (Figure 3.5), Darién Pacific Coast (Figure 3.15) and the Serranía de Baudó (Figure 3.24).

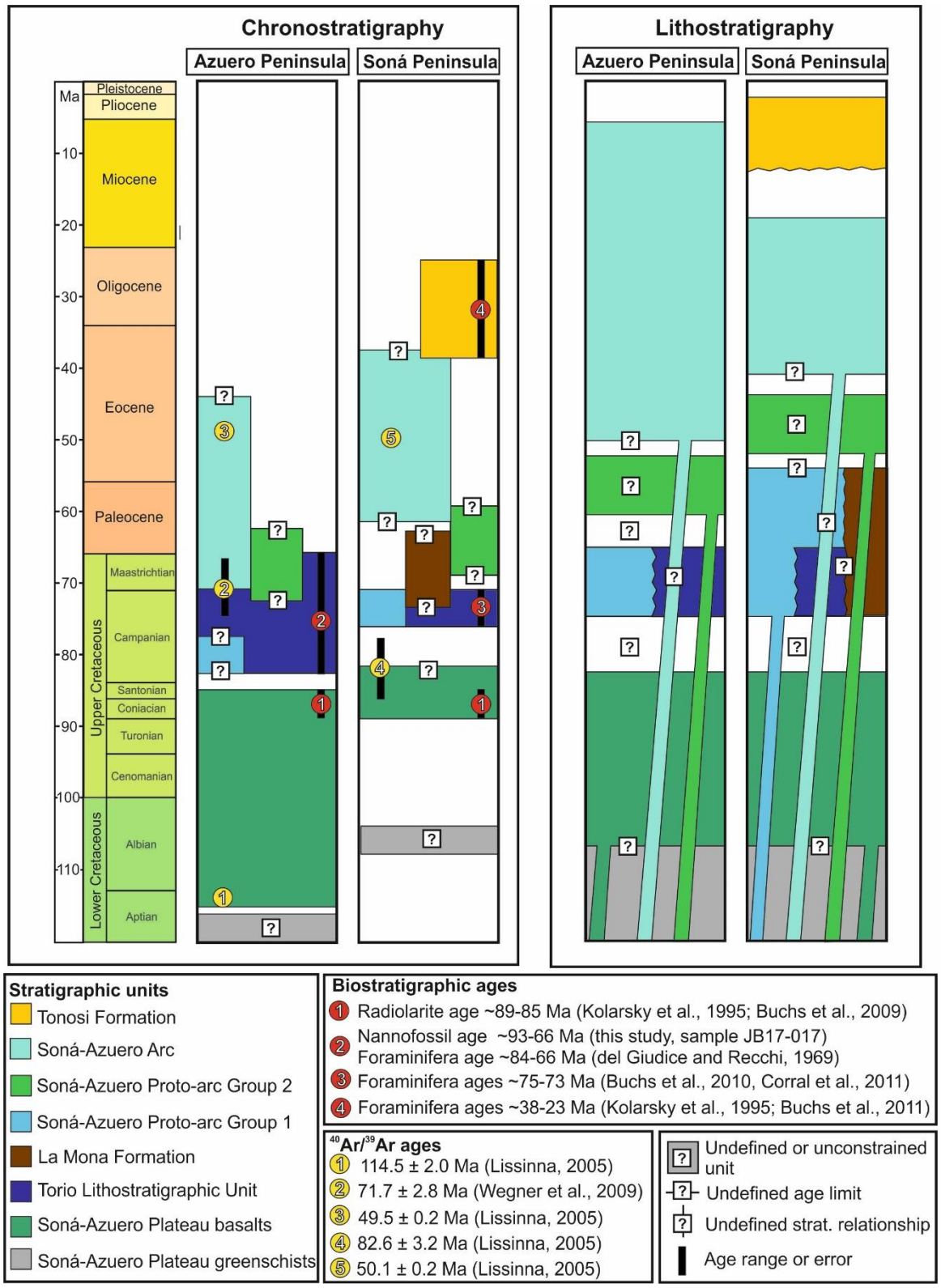

Figure 3.2: Chronostratigraphic and lithostratigraphic charts for the Azuero and Soná Peninsulas.

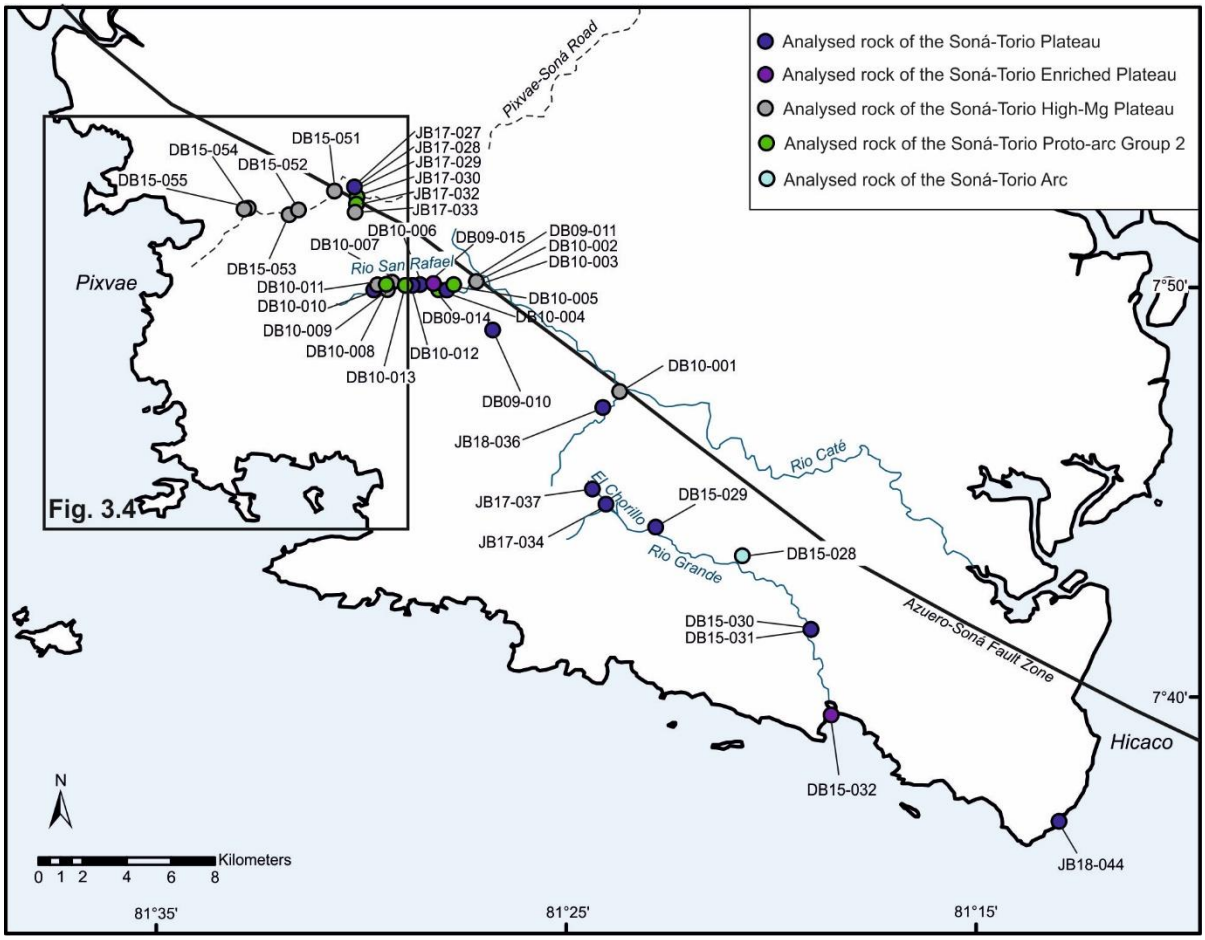

Figure 3.3: Map of the Soná Peninsula showing locations of samples with geochemical analyses

Chiriqui Gulf, there are also the Cebaco and Montusa basin complexes, which are estimated to have caused 7% of extension (Kolarsky and Mann, 1995). In coastal sections, units comprise a series of faulted blocks. The updated stratigraphic framework builds upon the model of Buchs et al. (2010) with new lithostratigraphic, geochemical and geochronological constraints, from across Soná peninsula and Rio Torio. It recognises 4 main groups: (1) The Soná-Torio Oceanic Plateau Complex, (2) the Soná-Torio Protoarc Group, (3) the Soná-Torio Arc Group (4) the Tonosí Formation (Figure 3.2).

3.2.1 Soná-Torio Oceanic Plateau Complex

The oldest group recognised in the Soná-Torio region was the Oceanic Plateau Complex. This complex can be separated into 3 units: (1) the Soná-Torio Oceanic Plateau Basalts (2) the Soná-Torio Oceanic Plateau Intrusions and (3) the Soná-Torio Greenschist unit (Figure 3.2).

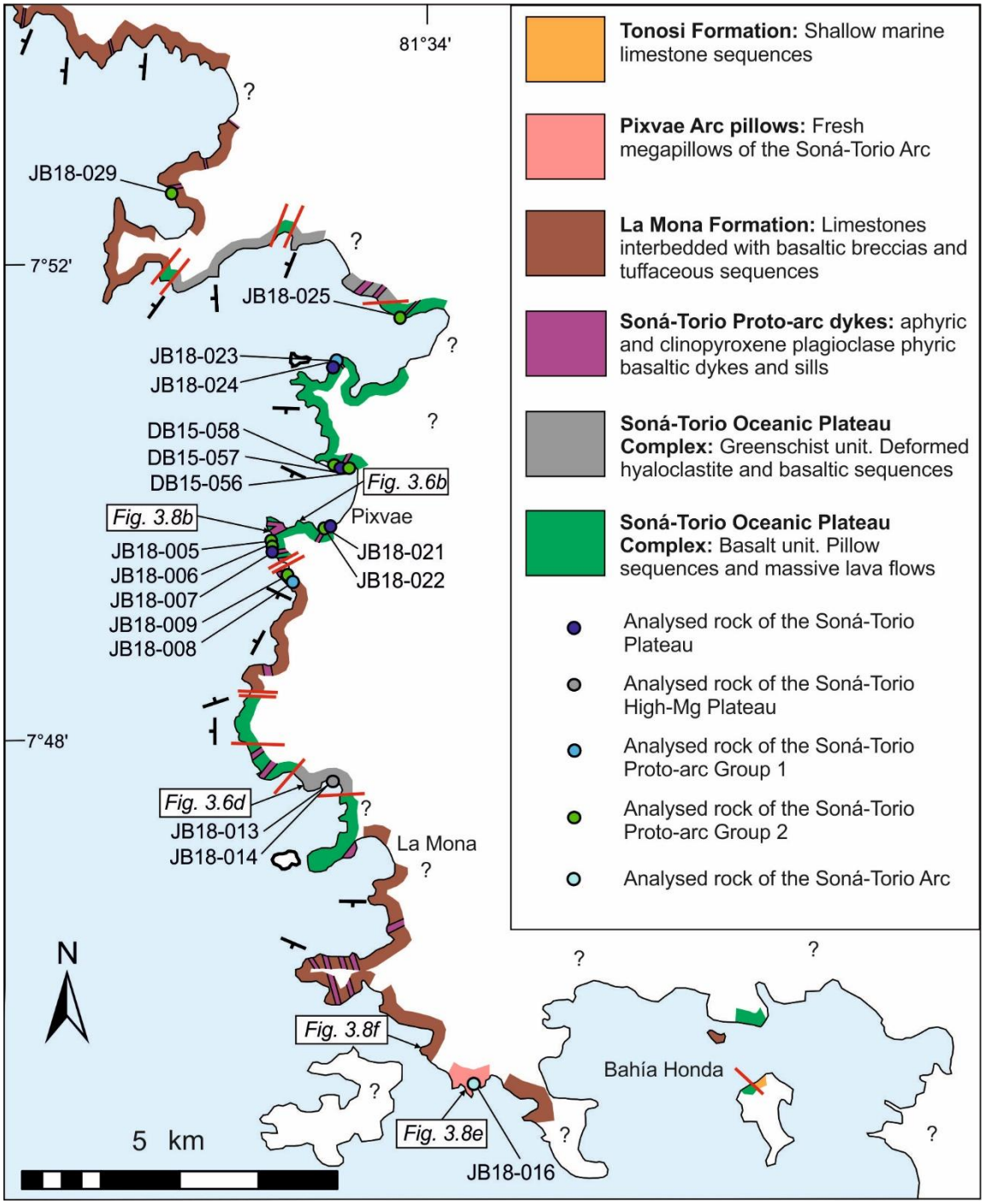

Figure 3.4: Map of the Pixvae coast showing exposure of lithostratigraphic units, locations of samples with geochemical analyses and locations of field photographs

Soná-Torio Oceanic Plateau Basalts: The Soná-Torio Oceanic Plateau Basalts are exposed across Soná and along the Rio Torio and are composed of pillow sequences and massive lava flows (Figure 3.6a-b). These plateau basalts represent an extension of the Azuero Plateau, previously described on Azuero Peninsula and Coiba Island (Buchs et al., 2010) and can be described together as the Soná-Azuero Plateau. The Oceanic Plateau Basalts includes samples from two geochemical groups. The majority of samples are part of the Soná-Torio Plateau, formed of samples with a flat pattern on primitive mantle-normalised

multielementary diagrams, while rare samples are part of the Soná-Torio Enriched Plateau, which is formed of samples with LREE enriched patterns on primitive mantle-normalised multielement diagrams (Chapter 5).

The pillows and lava flows of the Soná-Torio Oceanic Plateau basalts are often inclined, but there is not a consistent dip due to extensive faulting of lava sequences. The pillows and lava flows are typically deformed and cut heavily by calcite veins (Figure 3.6a). This deformation and veining increases with increased proximity to faulted regions, such as the main Azuero-Soná Fault Zone (Figure 3.3), along with more localised fault regimes. Within the basaltic sequences there are rare intervals of basaltic breccia and pillow breccia, which can exhibit layering. Rare interbeds of siliceous sediments are also found in basaltic sequences, composed of red-black pelagic chert and radiolarites. The plateau has previously been dated as Coniacian-early Santonian (89-85 Ma) based on radiolarite ages (Kolarsky et al. 1995; Buchs et al. 2009), but within the wider range of lower to upper Cretaceous (114.5 ± 2.0 to 71.3 ± 2.1 Ma) from $^{40}Ar/^{39}Ar$ incremental heating (Lissinna, 2005). Stratigraphically, the basalts form part of the arc basement, shown by plateau sequences crosscut by dykes of the proto-arc and arc groups, and plateau sequences which appear to underlie Campanian (ca. 75 Ma) limestones and basalts of the proto-arc group (Buchs et al., 2010).

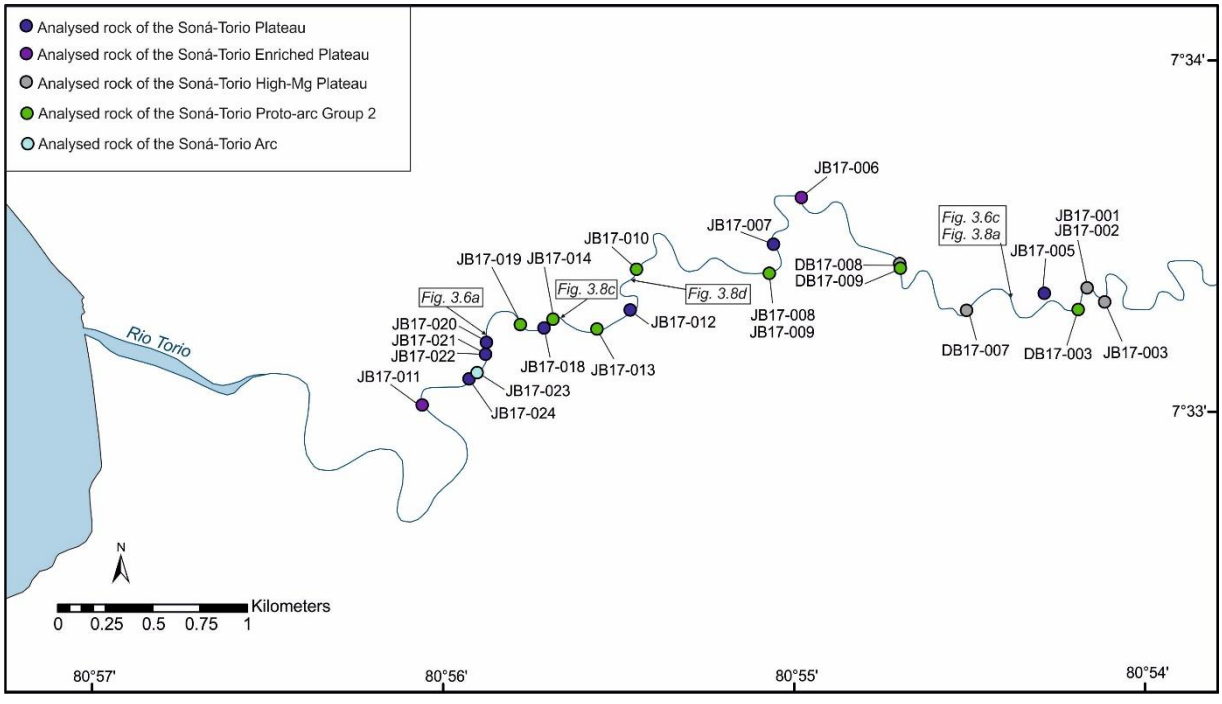

Figure 3.5: Map of Rio Torio, locations of samples with geochemical analyses and locations of field photographs.

Basalts of the Soná-Torio Oceanic Plateau are generally aphyric and fine grained with a grain size between <0.25mm to 0.5mm (Figure 3.7a-b). They generally comprise acicular to

lath shaped plagioclase, equant euhedral to anhedral clinopyroxene and cubic to irregular opaque oxides. Both holocrystalline and hypocrystalline textures are observed, but commonly rocks have an intersertal texture with rare subophitic samples. Rarely, there are porphyritic basalts, containing minor subhedral lath shaped plagioclase and/or equant subhedral clinopyroxene phenocrysts. These phenocrysts range in size from 1-3mm and can be fractured and pervasively altered (Figure 3.7d). The plagioclase phenocrysts are commonly replaced by up to 30% sericite and chlorite, while the clinopyroxene crystals are also generally altered to chlorite along fractures. The glassy groundmass is commonly completely altered to brown and green clays, while plagioclase groundmass crystals can be pervasively altered by both chlorite and sericite. Samples of the Soná-Torio Enriched Plateau can also occasionally contain olivine phenocrysts within porphyritic basalts. These olivine phenocrysts are typically extensively altered and fractured, often completely pseudomorphed by iddingsite or serpentine. Cross-cutting veins of quartz, calcite and zeolites all occur.

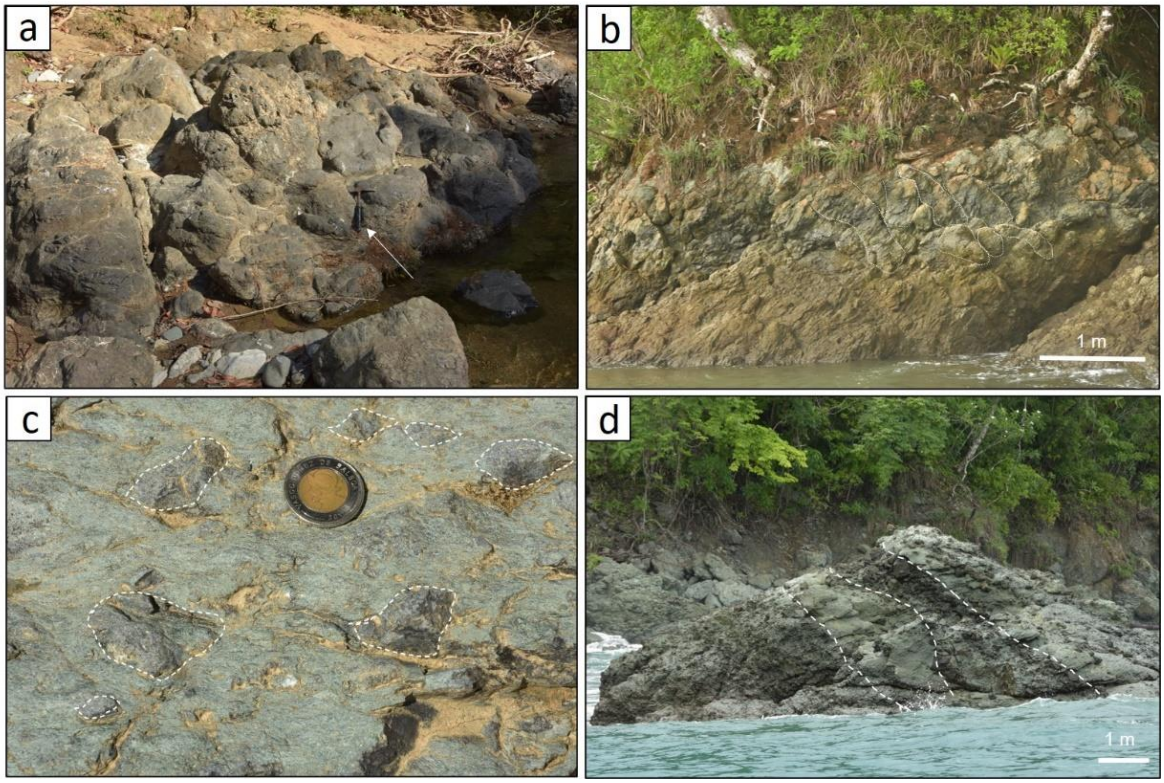

Figure 3.6: Pictures of typical exposures of the Soná-Torio Plateau Complex. (a) deformed pillow basalts heavily cut by veins (Rio Torio) (b) Lobate pillow lavas (Pixvae coast). (c) Hyaloclastite showing glassy clasts and schistose matrix (Rio Torio). (d) Layering within basaltic breccia (La Mona coast)

Soná-Torio Oceanic Plateau Intrusions: The basalts of the plateau are associated with doleritic to gabbroic intrusions of the Soná-Torio Oceanic Plateau, which were observed

along the Rio Torio, El Chorillo and the Hicaco coast, and are seen to crosscut basalts and greenschists of the plateau. These intrusions are from the Soná-Torio Plateau and Enriched Plateau geochemical groups. Grain sizes of gabbros and dolerites range from 2-4mm. The samples are typically comprised of lath shaped plagioclase, equant subhedral clinopyroxene and opaque oxides, with a hypocrystalline, intergranular texture (Figure 3.7c). Although intrusions are generally aphyric, the gabbros can have a “spotted” texture, with larger phenocrysts of clinopyroxene (up to 5mm) within a 2-3mm groundmass of plagioclase, pyroxene and opaque oxides. Occasionally, the groundmass within these samples displays an ophitic texture. Samples of the Oceanic Plateau Intrusions have generally undergone extensive alteration. Clinopyroxene crystals within the intrusions are typically extensively fractured and pervasively altered to chlorite, and occasionally can be completely replaced (Figure 3.7c). In many samples, the plagioclase has been largely replaced or pseudomorphed by both sericite and chlorite. Any glass within the sample has been altered to red and brown clays.

Soná-Torio Oceanic Plateau Greenschists: The Soná-Torio Plateau Greenschists are composed of deformed hyaloclastite and schistose basalt breccia sequences. These sequences are exposed across Soná and Azuero peninsulas and are found associated with the Soná-Torio Oceanic Plateau Basalts (Figure 3.6c-d). This unit correlates with the undifferentiated metamorphic rocks described in Buchs et al. (2011b), and may correlate with the picritic amphibolites reported by Tournon et al. (1989), although the origins of these amphibolites is unknown. The greenschists have a highly depleted geochemistry (i.e., very low incompatible trace element contents) with > 15 wt. % MgO, and form the geochemical group called the Soná-Torio High-Mg Plateau. The unit has poor exposure inland due to a extensive weathering but is seen in faulted blocks within coastal sections, and in limited road and river exposures. The greenschist unit is thought to form part of the oceanic plateau arc basement, below the Soná-Torio basalts. This is evidenced by intrusions of both the plateau and proto-arc groups intruding greenschists along the Rio Torio, along with arc-related dykes intruding the greenschists along the Rio San Rafael. The unit is also extensively deformed, which is not exhibited in other units, and the undeformed crosscutting dykes can follow the schistosity of the greenschist.

The hyaloclastites are formed of altered brown-green vesicular glass, which has been replaced by chlorite and actinolite with occasional prehnite. They also contain evidence of shearing, with elongated vesicles up to 1mm long which be filled with chlorite (Figure 3.7e). The replacement crystals of chlorite and actinolite are fine grained, fibrous and have a radiating texture. Some hyaloclastite samples also include glassy crystals, which are up to

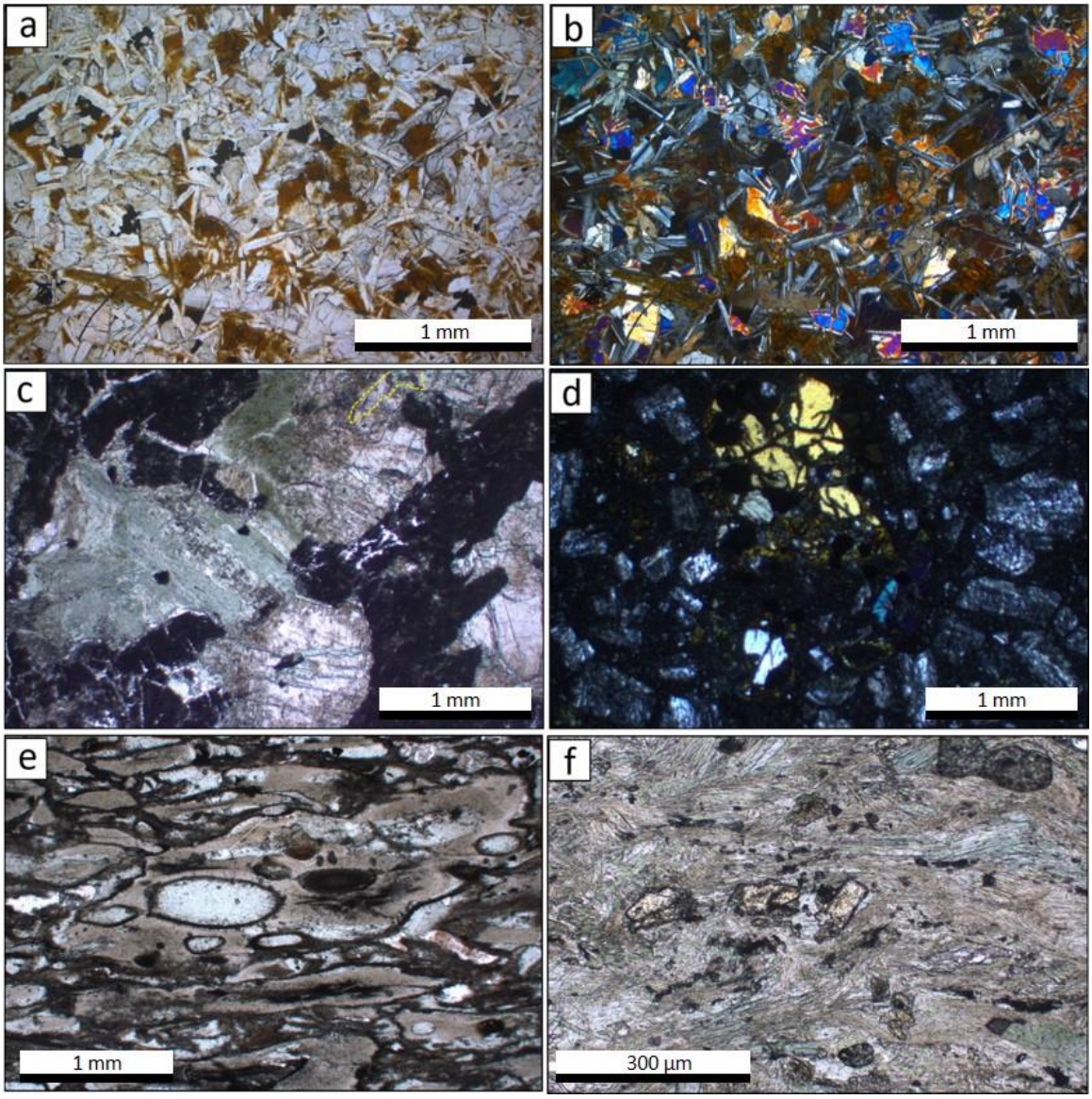

Figure 3.7: Photomicrographs of the Soná-Torio Plateau Complex. (a) PPL view of typical composition, texture and alterations of Soná-Torio Plateau basalts (sample DB15-030). (b) XPL view of typical composition, texture and alterations of Soná-Torio Plateau basalts (sample DB15-030). (c) PPL view of a highly altered gabbro of the Soná-Torio Plateau, showing replaced plagioclase and clinopyroxene (sample JB17-005). (d) XPL image of a porphyritic basalt of the Soná-Torio Enriched Plateau, with altered phenocrysts of plagioclase and olivine (sample DB15-032). (e) PPL view of a typical hyaloclastite of the Soná-Torio High-Mg Plateau, showing devitrified glass and elongate vesicles (sample DB17-007). (f) PPL view of a schistose basalt of the Soná-Torio High-Mg Plateau, with glassy clasts and needles of chlorite and actinolite (sample JB17-033).

2mm in size, generally altered to chlorite and actinolite and have extensive fractures due to shearing. Some samples do not exhibit any stretched vesicles or texture of parent rock. These rocks are completely recrystallised and are formed of fibrous chlorite and actinolite, with rare prehnite, epidote and sphene (Figure 3.7f). These samples also contain sheared serpentinised zones, which represent olivine pseudomorphs. Very rarely, small and altered fragments of olivine are still preserved.

The basaltic breccia sequences are composed of basaltic, amygdaloidal clasts within a green schistose matrix. These sequences are layered in places, with heterogeneous clast distribution, comprising 70% in some layers to only 10% in others (Figure 3.6d). Clasts size is variable, ranging from 1-30cm, with some larger clasts showing an internal schistose fabric. Typically, the matrix of the basaltic breccias is not as schistose as those of the hyaloclastites.

3.2.2 Soná-Torio Proto-arc Group

The second major stage of volcanism in Soná-Torio is associated with the Soná-Torio Proto-arc Group. These proto-arc rocks represent an extension of the Azuero Proto-arc Group, previously described on Azuero Peninsula and Coiba Island (Buchs et al., 2010). Geochemically, the Soná-Torio proto-arc is formed of two groups – the Proto-arc Group 1 is geochemically transitional between plateau and arc, whereas the Proto-arc Group 2 is more depleted in light REE (Chapter 5). The Proto-arc Complex is composed of basalts and dykes of the Soná-Torio Proto-arc Group 1, which are locally associated with pelagic to hemipelagic limestones and sandstones of the Torio Lithostratigraphic Unit and the shallow marine limestone and tuffaceous sequences of the La Mona Formation. This sequence is intruded by dykes of the Proto-arc Group 2.

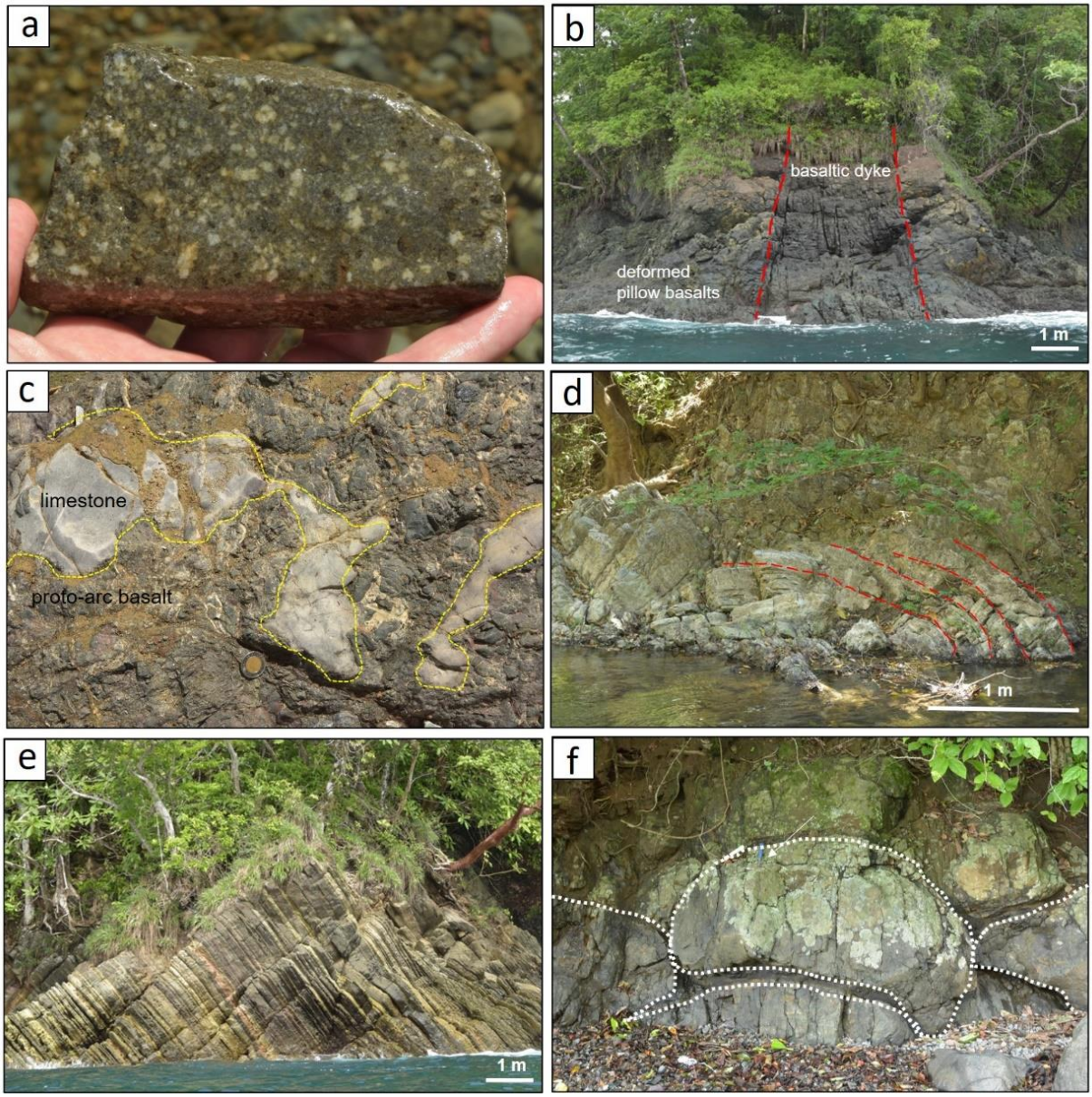

Figure 3.8: Pictures of typical exposures and stratigraphic relationships of the Soná-Torio Proto-arc Complex, arc pillows and volcaniclastic sediments. (a) Block of a proto-arc dyke, showing clinopyroxene and plagioclase phenocrysts. (Rio Torio). (b) Dyke of proto-arc crosscutting deformed pillows of the Oceanic Plateau Complex (Pixvae coast). (c) Soft sediment deformation within hemipelagic limestones intruded by a basaltic dyke of the proto-arc (possible peperite) (Rio Torio). (d) Folding within the hemipelagic limestones (Rio Torio). (e) Steeply dipping, finely laminated tuffaceous sediments of the La Mona Formation (Bahia Honda coast). (f) Mega-pillows of the Soná-Torio Arc with fresh glass. (Bahia Honda coast).

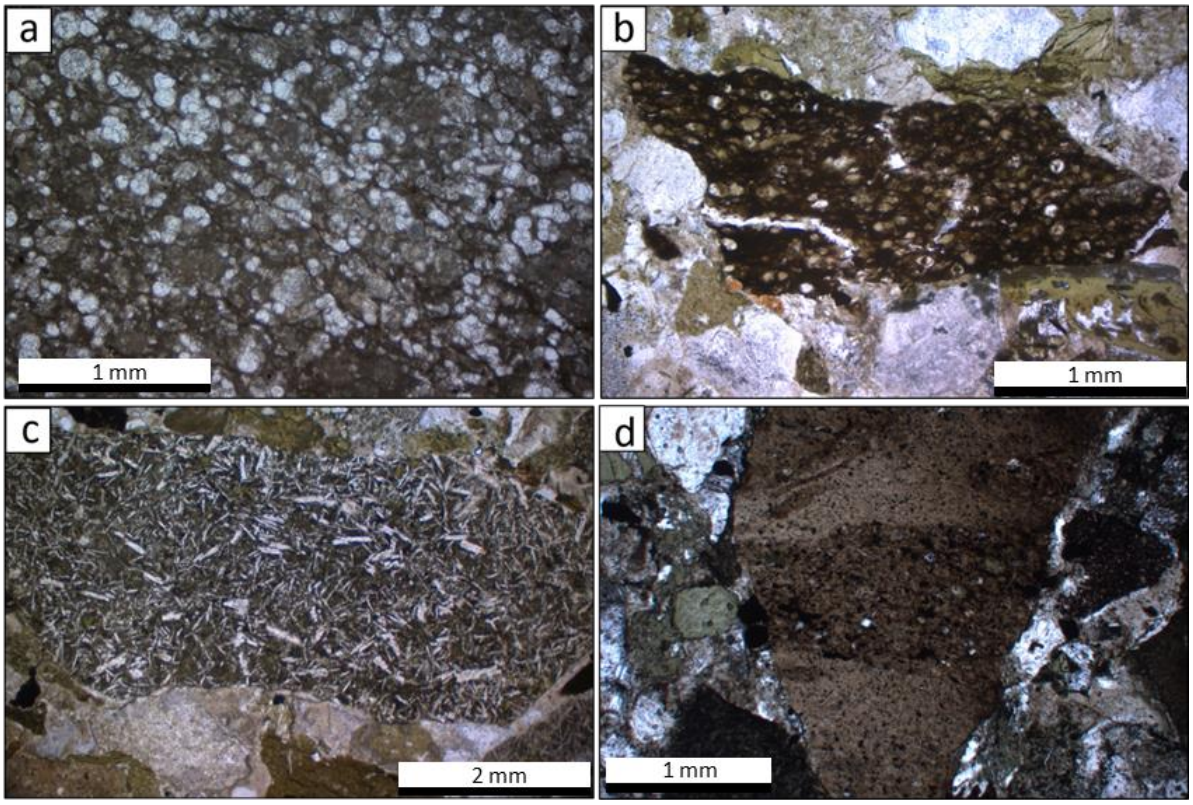

Figure 3.9: Photomicrographs of the Torio Lithostratigraphic Unit. (a) PPL view of a hemipelagic foraminiferal limestone (sample JB17-017). (b) PPL view of calcareous breccia with a radiolarite clast (sample JB17-016). (c) PPL view of calcareous breccia with a fine grained basaltic clast (sample JB17-016). (d) XPL view of calcareous breccia with a layered siliceous sediment clast (sample JB17-016).

Torio Lithostratigraphic unit: The pelagic to hemipelagic limestones of the Torio Lithostratigraphic Unit can be tuffaceous, and are observed in situ along Rio Torio and in blocks in rivers across Soná. They can be found in association with proto-arc sequences, intruded by proto-arc dykes and sills, and interbedded with proto-arc lava flows (Figure 3.8c). The limestones are locally folded and form ramps in close proximity to faults (Figure 3.8d). They are also occasionally bioturbated, and can exhibit small scale cross bedding and flaser bedding. Previously, these rocks were observed in situ across the Azuero Peninsula and on Coiba, with peperitic contacts between sediments and proto-arc dykes (Buchs et al., 2010). These limestones likely correlate with the non-tuffaceous pelagic Ocu Formation, which is exposed across Azuero Peninsula and has an Upper Campanian to Maastrichtian age (Kolarsky et al., 1995; Buchs et al., 2010). A sample from Rio Torio gave a nannofossil age of Turonian-Maastrichtian (sample JB17-017) (Chapter 4).

Locally along the Rio Torio, these limestones are found in sequences with basaltic sandstone breccias and graded sandstones. These sequences may correlate with the upper Ocu Formation, recognised by Kolarksy et al. (1995) on Soná Peninsula. These rocks contain fragments of basalt and radiolarites. This indicates that at the time of deposition of

the sandstone and breccias, the plateau and its Upper Cretaceous sedimentary cover was partially subaerially exposed. These sediments comprise the early forearc sediments in Soná.

Limestones from the Rio Torio are micritic and tuffaceous with little detrital material (Figure 3.9a). They contain abundant foraminifera which are largely recrystallised. These limestones can also contain fractures and calcite veins. The basaltic sandstones to conglomerate found in sequence with the limestones are polymictic, with a calcareous matrix containing both lithic and crystal fragments (Figure 3.9b-d). The sandstones have a grain size of 1 - 2mm and contain sub-rounded lithic fragments composed mainly of fine to medium grained basalt with acicular to tabular plagioclase. Crystal fragments are generally angular and are composed of large elongate plagioclase laths, quartz, and clinopyroxene. The lithic breccia is polymictic and clast supported, with angular to subrounded clasts up to 6mm in size. Angular crystal fragments are composed of clinopyroxene and plagioclase and are generally 0.2 - 0.7mm in size. Lithic clasts are composed mainly of subrounded basaltic to doleritic clasts, with minor clasts of subangular radiolarian chert, and layered siliceous sediments (Figure 3.9b-d). Many samples are altered and contain chlorite within the groundmass and within clasts. The clast composition in these sequences indicates that the source of the clasts was from the oceanic plateau.

La Mona Formation: The Soná forearc sediments of the La Mona Formation outcrop mainly along the Pixvae coast (Figure 3.4), with limited exposure at Hicaco point and inland across Soná Peninsula. They consist of limestones interbedded with basaltic breccias and tuffaceous sequences (Figure 3.8e). A sample of tuff from the La Mona Formation (sample JB18-008) has a Proto-arc Group 1 geochemistry.

Across the Pixvae and Hicaco coasts, the tuffaceous sequences are composed of thinly layered white-yellow or black-grey tuff, which can grade to more massive tuffs. The tuffs are interbedded with tuffaceous micritic limestones, which are locally siliceous. The tuffaceous units can be sandy, pumiceous or recrystallised in places, and display cross lamination, slumping and load structures. Interbedded with the tuffaceous sequences there are rare debris flow deposits, with rounded cobbles of cross-bedded sandstone and tuff. The tuffaceous sequences of the La Mona Formation are intruded by dykes of the Proto-arc Group 2.

Sequences of the La Mona Formation are also exposed in rivers and streams across the Soná Peninsula. Along El Chorillo, in southern Soná Peninsula, basaltic sandstones and siltstones are interbedded with beige siliceous limestone, containing radiolaria and

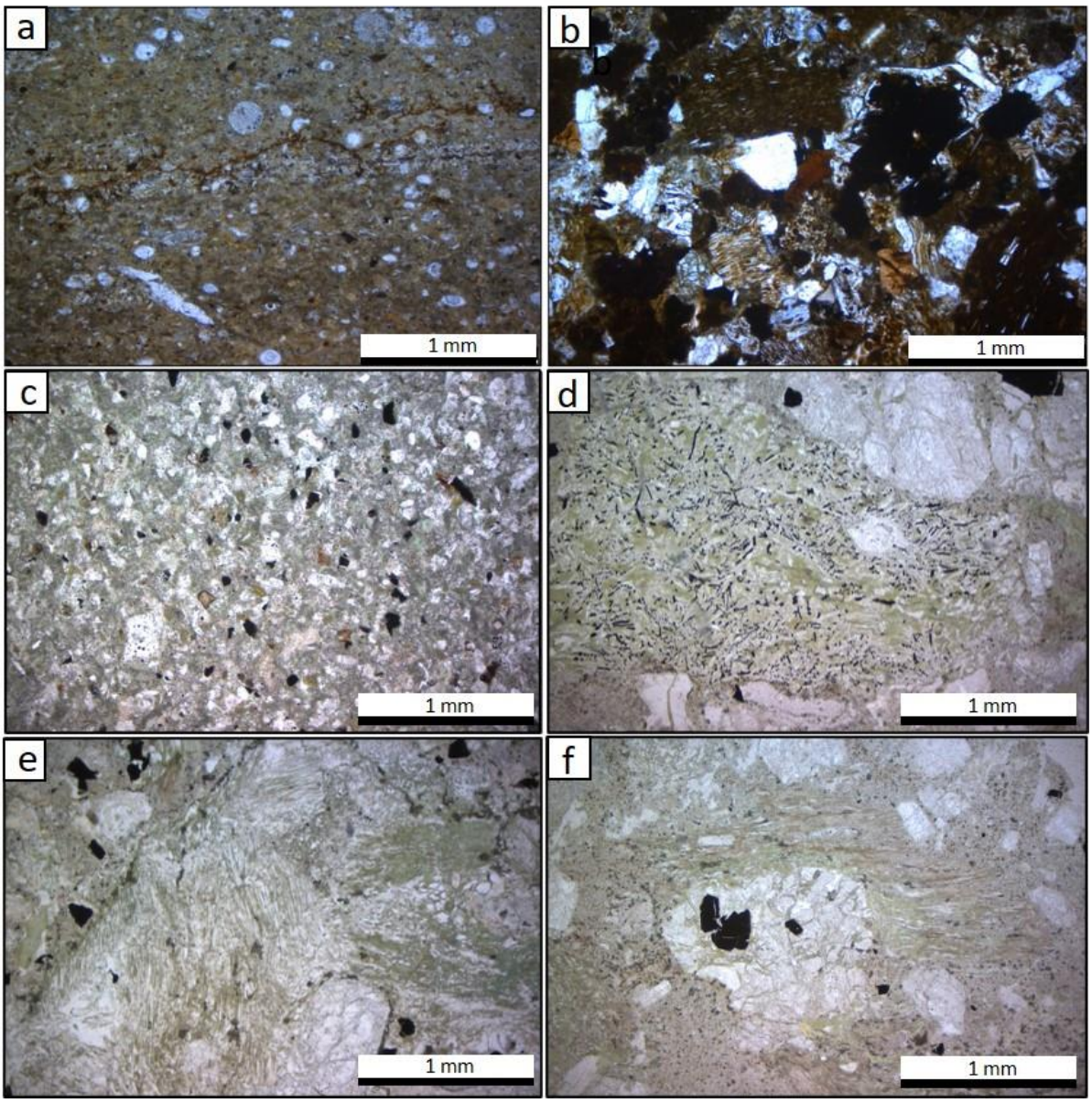

Figure 3.10: Photomicrographs of the La Mona Formation. (a) PPL image of tuffaceous fossiliferous sediment (sample JB17-036). (b) PPL image of sandstone with pumice clasts and fine grained basaltic clasts (sample JB17-035). (c) PPL image of tuffaceous sandstone (sample JB18-007). (d) PPL image of a glassy basaltic clast within a breccia (sample JB18-012). (e) PPL image of altered pumiceous groundmass of a breccia (sample JB18-012). (f) PPL image of pumice and pyroxene within a breccia (sample JB18-012).

recrystallised foraminifera (a). These sediments are crosscut by rare dykes of the proto-arc. Along El Tigre, a stream close to the Rio San Rafael, sequences of bedded sandstones and tuffs are exposed, with normal grading. Along the Quebrada Rosario, the La Mona Formation is exposed as sequences of volcanogenic basaltic breccia, which occasionally contains clasts of recrystallised limestone, interbedded with tuffaceous and siliceous limestones. Again, these sequences are intruded by plagioclase-phyric dykes of the Proto-Arc Group 2.

The sandstone observed along El Chorillo is polymictic, with subrounded to angular clasts (b). Crystal fragments are composed of microcrystals of glass and fractured clinopyroxene, whilst lithic clasts are primarily composed of fine grained basalts. These basalts can be highly amygdaloidal, while others contain aligned acicular plagioclase. There are multiple pumice clasts, between 0.7-1 mm in size, and rounded. The interbedded siliceous sediment is micritic and highly fractured, with multiple quartz veins (b). There is a detrital component formed of fragments of clinopyroxene and quartz, with very rare plagioclase. There are also abundant foraminiferal fragments, 100-500 µm in size, along with rare radiolaria.

Tuffaceous sandstones and breccia from the Pixvae Coast contain subrounded clasts of basalt along with subangular to subrounded fragments of both plagioclase and clinopyroxene (c-f). The basalt clasts are 1-3 mm in size, and contain acicular plagioclase and oxides in a chloritized glassy groundmass. These samples can be highly pumiceous, and in some cases, the pumice is deformed around clasts (f). Typically, the pumice is altered to chlorite. Plagioclase fragments are generally altered and in some cases are completely pseudomorphed by chlorite and sericite.

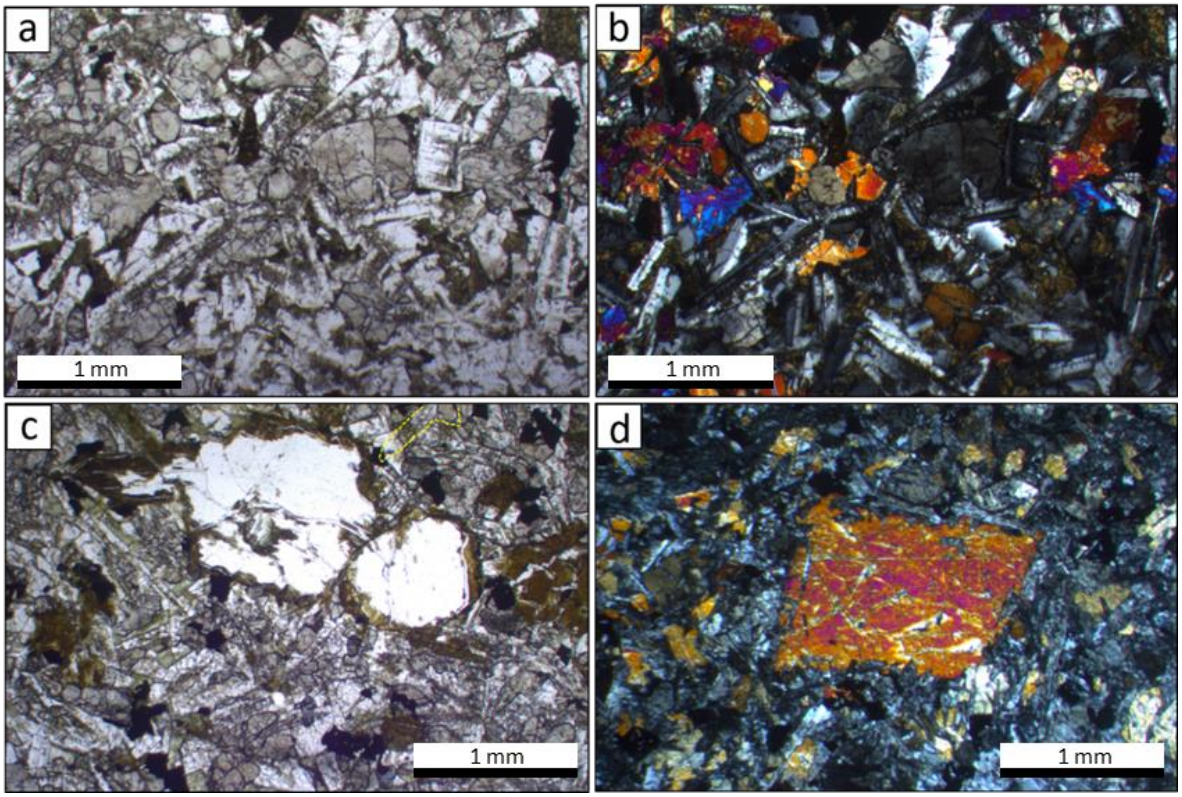

Figure 3.11: Photomicrographs of the Soná-Torio Proto-arc samples. (a) PPL view of a Proto-arc Group 1 basalt with typical composition and texture (sample JB18-023). (b) XPL view of a Proto-arc Group 1 basalt with typical composition and texture (sample JB18-023) (c) PPL view of a Proto-arc Group 2 porphyritic basalt with an altered olivine phenocryst (sample JB17-014). (d) XPL view of a Proto-arc Group 2 porphyritic basalt with a clinopyroxene phenocryst and plagioclase and clinopyroxene groundmass (sample JB18-025).

Soná-Torio Proto-arc Group 1 dykes and lavas: This group consists of basaltic dykes and lavas which are exposed across Soná close to the Oceanic Plateau Complex. Only one dyke with Proto-arc Group 1 geochemistry was observed in this study, but for this stratigraphic framework, this sample is combined with previously analysed dykes and lavas with Proto-arc Group 1 geochemistry from across Soná and Coiba (Lissinna, 2005; Buchs et al., 2010). The intrusions are observed to crosscut the sequences of the plateau complex along the Pixvae coast. Similar observations were previously reported in the region in Coiba Island where the limestone mingled with basalt hosts Campanian foraminifera (Buchs et al. 2010).

Samples of the Soná-Torio Proto-arc Group 1 lavas and dykes are generally aphyric and range from fine and glassy to coarser grained basalts (Figure 3.11a-b). Finer grained samples are composed of acicular plagioclase and equant clinopyroxene, with glass altered to green and brown clays. These samples can be pervasively altered, with chlorite forming up to 30% of the groundmass, and plagioclase showing some sericite alteration. The coarser basalts typically contain elongate laths of plagioclase, with equant subhedral to anhedral clinopyroxene and opaque oxides (Figure 3.11a-b). The groundmass is hypocrystalline to holocrystalline, and ranges from intersertal to intergranular in texture with rare subophitic samples. Samples can also be cut by veins of quartz and chlorite.

Soná-Torio Proto-arc Group 2 dykes and sills: The Proto-arc Group 2 consists of basaltic to doleritic dykes and sills, which are exposed across Soná and Rio Torio close to the Oceanic Plateau Complex. All samples of the Proto-arc Group 2 from across Soná and Rio Torio are intrusions, but there is a single Azuero Proto-arc basaltic lava sample from Buchs et al. (2010) which has Proto-arc Group 2 geochemistry. The dykes and sills of the Soná-Torio Proto-arc Group 2 range in width from minor dykes of around 50 cm to up to 4 m in thickness, with some having undergone slight deformation. Dykes and sills of the Proto-arc Group 2 intrude greenschists and basalts of the Oceanic Plateau complex along the Rio Torio, Rio San Rafael and Pixvae coast, the Torio Lithostratigraphic Unit along the Rio Torio, along with basaltic breccia and tuffaceous sequences of the La Mona Formation along the Quebrada Rosario and Pixvae Coast respectively.

Samples of the Proto-arc Group 2 are compositionally similar to those of the Proto-arc Group 1, but they are generally porphyritic. Phenocrysts are 1-3 mm in size and are composed of tabular shaped plagioclase and subhedral clinopyroxene, with very rare olivine (Figure 3.11c-d). The plagioclase phenocrysts are commonly fractured and replaced by up to 30 % of crystals by sericite and/or chlorite. The clinopyroxene phenocrysts are typically altered around the margins and along fractures by chlorite. The Proto-arc Group 2 also

includes some doleritic to gabbroic dykes, which are formed of laths of plagioclase with subhedral equant clinopyroxene with subophitic textures. The plagioclase in these samples can be 50% replaced by sericite alteration. Proto-arc Group 2 samples are also cut by veins of quartz and chlorite, with calcite cavity growths.

3.2.3 Soná-Torio Arc

The final major stage of volcanism in Soná-Torio is associated with the Soná-Torio Arc Group. The Soná-Torio Arc Group represents an extension of the Azuero Arc Group, as described by Buchs et al. (2010), which consists of arc samples from across the Azuero Peninsula. This complex is composed of the

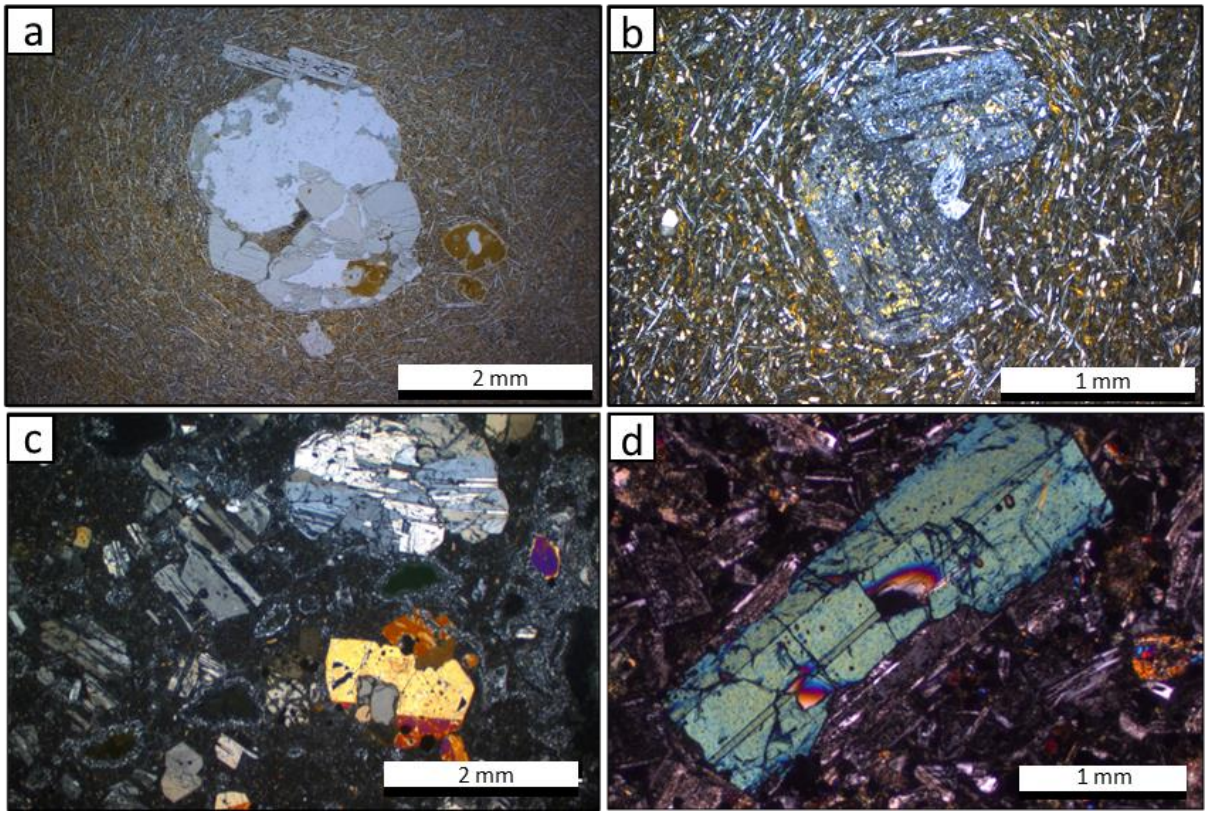

Figure 3.12: Photomicrographs of the Soná-Torio Arc. (a) PPL image of altered pyroxene and plagioclase glomerocryst in a fine grained groundmass (sample JB18-016). (b) XPL view of altered plagioclase phenocrysts in a fine grained matrix (sample JB18-016). (c) XPL view of a porphyritic andesite with phenocrysts and glomerocrysts of plagioclase and clinopyroxene (sample DB09-012). (d) XPL view of a porphyritic andesite with a tabular clinopyroxene phenocryst (sample DB15-045).

Pixvae pillow lavas, along with porphyritic basaltic to andesitic lavas and gabbroic to granodioritic intrusions from across the Soná Peninsula and Rio Torio.

In southern Soná, along the Pixvae coast, pillows with an arc-like geochemistry were recognised. These pillows are up 1.5 m wide, with thick glassy rims and phenocrysts of plagioclase (Figure 3.8f). These rims are well preserved, with celadonite forming in some areas. Overall, these pillows are much larger and fresher than those of the proto-arc or plateau, and are undeformed with less veining. The groundmass of the pillows has an intersertal texture, with brown glassy material between acicular plagioclase needles which have no preferential orientation (Figure 3.12a-b). Zoned plagioclase phenocrysts are 1 – 2 mm in size, and have typically been partially replaced by chlorite in the centre. Clinopyroxene and orthopyroxene phenocrysts form rare glomerocrysts with the plagioclase, and generally remain fresh.

Samples of the Soná-Torio Arc were also observed inland along the Rio San Rafael. Here they were observed as porphyritic basaltic to andesitic lavas and gabbros (Figure 3.12c-d). The porphyritic lavas contain phenocrysts and glomerocrysts of tabular to equant

clinopyroxene and lath shaped to rounded plagioclase, set in a very fine grained glassy matrix. The Soná-Torio Arc intrusions comprise lath shaped plagioclase, with equant clinopyroxene, amphibole and opaque oxides. Plagioclase is generally altered to sericite, Along the Rio Torio, Soná-Torio Arc dykes are basaltic, with phenocrysts of both plagioclase and clinopyroxene.

3.2.4 Tonosi Formation

Limited sequences of the Tonosi Formation were observed in Bahia Honda, along the Pixvae Coast. These sequences consist of shallow marine limestones containing algal fragments and rare small benthic foraminifera. Here, limestone sequences are in faulted contact with basalts of the Oceanic Plateau Complex.

The limestones in Bahia Honda correlate with sequences of the lower Tonosi Formation, as previously described on Coiba by Kolarsky et al. (1995) and Buchs et al. (2011b), which consists of transgressive sequences of turbidites and shallow marine limestones. These sequences have previously been assigned a late Eocene to Early Oligocene age based on nannofossils and larger benthic foraminifera (Kolarsky et al., 1995; Buchs et al., 2011b).

3.3 The Darién Pacific Coast

Fieldwork in the Darién was conducted along the Darién Pacific Coast (Figure 3.14), from La Palma to 20 km south of Jaqué, as well as inland along the Rio Jaqué and Rio Pavarando (Figure 3.15). The aim was to investigate and define the lithostratigraphy of the area, using a combination of field observations, geochemistry and geochronology. The lithostratigraphic subdivision for the Darién coast is as follows: (1) Jaqué Oceanic Plateau Complex, (2) the Jaqué Proto-arc Group, (3) the Darién Formation and (4) the Jaqué-La Palma Group (Figure 3.13).

3.3.1 Jaqué Oceanic Plateau Complex

The oldest unit exposed in the Darién is the Jaqué Oceanic Plateau Complex. This complex is composed of pillowed and massive basalts, interbedded with black to red chert, along with rare plateau related intrusions.

Jaqué Oceanic Plateau Basalts: The Jaqué Oceanic Plateau Basalts are composed of massive lava flows and pillow basalts (Figure 3.16a-b). The basalts have a plateau-like geochemistry, and are composed of samples from two geochemical groups: those with flat patterns on primitive mantle normalised multielementary diagrams (Jaqué Plateau), and those with light REE depleted patterns on primitive mantle normalised multielementary diagram (Jaqué Depleted Plateau) (Chapter 5).

Samples of the Jaqué Plateau and Jaqué Depleted Plateau are not lithologically distinct, and are exposed inland along Rio Pavarando, along the Jaqué Coast to Playa Muerto, and at La Palma (Figure 3.14, 3.15). These groups are largely composed of massive lava flows which can be interbedded with pillows, with beds of siliceous sediments and recrystallised limestone (Figure 3.16d). Pillows are deformed in places and can be extensively veined, with localised volcanic breccia. Pillow breccias can be interbedded with pillow lavas in layers of up to 4 m thick. Often the pillows have a green colour where they are deformed, due to alteration.

Basalts of the plateau are typically fine grained, aphyric and are composed of acicular to lath shaped plagioclase, equant subhedral clinopyroxene and opaque oxides (Figure 3.17a-d). Generally, these basalts are holocrystalline with an intergranular texture, but there are rare glassy samples with an intersertal texture. Plagioclase can be very fractured and altered to sericite and chlorite, and clinopyroxene is generally altered to chlorite. Rarely, the plagioclase is completely

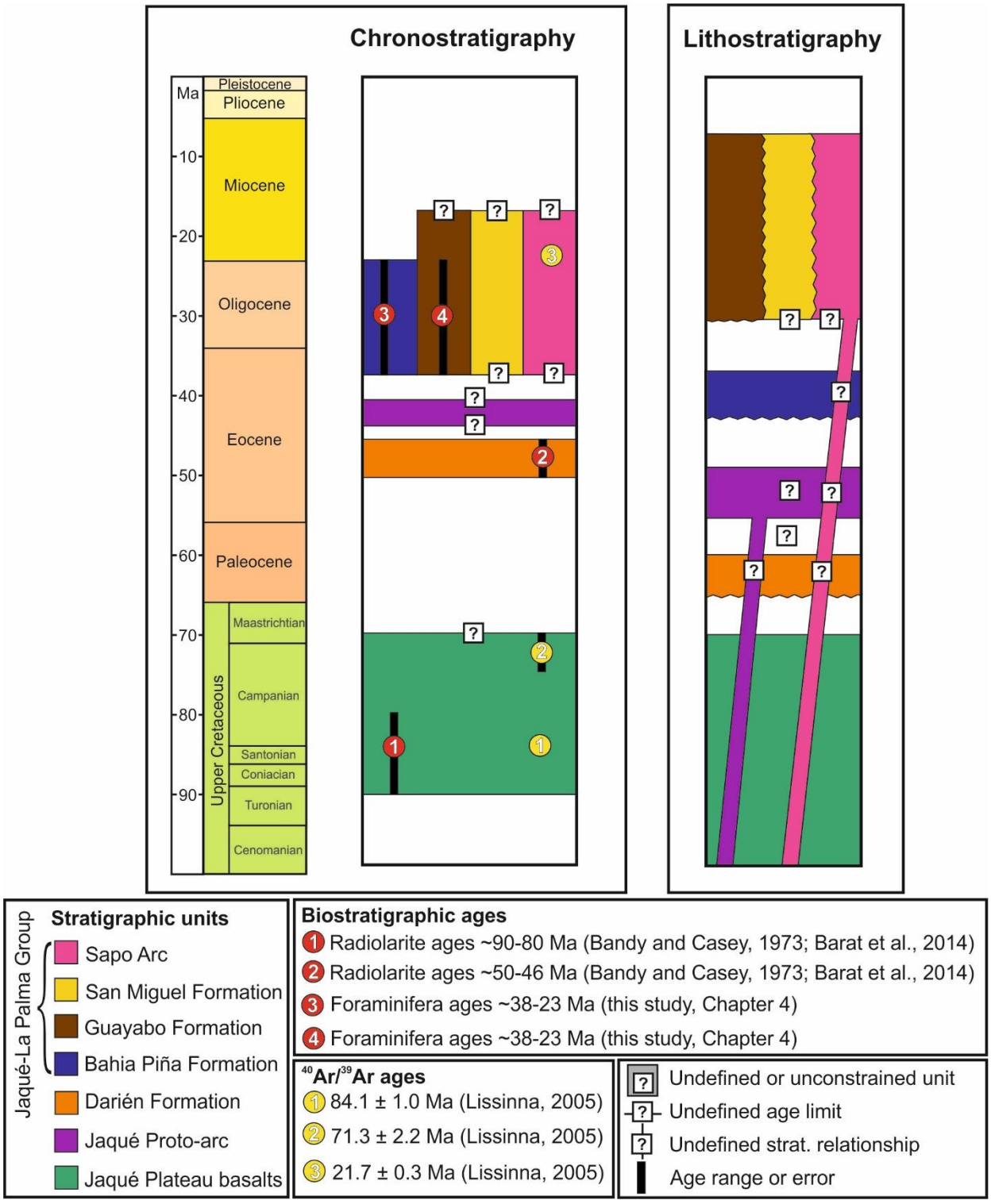

Figure 3.13: Chronostratigraphic and lithostratigraphic charts for the Darién Pacific Coast region

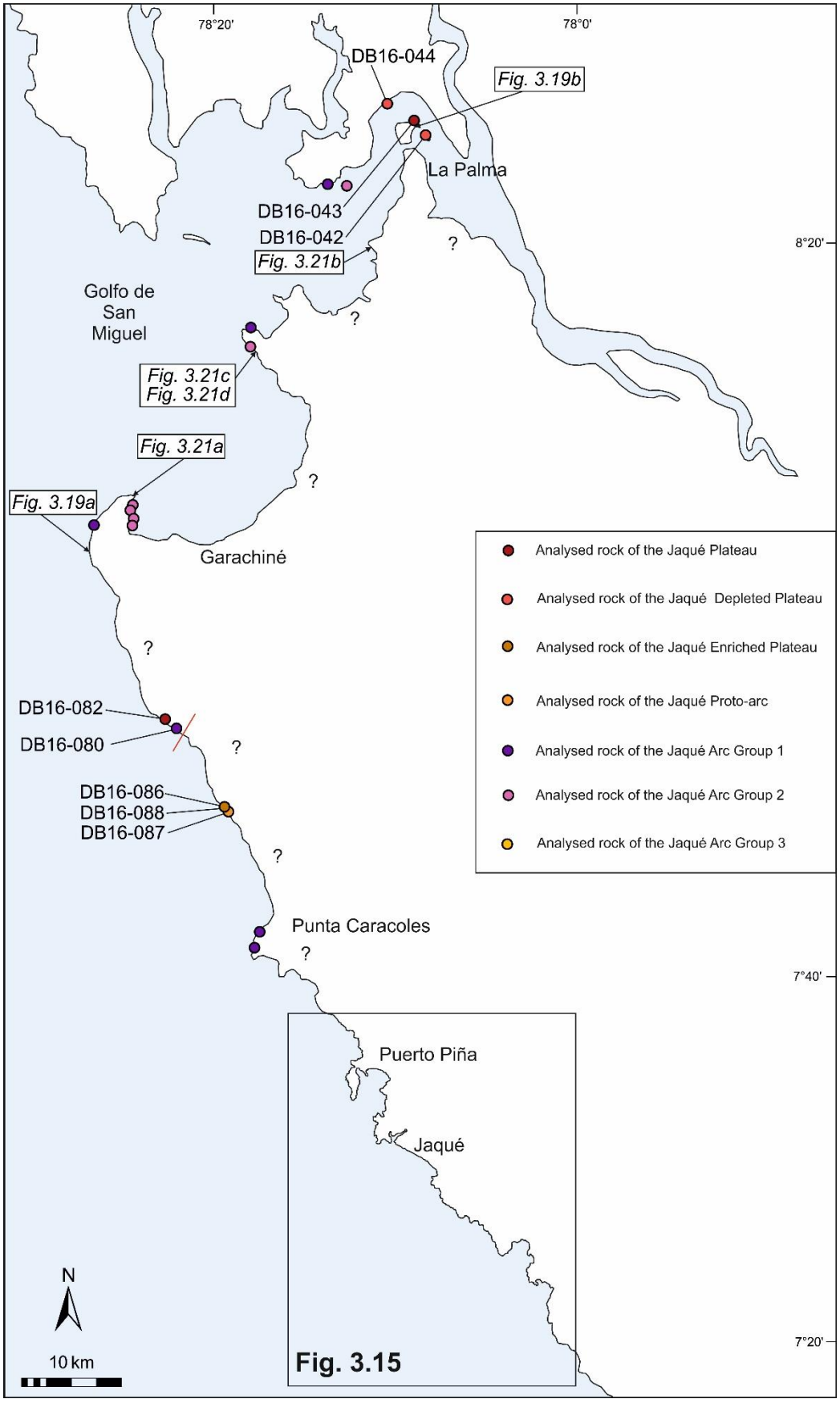

Figure 3.14: Map of the Darién Pacific Coast showing locations of samples with geochemical analyses and locations of field photographs.

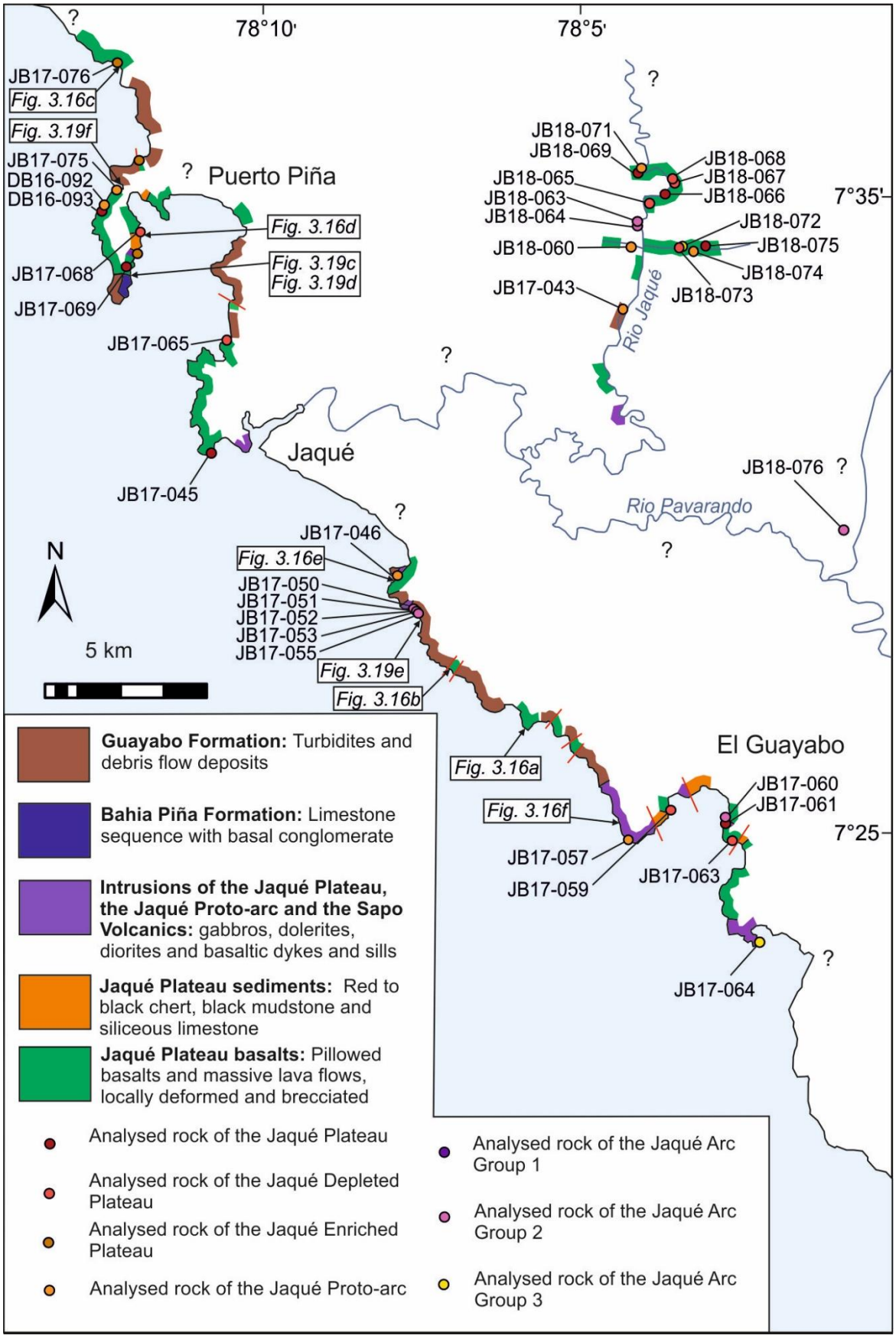

Figure 3.15: Map of the Jaqué coast showing exposure of lithostratigraphic units, locations of samples with geochemical analyses and locations of field photographs

replaced by sericite. The groundmass can also be altered and replaced by chlorite.

Rare porphyritic basalts of the plateau contain phenocrysts of equant subhedral plagioclase (3 mm) and equant subhedral clinopyroxene (1 mm). Plagioclase and clinopyroxene glomerocrysts are also observed. Some clinopyroxene phenocrysts contain plagioclase laths and exhibit ophitic textures. Phenocrysts are also pervasively fractured and altered by chlorite and sericite, with the plagioclase phenocrysts also occasionally replaced by sericite. Clay alteration was seen to rim clinopyroxene phenocrysts, while within the samples with a glassy component,

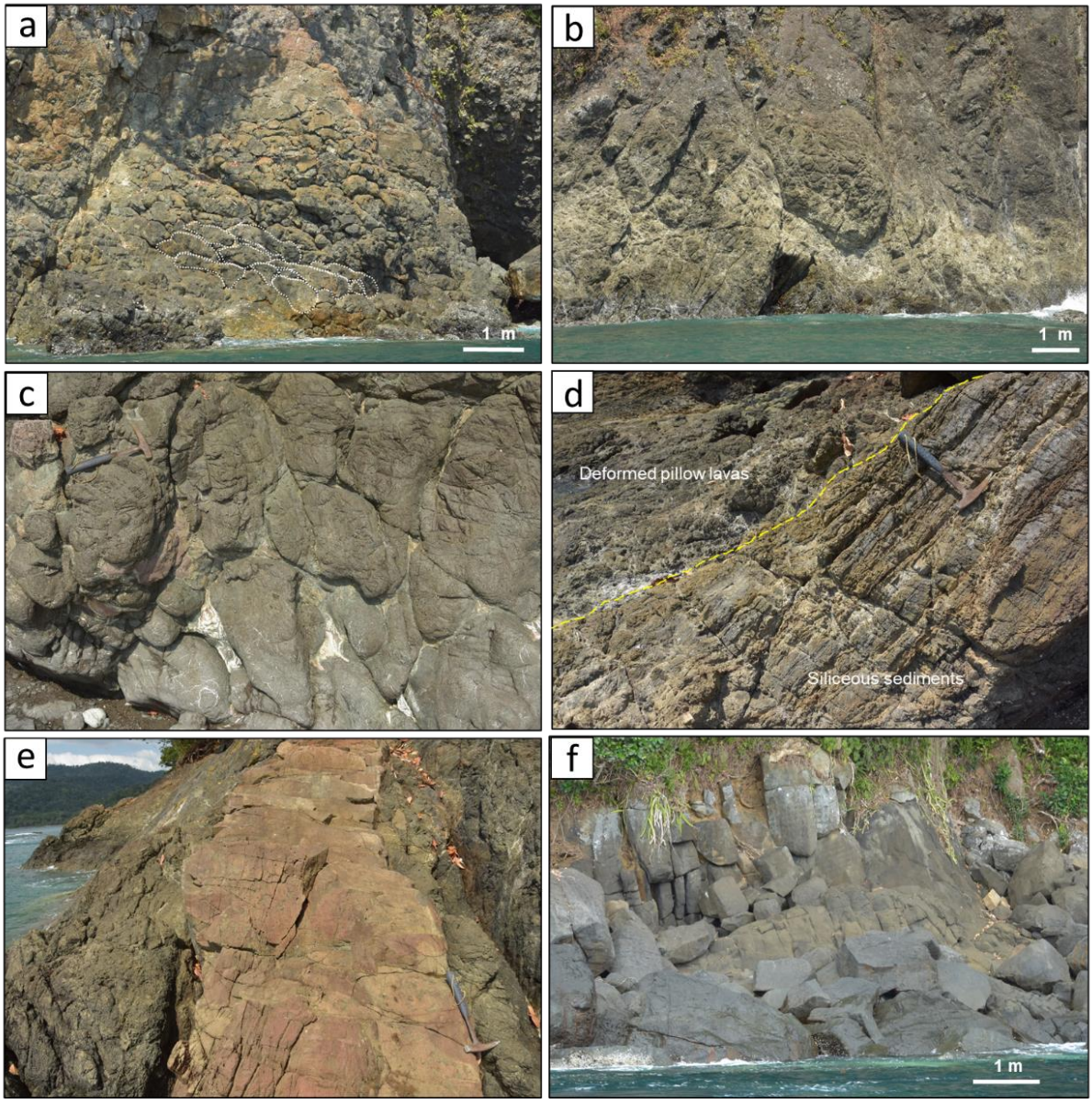

Figure 3.16: Pictures of exposures of the Jaqué Oceanic Plateau Complex and Proto-arc Complex. (a) Undeformed pillow basalts (coast south of Jaqué). (b) Deformed and heavily veined basalts (coast south of Jaqué). (c) Hyaloclastite in limestone (coast north of Aguacate). (d) Siliceous sediments interbedded with deformed plateau basalts (Puerto Piña coast). (e) Oxidised proto-arc dyke crosscutting deformed basalts (El Guayabo coast). (f) Columnar jointing within proto-arc intrusion (El Guayabo coast)

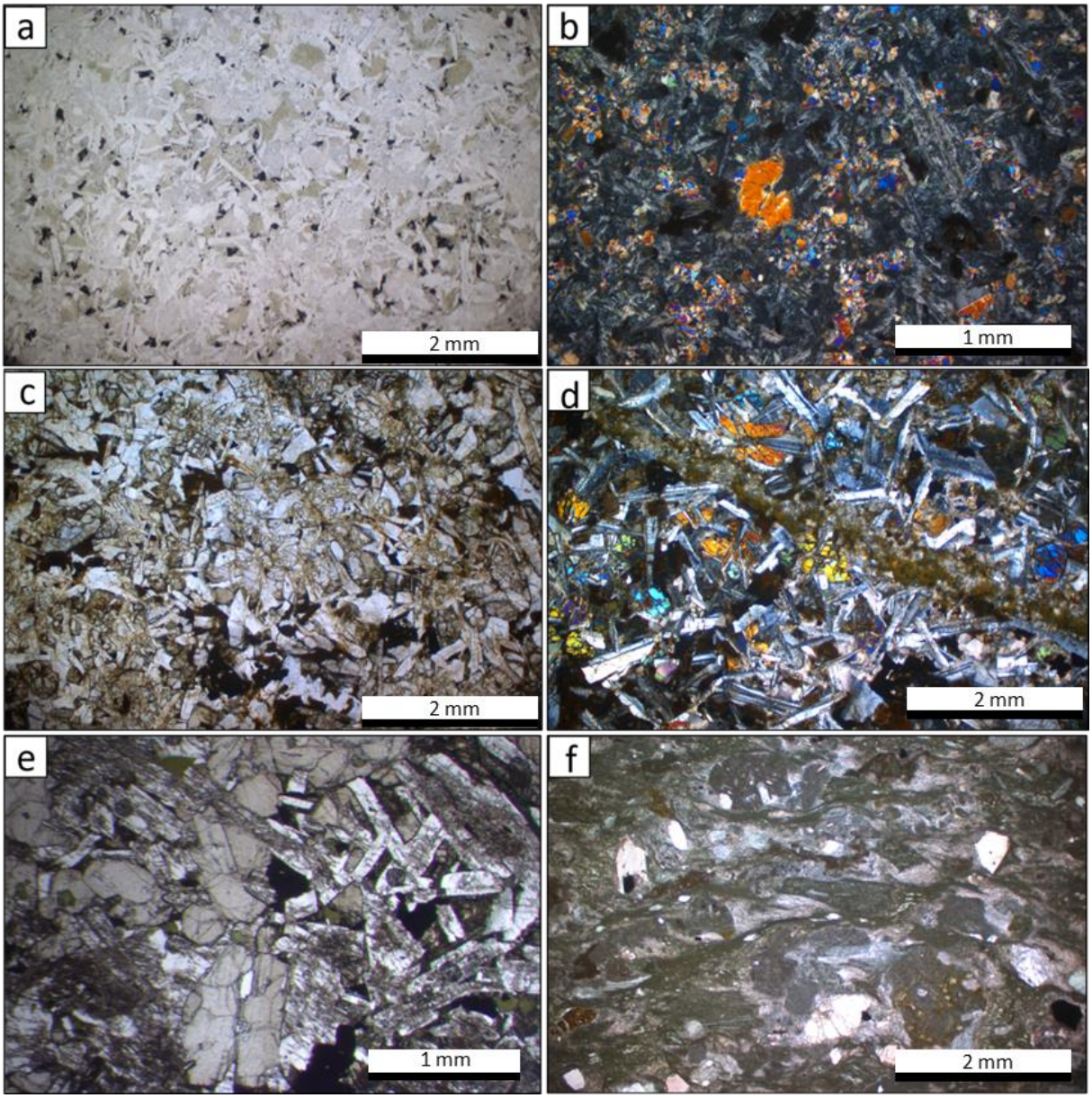

Figure 3.17: Microphotographs of the Jaqué Plateau Complex. (a) PPL view of a typical texture of a course basalt of the Jaqué Plateau (sample JB18-075). (b) XPL view of a fine grained porphyritic basalt of the Jaqué Plateau with a clinopyroxene phenocryst (sample DB16-082). (c) PPL view of a coarse basalt of the Jaqué Depleted Plateau with alteration (sample JB17-063). (d) XPL view of a coarse basalt of the Jaqué Depleted Plateau, crosscut by a calcite alteration vein and showing subophitic texture (sample JB17-059). (e) PPL view of a doleritic intrusion of the Jaqué Enriched Basalt (sample JB17-069). (f) PPL view of hyaloclastite of the Jaqué Enriched Plateau, showing glassy basaltic clasts and clinopyroxene fragments (sample JB17-077).

glass is altered to green and brown clays. Samples are often pervasively fractured, with calcite veining, and can show clay alteration along fractures.

Hyaloclastite intervals are rare within the plateau, and are found associated with basalts of the Jaqué Enriched Plateau (with light REE enriched patterns on primitive mantle normalised multielementary diagrams) exposed on the Puerto Piña peninsula and close to Playa

Muerto. These sequences are composed of deformed pillow basalts with extensive interpillow sediments, formed of red carbonate sediment to white pelagic limestone (Figure 3.16c). These pillows are found where pillows grade into limestone, creating limestone and hyaloclastite interbeds. The hyaloclastites are formed of devitrified vesicular glass, with fragments of plagioclase and clinopyroxene, ranging in size from 0.02 to 0.5mm (Figure 3.17f). There are also glassy clasts and basaltic clasts between 0.5-1.5mm in size, which can contain acicular to lath shaped plagioclase.

Jaqué Plateau Sediments: The Jaqué Plateau Sediments are exposed along the Jaqué coast, with limited exposure inland, mainly seen as blocks in the Rio Jaqué and Pavarando. They are found as small localised interbeds in the plateau, as well as continuous sections up to 6m thick (Figure 3.16d). Plateau sediments are composed of interbedded red chert, black chert, siliceous mudstones and rare limestones. The siliceous interbeds of red to black chert and mudstone are often recrystallized and deformed, with folding and small-scale faulting indicative of soft sediment deformation. The limestones are typically white and pelagic.

Jaqué Plateau Intrusions: The Jaqué Plateau Intrusions are composed of dolerites and gabbros which have Jaqué Enriched Plateau geochemistry. These samples intrude basalts and siliceous sediments of the plateau and are composed of lath shaped plagioclase with subhedral equant clinopyroxene and opaque oxides, with subophitic texture (Figure 3.17e). The intrusions can be porphyritic with a “spotted” appearance. These samples have a 1 mm grainsize groundmass and 1.5-3 mm phenocrysts of clinopyroxene and plagioclase. The clinopyroxene phenocrysts can exhibit twinning and can be fractured and altered to chlorite. The plagioclase is also altered to sericite, and can be completely replaced.

The Jaqué Oceanic Plateau Complex is the basement to the younger sedimentary and volcanic arc sequences. This is shown by an unconformable boundary between the Oceanic Plateau Basalts and overlying limestones of the Bahia Piña Formation, along with dykes of the volcanic arc crosscutting sequences of the Oceanic Plateau Basalts and Sediments. The Oceanic Plateau Complex has previously been described as the Punta Sabana Volcanics (Bandy and Casey, 1973), and as the San Blas Complex around the San Miguel Gulf (Coates et al., 2004; Barat et al., 2014). Previous $^{40}Ar/^{39}Ar$ dating of these basalts, yielded a matrix plateau age of 84.1 ± 1.0 Ma (error weighted mean stepheating age of to 71.3 ± 4.4 Ma for the same sample) (Lissinna, 2005). Previously cherts were dated as Lower Campanian (Bandy and Casey, 1973), with the radiolarian taxa revised by Barat et al. (2014) to give a Coniacian to lower Campanian age. Sampled siliceous sediments in the plateau

contained radiolarians, but due to poor preservation dating was not possible (Kukok, pers. comm. 2018).

3.3.2 Jaqué Proto-arc Intrusions

The Jaqué Proto-arc occurs as intrusions within the plateau basalts along the Jaqué Coast from El Guayabo to Puerto Piña and was only observed as blocks inland along the Rio Pavarando (Figure 3.15). The proto-arc represents the first subduction related magmatism, and exhibits an enriched plateau-like geochemistry with variable positive Th and negative Nb on primitive mantle normalised multielement diagrams. Dykes are seen to intrude deformed basalts of the plateau, and are formed of plagioclase-phyric basalts and are generally undeformed (Figure 3.16e). Dykes can be composite, with aphyric centres and plagioclase-phyric margins. Gabbros can intrude as large sills,

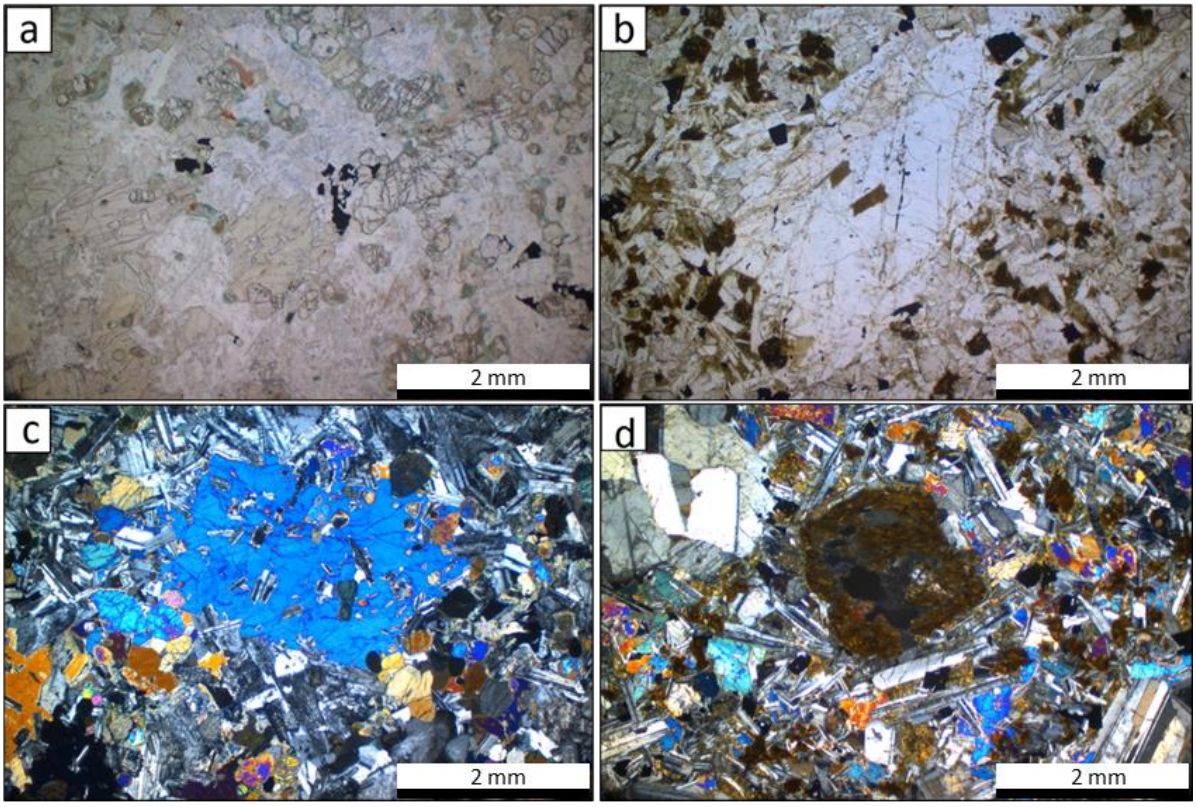

Figure 3.18: Photomicrographs of the Jaqué Proto-arc Group. (a) PPL view of a porphyritic dolerite, with phenocrysts of olivine and clinopyroxene (sample JB18-071). (b) PPL view of a porphyritic gabbro, with a large phenocryst of plagioclase (JB17-075). (c) XPL view of a porphyritic dolerite with a large clinopyroxene phenocrysts containing small crystals of plagioclase and olivine (sample JB18-071). (d) XPL view of a porphyritic gabbro, with phenocrysts of plagioclase and pseudomorphed olivine (sample JB17-075).

but are only seen in faulted contacts with basalts. A large gabbroic sill exhibited columnar jointing, with diffuse flow banding (Figure 3.16f).

The proto-arc dykes are generally formed of coarse porphyritic basalts (Figure 3.18). The groundmass is typically formed of interlocking acicular to lath shaped plagioclase along with equant subhedral to anhedral clinopyroxene, olivine and opaque oxides. Generally samples are holocrystalline and have a intergranular to subophitic texture. The groundmass typically is quite fresh, although there is some alteration to brown clays and limited sericite replacing plagioclase. Plagioclase phenocrysts are equant and can exhibit zoning. They are up to 2mm wide and can form glomerocrysts up to 4mm wide. These phenocrysts are quite fresh, with limited sericite alteration. There are also rare olivine phenocrysts, which can be pseudomorphed by iddingsite or serpentine. Clinopyroxene phenocrysts are up to 3 mm, and are quite fresh, with some alteration around the crystal rims. These phenocrysts are rimmed by smaller crystals of both plagioclase and olivine and can display an ophitic texture. Proto-arc gabbro intrusions have an intergranular to subophitic texture. They are formed of plagioclase laths, 1-2 mm long, with intergranular olivine and subhedral equant clinopyroxene. Plagioclase is altered to chlorite in places, and some olivine is heavily fractured, or completely pseudomorphed by iddingsite. The intrusions can be extensively fractured, with clay alteration along fractures.

3.3.3 Darién Formation

In this study, the Darién Formation is defined as an Early-Mid Eocene sequence of green-grey siliceous sediments, exposed around the San Miguel Gulf and along the Rio Jaqué (Figure 3.19a-b). Much of the sequence is formed of cherts, which can be tuffaceous and can contain minor fragments of plagioclase grains. Largely, sequences are thinly bedded, but can have beds up to 10cm thick. They are highly siliceous and can exhibit folding. In faulted areas, lenses of basalt up to 100m thick are found tectonically interbedded with siliceous sediment sequences. Tuffaceous chert overlying basalts close to the San Miguel Gulf have been dated as Late Ypresian to Early Lutetian based on radiolarian dating (Barat et al., 2014). A sequence of radiolarian rich volcanic sediments, part of the Morti Tuffs of Bandy and Casey (1983) which overlie plateau sequences, were dated as Early to Middle Eocene.

3.3.4 Jaqué-La Palma Group

The Jaqué-La Palma Group overlies the Jaqué Oceanic Plateau Complex, and is formed of 4 formations: (1) the Bahia Piña Formation (2) the Guayabo Formation (3) the San Miguel Formation and (4) the Sapo Arc

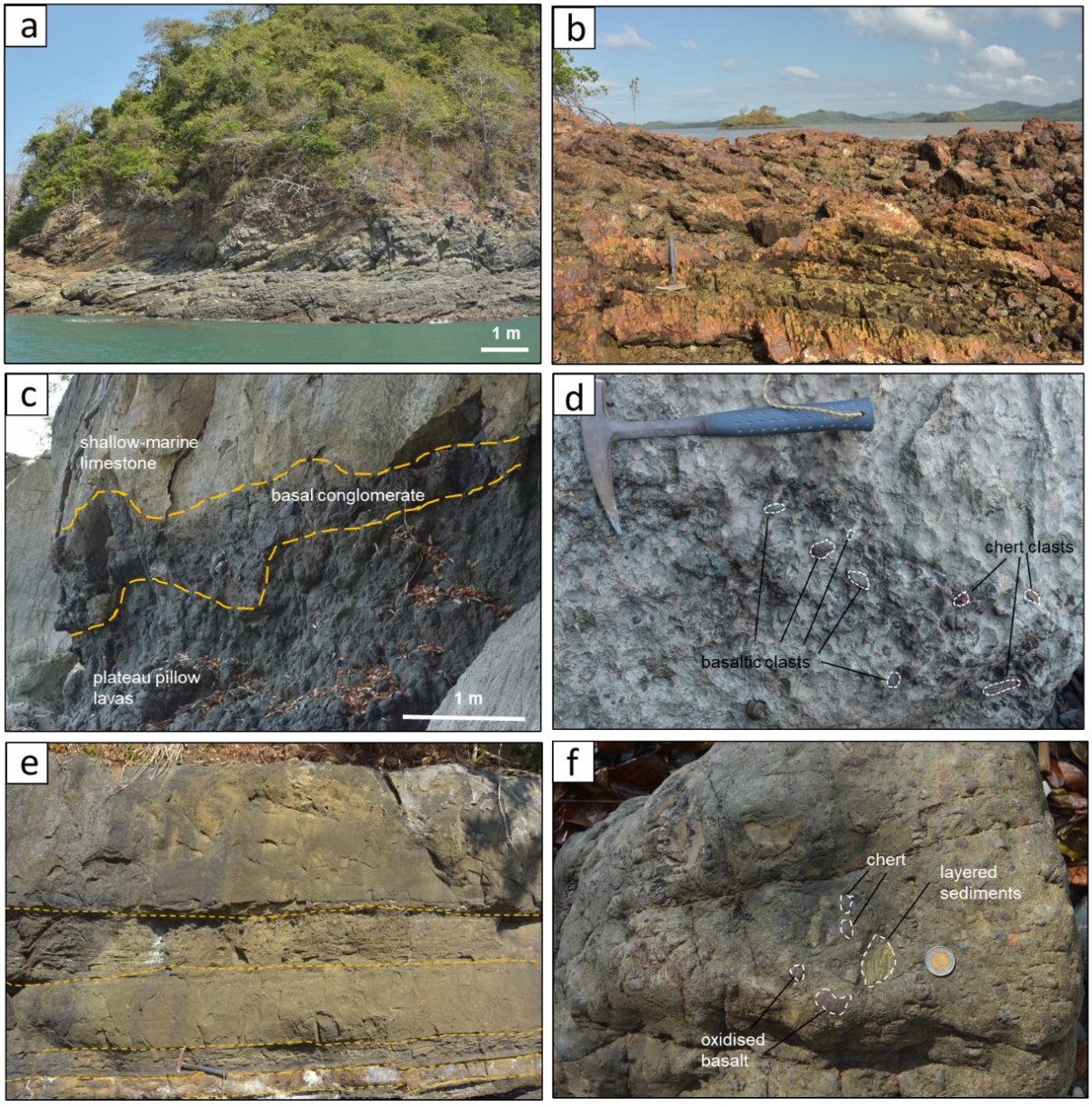

Figure 3.19: Photos of exposures and stratigraphic contacts of the Jaqué forearc sediments. (a)Dipping and folded grey tuffaceous siliceous sediments of the Darién Formation (Golfo de San Miguel). (b)Dipping bedded siliceous sediments of the Darién Formation (Golfo de San Miguel). (c) Limestones uncomformably overlying basalts of the plateau, with a basal conglomerate (Puerto Piña coast) (d) Basal conglomerate, showing clast assemblage (Puerto Piña coast). (e) Turbiditic deposits, showing massive and laminated layers (Jaqué coast). (f) Debris flow deposit, showing clast assemblage (Puerto Piña coast).

Bahia Piña Formation: At the base of the Jaqué-La Palma Group is the Bahia Piña Formation, formed of shallow marine limestone sequences. This formation is exposed along

the Bahia Piña coast, with blocks found inland along the Rio Jaqué and Pavarando (Figure 3.15). It is seen to locally uncomfortably overly the basalts on the Puerto Piña peninsula and is crosscut by gabbros (Figure 3.19c). Where the limestone overlies the basalt, there is a basal conglomerate (Figure 3.19c-d). This basal conglomerate is overlain by a shallow water limestone, with abundant broken large benthic foraminifera, which grades to a sandy foraminiferal limestone, to a bedded, bioturbated, darker limestone. Large benthic foraminifera from the limestone gave an overall age of Oligocene (Chapter 4).

The basal conglomerate is composed of a calcareous, tuffaceous matrix with foraminifera, radiolarites and basaltic clasts (Figure 3.20a). The groundmass contains planktonic foraminifera and crinoids (0.2-1 mm in size) along with abundant coralline algae. Basaltic clasts are up to 1-2 mm in size and have a glassy matrix with visible acicular plagioclase. Some of these clasts are extensively altered to clays. Clasts of radiolarite are subangular and up to 2 mm in size. There are also rounded clasts of micritic limestone. The rocks are extensively fractured, with many calcite veins up to 1.5 mm thick, which cut through both foraminifera and basaltic clasts. Overlying limestones have a micritic groundmass and are pervasively cut by calcite veins. They have a small detrital component composed of fragments of clinopyroxene. They also contain abundant corraline algae, and broken fragments of large benthic foraminifera, benthic foraminifera and shells (Figure 3.20b).

Guayabo Formation: The second formation of the Jaqué-La Palma Group is the Guayabo Formation, which consists of debris flow deposits and turbidites with intervals of calcareous hemipelagic mudstone (Figure 3.19e-f). The debris flow conglomerates and turbidites are exposed along the coast to the north of Jaqué, as well limited exposures inland on the Rio Pavarando (Figure 3.15). Along the Rio Pavarando and nearby low-lying ridges, debris-flow conglomerate blocks are found in abundance (with boulders up to 10 x 10m in size) but these conglomerates were not found in-situ. Blocks of turbidite deposits were also observed in Rio Pavarando and associated quebradas. Along the Puerto Piña Peninsula, the limestone of the Bahia Piña Formation is seen to grade into calcareous turbidites of the Guayabo Formation. This unit has been assigned an Oligocene age based on large benthic foraminifera and limestones.

Turbidites are composed of cross bedded and parallel laminated calcareous-tuffaceous siltstone-sandstone, which is locally graded. The base of turbidite beds were observed (T_a) with grain-supported basal conglomerates and load structures. Turbidites were often bioturbated, with limestone rich intervals. The unit is generally

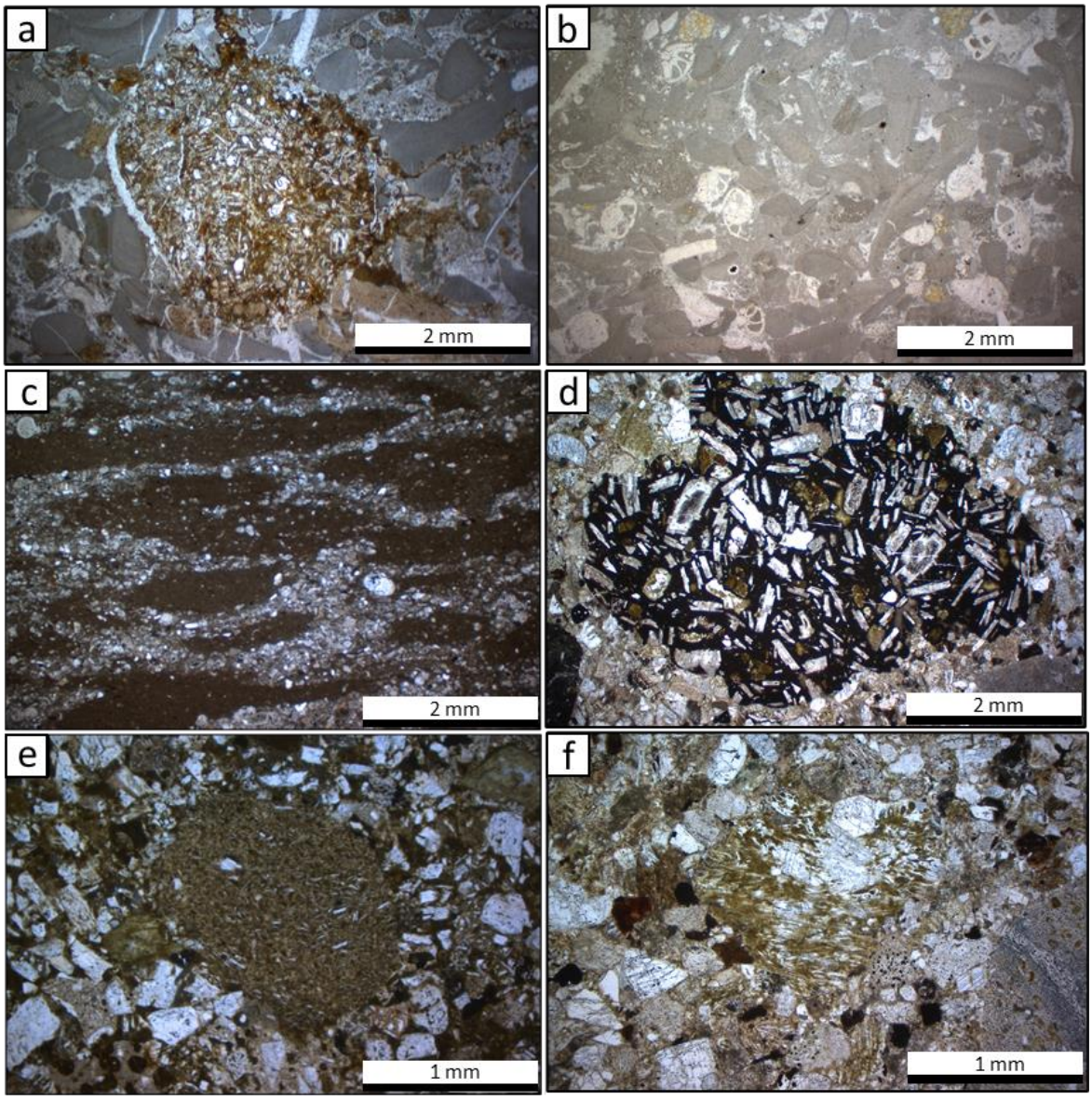

Figure 3.20: Photomicrographs of the Bahia Piña and Guayabo Formations. (a) PPL image of the basal conglomerate of the Bahia Piña Formation, containing an altered clast of basalt (sample JB17-070). (b) PPL image of limestone of the Bahia Piña Formation (sample JB17-073). (c) PPL image of a calcareous micritic interval in a turbiditic unit of the Guayabo Formation, showing flaser bedding (sample JB17-048). (d) PPL view of a coarse turbiditic conglomerate, containing a clast of porphyritic basalt with zones plagioclase phenocryst (sample JB17-074). (e) PPL view of a coarse turbiditic sandstone, showing a clast of fine grained basalt (sample JB17-049). (f) PPL view of a turbiditic conglomerate, containing a clast of pumice (sample JB17-074).

deformed and faulted, and extensively weathered with clasts weathered out in some areas. The turbidites are generally formed of fairly coarse sandstone, with a grain size between 0.1-0.7mm. Some samples have a calcareous matrix and a fossiliferous component, formed by up to 20 vol. % of recrystallised foraminifera fragments. Other samples have a much smaller calcareous component and are formed of subrounded to angular fragments of lithics and crystals, with a minor fossiliferous component. The fossiliferous component is formed of

broken fragments of large benthic foraminifera and planktonic foraminifera. The crystal component is formed of quartz, plagioclase and clinopyroxene grains. Plagioclase is seen as small needles as well as lath shaped zoned crystals up to 0.7 mm long and clinopyroxene fragments are up to 0.5mm in size, which are fractured and altered. Lithic clasts are primarily igneous, with fine grained basalt and porphyritic basalt clasts with zoned plagioclase phenocrysts.

Conglomerate from the base of a turbidite unit, close to the limestones is composed of a sandy groundmass, with igneous and sedimentary clasts (Figure 3.20d-f). Sedimentary clasts were formed of a fine grained calcareous sediment containing broken shell fragments. Igneous clasts were the most abundant, composed of pumice, gabbro, igneous clasts with visible acicular plagioclase, and plagioclase-phyric igneous clasts. Within some igneous clasts, the plagioclase can be preferentially aligned, with some flow banding present. Within the plagioclase-phyric clasts, the plagioclase can exhibit zoning.

The calcareous, tuffaceous sediments within the turbidite unit are fossiliferous with many broken fragments of foraminifera <0.1 mm in size, with rare larger foraminifera up to 0.4 mm in size (Figure 3.20c). The majority of foraminifera are recrystallised with calcite. The matrix is brown and micritic and exhibits lamination in areas, as well as flaser bedding with muddy lenses up to 1 cm long. These lenses are often surrounded by broken foraminifera fragments. There are pervasive fractures through the unit, with many quartz and calcite veins. There is a very limited lithic component, with only rare plagioclase observed.

The debris flow deposits are matrix supported, poorly sorted and polymictic. The matrix is typically sandy with a tuffaceous component. The clasts range from pebbles to cobbles and are subrounded to angular. Clast composition includes siliceous-tuffaceous layered sediments, more massive cherts, porphyritic and aphyric igneous clasts and micritic limestone. These clasts likely represent the composition of plateau through to arc sequences. Analysed andesitic clasts of the Guayabo Formation had a Jaqué Arc Group 2 geochemistry (Chapter 5).

San Miguel Formation: The next formation within the La Palma-Jaqué group is the San Miguel Formation. This formation is composed of arc derived volcaniclastic deposits and tuffs and is exposed mainly around the San Miguel Gulf, with limited exposures along the remainder of the Jaqué coast.

The arc-derived debris flows typically have a tuffaceous-sandy matrix, which is pumiceous in places. The debris flows can be monomictic with arc clasts of similar origin, but more often they are polymicitic (Figure 3.21c-d). In these debris flows, the clasts include tuffs, along

with igneous clasts with andesitic to dacitic compositions and different phenocryst assemblages. All igneous clasts have a petrographic composition which mimics those observed in lava flows of the Sapo Arc. These clasts can range from <1cm to large blocks 5m wide. Rare scoria, algae and biogenic clasts (mollusc shells and echinoderms) clasts are also seen in tuffaceous debris flow deposits. Although most debris flow deposits are matrix supported with rounded clasts, there are infrequent deposits of a grain-supported volcanic breccia.with angular porphyritic arc clasts. Some debris flows also contain large (>40 cm) rip up clasts.

These debris flows are interbedded with massive to finely laminated brown to yellow sandy-tuff units, which can exhibit small to large scale cross bedding, bioturbation and soft-sediment deformation. Some massive tuff beds represent fall-out deposits (Figure 3.21b). Channels of up to 10m wide were observed in these sequences, and were immature with visible fragments of clinopyroxene and amphibole. Rare granular beds contain small clasts of well-rounded tuff and some beds are rich in pumice.

These sequences are intruded by arc dykes, with a subvolcanic intrusion within the unit seen to contain sedimentary enclaves within the Golfo de San Miguel. They are also interbedded with lava flows from the Sapo Arc. These sequences formed on the later part of the volcaniclastic apron.

Sapo Arc: The final formation within the La Palma-Jaqué Group is the Sapo Arc. These volcanic arc sequences are comprised of mafic to felsic intrusive rocks and lava flows (Figure 3.21a). The intrusions and lava flows have an arc-like geochemistry, and include samples of three geochemical groups: Jaqué Arc Group 1, Jaqué Arc Group 2 and Jaqué Arc Group 3 (Chapter 5). These geochemical groups include samples previously analysed by Cavell (unpublished). This formation has not previously been described in detail for this area, and was considered to be part of the San Blas Complex associated with the oceanic plateau (Coates et al., 2004; Lissinna, 2005; Barat et al., 2014). A previous basaltic andesite with unknown field constraints from Bahia Piña was dated by $^{40}Ar/^{39}Ar$ laser step heating at 21.7 ± 0.3 Ma (Lissinna, 2005).

Lavas of the Sapo Arc Formation are exposed along the Jaqué coast, from Punta Caracoles to La Palma. Most lava flows are thick, ranging in thickness from

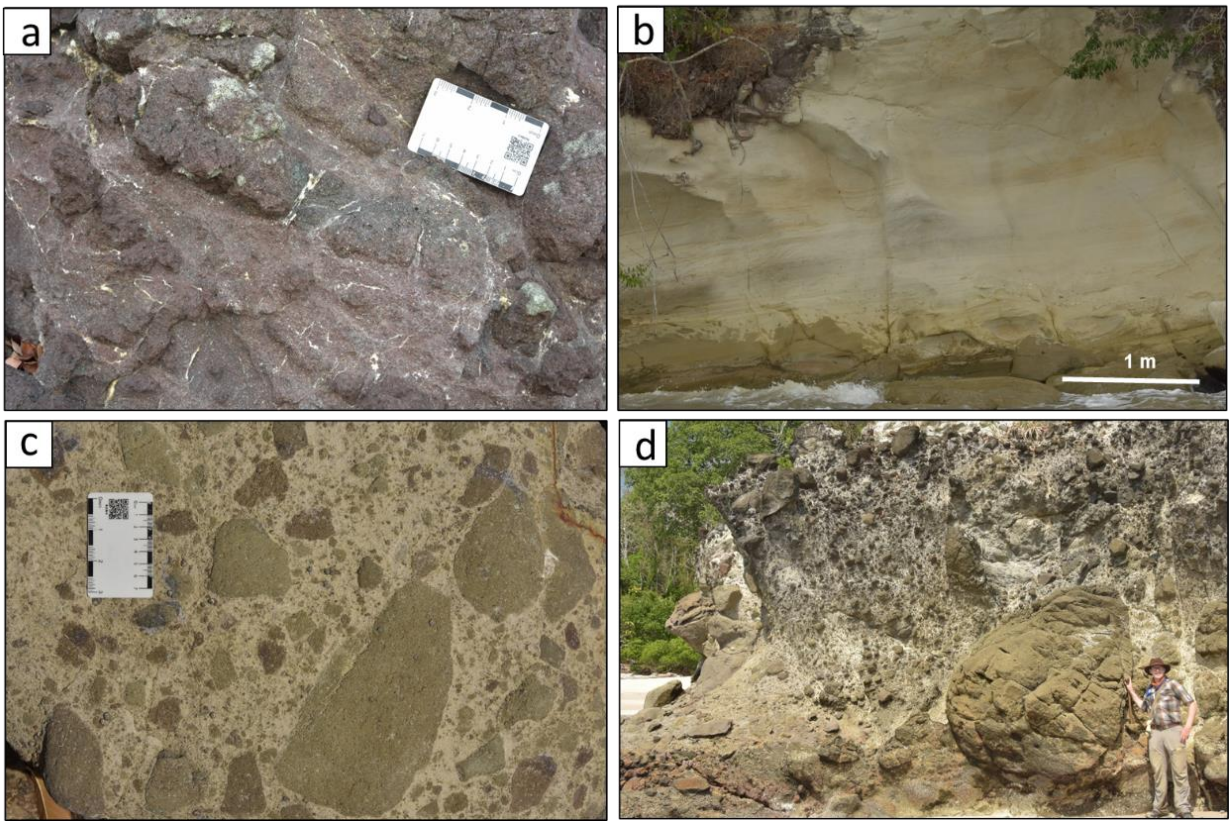

Figure 3.21: Pictures of exposures of the Jaqué Volcanic arc sequences. (a) Oxidised amygdalar lava flow (Garachine coast). (b) Massive tuff fall out deposit (La Palma coast). (c) Polymictic arc volcanic breccia with tuffaceous matrix (La Palma coast). (d) Volcanic breccia with large clasts and a tuffaceous matrix. (La Palma coast).

3-20 m. Breccias were observed at the base of some lava flows, with columnar jointing in flows with a thickness of 20 m. The lavas were interbedded with volcaniclastic sediments and tuffs of the San Miguel Formation. Lavas range in composition from basaltic to andesitic, and can be aphyric, although most have phenocrysts of plagioclase, clinopyroxene and/or amphibole (Figure 3.22). The groundmass of these samples is glassy, containing small acicular plagioclase and and equant clinopyroxene with brown glass with an intersertal texture. Plagioclase phenocrysts can comprise 30 vol. % of the rock and are between 2-5 mm in size. Generally these plagioclase phenocrysts are euhedral to subhedral lath shaped, and can be zoned. Some phenocrysts show sieve textures and others are replaced by chlorite. Euhedral to subhedral clinopyroxene crystals were also observed, sometimes forming glomerocrysts with plagioclase. In some samples, this clinopyroxene is fresh, with only limited alteration around the rim of crystals, but in others it has been pseudomorphed by calcite.

Intrusions of the Sapo Arc are exposed inland along the Rio Jaqué and Rio Pavarando as blocks, and in-situ along the Jaqué Coast to La Palma. They

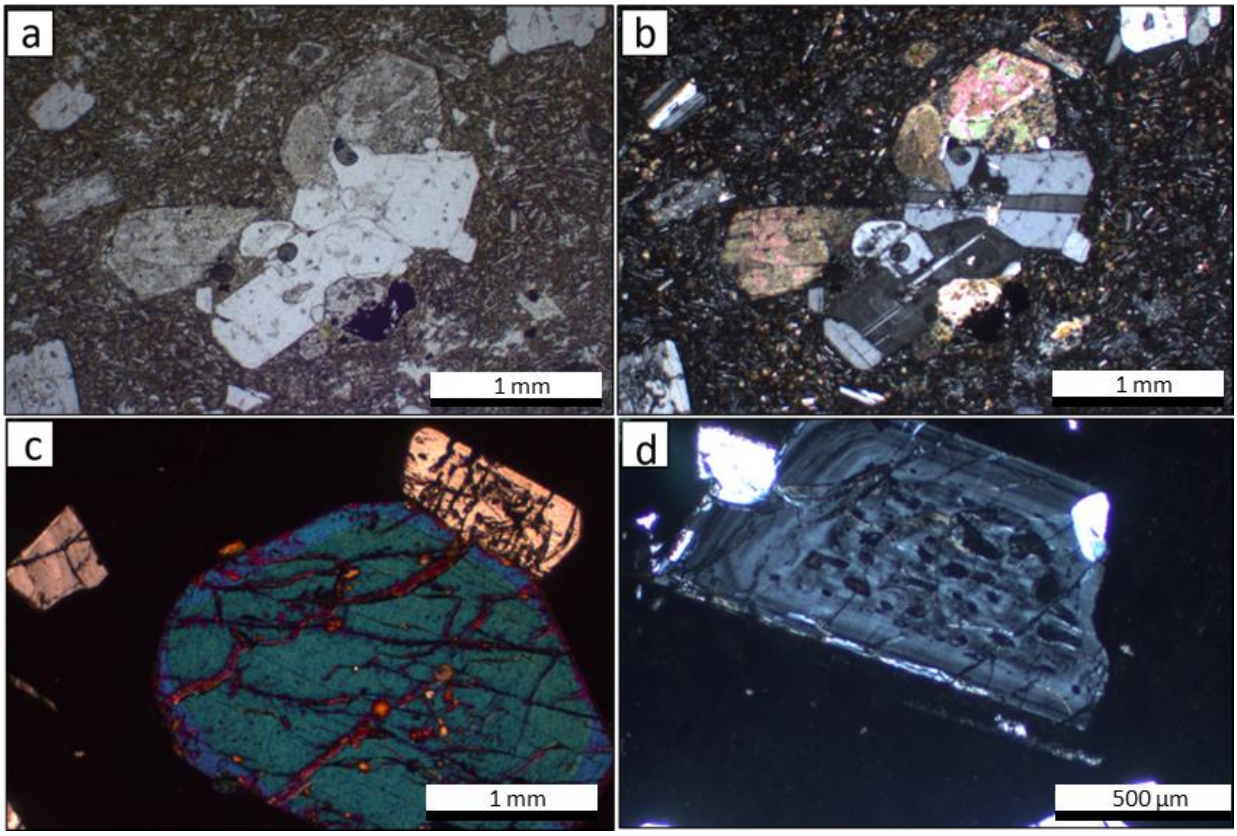

Figure 3.22: Photomicrographs of the Sapo Arc (a) and (b) PPL and XPL images of a clinopyroxene and plagioclase glomerocryst within a fine grained glassy andesitic matrix of Arc Group 2. Clinopyroxene has partially altered to calcite (sample JB18-064). (c) XPL image of a clinopyroxene phenocryst within a glassy andesitic matrix (sample DB15-019). (d) XPL view of a zoned plagioclase phenocryst within a glassy andesitic matrix (sample DB15-019).

range from gabbros, dolerites, diorites to plagioclase-phyric and aphyric basalt dykes with rare amygdaloidal dykes. Along Rio Pavarando and associated quebradas, there are abundant gabbro blocks up to 50cm, with rare megablocks up to 5m in diameter. Dolerites and gabbros of the Sapo Arc intrude the Oceanic Plateau Complex basalts as both dykes and sills. Plagioclase-phyric and aphyric basalts also intrude the basalts, siliceous sediments of the Oceanic Plateau Complex,and forearc sediments of the Guayabo and San Miguel Formations. They intrude as dykes and sills, up to 15m thick, and can exhibit flow banding and columnar jointing.

Samples of the Jaqué Arc Groups do not form distinct groups in the field, but they are exposed in different areas. Samples of the Jaqué Arc Group 1 are exposed from Punta Caracoles to La Palma. Only one sample with Arc Group 1 geochemistry was sampled in this study (sample DB16-080), but here it is combined with samples and field observations from Cavell (unpublished). Samples of the Arc Group 1 are largely composed of lava flows, along with rare dykes. Lava flows are basaltic to andesitic and can have phenocrysts of plagioclase and rare phenocrysts of amphibole. Lava flows of the Arc Group 1 were also

observed interbedded with tuffs of the San Miguel Formation. Dykes of the Arc Group 1 can also be plagioclase-phyric and intrude basalts of the Oceanic Plateau Complex.

Samples of the Arc Group 2 are exposed inland along the Rio Jaqué and Rio Pavarando, and along the Jaqué Coast up to La Palma. Samples of Sapo Arc with Jaqué Arc Group 2 geochemistry are composed of both intrusions and lava flows. Largely, Jaqué Arc Group 2 samples were found as clasts in debris flows of the San Miguel Formation. Inland along the Rio Pavarando and Rio Jaqué, Arc Group 2 samples are found as blocks of gabbros and plagioclase and amphibole-phyric basalts and andesites. They also occur as intrusions along the coast, and intrude tuffaceous sediments of the San Miguel Formation. Rare intrusions show flow banding.

Only two samples of the Arc Group 3 were found. These samples occur as a dacitic block from the Rio Pavarando, and a large sill from the Jaqué coast. This sill is part of a series of sills 10-15m thick, intruding turbidites of the Guayabo Formation. It exhibits large columnar joints, and is plagioclase-pyric.

The Sapo Arc Formation, the San Miguel Formation and the Guayabo Formation represent the formation of emerging volcanic islands. The Sapo Arc Formation represents the lavas and intrusions forming these islands, the San Miguel Formation represents proximal breccias and tuffaceous deposits from subaerial volcanism, and the Guayabo Formation represents more distal turbidites and debris flows. The transition from the basal conglomerate at the base of the limestone, which overlies the plateau and shows subaerial exposure of the plateau, through to shallow marine limestones, to turbidites and debris flow deposits, indicates a transgression at the time of deposition.

3.4 Serranía de Baudó

Fieldwork was undertaken along the Colombian coast of the Serranía de Baudó, from El Valle in the south to Aguacate in the north (Figure 3.24). The only inland location was the Rio Chocolotal. Based on observations made during fieldwork, combined with new geochemical and geochronological constraints, new lithostratigraphic subdivision can be described for the coast of Serranía de Baudó. These groups are (1) the Baudó Basalt Group, (2) the Baudó Sill Complex, (3) the Punta Lana Formation and (4) the Bahia Solano Mélange (Figure 3.23).

3.4.1 The Baudó Oceanic Plateau Complex

The Baudó Oceanic Plateau Complex is composed of pillow basalts and lava flows, along with interbedded sediments and sills.

The Baudó Oceanic Plateau Basalts: The Baudó Plateau Basalts are composed of series of pillow basalts and massive lava flows with rare intervals of pillow breccia and hyaloclastite, and local peperitic sequences (Figure 3.25). These basalts have a plateau-like geochemistry (Chapter 5) and are exposed along the coast from Bahia Solano to Aguacate, as well as along Rio Chocolotal (Figure 3.24). Towards Cupica and Aguacate there are extensive exposures of pillow basalts with inflated flows of 5-10m thick. Pillows are often seen to be deformed and elongated and are markedly veined in areas (Figure 3.25b) Locally at Cupica there are inflated mega-pillows with thick rims of glass and rare hyaloclastite, locally with pillow breccia in interpillow spaces (Figure 3.25d) Lavas of the plateau group are seen in faulted contact with dolerites and sediment and are intruded by plateau dolerites. Previous $^{40}Ar/^{39}Ar$ ages of Baudó lavas range between 73 and 78 Ma (Kerr et al., 1997b).

The plateau pillow basalts and lava flows are fine grained and aphyric, formed of acicular to elongate laths of plagioclase and equant clinopyroxene and opaque oxides (Figure 3.26). The texture ranges from holocrystalline to hypocrystalline, but typically textures are intergranular and can be subophitic. Plagioclase crystals are typically partially altered to sericite, while the glassy groundmass can be altered to palagonite, chlorite and actinolite. Rarely there are phenocrysts of both lath shaped plagioclase and subhedral clinopyroxene over 1mm in size, which can form glomerocrysts. These rocks can also be crosscut by veins of quartz and zeolites.

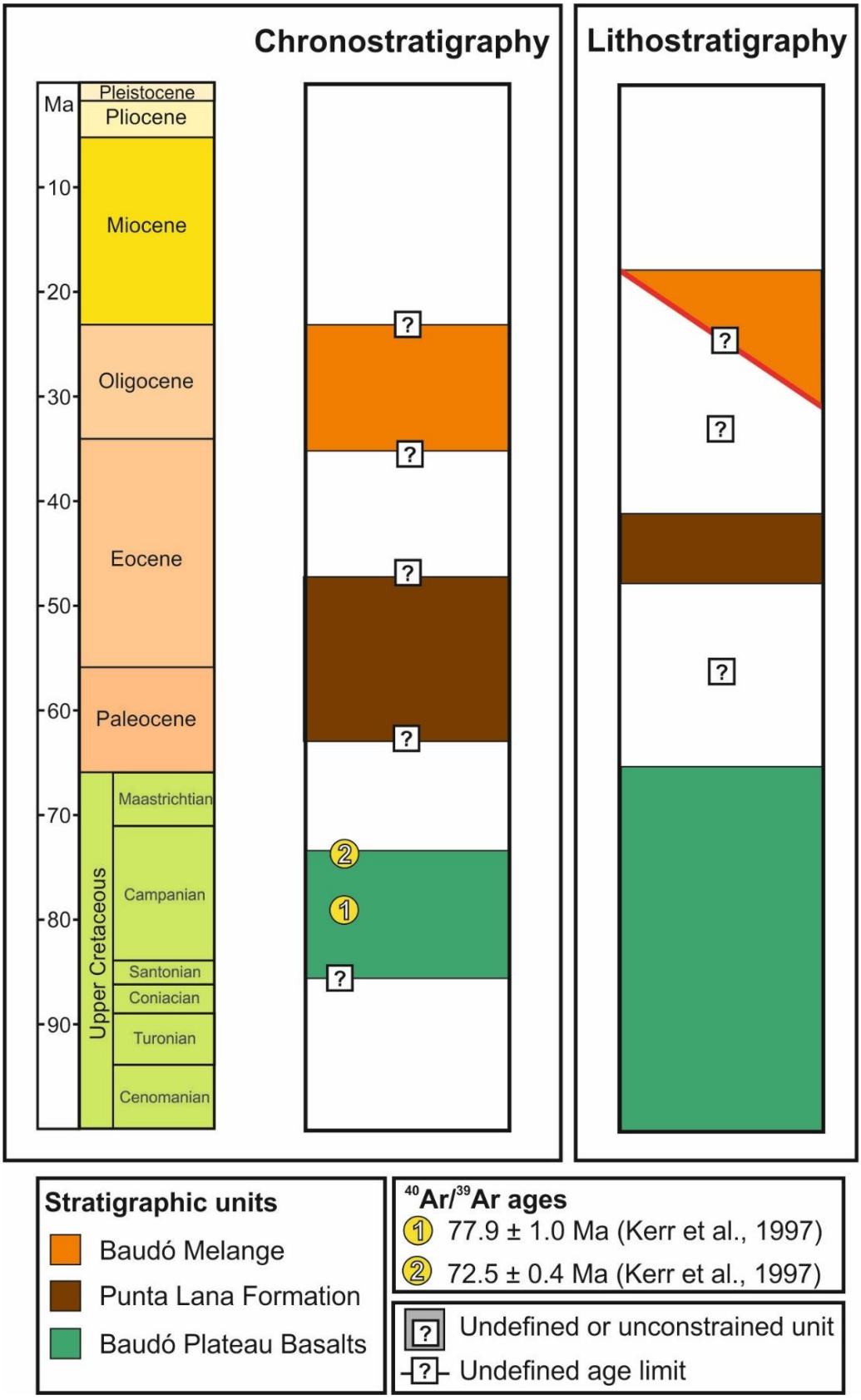

Figure 3.23: Chronostratigraphic and lithostratigraphic charts of the Serranía de Baudó region

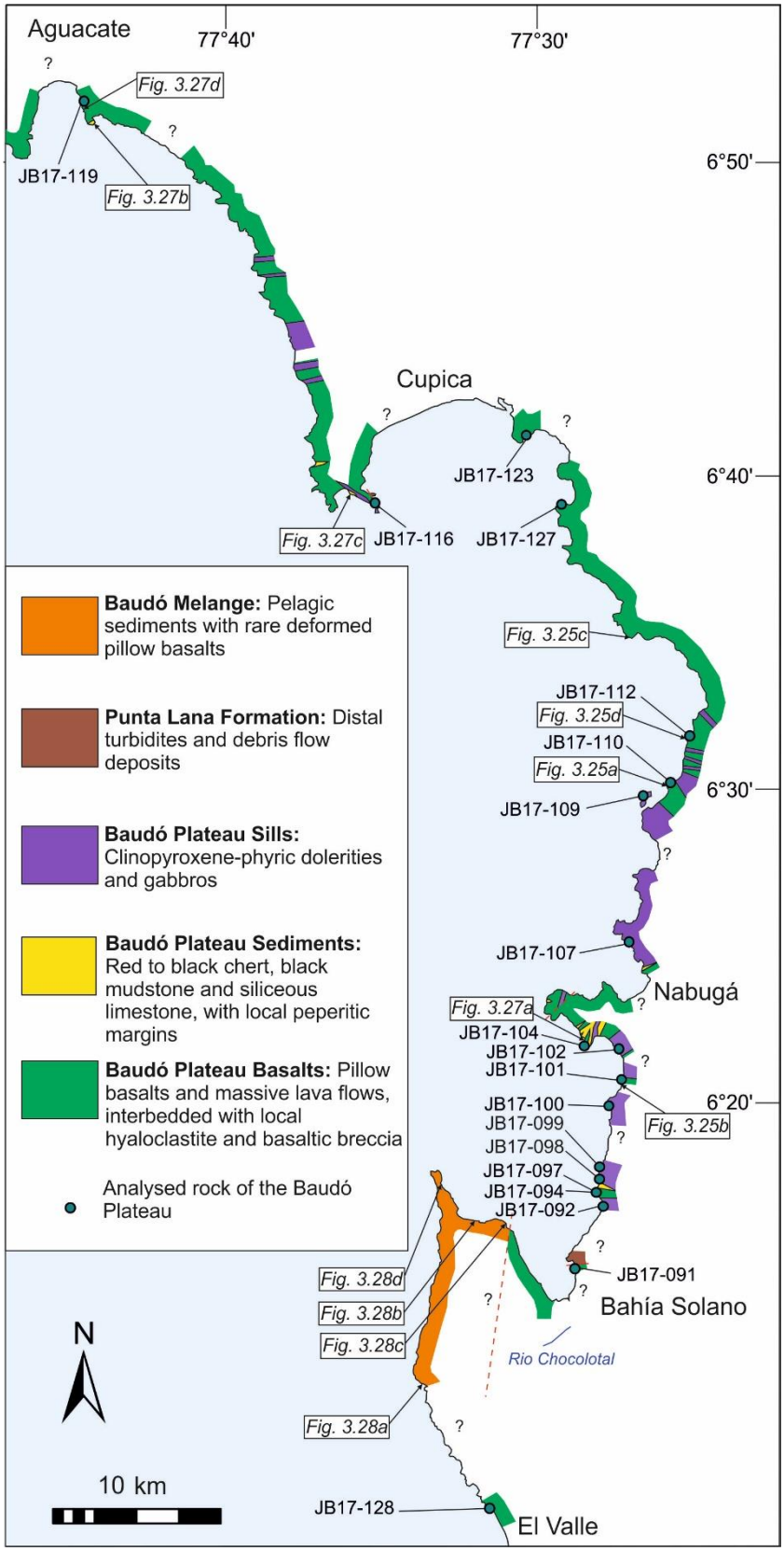

Figure 3.24: Geological map of coastal exposures of the Serranía de Baudó stratigraphic units along the Baudó from Cupica to El Valle, with locations of samples with geochemical analyses and locations of field photographs.

Within the plateau, plagioclase-megacryst basalt was also observed along Rio Chocolotal. This basalt formed of 4cm wide plagioclase crystals in a medium grained groundmass. The plagioclase megacrysts form up to 80 vol. % of the total sample and are rounded. They are fractured, with some sericite replacement, and have small clinopyroxene crystals within the larger plagioclases. The groundmass surrounding the megacrysts is ophitic, with large clinopyroxene crystals encompassing elongate laths of randomly oriented plagioclase (Figure 3.26c). This groundmass clinopyroxene has some chlorite replacement and the plagioclase has been partially altered to chlorite and sericite.

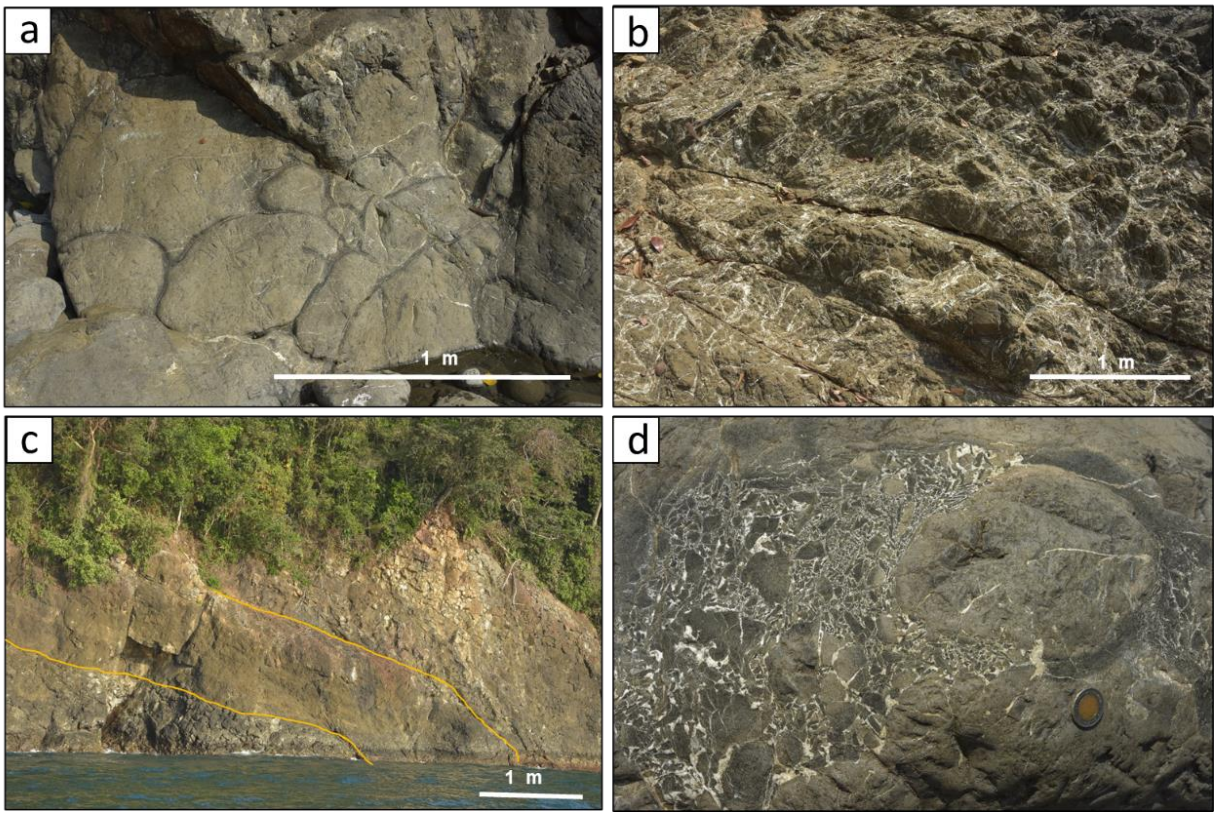

Figure 3.25: Pictures of exposures of the Baudó Oceanic Plateau Basalts. (a) Undeformed pillows with thick glassy rims (coast north of Nabuga). (b) Heavily deformed basalt, with intense veining (coast north of Bahia Solano). (c) Pillows interbedded with massive lava flows (coast north of Nabuga). (d) Interpillow breccia (coast north of Nabuga).

Baudó Oceanic Plateau Sediments: Pillows were observed to be interbedded with black to red chert, black mudstone, and grey siliceous limestone (Figure 3.27a-b). On the Nabuga peninsula and locally along the coast near Cupica, these sediments can form peperites with lavas or doleritic intrusions. Peperite textures vary from highly irregular, mingled margins to occasional more angular, quenched boundaries (Figure 3.27c-d). Often at the margins between igneous intrusion and sediment, there is some silicification with the formation of

silica nodules. In some places this silicified boundary is only a few cm thick, whereas in others it ranges from 20cm to 1m. Within the thicker silicified margins, silica nodules can be up to 3cm wide, along with lenses of both the mudstone and intruding dolerite.

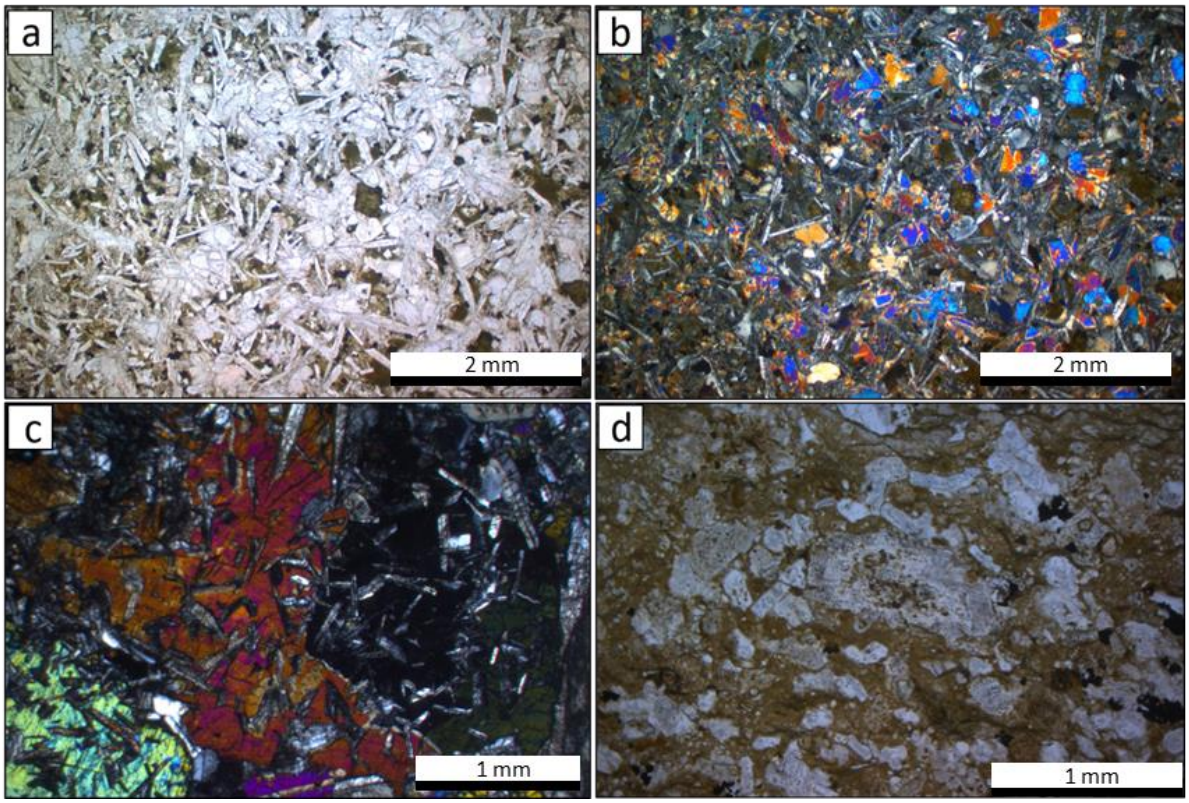

Figure 3.26: Photomicrographs of the Baudó Plateau and the Punta Lana Formation. (a) PPL view of a typical texture and composition of a Baudó Plateau Basalt (sample JB17-127). (b) XPL view of a typical texture and composition of Baudó Plateau Basalt (sample JB17-127). (c) XPL view of the ophitic texture of the groundmass of the plagioclase megacryst basalts of the Baudó Plateau (sample JB17-082). (d) PPL view of tuffaceous sandstone of the Punta Lana Formation (sample JB17-096).

Baudó Oceanic Plateau Sills: The Baudó Plateau Sills are exposed along the coast from Bahia Solano to north of Nabuga, with rare intrusions near Cupica (Figure 3.24). It is composed of clinopyroxene-phyric dolerites and gabbros, which have a plateau-like geochemistry. The sills are seen in faulted contact with pillow basalts and sediments. The sills intrude the basalts of the Baudó Plateau and intrudes sediments to form the peperites. Gabbros and dolerites are deformed in places, with both lenticular structures and foliated textures observed.

Intrusions in the plateau range from dolerite to gabbro. These rocks are composed of elongate laths of plagioclase, equant pyroxene, opaque oxides and rare olivine. They generally have a subophitic texture which can be ophitic in some samples. The groundmass displays both chlorite and actinolite alteration, and clinopyroxene phenocrysts are fractured and altered to chlorite along rims of crystals. Plagioclase crystals are also fractured and

altered to chlorite and sericite. Some gabbros have a “spotted” texture, with clinopyroxene phenocrysts of up to 4mm in size in a 2mm grain size groundmass.

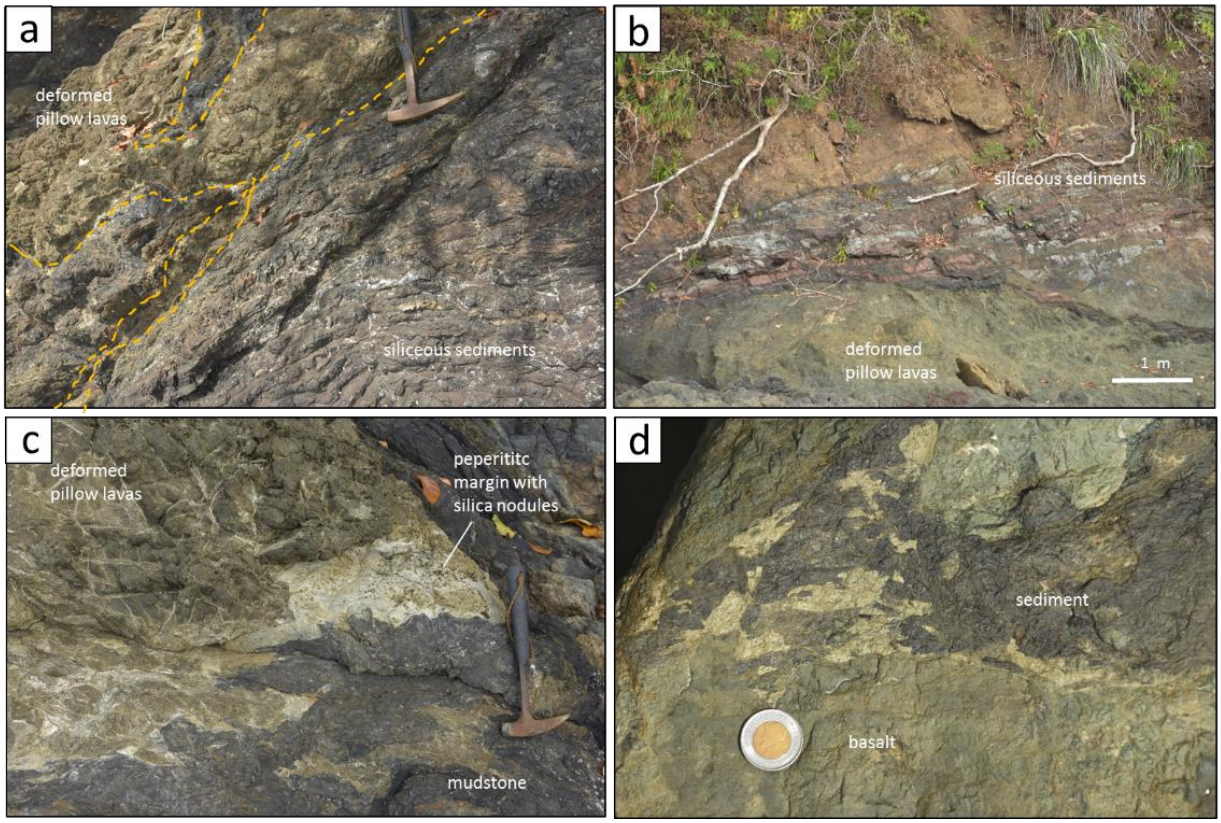

Figure 3.27: Pictures of exposures of the Baudó Oceanic Plateau Basalts and Sediments. (a) Black mudstones interbedded with deformed pillows (Nabuga peninsula). (b) Interbedded red to black chert and limestone, overlying deformed pillow lavas. (Cupica coast). (c) Peperitic margin between mudstone and deformed pillow lavas, showing silica nodules. (Nabuga peninsula). (d) Peperitic margin between sediments and basalt, showing highly irregular margins. (Nabuga peninsula).

3.4.2 Punta Lana Formation

Outcrops of undeformed volcaniclastic sediments are rare, with only 2 outcrops seen along the coast. The most southern of these is exposed at Bahia Solano, with layers of black siliceous mudstone and medium to coarse sandstone, interpreted to be a distal turbidite deposit. The second exposure is at Cupica, where a polymictic breccia is in faulted contact with plateau basalts. This breccia has clasts of fine to coarse basalt, cross laminated sandstone, black chert and limestone. These sediments are from a volcaniclastic apron, which could represent a syn-volcanic plateau debris flow.

Tuffaceous sandstones of the Punta Lana Formation is composed of a green tuffaceous matrix, with fragments of clinopyroxene and plagioclase crystals, 0.2-0.3mm in size, and small rounded clasts of fine-grained basalt (Figure 3.26d-e). The fragments are generally altered and can be fractured. Some larger plagioclase crystals are also observed, which

have an irregular shape and are zoned. These plagioclase phenocrysts are altered by both sericite and chlorite, preferentially in the centre. These sandstones are interbedded with layers of mudstone, and also contain small muddy lenses (Figure 3.26). Overall, the rock is very fractured and slightly deformed.

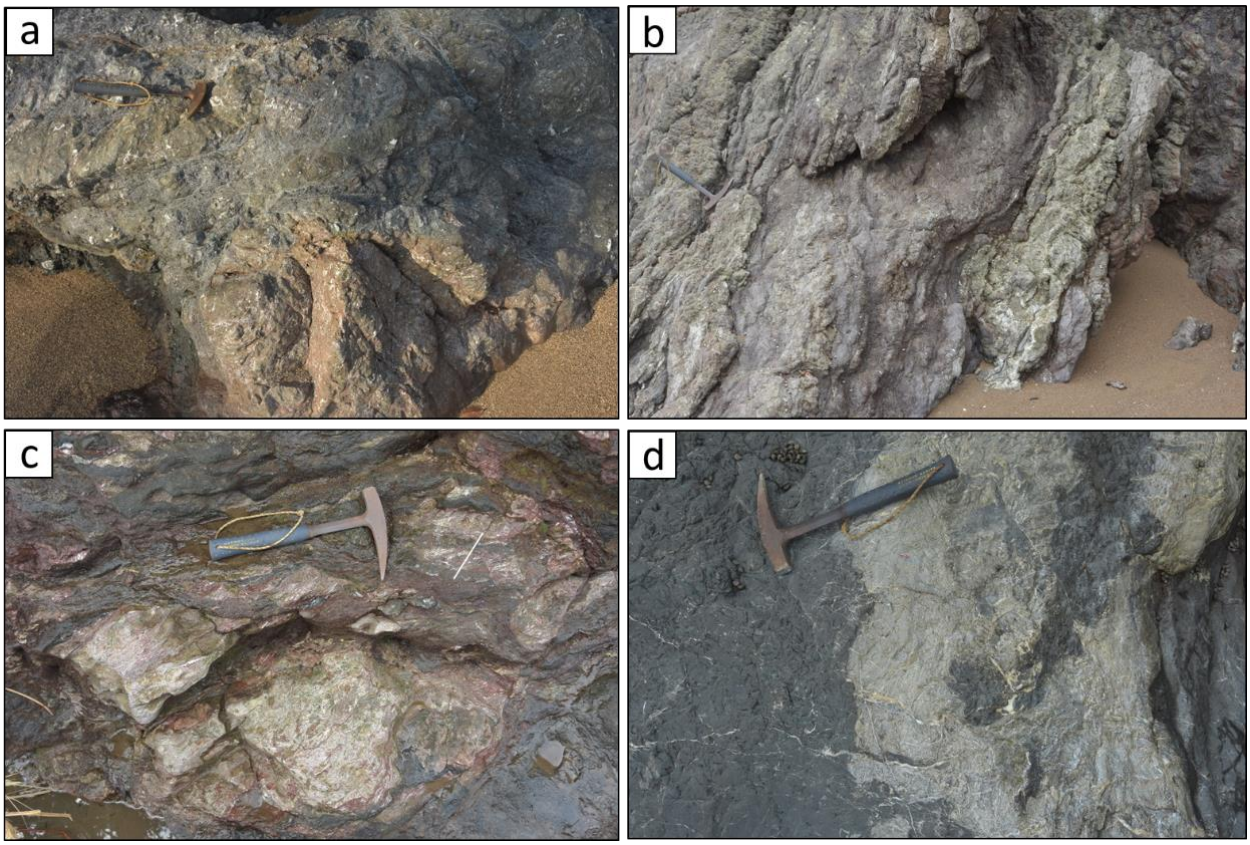

Figure 3.28 : Pictures of exposures of the Bahia Solano melange. (a) Heavily deformed pillow basalts (Bahia Solano peninsula). (b) Deformed, layered red chert and limestone (Bahia Solano peninsula). (c) Deformed red chert and white limestone (Bahia Solano peninsula). (d) Deformed grey siliceous and calcaresous sediments of the second unit. (Bahia Solano peninsula).

3.4.3 Baudó Mélange

The Baudó Melange is exposed on the Bahia Solano peninsula. It is largely composed of pelagic sediments with rare deformed pillow basalts and can be divided into 2 facies: A dark red unit with calcareous and siliceous blocks in a mudstone-sandstone matrix (Figure 3.28a-c), and a dark grey mudstone unit with blocks of pelagic sediment (Figure 3.28d).

The dark red unit comprises most of the melange from Bahia Solano to El Valle. The reddish matrix is composed of deformed mudstone to sandstone, with rare tuffaceous components. This matrix encloses blocks and brecciated lenses of siliceous and calcareous mudstone to siltstone with rare basalt (Figure 3.29). The blocks and lenses comprise 10% of the melange and range from small clasts to 10mx50m blocks. Some blocks of limestone were siliceous

with interbeds of red chert while larger blocks of limestone showed grading to red chert. Within the unit there was evidence of red chert and limestone showing disharmonic folding. Many of the limestone blocks showed evidence of ductile mudstone deformation, with a later brittle deformation shown by brecciation throughout the melange by intense calcite veining.

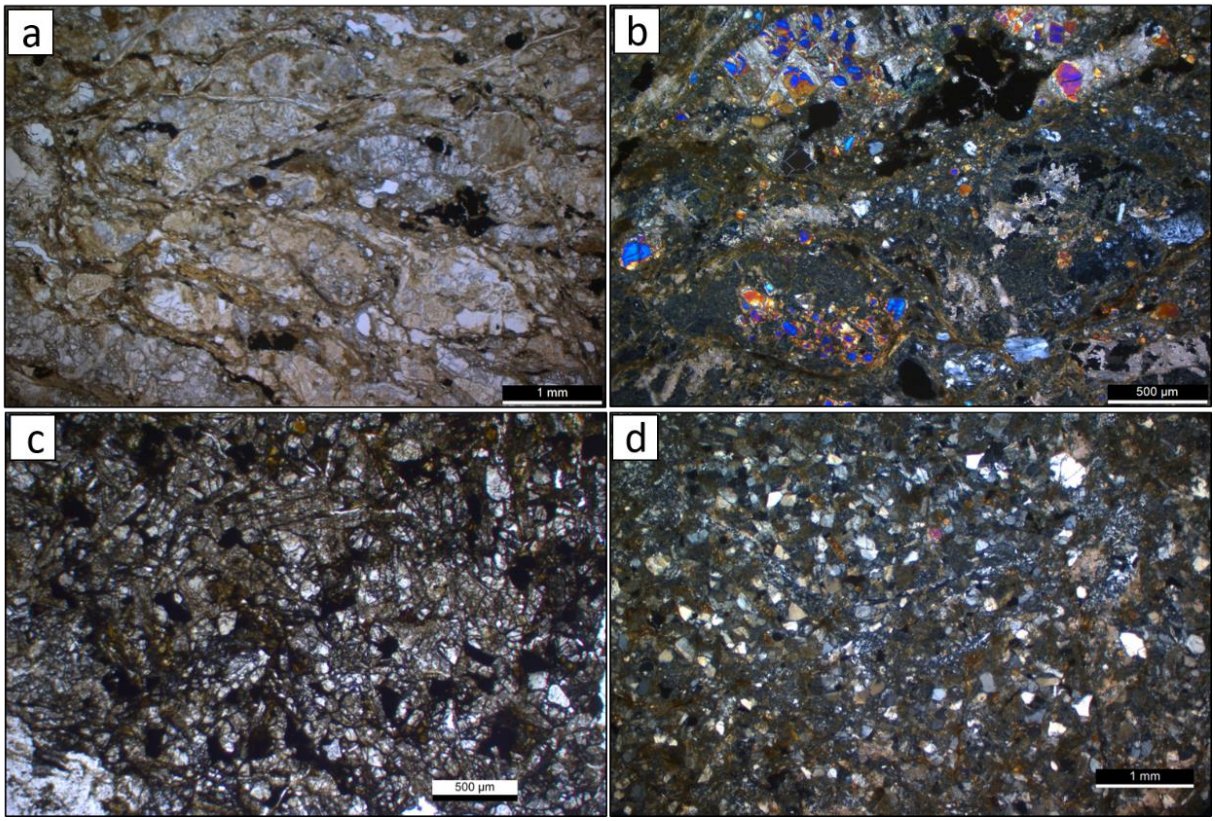

Figure 3.29: Photomicrographs of samples from the Bahia Solano Melange. (a) and (b) PPL and XPL views of heavily deformed conglomerate from the melange, showing extensive veining and fractures, and fractured and altered clinopyroxene crystals (sample JB17-089). (c) PPL view of a heavily deformed basalt from the melange (sample JB17-086). (d) XPL view of a basaltic sandstone from the melange, showing clasts of plagioclase and clinopyroxene (sample JB17-087).

Deformed sandstones and siltstones of the Baudó Melange are pervasively cut by both quartz and calcite veins. They are composed of fragments of quartz, clinopyroxene and plagioclase, with fine grained muddy lenses. These muddy lenses contain small fragments of clinopyroxene, quartz and plagioclase. Conglomerates of the melange also exhibit extensive veining and contain fragments of plagioclase and clinopyroxene, along with clasts of fine-grained basalt. These clasts are deformed, fractured and altered. The fragments of clinopyroxene are pervasively altered along fractures, and locally appear to have been fragmented due to shearing.

The second facies is fairly minor, comprising <10% of the melange, and also has blocks of siliceous and calcareous sediments with conglomeratic lenses. The matrix is deformed dark

mudstone with fluid structures showing soft sediment deformation. The unit is also extensively veined, showing later brittle deformation.

3.5 Summary

In the Soná-Torio region, the oceanic plateau is dominated by a basaltic unit which is largely formed of pillow basalts and lava flows, interbedded with radiolarites. Plateau basalts generally comprise acicular to lath shaped plagioclase, equant euhedral to anhedral clinopyroxene and cubic to irregular opaque oxides. The glassy groundmass of these samples is often altered to clays, while clinopyroxene can be altered to chlorite and plagioclase is altered to chlorite or sericite. Within the oceanic plateau there are also rare plateau-related intrusions, and a greenschist unit which is composed of deformed hyaloclastites and schistose basaltic breccias which have undergone greenschist facies metamorphism. The groundmass of the hyaloclastites is formed of green-brown vesicular glass, largely replaced by fibrous chlorite and actinolite. In other samples, the groundmass is completely recrystallised and there are serpentinised olivine psuedomorphs.

The plateau sequences are overlain by the Soná-Torio Proto-arc Group. At the base of this group is the Torio Lithostratigraphic Unit, largely formed of hemipelagic to pelagic limestones, which locally grade to basaltic sandstone breccias and graded sandstone. The limestones contain foraminifera but are largely recrystallised and fractured. The sandstones contain abundant clasts of basalt, dolerite and siliceous sediments, which indicates subaerial exposure of plateau sequences at the time of formation.

The next unit in the Soná-Torio Proto-arc Group is the La Mona Formation, which is composed of interbedded limestones, basaltic breccias and tuffaceous sequences. The tuffaceous sequences are composed thinly layered to massive tuffs, which can display cross lamination and are locally pumiceous. An analysed tuff sample has Proto-arc Group 1 geochemistry. These sequences are interbedded with tuffaceous micritic limestones, which can contain radiolaria and recrystallised foraminifera. The basaltic breccias contain basalts, fragments of plagioclase and clinopyroxene and pumiceous clasts.

The Proto-arc Group 1 is exposed as a series of lavas and dykes, which intrude sequences of the plateau, and intrude and are interbedded with the Torio Lithostratigraphic Unit. Where dykes of the Proto-arc Group 1 intrude limestones of the Torio Lithostratigraphic Unit, there are irregular margins due to soft-sediment deformation. Basalts of the Proto-arc Group 1 are composed of acicular to lath shaped plagioclase with equant subhedral to anhedral clinopyroxene and opaque oxides. In fine grained samples, the groundmass is often altered to green-brown clays, and plagioclase has been altered to sericite.

The Proto-arc Group 2 is exposed only as dykes and sills across the Soná, which intrude sequences of the oceanic plateau, the Torio Lithostratigraphic Unit, and the La Mona Formation. These intrusions are typically porphyritic with tabular plagioclase and subhedral clinopyroxene phenocrysts in a fine grained basalt groundmass. The groundmass and phenocrysts are typically altered to sericite and chlorite.

The Soná-Torio Arc is composed of gabbroic to granodioritic intrusions, and pillow basalts which were exposed on the Pixvae coast. The Soná-Torio Arc intrusions were generally formed of lath shaped plagioclase (typically with some sericite alteration), equant clinopyroxene, amphibole and opaque oxides. The Arc pillow basalts were larger and fresher than those associated with the plateau or proto-arc, and contained a glassy groundmass with acicular plagioclase with zoned plagioclase and pyroxene phenocrysts and glomerocrysts.

The Tonosi Formation is an overlap sequence which is composed of shallow marine limestones with algal fragments and small benthic foraminifera. In this study, this unit was only observed in limited sequences in Bahia Honda.

In the Darién Pacific Coast region, the oceanic plateau sequences are again dominated by massive lava flows and pillow basalts. These pillows can be deformed and extensively veined. The plateau basalts are typically composed of acicular to lath shaped plagioclase, equant subhedral clinopyroxene and opaque oxides. Plagioclase can be well fractured and altered to sericite and chlorite, and clinopyroxene is generally altered to chlorite. The plateau basalts can be interbedded with interbedded red chert, black chert, siliceous mudstones and rare limestones, which are often recrystallised and deformed. Intrusions associated with the plateau are composed of lath shaped plagioclase with subhedral equant clinopyroxene and opaque oxides, and can have phenocrysts of plagioclase and clinopyroxene.

The Jaqué Proto-arc Intrusions intrude plateau sequences, and are formed of dykes and gabbros. The dykes are generally coarse porphyritic basalts, composed of a groundmass of interlocking acicular to lath shaped plagioclase along with equant subhedral to anhedral clinopyroxene, olivine and opaque oxides. Phenocrysts of plagioclase and clinopyroxene are typically fresh, while the groundmass can be altered to brown clays, and groundmass plagioclase can be altered to sericite. Within the Proto-arc intrusions, there are also rare olivine phenocrysts, which are typically heavily fractured and can be completed psuedomorphed by iddingsite. Proto-arc gabbro intrusions are formed of plagioclase laths, 1-2mm long, with intergranular olivine and subhedral equant clinopyroxene.

The Darién Formation is composed of siliceous sequences of green-grey thinly bedded cherts which can be tuffaceous. These sequences overly the basalts of the plateau (Bandy and Casey, 1973; Barat et al., 2014).

The Jaqué-La Palma Group is formed of the Bahia Pina Formation, the Guayabo Formation, the San Miguel Formation and the Sapo Arc. The Bahia Pina Formation is formed of shallow marine limestones sequences, which unconformably overly basalts of the oceanic plateau. At this contact, there is a basal conglomerate which contains foraminifera, radiolarites and basaltic clasts. Overlying limestones contain abundant foraminifera, limited fragments of clinopyroxene and corraline algae, with a micritic groundmass which is extensively cut by veins.

The Bahia Pina Formation grades into the Guayabo Formation, which is composed of turbidites and debris flow deposits interbedded with calcareous hemipelagic mudstones. The turbidites are composed of cross bedded and parallel laminated calcareous-tuffaceous siltstone-sandstone, which is locally graded. Debris flow deposits contain clasts of siliceous and tuffaceous layered sediments, cherts, micritic limestone and igneous clasts. Although some igneous clasts may represent the plateau and proto-arc, analysed andesitic clasts from the Guayabo Formation were derived from the Sapo Arc.

The San Miguel Formation is formed of arc derived volcaniclastic deposits and tuffs. Tuffs are brown to yellow and can be finely bedded or massive. Arc derived debris flows have a tuffaceous-sandy matrix with clasts of tuff and igneous clasts with andesitic to dacitic compositions. These clasts are likely derived from the Sapo Arc.

The Sapo Arc is formed of mafic to felsic intrusive rocks and lava flows. Lava flows exhibited basal breccias and columnar jointing, and could be interbedded with units of the San Miguel Formation. Most lavas contain phenocrysts of plagioclase, clinopyroxene and/or amphibole, with a glassy fine-grained groundmass containing acicular plagioclase and equant clinopyroxene. These rocks are generally much fresher than those seen in the plateau, but plagioclase can exhibit sieve textures and limited chlorite alteration. Intrusions of the Sapo Arc consist of gabbros, dolerites, diorites with plagioclase-phyric and aphyric basalt dykes and rare amygdaloidal dykes. The intrude sequences of the oceanic plateau, the Guayabo Formation, and the San Miguel Formation.

The Baudó Oceanic Plateau is again dominated by pillow basalts and lava flows. They are fine grained and aphyric, formed of acicular to elongate laths of plagioclase and equant clinopyroxene and opaque oxides. Plagioclase crystals are typically partially altered to sericite, while the glassy groundmass can be altered to palagonite, chlorite and actinolite. The pillows are locally interbedded with black to red chert, black mudstone, and grey

siliceous limestone. Sills of the Baudó Oceanic Plateau are composed of clinopyroxene-phyric dolerites and gabbros. These sills intrude the basalts of the Baudó Plateau and intrude plateau sediments to form peperites. The intrusions are composed of elongate laths of plagioclase, equant pyroxene, opaque oxides and rare olivine. The groundmass displays both chlorite and actinolite alteration, and clinopyroxene phenocryst are fractures and altered to chlorite along rims of crystals. Plagioclase crystals are also fractured and altered to chlorite and sericite.

The Punta Lana Formation is composed of volcaniclastic tuffaceous sediments. Debris flow deposits contain clasts of fine to coarse basalt, cross laminated sandstone, black chert and limestone while tuffaceous sandstones are composed of a green tuffaceous matrix, with fragments of clinopyroxene and plagioclase crystals, and small rounded clasts of fine-grained basalt.

The Baudó Melange is composed of pelagic sediments with rare, deformed pillow basalts. Most of the melange consists of a dark red unit with calcareous and siliceous blocks in a mudstone-sandstone matrix, but there is a minor unit of dark grey mudstone unit with blocks of pelagic sediment. The age and geochemistry of this melange is unknown, but it is likely younger than the plateau and the Punta Lana Formation.

4. GEOCHRONOLOGY AND BIOSTRATIGRAPHY

4.1 Introduction

This section describes the new $^{40}Ar/^{39}Ar$ geochronology results alongside new biostratigraphic ages. A total of 17 samples of basaltic lavas and dykes were dated using the $^{40}Ar/^{39}Ar$ radiometric dating technique to attempt to constrain the age of formation of plateau and proto-arc sequences in the Soná-Torio, Darién Pacific Coast and Serranía de Baudó regions. Samples were selected based on location, geological context, and lack of alteration (assessed using Loss On Ignition (LOI) values and alteration levels in thin section). Samples were prepared at Cardiff University and SUERC (Scottish Universities Environmental Research Centre) by the author, while analysis was performed by Dan Barfod at SUERC. Full $^{40}Ar/^{39}Ar$ results can be found in Appendix E4 while full methods can be found in Appendix A.3. Biostratigraphic constraints from a selection of 5 sedimentary samples associated with the studied volcanic sequences were provided by Jonathan Bryan at the University of Florida, USA (larger benthic foraminifera), Raul Trejos Tamayo at the University of Caldas, Colombia (nannofossils), and Felipe Vallejo at the University of Caldas, Colombia (planktic foraminifera). The report provided by Jonathan Bryan is included in Appendix E5. This chapter provides a summary of the methods and a discussion of the results for each of the Soná-Azuero, Darién Pacific Coast, and Serranía de Baudó areas.

4.2 Summary of the methods

The $^{40}Ar/^{39}Ar$ radiometric dating technique is performed by step heating of groundmass or mineral separates at increasing temperatures and measuring the ratio of $^{40}Ar/^{39}Ar$ gas released at each step. These gas ratios are used to infer the age of the sample. This technique relies on the separates analysed not having ^{40}Ar removed or added through alteration, and where samples have not experienced addition or loss of ^{40}Ar, the gas ratios and inferred ages at each incremental step will remain constant and produce a good plateau (Dalrymple and Lanphere, 1974). However, where samples have been altered or Ar has been locally lost/inherited in the analysed material, there is more likely to be variation in the $^{40}Ar/^{39}Ar$ ratios of gas released. The samples analysed here were selected for their high relative freshness among available samples and separates were carefully hand-picked under a binocular to remove altered material. However, all samples in the study had undergone some amount of alteration (as documented in Chapter 3). To attempt to gain

reliable $^{40}Ar/^{39}Ar$ crystallization ages, all separates were analysed with an extended low temperature heating schedules, to remove gas released by alteration phases (e.g., sericite and clays) before plagioclase and clinopyroxene start degassing. Inverse isochrons are also produced by plotting the $^{39}Ar/^{40}Ar$ and $^{36}Ar/^{40}Ar$ ratios, which should form a straight line in the absence of alteration. In these isochrons the slope is proportional to the age of the sample, and the y-axis intercept represents the $^{40}Ar/^{36}Ar$ ratio of the trapped component composition.

Reliable age plateaus were defined using set criteria based on those used by Fleck et al. (1977) and Lanphere and Dalrymple (1978). These criteria state that there must be a minimum of three contiguous steps which overlap within 2σ uncertainty and which release at least 50% of ^{39}Ar. The inverse isochron formed by the plateau steps must also yield an age indistinguishable from the plateau age at 2σ uncertainty, while the trapped component composition must be indistinguishable from the atmospheric composition at 2σ uncertainty. The age and uncertainty of the plateau were calculated using the mean weighted by the inverse variance of each step.

Of the 17 samples analysed here, 6 were on groundmass separates and 11 on plagioclase separates of 7 lavas and 10 dykes of basalts to andesites. Two samples did not produce plateaus and so do not have a reliable $^{40}Ar/^{39}Ar$ crystallization age. Despite the remaining samples adhering to the above quality criteria and appearing to have reliable $^{40}Ar/^{39}Ar$ crystallization ages, most of these ages are inconsistent with existing dates or local to regional stratigraphic constraints. These results indicate significant issues with using $^{40}Ar/^{39}Ar$ dating on possibly altered (low-K) tholeiitic basalts, as detailed below and further discussed in Section 6.2.

New biostratigraphic ages were obtained from thin sections or poorly consolidated shallow-marine to pelagic limestones and tuffaceous calcareous marine sedimentary rocks. All biostratigraphic constraints and the location of the dated sedimentary samples are summarized in Table 4.1.

4.3 Soná-Torio

Seven samples from the Soná-Torio region were prepared for $^{40}Ar/^{39}Ar$ dating. Of these, 3 were from the Soná-Torio Plateau, 3 were from the Soná-Torio Proto-arc Group 2, and one was from the Soná-Torio Arc. A biostratigraphic age was also obtained for the Torio Lithostratigraphic Unit.

4.3.1 Soná-Torio Plateau

Three samples of the Soná-Torio Plateau were prepared for $^{40}Ar/^{39}Ar$ geochronology on groundmass separates. These samples yielded plateau ages ranging from 54.6 ± 1.3 to 87.0 ± 2.4 Ma.

Sample DB09-010 is an aphyric pillow basalt from Rio San Rafael on Soná Peninsula. Analysis of this sample gave a plateau age of 54.6 ± 1.3 Ma with 88.4 % of ^{39}Ar gas released within 12 contiguous steps (Figure 4.1). This sample has an isochron age of 48.6 ± 8.4 Ma, which is within error of the plateau age, and the initial $^{40}Ar/^{36}Ar$ ratio is within error of atmospheric values. Therefore, the sample satisfies quality criteria, and the age can be considered reliable. However, the lowest temperature steps of the plateau have more variable ages with high errors when compared to the remainder of the plateau. These low temperature steps also show high Ca/K ratios, indicating that degassing at the lower temperatures is associated with alteration phases. If these stages were removed from the plateau, there would still be a clear reliable plateau with a slightly younger age, 7 contiguous steps and 83.3 % of total ^{39}Ar gas released. This sample age is not consistent with previous $^{40}Ar/^{39}Ar$ ages for the area, where plateau basalts from across Soná and Azuero peninsulas have been dated as 93.5 ± 5.3 to 82.6 ± 3.2 Ma based on step heating of plagioclase separates, a 114.5 ± 2.0 Ma error weighted mean age (Lissinna, 2005), and a 71.3 ± 2.1 Ma matrix total fusion age (Hoernle et al., 2002). It is also not consistent with the age of radiolarite interbedded in plateau sequences, which was dated as ~89 – 85 Ma (Kolarsky et al., 1995; Buchs et al., 2009). This $^{40}Ar/^{39}Ar$ age would also contradict geological constraints, as it would be younger than the Torio Lithostratigraphic Unit, and the associated Soná-Torio Proto-arc Group 1 dykes and lavas, which locally overlie or crosscut the plateau.

Sample JB18-024 is an aphyric basalt from the Pixvae Coast, which gave a plateau age of 57.30 ± 0.38 Ma with 93.2 % of the total ^{39}Ar gas released within 24 contiguous steps (Figure 4.2). The isochron age is 58.2 ± 1.8 Ma, which is within error of the plateau age. The initial $^{40}Ar/^{36}Ar$ value is within error of atmospheric values. Therefore, this sample again adheres to quality criteria and could be considered as a reliable crystallization age. In this sample the plateau values and errors remain relatively constant from high to low temperatures. The Ca/K values are lower in the lower temperatures, with values of around 10, and rise to values largely ranging between 30 and 60 in the higher temperature steps. This suggests that different minerals are degassing at lower and higher temperatures. Again, this

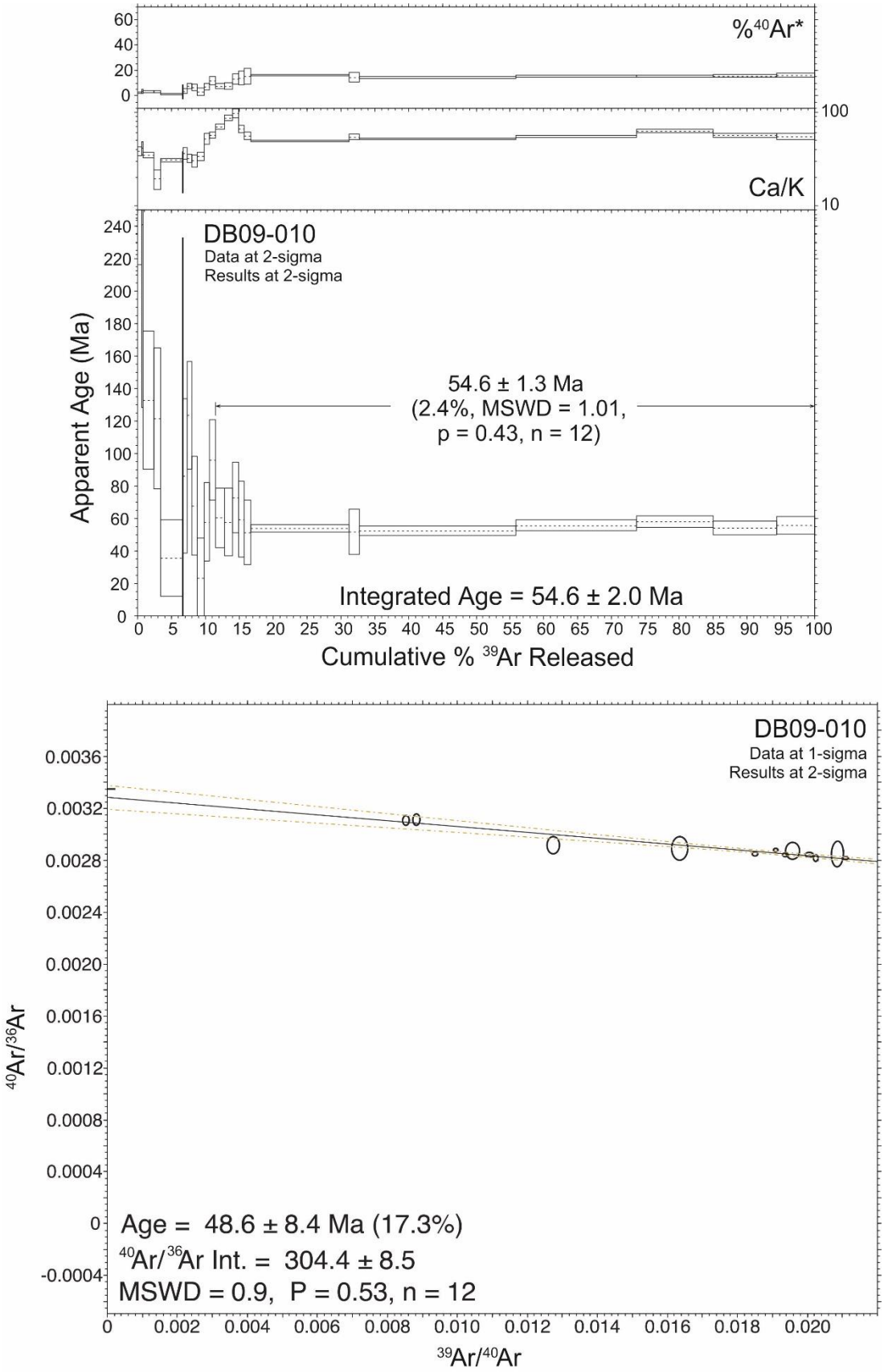

Figure 4.1: Ar-Ar step heating plateau plot and inverse isochron plot for sample DB09-010 (Soná-Torio Plateau).

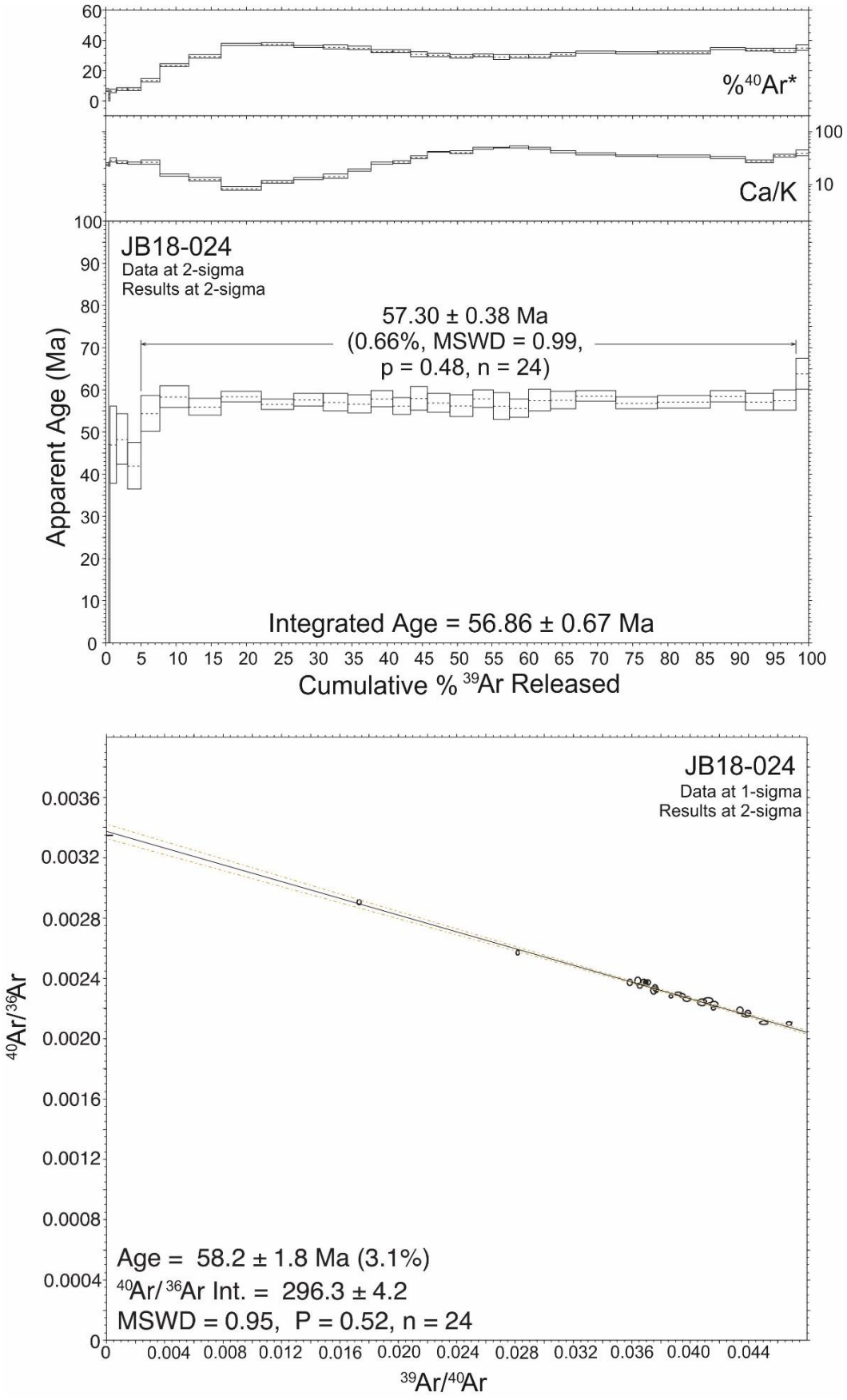

Figure 4.2: Ar-Ar step heating plateau plot and inverse isochron plot for sample JB18-024 (Soná-Torio Plateau).

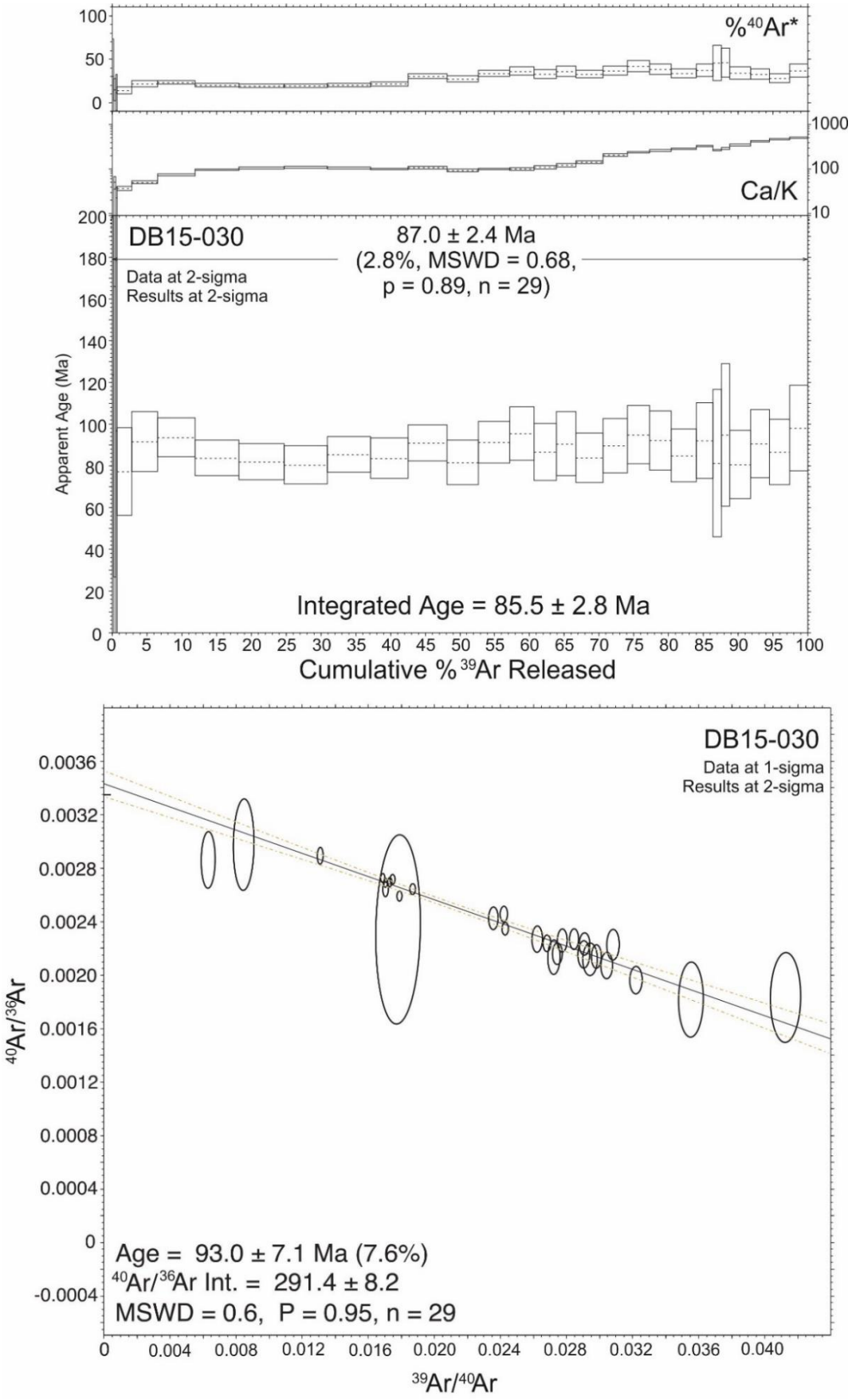

Figure 4.3: Ar-Ar step heating plateau plot and inverse isochron plot for sample DB15-030 (Soná-Torio Plateau).

sample does not agree with the previous ages of plateau samples and geological constraints in this region.

Sample DB15-030 is an aphyric basalt from southern Soná Peninsula, and gave a plateau age of 87.0 ± 2.4 Ma, with 100% of ^{39}Ar gas released in the plateau within 29 contiguous steps (Figure 4.3). The isochron age is 93.0 ± 7.1 Ma, within error of the plateau age, and the initial ^{40}Ar/^{36}Ar value is within error of atmospheric values. Again, this sample fulfils quality criteria and could be regarded as a reliable crystallization age. Within the plateau the ages and errors remain consistent with increasing temperature steps, apart from a single high error step at the lowest temperatures. The Ca/K appears to steadily increase with increasing temperatures, from initial values of ~30 up to final values of ~500. These final values are significantly higher than those seen in the other Soná-Torio Plateau samples. The age of this sample is within error of previous ages for the plateau in this region, and is also consistent with geological constraints.

4.3.2 Torio Lithostratigraphic Unit

Sample JB17-017 is a micritic (hemipelagic) limestone from the Torio Lithostratigraphic Unit from the Rio Torio. It was dated as Turonian-Maastrichtian (~93–66 Ma) based on nannofossils (Table 4.1). This age has a large range, but is in agreement with previous foraminifera ages for this unit from Azuero and Coiba, which have ages of ~ 75–73 Ma (Del Guidice and Recchi, 1969; Buchs et al., 2010; Corral et al., 2011).

4.3.3 Soná-Torio Proto-arc Group 2

Three samples of the Soná-Torio Proto-arc Group 2 were prepared for ^{40}Ar/^{39}Ar geochronology, each on plagioclase separates. These samples yielded 2 plateau ages of 50.09 ± 0.10 and 55.25 ± 0.13 Ma.

Sample JB17-008 is a coarse basaltic dyke from Rio Torio. This sample gave a plateau age of 55.25 ± 0.13 Ma, with 63.7 % of ^{39}Ar gas released in the plateau within 23 contiguous steps (Figure 4.4). The isochron age is 55.63 ± 0.99 Ma, within error of the plateau age, and the initial ^{40}Ar/^{36}Ar value is within error of atmospheric values. The age, errors and Ca/K ratios remain relatively constant within the plateau with increasing temperatures. This sample fulfils the quality criteria and could be

Table 4.1: Table with details of biostratigraphic ages

Sample	**Unit**	**Locality**	**Lat**	**Long**	**Nannofossils**	**Biozones**	**Age**
JB17-017	Torio L. U.	Rio Torio	7.554318	-80.92844	Q. gartneri, W. barnesae, Retecapsa spp.	UC7-UC20	Turonian-Maastrichtian
JB17-048	El Guayabo	Darién Coast	7.476776	-78.12665	C. floridanus, R. bisecta	NP17-NP26	Late Eocene-Late Oligocene
JB17-066	El Guayabo	Darién Coast	7.545428	-78.17542	R. bisecta, R. dictyoda	NP17-NP26	Late Eocene-Late Oligocene
Sample		**Locality**	**Lat**	**Long**	**Foraminifera**	**Biozones**	**Age**
JB17-048	El Guayabo	Darién Coast	7.476776	-78.12665	Globigerinatheka sp., Planktonic forams idet., Benthic foram indet.	E8-E16	Middle-Late Eocene
JB17-056	El Guayabo	Darién Coast	7.442198	-78.08812	Clavigerinella cf. Cl colombiana, Parasubbotina cf. griffinae, Parasubbotina sp., Alveolina sp.	E7-E10	Early-Middle Eocene
JB17-071	Bahia Piña	Darién Coast	7.561126	-78.20241	Lepidocyclina (Eulepidina) undosa		Oligocene
JB17-072	Bahia Piña	Darién Coast	7.561126	-78.20241	Lepidocyclina (Lepidocyclina) pustulosa, Amphistegina sp., Eoconuloides		Late Middle to Late Eocene

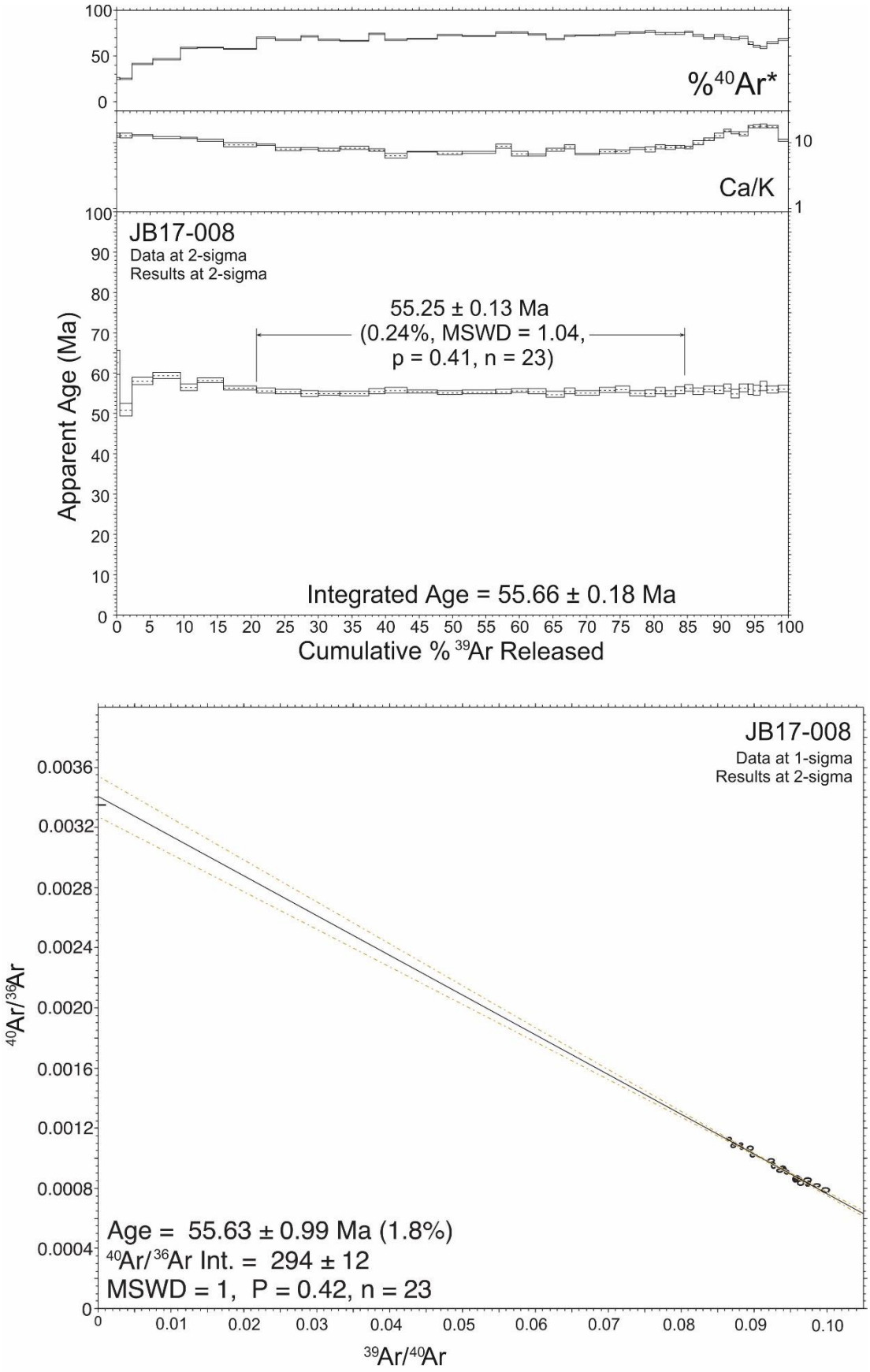

Figure 4.4: Ar-Ar step heating plateau plot and inverse isochron plot for sample JB17-008 (Soná-Torio Proto-arc Group 2).

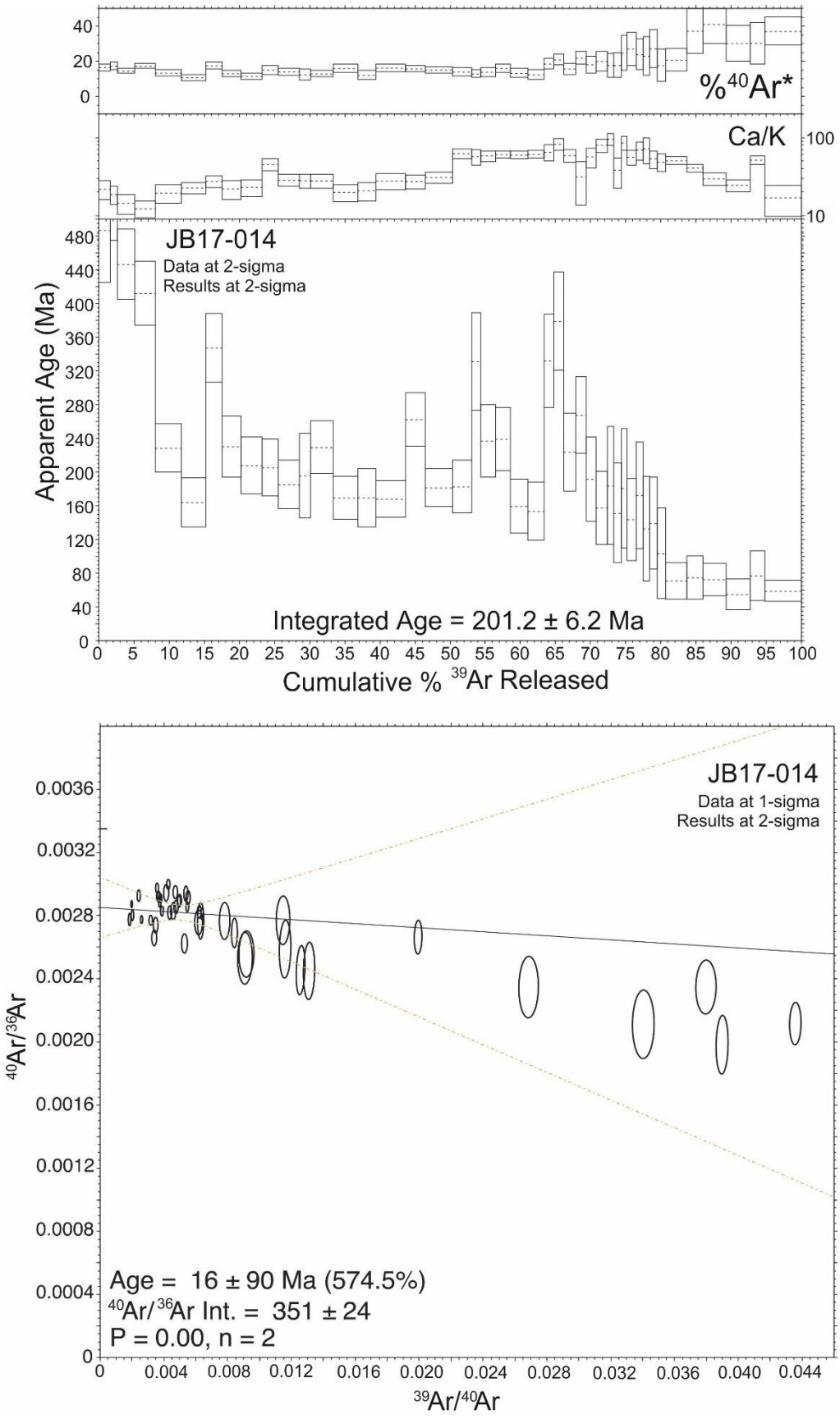

Figure 4.5: Ar-Ar step heating plateau plot and inverse isochron plot for sample JB17-014 (Soná-Torio Proto-arc Group 2).

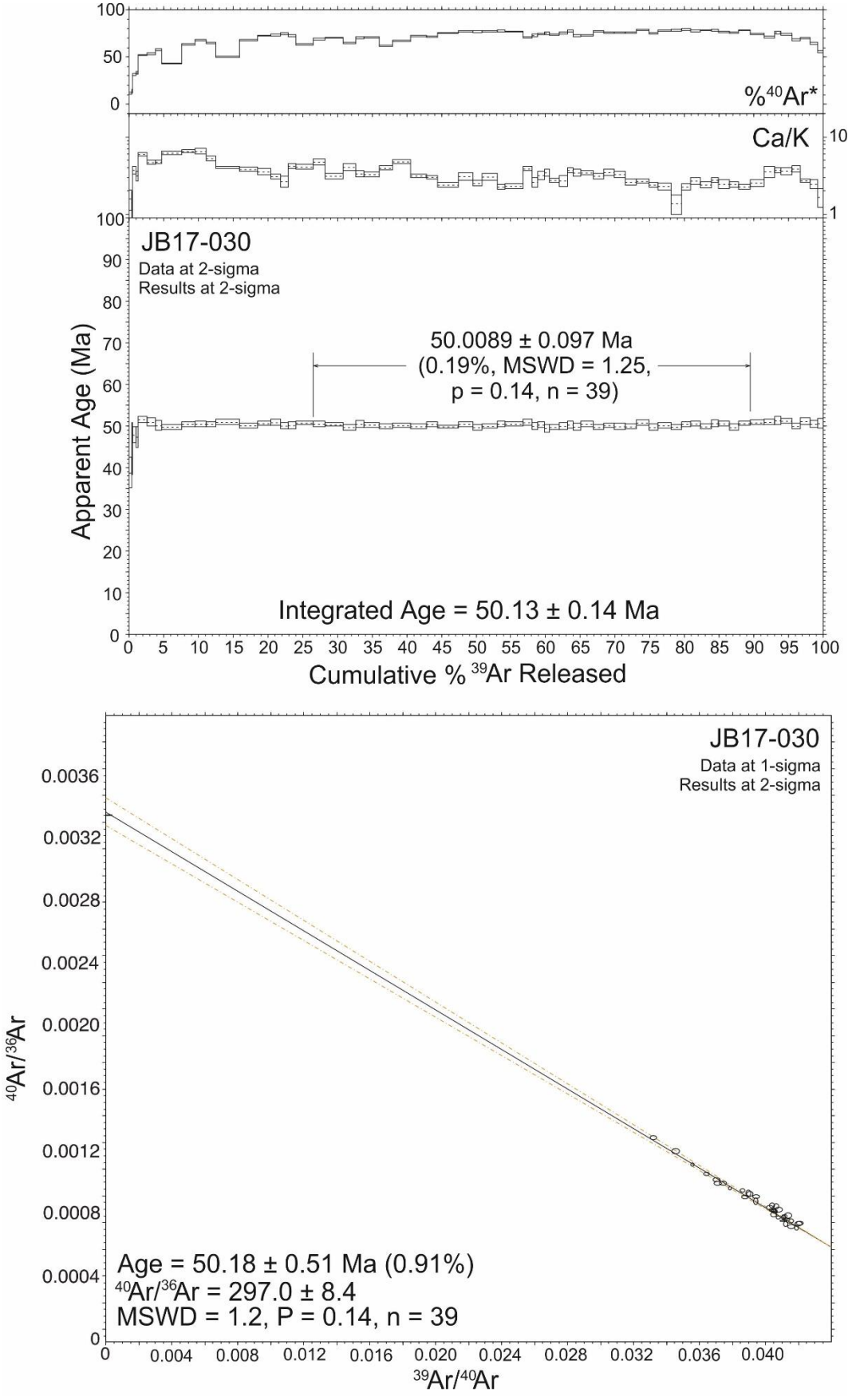

Figure 4.6: Ar-Ar step heating plateau plot and inverse isochron plot for sample JB17-030 (Soná-Torio Proto-arc Group 2).

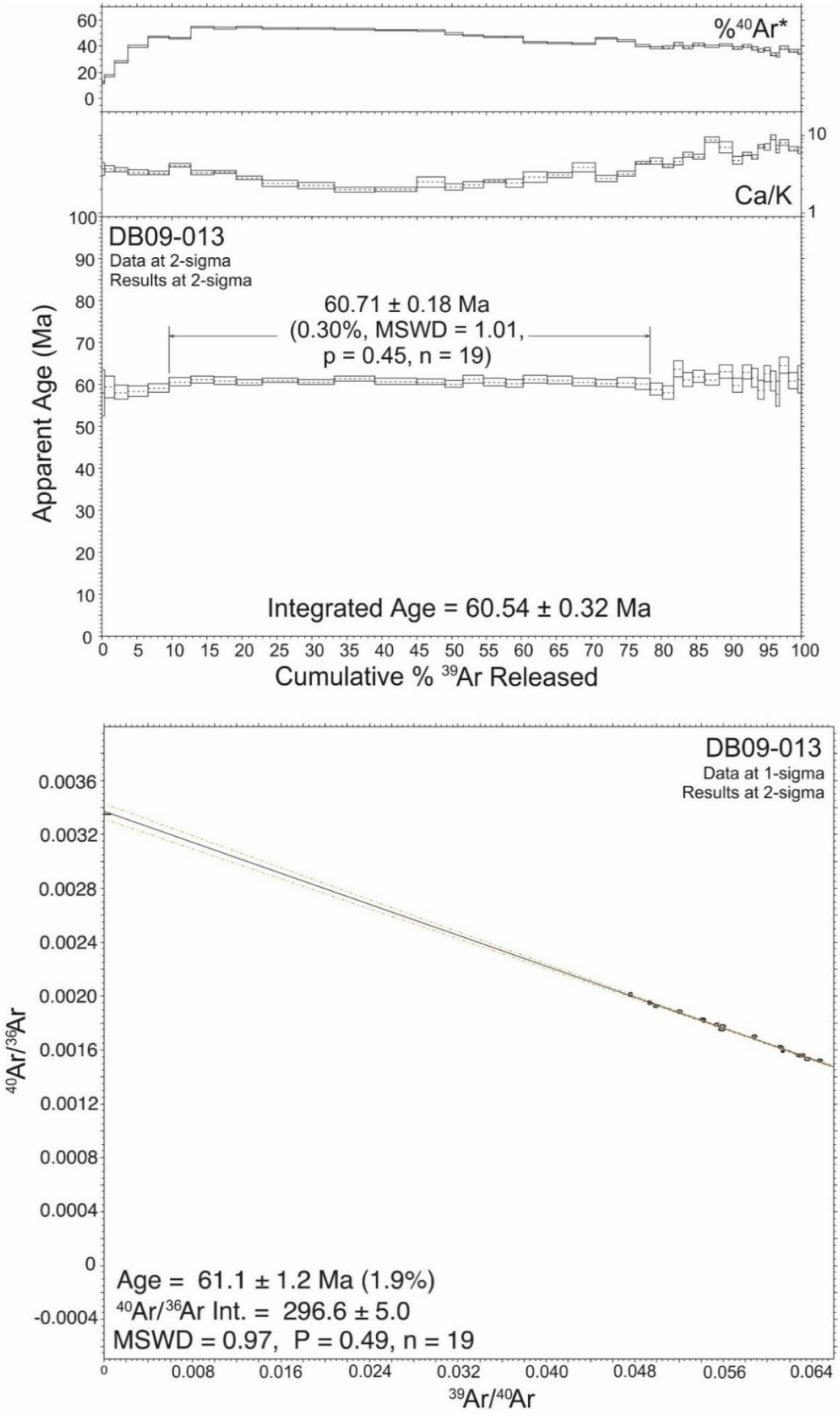

Figure 4.7: Ar-Ar step heating plateau plot and inverse isochron plot for sample DB09-013 (Soná-Torio Arc)

considered as a reliable age. There are no previous geochronological data for this group, but this age is younger than expected based on previous stratigraphic and biostratigrpahic constraints that support a Campanian (~73-72 Ma) age of emplacement (Buchs et al., 2010).

Sample JB17-014 is a porphyritic dyke from Rio Torio. This sample gave highly variable $^{40}Ar/^{39}Ar$ gas ratios and ages at different temperature steps, and many steps have high errors (Figure 4.5). The isochron also shows highly variable values. This data does not fufill the plateau criteria for a reliable age and it cannot be used.

Sample JB17-030 is a porphyritic dyke from Quebrada Rosario, and gave a plateau age of 50.09 ± 0.10 Ma with 63.0 % of total ^{39}Ar gas released within 39 contiguous steps (Figure 4.6). The isochron age is 50.18 ± 0.51 Ma and the $^{40}Ar/^{36}Ar$ initial value is within error of the atmospheric value. The plateau ages and errors remain fairly constant within the plateau, as do the Ca/K values which range between 1 and 7. This sample adheres to quality criteria and could again be accepted as a reliable age. Again, this sample is younger than expected based on geological constraints.

4.3.1 Soná-Torio Arc

Sample DB09-013 is doleritic dyke, which intrudes basalts of the Soná-Torio Plateau, and was the only Soná-Torio Arc sample prepared for $^{40}Ar/^{39}Ar$ geochronology in this study. Analysis was performed on plagioclase separates. This sample gave a plateau age of 60.71 ± 0.18 Ma, with 68.8 % of total ^{39}Ar gas released within 19 contiguous steps of the plateau (Figure 4.7). The isochron age is 61.1 ± 1.3 Ma, within the error of the plateau age, and the initial $^{40}Ar/^{36}Ar$ value is within error of the atmospheric value. The plateau ages and errors remain fairly constant within the plateau, and the Ca/K values which range between 1 and 5. Therefore, this sample fulfils quality criteria and could be considered as a reliable age. This age agrees with previous ages for the Arc in this region, with an existing age of the Arc on Soná as 50.1 ± 0.2 Ma based on $^{40}Ar/^{39}Ar$ step heating on biotite (Lissinna, 2005), and ages for the arc from across Azuero largely ranging from 70 – 40 Ma (Lissinna, 2005; Wörner et al., 2009; Corral et al., 2011). However, the new age appears to contradict another date from this study. Dyke DB09-013 intruded the plateau sequence along the Rio San Rafael, from which sample DB09-010 was taken. Sample DB09-010 gave an age of 54.6 ± 1.3 Ma. An older age of 60.71 ± 0.18 Ma for the intruding arc dyke indicates that there is an issue with these dates, most likely the low-K and more altered plateau sample, even if they pass the necessary plateau criteria.

4.4 Darién Pacific Coast

Eight samples from the Darién Pacific Coast region were prepared for $^{40}Ar/^{39}Ar$ dating. Of these, one sample was from the Jaqué Plateau, two were from the Jaqué Depleted Plateau, one was from the Jaqué Enriched Plateau, two were from the Jaqué Proto-arc and one was from the Jaqué Arc Group 2. Biostratigraphic ages were also obtained for the Bahia Piña and Guayabo Formations.

4.4.1 Jaqué Plateau

Two samples of the Jaqué Plateau were prepared for $^{40}Ar/^{39}Ar$ geochronology, both on groundmass separates. These samples gave ages of 39.51 ± 0.90 Ma and 59.8 ± 7.8 Ma.

Sample DB16-082 is an aphyric basalt from Playa Muerto on the Darién coast. This sample gave a plateau age of 59.8 ± 7.8 Ma, with 91.5 % of total ^{39}Ar gas released within 21 contiguous steps of the plateau (Figure 4.8). The isochron age is 53 ± 15 Ma, within the error of the plateau age, and the initial $^{40}Ar/^{36}Ar$ value is within error of the atmospheric value, and so this date passes quality criteria and could be accepted as a reliable plateau age. Within the plateau, the steps have fairly variable ages with larger errors than most plateaus of other samples in this study. This age is younger than existing $^{40}Ar/^{39}Ar$ geochronological ages obtained on groundmass for the plateau in this region, which gave a step heating age of 84.1 ± 1.0 Ma and mean apparent age (inverse variant weighted age) of 71.3 ± 2.2 Ma (Lissinna, 2005). In addition, Upper Cretaceous (Coniacian-Campanian) radiolarites have previously been reported from basaltic sequences of the nearby San Miguel Gulf (Bandy and Casey, 1973; Barat et al., 2014), which suggest the occurrence of an older oceanic basement along the Darién Pacific Coast. The occurrence of an older oceanic basement in the area is also supported by the occurrence of Campanian pelagic limestone that rests unconformably on top of folded basaltic and radiolarite sequences in the San Miguel Gulf (Barat et al., 2014). These sequences include unpublished analyses of plateau basalts (Buchs, pers. com. 2020) and are probably correlative to other oceanic plateau sequences in Panama, hence questioning the reliability of the new $^{40}Ar/^{39}Ar$ age. In addition, if deemed reliable, the new $^{40}Ar/^{39}Ar$ age would imply the occurrence of an undocumented Palaeogene oceanic plateau in the central eastern Pacific. This seems very unlikely given that a large number of studies in the accretionary complexes of Central America and northern South America have only reported Mesozoic ages for oceanic plateau sequences (e.g., Buchs et al., 2009; Villagomez et al., 2011; Andjic et al., 2019).

Sample JB18-075 is an aphyric basalt from Rio Pavarando. and gave a plateau age of 39.51 ± 0.90 Ma with 77.3 % of total ^{39}Ar released within 16 contiguous steps (Figure 4.9). The isochron age is 39.4 ± 3.6 Ma, well within error of the plateau age, and the initial ^{40}Ar/^{36}Ar value is within error of atmospheric values. This data fulfils quality criteria and could regarded as a reliable age. The ages and errors remain consistent within the plateau with increasing temperatures, but the Ca/K ratio appears to steadily increase with increasing temperatures within the plateau, from values of 20 up to values of 100. However, this age is in contradiction with the geochronological, biostratigraphic, and geological constraints discussed above. In addition, this age is around 20 Ma younger than the age of sample DB16-082, which seems problematical considering that these samples appear to be from the same oceanic plateau unit based on field geological and geochemical constraints.

4.4.2 Jaqué Depleted Plateau

Two samples of the Jaqué Depleted Plateau were prepared for ^{40}Ar/^{39}Ar geochronology, one on groundmass and one on plagioclase separates. These analyses yielded a single age of 22.52 ± 0.93 Ma.

Sample JB17-059 is a coarse lava flow from near El Guayabo on the Darién coast. Analysis of this sample was performed on plagioclase separate, and yielded a plateau age of 22.52 ± 0.93 Ma (Figure 4.10). This plateau contained 76.5 % of total ^{39}Ar gas released, within 22 contiguous steps. The isochron age is 22.7 ± 4.5 Ma, which is within error of the plateau age, and the initial ^{40}Ar/^{36}Ar ratio is within error of the atmospheric values. Therefore, this age could be accepted as a reliable crystallization age. Within the plateau, ages remain constant, although errors are smaller in the central temperature steps. Ca/K values are also higher and more variable at the lowest and highest temperatures. Although there are no existing ages for the Jaqué Depleted Plateau, this age is again in contradiction with a large range of geological constraints (see above). The Jaqué Plateau and Depleted Plateau are indistinguishable in the field, and therefore appear to have a similar age. Critically, these basaltic sequences also underlie sedimentary sequences which have dates older than 22 Ma (Section 4.3.4).

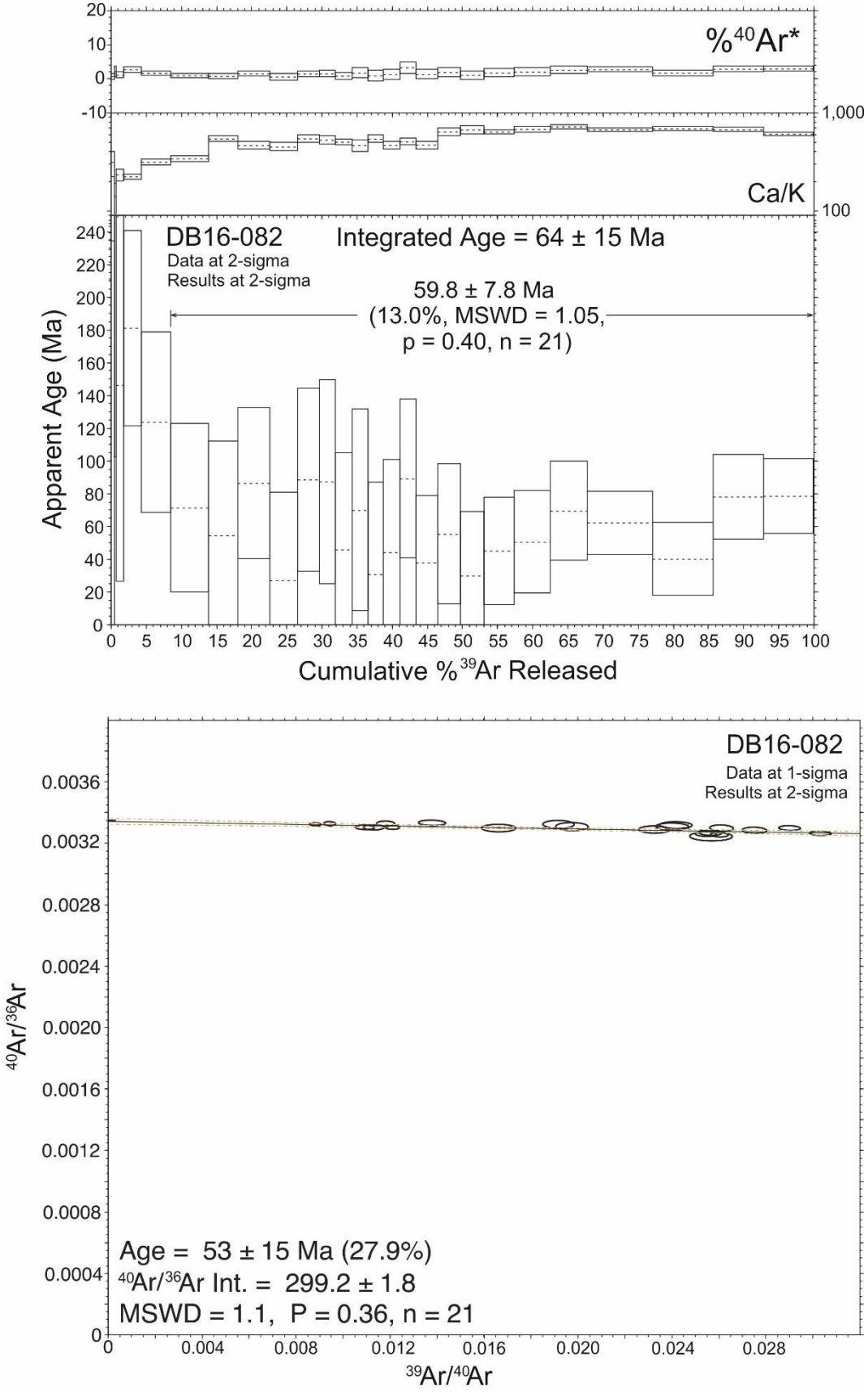

Figure 4.8: Ar-Ar step heating plateau plot and inverse isochron plot for sample DB16-082 (Jaqué Plateau).

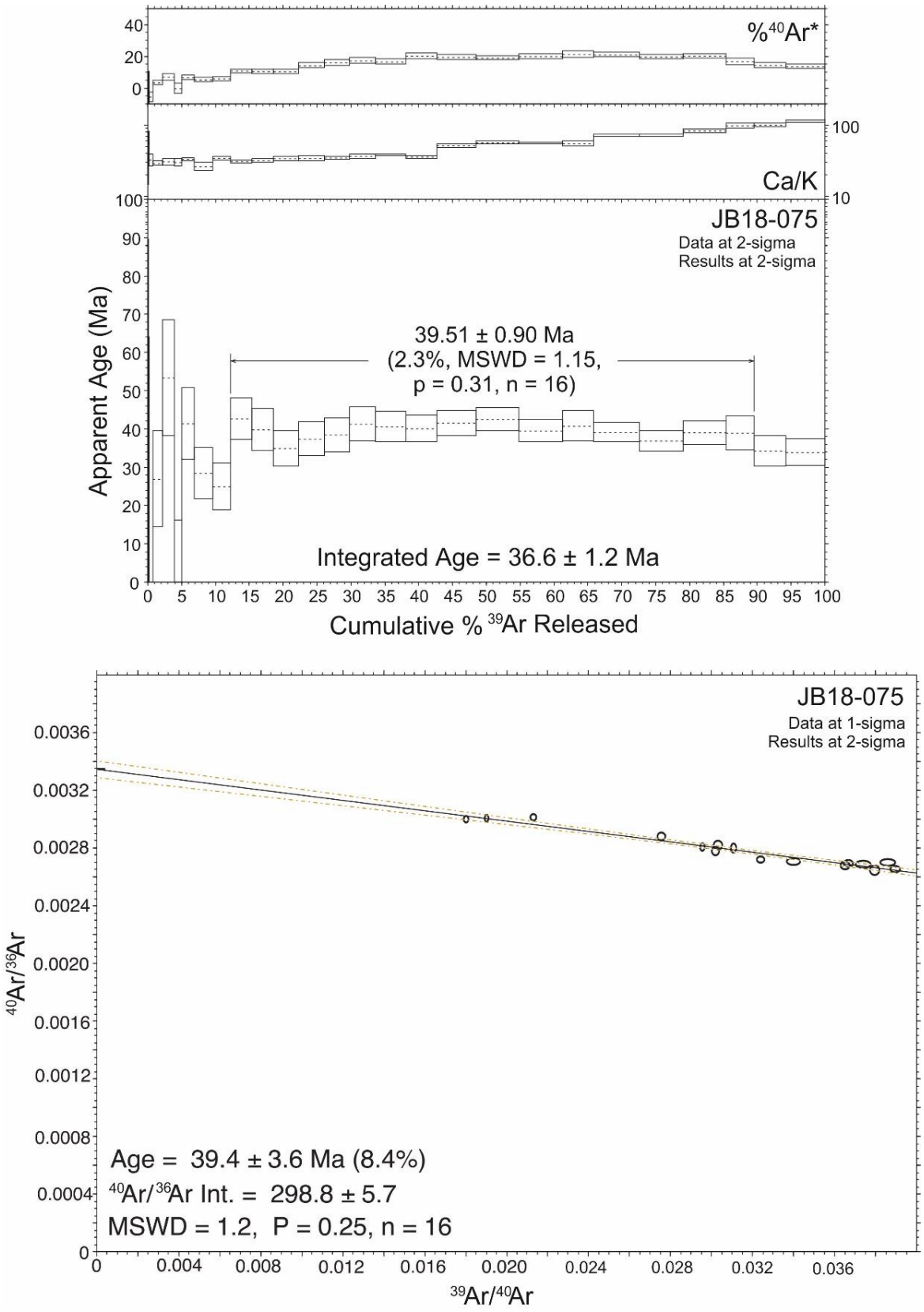

Figure 4.9: Ar-Ar step heating plateau plot and inverse isochron plot for sample JB18-075 (Jaqué Plateau).

Sample JB18-068 is a coarse basalt from Rio Pavarando, which did not give a plateau age. The step heating ages were highly variable and there were not contiguous steps releasing at least 50 % of the total ^{39}Ar (Figure 4.11). The data also did not produce a suitable isochron, and the initial $^{40}Ar/^{36}Ar$ did not align with atmospheric values. Therefore, this data cannot be used to provide a reliable age.

4.4.3 Jaqué Enriched Plateau

Sample JB17-069 was the only Jaqué Enriched Plateau sample to be prepared for $^{40}Ar/^{39}Ar$ geochronology. This sample is a coarse basalt and analysis was performed on plagioclase separates. This sample gave a plateau age of 18.13 ± 0.59 Ma, with 76.0 % of the total ^{39}Ar gas released within 25 contiguous steps (Figure 4.12). The isochron age was 17.5 ± 3.1 Ma, which is within error of the plateau age. The initial $^{40}Ar/^{36}Ar$ value was also within error of the accepted atmospheric value. There are no existing ages for the Jaqué Enriched Plateau, but this age is younger than expected based on geological constraints that suggest an age similar to the remainder of the Plateau groups (i.e., Late Cretaceous).

4.4.4 Bahia Piña Formation

Two samples of the Bahia Piña Formation were dated using larger benthic foraminifera. Sample JB17-072 was estimated to have an age of Late Middle to Late Eocene, while sample JB17-071 was determined to have an age of Oligocene (Table 4.1, Appendix E5). These two samples were taken from a ~3 metre sequence, and would be expected to have a similar age. As these samples were deformed and partly recrystalized, foraminifera identification was difficult due to poor preservation of fossils. Therefore, this formation has been assigned an Early Oligocene age (ca. 38-34 Ma), due to the clear abundance of *Lepidocyclina* (*Eulepidina*) *undosa* in sample JB17-071, which is a common Oligocene index species in the Caribbean.

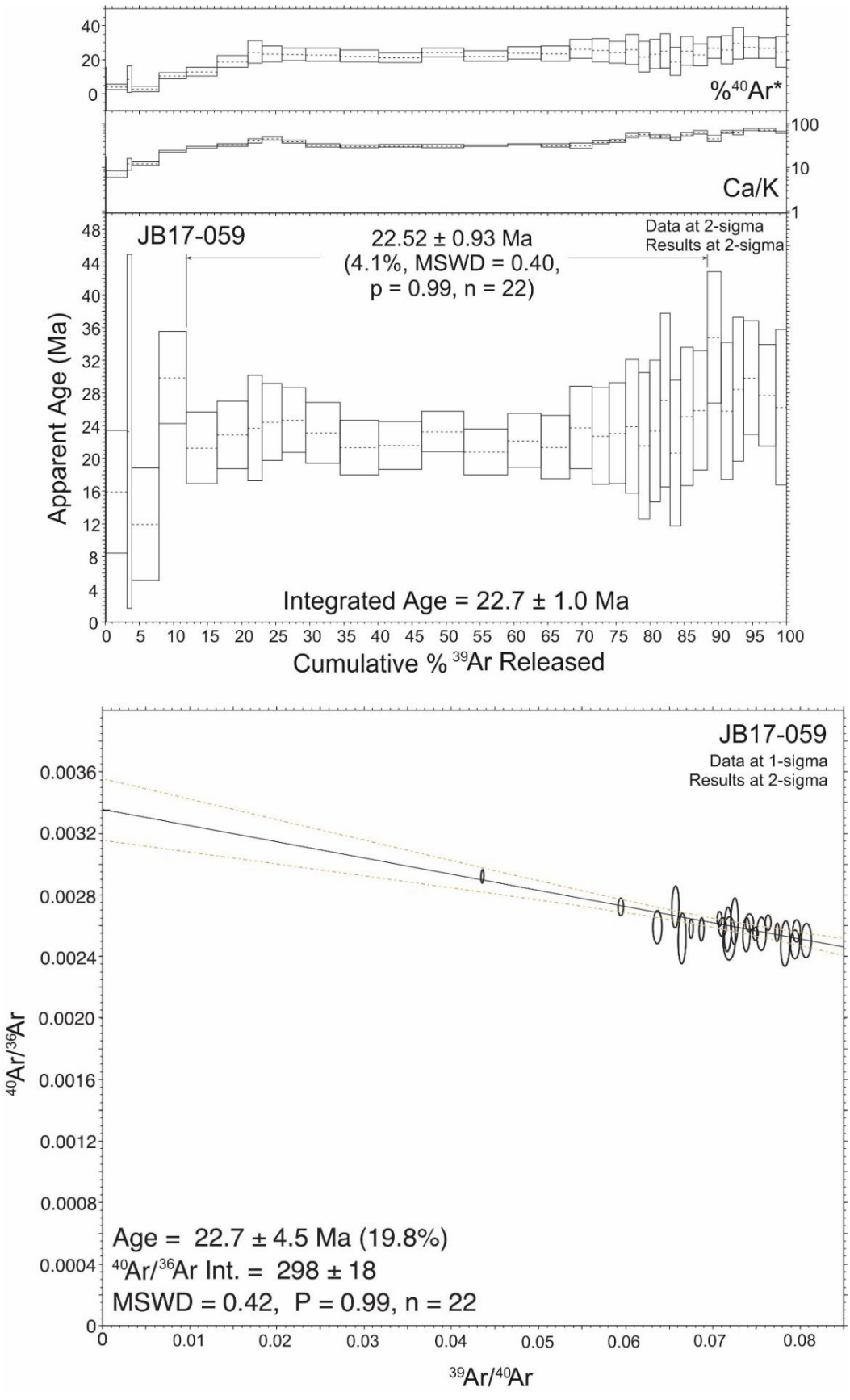

Figure 4.10: : Ar-Ar step heating plateau plot and inverse isochron plot for sample JB17-059 (Jaqué Depleted Plateau)

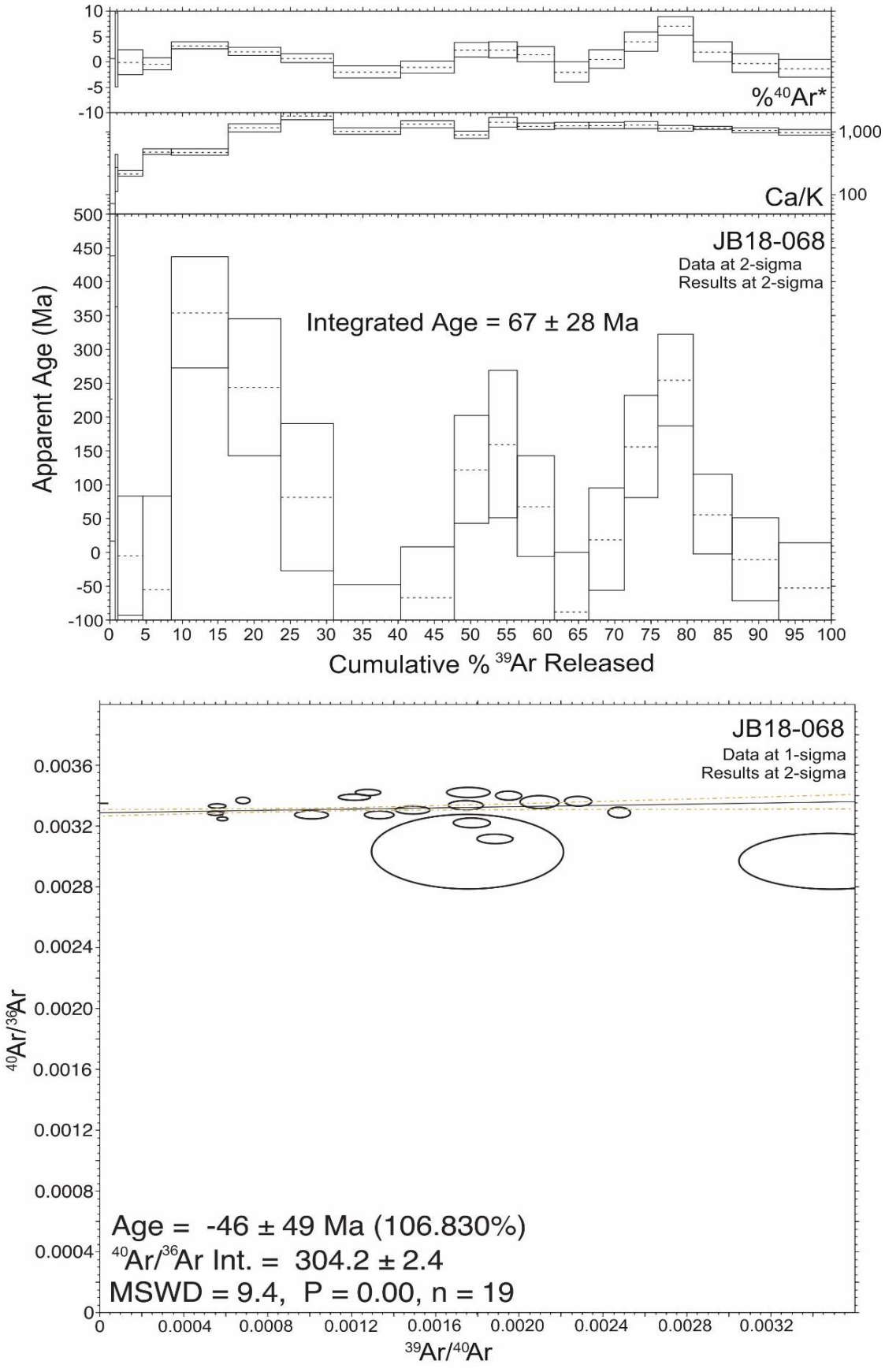

Figure 4.11: Ar-Ar step heating plateau plot and inverse isochron plot for sample JB18-068 (Jaqué Depleted Plateau)

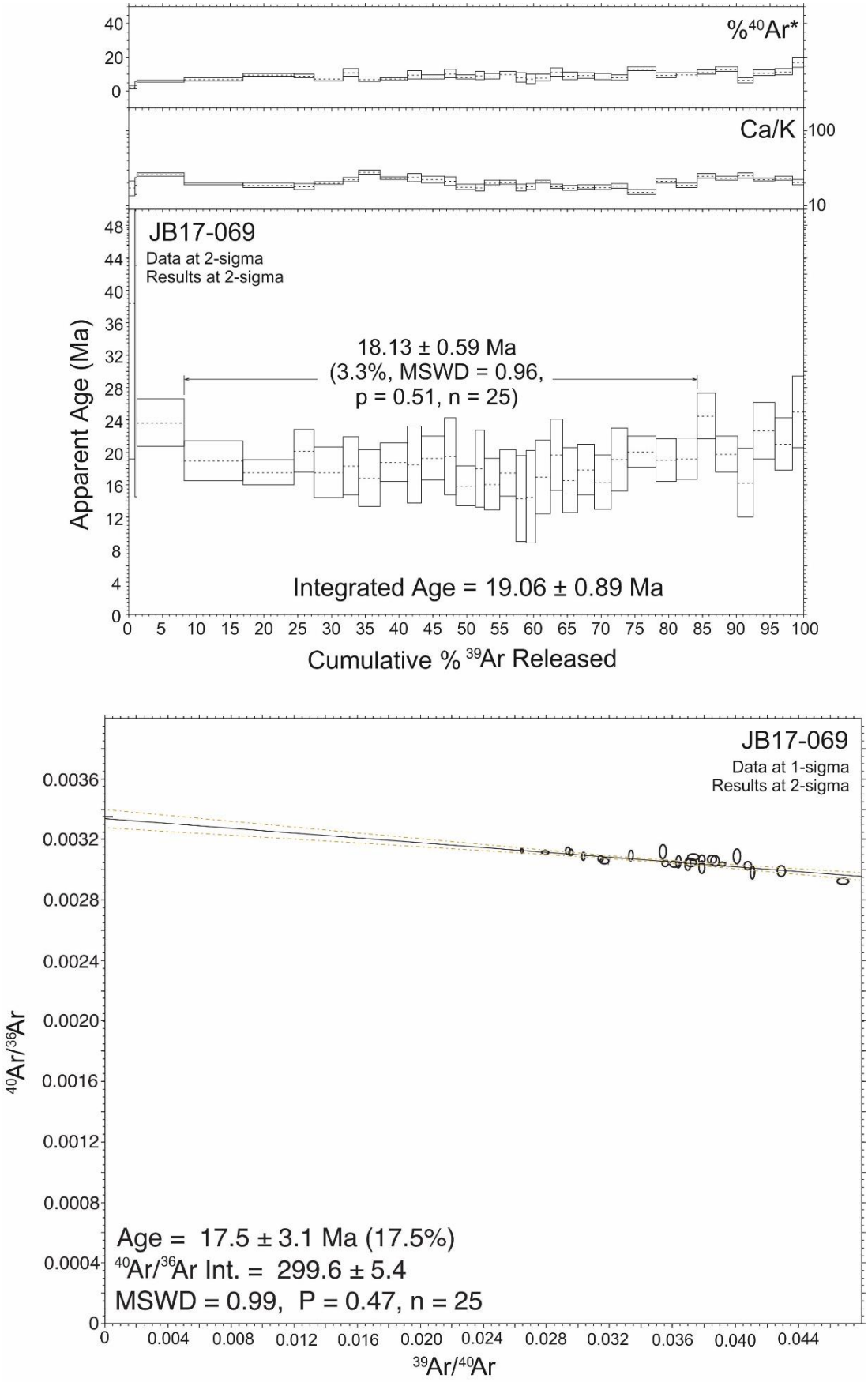

Figure 4.12: Ar-Ar step heating plateau plot and inverse isochron plot for sample JB17-069 (Jaqué Enriched Plateau)

4.4.5 Guayabo Formation

Two samples of the Guayabo Formation were dated using nannofossils, and two samples were dated using planktic foraminifera. Both samples JB17-048 (a bioturbated limestone) and JB17-066 (a calcareous sandstone) gave nannofossil ages of Late Eocene – Late Oligocene. Sample JB17-048 gave a foraminifera age of Middle – Late Eocene, and sample JB17-056 (a calcareous sandstone) gave an age of Early – Middle Eocene (Table 4.1). Again, detailed identification of nannofossils and foraminifera was made difficult due to poor preservation. In addition, these samples had low fossil abundances, which limited the biostratigraphic determinations. This unit is tentatively given an Early Oligocene age (ca. 38-34 Ma) based on partial consistency between the nannofossil and planktic foraminifera ages and because the Guayabo Formation apparently overlies the Bahia Piña Formation dated to the Oligocene by larger benthic foraminifera (see above). Occurrence of an Oligocene sedimentary sequence with shallow-marine limestone and deeper marine turbidites resting unconformably on top of a volcanic basement is consistent with lithostratigraphic and biostratigraphic constraints from the rest of the Panamanian forearc (e.g., Kolarsky et al., 1995; Buchs et al., 2011; Montes et al., 2012; Barat et al., 2014).

4.4.6 Jaqué Proto-arc Group

Two samples of the Jaqué Proto-arc were selected for $^{40}Ar/^{39}Ar$ geochronology, and both were analysed on plagioclase separates. These samples gave ages of 13.61 ± 0.63 Ma and 16.0 ± 1.1 Ma.

Sample JB17-075 is a plagioclase-phyric dyke from the Puerto Piña peninsula on the Darién Coast. This sample gave a plateau age of 16.0 ± 1.1 Ma, with 71.9 % of total ^{39}Ar gas released within 20 contiguous steps (Figure 4.13). The isochron age was 16.1 ± 3.4 Ma, within error of the plateau age, and the initial $^{40}Ar/^{36}Ar$ ratio was within error of atmospheric values. Within the plateau, the steps are quite variable, with higher errors than most other samples in this study. Ca/K values remain relatively constant within the plateau.

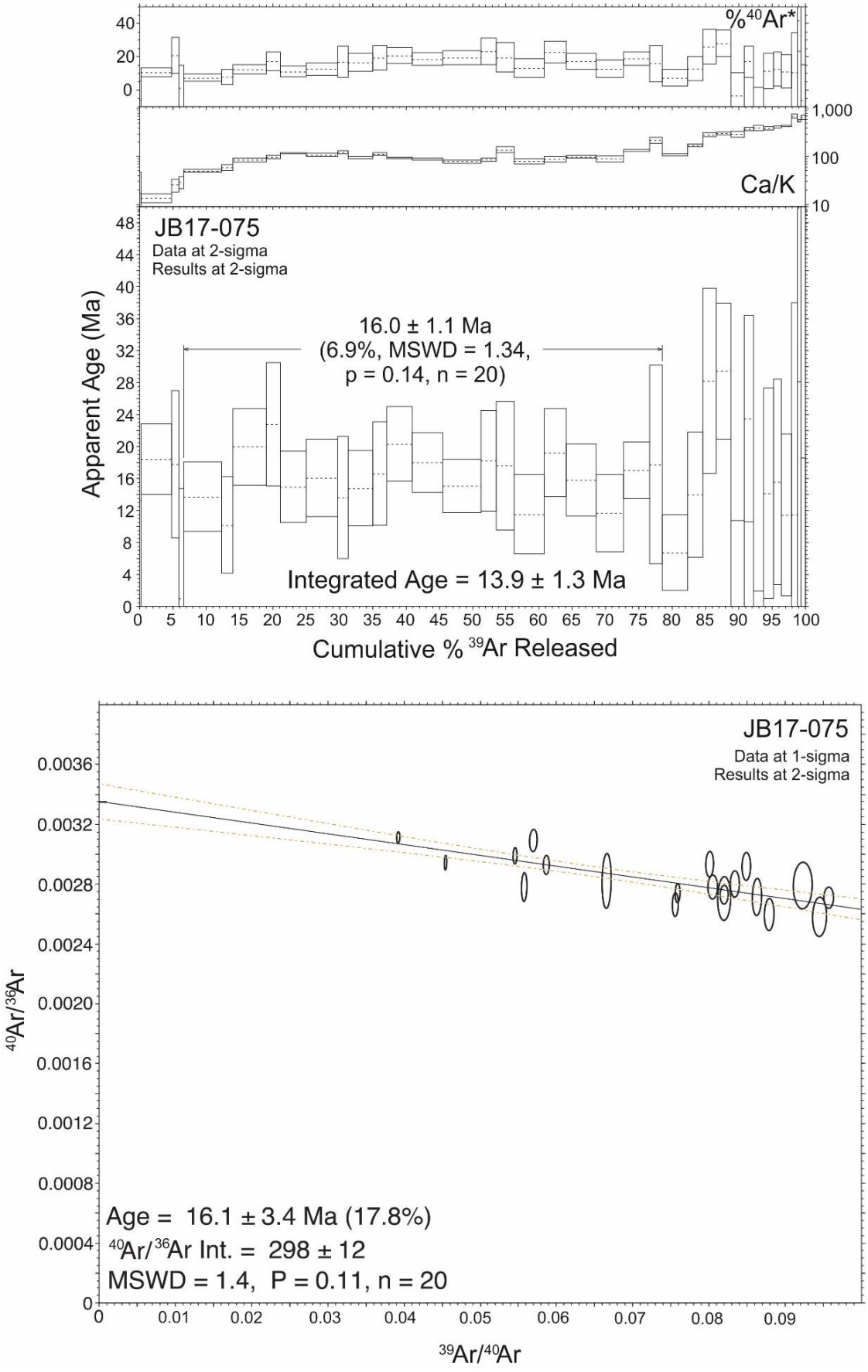

Figure 4.13: Ar-Ar step heating plateau plot and inverse isochron plot for sample JB17-075 (Jaqué Proto-arc).

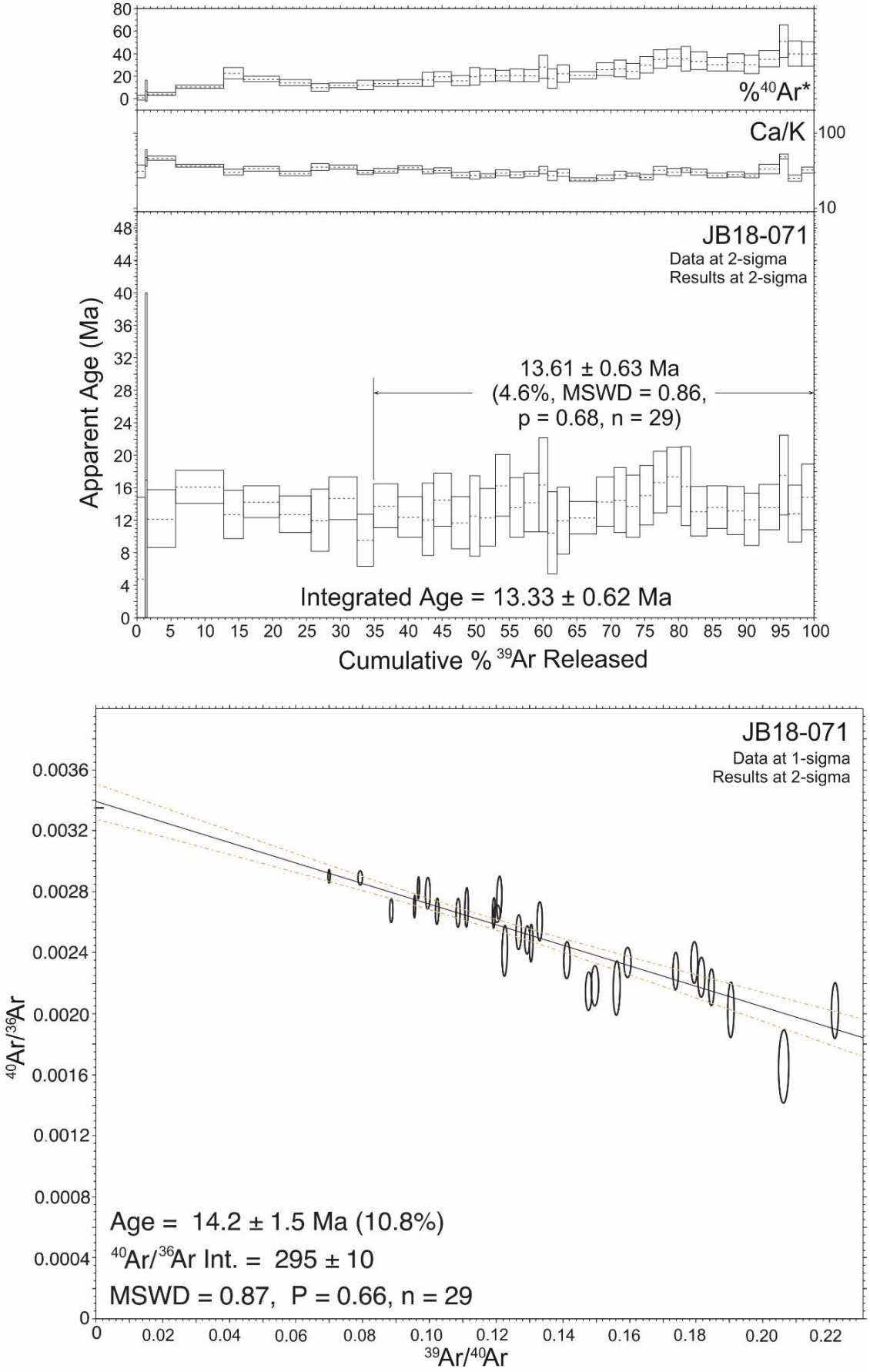

Figure 4.14: Ar-Ar step heating plateau plot and inverse isochron plot for sample JB18-071 (Jaqué Proto-arc).

This sample fulfils quality criteria and the age could be assumed to be reliable. There are no existing dates for this group. However, the Proto-arc Group should be older than the Lower Oligocene Bahia Piña and El Guayabo Formations, because dykes of the proto-arc were only seen to intrude the plateau, and no igneous clasts in the El Guayabo Formation have a Proto-arc geochemistry.

Sample JB18-071 is a gabbroic intrusion from Rio Pavarando. This sample gave a plateau age of 13.61 ± 0.63 Ma, with 65.0 % of the total ^{39}Ar gas released within 29 contiguous steps (Figure 4.14). The isochron age is 14.2 ± 1.5 Ma, within error of the plateau age, and the initial ^{40}Ar/^{36}Ar value is within error of atmospheric values. Ages, errors, and Ca/K values remain constant within the plateau with increasing temperatures. This sample adheres to the required criteria and can be used as a reliable age. However, this age is also younger than was estimated based on geological constraints, as detailed above.

4.4.7 Jaqué Arc Group 2

Sample JB18-064 is a porphyritic andesite from Rio Pavarando and was the only Jaqué Arc sample prepared for ^{40}Ar/^{39}Ar geochronology. Analysis was performed on plagioclase separates. The plateau age was 12.83 ± 0.69 Ma, with 72.6 % of the total ^{39}Ar released within 28 contiguous steps (Figure 4.15). The isochron age is 12.9 ± 1.5 Ma, within error of the plateau age, and the initial ^{40}Ar/^{36}Ar value is within error of atmospheric values. Within the plateau, Ca/K values increase from 1 to 80 with increasing temperatures, and ages and errors remain relatively consistent. This age is younger than the previous age of an arc sample from Puerto Piña, which was 21.7 ± 0.3 Ma based on ^{40}Ar/^{39}Ar step heating on a plagioclase separate (Lissinna, 2005). This age is also younger than the 18 ± 0.9 Ma volcanic activity in the nearby Majé Range, which was determined based on zircon U-Pb geochronology (Whattam et al., 2012). It is, however, similar to the apparent age of volcanic cessation ca. 15 Ma in Central Panama, which was determined by ^{40}Ar/^{39}Ar geochronology and might also correlate with the termination of magmatic activity in eastern Panama (Buchs et al., 2019b).

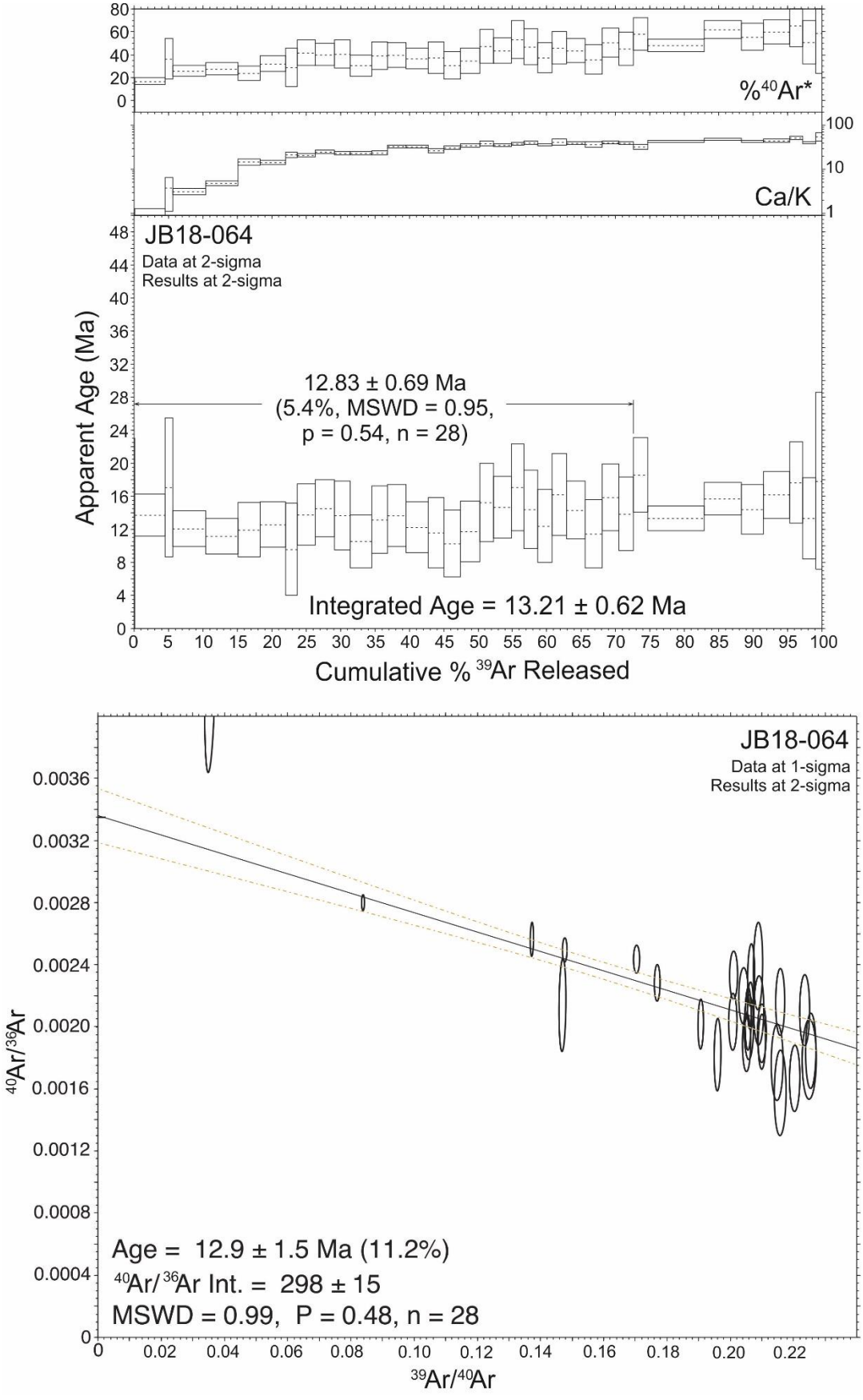

Figure 4.15: Ar-Ar step heating plateau plot and inverse isochron plot for sample JB18-064 (Jaqué Proto-arc).

4.5 Serranía de Baudó

Two samples from the Serranía de Baudó were selected for $^{40}Ar/^{39}Ar$ geochronology, both from the Baudó Plateau.

4.5.1 Baudó Plateau

Two samples from the Baudó Plateau were analysed for $^{40}Ar/^{39}Ar$ geochronology, both on plagioclase separates. These samples gave ages of 47 ± 15 Ma and 69.7 ± 2.0 Ma.

Sample JB17-092 is a dolerite sill from the Bahia Solano coast, and gave a plateau age of 69.7 ± 2.0 Ma, with 77.9 % of total ^{39}Ar released within 27 contiguous steps (Figure 4.16). The isochron age is 69.4 ± 3.4 Ma, within error of the plateau age, and the initial $^{40}Ar/^{36}Ar$ ratio was within error of atmospheric values. Within the plateau, ages and errors are variable, and generally errors are higher than most of the other samples in this study. Some of the highest errors occur at the lowest and highest temperatures. Ca/K values are also highly variable within the plateau, and there is no clear pattern with increasing temperatures. However, the data satisfies quality criteria and could be considered as a reliable age. This age is however much younger than the existing ages of the plateau in the Baudó region, which are 72.5 ± 0.4 Ma and 77.9 ± 1.0 Ma based on $^{40}Ar/^{39}Ar$ plateau step heat ages (Kerr et al., 1997b).

Sample JB17-127 is a basalt from the Cupica coast. This sample gave a plateau age of 47 ± 15 Ma, with a 75.8 % of total ^{39}Ar gas released within 21 contiguous steps. The isochron age was 34 ± 15 Ma, within error of the plateau age, and initial $^{40}Ar/^{36}Ar$ values were within error of atmospheric values. This sample satisfies all quality criteria and the data could be assumed to be reliable. However, this data has high errors for many of the temperature steps within the plateau, particularly at higher temperatures. Ca/K values are also highly variable with high errors at higher temperatures. This sample is again younger than the existing plateau ages from the Baudó region.

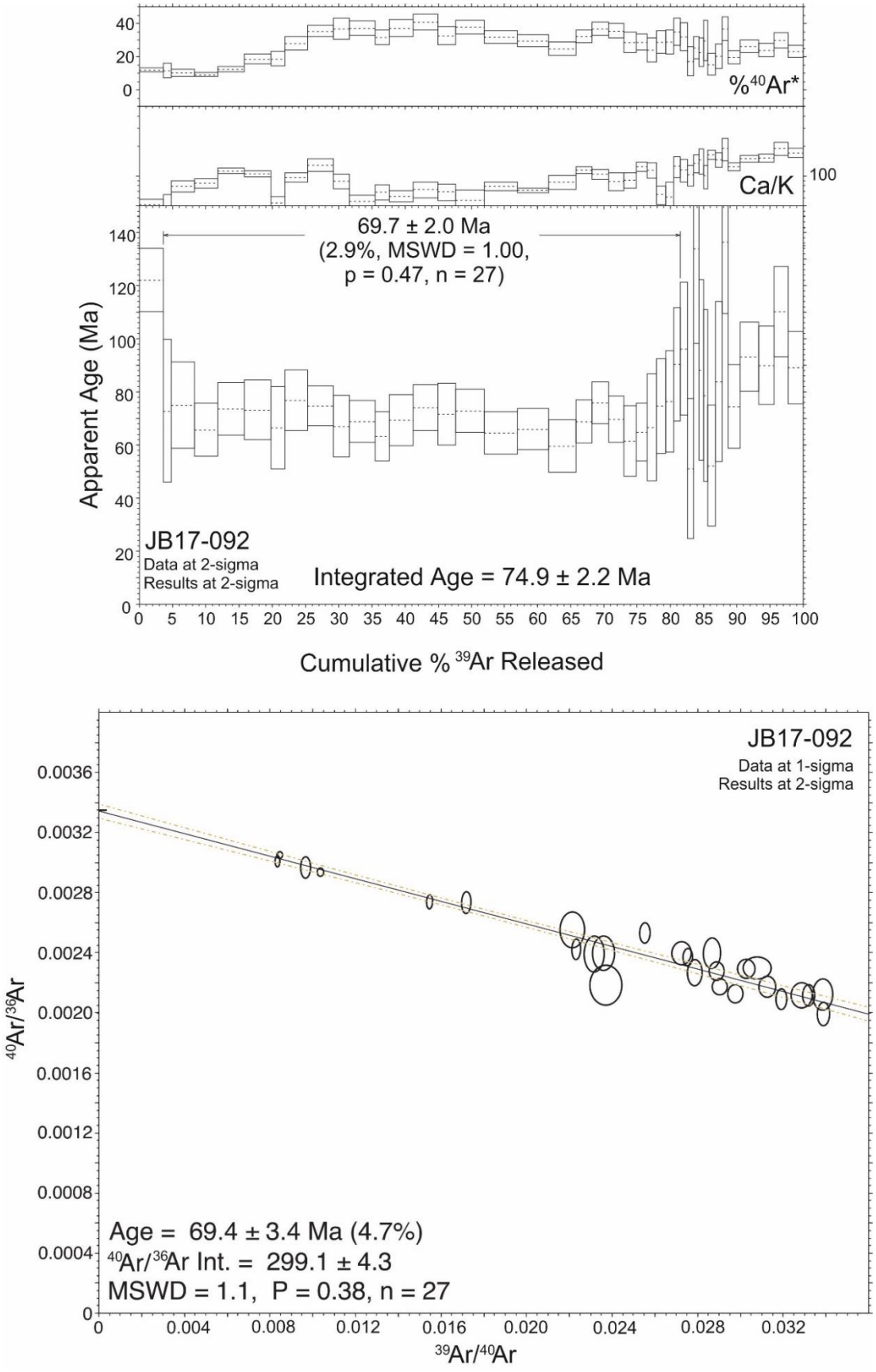

Figure 4.16: Ar-Ar step heating plateau plot and inverse isochron plot for sample JB17-092 (Baudó Plateau).

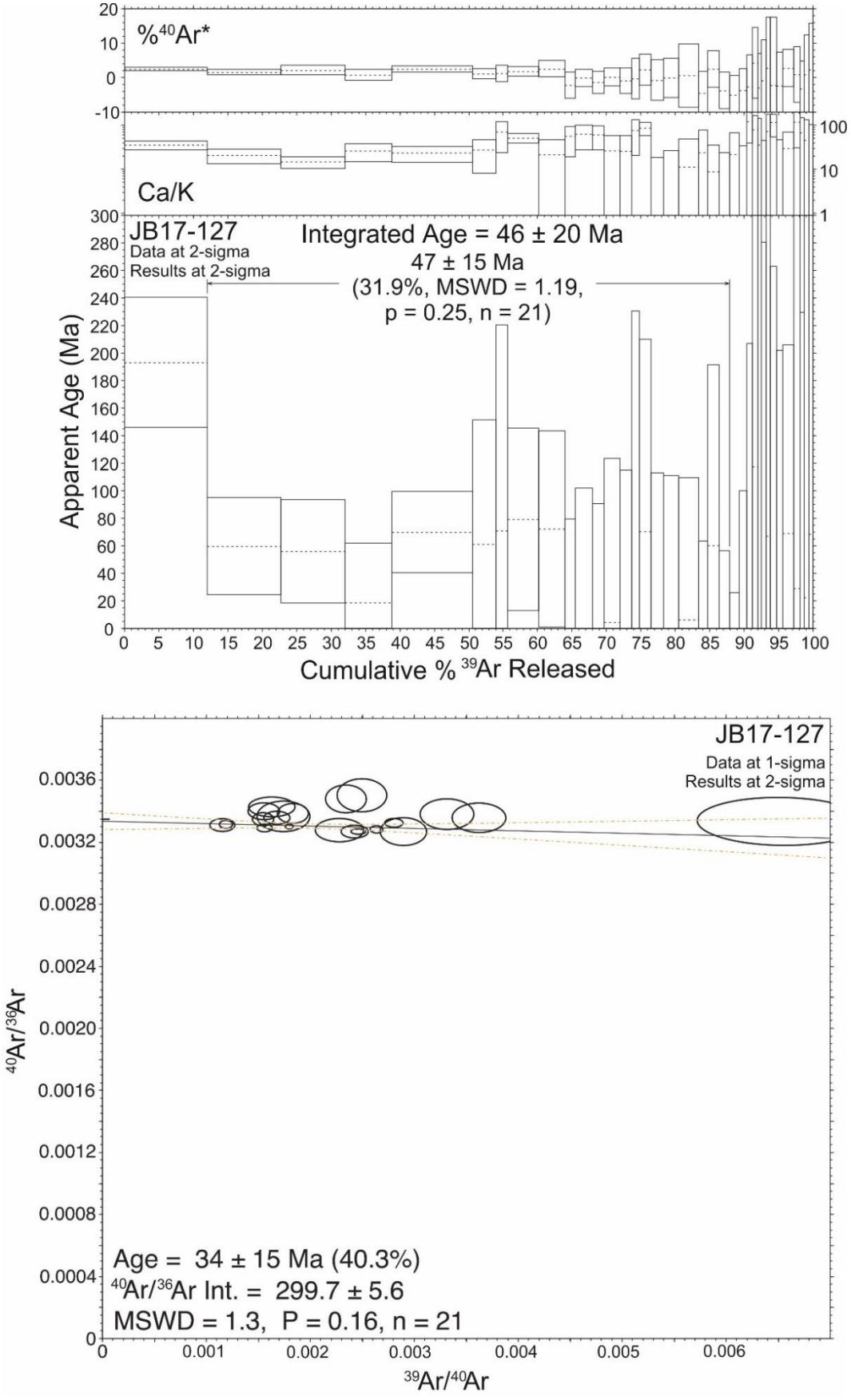

Figure 4.17: Ar-Ar step heating plateau plot and inverse isochron plot for sample JB17-127 (Baudó Plateau).

4.6 Summary

Overall, 15 samples gave new $^{40}Ar/^{39}Ar$ ages for plateau, proto-arc and arc groups from the Soná-Torio, Darién Pacific Coast and Serranía de Baudó regions. These ages ranged from 87 Ma through to 18 Ma. New biostratigraphic ages were also obtained for sedimentary formations from the Soná-Torio and Darién Pacific Coast regions, giving context to the surrounding igneous units.

Although new $^{40}Ar/^{39}Ar$ data successfully pass quality criteria and could be considered as reliable crystallization ages, most of them do not agree with previous and new geochronological, biostratigraphic, lithostratigraphic, and/or regional geological constraints. Although some of these new ages may be reliable and represent the true crystallisation age, there is no clear criterion to distinguish between those that clearly do represent the crystallisation age, and those that do not. For this reason, these new ages have not been used within the stratigraphic framework of this study. Reasons for this will be further discussed in Section 6.2.

5. GEOCHEMISTRY

5.1 Introduction

This section introduces the whole rock major and trace element results and whole rock Nd isotope results from Soná-Torio, Darién Pacific Coast and Serranía de Baudó regions. Laboratory methods, with a discussion of analytical issues encountered during this study, are described in Appendices A.1 and A.3 with datasets found in Appendices E2 and E3. All major element wt. % concentrations have been recalculated on an anhydrous basis. Fourteen geochemical groups were defined in the studied areas, which reflect the different stages of evolution of the southwest Caribbean margin, from oceanic plateau formation to subduction initiation and arc maturation.

The definition of the geochemical groups was primarily made based on geochemical criteria (as detailed below). However, as explained in Chapter 3, important guidance in the recognition and sampling of the groups was provided by field constraints because most igneous suites recognised in this study have distinctive petrographic and lithostratigraphic characteristics. Geochemical criteria for defining geochemical groups consisted of similarity of primitive mantle-normalised multielementary and chrondrite normalised REE patterns, along with similarity of key trace element ratio values and major element values.

This chapter will first assess the effects of secondary alteration and element mobility on the whole rock geochemical results, using petrography, LOI values and correlation of elements with Zr contents. Both major and trace elements will then be used to classify samples according to their rock type. Major and trace elements will additionally be used to review the major and trace element characteristics of each group, and to investigate the magmatic processes and tectonic setting of the magmatic suites. Nd radiogenic isotope results from samples across the 3 studied locations and associated magmatic groups from across southern Central America and the Caribbean will be used to assess the mantle source characteristics.

5.2 Alteration and element mobility

It is clear from their petrography that sampled rocks from across Panama and northwest Colombia have undergone variable amounts of alteration, up to greenschist facies. All samples show some degree of alteration and the LOI values mostly range between 0.5 and 4 wt. %. However, in some samples this can extend up to ~6 wt. %, and in rare samples with

extensive carbonate veining, LOI values can be as high as 13.9 wt. % (Figure 5.1). This indicates that some samples have undergone extensive alteration, which may be due to weathering and sub-solidus hydrothermal alteration. These processes can affect the composition of the samples due to mobility of some major and trace elements. Therefore, it is imperative to assess the effects of secondary alteration and element mobility on major and trace elements, before using the data to characterise petrogenetic processes.

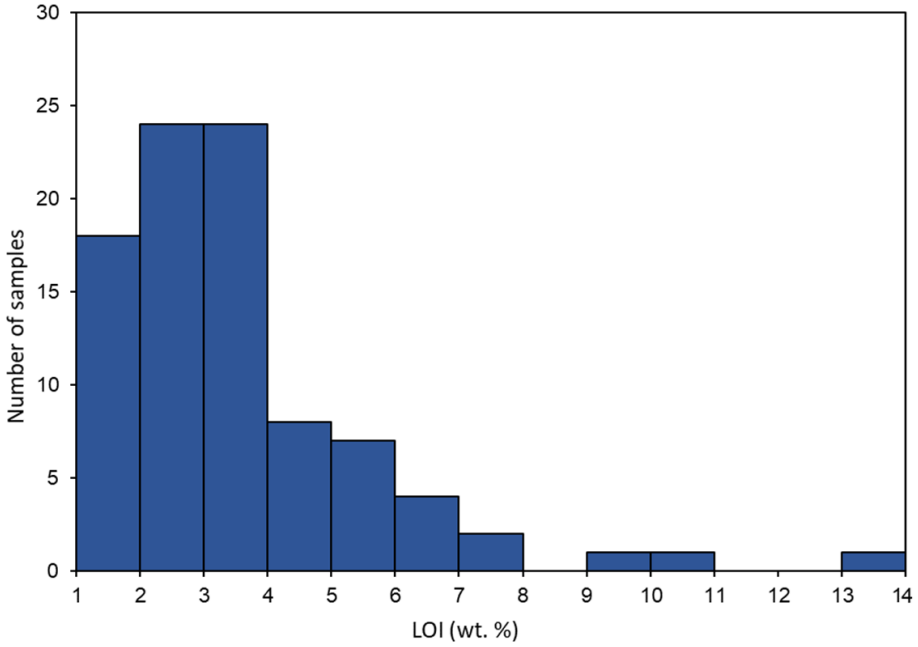

Figure 5.1: Histogram of LOI values for all samples analysed in this study

Many elements can become mobile during sub-solidus alteration, especially the Large-Ion Lithophile Elements (LILE) such as K, Ba, Rb, Pb and Sr (Pearce, 1996). Many of these elements are carried in subduction fluids, and can be used to trace slab component in fresh, unaltered samples. The most immobile elements generally do not go into solution during alteration, including the majority of the Rare Earth Elements (REE) and the High Field Strength Elements (HFSE) (Pearce, 1996). To assess the mobility of elements, they will be plotted against Zr. Zr is thought to be one of the most immobile elements during medium-high grade metamorphic conditions and is incompatible during basalt fractionation (Cann, 1970; Pearce, 1996). For immobile elements in a suite linked through fractional crystallisation, a clear correlation should be seen between each element and Zr. In contrast, for elements which have been mobilised, there will be more scatter. If scatter or multiple trends are observed in elements known to be immobile during alteration, such as the REEs and HFSEs, then it is likely that this scatter is due to primary petrological processes rather than secondary alteration (Pearce, 1996). To quantify the scatter between each element and Zr, bivariate plots of Zr and trace elements were constructed for each magmatic suite, along

with calculations of the R^2 correlation value. For this study, R^2 values > 0.7 are interpreted as having a good correlation, those between 0.4 - 0.7 a moderate correlation, and values < 0.4 a poor correlation. In this approach, the compositional range of the magmatic suites should be similar to avoid creating disparities in R^2 values that would be related to differentiation processes rather than alteration effects. One could expect that correlation between mobile elements and Zr may improve at lower LOI values. However, for the geochemical groups of this study, using samples only with LOI < 3 wt. % did not lead to an improvement of mobile elemental correlations with Zr. Geochemical groups with less than 7 samples will not be used for correlations with Zr as they cannot give statistically reliable trends and can produce an anomalously low R^2 value.

5.2.1 Soná-Torio region

Six geochemical groups have been identified in the Soná-Torio region: Soná-Torio Plateau, Soná-Torio Enriched Plateau, Soná-Torio High-Mg Plateau, Soná-Torio Proto-arc Group 1, Soná-Torio Proto-arc Group 2 and Soná-Torio Arc. Samples of the Soná-Torio region can show extensive clay alteration in thin section (as documented in Chapter 3) and the bulk of samples have LOIs ranging from 0.5 - 4 wt. %, with rare samples with values as high as 10.9 wt. % (Figure 5.2). This indicates that variable amounts of alteration have affected these rocks. The Enriched Plateau, Proto-arc Group 1 and Arc groups contain less than 7 samples, and so cannot be used to correlate with Zr. As these groups have similar LOI values and levels of alteration in thin section with other groups, the element mobility in these groups will be inferred.

The Zr correlations for the Soná-Torio Plateau, High-Mg Plateau and Proto-arc Group 2 will be calculated individually, as they are different magmatic suites. Both Plateau and Group III have relatively narrow ranges of Zr, with ranges of 49.2 – 79.7 ppm and 11.1 – 29.7 ppm respectively. As a result, the data for these points is clustered and may not give reliable R^2 values. Proto-arc Group 2 has a wider range

	Soná-Torio			Jaqué			Baudó
Element	Plateau (n = 24)	High MgO Plateau (n = 20)	Proto-arc Group 2 (n = 25)	Plateau (n = 8)	Depleted Plateau (n = 10)	Proto-arc (n = 8)	Plateau (n = 18)
SiO_2	0.00	0.13	0.03	0.11	0.35	0.25	0.09
TiO_2	0.43	0.86	0.71	0.77	0.64	0.96	0.98
Al_2O_3	0.03	0.56	0.14	0.25	0.28	0.58	0.33
Fe_2O_3	0.01	0.33	0.45	0.54	0.24	0.71	0.81
MnO	0.09	0.01	0.01	0.30	0.00	0.30	0.35
MgO	0.08	0.13	0.43	0.66	0.36	0.46	0.62
CaO	0.00	0.03	0.42	0.32	0.40	0.23	0.06
Na_2O	0.00	0.11	0.20	0.48	0.21	0.21	0.05
K_2O	0.01	0.08	0.07	0.21	0.01	0.16	0.00
P_2O_5	0.02	0.31	0.67	0.74	0.30	0.61	0.95
Sc	0.06	0.42	0.10	0.21	0.01	0.16	0.08
V	0.57	0.34	0.25	0.69	0.01	0.86	0.74
Cr	0.27	0.13	0.27	0.61	0.19	0.37	0.44
Co	0.20	0.09	0.16	0.29	0.00	0.26	0.11
Ni	0.24	0.29	0.14	0.08	0.05	0.35	0.54
Cu	0.00	0.01	0.49	0.23	0.13	0.24	0.01
Zn	0.17	0.59	0.30	0.38	0.08	0.43	0.04
Sr	0.00	0.23	0.02	0.17	0.24	0.05	0.07
Y	0.82	0.73	0.92	0.83	0.20	0.94	0.90
Ba	0.01	0.00	0.01	0.15	0.37	0.07	0.07
Rb	0.01	0.07	0.09	0.21	0.04	0.09	0.00
Nb	0.62	0.14	0.74	0.39	0.74	0.91	0.90
Mo	0.08	0.21	0.58	0.02	0.00	0.63	0.18
La	0.40	0.48	0.91	0.86	0.40	0.73	0.92
Ce	0.45	0.66	0.94	0.94	0.63	0.85	0.97
Pr	0.37	0.73	0.96	0.80	0.78	0.88	0.98
Nd	0.50	0.78	0.94	0.96	0.79	0.92	0.98
Sm	0.65	0.88	0.91	0.63	0.60	0.89	0.98
Eu	0.55	0.55	0.90	0.84	0.70	0.89	0.97
Gd	0.49	0.68	0.91	0.65	0.65	0.93	0.97
Tb	0.47	0.71	0.90	0.49	0.60	0.94	0.97
Dy	0.28	0.67	0.88	0.75	0.71	0.95	0.94
Ho	0.20	0.60	0.88	0.55	0.51	0.94	0.92
Er	0.25	0.55	0.86	0.77	0.46	0.93	0.88
Tm	0.67	0.71	0.85	0.84	0.37	0.95	0.80
Yb	0.28	0.50	0.81	0.88	0.44	0.94	0.84
Lu	0.51	0.68	0.82	0.54	0.24	0.95	0.72
Hf	0.47	0.85	0.96	0.77	0.93	0.99	0.99
Ta	0.77	0.28	0.72	0.52	0.81	0.93	0.88
Pb	0.25	0.06	0.19	0.33	0.32	0.02	0.02
Th	0.10	0.26	0.81	0.39	0.59	0.63	0.90
U	0.00	0.09	0.82	0.08	0.01	0.70	0.84

Table 5.1: R^2 values for elements with Zr for geochemical groups from the Soná-Torio region. Yellow indicates a moderate correlation with Zr and R^2 value of between 0.4 – 0.7 and green indicates a good correlation with Zr, and and R^2 value of > 0.7

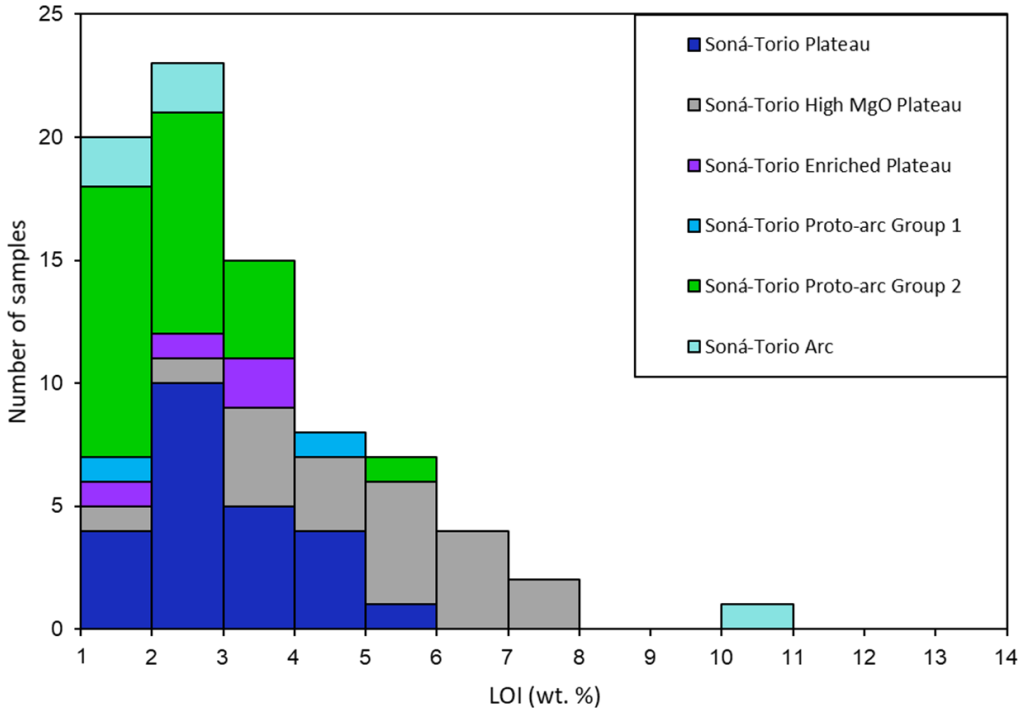

Figure 5.2: Histogram of LOI values for the Soná-Torio region samples

of Zr, from 59.6 – 175.3 ppm, and therefore R^2 values for these samples may more accurately assess element mobility.

The Soná-Torio Plateau has LOI values ranging from 1.24 to 5.99 wt. %, and shows extensive clay alteration in thin section. It shows only moderate correlations of Zr with TiO_2, V, Nb, La, Ce, Nd, Sm, Eu, Gd, Tb, Tm, Lu and Hf, good correlations with Y and Ta, with poor correlations for the remainder of major and trace elements (Figure 5.3, Table 5.1). Usually the REE show similar amounts of remobilisation, and so it is most likely that variations in correlations between the REE and Zr are due to petrological processes and not remobilisation. Many of these correlations are also likely to have been affected by the clustering effect of the data, as the group has a narrow range of Zr. As elements which are typically mobile (e.g., Rb, Ba, Sr) have very low correlations with Zr (<0.15), the scatter on the elements with low to moderate correlations is likely due to other petrological processes.

The High-Mg Plateau group has LOI values ranging from 1.67 - 6.18 wt. %, and has undergone greenschist facies metamorphism, with extensive actinolite-chlorite replacement. This group shows good correlations of Zr with TiO_2, Y, Pr, Nd, Sm, Tb, Tm and Hf, and moderate correlations with Al2O3, Sc, Zn, La, Ce, Eu, Gd, Dy, Ho, Er, Yb and Lu (Figure 5.3, Table 5.1). The remainder of trace and elements have R^2 values under 0.4 and show poor correlations. As elements which are typically

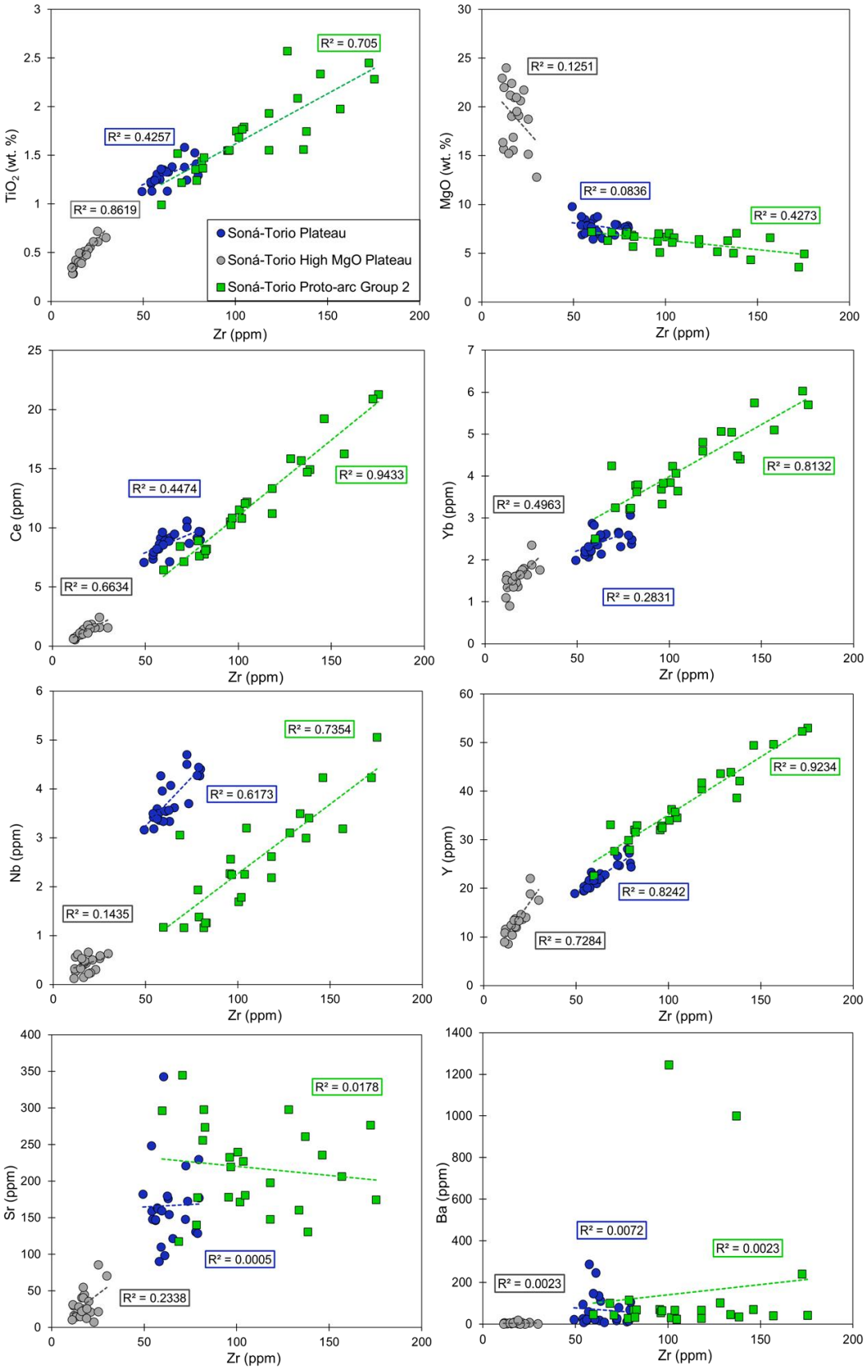

.

Figure 5.3: Bivariate diagrams of representative elements against Zr from the Soná-Torio Plateau, Soná-Torio High-Mg Plateau and Soná-Torio Proto-arc Group 2

mobile (e.g., Rb, Ba, Sr) have very low correlations with Zr (<0.15), the scatter on the elements with low to moderate correlations is likely due to other petrological processes. The Proto-arc Group 2 have a wider Zr range and so may give more reliable and informative Zr correlations. The group has LOI values ranging from 1.28 – 3.37 wt. %, and variable amounts of clay alteration as outlined in Chapter 3. This group has good correlations of Zr with TiO_2, Nb, Hf, Ta, Th, U and the REEs, with moderate correlations with Fe_2O_3, MgO, CaO, P_2O_5, Cu and Mo, and poor correlations with the remainder of the elements (Table 5.1, Figure 5.3). Again, the high amount of scatter and very low R^2 values for known mobile elements such as Rb and Ba indicates that for elements with moderate to poor correlations, the lower degree of scatter may not be due to mobilisation, but rather petrological processes.

5.2.2 Darién Pacific Coast

There are 7 geochemical groups within the Darién Pacific Coast region: Jaqué Plateau, Jaqué Depleted Plateau, Jaqué Enriched Plateau, Jaqué Proto-arc and Jaqué Arc Group 1, Arc Group 2, and Arc Group 3. Samples of the Darién region can show extensive clay alteration in thin section and have LOIs largely ranging

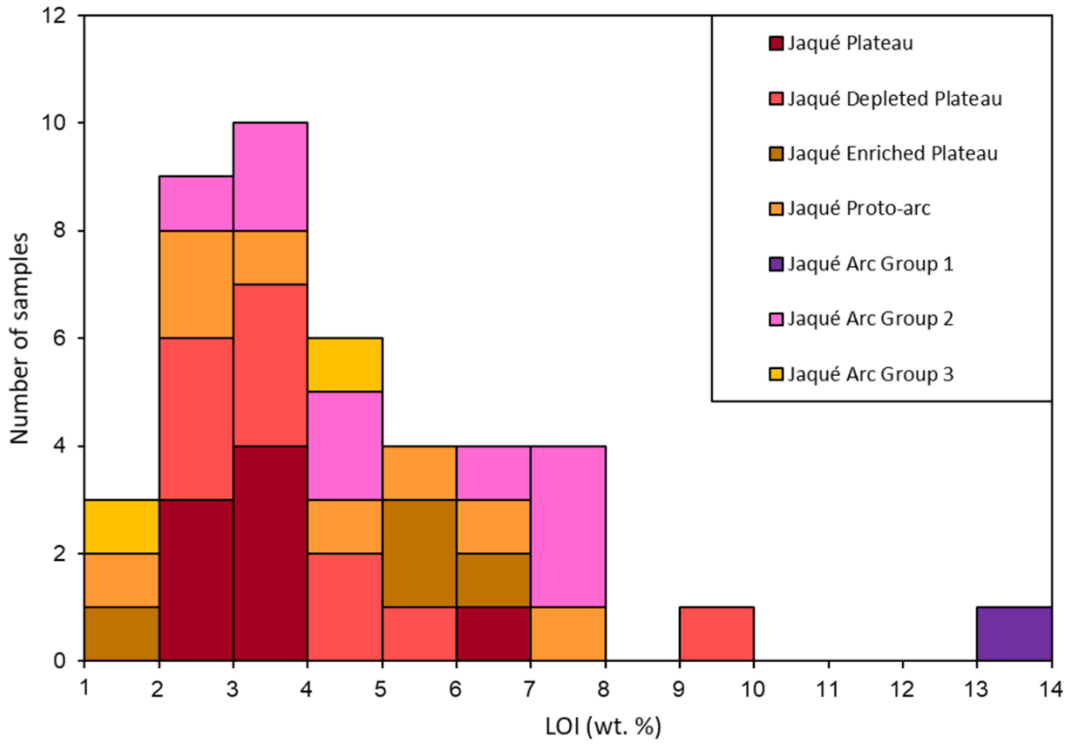

Figure 5.4: Histogram of LOI values for the Darién Pacific Coast samples

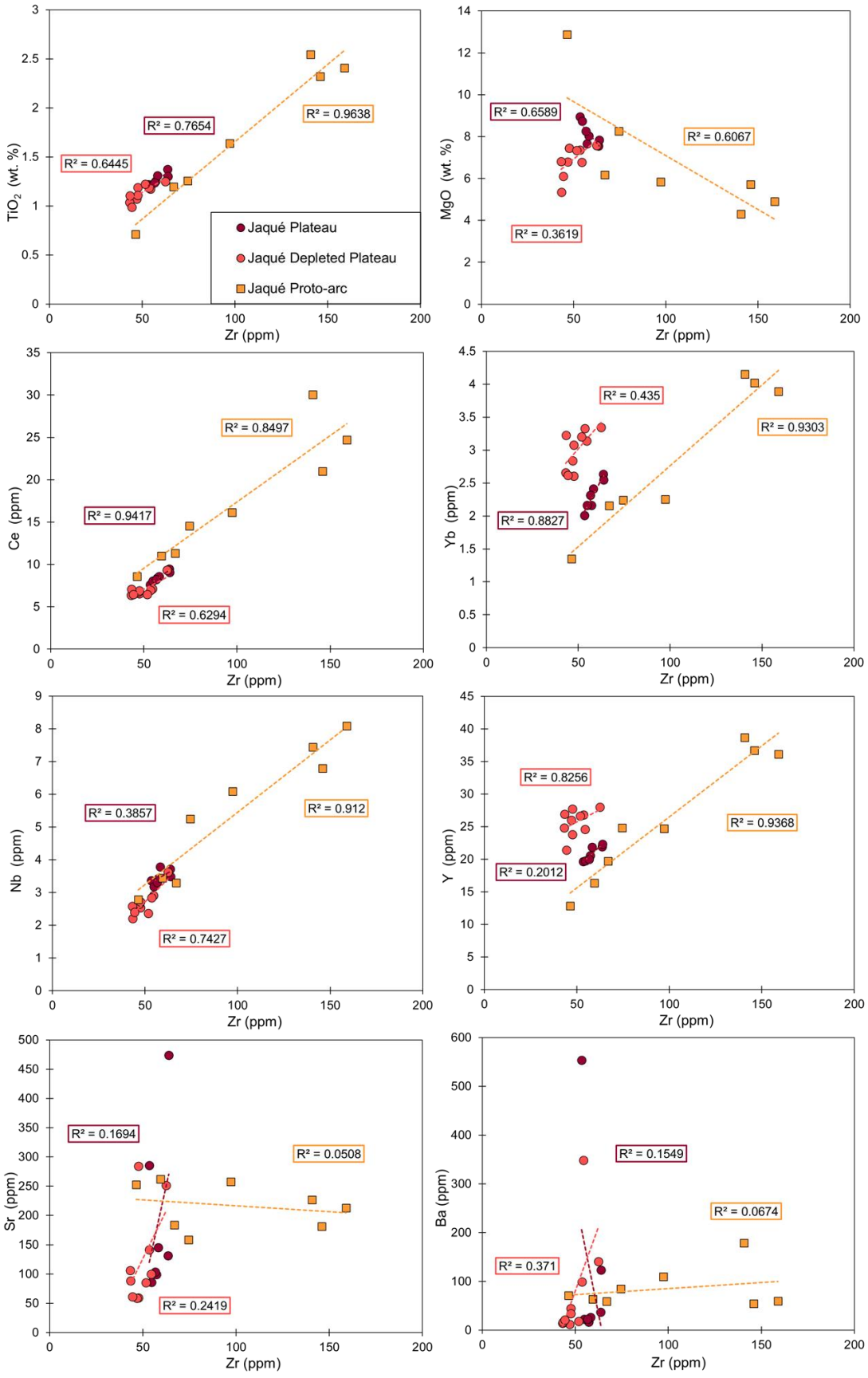

Figure 5.5: Bivariate diagrams of representative elements against Zr from the Jaqué Plateau, Jaqué Depleted Plateau and Jaqué Proto-arc

from 1.6 - 5 wt. Some samples have LOIs that extend up to 8 wt. %, with a single sample as high as 13.91 wt. % (Figure 5.4). Only the Jaqué Plateau, Jaqué Depleted Plateau and Jaqué Proto-arc Groups will be used to correlate against Zr as they represent individual magmatic suites and contain more than 7 samples. As these groups have similar LOI values and levels of alteration in thin section with Enriched Plateau and the Arc Groups, the element mobility in these groups will be inferred. The Zr correlations for the Jaqué Plateau, Depleted Plateau and Proto-arc will be calculated individually, as they are different magmatic suites. These groups all have relatively narrow ranges of Zr. For the Jaqué Plateau, the range of Zr is 53.4 – 63.5 ppm, with a single outlier sample with 115.05 ppm. The inclusion of this outlier sample gives anomalously positive R^2 values, so this point will be omitted for the purpose of accurately assessing element mobility. The Depleted Plateau has a Zr range of 43 – 63 ppm. The data for these groups can be clustered and may not give reliable R^2 values. Proto-arc has a wider range of Zr, from 46 – 159 ppm, and therefore R^2 values for these samples may more accurately show element mobility.

Jaqué Plateau samples have LOI values ranging from 2.23 to 3.63 wt. % and show extensive clay and chlorite alteration in thin section. The samples of this group show good correlations of Zr with TiO_2, P_2O_5, Y, La, Ce, Pr, Nd, Eu, Dy, Er, Tm, Yb and Hf and moderate correlations with Fe_2O_3, MgO, Na_2O, V, Cr, Nb, Sm, Gd, Tb, Ho, Lu and Ta. For the remainder of measured major and trace elements, Zr shows poor correlations (Table 5.1, Figure 5.5)

The Jaqué Depleted Plateau has LOI values ranging from 2.64 – 5.80 wt. %, with one sample with a higher value of 9.08 wt.%. In thin section there is again clay and chlorite alteration, with a similar amount of alteration as is seen in samples of the Jaqué Plateau. The Depleted Plateau shows good correlation of Zr only with Nb, Pr, Nd, Dy, Hf and Ta, moderate correlation with TiO_2, CaO, La, Ce, Sm, Eu, Gd, Tb, Ho, Er, Yb and Th and poor correlations with the remainder of major and trace elements (Table 5.1, Figure 5.5).

The Jaqué Proto-arc has LOI values ranging from 1.81 – 6.94 wt. %, and samples have clay and chlorite alteration in thin section, to a lesser extent than the plateau groups. Proto-arc samples show a good correlation of Zr with TiO_2, Fe_2O_3, V, Nb, Hf, Ta, U and the REEs. There are moderate correlations of Zr with Al_2O_3, MgO, P_2O_5, Zn, Mo, and Th and poor correlations with the remainder of measured elements (Table 5.1, Figure 5.5).

Usually the REE show equal amounts of remobilisation, so here it is likely that variations in correlations between the REE and Zr are due to petrological processes or the clustering effect of the data, due to the narrow range of Zr. As elements which are typically mobile (e.g., Rb, Ba, Sr) have very low correlations with Zr (<0.25), the scatter on the elements with

moderate correlations is likely due to other petrological processes, or again due to clustering of the data.

5.2.3 Serranía de Baudó

The igneous rocks of the Serranía de Baudó are composed of one geochemical group, the Baudó Plateau. This group has an LOI range from 2.19 – 5.29 wt. % (Figure 5.6), with clay and chlorite alteration in thin section. There is a narrow range of Zr values, from 31 – 80 ppm, which means that values are clustered and may not give accurate R^2 values. The Baudó Plateau shows good correlations with TiO_2, Fe_2O_3, P_2O_5, V, Nb, Hf, Ta, Th, U and the REEs, moderate correlations with MgO, Cr and Ni and poor correlations with the remaining elements (Table 5.1, Figure 5.7).

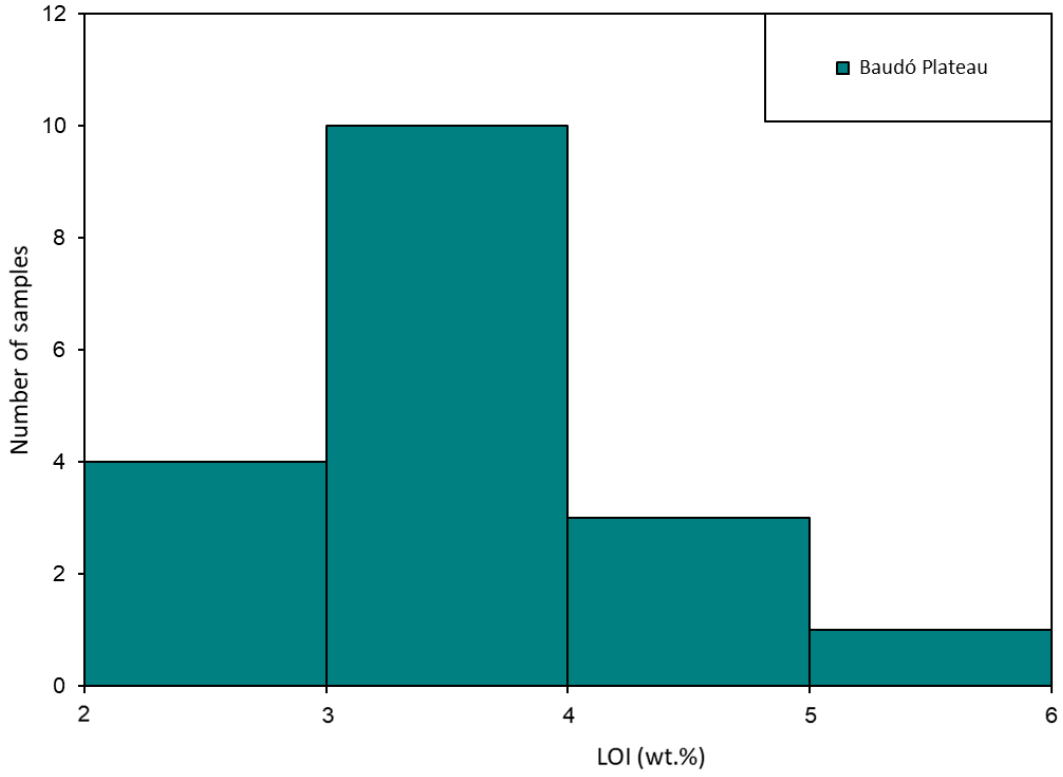

Figure 5.6: Histogram of LOI values for the Baudó Plateau samples

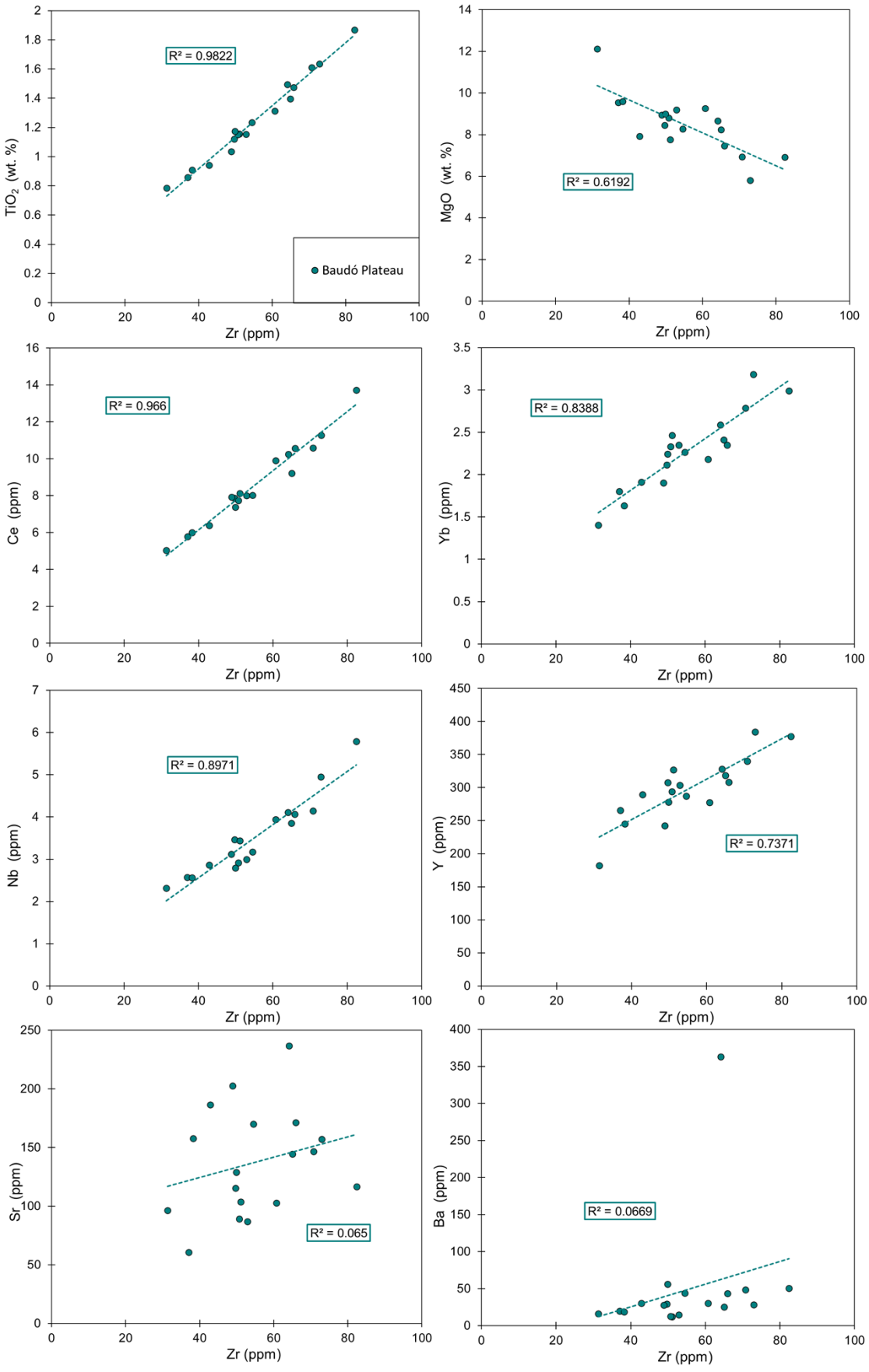

Figure 5.7: Bivariate diagrams of representative elements against Zr for the Baudó Plateau samples

5.2.4 Alteration Summary

As documented in Chapter 3, all groups have undergone significant levels of alteration, with the most alteration seen in the plateau groups. This is reflected in the variable correlations of Zr with major and trace elements shown above.

While some trace elements show good correlations with Zr for most groups, many trace elements show poor to moderate correlations with Zr for most groups. Generally, the REE and HFSE show good to moderate correlations for all groups, but rarely elements such as Nb, Hf, Ta and Th show poor correlations. However, these poor correlations with Zr for immobile trace elements are generally significantly higher than the correlations with Zr for the known mobile elements (e.g., Sr, Ba, K, Pb), which are largely <0.1. Poor correlations between Zr and elements may be caused by clustering of data due to a narrow range of MgO values, slight differences in source compositions or in petrographic processes, including accumulation and fractionation. Overall, the HFSE and REE do not appear to have been significantly mobilised during secondary alteration.

Many of the major elements appear to have become mobile during secondary alteration, as shown by poor to moderate correlations between major elements and Zr for most geochemical groups. SiO2, Na2O and K2O show particularly poor correlations with Zr for most groups, and caution should be exercised when using these elements.

5.3 Classification

Within this section, major and trace elements will be used to classify rocks in terms of their rock types. For this the TAS (Total Alkali Silica) (Le Bas et al., 1986) and Zr/Ti vs Nb/Yb (Pearce, 1996) diagrams will be used. Due to the potential mobility of Na_2O, K_2O and SiO_2, the TAS diagram may not be reliable, and caution must be used when using it for classification with altered samples. The Zr/Ti vs Nb/Yb diagram uses elements which are generally regarded to be immobile up to greenschist facies grades of metamorphism and is more likely to be accurate when used for classification.

5.3.1 Soná-Torio

On the TAS diagram (Figure 5.8A) and the Zr/Ti vs Nb/Y diagram (Figure 5.8B), most samples from all groups from the Soná-Torio region plot within the basalt field. For the Soná-Torio Plateau, most samples plot within the basalt field on the TAS diagram, with two samples lying on the basaltic andesite field boundary (samples JB17-022, JB17-024) and a

single sample lying on the trachybasalt and basaltic trachyandesite field boundary (sample DB15-029). On the Zr/Ti vs Nb/Yb diagram all Plateau samples lie within a tight cluster within the basalt field, confirming that the TAS diagram was affected by K_2O, Na_2O and/or SiO_2 mobility.

On the TAS diagram, most Soná-Torio Enriched Plateau samples plot within the basalt field, with a singular sample (sample JB17-006) plotting in the basaltic andesite field, and one sample plotting above the Alkaline Series line (sample DB15-032). On the Zr/Ti vs Nb/Yb diagram all samples plot in the basalt field with significantly less scatter. For the High-Mg Plateau, there is some scatter on the TAS diagram. Most samples still plot within the basalt field, with many close to the picrobasalt field boundary. The remainder of the samples plot within the picrobasalt field, with one sample plotting in the basanite field (sample DB15-051). On the Zr/Ti vs Nb/Y diagram all samples plot together in the basalt field. As these rocks are ultramafic, they cannot be further classified using these diagrams. The two Proto-arc Group 1 samples plot in different fields on the TAS diagram, with one plotting in the basalt field (sample JB18-023), and the other plotting in the andesite field (sample JB18-008). On the Zr/Ti vs Nb/Y, both samples plot in the basalt field, although one plots close to the basaltic andesite field boundary (sample JB18-008). The Proto-arc Group 2 samples largely plot within the basalt field on the TAS diagram, with one sample plotting within the basaltic andesite field (sample JB17-010), and one in the trachybasalt field (sample DB09-014), both of which lie close to the basalt field boundary.

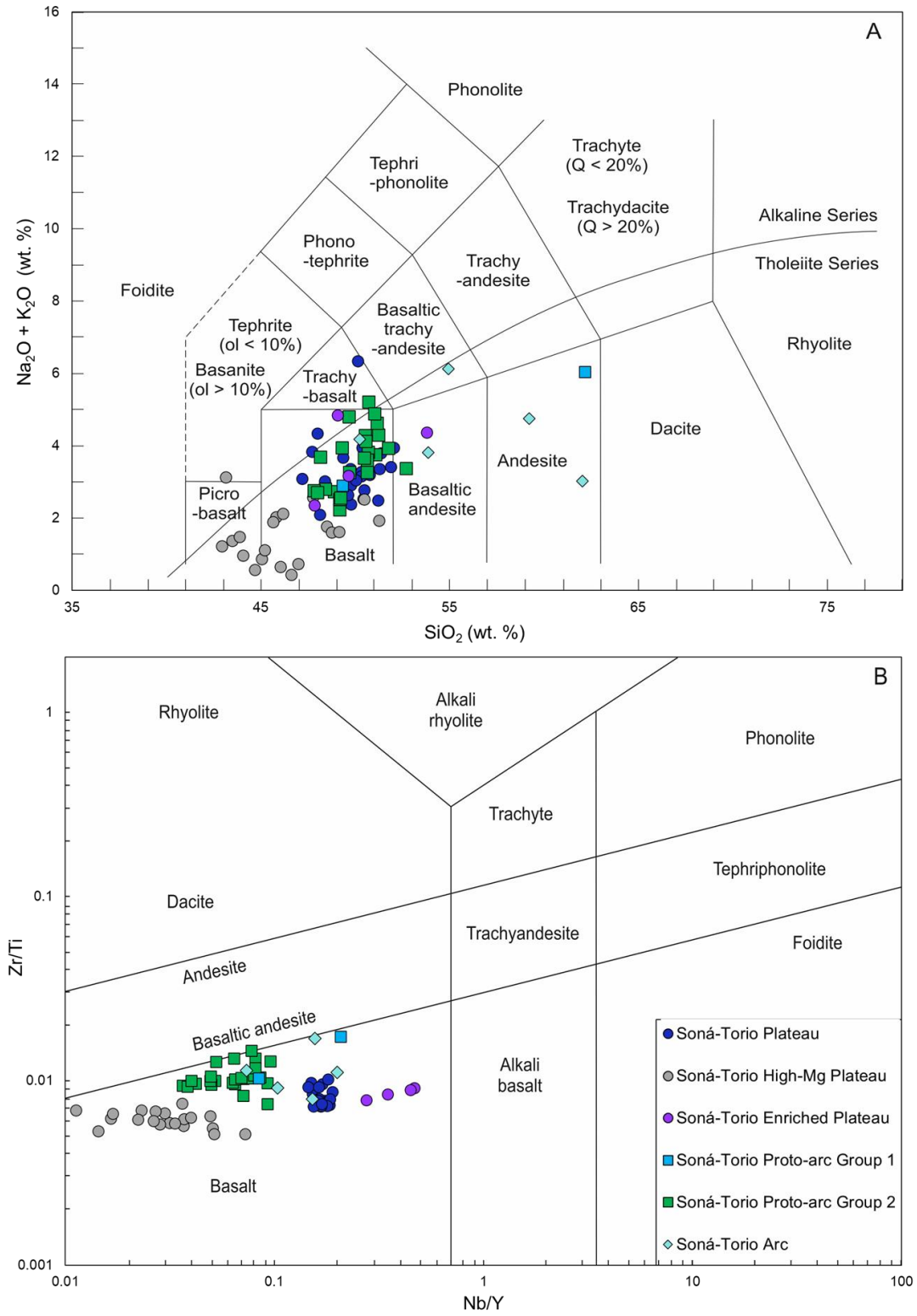

Figure 5.8: A) Total alkali silica classification diagram (Le Bas et al., 1986) and B) Zr/Ti vs Nb/Y classification diagram (Pearce, 1996) for the Soná-Torio region samples

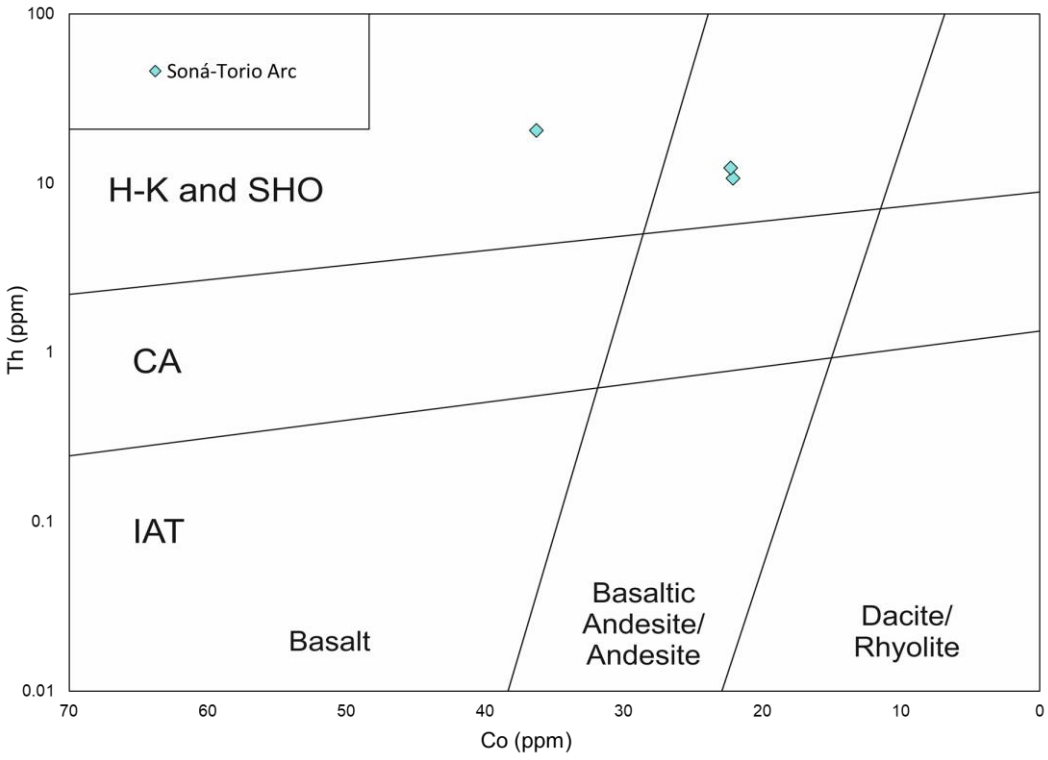

Figure 5.9: Th-Co discrimination diagram (Hastie et al., 2007) with the Soná-Torio Arc samples. IAT = Island arc tholeiite, CA = Calc-alkaline, H-K = High-K calc alkaline, SHO = shoshonitic

On the Zr/Ti vs Nb/Y diagram, the Proto-arc Group 2 samples lie within the basalt field, although some plot along the boundary with basaltic andesite (samples DB10-003, JB17-013, JB18-022). On the TAS diagram, the Arc samples are very scattered, with one sample in the basalt field (sample JB17-023), one in the basaltic andesite field (sample DB09-013), one in the basaltic trachyandesite field (sample JB18-016) and 2 in the andesitic field (samples DB09-012, DB15-028). On the Zr/Ti vs Nb/Y diagram, all Soná-Torio Arc samples plot within the basalt field, although one plots on the basaltic andesite boundary (sample DB15-028). On the Th-Co discrimination diagram of (Hastie et al., 2007), Soná-Torio Arc samples have a high-K calc-alkaline to shoshonitic affinity. One sample has a basaltic composition (sample JB17-023), while two samples have a basaltic andesite to andesitic composition (samples DB15-028, JB18-016).

5.3.2 Darién Pacific Coast

On the TAS diagram (Figure 5.10A) and Zr/Ti vs Nb/Y diagram (Figure 5.10B), the majority of geochemical groups from the Darién Pacific Coast plot within the basalt field. For the Jaqué Plateau, all samples plot within the basalt field on both diagrams, although they are more clustered on the Zr/Ti vs Nb/Y diagram. Depleted Plateau samples plot within the

basalt field on the TAS diagram, with one sample on the boundary of the basaltic andesite field (sample JB17-063). On the Zr/Ti vs Nb/Y diagram, all samples plot in a distinct cluster in the basalt field. Enriched Plateau samples also plot within the basalt field on both the TAS diagram and Zr/Ti vs Nb/Y diagram, but are more clustered on the Zr/Ti vs Nb/Y diagram. For the Proto-arc, all samples are scattered in the basalt field on the TAS diagram, and are clustered in the basalt field on the Zr/Ti vs Nb/Y diagram. Compared to the other geochemical groups, the arc samples show a larger diversity of rock types across both diagrams. The Arc Group 1 sample plots within the basalt field on both the TAS and Zr/Ti vs Nb/Y diagrams, close to the samples of the plateau groups and proto-arc. On the Th-Co diagram, the Arc Group 1 sample has a dacitic to rhyolitic composition with and island arc tholeiite affinity. Arc Group 2 samples are scattered across the TAS diagram, with three samples plotting within the trachybasalt field (samples JB17-050, JB17-052, JB17-053), one plotting in the basaltic andesite field (sample JB18-076), one within the basaltic trachyandesite field (sample JB17-051), one in the andesite field (sample JB18-064) and the remainder in the dacite field. On the Zr/Ti vs Nb/Y diagram, three samples plot in the basalt field, close to the samples of the Proto-arc (samples JB17-050, JB17-052, JB17-053), three samples plot in the basalt field close to the basaltic andesite boundary (samples JB17-051, JB18-064, JB18-076), two samples plot within the basaltic andesite field (samples JB17-055, JB17-060) and one plots within the trachyandesite field (sample JB18-063). On the Th-Co diagram, three samples have a dacitic to rhyolitic composition: two of these samples have a calc-alkaline affinity (samples JB17-050, JB17-055) while one plots just below the calc-alkaline boundary with an island-arc tholeiite affinity (sample JB17-052). The remainder of the Arc Group 2 samples have a basaltic andesite to andesitic composition on the Th-Co diagram. Five of these samples plot have a calc-alkaline affinity (samples JB17-051, JB17-053, JB17-060, JB18-063, JB18-064), while one has a high-K calc-alkaline to shoshonitic affinity (sample JB18-076). Arc Group 3 is composed of two samples, one of which plots in the dacite field (sample JB18-072), with the other in the trachyte field, on the boundary with

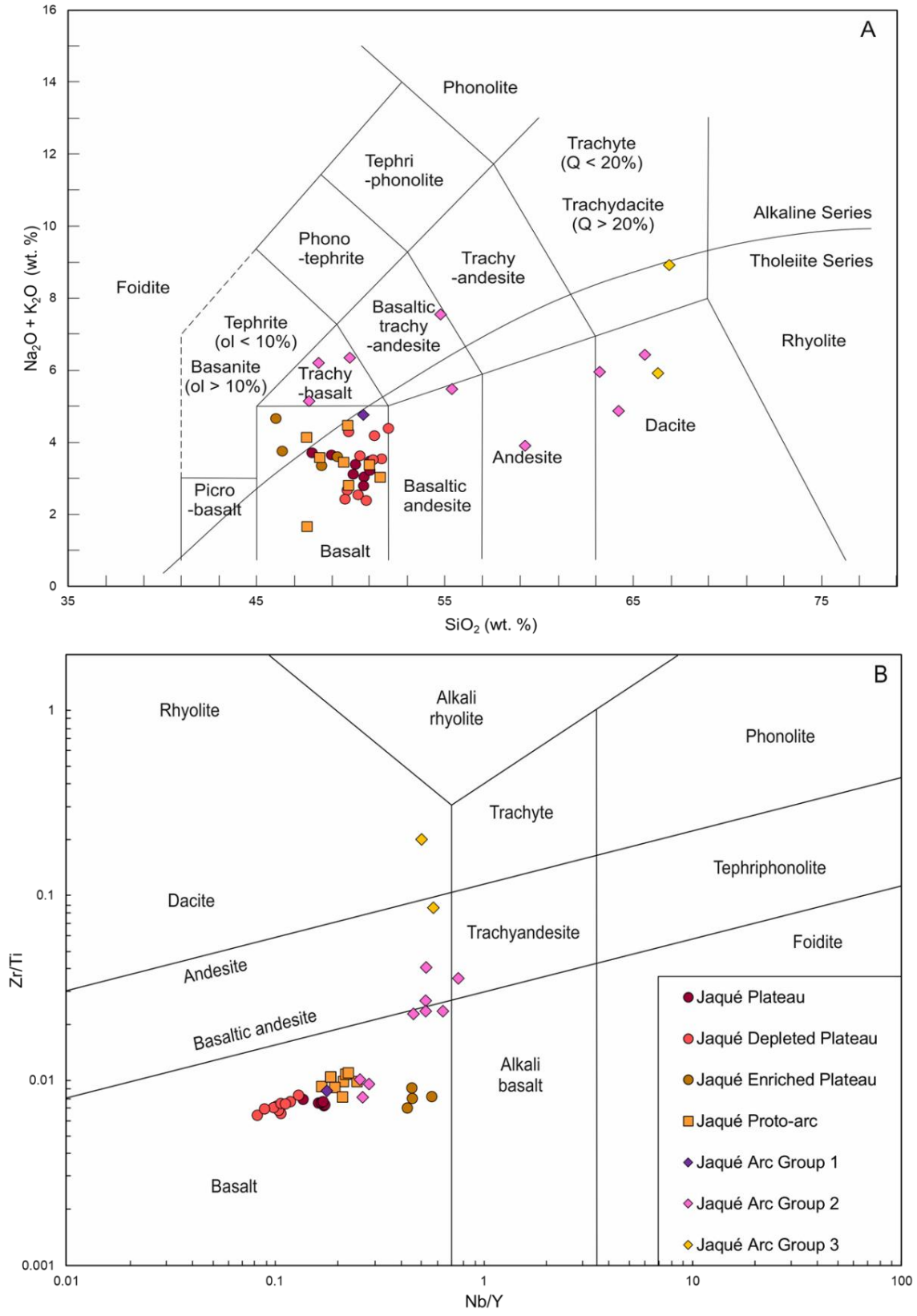

Figure 5.10: A) Total alkali silica classification diagram (Le Bas et al., 1986) and B) Zr/Ti vs Nb/Y classification diagram (Pearce, 1996) for the Darién Pacific Coast region samples

the alkaline series boundary (sample JB17-064) on the TAS diagram. On the Zr/Ti vs Nb/Y diagram, one sample plots within the andesite field (sample JB18-072) with the other in the dacite field (sample JB17-064). On the Th-Co diagram, both Arc Group 3 samples have a dacitic to rhyolitic composition with a calc-alkaline affinity.

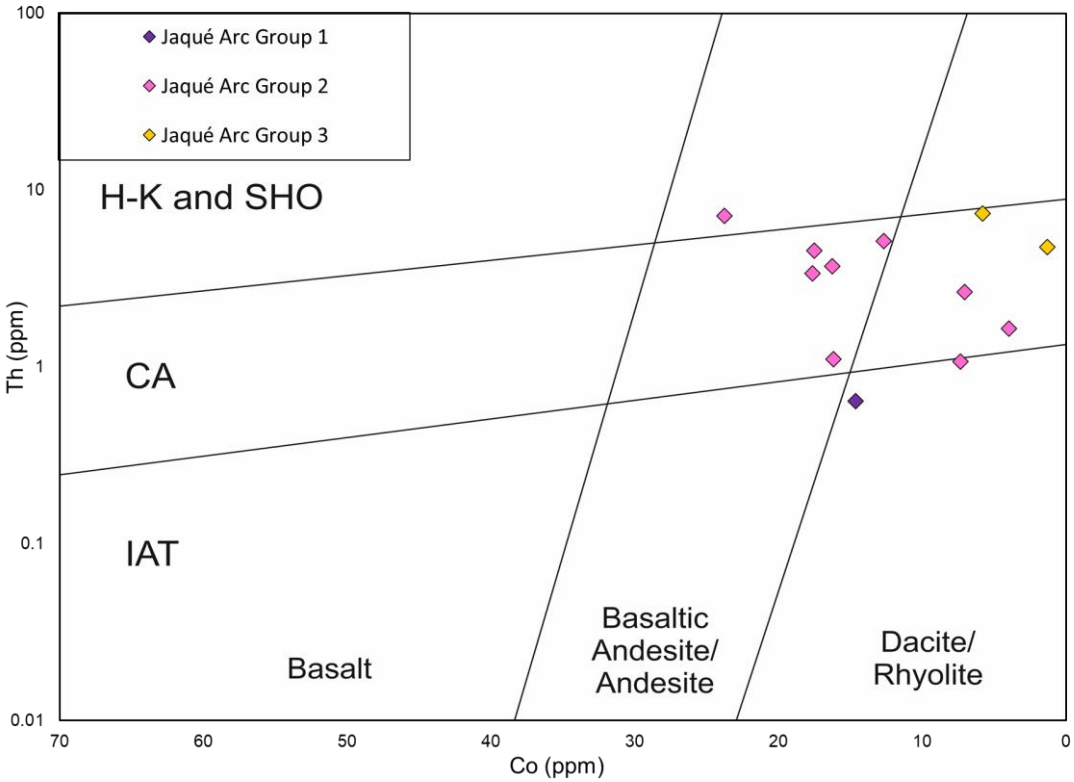

Figure 5.11: Th-Co discrimination diagram (Hastie et al., 2007) with the Jaqué Arc Groups 1-3 samples. IAT = Island arc tholeiite, CA = Calc-alkaline, H-K = High-K calc alkaline, SHO = shoshonitic

5.3.3 Serranía de Baudó

For the Serranía de Baudó Plateau samples, all lie within the basalt field on the TAS diagram (Figure 5.12A), with some plotting close to the basaltic andesite field boundary. On the Zr/Ti vs Nb/Y diagram (Figure 5.12B), all samples are clustered in the centre of the basalt field.

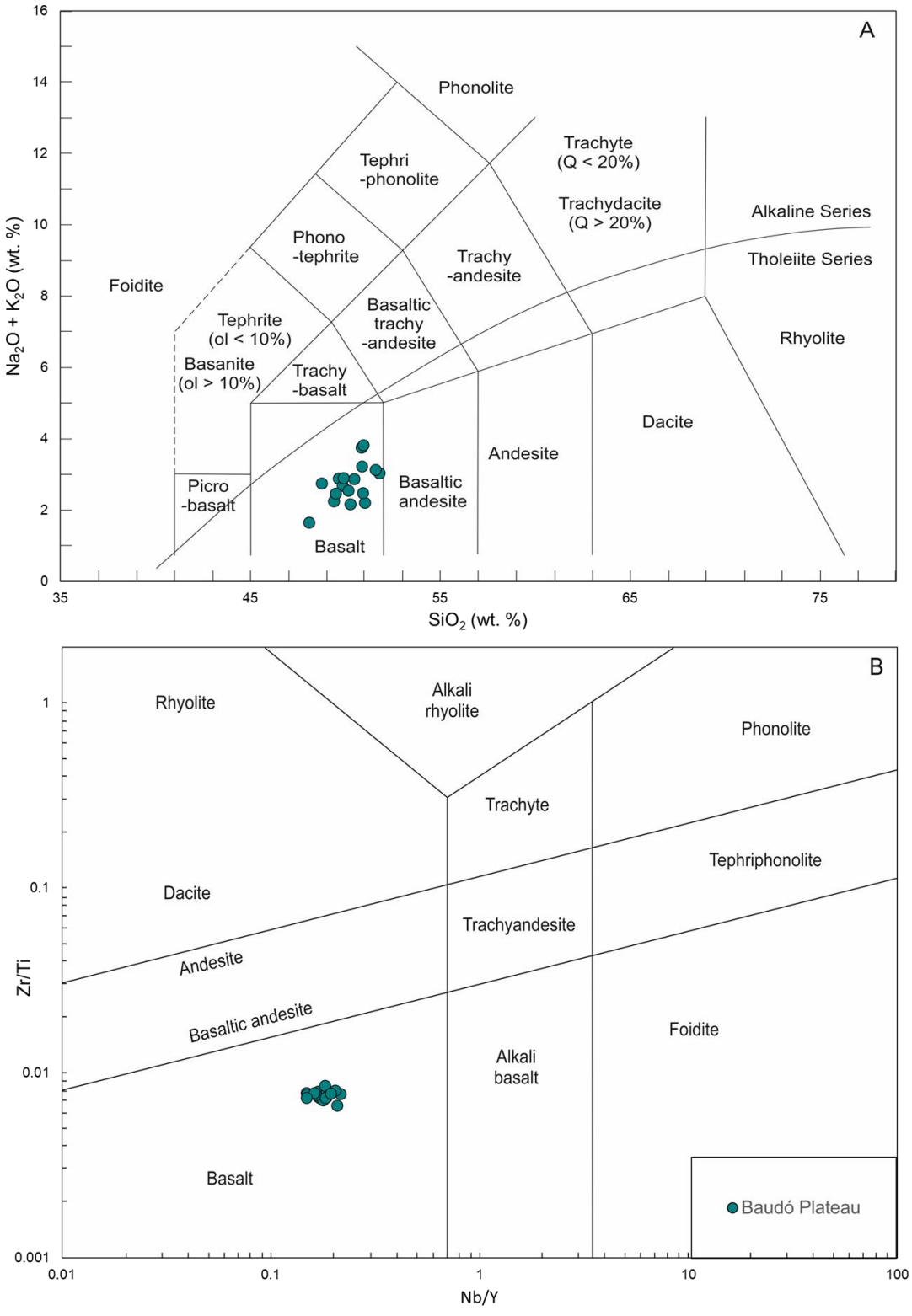

Figure 5.12: A) Total alkali silica classification diagram (Le Bas et al., 1986) and B) Zr/Ti vs Nb/Y classification diagram (Pearce, 1996) for the Serranía de Baudó region samples

5.4 **Major Elements**

In this section, the major element characteristics are presented for each geochemical group in each region. Samples from this study have been plotted alongside previously analysed samples from the same geochemical groups, to better assess the characteristics of each group. For the Soná-Torio region, these results are compiled from the studies of Lissinna (2005), Worner et al. (2009), Buchs et al. (2010) and Wegner et al. (2011). For the Darién Pacific Coast region, results are compiled from the studies of Lissinna (2005) and Cavell (unpublished). For the Serranía de Baudó, compiled data is from Kerr et al. (1997).

As previously discussed, as these rocks are altered, some major elements (such as SiO_2, K_2O) are mobile and measured values may not be indicative of igneous processes only. Therefore, much of the discussion is focussed on TiO_2, Al_2O_3, CaO, MgO and Fe_2O_3, which are more likely to accurately represent the geochemical groups and the geochemical processes which these groups may have undergone.

5.4.1 Soná-Torio

Overall, the geochemical groups of the Soná-Torio region have similar major element ranges, with the exception of High-Mg Plateau, which has much higher MgO values (Figure 5.13). Most groups have relatively narrow ranges of major elements, although the major elements identified as being the most mobile tend to show the most variability in concentration.

The Soná-Torio Plateau samples have been plotted alongside previously analysed samples of Lissinna (2005) and Buchs et al. (2010). Combined, these samples have ranges of 6.44 – 9.80 wt. % MgO, and 0.99 – 1.58 wt. % TiO_2 (Figure 5.13**Error! Reference source not found.**). Fe_2O_3, Al_2O_3 and CaO contents range from 9.36 – 14.23 wt. %, 13.00 – 15.13 wt. % and 8.54 – 13.74 wt. % respectively. Generally, the samples are clustered, and do not show clear trends of major element concentration with increasing MgO values. However, with increasing values of MgO, Soná-Torio Plateau samples and show a slight decrease in TiO_2 (Figure 5.13). Soná-Torio Enriched Plateau samples have again been plotted with previously analysed samples of Lissinna (2005) and Buchs et al. (2010). The Enriched Plateau samples have ranges similar to Plateau for most major elements, with slightly lower MgO values of 3.38 – 8.21 wt. %, and more variable TiO_2 (2.08 – 4.20 wt. %) (Figure 5.13). Fe_2O_3 ranges from 10.72 – 17.09

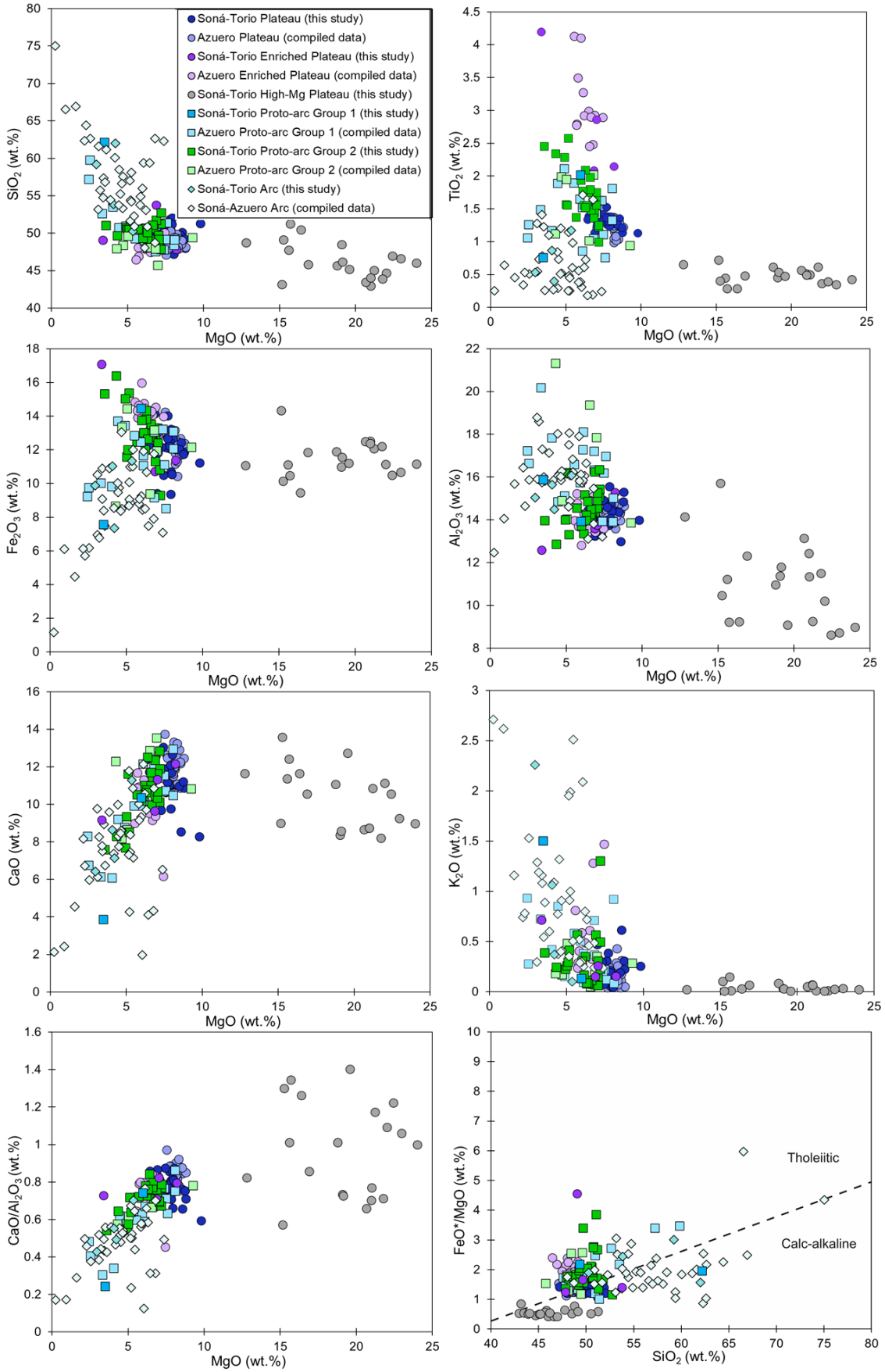

Figure 5.13: Bivariate diagrams of selected major elements vs MgO for the Soná-Torio samples

wt. %, Al_2O_3 ranges from 12.59 – 15.28 wt. %, and CaO contents ranges from 6.17 – 12.57 wt. %. With increasing MgO values, samples of the Enriched Plateau show strongly decreasing TiO_2 and Fe_2O_3 values and increasing CaO values. The Soná-Torio High-Mg Plateau samples are distinct from the remainder of the groups in MgO values, with a wide range from 12.8 – 24.0 wt. % MgO (Figure 5.13). The High-Mg Plateau samples also have lower TiO_2 values than the other plateau and proto-arc groups, with a narrow range of 0.28 – 0.72 wt. % TiO_2 (Figure 5.13). For the remainder of elements, the range is similar to the other plateau and proto-arc groups, with ranges of 9.45 – 14.34 wt. % Fe_2O_3, 8.62 – 15.71 wt. % Al_2O_3 and 8.19 – 13.59 wt. % CaO. Samples of the High-Mg plateau do not show clear trends with increasing MgO values.

The Proto-arc Groups overlap with the Soná-Torio Plateau and Enriched Plateau groups in most major elements. The Proto-arc Group 1 samples are plotted with previously analysed samples from Lissinna (2005) and Buchs et al. (2010) (Figure 5.13). While some of these samples were considered to be part of the Azuero Proto-arc (Buchs et al., 2010), other samples were considered to be part of the arc, or an accreted ocean island (Lissinna, 2005). Together, the samples of the Proto-arc Group 1 have ranges of 3.32 – 8.08 wt. % MgO and 0.76 – 2.12 wt. % TiO_2 (Figure 5.13). Fe_2O_3, Al_2O_3 and CaO range from 7.57 – 14.46 wt. %, 13.93 – 20.18 wt. % and 2.44 – 12.96 wt. % respectively (Figure 5.13). Generally, the samples of the Proto-arc Group 1 are scattered and do not show clear tends with increasing MgO contents. However, with increasing MgO, SiO_2, Al_2O_3 and K_2O decrease, and CaO increases (Figure 5.13). Soná-Torio Proto-arc Group 2 samples have been plotted alongside previously analysed data of the Proto-arc Group 2 from Lissinna (2005), Worner et al. (2009) and Buchs et al (2010). Some of these samples were considered to be part of the proto-arc (Buchs et al., 2010), while others were considered to be part of the Caribbean Oceanic Plateau (Wörner et al., 2009) or an ocean island basalt (Lissinna, 2005). Overall, the samples of Proto-arc Group 2 of have similar ranges to Proto-arc Group 1 samples, with TiO_2 and MgO values ranging from 0.94 – 2.57 wt. %, and 3.57 – 9.25 wt. % respectively (Figure 5.13). Samples also have ranges of 8.65 – 16.40 wt. % Fe_2O_3, 12.87 – 21.33 wt. % Al_2O_3 and 7.58 – 13.54 wt. % CaO. Proto-arc Group 2 samples show increasing CaO values and decreasing TiO_2, Fe_2O_3 and Al_2O_3 values with increasing MgO (Figure 5.13). The Soná-Torio Arc has been plotted with previously analysed Arc samples of Lissinna (2005), Worner et al. (2009), Buchs et al. (2010) and Wegner et al. (2011). Arc samples are distinct from the other groups in some major element values. Samples have a relatively narrow range of TiO_2 (values of 0.18 – 1.71 wt. %) and MgO (values of 0.24 – 7.37 wt. %) (Figure 5.13), with ranges of 1.16 – 13.34 wt.%, 12.47 – 18.59 wt. % and 1.98 – 12.14 wt. % for

Fe_2O_3, Al_2O_3 and CaO respectively. With increasing MgO values, Arc samples are generally scattered but show trends of decreasing SiO_2 and increasing Fe_2O_3.

On a graph of SiO_2 vs FeO*/MgO (Figure 5.13), the Plateau, Enriched Plateau and Proto-arc Group 2 samples are clustered across the tholeiitic/calc-alkaline boundary. Samples of the Proto-arc Group 1 are also scattered across the boundary, with most samples plotting in the tholeiitic domain. However, sample JB18-008 plots in the calc-alkaline domain. Samples of the Arc group are again scattered across the tholeiitic/calc-alkaline boundary, but the majority of samples plot in the calc-alkaline array. On a graph of MgO vs CaO/Al_2O_3 (Figure 5.13), samples of the Proto-arc Group 1, Proto-arc Group 2 and Arc lie on a clear trendline, which displays increasing CaO/Al_2O_3 with increasing MgO and may represent evidence of clinopyroxene fractionation. The Plateau and Enriched Plateau samples plot at the top of this trendline, but are clustered and do not show any trend clear trend with increasing MgO value. High-Mg Plateau samples are scatted and do not show a trend with increasing MgO value (Figure 5.13).

5.4.2 Darién Pacific Coast

The geochemical groups of the Darién Pacific Coast region generally have narrow ranges of major elements, with more variability in the most mobile elements. Most groups have similar values for most major elements, although the arc groups tend to be distinct from the plateau and proto-arc groups in major elements including SiO_2 and K_2O (Figure 5.14). The Jaqué Plateau has been plotted with a single previously analysed plateau sample from Lissinna (2005). Most samples of the Jaqué Plateau plot within a narrow range of MgO between 7.56 – 8.96 wt. %, while a distinct sample (sample DB16-043) has a lower MgO value of 4.13 wt. % (Figure 5.14). Similarly, most samples lie within the narrow range of TiO_2 between 1.20 and 1.40 wt. %, and sample DB16-043 has a value of 2.42 wt. % (Figure 5.14). For the remainder of major elements, most samples lie within narrow ranges, with 11.12 – 13.07 wt. % Fe_2O_3, 13.63 – 14.72 wt. % Al_2O_3 and 9.43 – 12.10 wt. % CaO. Sample DB16-043 has higher Fe_2O_3 (15.47 wt. %), higher CaO (13.07 wt. %) and lower

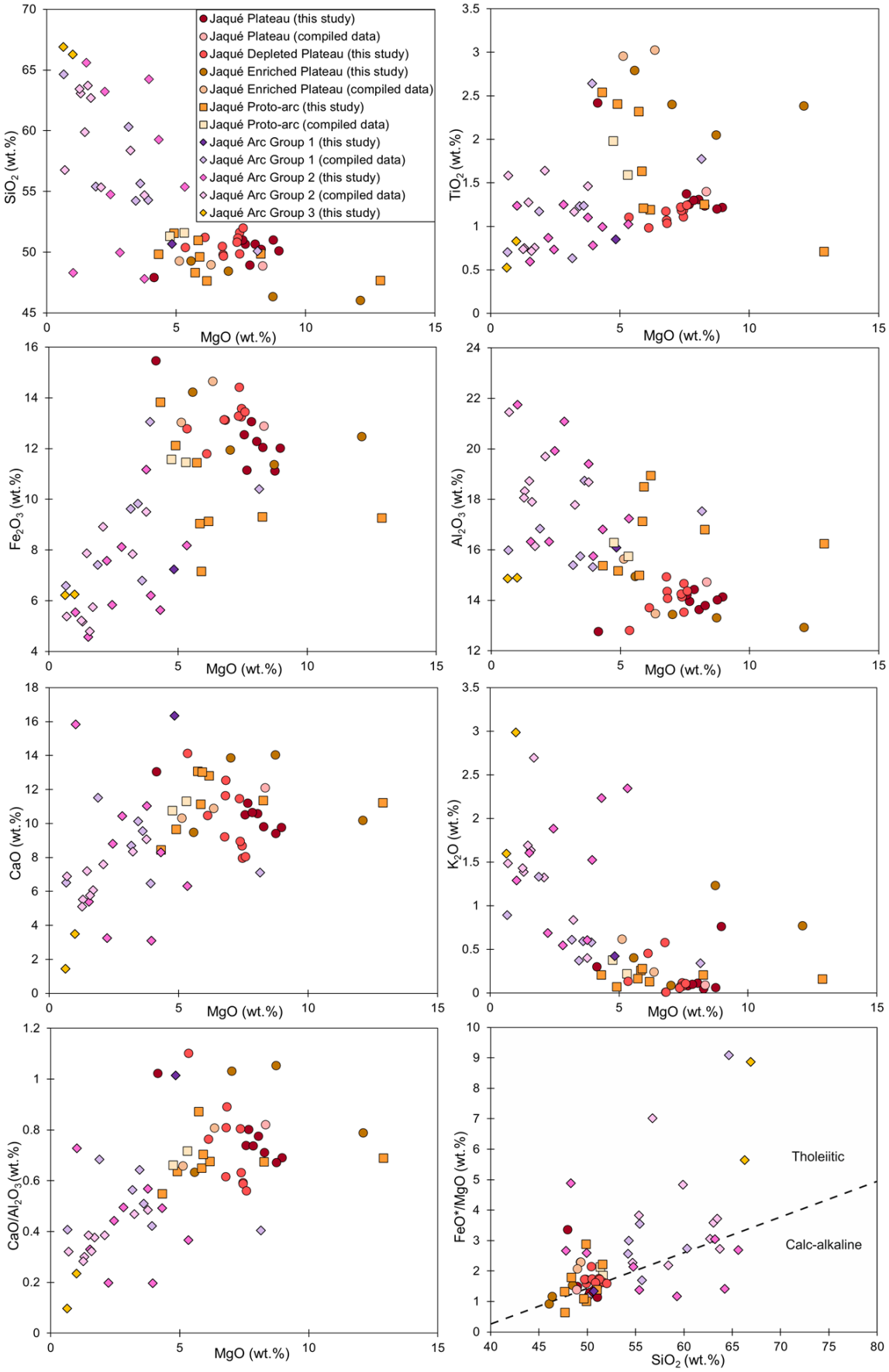

Figure 5.14: Bivariate diagrams of selected major elements vs MgO for the Darién Pacific Coast samples

Al_2O_3 (12.76 wt.%) (Figure 5.14). Overall, for all Plateau samples, MgO values increase with decreasing TiO_2, Fe_2O_3 and CaO values. Depleted Plateau samples again have relatively narrow major element ranges, with MgO and TiO_2 values slightly lower than those of the Jaqué Plateau (Figure 5.14). MgO values range from 5.34 – 7.58 wt. % and TiO_2 values range from 0.99 – 1.25 wt. %, while Fe_2O_3, Al_2O_3 and CaO values range from 11.80 – 14.43 wt. %, 12.82 – 14.94 wt. % and 7.96 – 14.14 wt. % respectively (Figure 5.14). With increasing MgO values, Depleted Plateau samples show scatter for most major elements, but TiO_2 values remain relatively constant and CaO values decrease (Figure 5.14). The Jaqué Enriched Plateau has been plotted with two previously analysed samples from Lissinna (2005). This group also generally has narrow ranges of major element values, with ranges of 11.38 – 14.65 wt. % Fe_2O_3, 12.93 – 14.95 wt. % Al_2O_3 and 9.49 – 14.05 wet. % CaO. Enriched Plateau samples have wider ranges of MgO and TiO_2 than the other plateau groups, with ranges of 5.56 – 12.11 wt. % and 2.05 – 2.80 wt. % values respectively (Figure 5.14). The samples show scatter and there are no clear major element trends with increasing MgO values. The Proto-arc group also has a wider range of MgO values, from 4.31 – 12.88 wt. %, and TiO_2 values, from 0.71 - 2.54 wt. % (Figure 5.14). For the remainder of the major elements, Proto-arc samples have narrow ranges similar to those of the plateau groups, with Fe_2O_3, Al_2O_3 and CaO ranges of 7.16 – 14.65 wt. %, 13.48 – 18.94 wt. % and 8.46 – 13.09 wt. % respectively. Again, with increasing values of MgO contents, there are no clear major elements trends, and samples are scattered (Figure 5.14).

The Arc Groups generally plot together and are distinct in major element values from the plateau and proto-arc groups. The Arc Group 1 sample has been plotted with previously analysed results of Cavell (unpublished). These samples have ranges of 0.65 – 8.15 wt. % MgO, 0.63 – 2.64 wt. % TiO_2, 6.60 – 13.05 wt. % Fe_2O_3, 15.33 – 18.74 wt. % Al_2O_3 and 6.47 – 16.34 wt. % CaO (Figure 5.14). With increasing MgO values, Arc Group 1 samples show decreasing SiO_2 and K2O and increasing Fe_2O_3, with no clear trends for the remainder of the elements. Arc Group 2 samples have been plotted with previously analysed samples of Cavell (unpublished). These samples have ranges similar to those of the Arc Group 1 in most major elements, with ranges of 0.69 – 5.33 wt. % MgO, 0.59 – 1.64 wt. % TiO_2, 4.57 – 11.17 wt. % Fe_2O_3, 15.75 – 21.75 wt. % Al_2O_3 and 3.09 – 15.84 wt. % CaO (Figure 5.14). Arc Group 2 samples show considerable scatter and there are no clear major element trends with increasing MgO. Arc Group 3 is the most evolved group, but most major elements plot within the ranges of the other arc groups, with MgO, TiO_2 and Fe_2O_3 values of 0.63 – 1.00 wt. %, 0.53 – 0.83 wt. % and 6.22 – 6.25 wt. % respectively. However, the Arc Group 3 samples have lower values of Al_2O_3 (14.86 – 14.89 wt. %) and CaO (1.45 – 3.49 wt. %) (Figure 5.14).

On a graph of SiO_2 vs FeO*/MgO (Figure 5.14), samples of the Jaqué Plateau, Depleted Plateau, Enriched Plateau and Proto-arc are clustered together across the tholeiitic/calc-alkaline boundary. However, all Jaqué Arc groups are very scattered. Jaqué Arc Group 1 samples plot across the tholeiitic/calc-alkaline boundary, with most samples plotting above the boundary in the tholeiitic array. Jaqué Arc Group 2 samples again plot across the tholeiitic/calc-alkaline boundary, and samples plot equally across the two domains. The two samples of the Jaqué Arc Group 3 both plot in the tholeiitic domain.

On a graph of MgO vs CaO/Al_2O_3 (Figure 5.14), there is an overall positive trend for all groups, with increasing CaO/Al_2O_3 with increasing MgO. However, the Jaqué Plateau and Depleted Plateau groups show decreasing CaO/Al_2O_3 with increasing MgO. The remainder of individual groups show scatter, and there are no clear trends with increasing MgO (Figure 5.14).

5.4.3 Serranía de Baudó

The Baudó Plateau basalts have been plotted with previously analysed samples of Kerr et al. (1997). Together, these samples have relatively wide ranges of major element values in comparison to the Plateau Groups of the Darién Pacific Coast and the Soná-Torio Plateau. These values range from 5.08 – 12.12 wt. % MgO, 0.57 – 2.91 wt. % TiO_2, 9.24 – 15.43 wt. % Fe_2O_3, 12.90 – 16.91 wt. % Al_2O_3 and 7.98 – 14.53 wt. % CaO (Figure 5.15). With increasing MgO values, TiO_2 and Fe_2O_3 values decrease, and Al_2O_3 and CaO values increase.

On a graph of SiO_2 vs FeO*/MgO, samples of the Baudó Plateau are clustered across the tholeiitic/calc-alkaline boundary. On a graph of MgO vs CaO/Al_2O_3, samples again are clustered, and show no clear trend with increasing MgO contents (Figure 5.15).

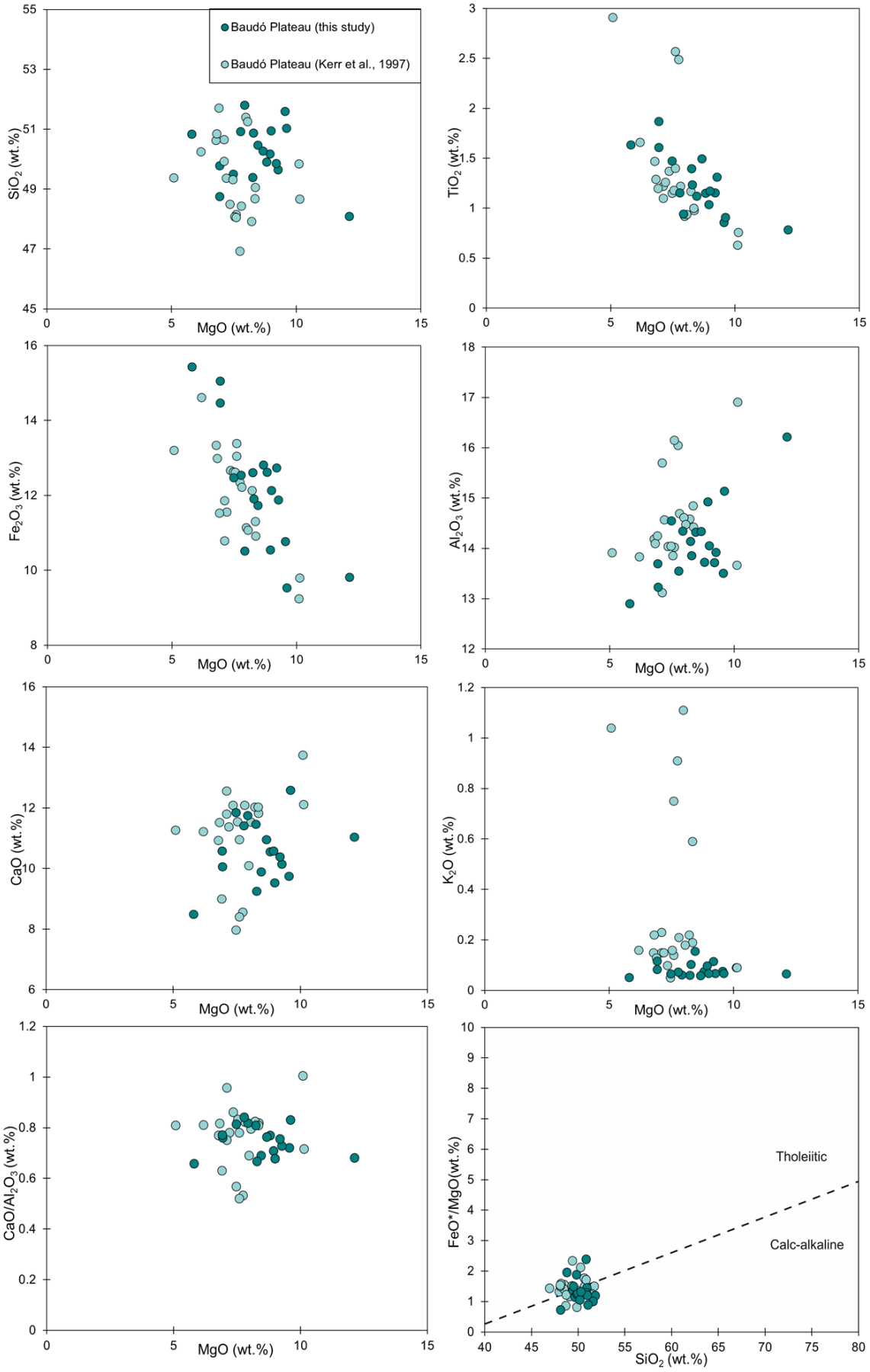

Figure 5.15: Bivariate diagrams of selected major elements vs MgO for the Baudó Plateau

5.5 **Trace Elements**

In this section, the trace element composition will be presented for each geochemical group from the Soná-Torio, Darién Pacific Coast, and Serranía de Baudó regions. Binary plots against MgO will be used to show the geochemical relationships between units for each region, alongside primitive mantle-normalised (Sun and McDonough, 1989) trace element variation diagrams, chondrite normalised (McDonough and Sun, 1995) REE diagrams and incompatible trace element ratio plots. On primitive mantle-normalised multielement diagrams, chondrite normalised REE diagrams, and incompatible trace element diagrams, geochemical groups from this study will be plotted with samples from previous studies (Lissinna 2005; Wörner et al. 2009; Buchs et al. 2010; Wegner et al. 2011; Cavell, unpublished).

5.5.1 Soná-Torio

On binary plots of trace element vs MgO contents, most geochemical groups of the Soná-Torio region have similar values, with the exception of the High MgO group (Figure 5.16). Most Soná-Torio Plateau samples lie within a narrow range of values for many of the trace elements (La = 2.33 – 5.05 ppm, Yb = 1.92 – 3.21 ppm) (Figure 5.16). Enriched Plateau samples generally have a wider range of trace element contents, with higher values particularly in the LREE and Th, Nb and Ta (La = 7.79 – 22.52 ppm, Yb = 2.20 – 4.34 ppm) (Figure 5.16). High-Mg Plateau samples have moderate to low values of HREE, with very low values of the LREE, Th, Nb and Ta (La = 0.14 – 0.80 ppm, Lu = 0.91 – 2.36 ppm) (Figure 5.16). This group also has very high values of Ni, and Cr. The Proto-arc Group 1 samples lie within a narrow range for most of the trace elements, with a wider range for HREE (La = 3.24 – 9.35 ppm, Yb = 1.82 – 4.86 ppm) (Figure 5.16). The Proto-arc Group 2 samples also generally have a wider range of trace element contents, similar to those of the Proto-arc Group 1 (La = 2.11 – 7.44 ppm, Yb = 2.51 – 6.04 ppm) (Figure 5.16). The Arc Group shows wide ranges of the LREE, HREE and Th, with a narrow range of both Nb and Ta. LREE contents reach to values higher than those of the Plateau and Proto-arc Group 1 and 2, whereas HREE contents reach to lower values (La = 2.29 – 19.20 ppm, Lu = 0.71 – 5.26 ppm) (Figure 5.16).

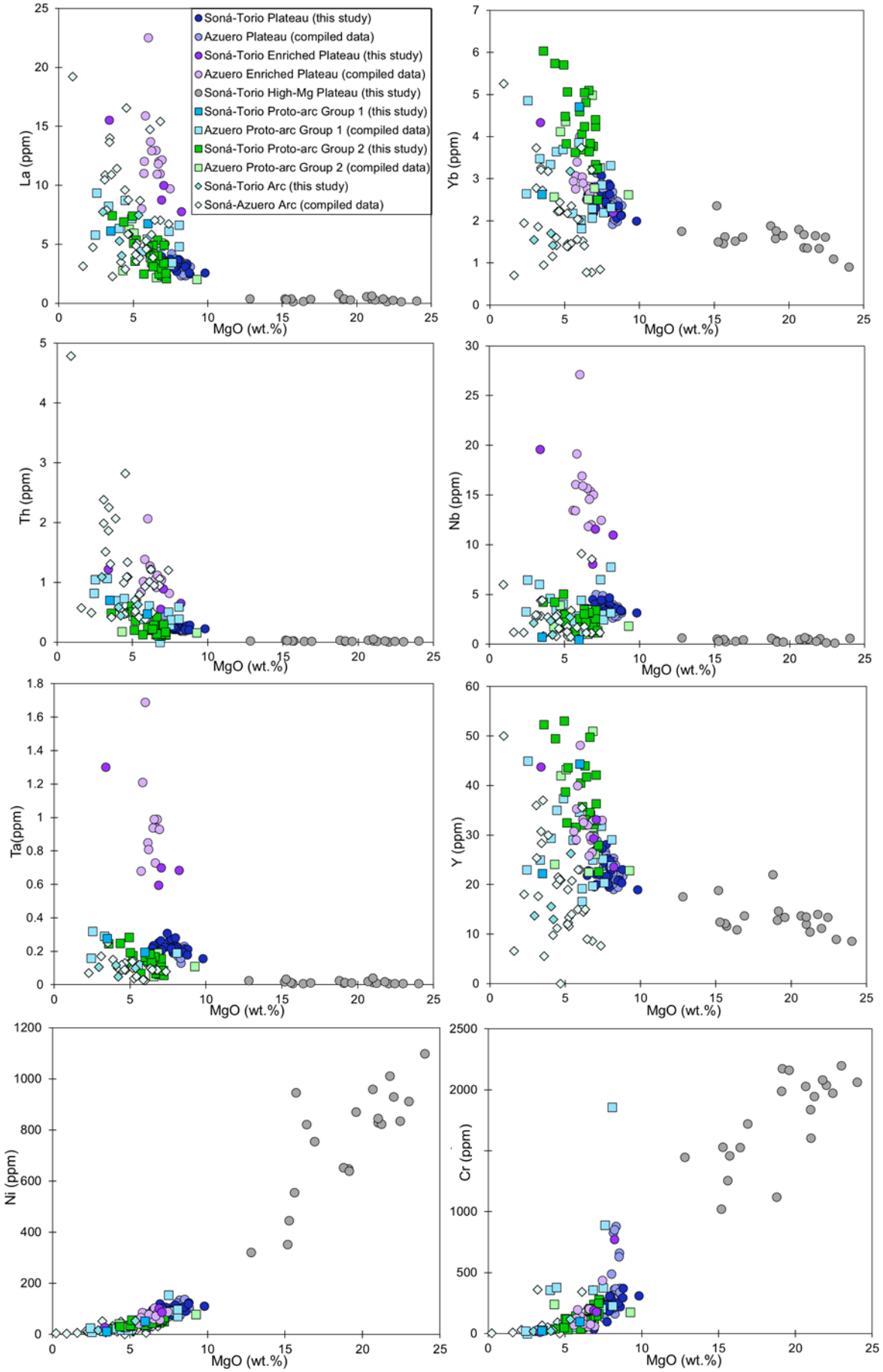

Figure 5.16: Bivariate diagrams of representative trace elements vs MgO for the Soná-Torio samples

Samples from Soná-Torio Plateau, Enriched Plateau and Proto-arc Group 1 and 2 show negative correlations between the REE and MgO contents. Samples of the Arc are generally scattered and do have a clear correlation. All groups (excluding the High-Mg Plateau) also show negative correlations for Th vs MgO, and a positive correlation for Ni vs MgO (Figure 5.16). For samples of the High-Mg Plateau, there is no correlation between most trace elements and MgO, as these trace elements are highly depleted with little variation. However, despite being pervasively recrystallised in thin section, these samples have preserved olivine fractionation/accumulation trends, shown by strong positive correlations between MgO and Cr and Ni. (Figure 5.16).

On chondrite normalised REE plots, Soná-Torio Plateau samples have flat REE patterns (Figure 5.17B). On primitive mantle-normalised multielement plots, the Soná-Torio Plateau samples have flat patterns ($La/Sm_{(PMn)}$ values of 0.63 – 0.95 and $Dy/Yb_{(PMn)}$ of 0.95 – 1.18) with a positive Nb anomaly (Figure 5.17A). Enriched Plateau samples have enriched signatures on chondrite normalised REE plots (Figure 5.17D), and on primitive mantle-normalised multielement plot (Figure 5.17C), samples have enriched profiles with slightly positive Nb anomalies, and $La/Sm_{(PMn)}$ ranging from 1.08 - 1.15, and $Dy/Yb_{(PMn)}$ from 1.35 – 1.48. Soná-Torio High-Mg Plateau samples are highly depleted in the LREE and on a chondrite normalised REE plot, they have flat HREE trends with highly depleted LREE (Figure 5.17F). On primitive mantle-normalised multielement diagrams (Figure 5.17E), samples again have flat to slightly depleted HREEs ($Dy/Yb_{(PMn)}$ = 0.80-1.20), are very depleted in Th and LREEs ($La/Sm_{(PMn)}$ = 0.14 – 0.41), and most samples have slight positive Nb anomalies.

The Proto-arc Group 1 samples have flat to LREE enriched patterns on a chondrite normalised REE diagram (Figure 5.18B). On a primitive mantle-normalised multielement diagram (Figure 5.18A), samples have relatively flat to slightly enriched signatures, with slight Ti negative anomalies, variable Nb negative anomalies, and variable negative to positive Th anomalies. $La/Sm_{(PMn)}$ values of the Proto-arc Group 1 samples ranges from 0.91 – 1.30 and from 1.07 – 1.09 for $Dy/Yb_{(PMn)}$ values. Proto-arc Group 2 samples have slightly depleted signatures on the chondrite normalised REE diagram (Figure 5.18D), with flat HREEs and a depletion of LREEs. On a primitive mantle-normalised multielement diagram (Figure 5.18C), samples have similar depleted patterns with $La/Sm_{(PMn)}$ ranging from 0.41 to 0.73 and $Dy/Yb_{(PMn)}$ ranging from 1.05 – 1.16, along with slight Ti depletions, Nd negative anomalies, and variable negative to positive Th anomalies.

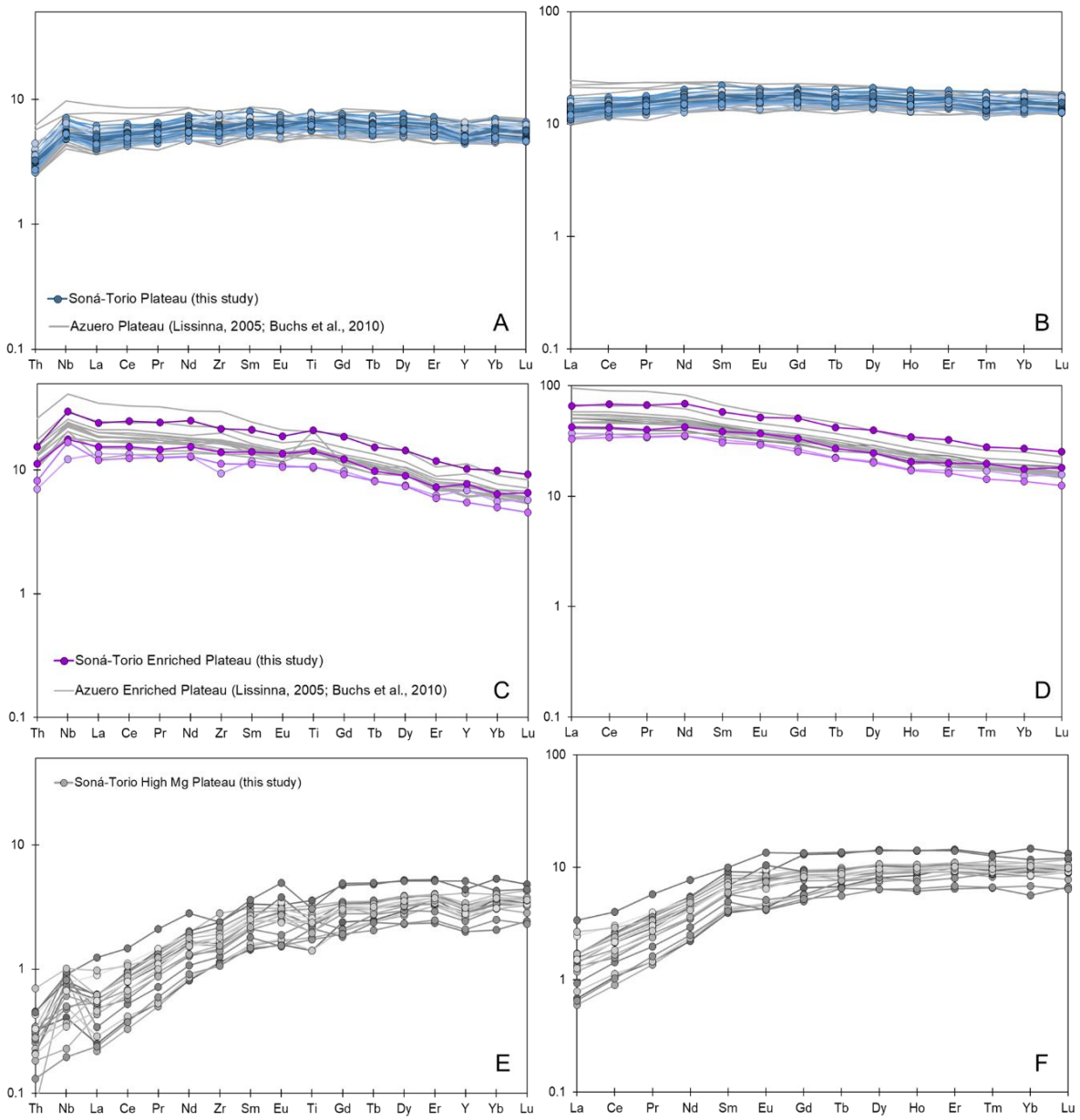

Figure 5.17: Primitive mantle-normalised multi-element diagrams (A, C, E) and chondrite normalised REE plots (B, D, F) for the Soná-Torio plateau groups. Compiled data of the Azuero Plateau shown for in grey in A-D. Plateau data compiled from (Lissinna, 2005; Wörner et al., 2009; Buchs et al., 2010), Enriched Plateau data compiled from (Lissinna, 2005; Buchs et al., 2010)

Samples of the Soná-Torio Arc have slight enriched patterns on chondrite normalised REE plots (Figure 5.18F). On a primitive mantle-normalised multielement diagram (Figure 5.18E), Arc samples are enriched ($La/Sm_{(PMn)}$ = 1.32 – 1.92, $Dy/Yb_{(PMn)}$ = 0.93 – 1.11), with variable Ti negative anomalies, Zr negative anomalies, and marked Nb negative anomalies.

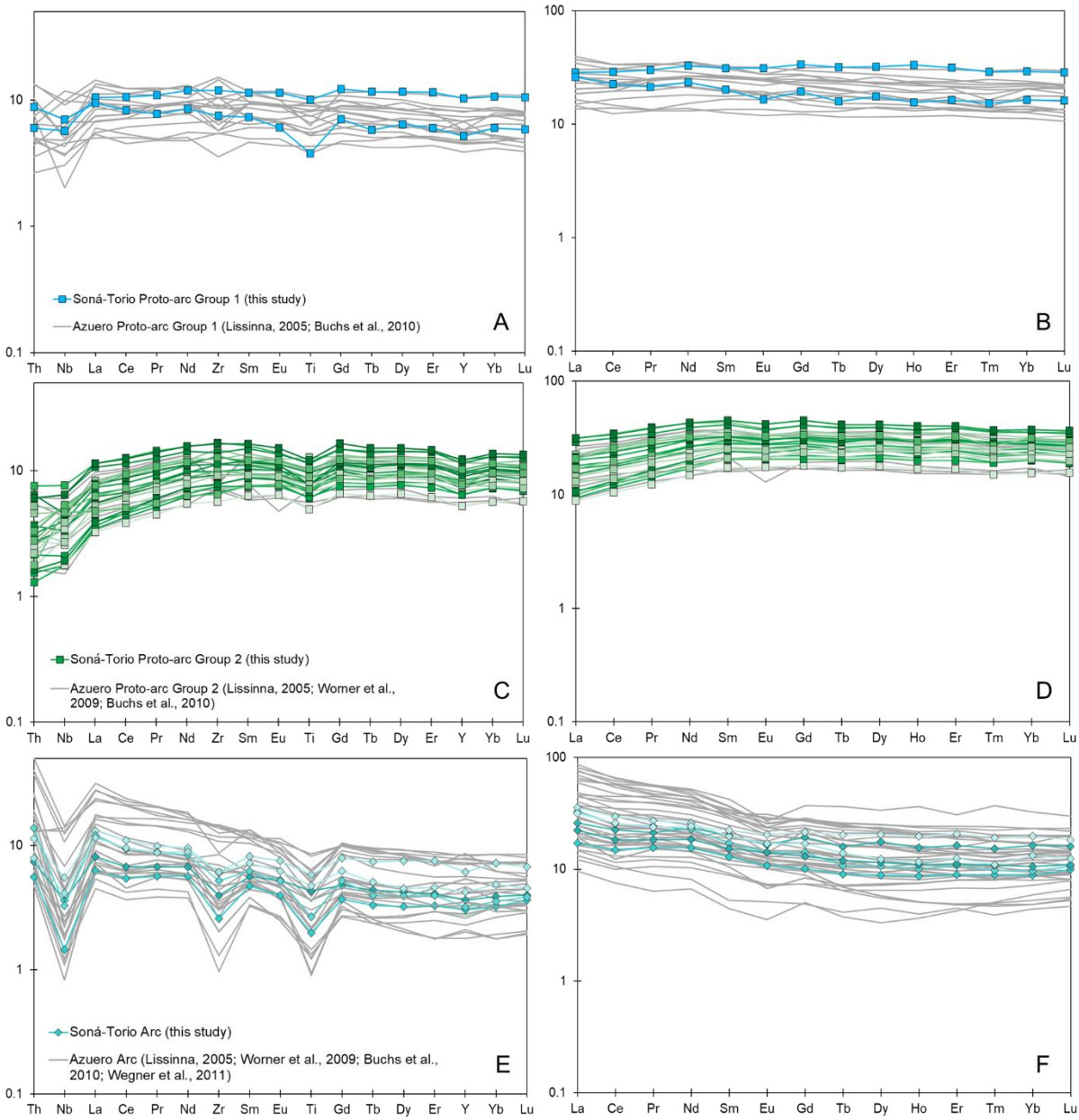

Figure 5.18: Primitive mantle-normalised multi-element diagrams (A, C, E) and chondrite normalised REE plots (B, D, F) for the Soná-Torio proto-arc and arc groups. Compiled data of the Azuero Proto-arc and Arc shown in grey in A-F. Proto-arc Group 1 data compiled from (Lissinna, 2005; Buchs et al., 2010), Soná-Torio Proto-arc Group 2 data from (Lissinna, 2005; Wörner et al., 2009; Buchs et al., 2010) and Arc data from ((Lissinna, 2005; Wörner et al., 2009; Buchs et al., 2010; Wegner et al., 2011)

On the Th/Yb vs Nb/Yb diagram (Figure 5.19A) Soná-Torio Plateau samples lie in the MORB-OIB array, between N-MORB and E-MORB. One sample (AZ-21 -1, Lissinna (2005)) lies on the upper margin of the MORB-OIB array. On the TiO_2/Yb vs Nb/Yb diagram (Figure 5.19B), most samples lie within the upper portion of the MORB array, lying across the boundary between the N-MORB and E-MORB arrays. One sample (DB05-080, Buchs et al., 2010) lies very close to N-MORB. On the Nb/Y vs Zr/Y diagram (Figure 5.19C), all samples plot within the Oceanic Plateau Basalt array, although many samples plot on the lower

margin. On the Zr/Nb vs Nb/Th (Figure 5.19D) plot, all samples lie within the Oceanic Plateau Array, with many overlapping the field between Oceanic Plateau and N-MORB. On the Dy/Yb vs Dy/Dy* diagram (Figure 5.19E), Plateau samples plot within the MORB array, towards the LREE depleted end of the field. On the La/Sm vs V/Ti diagram (Figure 5.19F), Soná-Torio Plateau samples are clustered centrally, between the Proto-arc Groups.

On the Th/Yb vs Nb/Yb diagram (Figure 5.19A), samples of the Enriched Plateau plot within the MORB-OIB array, close to E-MORB. On the TiO_2/Yb vs Nb/Yb plot (Figure 5.19B), samples plot in the tholeiitic OIB array, within the plume-ridge interaction section. On the Zr/Y vs Nb/Y diagram (Figure 5.19C), most samples lie within the Oceanic Plateau array, although some lie outside of the array boundary, close to the OIB array. On the Nb/Th vs Zr/Nb plot (Figure 5.19D), samples lie centrally in the Oceanic Plateau Basalt array, with lower Zr/Nb than the Soná-Torio Plateau samples. On the Dy/Yb vs Dy/Dy* diagram (Figure 5.19E), Soná–Torio Enriched Plateau samples plot between the MORB and OIB arrays, indicating a control of garnet in the source. On the La/Sm vs V/Ti diagram (Figure 5.19F), Soná-Torio Enriched Plateau samples are clustered, below Proto-arc Group 1 samples.

On the Nb/Yb vs Th/Yb diagram (Figure 5.19A), samples of the Soná-Torio High-Mg Plateau largely plot within the MORB-OIB array, with low values of both Nb/Yb and Th/Yb. On the TiO_2/Yb vs Nb/Yb diagram (Figure 5.19B), most samples plot within the MORB array, to the left of N-MORB, with 2 samples lying below the MORB array (samples JB17-002, JB17-003). On the Nb/Y vs Zr/Y plot (Figure 5.19C), samples of the High-Mg Plateau plot across the Plume Source boundary line, with some samples plotting inside the depleted section of the Oceanic Plateau array. On the Zr/Nb vs Nb/Th diagram (Figure 5.19D), samples are very scattered, with high Zr/Nb values and a wide range of Nb/Th. This scatter is likely due to inaccurate measurements at very low concentrations. Samples largely plot within, and close to, the N-MORB array. On the Dy/Yb vs Dy/Dy* diagram (Figure 5.19E), High-Mg Plateau samples plot above the MORB array, beyond the LREE depleted end of the field. On the La/Sm vs V/Ti diagram (Figure 5.19F), Soná-Torio High-Mg Plateau samples plot as a distinct group, with low La/Sm values, but high V/Ti values.

On the Th/Yb vs Nb/Yb diagram (Figure 5.19A), samples of the Proto-arc Group 1 lie both within the MORB-OIB array, and above the upper margin, between the

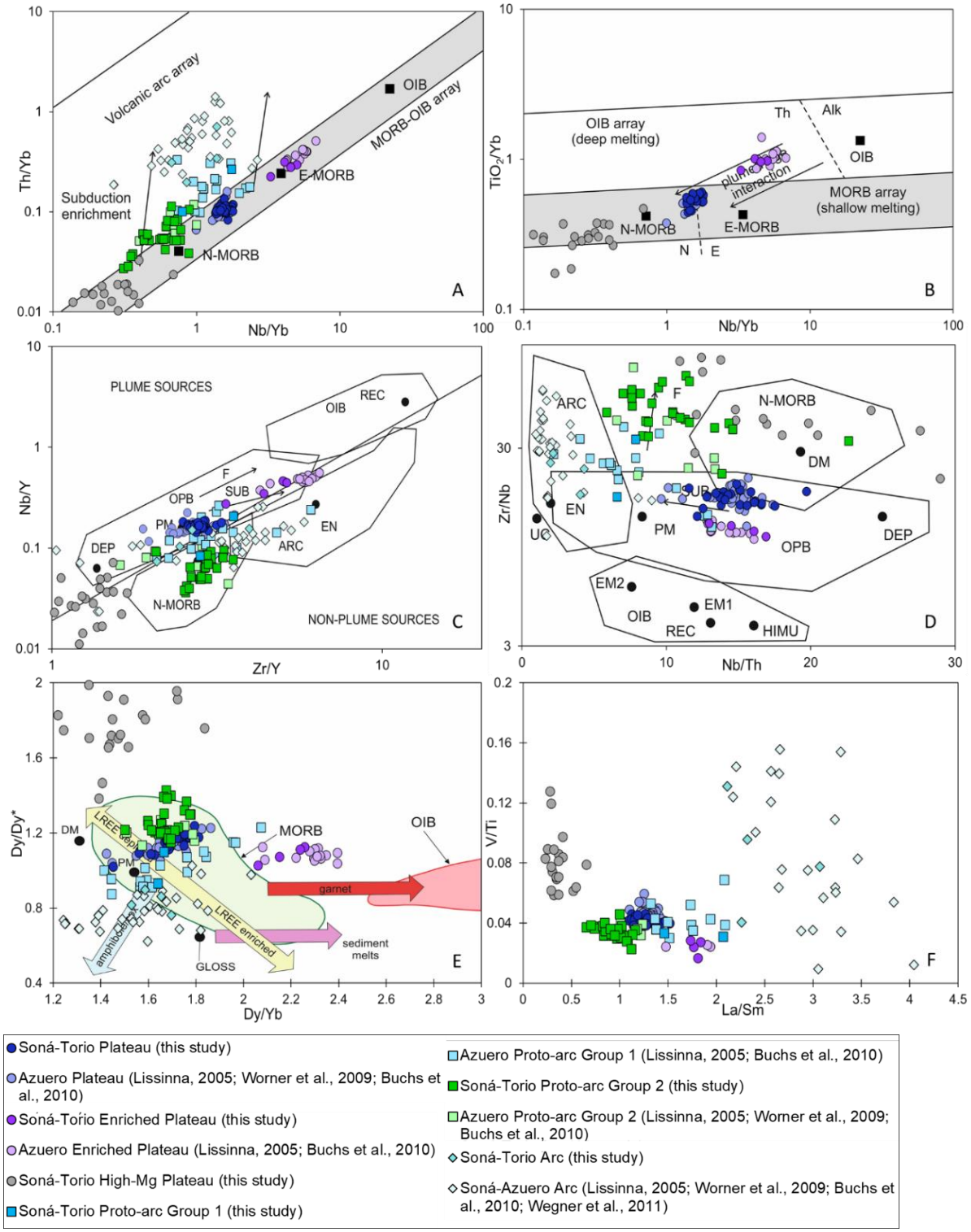

Figure 5.19: Tectonic discrimination diagrams with the Soná-Torio region samples A) Nb/Yb vs Th/Yb crustal input proxy diagram (Pearce, 2008), B) Nb/Yb vs TiO_2/Yb deep melting proxy diagram (Pearce, 2008), C) Zr/Y vs Nb/Y diagram (Condie, 2005), D) Nb/Th vs Zr/Nb diagram (Condie, 2005), E) Dy/Yb vs Dy/Dy* diagram (Davidson et al., 2013) and F) La/Sm vs V/Ti diagram. Abbreviations: UC = upper continental crust, PM = Primitive Mantle, DM = shallow depleted mantle, HIMU = high mu (U/Pb) source, EM1 and EM2 = enriched mantle sources, ARC = arc related basalts, N-MORB = normal mid-ocean ridge basalt, OPB = oceanic plateau basalt, OIB = oceanic island basalt, DEP = deep depleted mantle, EN = enriched component, F = effects of batch melting and SUB = subduction effect.

samples of the Plateau and Arc groups. On the Nb/Y vs Zr/Y diagram (Figure 5.19C), most samples lie within the Oceanic Plateau array, with some samples plotting within the N-MORB and Arc arrays. On the Zr/Nb vs Nb/Th diagram (Figure 5.19D), samples are split between the Oceanic Plateau array and the Arc array, and four samples plot between the two groups (sample JB18-023 (this study), DB05-043, DB05-087, DB07-049 (Buchs et al., 2010)). On the Dy/Yb vs Dy/Dy* diagram (Figure 5.19E), Soná-Torio Proto-arc Group 1 samples plot in a linear group across the centre of the MORB array, below the samples of the Soná-Torio Plateau. On the La/Sm vs V/Ti diagram (Figure 5.19F), the Proto-arc Group 1 samples plot as a transitional group between the Soná-Torio Plateau and Arc Groups.

On the Th/Yb vs Nb/Yb diagram (Figure 5.19A) samples of Proto-arc Group 2 plot within the MORB-OIB array and above the upper margin. This group has lower Th/Yb and Nb/Yb values than samples of the Proto-arc Group 1, and plot above the N-MORB array. On the Nb/Y vs Zr/Y plot (Figure 5.19C), most samples of the Proto-arc Group 2 plot below the Plume Source array, within the N-MORB array. However, some samples also lie within the depleted area of the Iceland Plume array. On the Zr/Nb bs Nb/Th diagam (Figure 5.19D), Proto-arc Group 2 samples are scattered, largely plotting between the Oceanic Plateau, N-MORB and Arc arrays. Six samples lie within the N-MORB array. On the Dy/Yb vs Dy/Dy* diagram (Figure 5.19E), Soná-Torio Proto-arc Group 2 samples largely plot within the MORB array, above the Soná-Torio Plateau, in the LREE depleted end of the field. On the La/Sm vs V/Ti diagram (Figure 5.19F), Proto-arc Group 2 samples are clustered close to the Soná-Torio Plateau group, with lower values of both V/Ti and La/Sm

On the Th/Yb vs Nb/Yb diagram (Figure 5.19A), Soná-Torio Arc samples plot above the MORB-OIB array, in the Volcanic Arc array. On the Nb/Y vs Zr/Y diagram (Figure 5.19C), most samples plot below the Plume Source line in the Arc array, with rare samples plotting in the Oceanic Plateau and N-MORB arrays. On the Zr/Nb vs Nb/Th diagram (Figure 5.19D), all samples lie in the Arc array, with rare samples plotting in the overlap with the Oceanic Plateau array. On the Dy/Yb vs Dy/Dy* diagram (Figure 5.19E), Soná-Torio Arc samples plot across the lower boundary of the MORB array, indicating the influence of fractionation of amphibole and clinopyroxene. On the La/Sm vs V/Ti diagram (Figure 5.19F), Soná-Torio Arc samples are scattered, with a wide range of V/Ti values.

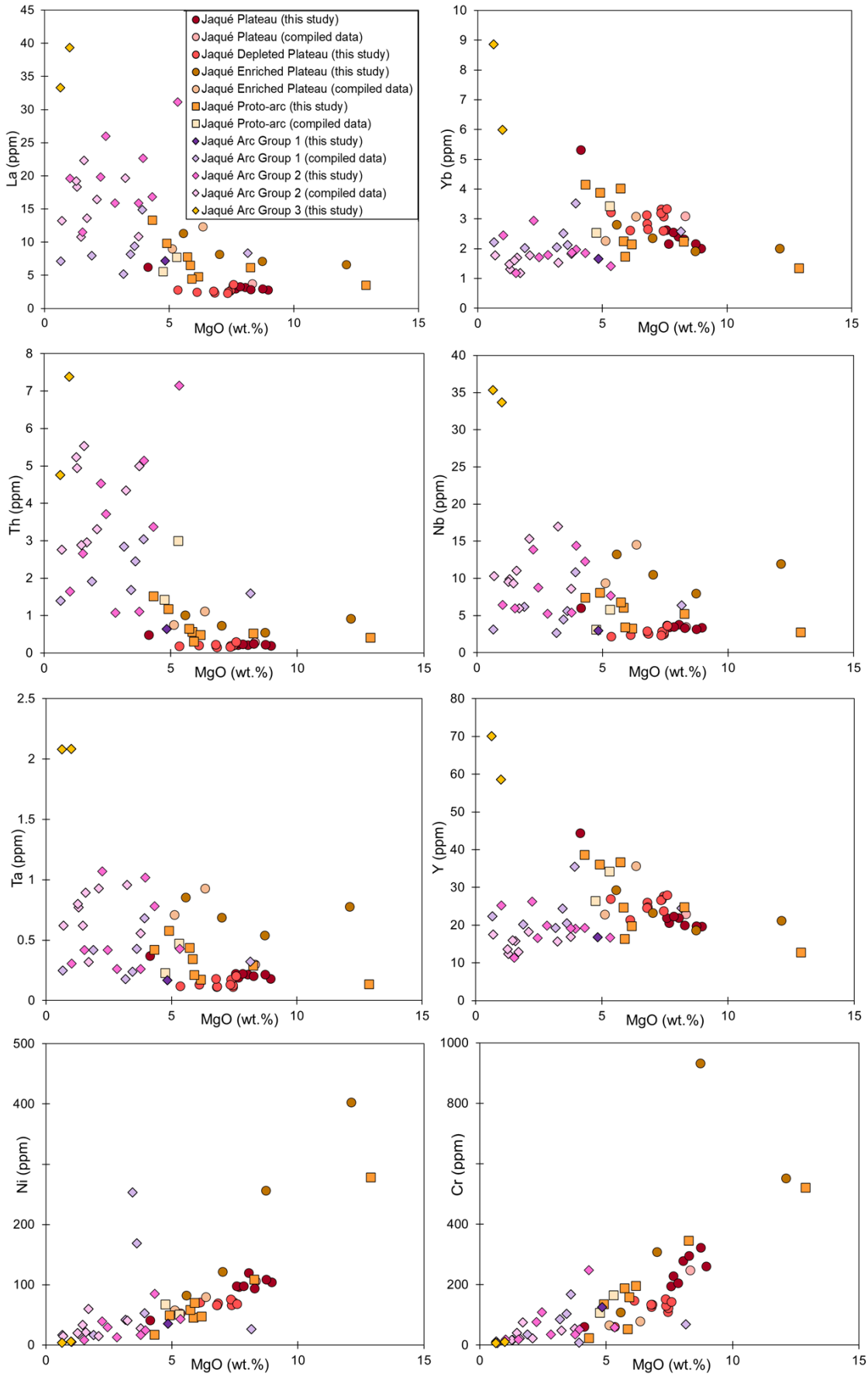

Figure 5.20: Bivariate diagrams of representative trace elements vs MgO for the Darién Pacific Coast samples

5.5.2 Darién Pacific Coast

On binary plots of trace element vs MgO contents (Figure 5.20), there is little variation of trace element values in most samples of the Jaqué Plateau (La = 2.82 – 3.76, Yb = 2.01 – 3.10), whilst sample DB16-043 has higher values of REE (La = 6.27, Yb = 5.32) and lower values of Cr and Ni (Figure 5.20). The Jaqué Depleted Plateau samples also have narrow ranges in most elements and have similar trace elements to the samples of the Jaqué Plateau (Figure 5.20), although the Depleted Plateau samples do have slightly higher HREE and lower LREE and Cr and Ni (La = 2.29 – 2.82, Yb = 2.61 – 3.35). Sample JB17-063 has slightly higher LREE (La = 3.64). Samples of Enriched Plateau can be much more variable, with fairly narrow ranges of the HREE and Th, but slightly wider ranges of LREE, Nb and Ta (La = 4.50 – 12.37, Yb = 1.74 – 3.08) (Figure 5.20). There are also very wide ranges of both Cr and Ni, although this is partially due to the wider range of MgO values. Proto-arc samples also have a wider range of trace element values across a wider MgO range, with values higher than the plateau groups for the REEs (La = 3.54 – 13.33, Yb = 1.35 – 4.16) (Figure 5.20). The Proto-arc samples also extend to high Ni and Cr values. The Arc Group 1 samples have trace element values generally similar to those of the Proto-arc, but with narrower ranges of the HREE (La = 5.17 – 14.87, Yb = 1.66 – 3.52) (Figure 5.20). The Arc Group 1 samples also have very narrow ranges of Cr, with a wider range of Ni values. Jaqué Arc Group 2 samples have similar HREE values to samples of the Plateau and Arc Group 1. In Th, Nb, Ta and the LREEs, samples reach higher values, with low values of Ni and Cr (La = 10.82 – 31.16, Yb = 1.18 – 2.95) (Figure 5.20). Arc Group 3 samples have values higher than all other samples for most trace elements, with Th values similar to Arc Group 2, and low Ni and Cr contents (La = 33.31 – 39.33, Yb = 5.99 – 8.86) (Figure 5.20).

Samples from of the Jaqué Plateau and Proto-arc groups show negative correlations between the REE and MgO contents. Samples of the Jaqué Plateau groups remain consistent in the LREE, Th, Nb, and Ta with increasing MgO contents, whereas the Proto-arc show negative correlations. Samples of the Jaqué Arc Groups are generally scattered and do have a clear correlation for any of these trace elements with MgO contents. All groups also show positive correlations for Ni and Cr vs MgO (Figure 5.20).

On the chondrite normalised REE plots, samples of the Jaqué Plateau have flat patterns (Figure 5.21B). Sample DB16-043 also has a flat pattern, but it has REE

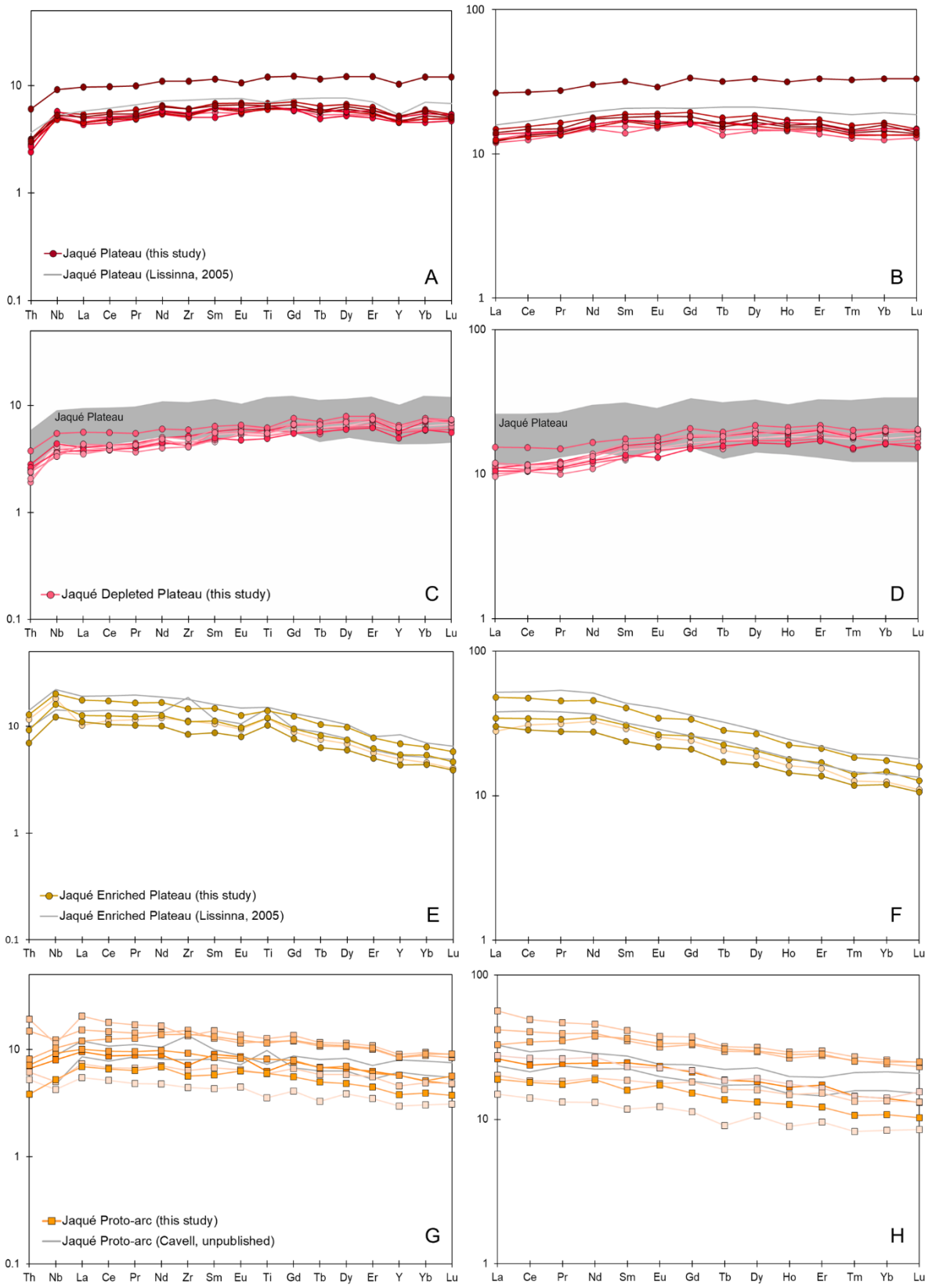

Figure 5.21: Primitive mantle-normalised multi-element diagrams (A, C, E, G) and chondrite normalised REE plots (B, D, F, H) for the Jaqué Plateau and Proto-arc groups. Compiled data shown in grey in A-H. Jaqué Plateau data compiled from (Lissinna, 2005), Soná-Torio Enriched Plateau data compiled from (Lissinna, 2005) and Jaqué Proto-arc data from (Cavell, unpublished)

contents 2.0x the average of other Jaqué Plateau samples. On primitive mantle-normalised multielement diagrams (Figure 5.21A), Jaqué Plateau samples have flat patterns ($La/Sm_{(PMn)}$ = 0.71 – 0.86, $Dy/Yb_{(PMn)}$ = 1.00 – 1.16) with positive Nb anomalies, and slightly negative Th contents. Jaqué Depleted Plateau samples have slightly depleted, flat patterns on chondrite normalised REE plots (Figure 5.21D), and sample JB17-063 has slightly higher values of the LREE in comparison to the remainder of the Depleted Plateau samples. On a primitive mantle-normalised multielement diagram (Figure 5.21C), samples again have depleted profiles, with $La/Sm_{(PMn)}$ = 0.59 – 0.88, and $Dy/Yb_{(PMn)}$ = 0.93 – 1.05, and slight positive Nb anomalies. Sample JB17-063 has relatively higher values of the LREE, Nb and Th. Jaqué Enriched Plateau samples have enriched patterns on a chondrite normalised REE plot (Figure 5.21F). On a primitive mantle-normalised multielement plot (Figure 5.21E), samples have enriched profiles, with ranges of $La/Sm_{(PMn)}$ = 0.97 – 1.27 and $Dy/Yb_{(PMn)}$ = 1.22 – 1.53, and normal to slightly enriched Ti, and generally positive Nb anomalies. Sample JB17-043 does not have a positive Nb anomaly. On chondrite normalised REE diagrams (Figure 5.21H), Jaqué Proto-arc samples have slightly enriched trends, whereas primitive mantle-normalised multielement diagrams (Figure 5.21G), have enriched trends with flat to slightly depleted Ti and normal to slightly depleted Zr. These samples have ranges of $La/Sm_{(PMn)}$ from 0.91 – 1.37 and $Dy/Yb_{(PMn)}$ from 1.19 – 1.37. Nb is depleted in all samples, and Th is variably enriched or depleted. Jaqué Arc Group 1 samples have slightly enriched trends on a chondrite normalised REE plot (Figure 5.22B), with slight depletion in Sm and Ce. On a primitive mantle-normalised multielement diagram (Figure 5.22A), the Jaqué Arc Group 1 samples have negative Nb and Ti anomalies, with variable positive and negative Zr anomalies. $La/Sm_{(PMn)}$ for the Jaqué Arc Group 1 sample from this study is 1.90, and $Dy/Yb_{(PMn)}$ is 1.24. Jaqué Arc Group 2 samples have an enriched profile on a chondrite normalised REE plot (Figure 5.22D), with an enrichment in the LREEs. On a primitive mantle-normalised multielement diagram (Figure 5.22C), samples have enriched profiles, with $La/Sm_{(PMn)}$ = 2.48 – 3.94 and $Dy/Yb_{(PMn)}$ = 1.08 – 1.53. The trends also show depletions in Ti relative to Eu and Gd, and marked depletions in Nb relative to Th and La, along with positive to negative Zr anomalies. Th values are flat to enriched relative to La. Arc Group 3 samples have enriched trends on chondrite normalised REE plots (Figure 5.22 F), with higher HREE values, (3.5x average HREEs of Arc Group 2). Arc Group 3 samples have slightly enriched patterns on a primitive mantle-normalised multielement plot (Figure 5.22E), with $La/Sm_{(PMn)}$ = 1.94 – 2.68 and $Dy/Yb_{(PMn)}$ = 1.00 – 1.14, and marked negative Ti anomalies

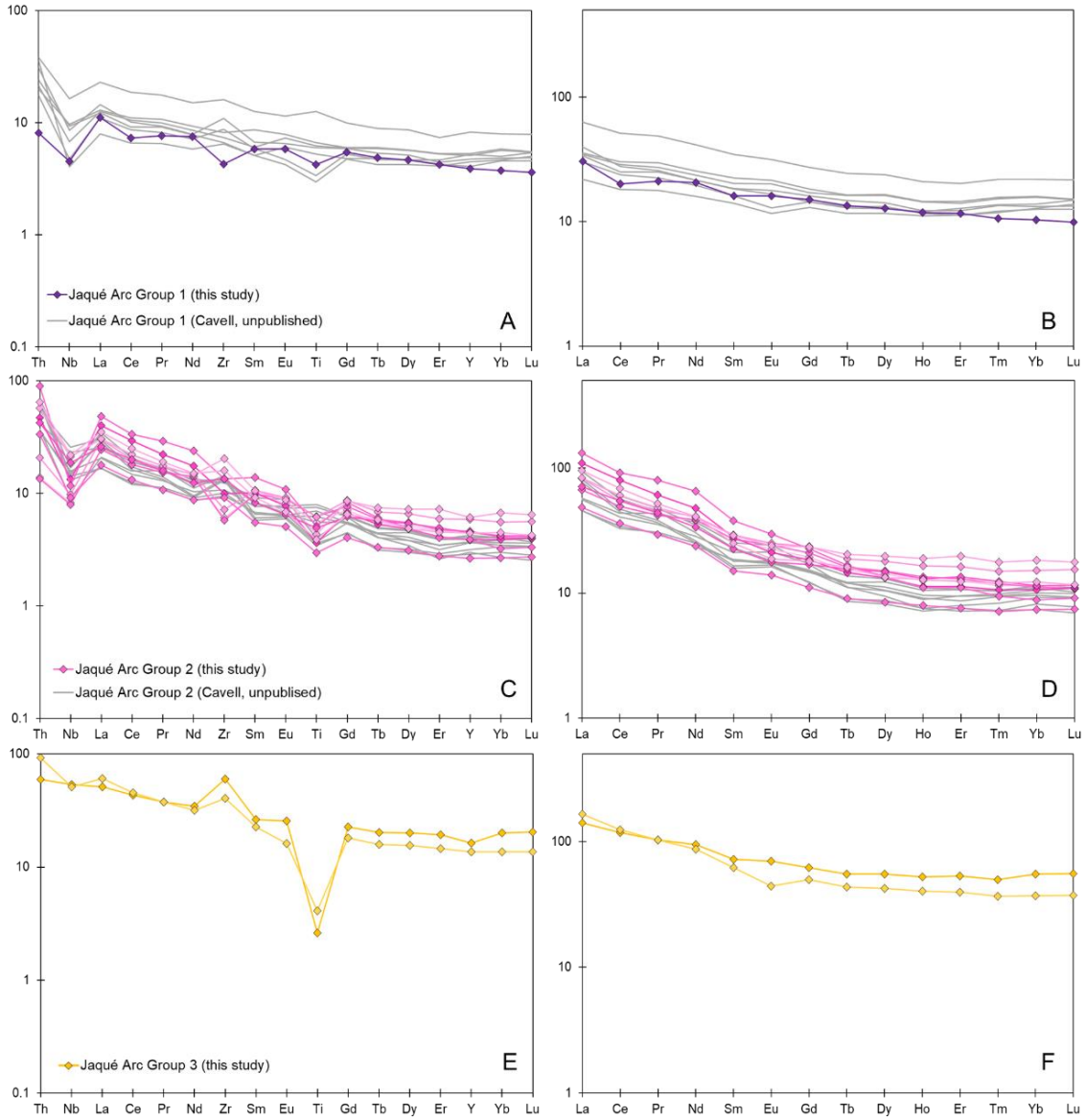

Figure 5.22: Primitive mantle-normalised multi-element diagrams (A, C, E) and chondrite normalised REE plots (B, D, F) for the Jaqué arc groups. Compiled data shown in grey in A-D. Jaqué Arc Group 1 data compiled from (Cavell, unpublished) and Jaqué Arc Group 2 data compiled from Cavell, unpublished

relative to Eu and Gd along with enriched Zr. Sample JB18-072 has a slight Nb depletion and Th enrichment.

On the Th/Yb vs Nb/Yb diagram (Figure 5.23A), samples of the Jaqué Plateau lie in the MORB-OIB array, midway between N-MORB and E-MORB. On the TiO_2/Yb vs Nb/Yb diagram (Figure 5.23B), samples lie within the upper section of the MORB array, across the boundary between N-MORB and E-MORB and close to the plume-ridge interaction area. On the Zr/Y vs Nb/Y diagram (Figure 5.23C), all samples plot centrally within the Oceanic Plateau array. On the Nb/Th vs Zr/Nb plot

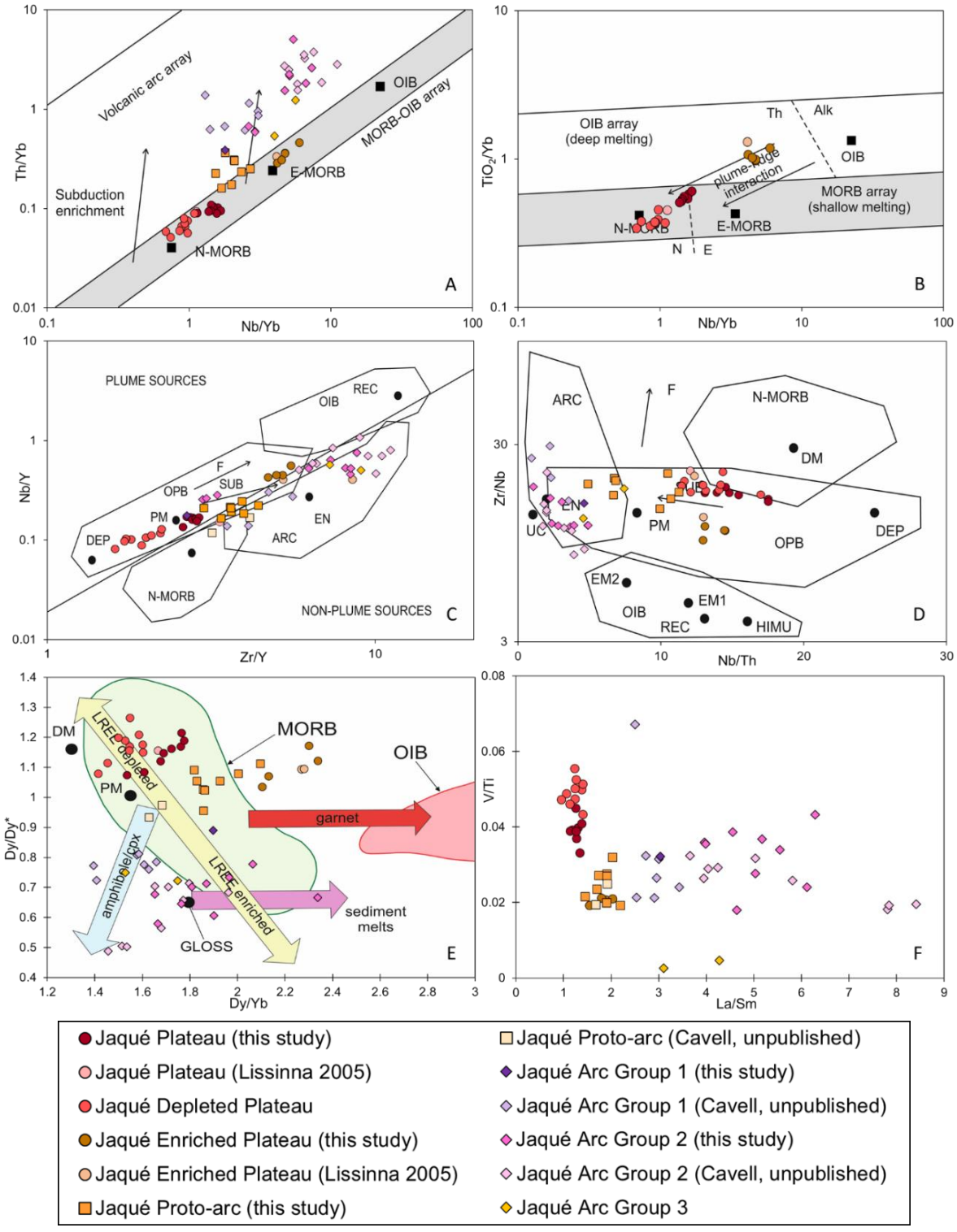

Figure 5.23: Tectonic discrimination diagrams with the Darién Pacific Coast region samples A) Nb/Yb vs Th/Yb crustal input proxy diagram (Pearce, 2008), B) Nb/Yb vs TiO_2/Yb deep melting proxy diagram (Pearce, 2008), C) Zr/Y vs Nb/Y diagram (Condie, 2005), D) Nb/Th vs Zr/Nb diagram (Condie, 2005), E) Dy/Yb vs Dy/Dy* diagram (Davidson et al., 2013) and F) La/Sm vs V/Ti diagram. Abbreviations: UC = upper continental crust, PM = Primitive Mantle, DM = shallow depleted mantle, HIMU = high mu (U/Pb) source, EM1 and EM2 = enriched mantle sources, ARC = arc related basalts, N-MORB = normal mid-ocean ridge basalt, OPB = oceanic plateau basalt, OIB = oceanic island basalt, DEP = deep depleted mantle, EN = enriched component, F = effects of batch melting and SUB = subduction effect

(Figure 5.23D), all samples lie within the Oceanic Plateau Array, with some samples plotting along the margin of the N-MORB array. On the Dy/Yb vs Dy/Dy* diagram (Figure 5.23E), Jaqué Plateau samples plot in a linear group across the MORB array, towards the LREE depleted end of the field. On the La/Sm vs V/Ti diagram (Figure 5.23F), samples of the Plateau are clustered centrally.

On the Th/Yb vs Nb/Yb diagram (Figure 5.23A), Jaqué Depleted Plateau samples plot within the MORB-OIB array, close to N-MORB, with values of Th/Yb and Nb/Yb both lower than those of the Jaqué Plateau. On the diagram of TiO_2/Yb vs Nb/Yb (Figure 5.23B), samples of the Depleted Plateau plot within the MORB array, close to N-MORB. On the Zr/Y vs Nb/Y diagram (Figure 5.23C), samples of the Jaqué Depleted Plateau plot within the Oceanic Plateau array, towards the depleted section of the array. Samples of the Depleted Plateau plot within the Oceanic Plateau array on the Zr/Nb vs Nb/Th diagram (Figure 5.23D), with rare samples lying in the overlap with the N-MORB array. On the Dy/Yb vs Dy/Dy* diagram (Figure 5.23E), Jaqué Depleted Plateau samples plot in the MORB array, above the samples of the Jaqué Plateau, in the LREE depleted end of the field. On the La/Sm vs V/Ti diagram (Figure 5.23F), samples of the Depleted Plateau are clustered above those of the Jaqué Plateau, with similar values of La/Sm, but higher values of V/Ti.

On the Th/Nb vs Nb/Yb diagram (Figure 5.23A), samples of the Enriched Plateau plot within the MORB-OIB array, above E-MORB. On the TiO_2/Yb vs Nb/Yb (Figure 5.23B), Enriched Plateau samples plot in the OIB tholeiitic array, at the top of the plume-ridge interaction trend. On the Nb/Y vs Zr/Y diagram (Figure 5.23C), samples plot towards the enriched end of the Oceanic Plateau array, close to the OIB array. On the Zr/Nb vs Nb/Th diagram (Figure 5.23D), samples of Jaqué Enriched Plateau plot centrally in the Oceanic Plateau array. On the Dy/Yb vs Dy/Dy* diagram (Figure 5.23E), Jaqué Enriched Plateau samples plot between the MORB and OIB arrays, indicating the influence of garnet in the source. On the La/Sm vs V/Ti diagram (Figure 5.23F), samples of the Enriched Plateau are clustered below those of the other plateau groups.

On the Th/Yb vs Nb/Yb diagram (Figure 5.23A), four samples of the Jaqué Proto-arc plot on the upper boundary of the MORB-OIB array between N-MORB and E-MORB (samples JB17-043, JB17-057, JB18-060, JB17-074), and the remainder above the MORB-OIB array. On the Nb/Y vs Zr/Y diagram (Figure 5.23C), most samples plot along the lower boundary of the Oceanic Plateau array, with some samples plotting in the N-MORB and Arc arrays. On the Zr/Nb vs Nb/Th diagram (Figure 5.23D), 4 samples of Jaqué Proto-arc (samples JB17-043, JB17-057, JB18-060, JB17-074) plot within the Oceanic Plateau array, close to the Plateau samples, whilst the remainder of samples plot within the overlap between Oceanic

Plateau and Arc arrays. On the Dy/Yb vs Dy/Dy* diagram (Figure 5.23E), Jaqué Proto-arc samples plot across the centre of the MORB array, with two samples plotting outside the boundary (samples DB16-092, JB18-071). On the La/Sm vs V/Ti diagram (Figure 5.23F), samples of the Jaqué Proto-arc are clustered with those of the Jaqué Enriched Plateau.

On the Th/Yb vs Nb/Yb diagram (Figure 5.23A), samples of the Jaqué Arc Group 1 plot solely within the Volcanic Arc array, above samples of the Proto-arc. On the Nb/Y vs Zr/Y diagram (Figure 5.23C), Jaqué Arc Group 1 samples largely plot within the Arc Array, with one sample plotting within Oceanic Plateau array, close to the Jaqué Plateau samples (sample DB16-080). On the Zr/Nb vs Nb/Th diagram (Figure 5.23D), three samples plot within the Oceanic Plateau and Arc array overlap, with two samples plotting in the Arc array only (samples DB15-018, DB15-019). On the Dy/Yb vs Dy/Dy* diagram (Figure 5.23E), Jaqué Arc Group 1 samples largely plot below the lower boundary of the MORB array indicating fractionation of amphibole and/or clinopyroxene, although sample DB16-082 plots within the MORB array. On the La/Sm vs V/Ti diagram (Figure 5.23F), samples of the Arc Group 1, samples plot to the right of the Enriched Plateau and Proto-arc, with one sample with a high V/Ti value (sample DB15-018).

On the Th/Yb vs Nb/Yb diagram (Figure 5.23A), Jaqué Arc Group 2 samples plot within the Volcanic Arc array, with two samples plotting close to those of the Arc Group 1 (samples JB17-050, JB17-052). On the Nb/Y vs Zr/Y diagram (Figure 5.23C), most samples lie within the arc array, or above the upper boundary of the Arc array. Three samples plotting within the oceanic plateau array, close to the plateau and proto-arc samples (samples JB17-050, JB17-052, JB17-053). On the Zr/Nb vs Nb/Th diagram (Figure 5.23D), most samples plot within the lower Arc array, with rare samples plotting outside the Arc array. On the Dy/Yb vs Dy/Dy* diagram (Figure 5.23E), Jaqué Arc Group 2 samples are scattered around the lower boundary of the MORB array, again showing evidence of fractionation of clinopyroxene and/or amphibole. The Arc Group 2 samples plot at higher values of Dy/Yb than the Arc Group 1 samples. On the La/Sm vs V/Ti diagram (Figure 5.23F), samples of the Arc Group 2 are scattered, and extend to higher La/Sm values than

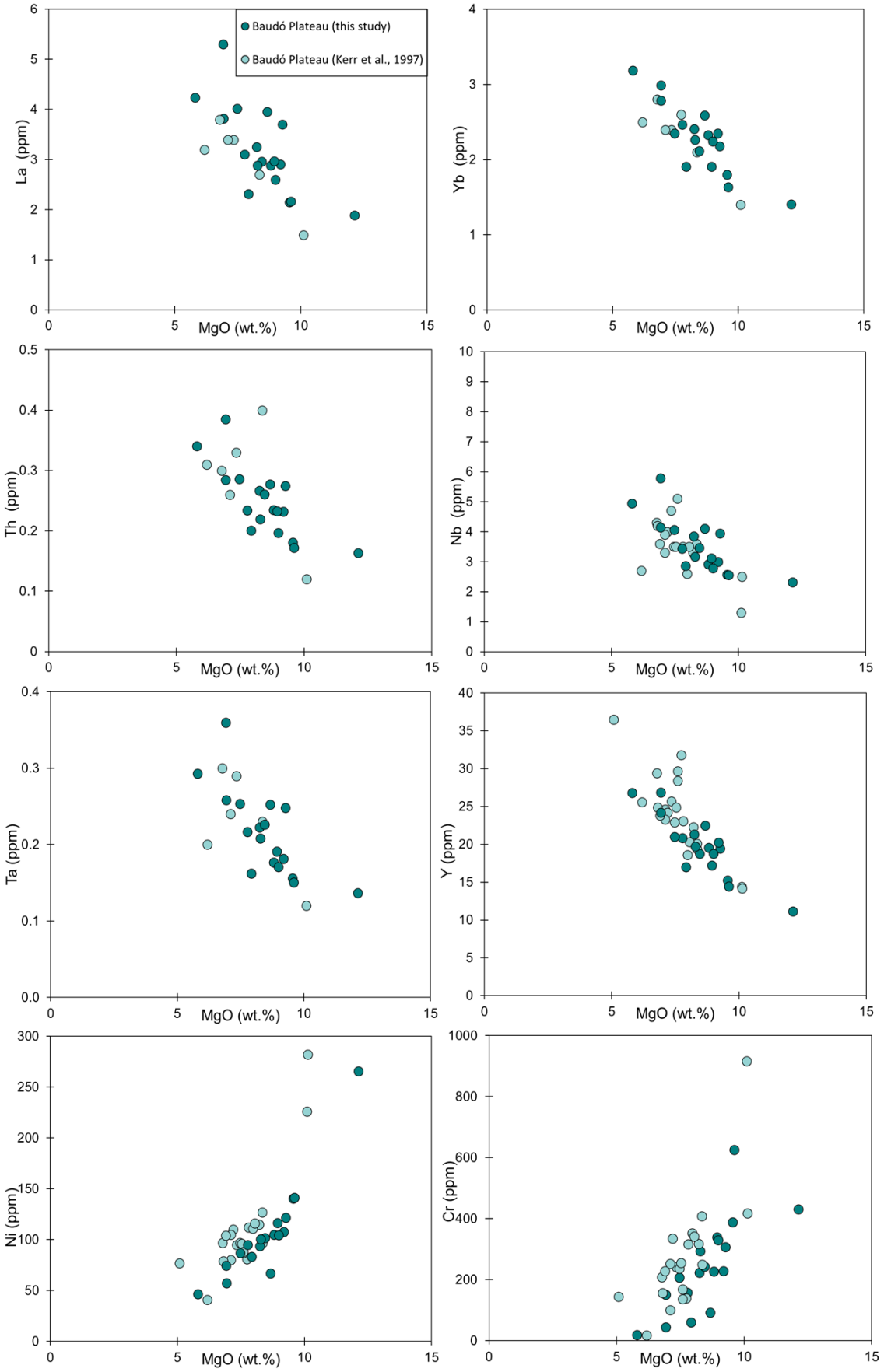

Figure 5.24: Bivariate diagrams of representative trace elements vs MgO for the Baudó region samples

the remainder of the Jaqué geochemical groups.

On the Th/Yb vs Nb/Yb diagram (Figure 5.23A), Jaqué Arc Group 3 samples plot within the Volcanic Arc array. On the Nb/Y vs Z/Y diagram (Figure 5.23C), samples plot with those of the Arc Group 2, below the Iceland Plume array lower boundary. On the Zr/Nb vs Nb/Th diagram (Figure 5.23D), one Arc Group 3 sample plots within the overlap of the Arc and Oceanic Plateau array (sample JB18-072), while the other plots on the boundary of the Arc array, within the Oceanic Plateau array (sample JB17-064). On the Dy/Yb vs Dy/Dy* diagram (Figure 5.23E), Jaqué Arc Group 3 samples plot below the lower boundary of the MORB array. On the La/Sm vs V/Ti diagram (Figure 5.23F), samples of the Arc Group 3 plot below the other Jaqué Arc groups, with low V/Ti values.

5.5.3 Serranía de Baudó

For all trace elements, samples of the Baudó Basalts cover slightly wider ranges than basalts of the Soná-Torio Plateau, Jaqué Plateau and Jaqué Depleted Plateau, with the ranges of La = 1.50 – 5.31, and Yb = 1.31 - 3.19. The REEs, Th, Nb, Ta and Y decrease with increasing MgO values, whilst Ni and Cr values for Baudó basalt samples form a positive correlation with MgO content (Figure 5.24).

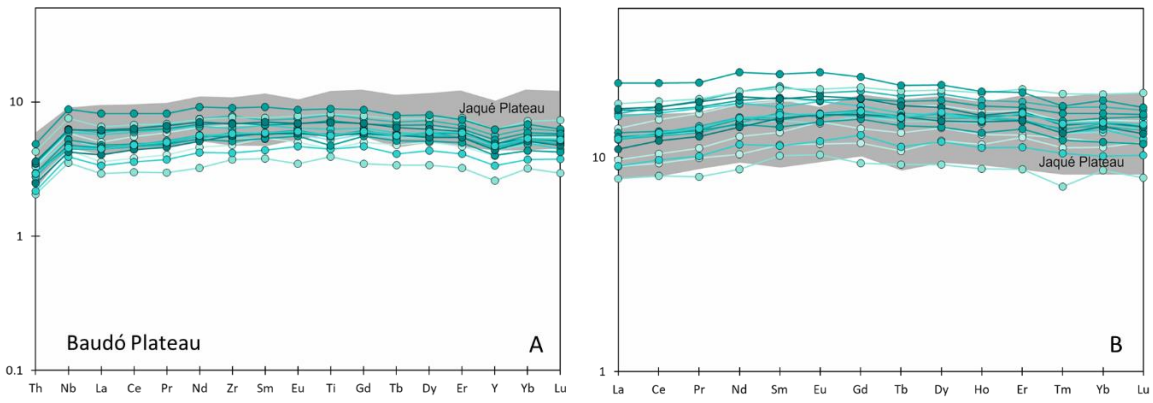

Figure 5.25: A) Primitive mantle-normalised multi-element diagrams and B) chondrite normalised REE plots for the Baudó Plateau samples

On chondrite normalised REE plots (Figure 5.25B), samples of the Baudó Basalts have relatively flat patterns. On primitive mantle-normalised multielement plots (Figure 5.25A), trends are flat ($La/Sm_{(PMn)}$ = 0.66 – 0.90, $Dy/Yb_{(PMn)}$ = 1.05 – 1.18) with slight positive Nb anomalies, and negative Th values.

On the Th/Yb vs Nb/Yb diagram (Figure 5.26A), samples of the Baudó Plateau largely lie along the upper margin of the MORB-OIB array, close to N-MORB, and as a cluster separate from that of the Jaqué Plateau. On the TiO_2/Yb vs Nb/Yb diagram (Figure 5.26B), samples plot in the upper portion of the N-MORB array, again in a

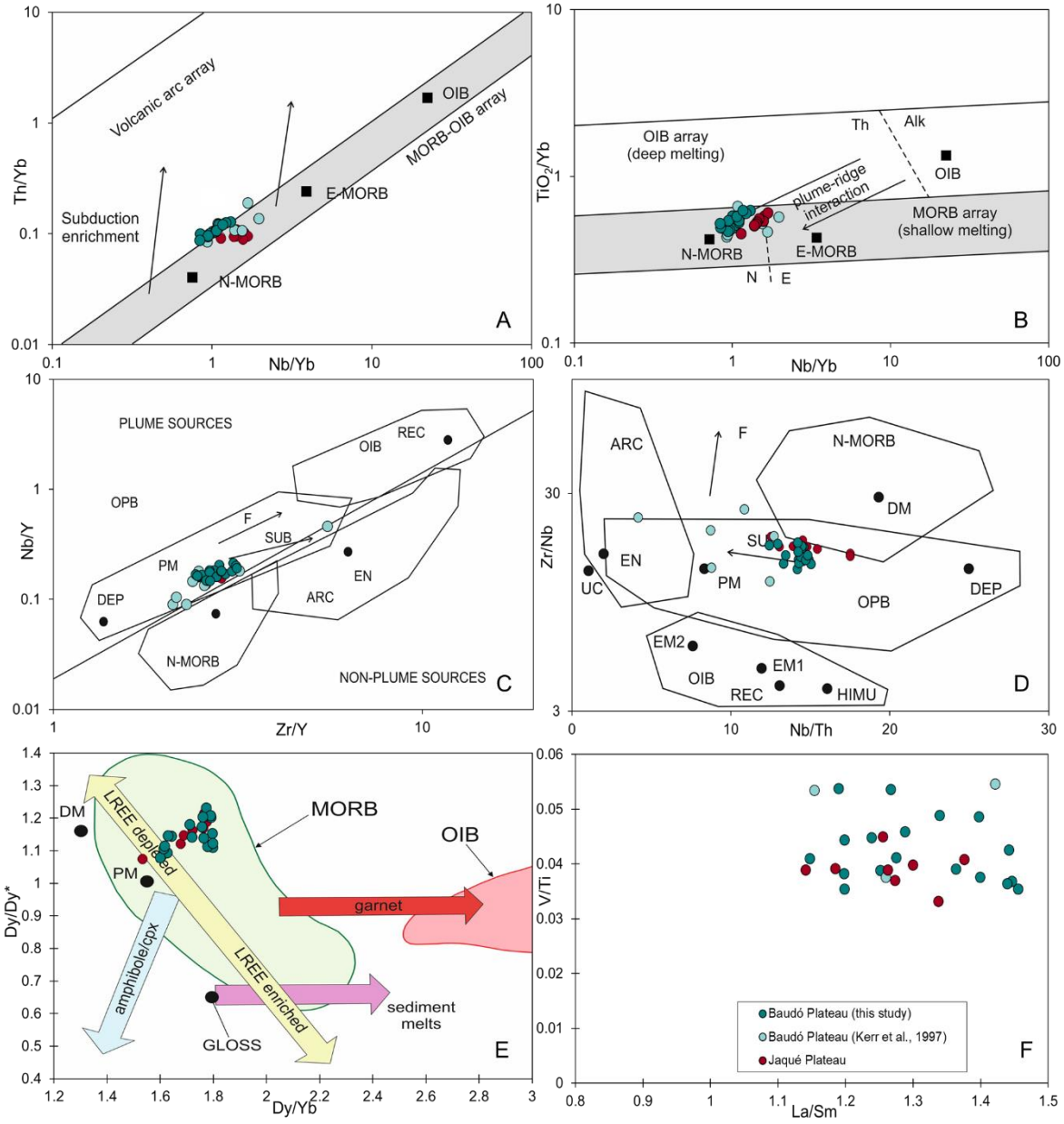

Figure 5.26: Tectonic discrimination diagrams with the Baudó Plateau samples, with Jaqué Plateau for comparison. A) Nb/Yb vs Th/Yb crustal input proxy diagram (Pearce 2008), B) Nb/Yb vs TiO_2/Yb deep melting proxy diagram (Pearce 2008), C) Zr/Y vs Nb/Y diagram (Condie 2005), D) Nb/Th vs Zr/Nb diagram (Condie, 2005), E) Dy/Yb vs Dy/Dy* diagram (Davidson et al., 2013) and F) La/Sm vs V/Ti diagram. Abbreviations: UC = upper continental crust, PM = Primitive Mantle, DM = shallow depleted mantle, HIMU = high mu (U/Pb) source, EM1 and EM2 = enriched mantle sources, ARC = arc related basalts, N-MORB = normal mid-ocean ridge basalt, OPB = oceanic plateau basalt, OIB = oceanic island basalt, DEP = deep depleted mantle, EN = enriched component, F = effects of batch melting and SUB = subduction effect

cluster separate from the Jaqué Plateau samples. On the Nb/Y vs Zr/Y diagram (Figure 5.26C), samples of the Baudó Plateau plot within the centrally in the Oceanic Plateau array. On the Zr/Nb vs Nb/Th diagram (Figure 5.26D), samples plot within the upper portion of the Oceanic Plateau array, close to the margin of the N-MORB array. On the Dy/Yb vs Dy/Dy* diagram (Figure 5.26E), Baudó Plateau samples plot centrally in the MORB array, towards the LREE depleted end of the field, close to those of the Jaqué Plateau. On the La/Sm vs V/Ti diagram (Figure 5.26F), samples of the Baudó Plateau are clustered, again overlapping with samples of the Jaqué Plateau.

5.5.4 Trace Element Summary

A comparison of all data presented in this section is presented in Figure 5.27. On these graphs the groups of the Soná-Torio Plateau, Jaqué Plateau and Baudó Plateau generally plot together. However, the Baudó Plateau samples extend to lower Zr/Nb and Nb/Yb values, along with higher V/Ti (Figure 5.27). The Jaqué Depleted Plateau also plots close to these plateau groups, although samples higher V/Ti values, and lower Nb/Yb, TiO_2/Yb, Zr/Y, Nb/Y and Dy/Yb values (Figure 5.27).

The Enriched Plateau groups of both Soná-Torio and Jaqué also plot together, with similar values of for all trace element ratios presented in Figure 5.27. The Soná-Torio High Mg Plateau plots as a distinct group on all plots, and does not have an equivalent in the Jaqué or Baudó regions (Figure 5.27). The Soná-Torio Proto-arc Group 1 samples plot with the Jaqué Proto-arc samples on the Th/Yb vs Nb/Yb, Nb/Y vs Zr/Y and Zr/Nb vs Nb/Th diagrams, but Soná-Torio samples do extend to lower V/Ti values (Figure 5.27). Soná-Torio Proto-arc Group 2 generally lies as a separate group, and is distinct from the other proto-arc groups, with no equivalent in Jaqué. The Soná-Torio Arc is also distinct from the Jaqué Arc Groups 1-3. The Jaqué Arc Groups have higher Nb/Yb and Zr/Y ratios, with lower Zr/Nb ratios and a narrow range of V/Ti ratios (Figure 5.27).

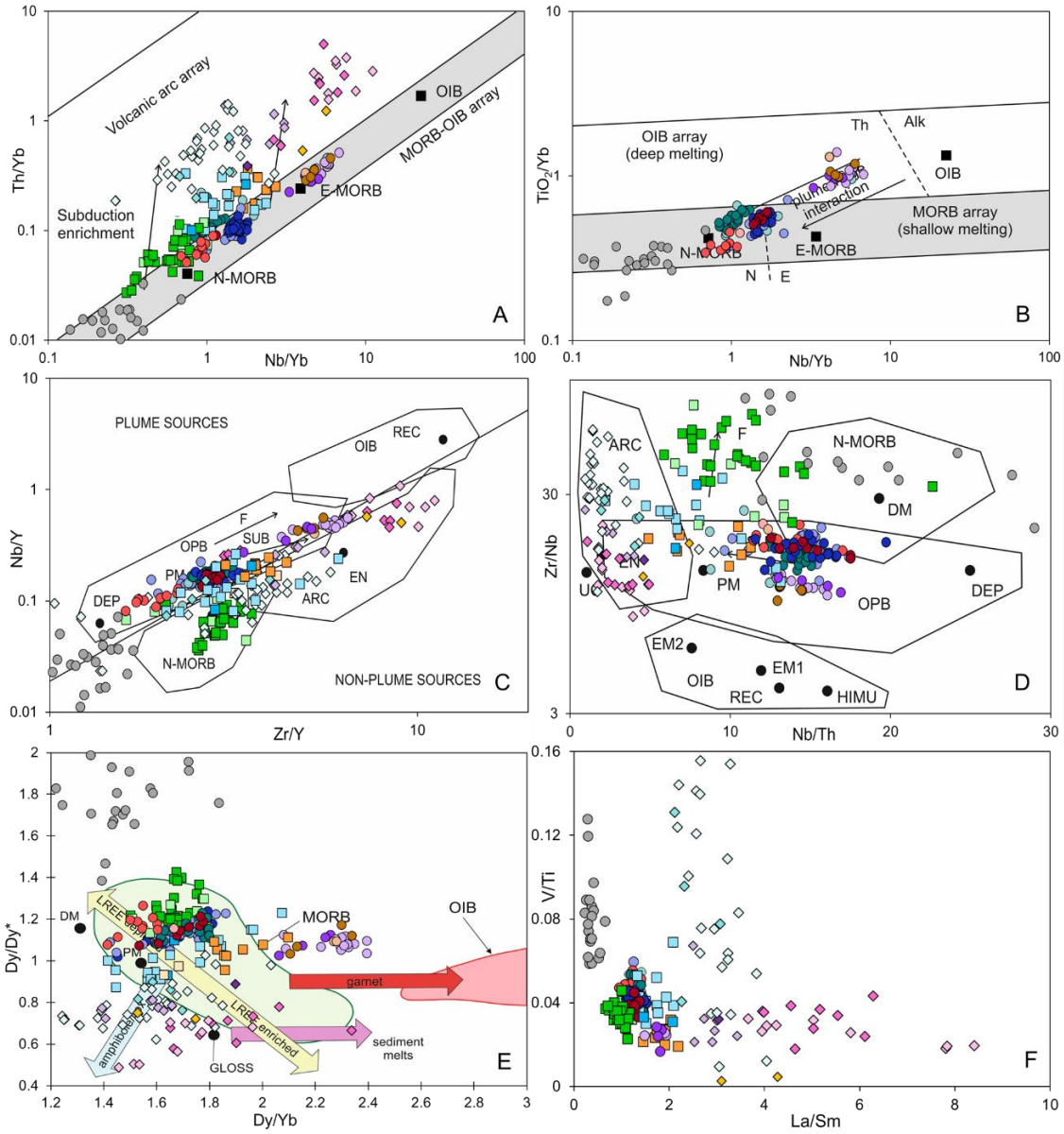

Soná-Torio Plateau (this study)	Jaqué Plateau (this study)
Azuero Plateau (Lissinna, 2005; Worner et al., 2009; Buchs et al., 2010)	Jaqué Plateau (Lissinna, 2005)
Soná-Torio Enriched Plateau (this study)	Jaqué Depleted Plateau (this study)
Azuero Enriched Plateau (Lissinna, 2005; Buchs et al., 2010)	Jaqué Enriched Plateau (this study)
Soná-Torio High Mg Plateau (this study)	Jaqué Enriched Plateau (Lissinna, 2005)
Soná-Torio Proto-arc Group 1 (this study)	Jaqué Proto-arc (this study)
Azuero Proto-arc Group 1 (Lissinna, 2005; Buchs et al., 2010)	Jaqué Proto-arc (Cavell, unpublished)
Soná-Torio Proto-arc Group 2 (this study)	Jaqué Arc Group 1 (this study)
Azuero Proto-arc Group 2 (Lissinna, 2005; Worner et al., 2009; Buchs et al., 2010)	Jaqué Arc Group 1 (Cavell, unpublished)
Soná-Torio Arc (this study)	Jaqué Arc Group 2 (this study)
Soná-Azuero Arc (Lissinna, 2005; Worner et al., 2009; Buchs et al., 2010; Wegner et al., 2011)	Jaqué Arc Group 2 (Cavell, unpublished)
Baudó Plateau (this study)	Jaqué Arc Group 3 (this study)
Baudó Plateau (Kerr et al., 1997)	

Figure 5.27: Tectonic discrimination diagrams for all samples from this study. A) Nb/Yb vs Th/Yb crustal input proxy diagram (Pearce 2008), B) Nb/Yb vs TiO_2/Yb deep melting proxy diagram (Pearce 2008), C) Zr/Y vs Nb/Y diagram (Condie 2005), D) Nb/Th vs Zr/Nb diagram (Condie, 2005), E) Dy/Yb vs Dy/Dy* diagram (Davidson et al., 2013) and F) La/Sm vs V/Ti diagram. Abbreviations: UC = upper continental crust, PM = Primitive Mantle, DM = shallow depleted mantle, HIMU = high mu (U/Pb) source, EM1 and EM2 = enriched mantle sources, ARC = arc related basalts, N-MORB = normal mid-ocean ridge basalt, OPB = oceanic plateau basalt, OIB = oceanic island basalt, DEP = deep depleted mantle, EN = enriched component, F = effects of batch melting and SUB = subduction effect

5.6 Neodymium Isotopes

In total, thirty-three representative samples were selected for Nd radiogenic isotope analyses from across the Soná-Torio, Darién Pacific Coast and Serranía de Baudó regions. The samples were selected based on lack of alteration and $^{40}Ar/^{39}Ar$ dating potential, alongside geographical and geochemical variability to ensure good coverage. Selected samples have LOI values largely ranging from 1.28 – 4.82 %, although 3 samples have higher values. (samples JB17-057 has an LOI value of 5.50 %, sample JB17-046 has an LOI value of 6.90 %, sample JB17-059 has an LOI value of 9.07 %). As both Sm and Nd are relatively immobile in fluids and partition similarly in most rock forming minerals, the Sm-Nd system is more likely to be resistant to metamorphism and alteration than other isotope systems (e.g., Sr isotopes, Pb isotopes).

Of the total samples, nineteen were from Soná-Torio (three from the Plateau, three from the High Mg Plateau, five from Proto-arc Group 1 and six from Proto-arc Group 2), eleven were from the Darién Pacific Coast (two from the Plateau, two from the Depleted Plateau, three from Enriched Plateau and four from Proto-arc) and three were from the Serranía de Baudó Plateau. This data is used to assess the characteristics of the mantle sources of the Plateau and Proto-arc Groups, including subduction-based contamination. The isotope ratios used in the study have been age corrected for in-situ decay (using ages between 85 - 60 Ma), using trace element abundances reported in Appendix E2. Both measured and initial values are reported in Appendix E3.

Nd is slightly more incompatible than Sm and is preferentially concentrated in the melt during melting of the mantle or crust. The initial Nd isotope ratio of a sample therefore acts as a tracer of the composition of the mantle source region, including potential contamination with crustal material, at the time of extraction of the magma. The initial Nd isotopic ratio can be derived using Equation 5.2.

Equation 5.2

$$\left(\frac{^{143}\mathrm{Nd}}{^{144}\mathrm{Nd}}\right)(i) = \left(\frac{^{143}\mathrm{Nd}}{^{144}\mathrm{Nd}}\right)(m) - \left(\frac{^{147}\mathrm{Sm}}{^{144}\mathrm{Nd}}\right)(m) \times \left(e^{\lambda \mathrm{t}-1}\right)$$

The initial isotope ratios for all samples for $(^{143}Nd/^{144}Nd)_i$ range from 0.51279 – 0.51313. In the Soná-Torio area the range is 0.51279 – 0.51313, in the Darién Pacific Coast the range is 0.51287 – 0.51300 and in the Serranía de Baudó, it is 0.51292 – 0.51295. Analysed samples have been plotted on $(^{143}Nd/^{144}Nd)_i$ bivariate diagrams (Figure 5.28) along with

previously analysed samples from respective regions, from Lissinna (2005) and Wegner et al. (2011).

Samples of the Soná-Torio Plateau have $(^{143}Nd/^{144}Nd)_i$ values of 0.51292 – 0.51296, which plot within the range of the CCOP array. Samples of the Enriched Plateau have lower $(^{143}Nd/^{144}Nd)_i$ values, with a range of 0.51288 – 0.51292, which also lie within the CCOP array. Samples of the High-Mg Plateau also have lower $(^{143}Nd/^{144}Nd)_i$ values, with a range of 0.51279 – 0.51289. Two of these samples plot at the lower margin of the CCOP array. Samples of the Soná-Torio Proto-arc Group 1 have more variable $(^{143}Nd/^{144}Nd)_i$ values, with a range of 0.51288 – 0.51300. These samples all lie within the range of the CCOP, but can overlap with the ERP MORB and Charges Bayano Arc arrays. Samples of the Soná-Torio Proto-arc Group 2 have higher $(^{143}Nd/^{144}Nd)_i$ values, ranging from 0.51302 – 0.51313. These samples plot higher than the CCOP array, and lie within the ranges of the EPR MORB and Depleted CCOP. No samples of the Soná-Torio Arc were analaysed, and therefore samples of the Azuero Arc have been plotted for comparison. Azuero Arc $(^{143}Nd/^{144}Nd)_i$ values typically plot within the Chagres Bayano array with a range of 0.51287 – 0.51295.

Samples of the Jaqué Plateau have a $(^{143}Nd/^{144}Nd)_i$ range of 0.51292 - 0.51296. These samples plot centrally in the CCOP array. Samples of the Jaqué Depleted Plateau plot on the upper margins of the CCOP array, with higher $(^{143}Nd/^{144}Nd)_i$ values of 0.51298 - 0.51299. Jaqué Enriched Plateau samples have $(^{143}Nd/^{144}Nd)_i$ ranges within the CCOP array, with values of 0.51287 - 0.51292. There was also a Jaqué Enriched Plateau sample which had an $(^{143}Nd/^{144}Nd)_i$ value of 0.51351, but this value was assumed to be erroneous as it is such an anomalously high value. Jaqué Proto-arc samples have $(^{143}Nd/^{144}Nd)_i$ values which plot on the margin between the EPR MORB and CCOP, with a range of 0.51297 – 0.51300.

Samples of the Baudó Plateau also plot within the CCOP array, with a range of values from 0.51292 – 0.51295.

Discounting the samples of the Soná-Torio High-Mg Plateau and Soná-Azuero Arc, there is a negative correlation with $(^{143}Nd/^{144}Nd)_i$ values for La/Sm, indicating the light REE contents correlates to source composition for most samples. Samples of the plateau and proto-arc groups also show negative correlations between ΔNb and $(^{143}Nd/^{144}Nd)_i$ contents, while proto-arc samples show negative correlations between Th/Nb ratios and $(^{143}Nd/^{144}Nd)_i$ values.

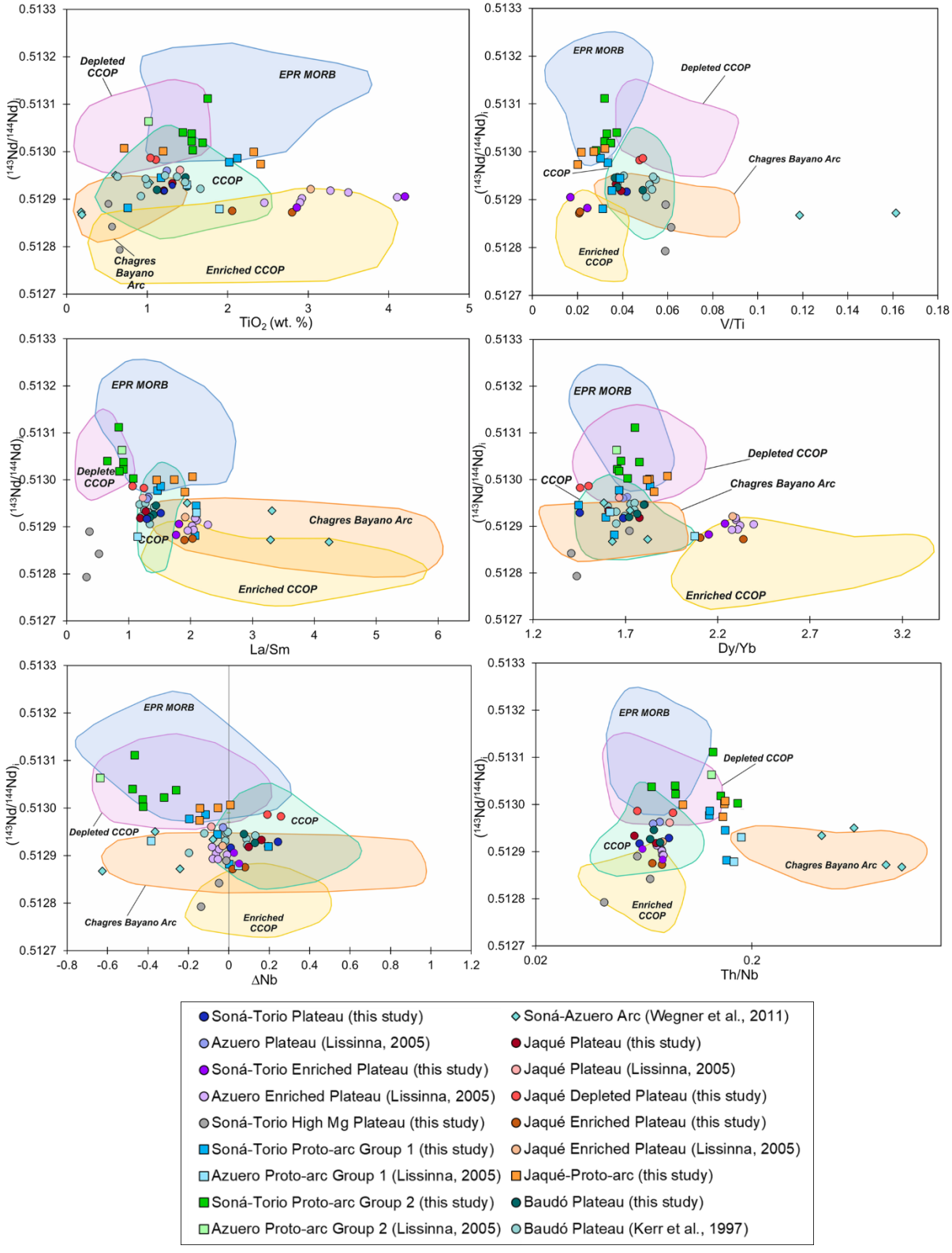

Figure 5.28: Bivariate diagrams of initial Nd isotopic ratios of the Soná-Torio, Darién Pacific Coast and Serranía de Baudó samples, with previously analysed samples of Lissinna (2005) and Wegner et al. (2011). Also displayed are the isotope fields for the Colombian-Caribbean Oceanic Plateau (CCOP) (La/Sm > 0.60, < 1.20), the Depleted CCOP (La/Sm < 0.60) and Enriched CCOP (La/Sm > 1.20) (all from GEOROC online database, age corrected to 90Ma), the East Pacific Rise MORB (EPR MORB) from (PetDB online database) and the Chagres Bayano Arc (Wegner et al., 2011).

5.7 **Summary**

The samples of the Soná-Torio, Darién Pacific Coast and Serranía de Baudó regions have LOI values ranging between 0.5 and 13.9 wt. %, and all samples show some degree of alteration in thin section. On plots of major and trace elements against Zr, many elements (K_2O, Ba, Rb, Sr) had poor correlations with Zr and it was clear that they may have been mobilised during alteration. However, major elements such as TiO_2, Al_2O_3, Fe_2O_3 and MgO, and trace elements including the REE and Th, Nb, Hf and Ta showed moderate to good correlations with Zr, and therefore remained immobile and are suitable to be used for further interpretation of geochemical groups.

Within the Plateau, Enriched Plateau and Depleted Plateau groups from the three regions, the majority of samples plotted as basalts on classification diagrams. The Soná-Torio High-Mg Plateau is distinct from the remainder of the plateau groups, and plotted as basalts and picro-basalts. The Soná-Torio and Jaqué Proto-arc groups also generally were classified as basalts. Soná-Torio Arc samples ranged from basalt to andesite, as well as plotting in the High-K calc alkaline array on the Th-Co diagram. Jaqué Arc samples ranged from basalt through to rhyolite, and largely plotted in the calc-alkaline array on the Th-Co diagram. Across, the three regions, the Plateau groups had MgO contents ranging from, 5.08 – 12.88 wt. %, the Jaqué Depleted Plateau had MgO contents ranging from 5.34 - 7.58 wt. % and the Enriched Plateau groups had MgO contents ranging from 3.38 – 12.11 wt. %. Again, the Soná-Torio High-Mg Plateau has values distinct from the remainder of the plateau groups, with MgO contents ranging from 12.8 – 24.0 wt. %. The Soná-Torio and Jaqué Proto-arc groups have MgO contents ranging from 3.32 – 12.88 wt. %, and Soná-Torio and Jaqué Arc groups have MgO contents ranging from 0.25 – 8.15 wt. %.

On primitive mantle-normalised multielementary diagrams, the Soná-Torio, Jaqué and Baudó Plateau groups show flat patterns with positive Nb anomalies, typical of a plateau signature. The Jaqué Depleted Plateau show similar patterns with a slight LREE depletion, while the Soná-Torio High-Mg plateau is highly depleted in the LREE. The Soná-Torio and Jaqué Enriched Plateaus have similar enriched patterns, with positive Nb anomalies. The Soná-Torio Proto-arc Group 1 has flat pattern on the primitive mantle-normalised multielementary diagram, with depleted Nb and variable enriched to depleted Th. The Soná-Torio proto-arc Group 2 show depleted LREE, again with negative Nb anomaly and enriched to depleted Th. The Jaqué Proto-arc has flat to enriched LREE, but again has depleted Nb and enriched Th. Soná-Torio Arc shows flat patterns, with a clear Ti and Nb depletion and more enrichment in Th. The Jaqué Arc shows more variation. Jaqué Group 1 samples have flatter patterns, again with Ti and Nb negative anomalies, and Th positive anomalies. The

Jaqué Arc Group 2 is more enriched in the LREE, with Ti and Nb negative anomalies, Th positive anomalies and variable enriched to depleted Zr. Jaqué Group 3 shows enriched patterns, with higher overall REE content, strong Ti negative anomaly, small Nb depletion and Th enrichment.

On tectonic discrimination diagrams, the Soná-Torio, Jaqué and Baudó Plateau samples generally plot close together in the MORB or oceanic plateau arrays. The Jaqué Depleted Plateau generally plots close to these groups but as a distinct group, generally towards the depleted margin of the array. The Soná-Torio High-Mg Plateau again are a distinct group, always plotting in or beyond the depleted margin of the MORB or oceanic plateau array. The Enriched Plateau groups also plot together, within the enriched margins of the arrays, close to the OIB array. Generally, the Soná-Torio Proto-arc Group 1 and the Jaqué Proto-arc plot together on the tectonic discrimination diagrams, between the MORB or oceanic plateau and arc arrays. The Soná-Torio Proto-arc Group 2 plots separately, generally towards the N-MORB or more depleted end of the MORB array. The Soná-Torio and Jaqué Arc groups plot in the Arc arrays on the tectonic discrimination diagrams, but the samples from each region generally plot as separate groups.

Using Nd isotope initial values, the Soná-Torio, Jaqué and Baudó Plateau plot together, within the CCOP array. Jaqué Depleted Plateau have slightly higher values, while the samples of the Soná-Torio and Jaqué Enriched Plateaus also plot together, at lower values, at the top of the Enriched CCOP array. The Soná-Torio High-Mg Plateau samples plot at low Nd_i values, some below the range of the CCOP, despite being highly depleted in the light REE. Soná-Torio Proto Group 1 samples have a range similar to the Plateau groups, plotting between the EPR MORB, Depleted CCOP and CCOP arrays. The Jaqué Proto-arc has slightly higher values than the Plateau groups, again plotting within the EPR MORB, Depleted CCOP and CCOP arrays. Soná-Torio Proto-arc Group 2 has the highest values in this study, and these samples plot within the EPR MORB or Depleted CCOP arrays. The Soná-Azuero Arc samples generally plot within Chagres-Bayano Arc array.

6. DISCUSSION

6.1 Introduction

The following chapter first synthesises the results previously outlined in Chapters 3-5. These results are then evaluated and discussed to assess how they help to meet the project aims outlined in Chapter 1. The results are investigated to determine the potential implications for models of subduction initiation and the tectonic evolution of the southwestern Caribbean in the Late Cretaceous through to the Eocene.

This chapter will first include a short discussion on the suitability of the $^{40}Ar/^{39}Ar$ radiometric dating technique on altered tholeiitic basalts in the Caribbean. This discussion will include an evaluation of the methods by which the $^{40}Ar/^{39}Ar$ ages may be offset and the implications this has on our understanding of the stratigraphy of sequences in the Caribbean. There is then a short synthesis of field geology, petrography, geochemistry and geochronology results to produce a stratigraphic and geochemical summary for the Soná-Torio, Darién Pacific Coast and Serranía de Baudó regions.

The main portion of this chapter will then evaluate the impact of these results on the understanding of the nature of the first subduction related magmas along the southwestern margin of the Caribbean plateau, and subsequently what this can infer about the model of subduction initiation in this region in the Late Cretaceous. This will be done by comparing the stratigraphy, geochemistry and lithologies to those recognised along the Izu-Bonin-Mariana forearc, where subduction initiation processes have been studied most intensely. There is also an evaluation and consideration of subduction initiation models previously suggested for the Caribbean region, including the Plume-Induced Subduction Initiation (PISI) model of Whattam and Stern (2015). This section is concluded with a suggestion and evaluation of a potential new model of subduction initiation for the southwestern margin of the Caribbean Plateau, that can explain both new and pre-existing field and geochemical results, whilst also fitting with regional and geodynamic constraints.

The next stage of the discussion will investigate the nature of the arc basement. This section will consider the relationship between the Soná-Torio, Jaqué and Baudó Plateau sequences, and discuss the origins of these plateaus. This includes whether all basement sequences do represent part of an oceanic plateau, and if all sequences are derived from the same hotspot and oceanic plateau. As has been suggested for sequences across the Caribbean, it is possible that these sequences could represent multiple separate oceanic plateaus. These issues will be investigated using geochemical and field constraints from this study.

Finally, the outcomes of the above discussions will be used to to propose a model of tectonic evolution in the Caribbean from the Cretaceous onwards. This model will consider previous constraints, and will highlight how our new results contribute to the understanding of Caribbean tectonics during this time period.

6.2 Reliability of $^{40}Ar/^{39}Ar$ dating on rocks of the CCOP and associated arc units.

As described in Chapter 4, many of the new $^{40}Ar/^{39}Ar$ dates for tholeiitic basalts satisfy all regular quality criteria for reliable plateau ages, but do not represent geologically feasible crystallization ages. In the $^{40}Ar/^{39}Ar$ geochronology results from this study, 15 new ages were produced from 5 groundmass separates and 10 plagioclase separates. All of these ages satisfied the criteria to give reliable ages, which required plateaus to be formed of a minimum of three contiguous steps which overlap within 2σ uncertainty and which release at least 50% of ^{39}Ar. The inverse isochron formed by the plateau steps must also yield an age indistinguishable from the plateau age at 2σ uncertainty, while the trapped component composition must be indistinguishable from the atmospheric composition at 2σ uncertainty (Fleck et al., 1977; Lanphere and Dalrymple, 1978). However, previous and new field, geochemical and biostratigraphic constraints provide a well-defined stratigraphic context that can be used to test the reliability of $^{40}Ar/^{39}Ar$ geochronological results to determine crystallization ages of low-K basalts in the Panamanian forearc.

Results of this study clearly show that some ages disagree with stratigraphic constraints. For example, the age of Soná-Torio Plateau sample DB09-010 gave a plateau age of 54.6 ± 1.3 Ma, but this sample is clearly intruded in the field by sample DB09-013 that apparently has an older crystallization age of 60.71 ± 0.18 Ma. Rarely, ages from this study do not contradict stratigraphic constraints and could potentially fit within the hypothesised stratigraphic framework. It is possible that stratigraphically younger samples (such as those from the Soná-Torio or Jaqué Arc Groups) may represent true crystallisation ages, whilst samples from older, and more altered sequences (samples of the Soná-Torio, Jaqué or Baudó Plateau) are more problematic. However, where the age spectra for these samples appear to be similar, it is assumed that these potentially reliable ages have also experienced some disturbance and may not represent true crystallisation ages. For this reason, as there are no clear criteria to distinguish between true crystallisation ages and other ages which do not represent the crystallisation, the new results have not been used in the stratigraphic framework. The ages which fit within the stratigraphic framework could potentially be used in the future, or as minimum crystallisation ages, but they need to be verified by another dating

technique. To gain reliable ages for low-K submarine basalts in the future, it is likely that the $^{40}Ar/^{39}Ar$ technique and procedure needs to be further refined, or techniques such as U-Pb zircon or baddeleyite dating need to be utilised.

Previous studies have shown that using $^{40}Ar/^{39}Ar$ to date Cretaceous low-K, basalts using groundmass and plagioclase separates is a viable and reliable technique (Koppers et al., 2000; Koppers et al., 2003). As it is easier to remove artefacts of alteration from plagioclase through leaching and hand-picking, this technique is utilised over groundmass where possible. However, it can be difficult to completely remove all alteration from sample separates. In this study, samples were selected based on their relative freshness, along with location and sample availability, to help minimise the effects of alteration. Despite selecting the freshest samples available, most samples from the study area showed signs of alteration. In thin section, the groundmass was typically altered to clays and chlorite, while plagioclase often showed sericite alteration. This alteration was more significant in the older plateau samples, but was also present in the younger arc-like samples. All groups also showed alteration through the mobility of the LILE's, as displayed in Section 5.2. Despite extensive leaching and an extensive amount of time spent hand-picking the separates, it was impossible to completely remove all artefacts of alteration in the rocks.

The most significant and problematic alteration issue may be the alteration of plagioclase to sericite. Sericite is highly problematic as it is a K-rich mineral, which can contain 10 wt. % K_2O, while plagioclase is typically K-poor, often with < 0.1 wt. % K_2O. This makes plagioclase particularly sensitive to sericite alteration, as even a small addition of sericite can have a large impact on the K contents of the plagioclase crystal, which in turn can affect the age spectra the plagioclase will produce. It has been estimated that even an addition of 0.1 – 0.2 % of sericite to plagioclase can shift the apparent age by several tens of millions of years (Verati and Jourdan, 2014). It has also been suggested that plagioclase crystals which include around 1 – 2 % of sericite may be indistinguishable from unaltered plagioclase under a stereomicroscope, even for an experienced eye (Verati and Jourdan, 2014). This highlights the difficulty in removing all traces of alteration from plagioclase separates, and the likelihood that the separates in this study contained some sericite despite leaching with HCl and HNO_3 until altered phases appeared to be removed, followed by hand-picking. Samples affected by sericite alteration can produce young apparent ages, with disturbed spectra, but they can also produce 'alteration plateaus' (Jourdan et al., 2003; Pati et al., 2010). In this case, the age spectra produce plateaus which can potentially satisfy the required criteria for reliable ages, but the ages do not reflect the true crystallisation age.

One way to assess the potential influence of sericite on the age spectra is to look at the Ca/K ratios produced within the plateau. As previously stated, sericite is rich in K, while plagioclase is K-poor. Although the Ca/K ratios of individual plagioclase crystals were not measured in this study, plagioclase typically has high Ca/K ratios in comparison to sericite. A normal plagioclase may have a Ca/K ratio of 36, whereas a K-rich plagioclase may have a Ca/K ratio of 14, and a K-poor plagioclase may have a Ca/K ratio of 239 (Verati and Jourdan, 2014). Where sericite has altered the plagioclase, this will reduce the Ca/K ratio due to the addition of the K-rich phase. Where samples have true crystallisation plateau ages, with no Ar loss or alteration, the Ca/K ratio should be constant within the plateau. However, that is not reflected in many of the samples of this study. Within the age plateaus, the Ca/K ratios can be highly variable within ages measured on plagioclase separates. In the case of the Soná-Torio Proto-arc Group 2 and Arc samples (JB17-008, JB17-030 and DB09-013, Figures 4.4, 4.5, 4.7), the Ca/K ratios are low overall, with values below 10. These samples also show a dip in Ca/K ratios within the age plateau, reaching values as low as 1, which has been suggested to be a sign of sericite alteration (Verati and Jourdan, 2014). Sample JB17-059 of the Jaqué Depleted Plateau has higher values of Ca/K overall, but shows a characteristic “staircase” at the start and end of the age plateau, with lower values in the centre of the plateau (Figure 4.10) which may be indicative of Ar loss (Boven et al., 2001). Sample JB17-069 of the Jaqué Enriched Plateau has an average Ca/K value of 19.6 within the age plateau, but this also varies to values as high as 27 and as low as 15, which indicates some disturbance of the original plagioclase Ca/K ratio (Figure 4.12). Sample JB17-075 also shows typical staircase pattern in Ca/K ratio values at the beginning of the age plateau, with values within the age plateau ranging from 59 to 218 (Figure 4.13). Overall, sample JB18-071 of the Jaqué Proto-arc has an average Ca/K ratio of 29 within the age plateau, but this sample also shows disturbed spectra (Figure 4.14). Sample JB18-064 of the Sapo Arc, Jaqué Arc Group 2 shows a clear staircase pattern of Ca/K values within the age plateau (Figure 4.15). This staircase begins with Ca/K values of 1, indicating degassing of a high-K phase which is unlikely to be plagioclase, and increases to values of 40, which may represent the actual plagioclase composition. The samples of the Baudó Plateau both show disturbed Ca/K ratios within the age plateaus. Sample JB17-092 has Ca/K ratios varying from 63 through to 128 within the age plateau, although these values occur within three steps of the other (Figure 4.15). Sample JB17-127 shows further disrupted spectra, with Ca/K values ranging from 70 to 8, with several negative ratios down to -23, which is clearly problematic (Figure 4.16).

Therefore, despite having an age plateau which satisfies quality criteria, many of the geochronological results from this study have disturbed Ca/K ratios. This indicates the

presence of sericite alteration, which has produced anomalously young apparent ages which do not represent crystallisation ages. Unfortunately, some of the most problematic samples, those of the Soná-Torio Plateau, are measured on groundmass separates. Although these samples also show irregular Ca/K ratios within the plateau, this may be linked to the degassing of different phases within the groundmass at different times. In this case, it is difficult to assess the impact of alteration on the apparent ages.

Although sericite has likely affected the apparent ages of the samples, alteration or deformation of these samples could also affect the apparent age by causing excess ^{40}Ar or loss of argon in the plagioclase or groundmass. During a heating event, possibly caused by increased fluid flow or heating due to a larger tectonic event, ^{40}Ar can be released from K-bearing minerals. This ^{40}Ar can become trapped in the minerals of interest, resulting in excess ^{40}Ar within these minerals (Kuiper, 2002). Assuming that the excess ^{40}Ar is homogenously distributed across the measured minerals, the excess ^{40}Ar does not cause a shift in the apparent age on an inverse isochron diagram and could also remain undetected within plateau age spectra (Kuiper, 2002). The inverse isochron diagram can however detect excess ^{40}Ar within the measured minerals. If the trapped component contains excess ^{40}Ar, the $^{36}Ar/^{40}Ar$ y-axis intercept will be below atmospheric values (Kuiper, 2002). In this study, the isochron ^{36}Ar /^{40}Ar trapped argon ratios are always within error of atmospheric values, and therefore do not appear to show evidence of excess ^{40}Ar*. However, if the excess ^{40}Ar is distributed heterogeneously, which is more probable than homogenous distribution, it can be difficult to detect the ^{36}Ar /^{40}Ar offset as false isochrons can be formed (Kuiper, 2002). These false isochrons can produce an incorrect apparent age, offset to older ages than expected, along with an incorrect trapped argon composition, making it difficult to detect any trace of excess ^{40}Ar. In this case, the plateau apparent age can also be offset to older ages, with “saddle-shaped” age spectra. This age spectra is typical of samples containing excess ^{40}Ar, where a component containing the excess ^{40}Ar is released both at the lowest and highest temperature steps (Harrison and McDougall, 1981). It is still possible that a plateau age which adheres to quality criteria can be produced in these circumstances, and that both the plateau and isochron can produce similar incorrect ages (Kuiper, 2002) However, in this study, the samples typically have younger ages than indicated by the stratigraphic framework, and it is unlikely that the cause of these ages is excess ^{40}Ar.

Argon loss can occur during reheating or fluid circulation, possibly related to a tectonic event (Kuiper, 2002). It can also be caused by deformation when the crystal lattice is disturbed, but the samples here do not appear to show tectonic deformation of the measured minerals. Argon isotopes remain unfractionated during degassing, and therefore the ^{36}Ar /^{40}Ar trapped argon composition will not be affected by argon loss, despite being affected by excess ^{40}Ar

(Kuiper, 2002). The $^{39}Ar/^{40}Ar$ ratio is however affected by argon loss. The concentration of ^{39}Ar will remain stable as it is produced from ^{39}K which will not be released, but the concentration of ^{40}Ar will decrease as it released from the mineral. This will cause an increase in the ^{39}Ar /^{40}Ar values leading to a lower inverse isochron apparent age (Kuiper, 2002). If the argon loss occurs homogeneously across the minerals, it would be very difficult to detect this argon loss, both on an inverse isochron diagram and on a plateau step-heat diagram. However, where it has occurred heterogeneously, the argon loss can be potentially be detected by younger age steps across the plateau spectra, but a plateau which adheres to the quality criteria could still potentially be generated in this scenario (Harrison and McDougall, 1981). This is especially likely if the argon loss has occurred within 20 Myr of the initial crystallisation age of the mineral, or if the argon loss is homogeneous, where both a false plateau and a false isochron could be produced (Kuiper, 2002). Of the samples measured here, all samples have somewhat heterogeneous plateau values, which often do not correlate with the heterogeneous K/Ca values, indicating that there two independent processes affecting these spectra. Therefore, it appears likely that these samples have been affected by Ar loss.

Where apparent ages are offset by alteration or argon loss, it is not clear if the ages represent the age of resetting, or if they represent a hybrid between the true crystallisation age and the age of resetting. As the ages across the regions do not appear to converge on a single age, it is likely that these ages represent an offset to the crystallisation age dependent on age, extent of alteration and extent of argon loss. Plagioclase separates with over 65 % sericite alteration have been shown to be within 1% of the age of alteration (Verati and Jourdan, 2014), but the samples selected here did not have this extent of sericite alteration. If all ^{40}Ar escaped from the minerals during a reheating event, then the apparent age would represent the age of reheating, but if some relic ^{40}Ar remained then the apparent age will represent an arbritary age between the age of reheating and crystallisation. It is also likely that samples which have experienced sericite alteration may also have experienced some argon loss, and it is difficult to assess the individual effects of each of these mechanisms at this stage. However, the samples of the Soná-Torio region do largely have ages ranging between 60 – 50 Ma, which may indicate an alteration or reheating event at this stage. The samples of the Darién Pacific Coast area also largely lie between 23 – 12 Ma, which could point to an alteration or reheating event. This event may be related to the collision between Panama and South America (Farris et al., 2011; Montes et al., 2012b), which could lead to reheating or increased alteration in the region due to tectonic uplift and/or increased fluid flow. Due to the heterogeneity of the regions, with multiple units and lithologies with few existing age constraints, it is difficult to assess the true age offset caused by alteration.

Despite the $^{40}Ar/^{39}Ar$ technique being extensively used, it is likely that many ages used in the literature do not represent true crystallisation ages (Baksi, 2007). Analysis of previous plagioclase $^{40}Ar/^{39}Ar$ ages from Gorgona, Curacao, DSDP Leg 150 and Nicoya Peninsula (all on low-K basalts and picrites similar to those dated in this study) showed that all samples were affected by alteration (Baksi, 2007). It was determined that the ages for Gorgona and Leg 150 could represent the minimum crystallisation age at best, while the samples of the Nicoya Peninsula were altered to the extent that they could not be expected to produce reliable ages (Baksi, 2007). It is likely that where low-K basalts are pervasively altered, like those within the CCOP, there will have been issues affecting $^{40}Ar/^{39}Ar$ ages. As altered samples can produce alteration plateaus, it can be very difficult to recognise these problematic ages without stratigraphic constraints or accompanying U/Pb or biostratigraphic ages. A recent unpublished Masters study which aimed to collect new ages for basalts from the Serranía de Baudó has shown that the $^{40}Ar/^{39}Ar$ ages likely do not represent crystallisation ages (Acero, 2019). In this case, low temperature steps had low Ca/K, representing the addition of an alteration phase to the original plagioclase, while higher temperature steps had higher Ca/K. By selectively using only the higher temperature steps, which are less likely to represent an alteration phase, they produced a $^{40}Ar/^{39}Ar$ age of 86.09 ± 6.26 Ma (Acero, 2019). This age represents the minimum age of crystallisation, as it is thought to still be affected by sericite alteration (Acero, 2019). This leads to questions about the reliability of existing $^{40}Ar/^{39}Ar$ ages in the Serranía de Baudó, such as those of Kerr et al. (1997a). These previous ages range between 78 – 72 Ma and are at least ~7 Ma younger than the ages of other accreted fragments of the CCOP, which has led to the interpretations that this part of the plateau may have had a different origin that other accreted fragments (e.g., Kerr and Tarney, 2005; Whattam and Stern, 2015). However, based on the findings of Acero (2019) and the impact of small amounts of sericite in plagioclase, it is likely that these ages have been offset by alteration. These issues may also be reflected in ages of the Jaqué Plateau from Lissinna (2005), where $^{40}Ar/^{39}Ar$ ages of basalts are 84.1 ± 1.0 Ma and 71.3 ± 2.2 Ma, while radiolarite ages based on sediments interbedded with the plateau are 90 – 80 Ma (Bandy and Casey, 1973; Barat et al., 2014). Although these samples may produce acceptable age plateaus, it is likely that this younger age has been affected by alteration as it is very young age for the oceanic plateau, and it does not correlate with the biostratigraphic age. On the Soná and Azuero Peninsulas, ages of the plateau range from 93.5 ± 5.3 Ma to 82.6 ± 3.2 Ma based on step heating of plagioclase, and a 71.3 ± 2.1 Ma matrix total fusion age, but the ages of radiolarites interbedded with plateau basalts are 89-85 Ma (Kolarsky et al., 1995; Buchs, 2008). The oldest apparent age in this study was from the Soná-Torio Plateau (sample DB15-030), with an age of 87.0 ± 2.4 Ma. This age is in agreement with the radiolarite ages and is within error of the oldest plateau ages, and

therefore this sample age could represent the minimum crystallisation age of the plateau in Soná-Torio. This age of the Soná-Torio Plateau also coincides with the older $^{40}Ar/^{39}Ar$ and radiolarite ages of the Jaqué Plateau, and the minimum crystallisation age of the plateau in the Serranía de Baudó from Acero (2019). Based on these ages, it appears that the plateau sequences from Soná-Torio, Darién and Baudó formed more contemporaneously than previously thought (discussed further in Section 6.5).

In the future, caution needs to be used when $^{40}Ar/^{39}Ar$ ages are collected on low-K basalts which have been altered, even if the alteration is only moderate. Efforts should be made to verify $^{40}Ar/^{39}Ar$ ages using biostratigraphic or U-Pb constraints, as these results have shown that even where age data satisfies reliable plateau criteria, they may still be affected by alteration processes.

6.3 Stratigraphic and Geochemical Summaries

6.3.1 Stratigraphy and geochemistry of the Soná-Torio Region

At the base of the Soná-Torio region stratigraphy is the Soná-Torio Oceanic Plateau, which was emplaced on top of an unknown basement (Figure 3.2, 3.6). This oceanic plateau was previously recognised as the base to the proto-arc and arc (Buchs et al., 2010; Corral et al., 2011) which is consistent with the observations within this study. The plateau is primarily composed of pillow basalts and lava flows, and can be interbedded with siliceous sediments. These basalts consist of two geochemical groups – the Soná-Torio Plateau and the Soná-Torio Enriched Plateau. Both the Plateau and Enriched Plateau samples are exposed along the Rio Torio and across the Soná Peninsula. The Soná-Torio Plateau samples have flat patterns with positive Nb anomalies on trace element primitive mantle normalised diagrams, typical of a plateau signature (Figure 5.17). The Enriched Plateau samples have an enrichment in the LREE, also with positive Nb anomalies on multielementary primitive mantle normalised diagrams (Figure 5.17). The Enriched Plateau group correlates with samples labelled as “Plateau Group II” by Buchs et al. (2010). The Soná-Torio Oceanic Plateau also includes greenschists, which are exposed largely close to the Soná-Azuero Fault Zone (Figure 3.6). These greenschists are formed of the Soná-Torio High Mg Plateau samples, which are high in MgO and have are heavily depleted in the LREE. It appears that the Greenschists are older than the plateau basalts, as the greenschists are intruded by plateau-like dykes. Basalts of the plateau have been dated as Coniacian-early Santonian (89-85 Ma) based on radiolarites ages (Kolarsky et al. 1995; Buchs et al. 2009), and as

Cretaceous (114.5 ± 2.0 to 71.3 ± 2.1 Ma) from Ar^{40}/Ar^{39} incremental heating (Lissinna, 2005).

Overlying the Soná-Torio Oceanic Plateau is the Soná-Torio Proto-arc Group. At the base of this group is the Torio Lithostratigraphic Unit, which has also been described as part of the Ocu Formation (Buchs et al., 2010; Corral et al., 2011). This unit is composed of hemipelagic to pelagic limestones, which can rarely be tuffaceous, and includes intervals of sandstone breccias to graded sandstones (Figure 3.8). The Torio Lithostratigraphic Unit has previously been dated as Upper Campanian to Maastrichtian (75 – 73 Ma), based on foraminifera (Buchs et al 2010, 2011, Kolarsky 1995) (Figure 3.2). In this study, a sample from Rio Torio gave a nannofossil age of Turonian-Maastrichtian. This limestone is interbedded with lavas of the Proto-arc Group 1, and also intruded by Proto-arc Group 1 dykes (Figure 3.8). The Proto-arc Group 1 has generally flat trace element patterns, variably enriched Th, depleted Nb and slight Ti negative anomalies (Figure 5.18). The Proto-arc Group 1 has only been dated relatively based on the intrusion of dykes into the Torio Limestone, associated with soft-sediment deformation. Therefore, the Proto-arc Group 1 is also assigned an age of 75 - 73 Ma (Figure 3.2).

Along the Pixvae Coast, the La Mona Formation is exposed (Figure 3.4). This formation is composed of limestone and tuffaceous sequences interbedded with basaltic breccias (Figure 3.8). A tuff sample from the La Mona Formation had Proto-arc Group 1 geochemistry, and the La Mona Formation is intruded by dykes of the Proto-arc Group 2. The Proto-arc 2 has not been otherwise dated, but based on this relationship it is assumed to be relatively younger than the Proto-arc Group 1 and thus is estimated to have formed at ca. 73-72 Ma (Figure 3.2). The Proto-arc Group 2 is composed of porphyritic basaltic to doleritic intrusions, and shows variable enriched to depleted Th and a negative Nb anomaly, but is also generally depleted in the LREE (Figure 5.18).

The next stage of volcanism in this region is the formation of the Soná Torio Arc. This unit is formed of porphyritic basaltic to andesitic lavas, gabbroic to granodioritic intrusions and pillow basalts, seen only in Pixvae (Figure 3.8). The Soná-Torio Arc geochemistry shows a typical arc signature, with enriched Th, and strong Nb and Ti negative anomalies (Figure 5.18). Ages of the Soná-Torio age range from 70 – 44 Ma (Lissinna, 2005; Wegner et al., 2011) (Figure 3.2).Overlying the Arc are cover sediments such as the Tonosi Formation, a shallow marine limestone which grades into turbiditic sandstones, dated as Mid Eocene based on nannofossils (~ 38-23 Ma) (Kolarsky et al., 1995; Buchs et al., 2011b) (Figure 3.2).

6.3.2 Stratigraphy and geochemistry of the Darién Pacific Coast region

At the base of the sequence is the Jaqué Oceanic Plateau, again emplaced on an unknown basement. This Plateau is formed again of three geochemical groups – the Jaqué Plateau, Depleted Plateau and Enriched Plateau. The Jaqué Plateau and Jaqué Depleted Plateau cannot be distinguished in the field, and are composed of pillow basalts, lava flows and rare intrusions (Figure 3.16). These pillow basalts and lava flows can be interbedded with sequences of black to red chert, siliceous mudstones and rare limestones. Both the Jaqué Plateau and Depleted Plateau groups have generally flat plateau-like signatures on multielementary primitive mantle normalised diagrams, but the Jaqué Depleted Plateau is more depleted in the LREE (Figure 5.21). The Jaqué Enriched Plateau is generally found in deformed pillows associated with interpillow sediments or hyaloclastite (Figure 3.16). The Enriched Plateau samples have LREE enriched patterns on multielementary primitive mantle normalised diagrams, similar to the samples of the Soná-Torio Enriched Plateau (Figure 5.21). Basalts of the Jaqué Plateau have previously been dated as 84.1 ± 1.0 Ma using $^{40}Ar/^{39}Ar$ dating, with an error weighted mean stepheat age of to 71.3 ± 4.4 Ma for the same sample (Lissinna, 2005). Radiolarians interbedded with the plateau were assigned a Coniacian to early Campanian age (90-80 Ma) (Bandy and Casey, 1973; Barat et al., 2014) (Figure 3.13).

Plagioclase-phyric dykes of the Jaqué Proto-arc intrude the sequences of the Jaqué Plateau (Figure 3.16). These intrusions exhibit an enriched plateau-like geochemistry with variable positive Th and negative Nb on primitive mantle normalised multielement diagrams (Figure 5.21). Compared to the Soná-Torio Proto-arc Group 1 samples, these samples are slightly more enriched in the LREE. Unfortunately, it has not been possible to date this unit.

The Darién Formation is composed of green-grey siliceous sediments, which was observed overlying basalts in the San Miguel Gulf (Barat et al., 2014) (Figure 3.19). Therefore, this formation is thought to overly the basalts of the Jaqué Plateau. The Darién Formation has been dated as Late Ypresian to Early Lutetian (~50-46 Ma) based on radiolarian dating (Barat et al., 2014) (Figure 3.13).

The next group exposed along the Darién Pacific Coast is the Jaqué – La Palma Group. This Group is composed of the Bahia Piña Formation, the Guayabo Formation, the San Miguel Formation and the Sapo Volcanic Group. The Bahia Piña Formation overlies the basalts of the plateau (Figure 3.19). This formation is a 3-5m sequence formed of shallow marine limestones. Based on foraminifera, this unit has been assigned an age of Mid Eocene – Oligocene (~38-23 Ma) (Figure 3.13). The Bahia Piña Formation is observed to

grade into to the Guayabo Formation, which is formed of debris flow conglomerates and turbidites, interbedded with calcareous hemipelagic mudstones (Figure 3.19). This Guayabo Formation contains clasts of fine grained calcareous sediments along with porphyritic igneous clasts. All analysed igneous clasts from the Guayabo Formation had a whole rock geochemistry similar to the Jaqué Arc Group 2 (Figure 5.22). The Guayabo Formation was dated as Mid Eocene - Oligocene based on foraminifera and nannofossils (Figure 3.13). The San Miguel Formation is formed of arc-derived debris flows and tuffs, while the Sapo Volcanic Group consists of mafic to felsic intrusive rocks and lava flows (Figure 3.21). The Sapo Volcanic Group contains samples of Jaqué Arc Groups 1, 2 and 3. All Jaqué Arc Groups show established volcanic arc geochemistry, with depleted Nb, and Ti, and enriched Th. The Jaqué Arc Group 1 has relatively flat LREE on multielementary primitive mantle normalised diagrams, while the Jaqué Arc Group 2 is more enriched in the LREE and also shows depleted to enriched Zr (Figure 5.22). The Jaqué Arc 3 is generally more enriched in all trace elements, and shows very pronounced negative Ti anomalies (Figure 5.22).

6.3.3 Stratigraphy and geochemistry of the Serranía de Baudó region

As the base of the stratigraphy of this region is the Baudó Oceanic Plateau. This plateau is again composed of pillow basalts and lava flows, with interbedded sediments, but here there is also an extensive sill complex (Figure 3.25). The interbedded sediments are composed of black to red chert, black mudstone and siliceous limestone, and locally these sediments form peperites with lavas or intrusions (Figure 3.27). The Baudó Oceanic Plateau is composed only of one geochemical group, which displays typical flat trace element patterns on a primitive mantle normalised diagram, with positive Nb anomalies (Figure 5.25). The only ages for this plateau are the ages of Kerr et al. (1997) (77.9 ± 1.0 – 72.5 ± 0.4 Ma) (Figure 3.23). As discussed above (Section 6.2), these ages do not represent the true crystallisation age, and the plateau in this region may be older than this.

The Punta Lana Formation overlies the plateau. This formation is composed of black mudstone, sandstone and breccias, and does not appear to previously have been documented (Figure 3.23, 3.27).

The Baudó Melange is exposed on the Bahia Solano peninsula and is formed of heavily deformed basalts and sediments (Figure 3.24, 3.28) The relationship of the Baudó Melange to the Baudó Oceanic Plateau is not clear (Figure 3.23). Unfortunately, this unit could not be geochemically analysed or dated due to extensive alteration.

6.4 Subduction initiation along the southwestern margin of the Caribbean Oceanic Plateau

Along the southwestern margin of the Caribbean Oceanic Plateau, subduction initiation occurred in the Late Cretaceous, leading to the generation of the Panama Arc on top of an oceanic plateau basement (Buchs et al., 2010, Wegner et al., 2011, Corral et al.). Due to uplift of the forearc in the Mid Eocene – Oligocene, likely due to shallow subduction of the Cocos Ridge and Nazca and Cocos Plates (Krawinkel et al., 1999; Saks et al., 2009; Buchs et al., 2011), the earliest subduction initiation sequences are preserved in Panama, particularly on the Soná and Azuero Peninsulas. The magmatic products generated during subduction initiation, and associated sedimentary deposits, are so often removed by erosion or covered by younger arc related magmatic and sedimentary products. Therefore, the forearc stratigraphy exposed on the Azuero and Soná Penisulas give us a unique opportunity to study subduction initiation along the margin of an oceanic plateau. As previously outlined, much of our current understanding of subduction initiation comes from the Izu Bonin Mariana (IBM) system, which has been studied in detail (Stern and Bloomer, 1992; Reagan et al., 2010; Reagan et al., 2017; Li et al., 2019; Shervais et al., 2019). This has led to significant breakthroughs in potential mechanisms of subduction initiation and the associated formation of magmatic products. The level of investigation along the IBM system would not have been possible without IODP expeditions, and significant drilling. On the Azuero and Soná Peninsulas in western Panama, we have an opportunity to study the forearc on land, although this is largely limited to coastal regions and rivers due to the presence of tropical vegetation. As the oceanic plateau forms the basement to the proto-arc and arc, studying the forearc stratigraphy on Azuero and Soná allows the opportunity to evaluate the role of the oceanic plateau or plume on the initiation of subduction, and the influence of the plume on the generation of the first magmatic products of subduction initiation.

6.4.1 The Izu-Bonin-Mariana Forearc and the “Subduction Initiation Rule”

The stratigraphic record of subduction initiation in the Izu-Bonin-Mariana forearc has been extensively studied over the last few decades, assisted by numerous IODP expeditions to the region in recent years (Reagan et al., 2010; Ishizuka et al., 2011; Reagan et al., 2017; Ishizuka et al., 2018). Based on the stratigraphic assemblage of the earliest IBM deposits, a “Subduction Initiation Rule” defining key secular chemo-temporal changes which might be applicable to all nascent subduction systems was proposed by Whattam and Stern (2011). This rule aimed to develop a universal model of subduction initiation, based on the model of

subduction initiation along the IBM, and was thought to explain the stratigraphy seen at the base of subduction-related ophiolites. However, subduction zones can form in vastly different settings, and models of subduction initiation need to consider the complex interplay between a number of components, such as the external tectonic forces on the initiation of subduction, the nature of both the overriding and subducting plates and the nature of the mantle (Mueller and Phillips, 1991; Toth and Gurnis, 1998; Hall et al., 2003; Gurnis et al., 2004; Billen and Hirth, 2005; Burov and Cloetingh, 2010; Nikolaeva et al., 2010; Leng et al., 2012). Due to the high number of variables associated with subduction zones in vastly different tectonic settings, with many possible geodynamic and geochemical processes, it is highly unlikely that there is a “one model fits all” case that can be applied to all subduction zones. However, no other subduction zone has been studied to the level of the IBM. It is imperative that subduction zones other than the IBM are studied with as much rigor, to identify the potential heterogeneity of subduction initiation processes in different settings, and ultimately gain a more thorough understanding of subduction initiation. Geodynamic modelling of subduction zone settings can provide important constraints on subduction initiation mechanisms, such as the amount of compression required for a fracture zone to evolve to a self-sustaining subduction zone (e.g., Hall et al., 2003; Gurnis et al., 2004); the influence of plumes on lithospheric weakening and the initiation of subduction (e.g., Ueda et al., 2008); and the influence of sedimentary loading at passive continental margins (e.g., Regenauer-Lieb et al., 2001). However, it is vital that geodynamic models consider the stratigraphic constraints of real forearc assemblages. When studying subduction initiation, it is important to take a multidisciplinary approach, and to create a geochemical and geochronological stratigraphic framework to help develop subduction initiation models.

The Izu-Bonin-Mariana forearc stratigraphy is based on results of diving, dredging and limited land studies (Ishizuka et al., 2011; Arculus et al., 2015). It is composed of a basal mantle peridotite, followed by gabbros, a sheeted dyke complex and FAB pillow lavas, then boninites, andesitic tholeiitic lava flows and dykes, followed by magnesian andesites through to tholeiitic to calc alkaline arc lavas (Ishizuka et al., 2011). Both the gabbros and sheeted dykes are geochemically linked to the FAB pillow lavas (Ishizuka et al., 2011). $^{206}Pb/^{238}U$ zircon analyses of gabbros from the Bonin and Mariana forearcs gave ages of 51.94 ± 0.13 Ma, 51.81 ± 0.03 Ma and 51.79 ± 0.05 Ma, while the oldest and most reliable age produced by $^{40}Ar/^{39}Ar$ geochronology on FAB lavas from the Bonin forearc gave an age of 51.34 ± 0.78 Ma (Reagan et al., 2019). Boninites found further from the trench in the Bonin forearc gave and $^{40}Ar/^{39}Ar$ age of 50.92 ± 0.08 Ma (Reagan et al., 2019). These close ages indicate that there was rapid evolution from the formation of the FAB to the formation of the boninites.

The FAB lavas, or “Early Basalts” by Crameri et al. (2020), are the first magmatic products of subduction initiation along the IBM system. They are moderately differentiated with ~7 wt. % MgO contents, and are typically aphyric (Reagan et al. 2017). These FAB have been described as MORB-like, but they are more depleted than MORB, with higher ratios of highly incompatible trace elements against less incompatible trace elements. This indicates higher degrees of partial melting, or iterative/repeated melting of a depleted upper mantle source. Importantly, there is little evidence that FAB have significant slab fluid or melt influence in their formation. The FAB are not homogenous, but include several groups: the Normal FAB (N-FAB), Enriched FAB (E-FAB), Depleted FAB (D-FAB) and Primitive FAB (P-FAB) (Shervais et al., 2019). These groups are largely defined based on REE concentrations: N-FAB are LREE depleted; the E-FAB are less depleted in the LREE than N-FAB, with overall REE contents similar to MORB; the D-FAB are more depleted overall than the other FAB groups, with lower concentrations of both LREE and HREE; and the P-FAB have REE patterns similar to the N-FAB, with very low overall REE contents, along with high MgO and TiO_2 concentrations (Shervais et al., 2019) The heterogeneity within the FAB is due to heterogeneous source compositions or different melting history (Shervais et al., 2019). There are also andesites found in the forearc which have similar geochemical characteristics to N-FAB lavas, with higher overall REE concentrations, indicating derivation from a common source.

As the earliest FAB show no influence of slab fluids or melts geochemically, and form from a depleted source relative to MORB, it is thought that the FAB formed due to extension in the forearc during the first stages of subduction initiation, leading to adiabatic decompression melting of a refractory upper mantle source from which MORB melts were extracted during the Mesozoic/Cenozoic. Later release of slab fluids and/or melts into the mantle wedge led to further melting of the refractory mantle, with addition of slab-derived elements (e.g., Th, LILE) and development of supra-subduction Nb-Ti negative anomalies to form the boninites. Justification for extensive spreading in the forearc appears to largely be based on the clear geochemical argument for adiabatic melting. However, it is important to note for the interpretation of new results from Panama that forearc spreading in the Izu-Bonin forearc is also supported by the presence of sheeted dykes (Ishizuka et al., 2011). Spreading in the forearc during subduction initiation could also correlate with the stratigraphy observed in subduction related ophiolites (Pearce and Robinson, 2010; Whattam and Stern, 2011)

It is suggested that this forearc stratigraphy represents “spontaneous” subduction along a pre-existing fracture (Arculus et al., 2015). This spontaneous model can justify the spreading in the forearc, which may not be possible in an induced subduction initiation setting where compression is expected to occur along a lithospheric discontinuity. However, it has also

been suggested in numerical modelling that extension is likely to occur in the forearc during subduction initiation, even if it is not spontaneous (Hall et al., 2003; Gurnis et al., 2004).For the Soná-Torio region to follow the “Subduction Initiation Rule”, the forearc stratigraphy would have to replicate that of the IBM arc. It may be possible for this mechanism of subduction initiation to have occurred in Panama. According to geodynamic models, it is possible that spontaneous subduction initiation can occur along a pre-existing fracture, or even due to a high compositional density contrast across the margin of the oceanic plateau (e.g., Niu et al., 2003). It has also been argued that the geochemistry of the forearc sequences in Panama follow the Subduction Initiation Rule, as they show a transition from MORB-like to volcanic arc-like (Whattam et al., 2020). In this section, we will compare the lithostratigraphy and geochemistry of the IBM and Azuero-Soná sequences, specifically focussing on the units thought to be the first products of subduction initiation – the fore arc basalts in the IBM, and the proto-arc groups in Panama.

As the first magmatic products of subduction initiation, the geochemical characteristics of the FAB or Proto-arc Groups can be key to understanding the processes that occur in the first stage of subduction, and also to recognising the model of subduction initiation. As a result, the FAB of the IBM forearc have been studied extensively, which has greatly advanced the understanding of subduction initiation in the IBM (Reagan et al., 2010; Reagan et al., 2017; Shervais et al., 2018; Li et al., 2019). Here we will compare the FAB and boninites of the IBM with the Proto-arc Groups of Soná-Torio and Jaqué, to assess geochemical similarities, and to assess if the proto-arc groups confirm a IBM-like model of subduction initiation for the southwestern margin of the Caribbean Plateau.

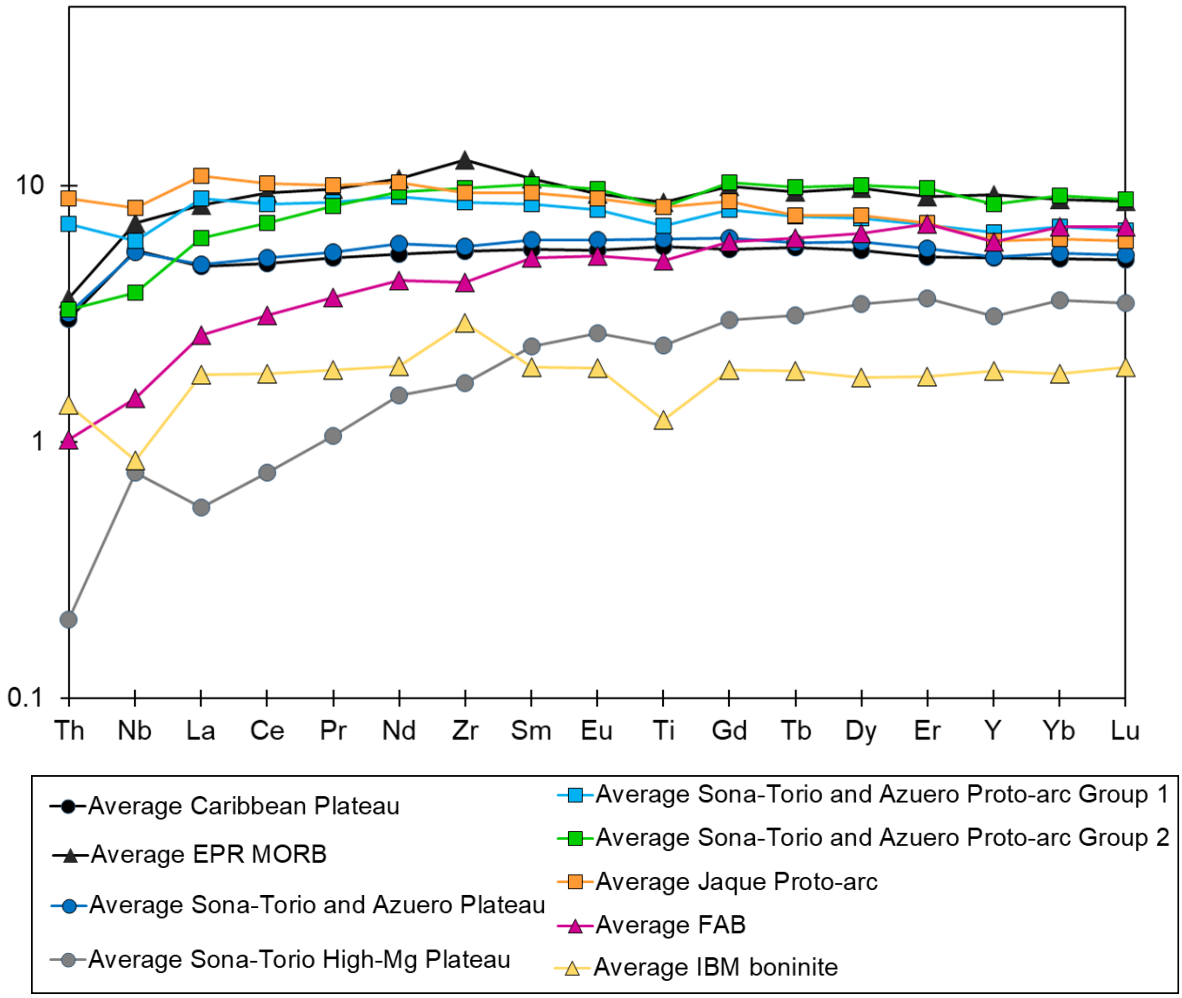

Figure 6.1: Multielementary primitive mantle normalised diagram, showing averages of key geochemical groups. Average Caribbean Plateau calculated from, GEOROC online database (n = 87); Average EPR MORB calculated from PetDB online database (n = 302); Average Soná-Torio and Azuero Plateau (n = 59), Proto-arc Group 1 (n = 18) and 2 (n = 32) from this study, Lissinna (2005), Buchs et al. (2010); Average Soná-Torio High-Mg Plateau from this study (n = 20); Average FAB (n = 63) and boninites (n = 34) from Reagan et al. (2010), Shervais et al. (2018) (n = 63).

6.4.1.1 Comparison of IBM FAB and Boninites with Proto-arc Groups

On multielementary primitive mantle normalised diagrams (Figure 6.1), FAB samples have highly depleted LREE, Nb and Th, with total REE lower than those of MORB. The IBM boninites have low overall REE concentrations, and flat REE patterns, with on average a Ti and Nb depletion and Zr enrichment. The Soná-Torio Proto-arc 1 have flat trace element patterns, similar to oceanic plateau patterns, but showing on average a slight Th enrichment and Nb depletion. The Jaqué Proto-arc samples have patterns similar to those of the Soná Torio Proto-arc Group 1, with a slightly higher average La/Yb. The Soná-Torio Proto-arc

Group 2 have a depleted LREE average pattern, very similar to average EPR MORB composition, with a negative Nb anomaly, lower Nb/La ratio and higher Th content. However, not all samples of the Proto-arc Group 2 have enriched Th.

On tectonic discrimination diagrams, FAB lavas largely plot within the Th/Yb vs Nb/Yb MORB-OIB array (Figure 6.2A), with a limited number of samples plotting above this array, showing a potential slab input. The FAB lavas also plot in the most depleted part of the array, below N-MORB, with values of both Nb/Yb and Th/Yb largely lower than the values of the Soná-Torio Proto-arc Group 1 and the Jaqué Proto-arc. However, FAB samples do show a significant overlap with samples of the Soná-Torio Proto-arc Group 2, although many samples of the Proto-arc Group 2 plot above the MORB-OIB array and generally show more signs of slab input. Both the Soná-Torio Proto-arc Group 1 and the Jaqué Proto-arc plot between N-MORB and E-MORB, and generally lie above the array, indicating some slab input. The IBM boninites also plot above the MORB-OIB array, again indicating slab input, On the plot of Nb/Y and Zr/Y, FAB lavas are again the most depleted in both Zr/Y and Nb/Y, plotting largely below or in the lowest section of the N-MORB array (Figure 6.2C). In this case, there is limited overlap with the Soná-Torio Proto-arc Group 2, which plot largely in the upper section of the N-MORB array, with limited samples plotting in the Oceanic Plateau Basalt array. Both the Jaqué Proto-arc and the Soná-Torio Proto-arc Group 1 samples plot between the Oceanic Plateau Basalt and Arc arrays, and show no overlap with FAB lavas. The IBM boninites plot in a relatively linear array from the FAB at the lower section of the N-MORB array through to the Arc array. They overlap with some samples of the Soná-Torio Proto-arc Group 2. On the Nb/Th and Zr/Nb plot Jaqué Proto-arc and Soná-Torio Proto-arc Group 2 samples again plot between the Oceanic Plateau Basalt and Arc arrays, showing

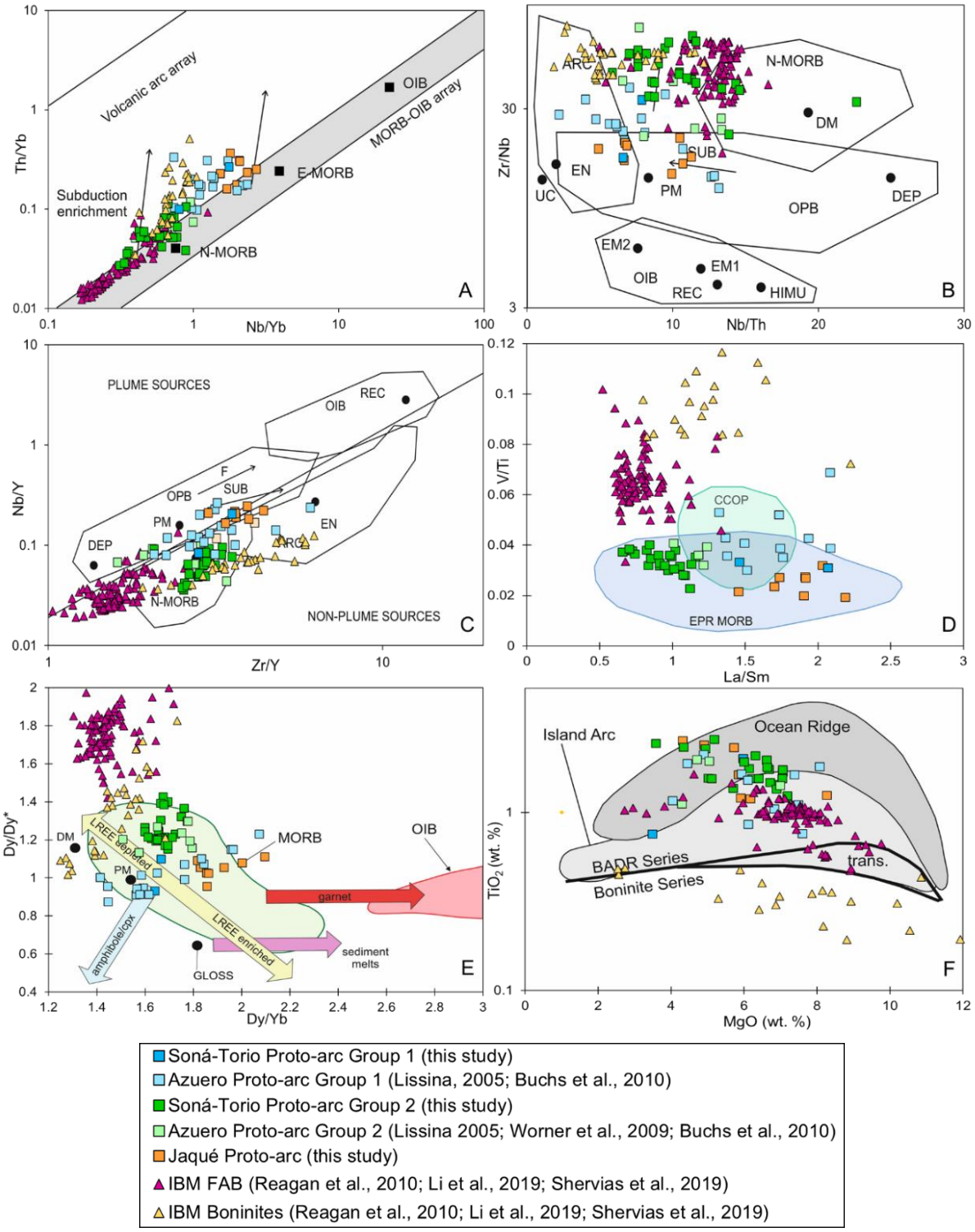

Figure 6.2: Tectonic discrimination diagrams with the Proto-arc and FAB samples. (A) Nb/Yb vs Th/Yb crustal input proxy diagram (Pearce, 2008), B) Nb/Th vs Zr/Nb diagram (Condie, 2005) C) Zr/Y vs Nb/Y diagram (Condie, 2005), D) La/Sm vs V/Ti diagram, E) Dy/Yb vs Dy/Dy* diagram (Davidson et al., 2013) and F) MgO vs TiO_2 diagram (Pearce and Robinson, 2010). Abbreviations: UC = upper continental crust, PM = Primitive Mantle, DM = shallow depleted mantle, HIMU = high mu (U/Pb) source, EM1 and EM2 = enriched mantle sources, ARC = arc related basalts, N-MORB = normal mid-ocean ridge basalt, OPB = oceanic plateau basalt, OIB = oceanic island basalt, DEP = deep depleted mantle, EN = enriched component, F = effects of batch melting and SUB = subduction effect.

very little overlap with the FAB or the Soná-Torio Proto-arc Group 1 samples (Figure 6.2B). The FAB and Soná-Torio Proto-arc Group 2 largely overlap, with the FAB lavas largely plotting on the margin of the N-MORB array, and the Proto-arc Group 2 samples largely plotting in the space between the N-MORB, Oceanic Plateau Basalt and Arc arrays. The IBM boninites plot between the margins of the N-MORB array to the upper section of the Arc array, overlapping with samples of the FAB and Proto-arc Group 2. On the Dy/Dy* and Dy/Yb plot, the FAB plot above the MORB array, separate from all Proto-arc Groups, with values of Dy/Dy* between 1.4 – 2 (Figure 6.2E). The IBM boninites plot in a quite linear array crossing the upper section of the MORB array. This group displays wide ranges of both Dy/Dy* and Dy/Yb, with values between 1 – 1.8 and 1.2 – 1.8 respectively. The Proto-arc Groups all plot within the MORB array, although Soná-Torio Proto-arc Group 2 shows higher Dy/Dy* values. On the plot of V/Ti vs La/Sm, the Proto-arc Groups have similar values of V/Ti, largely between 0.02 – 0.05, which is lower than the FAB groups, and overlapping with both the average Soná-Torio Plateau and EPR MORB arrays (Figure 6.2D). The Soná-Torio Proto-arc Group 1 and the Jaqué Proto-arc both have similar values of La/Sm (> 1.3) but the Soná-Torio Proto-arc Group 2 show LREE depletion as they did in the primitive mantle normalised diagrams, with values of La/Sm < 1.3. The FAB also have similar values of La/Sm, displaying a similar depletion in the LREE to the Soná-Torio Proto-arc Group 2, but the FAB have higher values of V/Ti, largely > 0.05. The IBM boninites have even higher values of V/Ti, with all samples having values > 0.07. On the boninite discrimination diagram of MgO and TiO2, the IBM boninites clearly plot in the boninite series, while the other geochemical groups plot within the BADR (Basalt, Dolerite, Andesite, Rhyolite) series (Figure 6.2F). The bulk of the FAB samples plot within the island arc array, with rare samples in the ocean ridge array. Some of these samples also plot in the transitional series between the BADR and Boninite series. All Proto-arc Groups plot together across the island arc and ocean ridge arrays, overlapping with some FAB samples but distinct from the boninite samples. In Nd_i isotopes, with FAB and boninites normalised to 50Ma and Proto-arc normalised to 75 Ma, FAB lavas have a relatively narrow range of values from 0.512977 – 0.513059 (Figure 6.3). This range overlaps with the isotopic range of the Soná-Torio Proto-arc Group 1, Group 2 and the Jaqué Proto-arc, which have ranges of 0.51288 – 0.51300, 0.51302 – 0.51313 and 0.51297 – 0.51300 respectively. The FAB range plots within the lower range of the EPR MORB and Depleted Plateau arrays, which are difficult to distinguish in Nd isotope space, and also overlap the upper margin of the Normal CCOP array. The IBM boninites have a range of 0.512912 – 0.513029, which overlaps with all Proto-arc Groups, and again

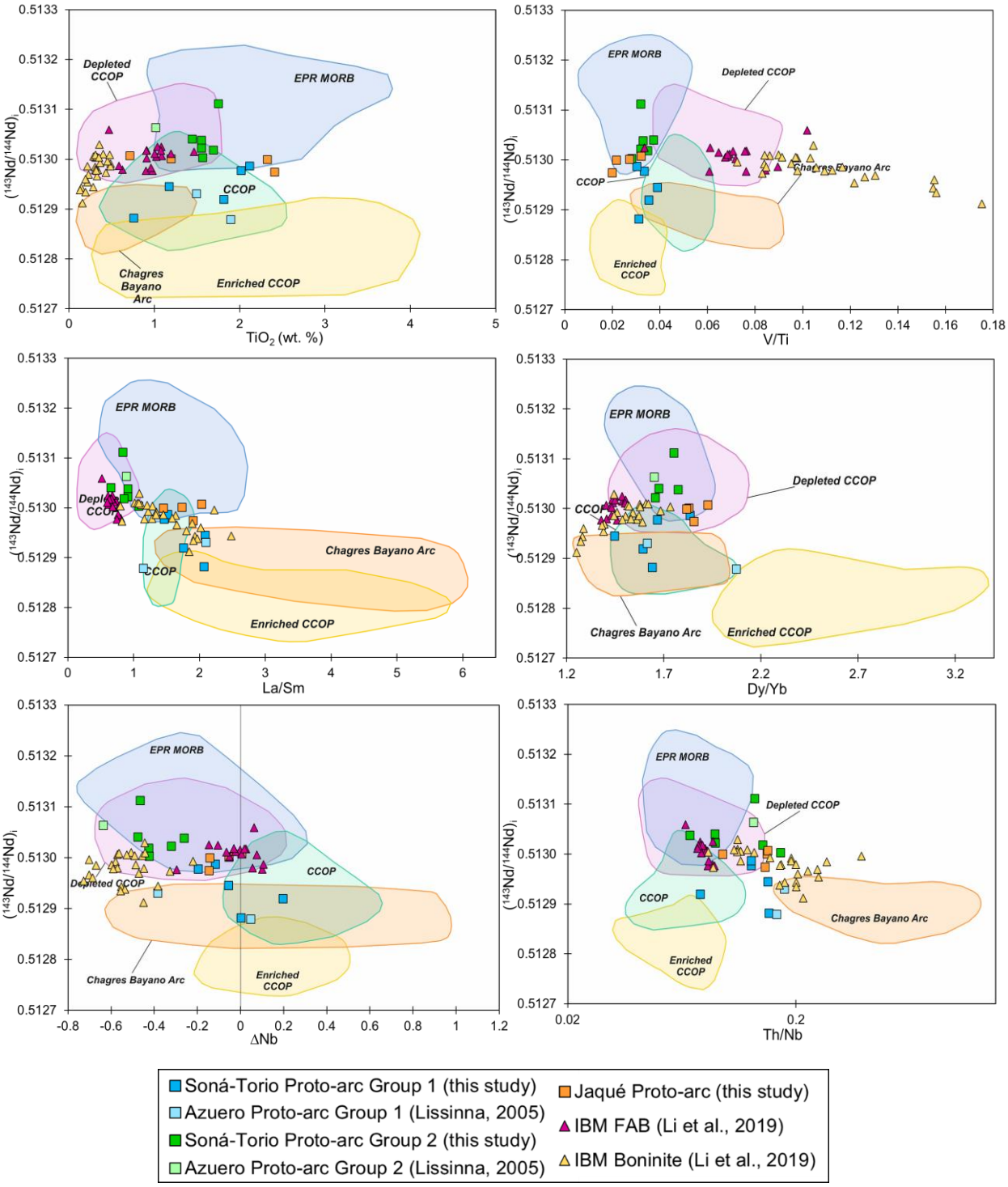

Figure 6.3: Bivariate diagrams of initial isotopic ratios of the Soná-Torio, Darién Pacific Coast Proto-arc samples, with previously analysed samples of Lissinna (2005) . IBM FAB and Boninite age corrected to 52 Ma and 50 Ma respectively, sourced from Li et al. (2019). Also displayed are the isotope fields for the Colombian-Caribbean Oceanic Plateau (CCOP) (La/Sm > 0.60, < 1.20), the Depleted CCOP (La/Sm < 0.60) and Enriched CCOP (La/Sm > 1.20) (all from GEOROC online database, age corrected to 90Ma), the East Pacific Rise MORB (EPR MORB) from (PetDB online database) and the Chagres Bayano Arc (Wegner et al., 2011).

plots within the EPR MORB, Depleted Plateau and Normal Plateau arrays, as well as overlapping with the upper margin of the Chagres-Bayano Arc.

Clearly, none of the Proto-arc Groups in Panama have geochemical characteristics similar to those of the FAB, or the IBM boninites. These observations do not support direct equivalence of the IBM or subduction initiation rule model in Panama (e.g., Whattam et al., 2020). However, it could be argued that Proto-arc Group 1 was produced by remelting of a plume-modified upper mantle (Buchs et al., 2010). On tectonic discrimination diagrams, the Soná-Torio Proto-arc Group 1 and the Jaqué Proto-arc consistently plot between the Oceanic Plateau Basalt and Arc arrays, suggesting influence of a plume component in their formation. The Soná-Torio Proto-arc Group 2 samples, however, have geochemical similarities to the IBM FAB, with similar primitive mantle normalised REE patterns. Most of the Proto-arc Group 2 samples also show a clear slab fluid or melt influence with elevated Th/Yb values, and they also have lower V/Ti than the FAB lavas.

As previously stated, FAB have lower ratios of more incompatible elements against less incompatible elements in comparison to those of typical MORB (e.g., FAB values: Ce/Yb = 1 – 2.6, Zr/Y = ~1.55, Zr/Hf = 26 – 30 vs MORB values: Ce/Yb > 2.0, Zr/Y > 2.5, Zr/Hf = 30 - 50). This indicates that FAB has been formed from a more refractory source than that of MORB, due to a higher level of previous melt extraction, or that there were higher degrees of partial melting in the generation of FAB (Shervais et al., 2018). Melting modelling by Shervais et al. (2019) indicated that the geochemical differences of FAB in comparison to MORB was due to higher degrees of partial melting than expected for typical MORB in the generation of FAB lavas, and a more refractory source. The high V/Ti ratio for FAB lavas, observed in Figure 6.2D could be due to higher oxygen fugacity during the generation of FAB, as it was interpreted by Reagan et al. (2010), due to MORB having a more reduced source. However the high V/Ti ratio for FAB in comparison to MORB is consistent with the lower ratios of more incompatible elements against less incompatible elements, and therefore the high V/Ti could be due to a more refractory source or higher degrees of partial melting (Shervais et al., 2019). Comparing elemental ratios of the Proto-arc and Plateau sequences in Panama with those of MORB can be used to make a first order assessment of the possible contribution of a refractory mantle source in of Panama. The Soná-Torio Proto-arc Group 1 (Ce/Yb = 2.9 – 5.9, Zr/Y = 2.3 – 3.7, Zr/Hf = 32 – 40) have similar ranges of immobile incompatible trace element ratios to the Proto-arc Group 2 (Ce/Yb = 2.0 – 3.5, Zr/Y = 2.1 – 3.3, Zr/Hf = 31 - 41) and the Jaqué Proto-arc (Ce/Yb = 5.2 – 7.2, Zr/Y= 3.0 – 4.4, Zr/Hf = 33.4 -37.9). These ranges of ratios are also similar to those of the Soná-Torio Plateau (Ce/Yb = 3.2 - 4.0, Zr/Y= 2.5 – 3.1, Zr/Hf = 30.4 – 42.0) and MORB. Therefore, unlike FAB, the Proto-arc Groups were not produced by simple remelting of a refractory

upper mantle source. The higher extent of partial melting in the generation of FAB is consistent with extensive decompressive melting due to extension in the forearc. If, based on the modelling of Shervais et al. (2018), the FAB source is refractory due to previous melt extraction at depth, prior to the initiation of subduction, it seems likely that this may be a geochemical characteristic that is unique to the IBM system, and may not be replicated in other subduction initiation sequences.

This geochemical evidence is further strengthened by the lack of field evidence for extension in the forearc during the formation of the Proto-arc. In the Soná-Torio region, there is evidence for compressive tectonics during the time of proto-arc magmatism, with folding observed within the Torio Lithostratigraphic Unit, possibly associated with ramps due to thrust faults. However, the timing of said folding is not clear, and this could be caused by a much later compression event.

There is also evidence for a low rate of eruption of the Soná-Torio Proto-arc Group 1 lavas, as they are interbedded with limestones of the Torio Lithostratigraphic Unit. Typically, this low eruption rate would not be expected in an extensional environment. Within the Torio Lithostratigraphic Unit there are basaltic sandstones and breccias, which contain clasts of basalt and radiolarites from the Soná-Torio Oceanic Plateau, as outlined in Section 3.2.2. This indicates that during the formation of the Torio Lithostratigraphic Unit the plateau was subaerially exposed and was reworked. Red conglomerate layers have also been described in the Ocu Formation (Buchs et al., 2010), which could represent palaeokarst infills which again indicates subaerial exposure of this formation. Within the Cretaceous limestones of Changuinola (which represent the lateral equivalent of the Ocu Formation in Central Panama), slumping has been observed (Buchs pers. comm., 2020). These features indicate uplift between the submarine formation of the plateau and the formation of the Torio Lithostratigraphic Unit, which is not consistent with extension in this region at this time. In the IBM system, the extension in the forearc is required to explain the formation of the FAB with no slab input, but there are also descriptions of sheeted dykes (Ishizuka et al. 2011) which supports the extensional model.

Based on field constraints in the Soná-Torio region, the plateau forms the base to the proto-arc and arc groups. If there was extension in the forearc as is predicted in the IBM, where FAB lavas form new oceanic crust, this plateau-proto-arc relationship may not have occurred. In this case, the proto-arc may also have formed new crust, not as lavas interbedded with limestone on top of the plateau. However, as oceanic plateaus are significantly thicker than typical oceanic crust (the Caribbean Plateau is estimated to vary between 8 – 20 km thickness across the plate, against typical oceanic crust of 5 -7 km thick

(Edgar et al., 1971; Mauffret and Leroy, 1997) rifting may not be as effective in opening new crustal space. The plateau assemblages observed across the Soná-Torio region clearly represent the upper section of the plateau, and gabbros and cumulates associated with the lower sections of the plateau are not observed (Section 3.2.1) (Kerr et al., 1997b).

It is also clear that the Proto-arc Group 2 of Soná-Torio have similar REE patterns to the FAB and MORB lavas. However, based on the lithostratigraphic relationships between volcanic deposits and dykes of the Proto-arc groups 1 and 2 in the Soná-Torio region, the formation of the Proto-arc Group 2 with MORB-like REE contents appears to postdate the emplacement of Proto-arc Group 1 with plateau-like REE contents. Although there might still be undocumented regional and/or temporal variability between these magmatic groups, new field and geochemical constraints from this study suggest that Proto-arc Group 1 cannot be a simple equivalent to FABs, because it appears that proto-arc groups in western Panama record increasing depletion of the source during the earliest stages of subduction (i.e., not just remelting of a residual refractory mantle as considered for FABs). In addition, the geochemistry of Proto-arc Group 2 also commonly exhibits some subduction influence, which is inconsistent with anhydrous decompression melting such as that associated with the formation of FABs. The petrogenesis of Proto-arc Group 2 will be discussed further in Section 6.4.3.

Interestingly, there are no boninites in the forearc of Azuero-Soná, which are thought to be a key component of intraoceanic subduction related magmatism. Although boninites are also seen in developed supra-subduction zones and not only during subduction initiation, High-Si boninites are thought to only be seen in subduction initiation assemblages (Shervais et al., 2018). In the IBM system, there is extensive shallow melting to form the FAB, leading to a highly depleted mantle source of the boninites. Boninities are formed when fluids are released from the downgoing slab, leading to further melting of this depleted mantle. In Panama, the first lavas produced during subduction initiation are the Proto-arc Group 1, which have not been sourced from a highly depleted mantle. The lack of boninites in Panama indicates that there was an absence of such depleted residual mantle, which would have been created through extensive melting to produce FAB-like lavas.

As the first subduction related magmatism in the Soná-Torio region, the Proto-arc Group 1 did not form from adiabatic meting due to extension in the forearc, evidenced by both geochemical and field studies. The FAB and Proto-arc Group 1 do not form from a similar source. On tectonic discrimination diagrams, the Proto-arc Group 1 consistently plots in the Oceanic Plateau Basalt array and this group has clearly been geochemically influenced by the presence of the plume and Caribbean Plateau. However, the differences in geochemistry

between the FAB and Proto-arc Group 1 cannot solely be explained by the presence of the Plateau as the basement to the proto-arc, as the Proto-arc Groups of Panama clearly show some slab fluid or melt influence and did not form solely by adiabatic decompression melting. Therefore, the forearc stratigraphy of the Soná-Torio region does not follow the model of the IBM subduction initiation.

6.4.2 The Plume-Induced Subduction Initiation Model

Whattam and Stern (2015) proposed a model for subduction initiation for the Leeward Antilles, the NW of South America and Central America, called the Plume Induced Subduction Initiation (PISI) model. Using the classification of Stern and Gerya (2018), this is a “spontaneous” model of subduction initiation, in that it does not necessarily need external plate tectonic forces, but it hypothesises that subduction could be induced along the margins of a plume head. They argued it is not coincidental that subduction occurred along the margins of the Plateau, but that it was induced due to the presence of a plume head in the Caribbean at this time. This model predicts that the impingement of a hot plume at the base of the lithosphere could lead to lithospheric rupture. As the plume thins the mantle and weakens the lithosphere, largely by heating and melt infiltration, plume related magmatism thickens the buoyant crust. This creates a strong density contrast, with the older, denser surrounding lithosphere sinking downwards around the plume margins, which could eventually lead to a self-sustaining subduction system (Ueda et al., 2008).

It was alleged that the forearc assemblages across Panama indicated that the record of subduction initiation was consistent with the PISI model (Whattam and Stern, 2015; Whattam et al., 2020). However, this model does not seem to be consistent with our new observations, or with other previous geochronologic constraints. The PISI model is based on three key observations or assumptions. These key observations are as follows: (1) major and trace element contents of plateau lavas show evidence of subduction related slab fluid or melt input, gradually increasing from 100 Ma, (2) there is no clear hiatus between the formation of the plateau lavas and the arc sequences, indicating that these units are part of the same tectono-magmatic sequence, and (3) the generation of plateau and arc related lavas overlap in time, space, and geochemical compositions.

Four methods were used to measure the progressive subduction addition to plateau through to arc units. These were the classification of tholeiitic or calc alkaline affinities of plateau and arc sequences, using Nb/Yb anomalies as a partial melting proxy (assuming that arc magmas are produced by a more depleted mantle than MORB), using Ti/V ratios as a proxy for the oxygen fugacity from plateau and arc magmas, and finally using trace element ratios

(Ba/Th, Ba/Nb and Th/Nb) to measure shallow to deep subduction related components (Whattam and Stern, 2015).

Primarily, these criteria aimed to recognise and document subduction influences on the plateau sequences around the Caribbean, beginning at 100 Ma. Therefore, we will focus on the plateau units from the Azuero-Soná unit and their geochemical characteristics. According to our results, the Soná-Torio and Azuero Plateaus do not appear to have a calc-alkaline affinity. On the SiO2 vs FeO*/MgO plot (Figure 5.13), the Soná-Torio Plateau samples are clustered across the tholeiitic-calc alkaline boundary, with no clear calc alkaline samples. As the first magmatic products of subduction initiation, Proto-arc samples from Soná-Torio also largely plot in the tholeiitic array, although some samples do plot below the calc-alkaline boundary. Whattam and Stern (2015) also used the Tholeiitic Index (THI), calculated by $Fe_{4.0}/Fe_{8.0}$ where $Fe_{4.0}$ is the average FeO* concentration of samples with 3 – 5 wt. % MgO, and $Fe_{8.0}$ is the average FeO* of samples with 7 – 9 wt. % MgO (Zimmer et al., 2010). The THI was used to assign tholeiitc or calc alkaline affinities to plateau samples, with tholieiitic samples giving a THI of >1 and calc alkaline <1. Only one sample from Azuero could be classified this way, and gave a calc alkaline affinity with a THI of 0.97. However, this is close to the margin of tholeiitic samples, and this does not show a trend of gradual subduction additions to the plateau beginning at 100 Ma.

Based solely on the clear subduction initiation forearc stratigraphy observed in the Azuero-Soná region, there is no increase in the Nb/Yb between the Plateau, Proto-arc Group 1 and the Arc group. The Proto-arc Group 2, however, does show a lower value of Nb/Yb, which is taken in this context to mean that there was a higher degree of partial melting to form these lavas. In Jaqué, Proto-arc and Arc lavas also show similar to higher ranges of Nb/Yb, and in the Serranía de Baudó there is a fairly narrow range of Nb/Yb. Ti/V ratios of the Soná-Torio Plateau and the Proto-arc Groups also largely overlap (Figure 5.27), which is again not consistent with PISI arguments, which suggest that the Ti/V values should steadily decrease until 70 Ma (Whattam and Stern, 2015). Although this Ti/V ratio may reflect the oxygen fugacity at the time of magma formation, this may in fact represent the degree of partial melting or depletion of the source as it is consistent with other ratios of more incompatible to less incompatible elements (as previously discussed in Section 6.4.1.1)

Based on trace elements, the samples of the Soná-Torio Plateau do not appear to show any subduction influence. Our plateau samples show typical plateau signatures, consistent with samples of the Caribbean Plateau that formed far from any potential subduction influence. In this model, the subduction influence in the formation of the plateau was predicted using the elemental ratios of Ba/Th, Ba/Nb and Th/Nb. Although it is ideal to use fluid mobile elements

as racers of subduction inputs, many of the rocks in this study have been heavily altered and therefore these elements have been mobilised and are not suitable to be used to trace a subduction component. In Chapter 5, it was shown that Ba has been mobilised due to the large degree of scatter when plotted against Zr concentrations. Therefore, we only use the Th/Nb ratio to reliably recognise a subduction addition to plateau units. Here, the samples of the Soná-Torio plateau again do not show any elevation of Th/Nb, and therefore show no influence of a subduction component.

As previously stated in Section 6.1, the ages that do exist and are used in the PISI model may be problematic. For example, plateau rocks of the Serranía de Baudó show progressive subduction influence according to the model of Whattam and Stern (2015). However, only two ages exist for this area, and therefore there is not a strong argument for this progressive addition. According to the $^{40}Ar/^{39}Ar$ results from this study and Acero (2019), these ages have likely been affected by post-crystallization alteration and degassing, and may be significantly younger than the age of formation of the plateau sequences. These arguments based on geochemical evolution through time are based on small sample sizes, due to a small number of ages for plateau and early arc sequences in Panama. Therefore, it is difficult to recognise this kind of progressive addition of a subduction component through time, and the geochemical criteria outlined in the PISI model do not appear to apply to the sequences of the Soná-Torio Plateau.

The second criteria to justify the PISI hypothesis is that there is no magmatic cessation between the formation of the Plateau and the Arc sequences in areas where PISI may apply. In the Soná-Torio region, this does not appear to be true. As previously documented (Buchs et al., 2010; Corral et al., 2011), and further confirmed in this study, the formation of the Torio Lithostratigraphic Unit indicates that there was a hiatus of magmatic activity between the formation of the Plateau and Proto-arc. Although there are potential issues with many of the $^{40}Ar/^{39}Ar$ dates for the Soná-Torio Plateau sequences, the biostratigraphic ages of the plateau (89-85 Ma (Kolarsky et al., 1995; Buchs et al., 2009) and limestones intruded by Proto-arc dykes (75-73 Ma, (del Giudice and Recchi, 1969; Buchs et al., 2010)) indicates that there was indeed a cessation of magmatism between the formation of the Plateau and the Proto-arc. New unpublished lithostratigraphic, biostratigraphic, and geochemical constraints (Buchs and Wang, com. pers. 2020) are also consistent with a ~10 Myr long magmatic gap between formation of the plateau and proto-arc sequences in central and eastern Panama. This indicates that there was not a continuous magmatic evolution from plateau through to arc sequences, a fundamental issue with the PISI model, which requires ongoing active plume magmatism at the onset of subduction initiation (Whattam and Stern, 2015).

The final assumption, that the sequences of the plateau and arc overlap in time, space, chemical and isotopic space is also not confirmed by evidence in the Soná-Torio region. Considering limited age constraints for plateau, proto-arc and arc sequences in Panama, it is impossible to capture the true complexity of the interplay between plateau and arc units, but as stated above, reliable biostratigraphic dates indicate that there is a significant hiatus between plateau and arc phases, and that they do not represent one continuous magmatic unit. In Nd isotopes, the Proto-arc Group 1 does appear to overlap with the samples of the Soná-Torio Plateau. Based on trace elements, the Soná-Torio Proto-arc Group 1 also has similar contents to samples of the Soná-Torio Plateau, with the addition of a slab derived fluid component, and could be considered to be somewhat intermediate between the Plateau and the Arc. Samples of the Soná-Torio Proto-arc Group 1 also consistently overlap with the Oceanic Plateau Basalt array on tectonic discrimination diagrams. This observation does not necessarily point towards a PISI model for Central America, only that the Proto-arc may have been sourced from plume modified sub plateau mantle. It remains however possible that the plume or the presence of the plateau indirectly influenced subduction initiation. For instance, large density contrast at the margin of the oceanic plateau could facilitated geodynamical conditions required for subduction initiation (Niu et al., 2003). Again, this does not mean that the plume directly caused subduction initiation to occur.

The PISI criteria were further supported by the claim that the forearc sequences in the Soná-Azuero and Chagres-Bayano regions follow the Subduction Initiation Rule (Whattam and Stern, 2011) following PISI, and that they transition from MORB-like to volcanic arc basalt-like (Whattam et al., 2020). They argue that the plateau, proto-arc and arc of the Soná-Azuero region are MORB-like, based on major and trace element geochemistry (Whattam et al., 2020). However, based on our geochemical and isotopic constraints outlined in Chapter 5, and further discussed in Section 6.5, the Soná-Torio Plateau has typical oceanic plateau geochemistry, and is sourced from a plume-like mantle. As outlined in this section, the Proto-arc Group 1 has plateau-like REE patterns and is also sourced from a plume-like mantle, and therefore these sequences cannot be classified as MORB-like.

Additionally, the PISI model indicates that the impingement of the plume will initially weaken and thin the lithosphere, leading to early forearc spreading (Whattam and Stern, 2015). This is similar to the model of the IBM above, and as described, there is a lack of field or geochemical evidence of early forearc extension in Azuero and Soná, with evidence for Early Cretaceous sequences (presumably plateau-related) preserved in central Panama (Kukok et al., 2017). However, in this case the first subduction initiation magmas could be sourced directly from the plume, and these lavas may be indistinguishable from the lavas

formed in the earlier phases of the Caribbean Plateau. This would likely lead to a clear continuous sequence from plateau-like through to proto-arc, which is not observed.

The evidence outlined above does not support a model of Plume Induced Subduction Initiation for Central America, or the remainder of the Caribbean region. At the time of subduction initiation (likely c. 75 Ma) n Central America, the Caribbean was a region with dynamic plate tectonic configurations and several volcanic arcs. During the Cretaceous, subduction zones formed along the southern and eastern margins of the Caribbean Plateau. The subduction zones on the eastern margin of the plateau are preserved in volcanic arc remnants and metamorphic complexes around the Caribbean (Pindell and Kennan, 2009; Neill et al., 2011; Wright and Wyld, 2011) and may have facilitated the movement of the plateau across the Caribbean. Subduction along the south eastern margin of the plateau has also been evidenced by the presence of plateau sequences interbedded with arc-like tuffs, and by plateau-like gabbros which have enriched Th relative to Nb, indicating the influence of a slab component (Buchs et al., 2018). During the Early to Late Cretaceous there was also active subduction along the eastern margin of Colombia, documented by the formation of the Quebradagrande Complex (Nivia et al., 2006; Villagómez and Spikings, 2013; Spikings et al., 2015; Jaramillo et al., 2017). Therefore, it seems unlikely that tectonic forces would not play an active role in the initiation of a new subduction zone in Central America. This critique of this model emphasises the importance of detailed field, geochemical and geochronological studies, which provide key geological criteria for models to follow.

6.4.3 Formation of the Soná-Torio Proto-arc Groups

In this section, the formation and petrogenesis of the Proto-arc Groups will be further discussed, to develop a model of subduction initiation which is consistent with both field and geochemical constraints. Largely this section will focus on the Soná-Torio Proto-arc Group 1 and Group 2, as the Soná-Torio region is where this study focussed, and where the most complete magmatic record of subduction initiation is exposed. However, this model is also in agreement with previous and new results from southern Costa Rica, eastern Panama, and western Colombia.

Rocks of the Soná-Torio Proto-arc Group 1 are seen as lava flows, which can be interbedded with the Torio Lithostratigraphic Unit, and as dykes crosscutting plateau sequences, and the Torio Lithostratigraphic unit, which can exhibit soft sediment (peperitic) deformation at intrusion boundaries. These dykes and lavas flows are observed across both Soná and Azuero Peninsulas. The Soná-Torio Proto-arc Group 2 is only observed as dykes. These dykes intrude sequences of the plateau, the Torio Lithostratigraphic Unit and

tuffaceous sequences of the La Mona Formation, which have a Proto-arc Group 1 geochemistry. Soft sediment deformation was not observed at the Proto-arc Group 2 boundaries in the Torio Lithostratigraphic Unit. While proto-arc group 1 lavas are largely aphyric, fine basalts, most samples of the Proto-arc Group 2 have phenocrysts of clinopyroxene and plagioclase.

Although a core aim of this study was to obtain new reliable $^{40}Ar/^{39}Ar$ ages to resolve the temporal evolution of subduction initiation magmas, this was not possible. There are no existing $^{40}Ar/^{39}Ar$ ages for these groups, but the age of Proto-arc Group 1 is constrained by the soft sediment deformation in the Torio Limestone Unit (75 - 73 Ma). $^{40}Ar/^{39}Ar$ ages obtained for the Proto-arc Group 2 in this study were 55.25 ± 0.13 Ma and 50.09 ± 0.10 Ma, and both samples adhered to the criteria for reliable ages. Although there are no clear stratigraphic relationships to rule these ages out, these ages will not be considered in this study. At 55 Ma in this region, there was an established subduction system forming the Soná-Azuero Arc, and it does not seem possible that the proto-arc could be forming at this time.

Based on the above stratigraphic constraints it is possible to somewhat constrain the relative timing of the Proto-arc Groups. It is possible that the formation of both the Soná-Torio Proto-arc Group 1 and Group 2 were somewhat coeval. However, based on our field constraints it does appear that the Group 2 are younger. This is largely based on field constraints: that dykes of the Proto-arc Group 2 intrude a La Mona tuffaceous sequence of the Proto-arc Group 1 along the Pixvae Coast, and that Proto-arc Group 1 lavas are interbedded with and intrude limestones of the Torio Lithostratigraphic unit exhibiting soft sediment deformation, while the Proto-arc Group are only seen as later intruding dykes.

The Soná-Torio Proto-arc Group 1 and Group 2 can largely be separated on their LREE contents, as Proto-arc 2 is more depleted. In tectonic discrimination diagrams, the Proto-arc Group 1 largely plots between the oceanic plateau basalt and arc arrays, whereas the Proto-arc Group 2 more often plots towards the MORB array, close to N-MORB. However, both groups show some subduction influence with the presence of variable Th anomalies relative to Nb. On trace element primitive-mantle normalised diagrams, Proto-arc Group 1 exhibits patterns similar to typical oceanic plateau, with variable Th, whereas Proto-arc Group 2 exhibits patterns similar to typical MORB, again with variable Th. However, some samples of the Proto-arc Group 2 do not have enriched Th, and instead are very similar to MORB. This indicates that these samples do not have a fluid input.

Nd isotopes can be utilised to gain understanding of the petrogenesis of the Proto-arc groups, as the system is resistant to alteration but can be modified by a slab component. Nd

isotope measurements can therefore be used along with trace element proxies (e.g., Th/Nb, Th/Yb) to identify additions of a slab component. The range of initial Nd in Proto-arc Group 1, 0.512879 – 0.513000, is largely similar the plateau groups (Figure 5.28). Therefore, consistent with trace elements, it appears that the Proto-arc Group 1 has a plateau-like source. When plotted against Th/Nb, a proxy for slab contribution, there is no clear change in Nd ratio with increasing Th/Nb between the plateau and proto-arc groups, or between the plateau and Soná-Azuero Arc samples (Figure 5.28). The Proto-arc Group 2 samples have higher initial Nd, largely plotting within the EPR MORB and depleted CCOP range (Figure 5.28). On plots of V/Ti vs Ndi, the Proto-arc Group 2 clearly shows affinity for the EPR MORB array, with lower values of V/Ti, while the Depleted CCOP array plots at higher values of V/Ti (Figure 5.28). Based on the previous trace element constraints and Nd isotopes, it appears that the Proto-arc Group 2 most likely has a MORB-like source. When plotted against Th/Nb, there is again no clear trend of decreasing Nd with increasing Th/Nb. Therefore, while both groups exhibit variable Th, reflecting variable amounts of subduction contribution, the source of the Proto-arc appears to initially be plume-like in the Proto-arc Group 1, evolving through to MORB-like in the Proto-arc Group 2.

We have attempted to estimate the sediment addition to the plume mantle and depleted upper mantle which could produce Proto-arc Group 1 and Group 2 respectively. This was done by constructing mixing lines between the likely initial mantle source composition and the subducting sediment composition. The end member compositions are outlined in Table 6.1. The depleted upper mantle (DMM) composition was sourced from Workman and Hart (2005) and Su (2003). The composition of the plume mantle is based on the CCOP source composition from Hastie et al. (2010), although Th concentration is adjusted to reflect the composition of the Soná-Torio Plateau samples. The plume Nd source is taken from the highest Soná-Torio Plateau value. However, the composition of the sediment to be used in constructing these mixing lines is not clear. An average Pacific pelagic sediment composition can be calculated from the samples of Pearce et al. (1999), which are Jurassic – Cretaceous cherts and radiolarites from the west Pacific, sampled during ODP Leg 129, Hole 801B. The averaged composition of these sediments gives Nd_i = 0.51249, Th/Nb = 0.36 and Th/Yb = 3.31. Mixing between a plume-like or MORB-like source and these sediments cannot explain the composition of the Proto-arc Groups or of the Soná-Azuero Arc (Figure 6.4). The average continental crust (Rudnick and Gao, 2003; Chauvel et al., 2014) also cannot explain the formation of the Proto-arc Groups, with Nd = 0.512101, Th/Nb = 0.875 and Th/Yb = 5.25. As the Soná-Azuero Arc is a more evolved group of the Proto-arc, with additional influence of the slab, it is necessary that the sediment composition can also explain the formation of the Soná-Azuero Arc. The Soná-Azuero Arc largely has values

Nd_i in line with those of the Plateau, and lower than MORB. Therefore, it is likely that the composition of the sediment here has an Nd value only slightly lower than the plateau, with Th/Nb higher than those seen in the Soná-Azuero Arc. Based the Th/Nb ratios of the Soná-Azuero and Chagres Bayano Arcs, Th/Nb of the slab component has to be at least 1.7.

The actual slab input to the plume and depleted upper mantle may be a fluid or a melt, and this is unlikely to represent the initial sediment composition (e.g., rutile in the slab may cause fractionation of Th/Nb during partial melting of the sediment). Therefore, without knowing the initial sediment composition, prior to any fractionation, it is difficult to ascertain the composition of the slab input. However, a hypothetical sediment composition based on existing constraints can be used for the purpose of evaluating the relative sediment input required to form the Soná-Torio Arc and Proto-arc groups. We have used a hypothetical sediment, with values of Th, Yb and Nd based on the continental crust, but with higher Nd (Nd = 0.5128), and modified Nb, which can explain the formation of the Proto-arc and Arc groups.

In Figure 6.4, mixing lines have been calculated using Nd isotope and the Th/Nb and Th/Yb proxies for sediment addition. These mixing lines indicate that addition of 0.2 – 0.8 % sediment to a plume-like mantle could produce the Soná-Torio Proto-Group 1 using both the Th/Nb and Th/Yb proxies. The mixing lines between DMM and the sediment indicate that the formation of the Proto-arc Group 2 requires < 0.4 % of sediment addition using the Th/Nb and Th/Yb proxies. The Soná-Torio Arc samples require an addition of 3 - 10% of sediment to a plume-like or DMM mantle using the Th/Yb proxy, and an addition of 0.6 – 8 % of sediment using the Th/Nb proxy.

Table 6.1: Isotope and trace element data for end members used in mixing calculations

	$^{143}Nd/^{144}Nd$	Nd (ppm)	Th (ppm)	Nb (ppm)	Yb (ppm)
DMM	0.51313	0.581	0.0079	0.365	0.1485
COP	0.51294	1.079	0.045	0.388	0.661
SED	0.5128	27	10.5	1.5	2

Based solely on Nd_i isotope values of the mantle sources plus continental crust, the range of the Proto-arc Group 1 could be explained with 0.1 and 0.3 % of sediment addition of the plume-like mantle, the Proto-arc Group 2 could be explained by 0.1 – 0.5 % of sediment addition to the depleted upper mantle , while the arc requires the addition of 0.1 – 0.7 % sediment.

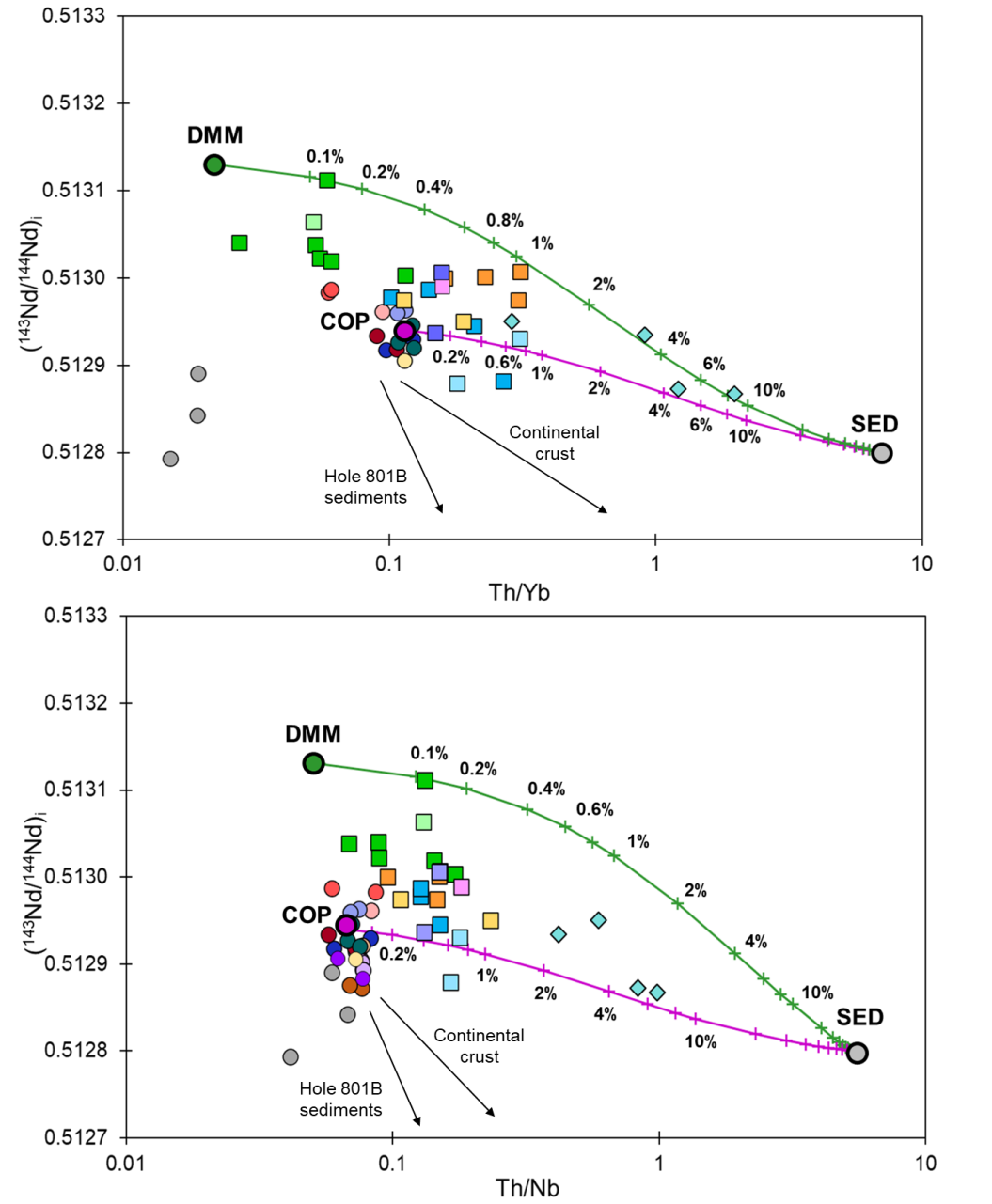

Figure 6.4: Initial Nd isotope plots. Lines show mixing between mantle end members and sediment. DMM = Depleted MORB Mantle, COP = Caribbean Oceanic Plateau mantle, SED = Sediment.

Not all Proto-arc Group 1 samples plot along the same mixing line. However, the variation of Nd_i in the Proto-arc Group 1 largely reflects the variation seen in the samples of the plateau. The oceanic plateau in the Caribbean is highly heterogeneous, shown in multiple previous studies (Kerr et al., 2002a; Kerr, 2005; Kerr et al., 2009; Hastie et al., 2016; Dürkefälden et al., 2019) and discussed in Section 6.5. If the Proto-arc Group 1 samples were produced due to melting of plume-like metasomatized mantle, this may lead to geochemical heterogeneity of the samples. Where a single Proto-arc Group 1 sample appears to plot at higher values than those of the Plateau, it is possible that this sample has also had the influence of a depleted component in the source. However, it is not clear whether this depleted component is from the depleted upper mantle or a depleted plume remnant mantle.

The Proto-arc Group 2 samples also display some heterogeneity. Many of the Proto-arc Group 2 samples do not plot along the mixing line between the DMM and the sediment. Instead, they plot in the area between the DDM-Sediment mixing line and the COP-Sediment mixing line. This indicates that the mantle source for the Proto-arc Group 2 may not have been solely depleted upper mantle, and may have also included a plume component. Although most of these samples show some degree of Th enrichment, some do not show any enrichment, and have Th/Nb similar to typical MORB. This indicates that these samples had no slab fluid or melt addition, as is reflected in the mixing lines above. Therefore, the melting which led to the formation of these Proto-arc 2 samples cannot be explained only by the release of fluids from the downgoing slab. Instead, the melting that produced some of the Proto-arc Group 2 lavas may have been due to decompression due to extension or due to additional heat.

Based on the depletion of the LREEs and the high Nd values, it is possible that the Proto-arc Group 2 could be related to a depleted plume mantle, rather than a depleted upper mantle. In Nd isotope space, the Proto-arc Group 2 samples largely like within the range of the Depleted CCOP Nd values. However, it appears that the most depleted and high Mg parts of the oceanic plateau in the Soná-Torio region have Nd values that are far more enriched than other LREE depleted plateau samples, such as the picrites and komatiites from Gorgona (Kerr et al., 1996c; Arndt et al., 1997). Additionally, rocks of the Proto-arc Group 2 also consistently plot within the MORB array on the tectonic discrimination diagrams, with ratios such as $Zr/Nb > 30$ and $Nb/Y < 0.1$, more in line with a MORB-like source than a plume source. Therefore, it seems more likely that the Proto-arc Group 2 samples are associated with a MORB source.

All samples of the Soná-Torio Proto-arc Group 1 show some amount of Th enrichment, and they are thought to be formed when the first slab fluids or melts were released from the early

downgoing slab, melting plume-related mantle. The Proto-arc Group 2 formed after this, after the source has evolved to a MORB-like mantle, and not all samples display the input of a slab component. This could mean that the first MORB-like Proto-arc melts was not caused by fluid addition, but potentially due to heating or decompression. This could be explained by minor spreading in the forearc and adiabatic melting of the underlying mantle at this time. However, as discussed above, there is a lack of evidence for this type of spreading in the forearc.

It is possible that the slab component in the Proto-arc Group 1 could be caused by fluids first coming from the arc further west, close to the margin of South America, and does not actually represent subduction initiation in the Soná-Torio region. This could mean that the Proto-arc Group 2 was first stage of subduction initiation related magmatism, and could have formed similarly to the FAB of the IBM. This would also explain why the Proto-arc Group 1 lavas all seem to have a slab related addition, whereas some of the Proto-arc Group 2 lavas do not. However, it is likely that if there was an arc close enough for the fluids to travel across, there would also be further evidence of volcanic activity, such as further tuffaceous deposits. The Torio Lithostratigraphic Unit, which formed at the same time as the Proto-arc Group 1, does not display a large enough tuffaceous component to indicate the proximity of a developed volcanic arc system.

Geochemically, the Proto-arc groups appear to show distinct compositions. This is especially reflected in the Nd isotope values. There is no clear spectrum of values from Proto-arc Group 1 through to Proto-arc Group 2, which could indicate a gradual change of source, but instead 2 distinct groups, which indicates a more rapid change. This is also verified by the lack of slab input in some of the Proto-arc Group 2 lavas, as this indicates a change in the melting mechanism and a significant change in the mantle wedge. The lack of a slab fluid signature in some of the Proto-arc Group 2 samples could be due to dilution of the slab input due to extensive melting of the mantle. During the first stage of subduction initiation magmatism, in the formation of the Soná-Torio Proto-arc Group 1, initial fluids from dehydration of the downgoing slab could have melted the most fertile remnant plume component, potentially plume related metasomatized lithospheric mantle. After extraction of these more fertile melts, the subsequent fluids from the downgoing slab melted the depleted upper mantle. It is possible that this depleted upper mantle was dragged into the early mantle wedge due to corner flow initiation. This mantle is likely to hold some residual heat from the presence of the plume (likely active ca. 10 Myr before subduction initiation) which will be retained due to subduction zones forming around the plateau, and the thermal lid of the oceanic plateau. Minor additions of a fluid component to this hot residual mantle could

therefore cause extensive melting, which would dilute the fluid signature, and explain why it is not observed in all samples of the Proto-arc Group 2.

Subsequently, during the establishment of a developed subduction zone and Soná-Torio Arc volcanism, downgoing slab will cool the surrounding mantle, which could terminate the melting observed in the Proto-arc Group 2. More fluids will be expelled from the downgoing slab, leading to normal mantle wedge melting and the formation of the Soná-Torio Arc with typical arc-like geochemical signatures showing clear Th and LREE enrichment.

6.4.4 Regional occurrences of the Proto-arc

The Late Campanian to Paleogene arc observed on the Soná and Azuero Peninsulas is also exposed along the Caribbean coastline of Panama, east of the Canal Zone (Maury et al., 1995; Wegner et al., 2011; Montes et al., 2012a) (Figure 6.5). Here, it is called the Chagres-Bayano Arc. These arc groups likely formed a continuous volcanic front in the Late Cretaceous to Paleogene, but were then offset between ca. 40 and 34 Ma due to the oroclinal bending of the isthmus, potentially caused by the collision of the arc with Colombia (Silver et al., 1990; Farris et al., 2011; Montes et al., 2012a; Buchs et al., 2019b). Sequences of the plateau and proto-arc have been recognised in Central Panama, as part of the Chagres Bayano Arc (Montes et al., 2012; Buchs and Wang, com. pers. 2020). The proto-arc samples of the Chagres-Bayano region appear to reflect the heterogeneity of the Soná-Torio Proto-arc groups. Previously, two groups for the proto-arc have been described in central Panama: one group (Group IIa) depleted in the LREEs which is equivalent to Proto-arc Group 2, and the other with slightly enriched LREEs (Group IIb) which is equivalent to Proto-arc Group 1 (Montes et al., 2012a). From the work of Buchs and Wang (com. pers. 2020) two samples (samples DB16-001, DB16-003) have REE patterns similar to those of the Proto-arc Group 1, with one sample showing a Th

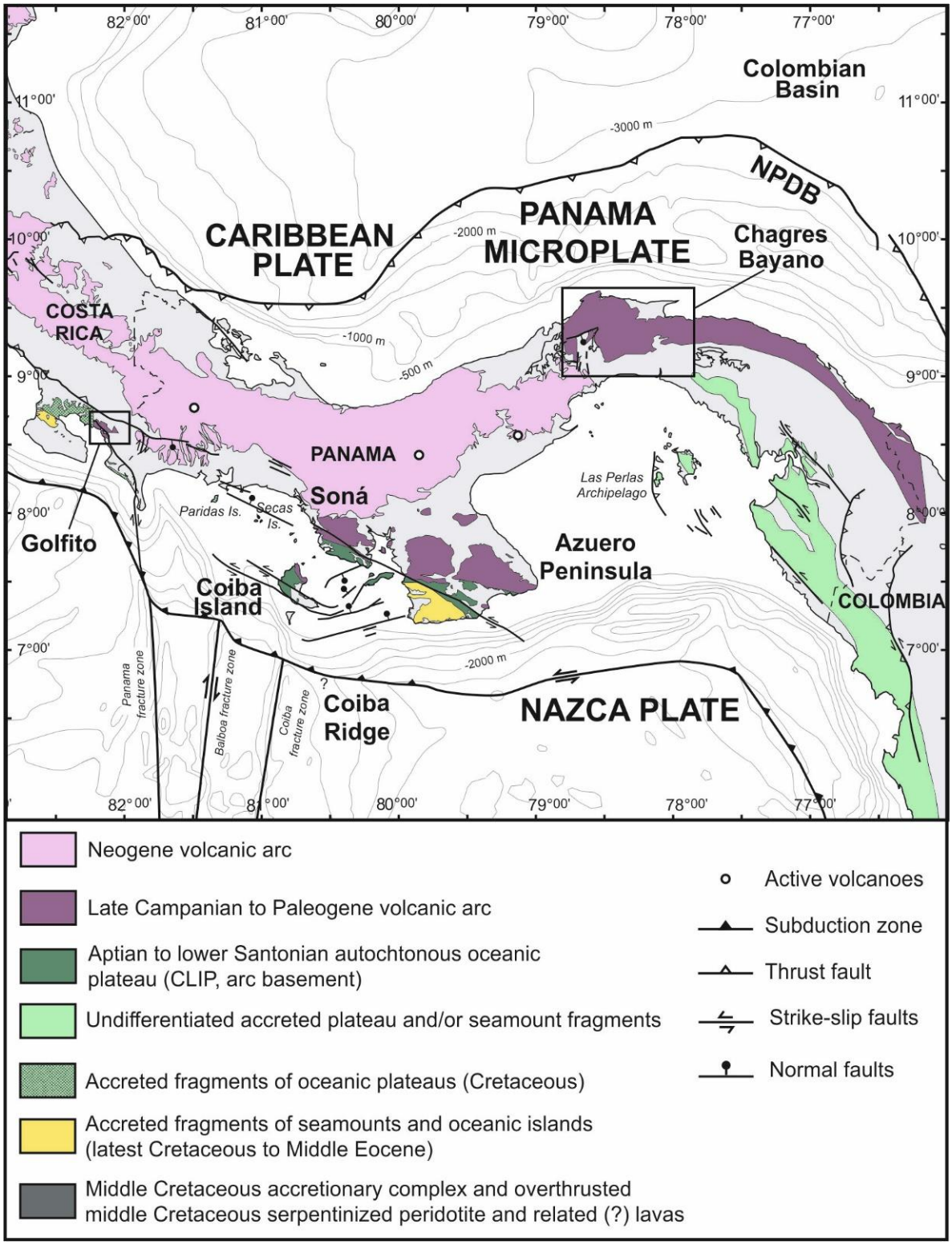

Figure 6.5: Simplified geological map of southern Central America modified after Buchs et al. (2011), showing location of the Golfito and Chagres Bayano regions.

enrichment relative to Nb, and another showing no Th enrichment (Figure 6.6). Sample J18-004 however, shows LREE depletion, with a similar pattern to samples of the Soná-Torio Proto-arc Group 2 (Figure 6.6). Using Nd_i isotopes, the two Group 1 samples plot within the range of the Soná-Torio Proto-arc Group 1 samples, with values of 0.51297 and 0.51295

(Figure 6.4). The sample with the enrichment in Th has a lower Nd_i value, consistent with addition of a slab component, and these samples follow the trend of the mixing line between a plume and sediment component. However, these samples have higher Nd_i than the central Panama plateau sample, potentially indicating the influence of a depleted component with the melt, but this is difficult to assess with such a limited number of analyses. The Group 2 sample plots on the margin between the Soná-Torio Proto-arc Group 1 and 2 ranges, but appears to plot on the trend of the Group 2 samples, with slightly higher Th. As this sample shows a depletion in the LREEs, but it is smaller than observed in the Soná-Torio Proto-arc Group 2, is it possible that this sample represents a transition between the Proto-arc Group 1 and Group 2 (Figure 6.4).

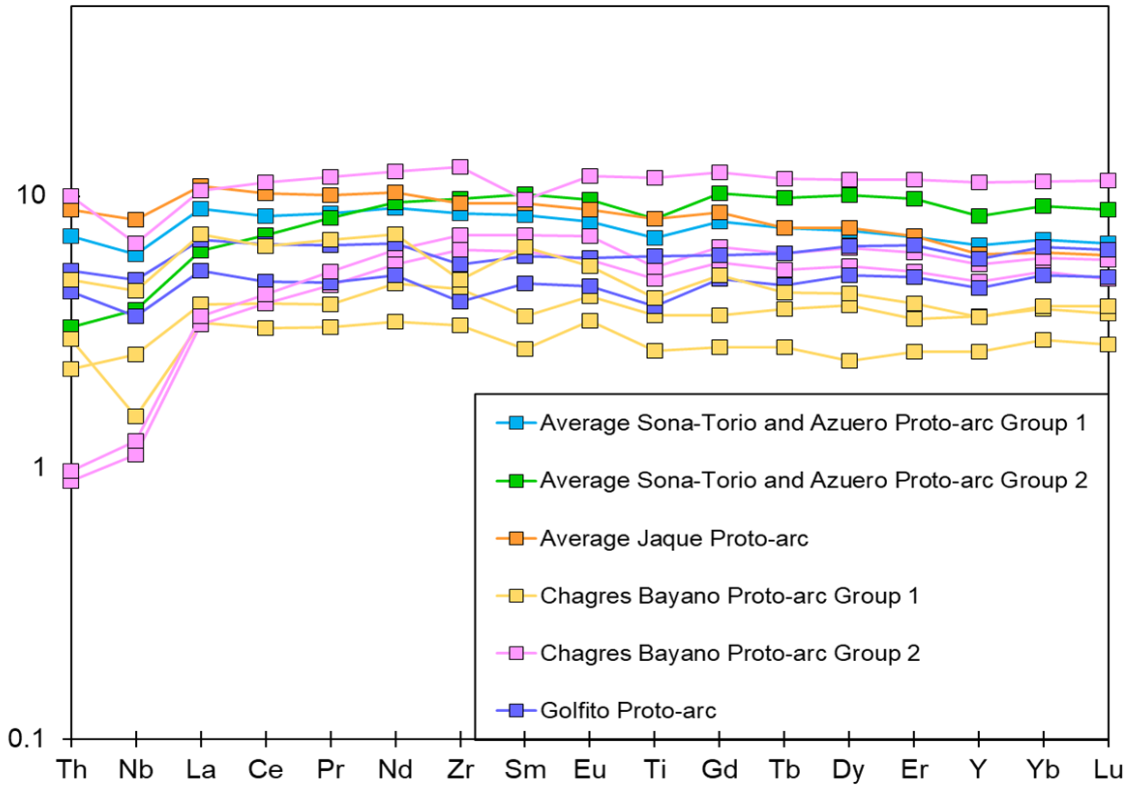

Figure 6.6: Primitive mantle-normalised multi element diagram for Proto-arc samples from across Central America. Chagres Bayano samples from Montes et al. (2012) and Wang (unpublished). Golfito Proto-arc from Buchs et al. (2010).

Proto-arc lavas have also been previously recognised in Golfito in Costa Rica, although no clear plateau basement has been observed in this region (Buchs et al., 2010) (Figure 6.5). These samples have REE patterns similar to those of the Proto-arc Group 1 (Figure 6.6). Based on Nd_i isotopes, the samples have a wide range; sample DB02-181 plots within the Proto-arc Group 1 range with a value of 0.51294 while sample DB02-174 plots on the margin of the two ranges, with a value of 0.51301 (Figure 6.4). This difference in values cannot be correlated to the varying contribution of slab fluids in each sample. This therefore

may represent the heterogeneity in the source, which is reflected in both Soná-Torio Proto-arc Groups. These results from central Panama and Golfito confirm that the Proto-arc is observed along strike and formed elsewhere along the southwestern margin of the Caribbean Plateau. It also shows that the heterogeneity of the Proto-arc is not unique to the Soná and Azuero Peninsulas.

Based on trace element characteristics, the Jaqué Proto-arc is similar to the Soná-Torio Proto-arc Group 1, while the Nd_i values of the Jaqué Proto-arc plot on the margin between the Soná-Torio Proto-arc Group 1 and 2. These samples are likely to represent the first stage of subduction magmatism in the Darién Pacific Coast region, although it is not clear when this began due to a lack of $^{40}Ar/^{39}Ar$ and/or biostratigraphic ages. After the oroclinal bending of the isthmus which led to offset of the Chagres-Bayano and Soná-Azuero Arcs, a younger volcanic front was established along the Darién Pacific Coast, south of the older Chagres-Bayano Arc (Lissinna, 2005). The only existing age for the arc along this coast is 21.7 ± 0.3 Ma, whilst ages for the Maje and Pearl Islands, which likely form the same volcanic front, range from ca. 18 – 20 Ma (Lissinna, 2005). However, it is possible that volcanism began earlier than this, as there are no existing ages for arc volcanism in eastern Panama between the ca. 40 Ma cessation of magmatism in the Chagres-Bayano Arc, and the 22 Ma age of volcanism above (Wegner et al., 2011; Buchs et al., 2019b). The mantle source of the Jaqué Proto-arc is also unknown. In Nd_i isotopes, these samples plot at higher values than those of the plateau samples, between the samples of the Soná-Torio Proto-arc Groups. Unfortunately, no samples of the Sapo Arc have been analysed for Nd isotopes, so these groups cannot be compared. However, the Jaqué Proto-arc samples do also have much higher Nd_i values than the samples of the Soná-Torio and Chagres-Bayano Arc and therefore it does not appear that they were sourced from a developed mantle wedge. The Jaqué Proto-arc most likely represents the lateral equivalent of the Soná-Torio Proto-arc.

6.4.5 Summary

Much of the current understanding of subduction initiation processes has come from the IBM system, which has been the focus of multiple drilling programs in recent years (Reagan et al., 2010; Ishizuka et al., 2011; Reagan et al., 2017; Ishizuka et al., 2018). Based on the stratigraphic assemblage of the first products of subduction initiation in the IBM, a “subduction initiation rule” was proposed (Whattam and Stern, 2011). This rule aimed to define the key stages of subduction initiation which could explain the formation of the IBM lavas and the stratigraphy seen in subduction zone ophiolites. In this subduction initiation rule, the first products of subduction initiation (FAB) are produced by adiabatic

decompression melting of a MORB-like asthenospheric source, due to early forearc spreading, with little to no slab fluid input (Whattam and Stern, 2011). In the IBM, these FAB lavas are formed from a source that is more refractory than that of MORB (Shervais et al., 2019). The FAB lavas are overlain by boninites, which formed when fluids released from the downgoing slab melted the depleted residual mantle (Whattam and Stern, 2011). It has been suggested that this subduction initiation rule may apply to the forearc assemblages which are uplifted in the Soná-Torio region (Whattam et al., 2020). It has also been suggested that the formation of these assemblages could be explained by the PISI model (Whattam and Stern, 2015), which dictates that the impingement of a plume head in the Caribbean could have caused sufficient lithospheric weakening to prompt the formation of subduction zones around the margins of the plateau.

However, the new field and geochemical results from this study, combined with previous constraints (Kolarsky et al., 1995; Lissinna, 2005; Buchs et al., 2010; Buchs et al., 2011b; Corral et al., 2011) do not support these models. Both the IBM subduction initiation rule and the PISI model require early extension in the forearc, which is not observed in the Soná-Torio region. In contrast, there is evidence of uplift in the region at the time of subduction initiation, in the form of breccias and sandstones which contain fragments of the oceanic plateau basement, and palaeokarst infills. There also does not appear to be a continuous evolution from plateau-like through to arc-like lavas in the forearc, with a clear cessation of magmatism between plateau and proto-arc lavas shown by the regional deposition of the Late Cretaceous Torio Lithostratigraphic Unit.

In the Soná-Torio region, the first magmatic products of subduction initiation (the proto-arc) can be divided into two groups. The first and oldest of these groups is the Soná-Torio Proto-arc Group 1. These samples are from a plume-like source, with Nd_i values within the range of normal CCOP and flat to slightly enriched primitive mantle normalised trace element patterns, with slight Nb negative anomalies and variably enriched Th. This group has clear slab fluid influence, and formed at ca. 75-73 Ma, based on the biostratigraphic ages of the Torio Lithostratigraphic Unit, which Proto-arc Group 1 dykes intrudes exhibiting soft sediment deformation and peperitic contacts. The Proto-arc Group 2 is the second group of the proto-arc and appears to be relatively younger than Group 1, as it intrudes tuffaceous sequences of the Proto-arc Group 1 and is not observed to be interbedded with the Torio Lithostratigraphic Unit. This group is thought to form at ca. 73-72 Ma. The Soná-Torio Proto-arc Group shows MORB-like primitive mantle normalised trace element patterns, with variable Th enrichment to depletion, and Nd_i values within the range of EPR MORB. Although the forearc stratigraphy has not yet been described in detail in central Panama,

samples of the Proto-arc Group 1 and Group 2 have been detected in the Chagres-Bayano region, so this heterogeneity continues along strike.

The geochemistry of the proto-arc groups indicates that there was a change in the mantle source during the first stages of subduction initiation magmatism. The formation of the Proto-arc Group 1 could have formed when the first fluids were released from the downgoing slab, prompting melting of a the most fusible and fertile plume-like heterogeneous metasomatized lithospheric mantle. The composition of the Proto-arc Group 1 requires the addition of 0.2 – 0.8 % sediment to a plume-like mantle. The Proto-arc Group 2 was then formed by melting of a MORB-like depleted upper mantle. This depleted upper mantle is likely hot, due to the residual heat of the plume which was active ca. 10 Ma earlier, and may be introduced into the mantle wedge due to the initiation of corner flow. Not all samples of the Proto-arc Group 2 show slab fluid input, and their formation can be explained by less than 0.4 % sediment addition to a DMM source. If this depleted mantle holds residual heat from the plume, the addition of fluids could cause extensive partial melting which will in turn dilute the fluid signature. Subsequently, during the establishment of an established volcanic arc, the downgoing slab will cool the mantle wedge, prompting less melting with the addition of fluids, leading to a stronger subduction related signature.

Subduction initiation along the southwestern margin of the Caribbean Plateau was likely to be tectonically induced, due to the complex tectonic configuration of the region at this time. In the Late Cretaceous, the Caribbean Plateau collided with the South American continent (Pindell and Kennan, 2001; Vallejo et al., 2006; Villagómez and Spikings, 2013). This collision may have prompted the propagation of subduction along the margin of the plateau, leading to subduction initiation in Panama. This induced model of subduction initiation is supported by the lack of evidence for extension in the forearc in the Late Cretaceous. Considering this lack of evidence for extension and the complex tectonic configuration in Central America, it appears unlikely that subduction initiation would occur spontaneously. However, the subduction initiation process could have been supported by the compositional density contrast across the margin of the oceanic plateau.

6.5 Origins of the Soná-Torio, Jaqué and Serranía de Baudó plateau assemblages

The CCOP is the oceanic plateau which forms most of the Caribbean Plate, along with many accreted fragments along the coast of north western South America, particularly in Colombia (Kerr et al., 1996b; Kerr et al., 1997b; Lapierre et al., 1999; Hauff et al., 2000a; Sinton et al., 2000; Kerr et al., 2002a; Kerr et al., 2003; Escuder-Viruete et al., 2007; Kerr et al., 2009). Although it could be thought that mantle plumes would produce homogenous plateaus due to the high degree of partial melting, previous work has shown that rocks from across the CCOP are highly heterogeneous (e.g., Kerr et al., 1996a; Lissinna et al., 2002; Escuder-Viruete et al., 2007; Kerr et al., 2009; Dürkefälden et al., 2019). These heterogeneous plateau assemblages can be categorised into three geochemical groups based on trace elements: (1) typical, “normal” oceanic plateau basalts and dolerites with flat primitive mantle normalised trace element patterns typically with positive Nb anomaly, which form the bulk of the oceanic plateau basalts; (2) an enriched group, typically enriched in the LREES, again with a positive Nb anomaly; and (3) a depleted group, with depletions in the LREES. Based on a compilation of CCOP assemblages from the GEOROC online database, the typical oceanic plateau basalts have values of La/Sm between 0.60 – 1.20, the enriched group have La/Sm values > 1.20 and the depleted group have La/Sm values < 0.60. Typically, these trace element patterns correlate with Nd isotope contents, as Nd_i values for normal CCOP basalts range from 0.51283 – 0.51304, the enriched CCOP range from 0.51277 – 0.51291 and depleted CCOP range from 0.51299 – 0.51312. Normal, enriched and depleted geochemical groups can occur in close stratigraphic association, as notably exemplified by rock sequences (komatiites, picrites, basalts, and gabbros) on the island of Gorgona, which is located approximately 30 km off the coast of south western Colombia in the Pacific Ocean, and is only 2.5 km wide (Figure 2.7) (Kerr et al., 1996b).

The geochemical heterogeneity within the CCOP cannot be explained only through varying degrees of partial melting, and therefore, it is necessary for the source to be a heterogeneous mantle plume with intrinsic depleted and enriched components (Kerr et al., 1996b; Révillon et al., 2000b; Kerr et al., 2009; Hastie et al., 2016; Dürkefälden et al., 2019). Generally, the accreted oceanic plateau rocks in Colombia and Ecuador, the uplifted portions of the plateau around the margins of the Caribbean Plate, and plume-sourced rocks drilled in the centre of the Caribbean Plate are thought to be part of the same oceanic plateau, sourced from the same mantle plume (Révillon et al., 2000a; Hoernle et al., 2002; Thompson et al., 2004). This plume is likely associated with the initiation of the Galapagos hotspot in the Cretaceous, which formed the oceanic plateau in the Pacific Ocean, before it drifted between the Americas (Duncan and Hargraves, 1984; Burke, 1988; Kerr et al., 2003; Thompson et al., 2004; Mann, 2007). It has also been suggested that the CCOP is actually

formed by more than one oceanic plateau, potentially attributed to multiple plumes (Kerr and Tarney, 2005). Kerr and Tarney (2005) suggested based on geochemistry, ages and paleomagnetic data that Gorgona Island and parts of the Serranía de Baudó form a separate oceanic plateau, called the Gorgona Plateau, with a different mantle plume source (potentially the Sala y Gomez hotspot) from further south in the Pacific (Kerr and Tarney, 2005). Comparing the nature and composition of the oceanic plateau sequences exposed across the Soná-Torio, Darién Pacific Coast and Serranía de Baudó regions will help us understand the origin of oceanic plateau sequences in Panama and north western Colombia. This will assist in understanding the tectonic configuration of the Caribbean Plateau and Panama Arc in the Cretaceous, and ultimately the mechanisms by which the Panama Arc formed along the margin of an oceanic plateau.

In this study, seven geochemical groups were recognised within the oceanic plateau sequences: The Soná-Torio Plateau, Enriched Plateau, and High-Mg Plateau; The Jaqué Plateau, Depleted Plateau and Enriched Plateau; and the Baudó Plateau. Here, the origin of these groups will be discussed, including the plume source to these plateaus. This will be done by evaluating the geochemical and field evidence presented for each oceanic plateau regions. Where there are geochemical or geological differences between the plateau groups, arguments for a heterogeneous plume source or separate plume sources will be considered.

6.5.1 Soná-Torio

In the Soná-Torio Region, most lavas and intrusions of the plateau are in the Soná-Torio Plateau geochemical group. However, locally, there are more enriched rocks with Soná-Torio Enriched Plateau geochemistry (Figure 3.3, 3.5). Also exposed locally, largely in heavily faulted regions, there are depleted hyaloclastites and basaltic breccias of the Soná-Torio High Mg Plateau.

6.5.1.1 Soná-Torio Plateau

The Soná-Torio Plateau group samples consist largely of pillow basalts and massive lava flows, along with rare dykes, indicating a submarine origin. Generally, these samples show typical oceanic plateau signatures on multielementary trace element normalised diagrams, within the range of normal CCOP values (Figure 6.7). On tectonic discrimination diagrams, these samples also plot within the array of typical CCOP values, showing trace element contents expected of typical oceanic plateau basalts (Figure 6.8). On the Nb/Yb vs Th/Yb diagram the Soná-Torio and Azuero Plateau samples plot within the MORB-OIB array, on

the TiO_2/Yb vs Nb/Yb diagram they plot within the MORB array, and on the Nb/Yb vs Zr/Y and Nb/Th vs Zr/Nb diagrams they plot in the OPB arrays. On Nd_i diagrams, these samples also plot within the range of normal CCOP (Figure 6.9). These observations confirm an oceanic plateau origin for these samples, and they represent the typical, “normal” oceanic plateau basalts observed across the CCOP.

6.5.1.2 Soná-Torio Enriched Plateau

The Soná-Torio Enriched Plateau is plotted with samples that were previously interpreted as Plateau Group II by Buchs et al. (2010), and some samples interpreted as OIB by Lissinna (2005). Generally, these samples are exposed close to the Soná-Azuero Fault zone. They are formed of pillow basalts, lava flows and intrusions, again indicating a submarine origin. Enriched components of the plateau have previously been recognised on the previously mentioned Gorgona Island, where they are called E-Basalts, as well as in the Duarte Complex on Hispaniola, Site 151 from the Beata Ridge, on the Lower Nicaraguan Rise (LNR) and in Tortugal in Costa Rica (Echeverria, 1980; Aitken and Echeverría, 1984; Kerr et al., 1996b; Arndt et al., 1997; Hauff et al., 2000a; Hauff et al., 2000b; Escuder-Viruete et al., 2007; Dürkefälden et al., 2019). Some of the enriched groups have been attributed to be the products of melting of an enriched component of a heterogeneous mantle plume (Kerr et al., 1996b; Arndt et al., 1997; Dürkefälden et al., 2019). It is thought that in a heterogeneous mantle plume containing an enriched and depleted component, the enriched basalts of the CCOP could form by limited melting within the plume which preferentially samples the enriched component, while later melting homogenises the enriched component with the depleted component, leading to the geochemistry seen in typical plateau basalts across the CCOP (Kerr et al., 1996c).

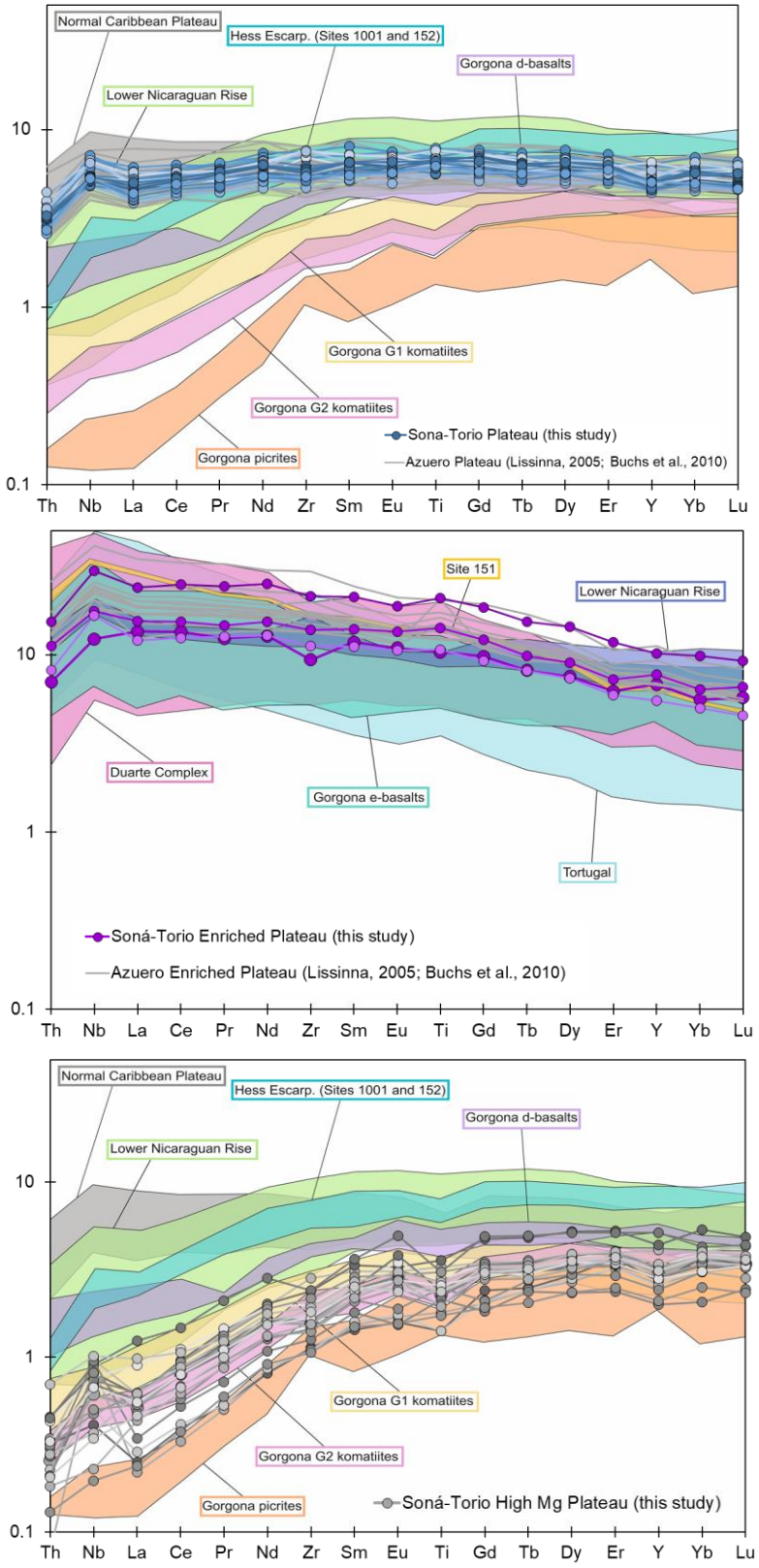

Figure 6.7: Primitive mantle-normalised multi-element diagrams for the Soná-Torio and Azuero Plateau, Enriched Plateau and High-Mg Plateau. Data sources: Normal Caribbean Plateau from GEOROC online database; Enriched and Depleted Lower Nicaraguan Rise (Durkefalden et al., 2018); Site 1001 (Kerr et al., 2009); Sites 151 and 152 (Hauff et al., 2000b); Duarte Complex (Escuder-Viruete et al., 2007); Tortugal (Hauff et al., 2000a); Gorgona e-basalts, d-basalts, G1 and G2 komatiites and picrites (Aitken and Echeverria, 1984; Kerr et al., 1996; Arndt et al., 1997; Revillon et al., 2000; Kerr, 2005)

It has also been suggested that enriched plateau basalts may have formed from melting of the more enriched plume tail or related to recycling of continental sediments or contribution from continental crust (Escuder-Viruete et al., 2007). The Tortugal rocks have also been attributed to be part of an accreted oceanic island (Hauff et al., 2000a), although most recent studies suggest it also belongs to the CCOP (Alvarado et al., 1997; Kerr et al., 2002a; Ludwig, 2017; Trela et al., 2017).

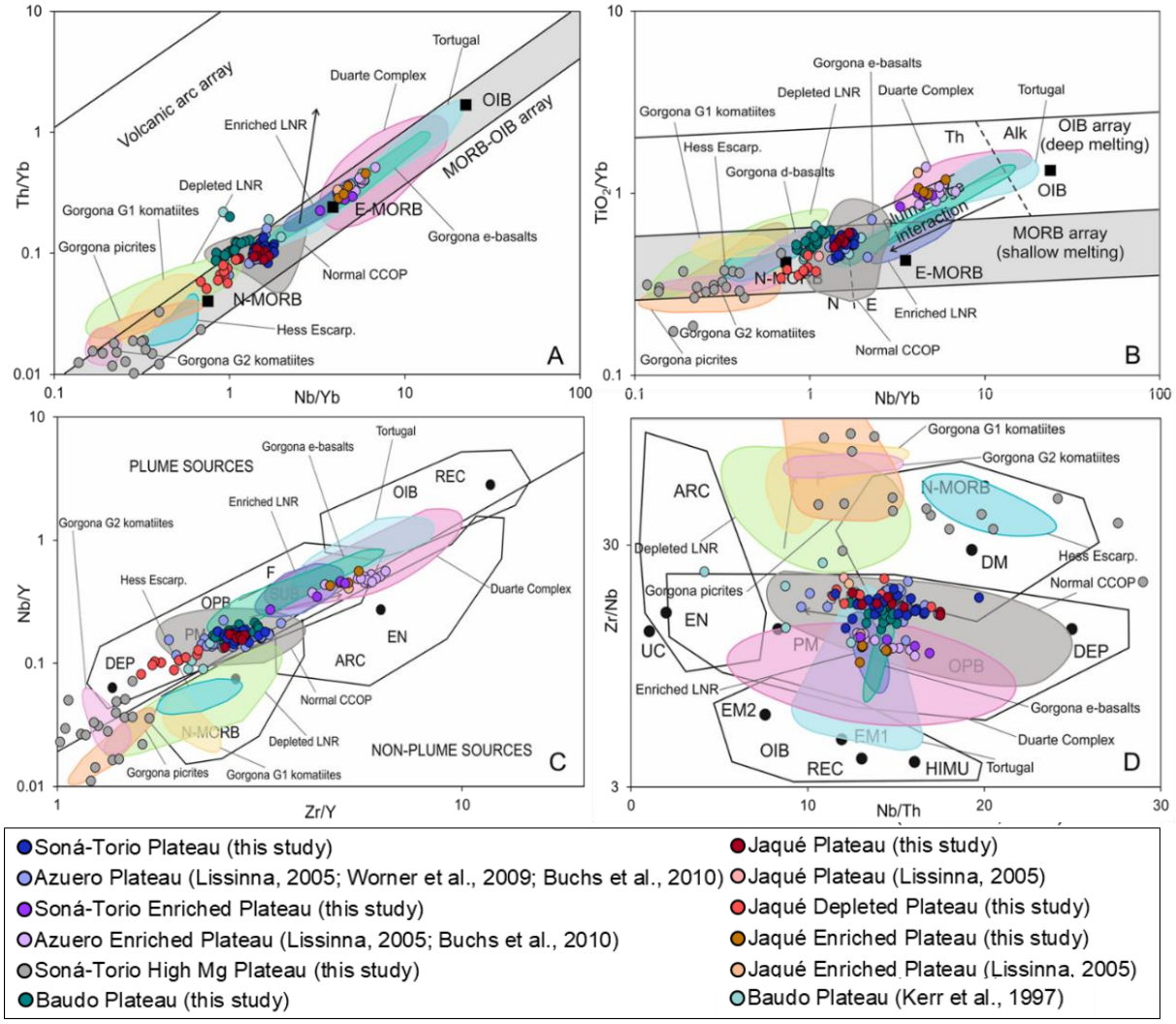

Figure 6.8: Tectonic discrimination diagrams for plateau samples. A) Nb/Yb vs Th/Yb crustal input proxy diagram (Pearce 2008), B) Nb/Yb vs TiO_2/Yb deep melting proxy diagram (Pearce 2008), C) Zr/Y vs Nb/Y diagram (Condie 2005), D) Nb/Th vs Zr/Nb diagram (Condie, 2005), Abbreviations: UC = upper continental crust, PM = Primitive Mantle, DM = shallow depleted mantle, HIMU = high mu (U/Pb) source, EM1 and EM2 = enriched mantle sources, ARC = arc related basalts, N-MORB = normal mid-ocean ridge basalt, OPB = oceanic plateau basalt, OIB = oceanic island basalt, DEP = deep depleted mantle, EN = enriched component, F = effects of batch melting and SUB = subduction effect. Data sources are as in Figure 6.5.

On primitive mantle normalised multielementary groups, the patterns of the Soná-Torio Enriched Plateau overlap with the other enriched plateau groups, although the La/Yb slope

is lower than samples of the Tortugal and Duarte complexes, and slightly higher than the Gorgona e-basalts (Figure 6.7). The depleted signature of the HREEs (Gd/Yb = 1.64 – 1.91) indicates deeper melting with the influence of garnet in the source. On tectonic discrimination diagrams, the Enriched Plateau samples again overlap with all arrays of other enriched CCOP units (Figure 6.8). On the Nb/Yb vs Th/Yb plot, the samples plot in the MORB-OIB array close to E-MORB and within the e-basalt, enriched LNR, Duarte Complex and Tortugal arrays, above the normal CCOP array. On the TiO_2/Yb vs Nb/Yb plot, all Soná-Torio Enriched Plateau samples plot above the MORB array, which indicates that they were produced by deeper melting with the presence of garnet. On this plot the Enriched Plateau samples plot above the Enriched LNR and Gorgona e-basalt arrays, but plot within the Tortugal and Duarte Complex arrays. Again, they are clearly distinct from the normal CCOP array. On the Zr/Y vs Nb/Y plot, the Soná-Torio Enriched Plateau samples plot in the upper section of the OPB array and below the OIB array, overlapping all enriched CCOP arrays. On the Nb/Th vs Zr/Nb plot, the Enriched Plateau samples lie in a somewhat linear array, again overlapping with all enriched CCOP arrays. On this plot, the Enriched Plateau samples also plot within the array of Normal CCOP rocks. Overall, on tectonic discrimination diagrams, the Enriched Plateau samples do not plot in typical OIB array but they are clearly more enriched than the normal CCOP basalts. This is in contrast to the Tortugal and Duarte complexes that plot within the OIB field.

Higher La/Sm (enriched) samples of the Soná-Torio and Azuero Enriched Plateau have Nd_i values lower than those of the normal Soná-Torio Plateau. On plots using Nd_i, samples of the Enriched Plateau generally plot on the upper margins of the Enriched CCOP array, defined by rocks of the CCOP with La/Sm > 1.2 (Figure 6.9).

From the trace elements and isotopes, it is clear that samples of the Soná-Torio and Azuero Enriched Plateau are not from a shallow depleted upper mantle MORB-like source, and that they are from a plume source. However, it is also clear that they have a composition which is distinct from the bulk of the CCOP lavas, and appear to have a more enriched source which may be similar to the sources of other enriched CCOP products, such as the e-basalts of Gorgona. As samples of the Soná-Torio Enriched Plateau consist of plateau lavas and sills which appear to form the same plateau sequences as samples of the Soná-Torio Plateau, these groups are likely to be from a single, compositionally heterogeneous mantle plume source.

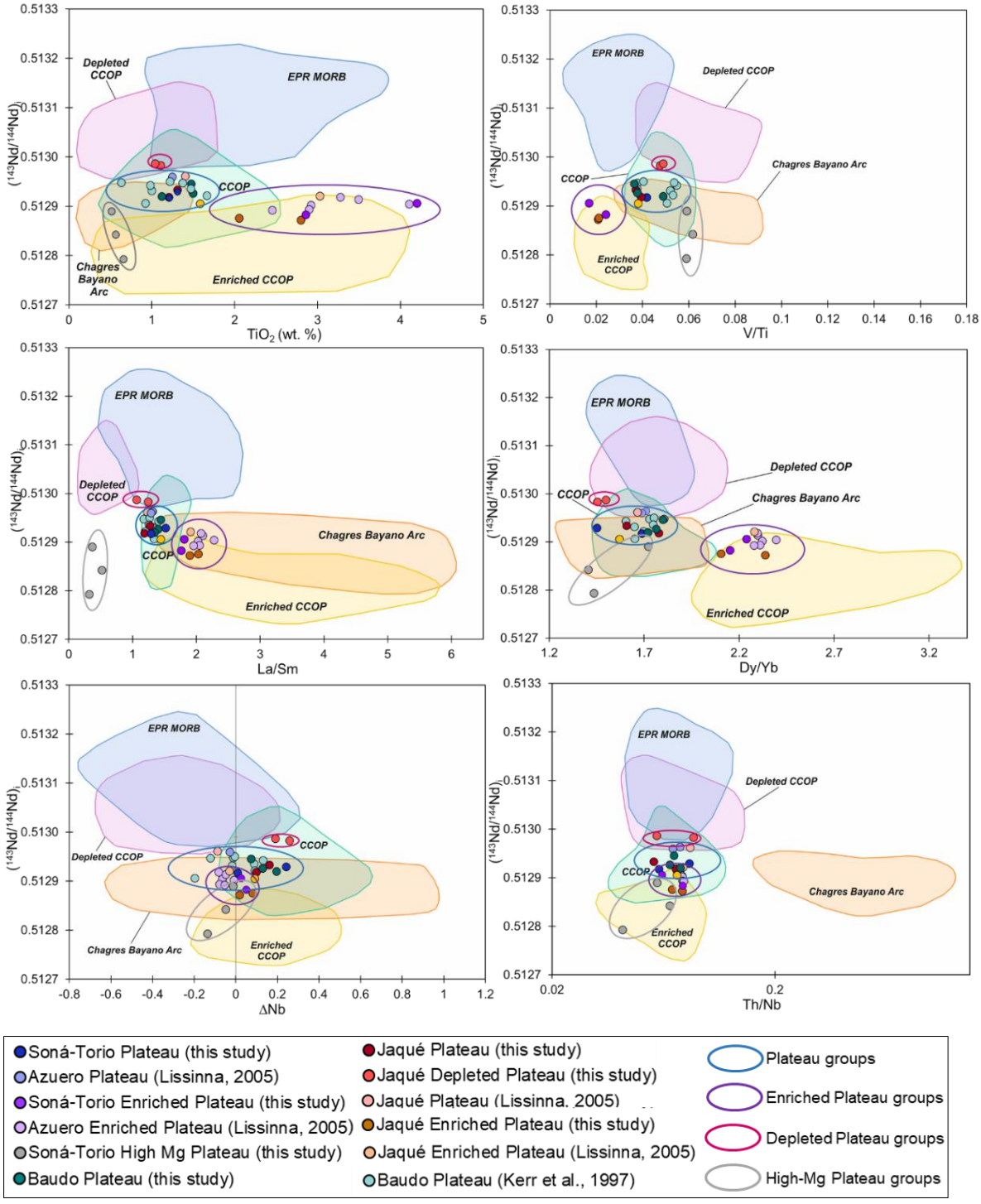

Figure 6.9: Bivariate diagrams of initial Nd isotopic ratios of the Soná-Torio, Darién Pacific Coast and Serranía de Baudó plateau samples, with previously analysed samples of Lissinna (2005) and Wegner et al. (2011). Also displayed are the isotope fields for the Colombian-Caribbean Oceanic Plateau (CCOP) (La/Sm > 0.60, < 1.20), the Depleted CCOP (La/Sm < 0.60) and Enriched CCOP (La/Sm > 1.20) (all from GEOROC online database, age corrected to 90Ma), the East Pacific Rise MORB (EPR MORB) from (PetDB online database) and the Chagres Bayano Arc (Wegner et al., 2011).

6.5.1.3 Soná-Torio High-Mg Plateau

The geochemistry of the Soná-Torio High-Mg Plateau samples has not previously been described. These samples represent the rocks described as greenschists by Del Guidice and Recchi (1969), as 'metamorphic rocks of unclear origin' by Buchs et al. (2011) and may be related to the amphibolites by Tournon et al. (1989). These samples are composed of greenschists and basaltic breccias/hyaloclastites, and petrography indicates that they have undergone greenschist facies metamorphism.

The samples of the Soná-Torio High-Mg Plateau will be compared with other similarly depleted rocks of the CCOP, which have so far been found on the Lower Nicaraguan Rise, Hess Escarpment (in Site 1001 and 152) and Gorgona Island (Hauff et al., 2000b; Kerr et al., 2009; Dürkefälden et al., 2019). On Gorgona Island depleted rocks have been subdivided into depleted (d-)basalts, G1 and G2 komatiites, and picrites (Echeverria, 1980; Aitken and Echeverría, 1984; Kerr et al., 1996b; Arndt et al., 1997; Révillon et al., 2000b). The Gorgona komatiites have been extensively studied as they are the only known post-Archean komatiites with spinifex texture. The picrites and komatiites of Gorgona are interpreted to have formed from a depleted plume component, potentially in the hottest, central part of the plume, which has undergone more extensive partial melting (estimated to be between 14-25 %) (Kerr et al., 1996c; Arndt et al., 1997; Révillon et al., 2000b). Despite having patterns in primitive mantle normalised trace elements similar to the Gorgona d-basalts and picrites, depleted basalts of the Hess Escarpment and Lower Nicaraguan Rise have been interpreted to have formed due to second stage melting of a residual mantle plume source, after the main phase of plateau magmatism (Kerr et al., 2009; Dürkefälden et al., 2019). It is possible that lithospheric thinning caused the upwelling and melting of this residual material which led to formation of LREE and isotopically depleted lavas (Dürkefälden et al., 2019).

On multielementary primitive mantle normalised diagrams, the samples of the Soná-Torio High-Mg Plateau show patterns similar to most of the other depleted CCOP groups (Figure 6.5). They most closely resemble G2 komatiites of Gorgona Island, but most samples of the High-MgO plateau show positive Nb anomalies, which are not seen in the Gorgona groups, but are observed in the Lower Nicaraguan Rise and Hess Escarpment samples. On tectonic discrimination diagrams, the High-Mg Plateau samples generally overlap with many of the arrays of depleted CCOP rocks (Figure 6.6). On the Th/Yb vs Nb/Yb diagram, the High-Mg Plateau samples plot within the MORB-OIB array, but with an incompatible element depletion below that of N-MORB. Some samples plot within the Gorgona, Lower Nicaraguan Rise and Hess Escarpment arrays, but many samples plot outwith these arrays. On the

TiO_2/Yb vs Nb/Yb plot, most samples plot within the MORB array, although some samples plot below. On this diagram, most High-Mg Plateau samples are most similar to Gorgona picrite and G2 komatiites. On the Nb/Y vs Zr/Y plot, the High-Mg samples plot within the LNR and Gorgona picrite and G2 Komatiite arrays, with most samples plotting outside of the OPB and N-MORB arrays, both above and below the plume source line. Although this indicates that some of the High-Mg Plateau samples may not have formed from a plume source, this plot was designed using a more homogenous plateau, and none of the other depleted CCOP arrays plot within the OBP array, most overlapping with N-MORB. Once again these samples are clearly distinct from the range of normal CCOP, with lower values of both Nb/Y and Zr/Y. On the Zr/Nb vs Nb/Th diagram, the High-Mg Plateau are dispersed across the plot, overlapping with all depleted CCOP groups, with higher Zr/Nb ratios than the normal CCOP plateau.

Using Nd_i isotopes, the Soná-Torio High-Mg Plateau shows very different results to the remainder of the depleted CCOP rocks (Figure 6.9). While these rocks have a Nd_i range of 0.51299 – 0.51312, the High-Mg Plateau has a Nd_i range of 0.51279 – 0.51289. This range is lower than the Soná-Torio Plateau range, and two of the samples also have lower values than the Soná-Torio Enriched Plateau. The Soná-Torio High-Mg Plateau group shows more of a range than other plateau groups, with all samples plotting within the Enriched CCOP array. In contrast to trace elements contents, Nd isotopes clearly show that the source of High-Mg Plateau rocks is different from that of the other depleted CCOP units, including Gorgona G2 komatiites. Overall, these results suggest that High-Mg Plateau rocks were produced from a (heterogenous) mantle plume source similar to that of the rest of the CCOP. However, Nd isotopes in High-Mg Plateau samples support a more enriched source than that commonly associated with depleted basalts, picrites and komatiites of the CCOP, suggesting that High-Mg Plateau rocks represent a new type of rock composition within the CCOP.

The timing of formation of the geochemical groups of the Soná-Torio Oceanic Plateau Complex remains poorly constrained due to the scarcity of $^{40}Ar/^{39}Ar$ and biostratigraphic ages. Although the previously outlined ages of 89 – 85 Ma (Kolarsky et al., 1995; Buchs et al., 2010) and 114.5 ± 2.0 to 71.3 ± 2.1 Ma from $^{40}Ar/^{39}Ar$ (Lissinna, 2005) exist for oceanic plateau sequences across Soná and Azuero, these are only for “normal” plateau basalts (Soná-Torio Plateau geochemical group of this study). There are no ages for the Soná-Torio and Azuero Enriched Plateau rocks, and High-Mg Plateau rocks. However, the Soná-Torio Enriched Plateau are found as lava flows and sills within the normal plateau sequences, indicating that at least some of the studied sequences formed contemporaneously from the

same mantle plume. There is no evidence supporting late stage, in situ emplacement, or accretion, of the enriched rocks.

A lack of interbedded sediments and a high degree of metamorphism and alteration means that there is no age for the High-Mg Plateau sequences. Detailed stratigraphic relationships were also not observed due to extensive faulting and scarce exposure where these rocks occur. However, High-Mg Plateau schistose hyaloclastites are intruded by undeformed plateau-like, proto-arc and arc dykes along the Torio and San Rafael rivers. Assuming that cross-cutting plateau-like dykes belong to the proto-arc magmatic phase, this indicates that the formation and main deformation phase of the High-Mg Plateau sequence predate the emplacement of the proto-arc in the Campanian ca. 72-73 Ma. Possibly, High-Mg Plateau sequences are part of a deeper crustal level of the oceanic plateau, which could have been deformed and partially exhumed due to subduction initiation tectonics. Early formation of these sequences during CCOP magmatism would be consistent with the occurrence of other high-Mg rocks in the CCOP, which have been associated with higher T mantle melting during incipient plume head magmatism (Kerr, 2005). In any case, our field observations indicate that the High-Mg Plateau sequences are unlikely to have formed through the same process as the Lower Nicaraguan Rise and Beata Ridge, which are younger sequences produced by the remelting of residual mantle, likely > 10 Myr after the main phase of formation of the CCOP ca. 90 Ma (Kerr et al., 2009; Dürkefälden et al., 2019). It is more likely that the Soná-Torio High-Mg Plateau hyaloclastites were produced during the main phase of plume-related submarine volcanism.

6.5.2 Darién Pacific Coast

In the Darién Pacific Coast region, most of the plateau is formed of pillow basalts and lava flows which form the Jaqué Plateau and Jaqué Depleted Plateau. Although these geochemical groups are commonly indistinguishable in the field, the Jaqué Enriched Plateau locally occurs with small volumes of interpillow, recrystalized carbonate sedimentary rocks, which indicates emplacement above the CCD (Carbon Compensation Depth) and suggests a lower effusion rates than in the bulk of the plateau sequences.

6.5.2.1 The Jaqué Plateau

The pillow lavas and lava flows of the Jaqué Plateau indicate a submarine origin. On primitive mantle normalised multielementary diagrams, most Jaqué Plateau

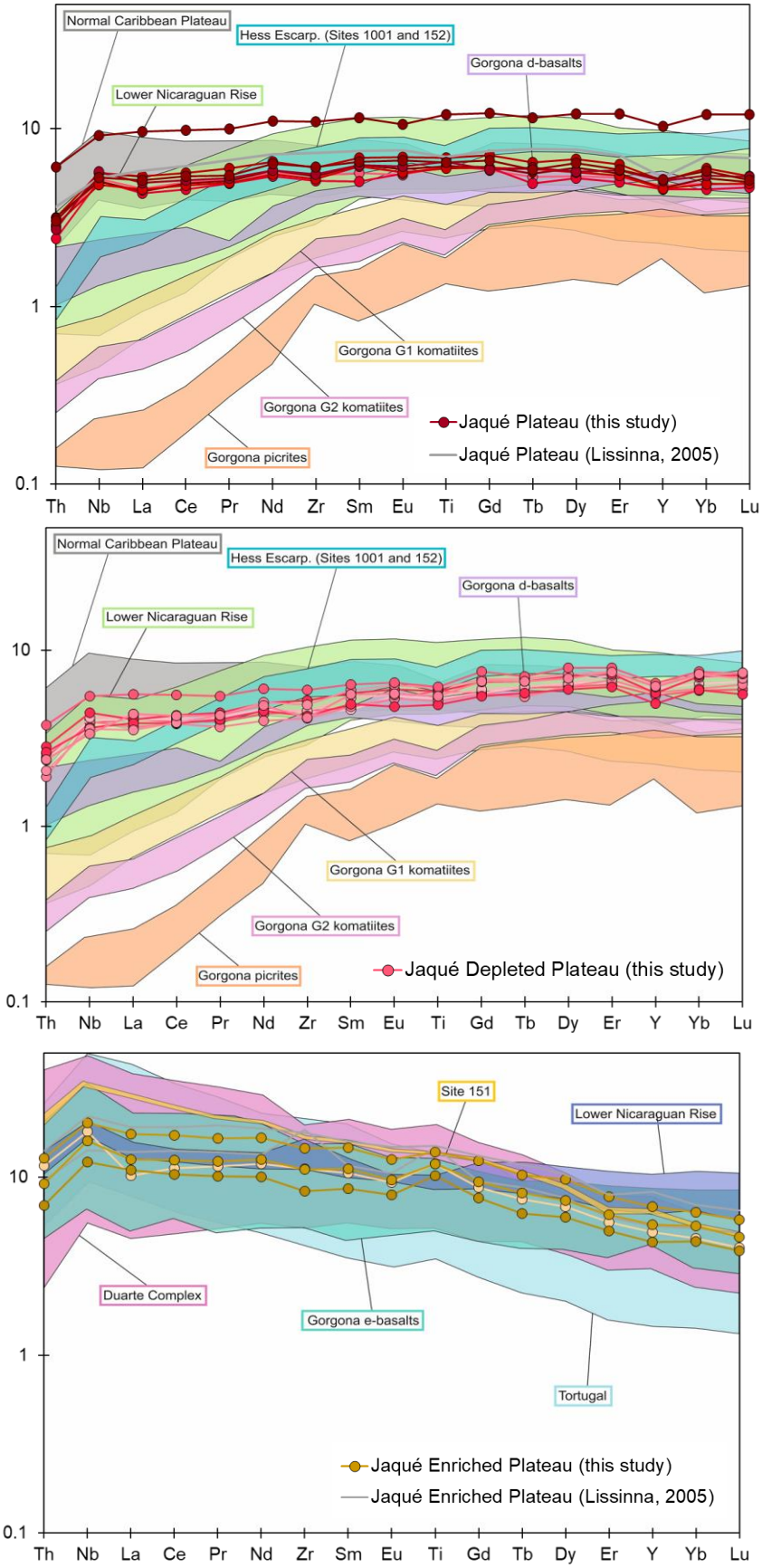

Figure 6.10: Primitive mantle-normalised multi-element diagrams for the Jaqué Plateau, Enriched Plateau and High-Mg Plateau. Data sources are as in Figure 6.5.

samples plot within the Normal CCOP array, showing typical oceanic plateau basalt signatures (Figure 6.10). However, the more enriched sample (sample DB16-043) plots above the typical oceanic plateau array, and is marginally more depleted in the LREEs than typical CCOP. On tectonic discrimination diagrams, the Jaqué Plateau samples plot within the normal CCOP arrays and the field defined by the Soná-Torio Plateau (Figure 6.8). The Nd_i values of the Jaqué Plateau samples range between 0.51292 - 0.51296 and are similar to the Soná-Torio Plateau samples and the normal CCOP array (Figure 6.9). These characteristics indicate that these samples have a mantle plume signature similar to that of the bulk of the CCOP and Soná-Torio Plateau.

6.5.2.2 Jaqué Depleted Plateau

The Jaqué Depleted Plateau is formed of pillow basalts and lava flows, and therefore also has a submarine origin. On the primitive mantle normalised diagram, samples of this group are compared with other depleted units from the CCOP (Figure 6.10). In this figure, the Jaqué depleted samples have distinct, less depleted LREE, Th and Nb than other depleted samples from the CCOP, with a positive Nb anomaly relative to Th. On tectonic discrimination diagrams, the Jaqué Depleted Plateau samples plot separately from the Jaqué Plateau samples, often outside of the normal CCOP array (Figure 6.8). On the Th/Yb vs Nb/Yb diagram, Jaqué Depleted Plateau samples plot within the MORB-OIB array, close to N-MORB. All samples plot within the depleted LNR array, and only one sample plots within the normal CCOP array. On the TiO_2/Yb vs Nb/Yb diagram, all samples plot close to N-MORB in the MORB array, on the margins of the normal CCOP and Gorgona picrite arrays; they plot separately from the Jaqué Plateau samples. On the Zr/Y vs Nb/Y diagram, the Jaqué Depleted Plateau samples plot within the depleted portion of the OPB array, with some samples plotting within the normal CCOP array; once again they plot separately from the Jaqué “normal” plateau samples. On the Zr/Nb vs Nb/Th diagram, the Depleted Plateau samples plot with the Jaqué Plateau samples, within the normal CCOP arrays. The Jaqué Depleted Plateau samples have more radiogenic Nd_i isotopic ratios than the Jaqué Plateau samples, with values overlapping with the normal CCOP, depleted CCOP and EPR MORB arrays (Figure 6.9).

The Jaqué Depleted Plateau is slightly more depleted in the LREE and has slightly higher Nd_i ratios than the typical “normal” oceanic plateau basalts of the Jaqué Plateau. The depleted LREE signature could be caused by more extensive partial melting in the Depleted Plateau in comparison to the Jaqué Plateau, but the distinctly higher Nd_i composition indicates that this is related to a difference in the plume source. Therefore, it is likely that

although the Jaqué Depleted Plateau has a plume source, this source is more depleted than the source of the Jaqué Plateau.

6.5.2.3 Jaqué Enriched Plateau

The Jaqué Enriched Plateau is exposed along the Darién Pacific Coast as lavas mingled with pelagic sediments, indicating a submarine origin. On multielementary primitive mantle normalised diagrams, the Jaqué Enriched Plateau samples show patterns similar to the Soná-Torio Enriched Plateau, with a depletion in the HREEs indicating the presence of garnet in the source (Figure 6.10). The Jaqué Enriched Plateau has trace element patterns similar to all other CCOP arrays, but with lower La/Yb than Tortugal, Site 151 and some of the Duarte Complex, and higher La/Yb than Gorgona e-basalts and enriched basalts from the Lower Nicaraguan Rise. On tectonic discrimination diagrams, the Jaqué Enriched Plateau samples overlap with the Soná-Torio Enriched Plateau, displaying overall very similar trace element characteristics (Figure 6.8). The Jaqué Enriched Plateau samples have similar Ndi ratios to the Soná-Torio Enriched Plateau, plotting within the upper margin of the Enriched CCOP array (Figure 6.9). This indicates that these units may also have formed from the same plume source.

Similarly to the Soná-Torio Oceanic Plateau Complex, the timing of formation of the geochemical groups of the Jaqué Oceanic Plateau Complex is difficult to constrain. The only existing ages (radiolarites ages: ~90-80 Ma (Bandy and Casey, 1973; Barat et al., 2014); $^{40}Ar/^{39}Ar$ ages: 84.1 ± 1.0 - 71.3 ± 2.2 Ma (Lissinna, 2005)) date the “normal” plateau volcanism of the Jaqué Plateau group. However, as the Jaqué Plateau and Jaqué Depleted Plateau are derived from the same basaltic sequences, these groups likely formed contemporaneously from a heterogeneous plume source ca. 90-85 Ma. Although the Jaqué Enriched Plateau samples have not been dated, the oceanic plateau origin indicates that they likely have a similar age to the other Jaqué Plateau groups. This group appear to form a distinct part of the oceanic plateau mingled with sediments, and it appears that they may have formed at a shallower depth above the CCD, with a lower effusion rate than the basalts of the Jaqué Plateau and Jaqué Depleted Plateau. This could potentially indicate a younger emplacement age for the Jaqué Enriched Plateau, but this remains unconstrained. There is no evidence that these basalts accreted to the plateau margin. Similarly to the Soná-Torio Enriched Plateau, these samples appear to be sourced from a more enriched component of the plume in comparison to the Jaqué Plateau and Jaqué Depleted Plateau. Therefore, the plateau sequences of the Jaqué Oceanic Plateau Complex also indicate the presence of a heterogeneous plume source.

6.5.3 Serranía de Baudó

In the Serranía de Baudó region, the oceanic plateau is formed by pillow basalts interbedded with lava flows, with locally a large abundance of sills that can form most of the sequences. Rarely, recrystalized siliceous pelagic sediments occur interbedded between the lavas and/or are locally intruded by sills with peperitic textures. Only rare hyaloclastites and basalt breccias were observed. Only one geochemical group occurs in the area – the Baudó Plateau.

The Baudó Plateau is composed of the aforementioned pillow basalts, lava flows and sills, with rare hyaloclastites, which clearly indicate a a submarine origin. On multielementary primitive mantle normalised diagrams, the Baudó Plateau samples have a typical plateau patterns and largely plot within the normal Caribbean Plateau array (Figure 6.11). However, the Baudó Plateau samples appear to have a larger variation in total trace element contents compared to normal Caribbean plateau and the Soná-Torio and Jaqué Plateau samples, which generally have a more uniform composition. Several Baudó Plateau samples plot below the normal Caribbean Plateau array. On tectonic discrimination diagrams, the Baudó Plateau samples generally plot within the normal CCOP array (Figure 6.8). On the Th/Yb vs Nb/Yb diagram, all samples plot within the normal CCOP array, although they are on the outer margin of the MORB-OIB array. Several samples also overlap with the depleted LNR array. On this plot, the Baudó plateau plots separately from the Soná-Torio and Jaqué Plateau samples. On the TiO_2/Yb vs Nb/Yb plot, the Baudó Plateau samples lie within the MORB array, and plot along the margins of the normal CCOP array, with some samples plotting in the depleted LNR, Gorgona d-basalt and Hess Escarpment arrays, without significant overlap with the Soná-Torio and Jaqué Plateau samples. On the Nb/Y vs Th/Y plot, the Baudó Plateau samples largely plot within the normal CCOP array, together with the Soná-Torio and Jaqué Plateau

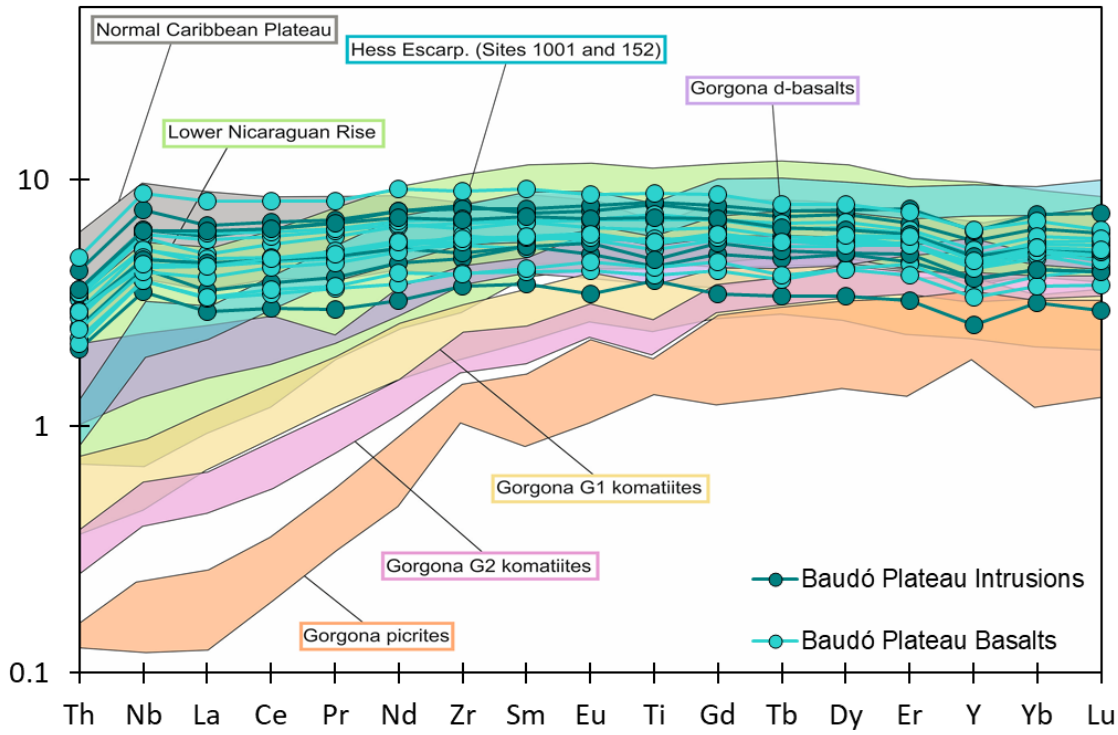

Figure 6.11: Primitive mantle-normalised multi-element diagrams for the Baudó Plateau. Data sources are as in Figure 6.5.

samples. On the Zr/Nb vs Nb/Th diagram the Baudó Plateau samples largely plot within the normal CCOP array, although just below the Soná-Torio and Jaqué Plateau samples. In this case, some samples plot in the overlap between the normal CCOP array and the enriched CCOP arrays. The Baudó Plateau samples have similar ranges of Nd_i to the Soná-Torio and Jaqué Plateau groups, plotting within the normal CCOP array (Figure 6.9).

This confirms an oceanic plateau, plume-sourced origin for the Baudó Plateau. Although the Nd isotope values indicate a common origin for all the Soná-Torio, Jaqué and Baudó Plateau groups, the Baudó Plateau has consistent, albeit slight differences in trace elements in tectonic discrimination diagrams, which may indicate that it is not simply a lateral extent of plateau rocks from Panama. Together with the larger abundance of sills found in the Baudó Plateau relative to Panamanian plateau rocks, this supports different formation histories within the studied oceanic sequences. This is a significant result from this study, because small, but systematic regional differences in the geochemistry of the studied sequences cannot be explained by inter-laboratory analytical bias (samples were processed in several batches in the same laboratory – see discussion in Appendix A.1.5.4), and the subtle geochemical variability documented here has not been reported in previous regional studies on the bulk of the CCOP.

6.5.4 Nature of the Plume Source

Each of the studied regions contains a unique plateau assemblage defined by specific lithological and geochemical characteristics, which highlights heterogeneity within plateau sequences across a c. 650 km transect. However, as documented above, all groups from the basement sequences have geochemical affinities consistent with derivation from a mantle plume source. Previous studies have noted that geochemical heterogeneities in the oceanic plateau, in particular in radiogenic isotope systems, require a heterogeneous plume source, and cannot be explained solely by different degrees of partial melting of a compositionally homogenous source (Kerr et al., 1996c; Arndt et al., 1997; Hauff et al., 2000b; Kerr et al., 2002a; Hastie et al., 2016).

Within the plateau sequences from this study, there appear to be four geochemical groups overall. The first of these are the typical plateau basalts, represented by the Soná-Torio Plateau, Jaqué Plateau and Baudó Plateau. While the Soná-Torio Plateau might be the lateral equivalent of the Jaqué Plateau, the Baudó Plateau appears to have slight geochemical differences, which plot as a separate group on some tectonic discrimination diagrams. However, the main geochemical characteristics of the Baudó Plateau samples are still consistent with derivation from the dominant source (or assemblage of sources) that formed most of the CCOP. The second group, the enriched member of the plateau, is represented by the Soná-Torio Enriched Plateau and the Jaqué Enriched Plateau, which have LREE enriched and HREE depleted patterns, respectively, and Nd_i isotopes lower than those of the normal CCOP. The third group is the depleted group. This group is represented by the Jaqué Depleted Plateau, which has depleted LREEs when compared to the normal plateau groups, along with higher Nd_i values. The Soná-Torio High-Mg Plateau forms the fourth group, with Nd_i values similar to those of the enriched plateau group, paired with highly depleted LREEs, similar to those of Gorgona komatiites.

The geochemical variation within these heterogeneous plateau sequences is consistent with formation from a heterogeneous mantle plume containing at least 2 end member components. This interpretation is consistent with previous studies of the CCOP (Kerr et al., 1996c; Arndt et al., 1997; Hauff et al., 2000b; Kerr et al., 2002a; Hastie et al., 2016). Previous models have envisioned a plume composed largely of a depleted component, with blobs, streaks or veins of variably enriched material (Kerr et al., 1995; Arndt et al., 1997). Deeper and more limited melting will preferentially sample more of the enriched component of the plume. Shallower and more extensive melting will melt more of the depleted component, which will dilute the melts of the enriched component and could produce the typical oceanic plateau basalts (Kerr et al., 2002a).

The enriched component may be sourced from enriched recycled oceanic crust, which could be pooled at the core mantle boundary, or dispersed in the lower mantle, before being entrained into the plume (Hofmann and White, 1982; Phipps Morgan and Morgan, 1999; Fitton, 2007; Hastie et al., 2016). This is supported by the presence of positive Nb anomalies in the plateau lavas, which could be sourced from rutile-bearing oceanic crust (Hastie et al., 2016). The depleted component of the plume may be derived from a more depleted recycled oceanic lithosphere (Kerr et al., 1995; Kerr et al., 2002a).

In this model, the Soná-Torio and Jaqué Enriched Plateau samples could be produced by deeper melting of a more enriched component. This is supported by HREE depletion in these groups, indicating deeper melting in a garnet-bearing lithology, with trace element and Nd isotope composition indicating an enriched source. The shallower more extensive melting, which melts both the enriched and depleted components could produce the Soná-Torio, Jaqué and Baudó Plateau groups. As the Jaqué Depleted Plateau are quite subtly different from the Jaqué Plateau, it is possible that these samples formed in an area (or time) where (or when) more of the enriched component had been extracted, leaving a more depleted source to produce more depleted lavas. The highly depleted components described elsewhere in the CCOP (e.g., komatiites and picrites of Gorgona) are thought to be sourced from the hottest, most depleted part of the plume (Arndt et al., 1997). Although this type of depleted material is not observed here, they could represent the depleted end member which played a higher contribution to the formation of the Jaqué Depleted Plateau.

The formation of rocks such as the Soná-Torio High-Mg Plateau have not yet been described in the CCOP. These samples appear to be sourced from an enriched plume based on Nd isotopes, but they are highly depleted in the LREE. These samples could have formed through extensive partial melting of the enriched plume component shortly prior to the extraction of these lavas. It would have been useful in this case to gain Pb isotope analyses to further understand the plume source of this group. However, these rocks have undergone greenschist facies metamorphism and original mineralogy is not preserved. Pb isotopes may be problematic, as the Pb isotope system is commonly sensitive to alteration in the CCOP (Hoernle, 1998; Hauff et al., 2000b).

Previous studies of the CCOP and Ontong Java Plateau been able to further constrain the temporal or lateral controls on geochemical heterogeneity in plateau sequences (e.g., Kerr et al., 2002a; Fitton and Godard, 2004; Kerr et al., 2009; Dürkefälden et al., 2019). However, these studies largely involve ocean floor drilling and/or high precision dating of plateau sequences. In a field-based study with no continuous exposure of undisturbed plateau sequences and a lack of reliable $^{40}Ar/^{39}Ar$ ages, the control on geochemical heterogeneity is

more difficult to assess. Based on the model of formation for the CCOP from outlined above, the geochemical variability is controlled somewhat temporally. In Curacao, picrites are exposed at the base of the plateau, indicating that these units often form in the earliest stages of plateau formation (Campbell and Griffiths, 1992; Kerr et al., 1995; Kerr et al., 1996a; Kerr et al., 1997b). This is consistent with the model of formation which requires them to form in the hottest part of the plume, prior to the extensive shallow melting which homogenises the depleted and enriched components (Arndt et al., 1997; Herzberg and O'Hara, 2002). Therefore, the Soná-Torio High Mg Plateau may represent an early stage of formation of the plateau. Although is sourced from a more enriched component of the plume than the Gorgona picrites and komatiites, it is possible that they both formed during the same stage of plume magmatism, sampling different components of the plume.

The enriched basalts of the CCOP are thought to form from limited early melting in the garnet stability zone. It has previously been estimated that the enriched basalts could be generated by a degree of melting as low as 3 % (Kerr et al., 2002a). The early formation of these enriched basalts is consistent with the idea that magma chambers may not have developed at this stage of plateau formation, allowing these enriched basalts to reach the surface while preserving their distinctive geochemistry (Kerr et al., 1997b). A spatial control has been suggested for the enriched basalts, as they largely form around the margins of the CCOP (e.g., in Central America and Hispaniola) (Kerr et al., 1997b). It is possible that the enriched components of the plume may have been swept out the margins of the plume head (Arndt et al., 1997; Révillon et al., 2000b) or that the small degrees of partial melting which preferentially sample the enriched component may be more likely to occur in the cooler peripheral regions of the plume head (Kerr et al., 1997b). The Soná-Torio and Jaqué Enriched Plateau groups may therefore represent this small degree partial melting along the cooler margins of the plume head

The Soná-Torio, Jaqué and Baudó Plateau and the Jaqué Depleted Plateau are formed during more extensive shallow melting (estimated to be between 10 – 20 % (Kerr et al., 2002a) which dilutes the enriched component of the plume (Kerr et al., 2002a). The timing of this magmatism is not clear. Although this could be considered to be a late stage of plateau formation,the 114.5 Ma age of the plateau from Azuero (Lissinna, 2005) indicates that the plume head was producing typical oceanic plateau basalts in an early stage of plateau formation. As the Jaqué Depleted Plateau is more depleted in the LREEs and has higher Nd_i isotope values than the typical plateau groups, it appears that it has sampled a mantle which has less contribution from the enriched plume component than the typical plateau basalts. This could be because the enriched component of the plume has been extracted from where or when the depleted plateau lavas are sourced. In Jaqué, the Depleted Plateau and Plateau

are indistinguishable in the field, and the Depleted Plateau was not recognised to overlie sequences of the Jaqué Plateau. It does not seem to be controlled spatially as samples of the Jaqué Plateau and Depleted Plateau are were sampled in situ ca. 150m apart. The simplest model in this case is to assume that the plateau is heterogeneous on a small scale, and that the Depleted Plateau may have formed in locations where relatively more of the enriched component was extracted previously to form Enriched Plateau basalts. This is in agreement with previous studies of the CCOP which have indicated the presence of a heterogeneous mantle on a < 10km scale, where enriched and depleted groups on Gorgona are exposed within 1 km of the other (Kerr, 2005). To properly address this question and to fully understand the temporal and spatial evolution of the oceanic plateau in Panama, sequences of the plateau need to be dated using a high precision technique such as U-Pb baddeleyite.

6.5.5 Origin of Serranía de Baudó plateau assemblages

The Serranía de Baudó is thought to be part of the Panama Microplate (or the Panama-Choco block), bound to the South American continent along the Uramita Suture (Figure 2.7). West of the suture, the Western Cordillera is formed of fault bounded slices of volcanic and sedimentary rocks predominantly composed of fragments of the CCOP, an Upper Cretaceous volcanic arc, and Upper Cretaceous hemipelagic sedimentary sequences that accreted to the continental margin in the Late Cretaceous (Kerr et al., 1997a; Villagómez et al., 2011; Villagómez and Spikings, 2013). From this general tectonic setting and the occurrence of the Jaqué Plateau west of the Uramita Suture along the Panama Microplate, the Baudó Plateau could represent an extension of the Jaqué Plateau. No major structure exists between these plateau sequences and, at the narrowest point, these two units are only 65 km apart. It is therefore surprising that each region has distinct geochemical and lithological characteristics.

The Soná-Torio region represents a forearc environment, where submarine plateau sequences form the basement to the Panama Arc intrusions and lavas. The plateau sequences from the Darién Pacific Coast also form the basement to proto-arc and arc assemblages. Although the arc assemblages are associated with the younger pre-Eocene arc, the Jaqué Proto-arc dykes are likely part of the older stage of arc magmatism associated with subduction initiation. However, the Baudó Plateau does not appear to be associated with any arc-like assemblages. The Baudó Plateau basalts are interbedded with tuffaceous and siliciclastic sediments which may be arc-related, but the geochemistry of these is unknown. In the Darién Pacific Coast region, the plateau is dominated by pillow

basalts and lava flows, with very rare plateau-related intrusions. However, in the Serranía de Baudó, the pillow and lava flow sequences are accompanied by a significant proportion of plateau-related sills, which form c. 20 % of the total mapped coastal section (Figure 3.24). This indicates that a deeper level of the plateau is exposed in the Serranía de Baudó, and that this section of the plateau may have been uplifted relative to the Darién Pacific Coast section. Using the hypothetical cross section of the CCOP by Kerr et al. (1997b), based on studies of Bolivar and other accreted fragments, the Serranía de Baudó exposures would be within the top 8 km of the oceanic plateau. However, this does not explain the lack of arc assemblages overlying the Baudó Plateau, as arc-related intrusions would still be observed at deeper plateau levels if they are present.

The origin of the Serranía de Baudó has previously been attributed to a different plume source than the remainder of the CCOP, based on palaeomagnetic data and geochemical differences (Kerr and Tarney, 2005). However, based on the geochemical characteristics outlined above, there appears to be no geochemical argument for the Baudó Plateau to be sourced from a separate plume source. Although the Baudó Plateau samples were previously noted to have higher Nd isotope values than other CCOP assemblages (Kerr and Tarney, 2005), here they are have values similar to those of the Jaqué Plateau and Soná-Torio Plateau. The existing ages for the plateau in the Serranía de Baudó are younger than the majority of those for the remainder of the Caribbean, which potentially justified formation from a different plume head. However these ages have likely been affected by alteration and/or degassing, and are likely to be younger that the true plateau age (Section 6.2) (Acero, 2019). Therefore, it seems consistent that the Baudó Plateau may have formed along the south western edge of the Caribbean Plateau, part of the same assemblage as the Soná-Torio and Jaqué Plateaus. Although there is some minor geochemical heterogeneity, the plume source has been shown to be heterogeneous and these minor differences cannot justify a different plume source. The lack of arc assemblages also does not justify a different source for the Serranía de Baudó lavas. The Jaqué Plateau is intruded by dykes of the Jaqué Proto-arc and by dykes and sills of the Sapo Arc, which is thought to have formed in the Oligocene – Miocene based on existing field constraints and a single $^{40}Ar/^{39}Ar$ age (21.7 ± 0.3 Ma (Lissinna, 2005)). Some tectonic reconstructions indicate that it is possible that the Panama Microblock was already accreting to the South American margin at this time (Montes et al., 2012a; Barat et al., 2014; Buchs et al., 2019b). It is possible that subduction dynamics at this time of accretion may not have allowed arc magmatism to occur along the Serranía de Baudó. It is also possible that the Baudó Plateau simply may have been closer to the trench than the Soná-Torio Plateau or Jaqué Plateau, meaning that it was not intruded by proto-arc or arc dykes. In Soná-Torio, the outer forearc has clearly been lost through

subduction erosion as a seamount is accreted to the Cretaceous volcanic front in this region (Buchs et al., 2011a). Alternatively, the Baudó Plateau reflects a later accreted fragment of the CCOP, but this is difficult to constrain at this stage.

When considering the origin of the plateau sequences of the Serranía de Baudó, the origin of the Baudó Melange also needs to be considered. This melange has not previously been recognised, and is formed of fault bounded and deformed basalts and sediments. As this melange has not been documented there is little to no existing data for this assemblage, and its origin is unclear. It is possible that this melange could also be sourced from the CCOP, and could represent a younger, accreted fragment that has been dismembered and moved along the margin of the Baudó coast. However, it is also possible that this melange represents an different allochthonous sequence, possibly representing an ocean island assemblage associated with the Galapagos plume head, or possibly another plume head, as was previously suggested for Gorgona and the Serranía de Baudó (Kerr and Tarney, 2005). Unfortunately it is impossible to assess the origin of the melange without further detailed work, including mapping of structures, geochemical analyses of basalt and analyses of the detrital component in melange sediments.

6.5.6 The oceanic plateau in central Panama

Samples of an oceanic plateau are also exposed in Central Panama, as the basement to the Chagres-Bayano Arc (Wegner et al., 2011; Montes et al., 2012; Wang, unpublished). The plateau basalts of the Chagres Bayano region will here be compared to those of the Soná-Torio, Darién Pacific Coast and Serranía de Baudó regions to assess the source region and identify any geochemical heterogeneities.

On multielementary primitive mantle normalised diagrams, 2 samples of the Chagres Bayano Plateau show flat patterns similar to the typical plateau basalts of the Jaqué Plateau (samples DB16-018, DB16-020 (Wang, unpublished)) (Figure 6.12). The remainder of the samples are more depleted in the REE, with patterns similar to those of the Jaqué Depleted Plateau (Wegner et al., 2011; Montes et al., 2012a). On tectonic discrimination diagrams, the Chagres Bayano Plateau samples overlap with samples of the Plateau and Depleted Plateau groups (Figure 6.13). On the Th/Yb vs Nb/Yb diagram, the Chagres Bayano Plateau samples plot within the MORB-OIB array, above N-MORB. Some samples plot with the Soná-Torio, Jaqué

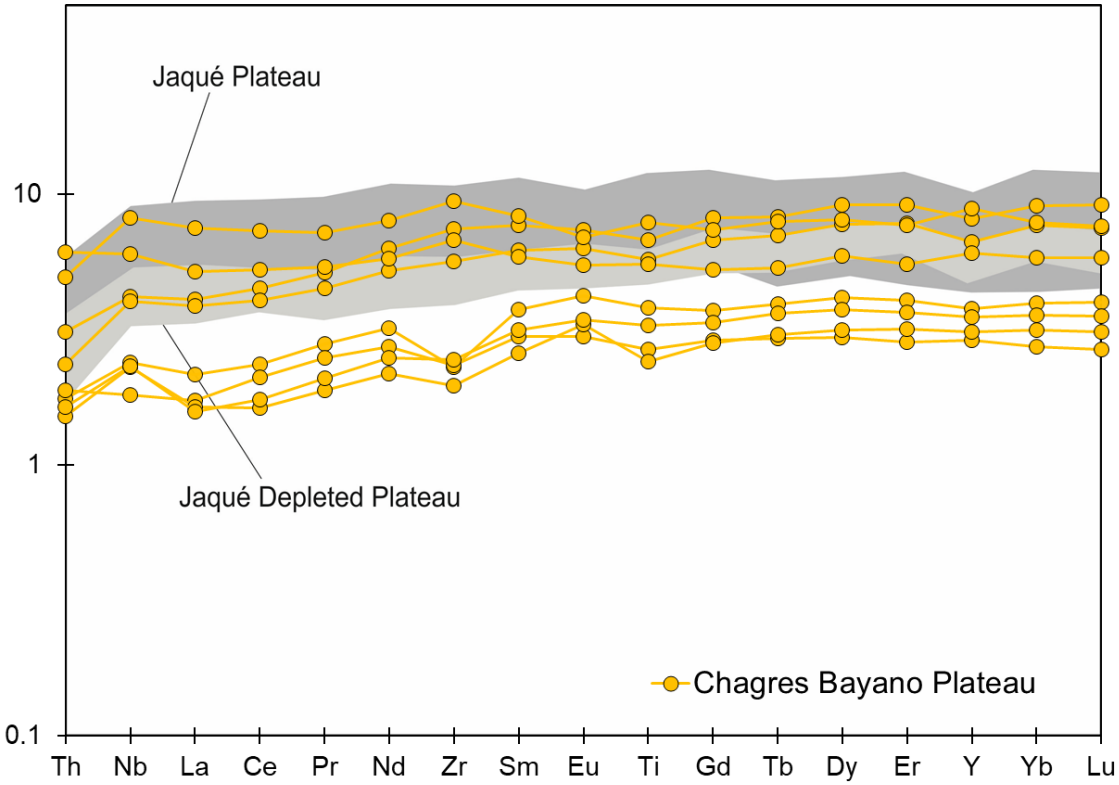

Figure 6.12: Primitve mantle normalised mutielementary diagram showing arrays of the Jaqué Plateau and Jaqué Depleted Plateau with samples of the Chagres Bayano Plateau. Geochemistry of Chagres Bayano Plateayu samples from Wegner et al. (2011), Montes et al. (2012) and Wang (unpublished).

and Baudó Plateau groups, but many samples plot with the Jaqué Depleted Plateau (Figure 6.13). On the TiO_2/Yb vs Nb/Yb plot, the Chagres Bayano samples plot within the MORB array close to N-MORB. The majority of samples again plot with the Jaqué Depleted Plateau while rare samples plot with the typical Plateau groups. On the Nb/Y vs Zr/Y plot, the Chagres Bayano samples plot within the Oceanic Plateau Basalt array, clearly distinct from the N-MORB array. In this diagram, most samples again plot with the Jaqué Depleted Plateau and 2 samples plot with the Plateau groups. On the Zr/Nb vs Nb/Th diagram, the Chagres Bayano largely plot within the Oceanic Plateau Basalt array, although one sample

overlaps with the N-MORB array and one sample plots outside both of these arrays. On this diagram the Chagres Bayano Plateau samples are more dispersed, but they plot with other samples of the Soná-Torio, Jaqué and Baudó Plateaus and Jaqué Depleted Plateau. Only one sample of the Chagres Bayano Plateau (sample DB16-020) has been analysed for Nd isotopes. This sample is has flat primitive mantle normalised patterns and plots with the typical plateau basalts on the tectonic discrimination diagrams. It has a Nd_i of 0.51291, within the range of the typical plateau basalts of this study and within the normal CCOP array (Figure 6.9).

It appears that the geochemical heterogeneity observed elsewhere in Panama is also observed in Central Panama. The plateau samples from the Chagres Bayano region display both typical oceanic plateau trace element contents and a more depleted group, similar to the samples observed in the Darién Pacific Coast region. Based on the single sample with Nd_i analysis, these plateau basalts are consistent with being derived from the same plume source as the plateau sequences of the Soná-Torio, Darién and Baudó regions

This plateau has not yet been dated using $^{40}Ar/^{39}Ar$ or U-Pb zircon or baddeleyite techniques. However, radiolarians found in chert pebbles from a Miocene fluvial conglomerate in central Panama have given a biostratigraphic age of Early Cretaceous (late Hauterivian – Barremian, ca. 130 - 125 Ma) (Kukok et al., 2017). This is the oldest reported age in Panama, significantly older than the bulk of the ages for the oceanic plateau across Soná-Azuero and the Darién, although one oceanic plateau basalt from Azuero has been previously been dated as 114.5 ± 2.0 Ma based on a $^{40}Ar/^{39}Ar$ mean apparent age (Lissinna, 2005). Although the radiolarians have not been sampled in situ, radiolarites are commonly observed to be interbedded with plateau sequences across the Soná-Torio region and the Darién region, as documented in Chapter 3. The presence of these radiolarites in central Panama, in the Chagres Bayano region, indicates that the oceanic plateau basement began forming in the Early Cretaceous in this region, approximately 40 Myr before the formation of the bulk of the oceanic plateau basalts exposed in Panama and around the CCOP (93 – 89 Ma (Kerr et al., 2003)).

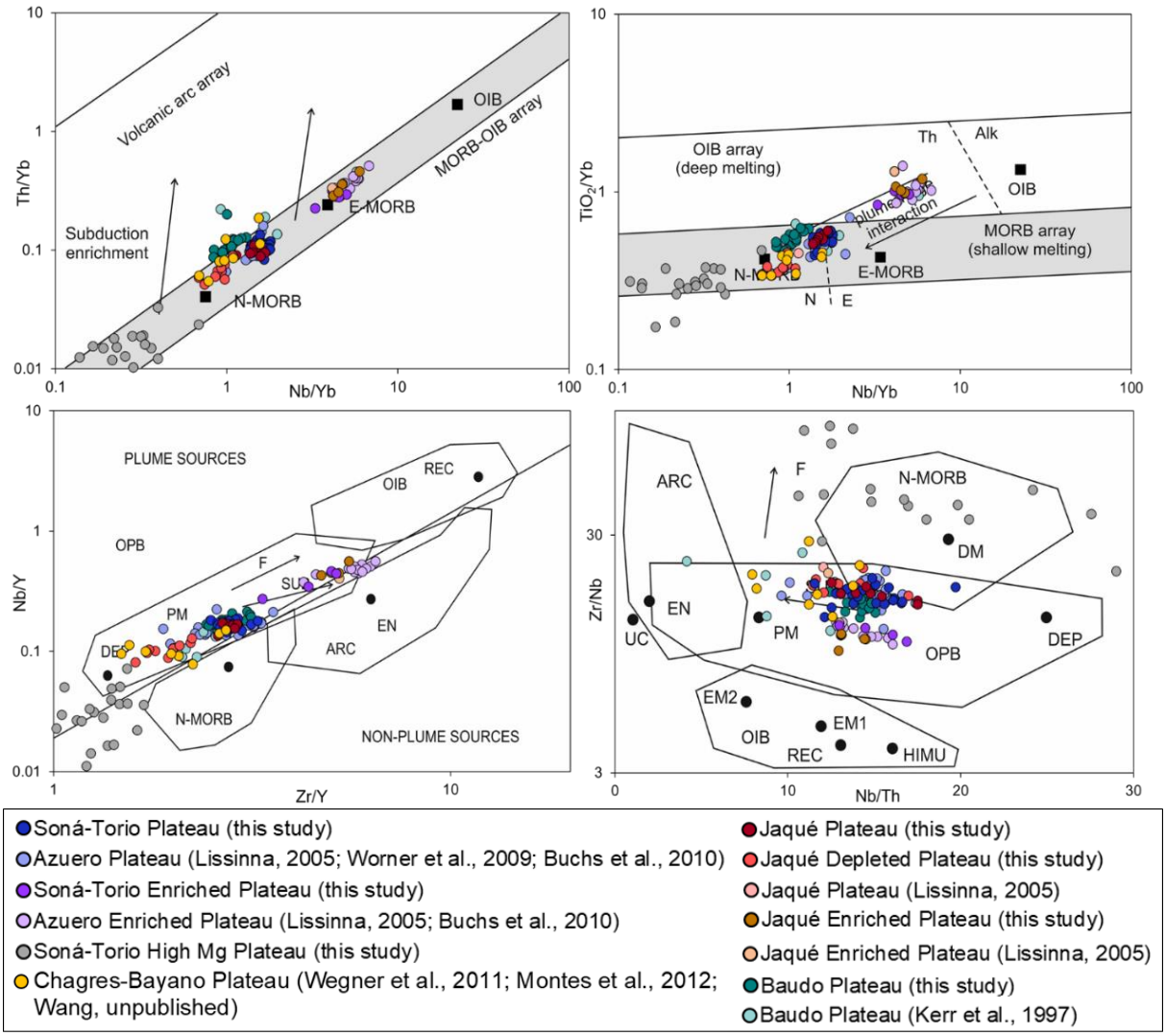

Figure 6.13*:* Tectonic discrimination diagrams for the Soná-Torio Jaqué, Baudó and Chagres Bayano Plateau samples. A) Nb/Yb vs Th/Yb crustal input proxy diagram (Pearce 2008), B) Nb/Yb vs TiO_2/Yb deep melting proxy diagram (Pearce 2008), C) Zr/Y vs Nb/Y diagram (Condie 2005), D) Nb/Th vs Zr/Nb diagram (Condie, 2005), Abbreviations: UC = upper continental crust, PM = Primitive Mantle, DM = shallow depleted mantle, HIMU = high mu (U/Pb) source, EM1 and EM2 = enriched mantle sources, ARC = arc related basalts, N-MORB = normal mid-ocean ridge basalt, OPB = oceanic plateau basalt, OIB = oceanic island basalt, DEP = deep depleted mantle, EN = enriched component, F = effects of batch melting and SUB = subduction effect.

The deposition of the Miocene fluvial conglomerate containing radiolarite pebbles indicates that the radiolarites and associated plateau sequences were subaerially exposed at this time. The plateau basalts which are currently exposed across the Chagres Bayano region are not necessarily associated with these radiolarites and the early phase of plateau volcanism, and could represent a younger phase. Although these heterogeneous plateau sequences are not necessarily associated with the Early Cretaceous radiolarians, the geochemistry of the Chagres Bayano Plateau samples indicates that the plateau may also been heterogeneous in the earliest stage of formation.

The bulk of the Caribbean Plateau ages lie between 93 – 89 Ma (Kerr, 2003). However, $^{40}Ar/^{39}Ar$ isochron and step heat ages of ca. 111–139 Ma have been measured on plateau basalts from the Nicoya Peninsula (Hoernle et al., 2004). The Nicoya Complex, located along the western margin of the Nicoya Peninsula, represents a composite plateau which formed in 3 stages (139-132, 118-110, 92-77 Ma) (Alvarado et al., 1997; Sinton et al., 1997; Hauff et al., 2000a; Hoernle et al., 2004; Denyer et al., 2006). Although the younger sequences are thought to be part of the main stage of CCOP formation, associated with the Galapagos plume (Sinton et al., 1997; Sinton et al., 1998; Kerr et al., 2002a; Kerr, 2003; Loewen et al., 2013), older stages of formation have been attributed to distinct Pacific hotspots (Hoernle et al., 2004; Baumgartner et al., 2008; Boschman et al., 2014; Madrigal et al., 2016; Andjić et al., 2018).Therefore, the plateau associated with the Early Cretaceous radiolarites could also have formed from these distinct Pacific hotspots. However, the plateau basalts currently exposed in the Charges Bayano region display similar geochemical characteristics to other plateau assemblages in Panama. The 114.5 ± 2.0 Ma plateau basalt of Azuero is also geochemically indistinguishable from the remainder of the typical plateau basalts across Panama, and appears to be part of the same plateau assemblages as samples which are thought to have formed during the main stage of CLIP formation. It is again difficult to fully assess this question without further context of the radiolarite ages and further high precision ages for plateau sequences across Panama.

6.5.7 Summary

In this study, oceanic plateau assemblages were studied across the Soná-Torio, Darién Pacific Coast and Serranía de Baudó regions, with the aim to characterise the plateau sequences and to recognise their sources and origins. Through better understanding of the formation of these sequences along the southwestern margin of the Caribbean Plateau, we can improve understanding of the tectonic configuration of the western Caribbean in the Late Cretaceous, which can help to constrain the evolution of the Panama Arc. Across the three regions, seven geochemical groups were recognised within the heterogeneous oceanic plateau sequences: The Soná-Torio Plateau, Enriched Plateau, and High-Mg Plateau; The Jaqué Plateau, Depleted Plateau and Enriched Plateau; and the Baudó Plateau.

Although the transect through the three regions is only ca. 650 km long, each region shows distinct plateau assemblages. In the Soná-Torio region, the Soná-Torio Plateau represents the typical, normal CCOP plateau member which dominates the plateau assemblages around the Caribbean and into South America. These basalts have flat primitive mantle normalised trace element patterns with positive Nb anomalies, and Nd_i values are within the

range of normal CCOP. The Soná-Torio Enriched Plateau represents an enriched member of the plateau, most similar to the Gorgona e-basalts. These samples have LREE enriched and HREE depleted patterns on primitive mantle normalised multielementary diagrams which indicate melting in the garnet stability zone, and their Nd_i values are consistent with other enriched samples of the CCOP. The Soná-Torio High Mg Plateau samples do not have an equivalent geochemical group which has previously been recognised in the Caribbean. They have highly LREE depleted primitive mantle normalised trace element contents and high MgO wt. % concentrations like Gorgona komatiites. They also have enriched Nd_i values, similar to those of the enriched CCOP samples, in contrast to the high Nd_i values of the Gorgona komatiites which indicates a more depleted source. In the Darién Pacific Coast region, the Jaqué Plateau is directly comparable to Soná-Torio Plateau, and the Jaqué Enriched Plateau is directly comparable to the Soná-Torio Enriched Plateau. However, the Jaqué Depleted Plateau does not have a lateral equivalent in the Soná-Torio or Baudó regions.It is not as depleted as other depleted basalts of the CCOP (e.g., the d-basalts of Gorgona) but it has LREE depleted patterns on primitive mantle normalised multielementary diagrams, and has higher Nd_i values than the typical CCOP basalts. The oceanic plateau in the Serranía de Baudó, exposed only 65 km from the Darién region, appears to only include a single geochemical group. The Baudó Plateau is typical oceanic plateau basalt, again with flat primitive mantle normalised trace element patterns and Nd_i contents consistent with the other normal CCOP samples. However, this group is not geochemically identical to the Soná-Torio and Jaqué Plateau samples and generally has a greater range of trace element contents. In the Chagres-Bayano region in central Panama, samples of the Plateau and Depleted Plateau have been observed, suggesting that the heterogeneous plateau basement occurs across Panama.

The formation of these plateau assemblages requires a heterogeneous plume source, which may consist of a dominant depleted component with blobs, streaks or veins of an enriched component. This type of plume model has been used to explain the formation of plateau assemblages across the CCOP. In this model, the High-Mg Plateau samples of the Soná-Torio region are formed by melting in the hottest part of the plume, with a high degree of partial melting of an enriched component. These basalts may be more likely to form lower within the oceanic plateau, and are only exposed in Soná-Torio due to uplift and faulting related to subduction dynamics. The Enriched Plateau groups are formed by low degrees of melting which preferentially samples the more enriched component of the plume, which may be swept out towards the margins. Extensive, shallower melting within the plume would then homogenise the depleted and enriched components of the plume and form the Plateau groups. Where the enriched component has been extracted, the Depleted Plateau of Jaqué

and Chagres Bayano will form, as these groups have a smaller contribution of an enriched component in comparison to the Plateau groups. It is difficult to further assess the petrogenesis of the plateau lavas across Panama and Baudó without further isotopes, primary magma compositions and high precision dates. It is also difficult to assess the temporal or spatial control on heterogeneity within the plateau without further stratigraphic constraints or high precision ages. Based on the indistinguishable and close nature of outcrops of the Jaqué Plateau and Depleted Plateau, it is likely that the plume source needs to be heterogeneous on a small scale.

Although it has previously been suggested that the Serranía de Baudó Plateau is from a different oceanic plateau (Kerr and Tarney, 2005) that does not appear to be justified here, based on field and geochemical constraints. The Baudó Plateau is geochemically consistent with other lavas of the CCOP, and appears to be from the same plume source as the other plateau assemblages. Although the existing ages of the Baudó Plateau are younger than the main pulse of plateau formation, it is likely that these ages have been affected by alteration and degassing (Section 6.2) (Acero, 2019). Investigation of the Baudó Melange could give important constraints on the origins of the Baudó Plateau, but this requires further detailed work.

Most of the reliable $^{40}Ar/^{39}Ar$ and biostratigraphic plateau ages from across Panama range between ca. 90-80 Ma (Bandy and Casey, 1973; Kolarsky et al., 1995; Lissinna, 2005; Buchs et al., 2010; Barat et al., 2014). However, there is also a single age of 114.5 ± 2.0 Ma for a normal plateau basalt from Azuero Peninsula and Early Cretaceous ages for assemblages is also found in central Panama This indicates that plateau formation was two-stage, although the early plateau basalts appear to be indistinguishable from the plateau basalts produced in the main phase of plateau volcanism.

6.6 Model of oceanic plateau formation and subduction initiation

This section presents a model of oceanic plateau formation and subduction initiation along the south western margin of the Caribbean Plate, based on the new results and arguments presented above.

In this model, the Caribbean Oceanic Plateau forms in the Pacific during the Cretaceous, likely above the Galapagos plume head (Figure 6.14, 6.15A). The ages for the entire plateau range from 139-69 Ma based on $^{40}Ar/^{39}Ar$ ages, while the main stage of volcanism appears to occur in the Late Cretaceous between 94-89 Ma (Walker et al., 1991; Kerr et al., 1997a; Sinton et al., 1998; Lapierre et al., 1999; Walker et al., 1999; Hauff et al., 2000a; Sinton et al., 2000; Kerr et al., 2003; Hoernle et al., 2004). Along the southwestern margin of the plateau, there appears to be an early phase of plateau formation, shown by Early Cretaceous ages of the plateau in Nicoya ($^{40}Ar/^{39}Ar$ ages: 139 – 111 Ma, Hoernle et al., 2004) , Azuero ($^{40}Ar/^{39}Ar$ age: 114.5 ± 2.0 Ma, Lissinna, 2005) and Chagres-Bayano (radiolarite age ca. 130-125 Ma, Kukok et al., 2017). However, the majority of ages for plateau units from this study (from Soná-Torio, Darién Pacific Coast and Serranía de Baudó) indicate a main stage of formation in the Late Cretaceous. The Soná-Torio Oceanic Plateau formed between 89-85 Ma based on radiolarites interbedded in plateau sequences (Kolarsky et al., 1995; Buchs et al., 2010), in agreement with the minimum age of plateau formation from this study (87.0 ± 2.4 Ma) and also with previous $^{40}Ar/^{39}Ar$ step heating ages (i.e.., 93.5 ± 5.3 to 82.6 ± 3.2 Ma (Lissinna, 2005). Ages for the plateau in the Darién range from ca. 90-70 Ma, based on 90-80 Ma ages of radiolarite interbedded with plateau lavas (Bandy and Casey, 1973; Barat et al., 2014) and existing $^{40}Ar/^{39}Ar$ ages of 84.1 ± 1.0 to 71.3 ± 2.2 (Lissinna, 2005). The Baudó plateau is dated only by existing $^{40}Ar/^{39}Ar$ ages of 77.9 ± 1.0 Ma and 72.5 ± 0.4 Ma (Kerr et al., 1997a). However, it is likely that these ages are offset due to alteration, as shown by Acero (2019) and discussed in Section 6.2. Biostratigraphic data from siliceous sediments that are stratigraphically interbedded with plateau lavas in Central America consistently support pre-Campanian ages of plateau formation (Bandy and Casey, 1973; Kolarsky et al., 1995; Buchs et al., 2010; Barat et al., 2014).

New and existing geochemical constraints indicate that the SW Caribbean Plateau is heterogenous, and formed from a heterogeneous plume with more enriched and depleted components (Figure 6.15A). Deeper, lower degrees of partial melting preferentially samples enriched components of the plume in the field stability of garnet, forming lavas such as the Soná-Torio Enriched Plateau and the Jaqué Enriched Plateau. More extensive partial melting of this more enriched component during rise to shallower depth (out of the field stability of garnet) forms rocks such as the Soná-Torio High-Mg Plateau. The Soná-Torio,

Jaqué and Baudó Plateau geochemical groups are produced due to more extensive, shallower melting of depleted and enriched components, which dilutes the enriched component to form typical plateau lavas, as previously described by Kerr et al. (2002). Where the enriched component is further diluted, due to more melting of the depleted component or due to the absence of the enriched component, lavas such as those of the Jaqué Depleted Plateau form.

During the Early to Late Cretaceous, subduction zones formed around the Caribbean Plateau which caused it to drift across the Caribbean and between the American plates (Pindell et al., 2011; Wright and Wyld, 2011) (Figure 6.14). Arc volcanism occurred along the eastern and southern margins of plateau, due to west- to north-dipping subduction beneath the plateau. This is notably evidenced by plateau sequences interbedded with arc-related tuffs in Altamira, now preserved in Upper Cretaceous accreted oceanic sequences in the Western Cordillera of Colombia (Buchs et al., 2018). Additional evidence for coeval plume and supra-subduction magmatism in the southern Caribbean during the Late Cretaceous is provided by plateau and arc sequences preserved in Aruba, in the Lesser Antilles (Wright and Wyld, 2011). Concurrently, volcanism occurred along northern South America due to east-dipping subduction of the Farallon Plate (Figure 6.14). Evidence of this subduction is preserved in the volcanic and plutonic rocks of the Quebradagrande Complex, which emplaced in an intra-oceanic volcanic arc along a rifted continental margin (Nivia et al., 2006; Villagómez and Spikings, 2013; Jaramillo et al., 2017)

This western dipping subduction along northern South America closed the gap between the Caribbean plateau and the continent, eventually leading to oblique collision of the Plateau with South America in the Late Cretaceous (Pindell and Kennan, 2001; Vallejo et al., 2006; Villagómez and Spikings, 2013) (Figure 6.14) Fragments of the oceanic plateau and associated arc remnants, including Altamira sequences, accreted as a result of this collision, forming parts of the Central and Western Cordilleras (Millward et al., 1984; Kerr et al., 1996b; Kerr et al., 1997a; Villagómez and Spikings, 2013; Buchs et al., 2018). Plateau and arc sequences from western dipping subduction along the north eastern margin of the plateau (e.g., those in Aruba) migrated around the top of South America, and are now exposed in the Lesser Antilles. By this time, (c. 80 Ma) the magmatism associated with the mantle plume has likely stopped (Figure 6.15B). Although there are younger ages for the plateau, this may be due to $^{40}Ar/^{39}Ar$ ages offset by alteration/deformation, or “rejuvenated” magmatic phases related to lithospheric extension several tens of million years after the end of the plume magmatism. In addition, some of the younger ages might be derived from accreted seamounts not associated with the oceanic plateau.

In this model, the collision of the plateau with south America terminated the west-dipping subduction beneath the plateau. This collision prompted the propagation of subduction along the margin of the Caribbean Plateau, causing the older, denser Farallon Plate to sink beneath the young, buoyant oceanic plateau (Figure 6.14, 6.15B). The first stage of subduction related magmatism is formed when the first fluids are released from the downgoing slab. These fluids percolate into the sub-plateau lithosphere and melt the most fertile mantle components which most likely included areas previously metasomatized by plume melts (Figure 6.15C). This process might have been facilitated by high thermal gradients in the lithosphere due to the emplacement of the oceanic plateau only ~10-5 Ma earlier. Resulting magmas formed the Proto-arc Group 1 lavas, which are from a plume-like source based on Nd isotopes, and have immobile trace element contents consistent with the addition of slab derived fluids (i.e., variable enriched Th and depleted Nb). This could be produced by the addition of only 0.2-0.8 % of a sediment component to a plume-like source. The Proto-arc Group 1 forms between 75-73 Ma, based on the age of the limestone which the proto-arc group 1 intrudes, exhibiting soft sediment deformation. There is then an influx of hot depleted upper mantle in the nascent subduction zone, potentially due to the initiation of corner flow in the developing mantle wedge (Figure 6.15D). A small addition of slab derived fluids to mantle will cause a higher degree of melting, which will dilute the fluid signature. This melting forms the Proto-arc Group 2, which is from a MORB-like source, with variable enriched to depleted Th. The Proto-arc Group 2 could be formed with the addition of <0.4 % sediment to a DMM mantle or DMM and plume hybrid source. Although local lithospheric extension could have occurred due to rifting of the forearc during the earliest stages of subduction of the Farallon plate, the occurrence of oceanic plateau sequences stratigraphically underlying proto-arc units and the absence of peridotite and sheeted dyke complexes in the studied area and Costa Rica indicate that rifting was only minor. If present, rifting was clearly less than that associated with areas subject to spontaneous subduction initiation (e.g., IBM system, Arculus et al., 2015). Significantly, there is no evidence in the early Panama subduction zone for widespread melting induced by lithospheric extension along the margin of the Caribbean Plateau (Whattam and Stern, 2015; Whattam et al., 2020). Regional occurrence of Campanian pelagic limestone on top of the plateau, which clearly emplaced before Proto-arc Group 1, strongly suggests that subduction occurred several Myr. after magmatic cessation of the Caribbean Plateau. Although in agreement with a tectonically induced subduction model, this is not supportive of plume-induced subduction initiation models that require temporal continuity between plume and supra-subduction magmatism (Whattam and Stern, 2015; Whattam et al., 2020). Following the emplacement of Proto-arc Group 2 in Panama, the downgoing slab cooled the surrounding mantle which led to the formation of developed volcanic arc lavas, with more pronounced supra-

subduction signatures and the apparition of calc-alkaline differentiation trends (e.g., Lissinna, 2005; Buchs et al., 2010; Wegner et al., 2011) (Figure 6.15E). Based on the ages of the first Proto-arc Group 1 lavas (ca. 75 Ma) and the oldest age of the Soná-Azuero Arc (ca. 71 Ma, Wegner et al., 2011), it appears that the time taken for the evolution from a nascent subduction zone to the formation of a developed arc was ~4 Myr.

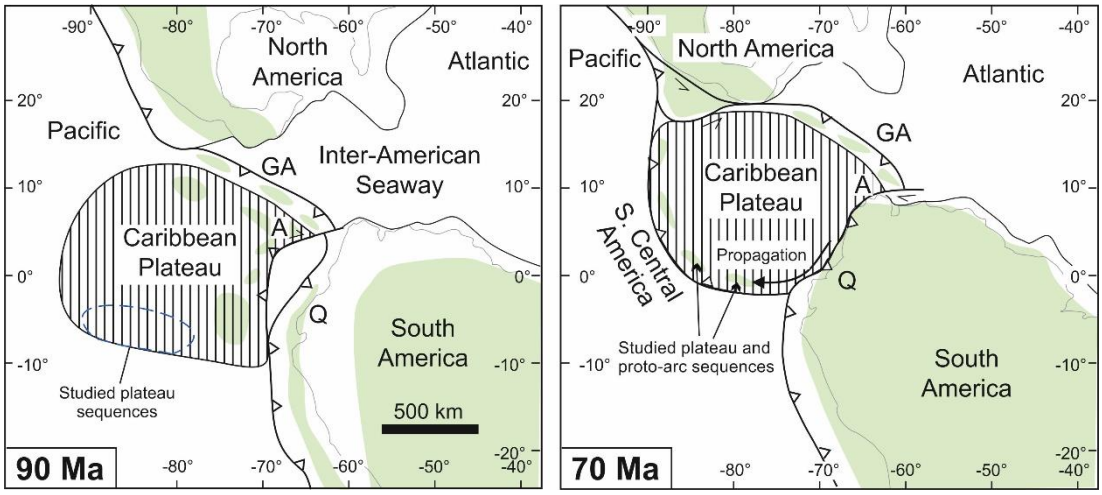

Figure 6.14: Tectonic model of the inter-American seaway in the Late Cretaceous after Buchs et al. (2018). Possible land exposures are shown in green. GA: Greater Antilles arc; A: Aruba Island part of the Colombian-Leeward Antilles arc (Wright and Wyld, 2011); Q: Quebradagrande complex.

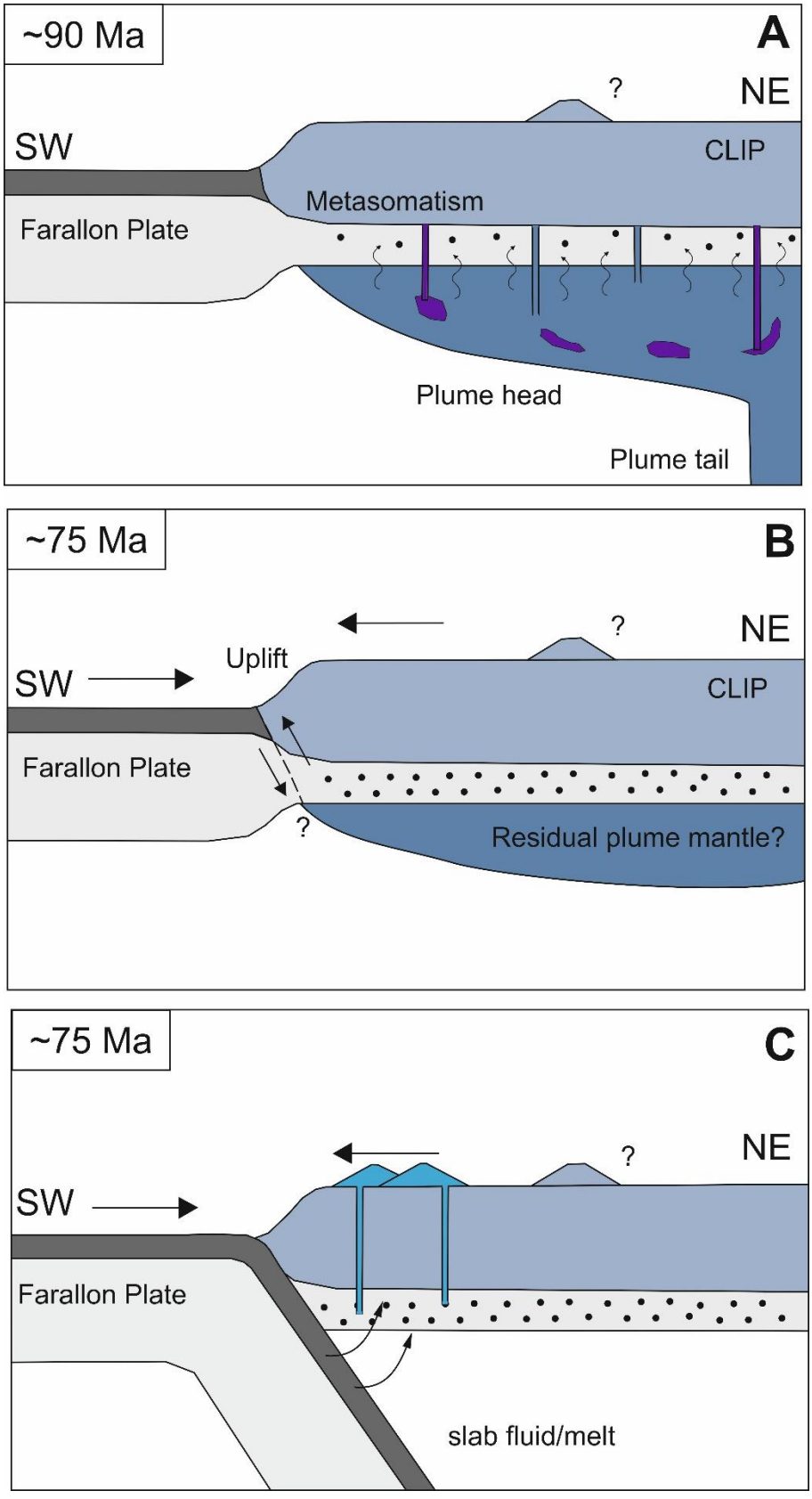
~90 Ma
A
?
NE
SW
CLIP
Metasomatism
Farallon Plate
Plume head
Plume tail
~75 Ma
B
?
NE
Uplift
SW
CLIP
Farallon Plate
?
Residual plume mantle?
~75 Ma
C
?
NE
SW
Farallon Plate
slab fluid/melt

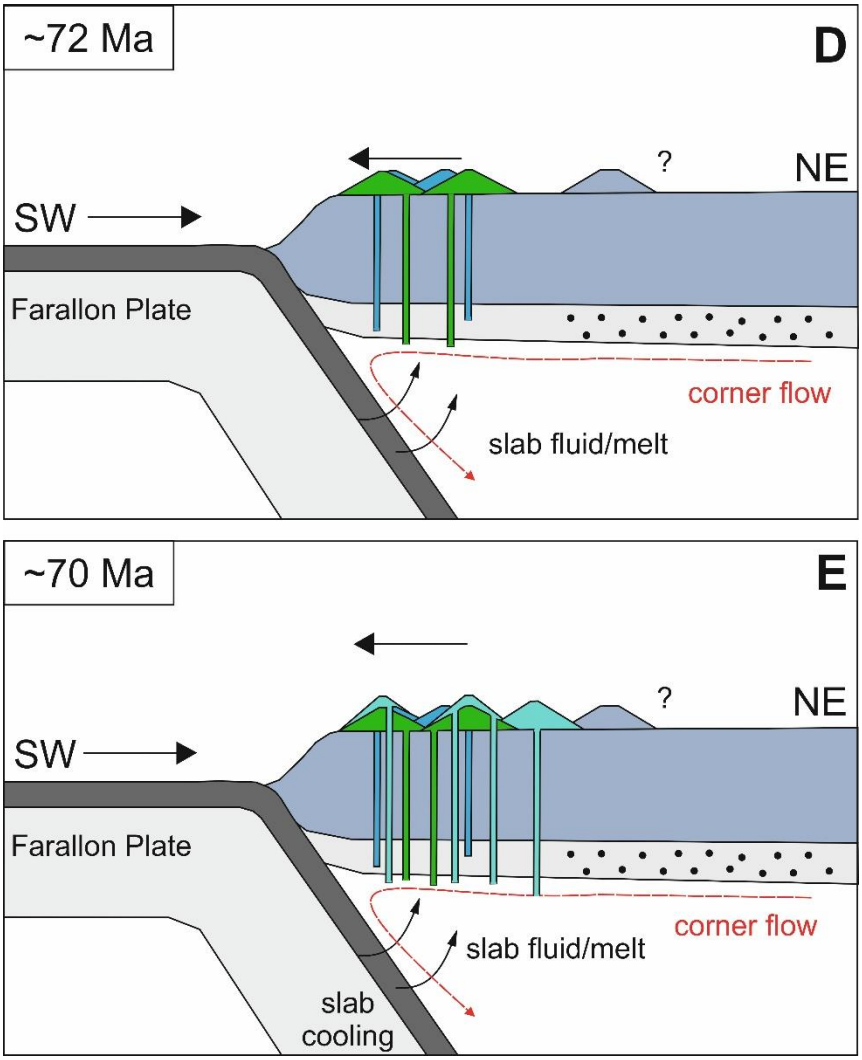

Figure 6.15*:* Model of subduction initiation and formation of the Proto-arc Groups along the south western marginof the Caribbean plateau. A) Formation of the Caribbean Plateau in the Cretaceous from a heterogeneous mantle plume, B) Initiation of subduction at around 75 Ma, due to propagation of subduction along the margin of the Caribbean Plateau, C) Release of fluids from the downgoing slab, prompting melting of the metasomatized lithospheric mantle forming the Proto-arc Group 1 at 75-73 Ma, D) An influx of hot depleted upper mantle due to initiation of corner flow. Fluids from the slab melt this upper mantle to form the Proto-arc Group 2 at around 72 Ma. E) Continued development of the mantle wedge and cooling associated with the downgoing slab forms the Soná-Torio Arc at around 70 Ma.

6.7 Future work

This study produced coherent and comprehensive geochemical data sets to characterise the geochemical heterogeneity of the oceanic plateau and proto-arc groups across Panama and the Serrania de Baudó. Using these geochemical results in combination with stratigraphic constraints, existing reliable $^{40}Ar/^{39}Ar$ ages and biostratigraphic ages, a model of oceanic plateau formation and subduction initiation was suggested. However, a key aim of the study was to produce new $^{40}Ar/^{39}Ar$ ages to constrain the temporal evolution of the plateau and proto-arc. Although samples were prepared and analysed for $^{40}Ar/^{39}Ar$ ages, it is clear that in low-K tholeiitic submarine basalts of the plateau and proto-arc, the $^{40}Ar/^{39}Ar$ system is sensitive to alteration and degassing, even when ages appear reliable and adhere to quality criteria. There is also evidence that existing $^{40}Ar/^{39}Ar$ ages from plateau sequences, which have previously been accepted to represent the true crystallisation age, may also have been affected by alteration and/or degassing (Baksi, 2007; Acero, 2019). Therefore, the $^{40}Ar/^{39}Ar$ technique needs to undergo further testing to confirm if it can be used reliably on rocks of this type. Further work also needs to be done to ensure that existing $^{40}Ar/^{39}Ar$ ages from around the CCOP are reliable and can be confirmed by stratigraphic constraints and/or biostratigraphic ages.

Despite the additional insights from this study, the temporal evolution of the plateau and proto-arc sequences remains relatively unconstrained. As $^{40}Ar/^{39}Ar$ dating does not appear to be suitable for these rocks, it may be feasible to investigate using baddeleyite to produce high precision ages for the plateau and proto-arc sequences. High precision ages could constrain the temporality of heterogeneity within the oceanic plateau sequences, and detect further evidence of an Early Cretaceous phase of formation. With the understanding of the plateau heterogeneity across the regions from this study, this dating could be accompanied by detailed sampling of plateau sequences to further constrain the temporal and spatial heterogeneity at a smaller scale. This work could be accompanied by Pb, Sr and Hf isotope work to gain further insight into the nature of the plume source through time.

High precision ages could also help to constrain the timing of subduction initiation magmatism, while further isotope work would assist in characterising the sources to the proto-arc lavas. Further exploration of plateau and proto-arc sequences in the Chagres Bayano and Darién Pacific Coast regions, with further stratigraphic constraints, geochemical analysis and high precision ages would also help us to understand the initiation of subduction and the associated magmatic processes.

Within this study, the Baudó Melange was recognised along the Bahia Solano coast. The formation of this melange could offer valuable insights into the origins of the Baudó Plateau

and the evolution of the continental margin, but the origins of the melange are unclear. To understand the formation of this melange, a detailed study is required, involving geochemical analyses of melange basalts, an investigation of the age and provenance of melange sediments and an investigation of structural relationships, both between the units of the melange and between the melange and the Baudó Plateau.

7. CONCLUSIONS

The uplifted and accreted oceanic plateau assemblages across Panama and northwestern Colombia provide an opportunity to investigate the nature and formation of the oceanic plateau arc basement across the southwestern margin of the Caribbean Plate. Uplifted segments of the forearc, particularly in the Soná-Torio region, allow investigation of the nature of the first subduction related magmas following the initiation of subduction along the margin of the plateau. Study of these assemblages, using field constraints, geochemical analyses and $^{40}Ar/^{39}Ar$ and biostratigraphic ages allowed us to produce a model of subduction initiation along the southwestern margin of the Caribbean Plateau in the Late Cretaceous.

In the Soná-Torio region, the Oceanic Plateau is dominated by submarine pillow basalts and lava flows, interbedded with radiolarites. Some of the radiolarites have been dated as 89-85 Ma, while $^{40}Ar/^{39}Ar$ ages of plateau lavas range from 114.5 ± 2.0 to 71.3 ± 2.1 Ma (Kolarsky et al., 1995; Hoernle et al., 2002; Lissinna, 2005; Buchs et al., 2010). The oceanic plateau in this region also includes limited outcrops of hyaloclastite and basaltic breccias, which are preferentially exposed along faults. In the Darién Pacific Coast region, the oceanic plateau sequences are also dominated by pillow basalts and lava flows. The $^{40}Ar/^{39}Ar$ ages of the plateau basalts range from 84.1 ± 1.0 to 71.3 ± 2.2 Ma while ages of radiolarites interbedded with the plateau are dated as 90-80 Ma (Bandy and Casey, 1973; Lissinna, 2005; Barat et al., 2014). In the Serranía de Baudó region, plateau sequences are formed of pillow basalts and lava flows, but there are also locally abundant plateau sills intruding the plateau basalt sequences. Plateau basalts in this region have been dated using $^{40}Ar/^{39}Ar$ as 77.9 ± 1.0 to 72.5 ± 0.4 Ma (Kerr et al., 1997), but there are currently no biostratigraphic ages.

Across the three regions, the plateau assemblages are geochemically heterogeneous, with 4 main geochemical groups: (1) normal plateau, consisting of the Soná-Torio, Jaqué and Baudó Plateau basalts, which represent the typical oceanic plateau basalts as also observed across the Caribbean; (2) enriched plateau, comprised of the Soná-Torio and Jaqué Enriched Plateau basalts, comparable to the e-basalts of Gorgona; (3) depleted plateau, represented by the Jaqué Depleted Plateau, which is more depleted than the normal plateau group, but not as depleted as previously recognised depleted basalts of the CCOP (e.g., the d-basalts of Gorgona) and (4) high-Mg plateau, exposed in the Soná-Torio region as hyaloclastites and basaltic breccias, which is highly depleted in LREE, and is compositionally similar to the Gorgona komatiites with a more enriched source based on Nd_i isotopes. In the Chagres Bayano region in central Panama, the normal plateau and depleted

plateau groups are also observed, showing that the arc basement in Panama is heterogeneous throughout.

Geochemical and field constraints suggest that the plateau assemblages in the Serrania de Baudó are part of the CCOP and formed along the southwestern margin of the oceanic plateau with the Soná-Torio and Jaqué Plateau assemblages. The Baudó Plateau group has trace element and Nd isotope composition which correlates with the normal oceanic plateau basalts of the remainder of the CCOP. The Baudó Plateau displays a sill complex which is not exposed in the other studied plateau regions, suggesting that it has been further uplifted and eroded, potentially due to distinct subduction dynamics along the margin of South America. The lack of arc- and proto-arc-related intrusions in Baudó may be due to the location of these plateau assemblages in the outer forearc, where subduction-related magmatism did not occur. In contrast, it is clear that the outermost Upper Cretaceous forearc has been eroded in the Soná-Torio region, where accreted Palaeocene ocean islands are juxtaposed to assemblages of the latest Cretaceous to Eocene Panama Arc (Buchs et al., 2011).

The formation of the four plateau geochemical groups requires a heterogeneous plume source, which may consist of a dominant depleted component with blobs, streaks or veins of an enriched component. This type of plume model has largely been used to explain the formation of plateau igneous rocks elsewhere in the CCOP (Kerr et al., 1996; Arndt et al., 1997; Hauff et al., 2000; Kerr et al., 2002; Hastie et al., 2016). The enriched member of the plateau could be produced by limited, deeper melting which could preferentially sample the most fertile enriched component of the plume. Shallower, more extensive melting could have sampled both the enriched and depleted plume components to produce the normal plateau groups. As the Jaqué Depleted Plateau are compositionally distinct from the Jaqué Plateau, it is possible that these samples formed from by more extensive melting of a similar, heterogenous plateau source. The occurrence of rocks such as the Soná-Torio High-Mg Plateau have not yet been described in the CCOP. These samples could have formed through extensive partial melting of the enriched plume component shortly prior to the extraction of these lavas. Without further stratigraphic constraints and high precision ages, it is difficult to constrain the temporal or spatial evolution of the heterogeneity of the plateau sequences. Based the Jaqué Plateau and the Jaqué Depleted Plateau groups, which are indistinguishable in the field and located only ca 150m apart without being separated by a major structure, the plume head must be heterogeneous on a small scale. To further investigate the temporal evolution of the plume head, as has been done for other Ontong Java Plateau and other sections of the CCOP, the detailed stratigraphy of the plateau needs to be further investigated.

Although this study attempted to gain new $^{40}Ar/^{39}Ar$ ages, many of the dates for the plateau assemblages were significantly younger than expected based on previous and new stratigraphic constraints or the existing biostratigraphic ages. Despite this, most of the $^{40}Ar/^{39}Ar$ dates adhered to quality criteria and, without stratigraphic control, could have be accepted as reliable crystallization ages. This highlights the difficulty in getting accurate and reliable $^{40}Ar/^{39}Ar$ ages from low-K, altered submarine basalts. This suggests that other dating techniques may be more suitable to constrain the timing of formation of plateau sequences from the Caribbean (e.g., U-Pb on micro-zircons or baddeleyite). It is likely that many of the ages previously published for the oceanic plateau around the Caribbean, such as those in the Serrania de Baudó, are offset by alteration or degassing, and may not represent a true crystallisation age (Baksi, 2007; Acero, 2019).

Several Proto-arc groups, formed during the first stages of subduction initiation, were recognised in the Soná-Torio and Darién Pacific Coast regions. Two main geochemical groups occur in the Soná-Torio region. The Proto-arc Group 1 is formed of pillow basalts, dykes and lava flows, which intrude sequences of the plateau and limestones of the Torio Lithostratigraphic Unit. The Torio Lithostratigraphic Unit is a hemipelagic limestone with interbeds of basaltic breccias and sandstones, which formed regionally in the Late Cretaceous. The Proto-arc Group 1 has only been dated based on peperitic intrusions into the Torio Limestone, associated with soft-sediment deformation (Buchs et al., 2010). Therefore, the Proto-arc Group 1 is also assigned an age of 75 - 73 Ma. The Proto-arc Group 2 is exposed only as dykes which intrude sequences of the oceanic plateau and tuffaceous sequences of the Proto-arc Group 1. The Proto-arc 2 has not been otherwise dated, but based on this relationship it is assumed to be at least partly younger than the Proto-arc Group 1 and thus is estimated to have formed at ca. 73-72 Ma (Figure 3.2). In the Darién Pacific Coast region, the nature of the Proto-arc is not as clear. It is observed only as intrusions in the plateau sequences, but remains unconstrained with no other stratigraphic or geochronologic constraints

The Soná-Torio Proto-arc Group 1 has generally flat trace element patterns with variably enriched Th, depleted Nb and slight Ti negative anomalies. Nd isotopes indicate a plume-like source, similar to the normal plateau sequences of the CCOP. The Soná-Torio Proto-arc Group 2 is depleted in the LREE, with variable enriched to depleted Th and a negative Nb anomaly. Nd isotopes are higher than the values of the Proto-arc Group 1, indicating a MORB-like source. Samples of the Jaqué Proto-arc are similar to the Proto-arc Group 1, although they are slightly more enriched in the LREE.

It has previously been suggested that the forearc assemblages in Panama may follow the "subduction initiation rule", based on studies of the forearc of the IBM and ophiolites (Whattam and Stern, 2011; Whattam and Stern, 2015; Whattam et al., 2020). This subduction initiation rule dictates that forearc assemblages begin with FAB, overlain by boninites. The FAB are formed by adiabatic melting due to forearc spreading, with little influence from slab derived fluids (Whattam and Stern, 2011). The overlying boninites are produced when fluids are released into depleted residual mantle. Clearly, the forearc assemblages in the Soná-Torio region do not agree with this model. The Proto-arc Group 1, the first magmatic product of subduction initiation along the margin of the Caribbean, shows the influence of a slab derived fluid through the variable Th enrichment. The Proto-arc Group 1 is also not derived from a refractory MORB-like source, as required in the subduction initiation rule. There is no evidence for spreading in the forearc in the Soná-Torio region during subduction initiation, while there is evidence of uplift in the region at this time. Finally, there is no evidence of boninites in the Soná-Torio region.

The uplifted forearc in the Soná-Torio region displays a unique stratigraphic assemblage, as the proto-arc and arc have formed on an oceanic plateau basement. This allows for an assessment of the influence of the plateau on subduction initiation. It has previously been suggested that subduction was initiated in the southwestern Caribbean by the plume, in the PISI model (Whattam and Stern, 2015). However, this model does not correlate with field and geochemical constraints from the Soná-Torio region. The PISI model also requires extensive spreading in the forearc, which is not observed. The PISI model also requires a continuous evolution from plume-like to arc-like magmas, with the progressive addition of a slab derived fluid. However, there is a clear cessation of magmatism between the plateau and proto-arc, which is evidenced regionally by the deposition of the Torio Lithostratigraphic Unit limestone on top of plateau sequences. The PISI model is also inconsistent with the newly-documented geochemical transition between Proto-arc Group 1 and Group 2.

The formation of the proto-arc groups in the Soná-Torio region can be explained by a new model of subduction initiation along the margin of the Caribbean plateau. Subduction initiation along the southwestern plateau margin may have occurred due to propagation of a subduction zone from the eastern margin of the plateau. When the first fluids were released from the downgoing slab during the early stages of subduction initiation, they melted the most fertile mantle components in the lithosphere/asthenosphere (presumably plume-metasomatized mantle) to produce the Proto-arc Group 1. Simple two component modelling indicates that the Proto-arc Group 1 could be produced by the addition of 0.2 – 0.8 % of pelagic sediment to a heterogeneous plume-like mantle. Depleted upper mantle, possibly holding residual heat from the mantle plume, subsequently reached the melting region due

to incipient corner flow in the supra-subduction mantle wedge. Small additions of fluid from the slab caused increasing partial melting of the hot depleted upper mantle, which could dilute the fluid signature to produce Proto-arc Group 2. Modelling suggests that some the Proto-arc Group 2 could be generated by the addition of less than 0.4 % of a sediment to a DDM source. However, some of the Proto-arc Group 2 may have been generated by sediment addition to a source intermediate between plume-like and DMM, hence pointing toward melting of a compositionally heterogenous mantle source under variable influence of slab-derived fluids Subsequent development of the mantle wedge and the cooling effect of the downgoing slab prompted less melting with the addition of fluids from the slab, allowing the Soná-Torio Arc to generate a developed arc-like signature form the addition of 0.6 – 10 % sediment to a plume to DDM source.

Samples of the Proto-arc Group 1 and Group 2 have also been recognised in the Chagres Bayano region in Central Panama, which indicates that similar petrogenetic processes occurred during subduction initiation along the plateau margin ca. 300 km to the east. Although the Proto-arc Group 2 was not identified in Jaqué, it may be discovered with further sampling in the region.

The models of plateau formation and subduction initiation can be brought together to describe the evolution of the plateau basement and early subduction products throughout the Cretaceous. The oceanic plateau began forming in the Early Cretaceous from heterogenous plume. The plateau collided with south America, which terminated the east-dipping subduction beneath the plateau. The Panama Arc formed due to subduction initiation along the southwestern margin of the Caribbean Plateau in the Late Cretaceous, likely due to propagation of subduction along the margin of the plateau, potentially from collision of the plateau with the South American continent.

REFERENCES

Acero, M.M.A., 2019. *Geochemical and Geochronological Characterization of the Mafic Basement of Northwestern Colombia (Chocó-Panamá Block)*. Section des Sciences de la Terre et de l'environnement [de] l'Université.

Acton, G.D., Galbrun, B. and King, J.W., 2000. 9. Paleolatitude of the Caribbean Plate since the Late Cretaceous. In: *Proceedings of the Ocean Drilling Program: Scientific results* 165 pp. 149-173

Aitken, B.G. and Echeverría, L.M., 1984. Petrology and geochemistry of komatiites and tholeiites from Gorgona Island, Colombia. *Contributions to Mineralogy and Petrology* 86(1), pp. 94–105.

Alvarado, G.E., Denyer, P. and Sinton, C.W., 1997. The 89 Ma Tortugal komatiitic suite, Costa Rica: implications for a common geological origin of the Caribbean and Eastern Pacific region from a mantle plume. *Geology* 25(5), pp. 439–442.

Andjić, G., Baumgartner, P.O. and Baumgartner-Mora, C., 2018. Rapid vertical motions and formation of volcanic arc gaps: Plateau collision recorded in the forearc geological evolution (Costa Rica margin). *Basin Research* 30(5), pp. 863–894.

Arculus, R.J., Ishizuka, O., Bogus, K.A., Gurnis, M., Hickey-Vargas, R., Aljahdali, M.H., Bandini-Maeder, A.N., Barth, A.P., Brandl, P.A., Drab, L. and do Monte Guerra, R., 2015. A record of spontaneous subduction initiation in the Izu–Bonin–Mariana arc. *Nature Geoscience* 8, p. 728.

Arndt, N.T., Kerr, A.C. and Tarney, J.,1997. Dynamic melting in plume heads: the formation of Gorgona komatiites and basalts. *Earth and Planetary Science Letters* 146(1–2), pp. 289–301.

Bandy, O.L., 1970. Upper Cretaceous-Cenozoic paleobathymetric cycles, eastern Panama and northern Colombia. *AAPG Bulletin* 54(9), p. 1782.

Bandy, O.L. and Casey, R.E., 1973. Reflector horizons and paleobathymetric history, eastern Panama. *Geological Society of America Bulletin* 84(9), pp. 3081–3086.

Baksi, A.K., 2007. A quantitative tool for detecting alteration in undisturbed rocks and minerals-II: application to argon ages related to hotspots. *Special Papers-Geological Society of America* 430, p. 305.

Barat, F., de Lépinay, B.M., Sosson, M., Müller, C., Baumgartner, P.O. and Baumgartner-Mora, C., 2014. Transition from the Farallon Plate subduction to the collision between South and Central America: Geological evolution of the Panama Isthmus. *Tectonophysics* 622(0), pp. 145–167.

Barlow, C.A., 1981. Radar geology and tectonic implications of the Chocó Basin, Colombia, South America.

Le Bas, M.J.L.E., Maitre, R.L., Streckeisen, A. and Zanettin, B. 1986. A chemical classification of volcanic rocks based on the total alkali-silica diagram. *Journal of petrology* 27(3), pp. 745–750.

Baumgartner, P.O., Flores, K., Bandini, A.N., Girault, F. and Cruz, D., 2008. Upper Triassic to Cretaceous radiolaria from Nicaragua and northern Costa Rica-The Mesquito composite oceanic terrane. *Ofioliti* 33(1), pp. 1–19.

Ben-Avraham, Z.V.I., Nur, A., Jones, D. and Cox, A., 1981. Continental accretion: from

oceanic plateaus to allochthonous terranes. *Science* 213(4503), pp. 47–54.

Bence, A.E., Papike, J.J. and Ayuso, R.A., 1975. Petrology of submarine basalts from the Central Caribbean: DSDP Leg 15. *Journal of Geophysical Research* 80(35), pp. 4775–4804.

Billen, M.I. and Hirth, G., 2005. Newtonian versus non-Newtonian upper mantle viscosity: Implications for subduction initiation. *Geophysical Research Letters* 32(19)

Boschman, L.M., van Hinsbergen, D.J., Torsvik, T.H., Spakman, W. and Pindell, J.L., 2014. Kinematic reconstruction of the Caribbean region since the Early Jurassic. *Earth-Science Reviews* 138, pp. 102–136.

Bryan, S.E. and Ernst, R.E., 2008. Revised definition of large igneous provinces (LIPs). *Earth-Science Reviews* 86(1–4), pp. 175–202.

Boven, A., Pasteels, P., Kelley, S.P., Punzalan, L., Bingen, B. and Demaiffe, D., 2001. $^{40}Ar/^{39}Ar$ study of plagioclases from the Rogaland anorthosite complex (SW Norway); an attempt to understand argon ages in plutonic plagioclase. *Chemical Geology* 176(1), pp. 105–135.

Buchs, D.M., 2008. *Late Cretaceous to Eocene geology of the South Central American forearc area (southern Costa Rica and western Panama): Initiation and evolution of an intra-oceanic convergent margin*. Lausanne: Lausanne.

Buchs, D.M., Arculus, R.J., Baumgartner, P.O., Baumgartner-Mora, C. and Ulianov, A., 2010. Late Cretaceous arc development on the SW margin of the Caribbean Plate: Insights from the Golfito, Costa Rica, and Azuero, Panama, complexes. *Geochemistry Geophysics Geosystems* 11(7), p. Q07S24.

Buchs, D.M., Arculus, R.J., Baumgartner, P.O. and Ulianov, A., 2011a. Oceanic intraplate volcanoes exposed: Example from seamounts accreted in Panama. *Geology* 39(4), pp. 335–338.

Buchs, D.M., Baumgartner, P.O., Baumgartner-Mora, C., Flores, K. and Bandini, A.N., 2011b. Upper Cretaceous to Miocene tectonostratigraphy of the Azuero area (Panama) and the discontinuous accretion and subduction erosion along the Middle American margin. *Tectonophysics* 512(1–4), pp. 31–46.

Buchs, D.M., Kerr, A.C., Brims, J.C., Zapata-Villada, J.P., Correa-Restrepo, T. and Rodríguez, G., 2018. Evidence for subaerial development of the Caribbean oceanic plateau in the Late Cretaceous and palaeo-environmental implications. *Earth and Planetary Science Letters* 499, pp. 62–73.

Buchs, D.M., Irving, D., Coombs, H., Miranda, R., Wang, J., Coronado, M., Arrocha, R., Lacerda, M., Goff, C., Almengor, E. and Portugal, E., 2019a. Volcanic contribution to emergence of Central Panama in the Early Miocene. *Scientific Reports* 9(1), p. 1417.

Buchs, D.M., Coombs, H., Irving, D., Wang, J., Koppers, A., Miranda, R., Coronado, M., Tapia, A. and Pitchford, S., 2019b. Volcanic shutdown of the Panama Canal area following breakup of the Farallon plate. *Lithos* 334–335, pp. 190–204.

Burke, K., 1988. Tectonic evolution of the Caribbean. *Annual Review of Earth and Planetary Sciences* 16(1), pp. 201–230.

Burov, E. and Cloetingh, S., 2010. Plume-like upper mantle instabilities drive subduction initiation. *Geophysical Research Letters* 37(3), p. L03309.

Busby, C.J., Tamura, Y, Blum, P, Guerin, G, Andrews, GDM, Barker, AK, Berger, JLR, Bongiolo, EM, Bordiga, M, DeBari, SM, Gill, JB, Hamelin, C, Jia, J, John, EH, Jonas, A-S, Jutzeler, M, Kars, MAC, Kita, ZA, Konrad, K, Mahony, S, Martini, M, Miyazaki, T, Musgrave,

RJ, Nascimento, DB, Nichols, ARL, Ribero, JM, Sato, T, Schindlbeck, JC, Schmitt, AK, Straub, SM, Mleneck-Vautravers, MJ & Yang Yang, A., 2017. The missing half of the subduction factory: shipboard results from the Izu rear arc, IODP Expedition 350. *International Geology Review* 59(13), pp. 1677–1708.

Campbell, I.H., Griffiths, R.W. and Hill, R.I., 1989. Melting in an Archaean mantle plume: heads it's basalts, tails it's komatiites. *Nature* 339(6227), p. 697.

Campbell, I.H., 2007. Testing the plume theory. *Chemical Geology* 241(3–4), pp. 153–176.

Campbell, I.H. and Griffiths, R.W., 1990. Implications of mantle plume structure for the evolution of flood basalts. *Earth and Planetary Science Letters* 99(1–2), pp. 79–93.

Campbell, I.H. and Griffiths, R.W., 1992. The changing nature of mantle hotspots through time: implications for the chemical evolution of the mantle. *The Journal of Geology* 100(5), pp. 497–523.

Cann, J.R., 1970. Rb, Sr, Y, Zr and Nb in some ocean floor basaltic rocks. *Earth and Planetary Science Letters* 10(1), pp. 7–11.

Case, J.E., Duran S, L.G., Alfonso, L.R. and Moore, W.R., 1971. Tectonic investigations in western Colombia and eastern Panama. *Geological Society of America Bulletin* 82(10), pp. 2685–2712.

Case, J.E., Barnes, J., PARÍS Q, G., GONZÁLEZ I, H. and Viña, A.,1973. Trans-Andean geophysical profile, southern Colombia. *Geological Society of America Bulletin* 84(9), pp. 2895–2904.

Case, J.E., 1974. Oceanic Crust Forms Basement of Eastern Panamá. *Geological Society of America Bulletin* 85(4), pp. 645–652.

Chambers, L.M., Pringle, M.S. and Fitton, J.G., 2004. Phreatomagmatic eruptions on the Ontong Java Plateau: An Aptian $^{40}Ar/^{39}Ar$ age for volcaniclastic rocks at ODP Site 1184. *Geological Society, London, Special Publications* 229(1), pp. 325–331.

Chauvel, C., Garçon, M., Bureau, S., Besnault, A., Jahn, B.M. and Ding, Z., 2014. Constraints from loess on the Hf–Nd isotopic composition of the upper continental crust. *Earth and Planetary Science Letters* 388, pp. 48–58.

Cloos, M., 1993. Lithospheric buoyancy and collisional orogenesis: Subduction of oceanic plateaus, continental margins, island arcs, spreading ridges, and seamounts. *Geological Society of America Bulletin* 105(6), pp. 715–737.

Coates, A.G., Collins, L.S., Aubry, M.P. and Berggren, W.A., 2004. The geology of the Darien, Panama, and the late Miocene-Pliocene collision of the Panama arc with northwestern South America. *Geological Society of America Bulletin* 116(11–12), pp. 1327–1344.

Coffin, M.F., Pringle, M.S., Duncan, R.A., Gladczenko, T.P., Storey, M., Müller, R.D. and Gahagan, L.A., 2002. Kerguelen hotspot magma output since 130 Ma. *Journal of Petrology* 43(7), pp. 1121–1137.

Coffin, M.F. and Eldholm, O., 1992. Volcanism and continental break-up: a global compilation of large igneous provinces. *Geological Society, London, Special Publications* 68(1), pp. 17–30.

Condie, K.C., 2005. High field strength element ratios in Archean basalts: a window to evolving sources of mantle plumes? *Lithos* 79(3–4), pp. 491–504.

Cooper, P.A. and Taylor, B., 1985. Polarity reversal in the Solomon Islands arc. *Nature* 314(6010), pp. 428–430.

Corral, I., Griera, A., Gómez-Gras, D., Corbella, M., i Sabaté, À.C., Falconett, M.P. and Cardellach, E., 2011. Geology of the Cerro Quema Au-Cu deposit (Azuero Peninsula, Panama). *Geologica Acta* 9(3–4), pp. 481–498.

Corral, I., Corbella, M., Griera, A., Gómez-Gras, D., Cosca, M.A. and Cardellach, E., 2012. Age of the Cerro Quema Au-Cu deposit (Azuero Peninsula, Panama): insights from biostratigraphy and Ar/Ar geochronology/Edad del depósito de Oro-Cobre de Cerro Quema (Península de Azuero, Panama): Evidencias bioestratigraficas y geocronologicas (Ar/Ar). *Geo-Temas* 13, p. 114.

Corral, I., Gómez-Gras, D., Griera, A., Corbella, M. and Cardellach, E., 2013. Sedimentation and volcanism in the Panamanian Cretaceous intra-oceanic arc and fore-arc: New insights from the Azuero peninsula (SW Panama). *Bulletin de la Societe Geologique de France* 184(1–2), pp. 35–45.

Cossio, U., 2003. *Geologia de las planchas 127 Cupica, 128 Rio Murri, 143 Bahia Solano y 144 Tagachi*.

Crameri, F., Magni, V., Domeier, M., Shephard, G.E., Chotalia, K., Cooper, G., Eakin, C.M., Grima, A.G., Gürer, D., Király, Á. and Mulyukova, E., 2020. A transdisciplinary and community-driven database to unravel subduction zone initiation. *Nature communications*, *11*(1), pp.1-14.

Dalrymple, G.B. and Lanphere, M.A., 1974. $^{40}Ar/^{39}Ar$ age spectra of some undisturbed terrestrial samples. *Geochimica et Cosmochimica Acta* 38(5), pp. 715–738.

Davaille, A., Girard, F. and Le Bars, M., 2002. How to anchor hotspots in a convecting mantle? *Earth and Planetary Science Letters* 203(2), pp. 621–634.

Davaille, A. and Vatteville, J., 2005. On the transient nature of mantle plumes. *Geophysical Research Letters* 32(14)

Davies, J.H., 1999. The role of hydraulic fractures and intermediate-depth earthquakes in generating subduction-zone magmatism. *Nature* 398(6723), pp. 142–145.

Denyer, P., Baumgartner, P.O. and Gazel, E., 2006. Characterization and tectonic implications of Mesozoic-Cenozoic oceanic assemblages of Costa Rica and Western Panama. *Geologica Acta* 4(1–2), pp. 219–235.

Donnelly, T.W., Kay, R. and Rogers, J.J.W., 1973. Chemical Petrology of Caribbean Basalts and Dolerites-Leg 15, Deep-Sea Drilling Project. In: *Transactions-American Geophysical Union*. pp. 1002–1004.

Donnelly, T.W., 1973. Late Cretaceous Basalts from Caribbean-Possible Flood Basalt Province of Vast Size. In: *Transactions-American Geophysical Union*. p. 1004.

Duncan, R.A., 2002. A time frame for construction of the Kerguelen Plateau and Broken Ridge. *Journal of Petrology* 43(7), pp. 1109–1119.

Duncan, R.A. and Hargraves, R.B., 1984. Plate tectonic evolution of the Caribbean region in the mantle reference frame. *Geological Society of America Memoirs* 162, pp. 81–94.

Dürkefälden, A., Hoernle, K., Hauff, F., Werner, R. and Garbe-Schönberg, D., 2019. Second-stage Caribbean Large Igneous Province volcanism: The depleted Icing on the enriched Cake. *Chemical Geology* 509, pp. 45–63.

Duque-Caro, H., 1990a. El Bloque del Choco en el noroccidente Suramericano: Implicaciones estructurales, tectonosstratiqraficas y paleogeograficas. *Boletin Geologico de Ingeominas* 31(1), pp. 1–45.

Duque-Caro, H., 1990b. Estratigrafía, paleoceanografía y paleobiogeografía de la cuenca

del Atrato y la evolución del Istmo de Panamá. *Boletín Geológico* 31(1), pp. 4–45.

Duque-Caro, H., 1990c. Neogene stratigraphy, paleoceanography and paleobiogeography in northwest South America and the evolution of the Panama Seaway. *Palaeogeography, Palaeoclimatology, Palaeoecology* 77(3–4), pp. 203–234.

Duque-Caro, H., 1990d. The Choco Block in the northwestern corner of South America: Structural, tectonostratigraphic, and paleogeographic implications. *Journal of South American Earth Sciences* 3(1), pp. 71–84.

Dymkova, D. and Gerya, T., 2013. Porous fluid flow enables oceanic subduction initiation on Earth. *Geophysical Research Letters* 40(21), pp. 5671–5676.

Echeverria, L.M., 1980. Tertiary or Mesozoic komatiites from Gorgona Island, Colombia: field relations and geochemistry. *Contributions to Mineralogy and Petrology* 73(3), pp. 253–266.

Edgar, N.T., Ewing, J.I. and Hennion, J., 1971. Seismic refraction and reflection in Caribbean Sea. *AAPG Bulletin* 55(6), pp. 833–870.

Eggins, S.M., 2003. Laser ablation ICP-MS analysis of geological materials prepared as lithium borate glasses. *Geostandards Newsletter* 27(2), pp. 147–162.

Eldholm, O. and Coffin, M.F., 2000. Large igneous provinces and plate tectonics. *Geophysical Monograph-American Geophysical Union* 121, pp. 309–326.

Escuder-Viruete, J., Pérez-Estaún, A., Contreras, F., Joubert, M., Weis, D., Ullrich, T.D. and Spadea, P., 2007. Plume mantle source heterogeneity through time: Insights from the Duarte Complex, Hispaniola, northeastern Caribbean. *Journal of Geophysical Research: Solid Earth* 112(B4)

Esso Exploration and Production Panama 1970. *Unpublished Annual Report Corresponding to the Second Year of Exploration Conforming to Contract 59, Darien Basin, October 1969-September 1970 (for Department of Mineral Resources, Government of Panama)*.

Esso Exploration and Production Panama 1971. *Unpublished Annual Report Corresponding to the Third Year of Exploration Conforming to Contract 59, Darien Basin, October 1970-March 1971 (for Department of Mineral Resources, Government of Panama)*.

Farnetani, C.G. and Samuel, H., 2005. Beyond the thermal plume paradigm. *Geophysical Research Letters* 32(7)

Farnetani, D.G. and Richards, M.A., 1995. Thermal entrainment and melting in mantle plumes. *Earth and Planetary Science Letters* 136(3–4), pp. 251–267.

Farris, D.W., Jaramillo, C., Bayona, G., Restrepo-Moreno, S.A., Montes, C., Cardona, A., Mora, A., Speakman, R.J., Glascock, M.D. and Valencia, V., 2011. Fracturing of the Panamanian Isthmus during initial collision with South America. *Geology* 39(11), pp. 1007–1010.

Fitton, J.G., 2007. The OIB paradox. In: Foulger, G. R. and Jurdy, D. M. eds. *Plates, Plumes and Planetary Processes*. Geological Society of America,

Fitton, J.G. and Godard, M., 2004. Origin and evolution of magmas on the Ontong Java Plateau. *Geological Society, London, Special Publications* 229(1), pp. 151–178.

Fleck, R.J., Sutter, J.F. and Elliot, D.H., 1977. Interpretation of discordant 40Ar/39Ar age-spectra of Mesozoic tholeiites from Antarctica. *Geochimica et Cosmochimica Acta* 41(1), pp. 15–32.

Gansser, A., 1973. Facts and theories on the Andes: Twenty-sixth William Smith Lecture.

Journal of the Geological Society 129(2), pp. 93–131.

Gao, H., Humphreys, E.D., Yao, H. and van der Hilst, R.D., 2011. Crust and lithosphere structure of the northwestern U.S. with ambient noise tomography: Terrane accretion and Cascade arc development. *Earth and Planetary Science Letters* 304(1), pp. 202–211.

Gardner, T., Marshall, J., Merritts, D., Bee, B., Burgette, R., Burton, E., Cooke, J., Kehrwald, N., Protti, M., Fisher, D. and Sak, P., 2001. Holocene forearc block rotation in response to seamount subduction, southeastern Peninsula de Nicoya, Costa Rica. *Geology* 29(2), pp. 151–154.

Gazel, E., Hayes, J.L., Hoernle, K., Kelemen, P., Everson, E., Holbrook, W.S., Hauff, F., Van Den Bogaard, P., Vance, E.A., Chu, S. and Calvert, A.J., 2015. Continental crust generated in oceanic arcs. *Nature Geoscience* 8(4), pp. 321–327.

Gerya, T. V., Stern, R.J., Baes, M., Sobolev, S.V. and Whattam, S.A., 2015. Plate tectonics on the Earth triggered by plume-induced subduction initiation. *Nature* 527, p. 221.

Del Giudice, D. and Recchi, G., 1969. *Geología del área del Proyecto Minero de Azuero*. Gobierno de la República de Panamá.

Giunta, G. and Oliveri, E., 2009. Some remarks on the Caribbean Plate kinematics: facts and remaining problems. *Geological Society, London, Special Publications* 328(1), pp. 57–75.

Goossens, P.J., Rose Jr, W.I. and Flores, D., 1977. Geochemistry of tholeiites of the Basic Igneous Complex of northwestern South America. *Geological Society of America Bulletin* 88(12), pp. 1711–1720.

Del Guidice, D. and Recchi, G., 1969. Geologia del areá del projecto minero de Azuero: Projecto Minero Panama, Fase I. *Naciones Unidas, Panama*

Gurnis, M., Hall, C. and Lavier, L., 2004. Evolving force balance during incipient subduction. *Geochemistry, Geophysics, Geosystems* 5(7).

Haffer, J., 1967. On the geology of the Urabá and northern Chocó regions. *NW Colombia: Bogotá, Empresa Colombiana de Petróleos (ECOPETROL), Reporte interno*

Hager, B.H. and O'Connell, R.J., 1981. A simple global model of plate dynamics and mantle convection. *Journal of Geophysical Research: Solid Earth* 86(B6), pp. 4843–4867.

Hall, C.E., Gurnis, M., Sdrolias, M., Lavier, L.L. and Müller, R.D., 2003. Catastrophic initiation of subduction following forced convergence across fracture zones. *Earth and Planetary Science Letters* 212(1–2), pp. 15–30.

Harrison, T.M. and McDougall, I., 1981. Excess40Ar in metamorphic rocks from Broken Hill, New South Wales: implications for40Ar/39Ar age spectra and the thermal history of the region. *Earth and Planetary Science Letters* 55(1), pp. 123–149.

Harland, W.B., Armstrong, R.L., Cox, A.V., Craig, L.E., Smith, A.G. and Smith, D.G., 1989. *A Geologic Time Scale*.

Hastie, A.R., Kerr, A.C., Pearce, J.A. and Mitchell, S.F., 2007. Classification of Altered Volcanic Island Arc Rocks using Immobile Trace Elements: Development of the Th–Co Discrimination Diagram. *Journal of Petrology* 48(12), pp. 2341–2357.

Hastie, A.R., Mitchell, S.F., Treloar, P.J., Kerr, A.C., Neill, I. and Barfod, D.N., 2013. Geochemical components in a Cretaceous island arc: The Th/La-(Ce/Ce*)Nd diagram and implications for subduction initiation in the inter-American region. *Lithos* 162–163(0), pp. 57–69.

Hastie, A.R., Fitton, J.G., Kerr, A.C., McDonald, I., Schwindrofska, A. and Hoernle, K., 2016. The composition of mantle plumes and the deep Earth. *Earth and Planetary Science Letters* 444, pp. 13–25.

Hastie, A.R. and Kerr, A.C., 2010. Mantle plume or slab window?: Physical and geochemical constraints on the origin of the Caribbean oceanic plateau. *Earth-Science Reviews* 98(3–4), pp. 283–293.

Hauff, F., Hoernle, K., van den Bogaard, P., Alvarado, G. and Garbe-Schönberg, D., 2000a. Age and geochemistry of basaltic complexes in western Costa Rica: Contributions to the geotectonic evolution of Central America. *Geochemistry, Geophysics, Geosystems* 1(5)

Hauff, F., Hoernle, K., Tilton, G., Graham, D.W. and Kerr, A.C., 2000b. Large volume recycling of oceanic lithosphere over short time scales: geochemical constraints from the Caribbean Large Igneous Province. *Earth and Planetary Science Letters* 174(3–4), pp. 247–263.

Herzberg, C., 2004. Partial melting below the Ontong Java Plateau. *Geological Society, London, Special Publications* 229(1), pp. 179–183.

Herzberg, C. and O'Hara, M.J., 2002. Plume-associated ultramafic magmas of Phanerozoic age. *Journal of Petrology* 43(10), pp. 1857–1883.

Hickey-Vargas, R., Yogodzinski, G.M., Ishizuka, O., McCarthy, A., Bizimis, M., Kusano, Y., Savov, I.P. and Arculus, R., 2018. Origin of depleted basalts during subduction initiation and early development of the Izu-Bonin-Mariana island arc: Evidence from IODP expedition 351 site U1438, Amami-Sankaku basin. *Geochimica et Cosmochimica Acta* 229, pp. 85–111.

Hill, R.I., Campbell, I.H., Davies, G.F. and Griffiths, R.W., 1992. Mantle plumes and continental tectonics. *Science* 256(5054), pp. 186–193.

Hill, R.I., 1993. Mantle plumes and continental tectonics. *Lithos* 30(3–4), pp. 193–206.

Hoernle, K., 1998. Geochemistry of Jurassic Oceanic Crust beneath Gran Canaria (Canary Islands): Implications for Crustal Recycling and Assimilation. *Journal of Petrology* 39(5), pp. 859–880.

Hoernle, K., Werner, R., Morgan, J.P., Garbe-Schönberg, D., Bryce, J. and Mrazek, J., 2000. Existence of complex spatial zonation in the Galápagos plume. *Geology* 28(5), pp. 435–438.

Hoernle, K., van den Bogaard, P., Werner, R., Lissinna, B., Hauff, F., Alvarado, G. and Garbe-Schönberg, D., 2002. Missing history (16–71 Ma) of the Galápagos hotspot: Implications for the tectonic and biological evolution of the Americas. *Geology* 30(9), pp. 795–798.

Hoernle, K., Hauff, F. and van den Bogaard, P., 2004. 70 my history (139–69 Ma) for the Caribbean large igneous province. *Geology* 32(8), pp. 697–700.

Hofmann, A.W. and White, W.M., 1982. Mantle plumes from ancient oceanic crust. *Earth and Planetary Science Letters* 57(2), pp. 421–436.

Ishizuka, O., Tani, K., Reagan, M.K., Kanayama, K., Umino, S., Harigane, Y., Sakamoto, I., Miyajima, Y., Yuasa, M. and Dunkley, D.J., 2011. The timescales of subduction initiation and subsequent evolution of an oceanic island arc. *Earth and Planetary Science Letters* 306(3–4), pp. 229–240

Ishizuka, O., Hickey-Vargas, R., Arculus, R.J., Yogodzinski, G.M., Savov, I.P., Kusano, Y., McCarthy, A., Brandl, P.A. and Sudo, M., 2018. Age of Izu–Bonin–Mariana arc basement. *Earth and Planetary Science Letters* 481, pp. 80–90.

James, K.H., 2006. Arguments for and against the Pacific origin of the Caribbean Plate: discussion, finding for an inter-American origin. *Geologica Acta: an international earth science journal* 4(1–2), pp. 279–302.

Jaramillo, J.S., Cardona, A., León, S., Valencia, V. and Vinasco, C., 2017. Geochemistry and geochronology from Cretaceous magmatic and sedimentary rocks at 6 35′ N, western flank of the Central cordillera (Colombian Andes): Magmatic record of arc growth and collision. *Journal of South American Earth Sciences* 76, pp. 460–481.

Jourdan, F., Marzoli, A., Bertrand, H., Cosca, M. and Fontignie, D., 2003. The Northernmost CAMP: 40Ar/39Ar age, petrology and Sr-Nd-Pb Isotope Geochemistry of the Kerforne Dyke, Brittany, France. In: *The Central Atlantic Magmatic Province: Insights from Fragments of Pangea*. American Geophysical Union, pp. 209–226.

Kanayama, K., Kitamura, K. and Umino, S., 2013. New geochemical classification of global boninites. *IAVCEI 2013 Scientific Assembly Abstracts*, *99*.Keigwin Jr., L.D. 1978. Pliocene closing of the Isthmus of Panama, based on biostratigraphic evidence from nearby Pacific Ocean and Caribbean Sea cores. *Geology* 6(10), pp. 630–634. A

Kennan, L. and Pindell, J.L., 2009. Dextral shear, terrane accretion and basin formation in the Northern Andes: best explained by interaction with a Pacific-derived Caribbean Plate? *Geological Society, London, Special Publications* 328(1), pp. 487–531.

Kerr, A.C., Saunders, A.D., Tarney, J., Berry, N.H. and Hards, V.L., 1995. Depleted mantle-plume geochemical signatures: No paradox for plume theories. *Geology* 23(9), pp. 843–846.

Kerr, A.C., Tarney, J., Marriner, G.F., Klaver, G.T., Saunders, A.D. and Thirlwall, M.F., 1996a. The geochemistry and petrogenesis of the late-Cretaceous picrites and basalts of Curaçao, Netherlands Antilles: a remnant of an oceanic plateau. *Contributions to Mineralogy and Petrology* 124(1), pp. 29–43.

Kerr, A.C., Tarney, J., Marriner, G.F., Nivia, A., Klaver, G.T. and Saunders, A.D., 1996b. The geochemistry and tectonic setting of late Cretaceous Caribbean and Colombian volcanism. *Journal of South American Earth Sciences* 9(1–2), pp. 111–120.

Kerr, A.C., Marriner, G.F., Arndt, N.T., Tarney, J., Nivia, A., Saunders, A.D. and Duncan, R.A., 1996c. The petrogenesis of Gorgona komatiites, picrites and basalts: new field, petrographic and geochemical constraints. *Lithos*- 37(2), pp. 245–260.

Kerr, A.C., Marriner, G.F., Tarney, J., Nivia, A., Saunders, A.D., Thirlwall, M.F. and Sinton, C.W., 1997a. Cretaceous basaltic terranes in western Colombia: Elemental, chronological and Sr-Nd isotopic constraints on petrogenesis. *Journal of Petrology* 38(6), pp. 677–702.

Kerr, A.C., Tarney, J., Marriner, G.F., Nivia, A. and Saunders, A.D., 1997b. The Caribbean-Colombian Cretaceous igneous province: The internal anatomy of an oceanic plateau. In: Mahoney, J. J. and Coffin, M. F. eds. *Large Igneous Provinces: Continental, Oceanic and Planetary Flood Volcanism*., pp. 123–144.

Kerr, A.C., Tarney, J., Nivia, A., Marriner, G.F. and Saunders, A.D., 1998. The internal structure of oceanic plateaus: inferences from obducted Cretaceous terranes in western Colombia and the Caribbean. *Tectonophysics* 292(3–4), pp. 173–188.

Kerr, A.C., Tarney, J., Kempton, P.D., Spadea, P., Nivia, A., Marriner, G.F. and Duncan, R.A., 2002a. Pervasive mantle plume head heterogeneity: Evidence from the late Cretaceous Caribbean-Colombian oceanic plateau. *Journal of Geophysical Research-Solid Earth* 107(B7), p. 2140.

Kerr, A.C., Aspden, J.A., Tarney, J. and Pilatasig, L.F., 2002b. The nature and provenance of accreted oceanic terranes in western Ecuador: geochemical and tectonic constraints.

Journal of the Geological Society 159(5), pp. 577–594.

Kerr, A.C., White, R.V., Thompson, P.M., Tarney, J. and Saunders, A.D., 2003. No Oceanic Plateau—No Caribbean Plate? The Seminal Role of an Oceanic Plateau in Caribbean Plate Evolution. *AAPG Memoir*, *79*, pp.126-168.

Kerr, A.C., 2003. Oceanic plateaus. *Treatise on geochemistry* 3, p. 659.

Kerr, A.C., 2005. La Isla de Gorgona, Colombia: A petrological enigma? *Lithos* 84(1), pp. 77–101.

Kerr, A.C., Pearson, D.G. and Nowell, G.M., 2009. Magma source evolution beneath the Caribbean oceanic plateau: new insights from elemental and Sr-Nd-Pb-Hf isotopic studies of ODP Leg 165 Site 1001 basalts. *Geological Society, London, Special Publications* 328(1), pp. 809–827.

Kerr, A.C. and Mahoney, J.J., 2007. Oceanic plateaus: problematic plumes, potential paradigms. *Chemical Geology* 241(3–4), pp. 332–353.

Kerr, A.C. and Tarney, J., 2005. Tectonic evolution of the Caribbean and northwestern South America: The case for accretion of two Late Cretaceous oceanic plateaus. *Geology* 33(4), pp. 269–272.

Kesler, S.E., Campbell, I.H. and Allen, C.M., 2005. Age of the Los Ranchos Formation, Dominican Republic: Timing and tectonic setting of primitive island arc volcanism in the Caribbean region. *Geological Society of America Bulletin* 117(7–8), pp. 987–995.

Kimura, G. and Ludden, J., 1995. Peeling oceanic crust in subduction zones. *Geology* 23(3), pp. 217–220.

Kolarsky, R.A., Mann, P., Monechi, S., Meyerhoff-Hull, D. and Pessagno, E.A., 1995. Stratigraphic development of southwestern Panama as determined from integration of marine seismic data and onshore geology.; Geologic and tectonic development of the Caribbean Plate boundary in southern Central America. In: Mann, P. ed. *Geologic and tectonic development of the Caribbean Plate boundary in southern Central America*., pp. 159–200.

Kolarsky, R.A. and Mann, P., 1995. Structure and neotectonics of an oblique-subduction margin, southwestern Panama.; Geologic and tectonic development of the Caribbean Plate boundary in southern Central America. In: Mann, P. ed. *Geologic and tectonic development of the Caribbean Plate boundary in southern Central America*., pp. 131–157.

Koppers, A.A.P., Staudigel, H. and Wijbrans, J.R., 2000. Dating crystalline groundmass separates of altered Cretaceous seamount basalts by the $^{40}Ar/^{39}Ar$ incremental heating technique. *Chemical Geology* 166(1), pp. 139–158.

Koppers, A.A.P., Staudigel, H. and Duncan, R.A., 2003. High-resolution $^{40}Ar/^{39}Ar$ dating of the oldest oceanic basement basalts in the western Pacific basin. *Geochemistry, Geophysics, Geosystems* 4(11)

Krawinkel, H., Wozazek, S., Krawinkel, J. and Hellmann, W., 1999. Heavy-mineral analysis and clinopyroxene geochemistry applied to provenance analysis of lithic sandstones from the Azuero–Sona Complex (NW Panama). *Sedimentary Geology* 124(1–4), pp. 149–168.

Kroenke, L.W., 1974. Origin of continents through development and coalescence of oceanic flood basalt plateaus. In: *Transactions-American Geophysical Union*. p. 443.

Kuiper, Y.D., 2002. The interpretation of inverse isochron diagrams in 40Ar/39Ar geochronology. *Earth and Planetary Science Letters* 203(1), pp. 499–506.

Kukok, D., Buchs, D., Baumgartner, P., Miranda, R. and Irving, D., 2017. Discovery of the

oldest fossils of Panama: Early Cretaceous radiolarians from Miocene conglomerate in the Canal Zone. In: *Proceedings of InterRad XV in Niigata 2017*.

Lanphere, M.A. and Dalrymple, G., 1978. The use of 40Ar/39 Ar data in evaluation of disturbed K-Ar systems. *US Geol. Surv. Open-File Rept.* 78, pp. 241–243.

Lapierre, H., Dupuis, V., Mercier de Lépinay, B., Bosch, D., Monié, P., Tardy, M., Maury, R.C., Hernandez, J., Polve, M., Yeghicheyan, D. and Cotten, J., 1999. Late Jurassic oceanic crust and Upper Cretaceous Caribbean plateau picritic basalts exposed in the Duarte igneous complex, Hispaniola. *The Journal of geology* 107(2), pp. 193–207.

Lapierre, H., Bosch, D., Dupuis, V., Polvé, M., Maury, R.C., Hernandez, J., Monié, P., Yeghicheyan, D., Jaillard, E., Tardy, M. and de Lépinay, B.M., 2000. Multiple plume events in the genesis of the peri-Caribbean Cretaceous oceanic plateau province. *Journal of Geophysical Research: Solid Earth* 105(B4), pp. 8403–8421.

Lebrón, M.C. and Perfit, M.R., 1994. Petrochemistry and tectonic significance of Cretaceous island-arc rocks, Cordillera Oriental, Dominican Republic. *Tectonophysics* 229(1–2), pp. 69–100.

Lee, S.M., 2004. Deformation from the convergence of oceanic lithosphere into Yap trench and its implications for early-stage subduction. *Journal of Geodynamics* 37(1), pp. 83–102.

Leng, W., Gurnis, M. and Asimow, P., 2012. From basalts to boninites: The geodynamics of volcanic expression during induced subduction initiation. *Lithosphere* 4(6), pp. 511–523.

Lewis, S.D. and Hayes, D.E., 1983. The tectonics of northward propagating subduction along eastern Luzon, Philippine Islands. *Washington DC American Geophysical Union Geophysical Monograph Series* 27, pp. 57–78.

Li, H.-Y., Taylor, R.N., Prytulak, J., Kirchenbaur, M., Shervais, J.W., Ryan, J.G., Godard, M., Reagan, M.K. and Pearce, J.A., 2019. Radiogenic isotopes document the start of subduction in the Western Pacific. *Earth and Planetary Science Letters* 518, pp. 197–210.

Lin, S. and van Keken, P.E., 2006a. Dynamics of thermochemical plumes: 1. Plume formation and entrainment of a dense layer. *Geochemistry, Geophysics, Geosystems* 7(2)

Lin, S. and van Keken, P.E., 2006b. Dynamics of thermochemical plumes: 2. Complexity of plume structures and its implications for mapping mantle plumes. *Geochemistry, Geophysics, Geosystems* 7(3)

Lissinna, B., 2005. *A profile though the Central American Landbridge in western Panama: 115 Ma Interplay between the Galápagos Hotspot and the Central American Subduction Zone*. Kiel: Christian-Albrechts University.

Lissinna, B., Hoernle, K. and Van Den Bogaard, P., 2002. Northern migration of arc volcanism in western Panama: evidence for subduction erosion? *Eos Transactions, American Geophysical Union* 83(47, Suppl.), pp. 1463–1464.

Loewen, M.W., Duncan, R.A., Kent, A.J. and Krawl, K., 2013. Prolonged plume volcanism in the Caribbean Large Igneous Province: new insights from Curaçao and Haiti. *Geochemistry, Geophysics, Geosystems* 14(10), pp. 4241–4259.

Loper, D.E., 1991. Mantle plumes. *Tectonophysics* 187(4), pp. 373–384.

Ludwig, K., 2017. Highly siderophile element abundances and 187 Re-187 Os isotope systematics of Gorgona Island komatiites and Costa Rican picrites.

MacMillan, I., Gans, P.B. and Alvarado, G., 2004. Middle Miocene to present plate tectonic history of southern Central American volcanic arc. *Tectonophysics* 392, p. 348.

Madrigal, P., Gazel, E., Flores, K.E., Bizimis, M. and Jicha, B., 2016. Record of massive upwellings from the Pacific large low shear velocity province. *Nature Communications* 7(1), pp. 1–12.

Mahoney, J.J., Storey, M., Duncan, R.A., Spencer, K.J. and Pringle, M., 1993. Geochemistry and age of the Ontong Java Plateau. *The Mesozoic Pacific: Geology, Tectonics, and Volcanism, Geophys. Monogr. Ser* 77, pp. 233–261.

Mann, P., 2007. Overview of the tectonic history of northern Central America. Geologic and tectonic development of the Caribbean Plate boundary in northern Central America. In: Mann, P. ed. *Geologic and tectonic development of the Caribbean Plate boundary in northern Central America*., pp. 1–19.

Mann, P. and Kolarsky, R.A., 1995. East Panama deformed belt; structure, age, and neotectonic significance.; Geologic and tectonic development of the Caribbean Plate boundary in southern Central America. *Special Paper - Geological Society of America* 295, pp. 111–130.

Marchesi, C., Jolly, W.T., Lewis, J.F., Garrido, C.J., Proenza, J.A. and Lidiak, E.G., 2011. Petrogenesis of fertile mantle peridotites from the Monte del Estado massif (Southwest Puerto Rico): a preserved section of Proto-Caribbean lithospheric mantle? *Geologica Acta* 9(3–4), pp. 289–306.

Di Marco, G., Baumgartner, P.O. and Channell, J.E.T., 1995. Late Cretaceous-early Tertiary paleomagnetic data and a revised tectonostratigraphic subdivision of Costa Rica and western Panama. *Geologic and Tectonic Development of the Caribbean Plate Boundary in Southern Central America, edited by P. Mann, Spec. Pap. Geol. Soc. Am.,* 295, pp. 1–27.

Matsumoto, T. and Tomoda, Y., 1983. Numerical simulation of the initiation of subduction at the fracture zone. *Journal of Physics of the Earth* 31(3), pp. 183–194.

Maury, R.C., Defant, M.J., Bellon, H., de Boer, Z.J., Stewart, R.H. and Cotton, J., 1995. Early Tertiary arc volcanics from eastern Panama: Geologic and tectonic development of the Caribbean Plate boundary in southern Central America. In: Mann, P. ed. *Geological Society of America Special Paper*., pp. 29–34.

Maya, M. and González, H., 1995. Unidades litodémicas en la Cordillera Central de Colombia. *Boletín Geológico* 35(2–3), pp. 44–57.

McCoy-West, A.J., Millet, M.A. and Burton, K.W., 2017. The neodymium stable isotope composition of the silicate Earth and chondrites. *Earth and Planetary Science Letters* 480, pp. 121–132.

McKenzie, D. and Bickle, M.J., 1988. The volume and composition of melt generated by extension of the lithosphere. *Journal of petrology* 29(3), pp. 625–679.

Mckenzie, D.P., 1977a. The Initiation of Trenches: A finite amplitude instability BT - Island Arcs, Deep Sea Trenches and Back-Arc Basins. Washington, DC: American Geophysical Union.

Mckenzie, D.P., 1977b. The Initiation of Trenches. *Island Arcs, Deep Sea Trenches and Back-Arc Basins* .

Meschede, M. and Frisch, W., 1998. A plate-tectonic model for the Mesozoic and early Cenozoic history of the Caribbean Plate. *Tectonophysics* 296(3–4), pp. 269–291.

Metti, A., Recchi, G. and Esquivel, D., 1972. Mapa geológico Sona-Isla de Coiba: scale 1: 250.000. *Ministerio de Comercio e Industrias, Panama City (Republica de Panamá)*

Metti, A., 1976. Geologia De La Peninsula De Sona E Isla De Coiba.

Meyerhoff, A.A. and Meyerhoff, H.A., 1972. Continental Drift, IV: The Caribbean" Plate". *The Journal of Geology* 80(1), pp. 34–60.

Millward, D., Marriner, G.F. and Saunders, A.D., 1984. Cretaceous tholeiitic volcanic rocks from the Western Cordillera of Colombia. *Journal of the Geological Society* 141(5), pp. 847–860.

Miyazaki, T. and Shuto, K., 1998. Sr and Nd isotope ratios of twelve GSJ rock reference samples. *Geochemical Journal* 32(5), pp. 345–350.

Montes, C., Bayona, G., Cardona, A., Buchs, D.M., Silva, C.A., Morón, S., Hoyos, N., Ramírez, D.A., Jaramillo, C.A. and Valencia, V., 2012a. Arc-continent collision and orocline formation: Closing of the Central American seaway. *Journal of Geophysical Research* 117(B4), p. B04105.

Montes, C., Cardona, A., McFadden, R., Morón, S.E., Silva, C.A., Restrepo-Moreno, S., Ramírez, D.A., Hoyos, N., Wilson, J., Farris, D. and Bayona, G.A., 2012b. Evidence for middle Eocene and younger land emergence in central Panama: Implications for Isthmus closure. *Geological Society of America Bulletin* .

Montes, C., Cardona, A., Jaramillo, C., Pardo, A., Silva, J.C., Valencia, V., Ayala, C., Pérez-Angel, L.C., Rodriguez-Parra, L.A., Ramirez, V. and Niño, H., 2015. Middle Miocene closure of the Central American Seaway. *Science* 348(6231), pp. 226–229.

Morgan, W.J., 1971. Convection plumes in the lower mantle. *Nature* 230(5288), p. 42.

Mueller, S. and Phillips, R.J., 1991. On the initiation of subduction. *Journal of Geophysical Research: Solid Earth* 96(B1), pp. 651–665.

Nair, R. and Chacko, T., 2008. Role of oceanic plateaus in the initiation of subduction and origin of continental crust. *Geology* 36(7), pp. 583–586.

Natland, J.H., 1981. Petrologic evolution of the Mariana arc and back-arc basin system: a synthesis of drilling results in the south Philippine Sea. *Initial reports of the deep sea drilling project* 60, pp. 877–908.

Neill, I., Kerr, A.C., Hastie, A.R., Stanek, K.P. and Millar, I.L., 2011. Origin of the Aves Ridge and Dutch-Venezuelan Antilles: interaction of the Cretaceous Great Arc and Caribbean-Colombian Oceanic Plateau? *Journal of the Geological Society* 168(2), pp. 333–348. Available at: http://jgs.lyellcollection.org/content/168/2/333.abstract.

Niespolo, E.M., Rutte, D., Deino, A.L. and Renne, P.R., 2017. Intercalibration and age of the Alder Creek sanidine 40Ar/39Ar standard. *Quaternary Geochronology* 39, pp. 205–213.

Nikolaeva, K., Gerya, T.V. and Marques, F.O., 2010. Subduction initiation at passive margins: numerical modeling. *Journal of Geophysical Research: Solid Earth* 115(B3)

Niu, Y.L., O'Hara, M.J. and Pearce, J.A., 2003. Initiation of subduction zones as a consequence of lateral compositional buoyancy contrast within the lithosphere: A petrological perspective. *Journal of Petrology* 44(5), pp. 851–866.

Nivia, A., 1996. The Bolivar mafic-ultramafic complex, SW Colombia: the base of an obducted oceanic plateau. *Journal of South American Earth Sciences* 9(1), pp. 59–68.

Nivia, A., Marriner, G.F., Kerr, A.C. and Tarney, J., 2006. The Quebradagrande complex: a lower cretaceous ensialic marginal basin in the Central Cordillera of the Colombian Andes. *Journal of South American Earth Sciences* 21(4), pp. 423–436.

Oliver, J. and Isacks, B., 1967. Deep earthquake zones, anomalous structures in the upper mantle, and the lithosphere. *Journal of Geophysical Research*, *72*(16), pp.4259-4275.

Orihashi, Y., Maeda, J., Tanaka, R., Zeniya, R. and Niida, K., 1998. Sr and Nd isotopic data for the seven GSJ rock reference samples; JA-1, JB-1a, JB-2, JB-3, JG-1a, JGb-1 and JR-1. *Geochemical Journal* 32(3), pp. 205–211.

Ozawa, A., Tagami, T., Listanco, E.L., Arpa, C.B. and Sudo, M., 2004. Initiation and propagation of subduction along the Philippine Trench: evidence from the temporal and spatial distribution of volcanoes. *Journal of Asian Earth Sciences* 23(1), pp. 105–111.

Parra, E. and Gonzalez, E.M., 2002. *Geologia de la plancha 122 Bis Jurado*.

Pati, J.K., Jourdan, F., Armstrong, R.A., Reimold, W.U. and Prakash, K., 2010. First SHRIMP U-Pb and $^{40}Ar/^{39}Ar$ chronological results from impact melt breccia from the Paleoproterozoic Dhala impact structure, India. *Large Meteorite Impacts and Planetary Evolution IV, Special Paper* 465, pp. 571–591.

Pearce, J.A., 1996. A user's guide to basalt discrimination diagrams. *Trace element geochemistry of volcanic rocks: applications for massive sulphide exploration. Geological Association of Canada, Short Course Notes* 12, pp. 79–113.

Pearce, J.A., 2008. Geochemical fingerprinting of oceanic basalts with applications to ophiolite classification and the search for Archean oceanic crust. *Lithos* 100(1–4), pp. 14–48.

Pearce, J.A. and Robinson, P.T., 2010. The Troodos ophiolitic complex probably formed in a subduction initiation, slab edge setting. *Gondwana Research* 18(1), pp. 60–81.

Pearce, J. A., Kempton, P.D., Nowell, G.M. and Noble, S.R., 1999. Hf-Nd element and isotope perspective on the nature and provenance of mantle and subduction components in Western Pacific arc-basin systems.*Journal of Petrology* 40(11) pp. 1579-1611.

Pearce, J.A., Reagan, M.K., Petronotis, K., Morgan, S., Almeev, R., Avery, A.J., Carvallo, C., Chapman, T., Christeson, G.L., Ferre, E.C. and Godard, M., 2015. International Ocean Discovery Program Expedition 352 Preliminary Report; Izu-Bonin-Mariana fore arc; testing subduction initiation and ophiolite models by drilling the outer Izu-Bonin-Mariana fore arc; 30 July-29 September 2014. *Preliminary Reports (International Ocean Discovery Program)* 352

Petterson, M.G., Babbs, T., Neal, C.R., Mahoney, J.J., Saunders, A.D., Duncan, R.A., Tolia, D., Magu, R., Qopoto, C., Mahoa, H. and Natogga, D., 1999. Geological–tectonic framework of Solomon Islands, SW Pacific: crustal accretion and growth within an intra-oceanic setting. *Tectonophysics* 301(1–2), pp. 35–60.

Phipps Morgan, J. and Morgan, W.J., 1999. Two-stage melting and the geochemical evolution of the mantle: a recipe for mantle plum-pudding. *Earth and Planetary Science Letters* 170(3), pp. 215–239.

Pindell, J., Kennan, L., Maresch, W.V., Stanek, K., Draper, G. and Higgs, R., 2005. Plate kinematics and crustal dynamics of circum-Caribbean arc-continent interactions; tectonic controls on basin development in proto-Caribbean margins.; Caribbean-South American plate interactions, Venezuela. *Special Paper - Geological Society of America* 394, pp. 7–52.

Pindell, J., Kennan, L., Stanek, K.P., Maresch, W.V. and Draper, G., 2006. Foundations of Gulf of Mexico and Caribbean evolution: eight controversies resolved. *Geologica Acta: an international earth science journal* 4(1–2), pp. 303–341.

Pindell, J., Maresch, W.V., Martens, U. and Stanek, K., 2011. The Greater Antillean Arc: Early Cretaceous origin and proposed relationship to Central American subduction mélanges: implications for models of Caribbean evolution. *International Geology Review* , pp. 1–13.

Pindell, J. and Kennan, L., 2009. Tectonic evolution of the Gulf of Mexico, Caribbean and northern South America in the mantle reference frame: an update. In: James, K. et al. eds.

The Origin and Evolution of the Caribbean Plate., pp. 1–55.

Pindell, J.L. and Kennan, L., 2001. Kinematic evolution of the Gulf of Mexico and Caribbean. In: *Transactions of the Gulf Coast Section Society of Economic Paleontologists and Mineralogists (GCSSEPM) 21st Annual Bob F. Perkins Research Conference, Petroleum Systems of Deep-Water Basins, Houston, Texas, December*., pp. 2–5.

Putirka, K.D., 2008. Thermometers and barometers for volcanic systems. *Reviews in mineralogy and geochemistry* 69(1), pp. 61–120.

Reagan, M.K., Ishizuka, O., Stern, R.J., Kelley, K.A., Ohara, Y., Blichert-Toft, J., Bloomer, S.H., Cash, J., Fryer, P., Hanan, B.B. and Hickey-Vargas, R., 2010. Fore-arc basalts and subduction initiation in the Izu-Bonin-Mariana system. *Geochemistry, Geophysics, Geosystems* 11(3).

Reagan, M.K., Pearce, J.A., Petronotis, K., Almeev, R.R., Avery, A.J., Carvallo, C., Chapman, T., Christeson, G.L., Ferré, E.C., Godard, M. and Heaton, D.E., 2017. Subduction initiation and ophiolite crust: new insights from IODP drilling. *International Geology Review* 59(11), pp. 1439–1450.

Reagan, M.K., Heaton, D.E., Schmitz, M.D., Pearce, J.A., Shervais, J.W. and Koppers, A.A., 2019. Forearc ages reveal extensive short-lived and rapid seafloor spreading following subduction initiation. *Earth and Planetary Science Letters* 506, pp. 520–529.

Recchi, G., 1976. Notas sobre la geologia de Panama. *Dir. Gen. Recur. Miner*

Recchi, G. and Miranda, R., 1977. Calizas de los Planes-Guaniquito (Tonosí). *Unpublished report, Panama City, Dirección General de Recursos Minerales* 27

Regenauer-Lieb, K., Yuen, D.A. and Branlund, J., 2001. The initiation of subduction: criticality by addition of water? *Science* 294.

Renne, P.R., Balco, G., Ludwig, K.R., Mundil, R. and Min, K., 2011. Response to the comment by WH Schwarz et al. on “Joint determination of ^{40}K decay constants and ^{40}Ar*/^{40}K for the Fish Canyon sanidine standard, and improved accuracy for ^{40}Ar/^{39}Ar geochronology” by PR Renne et al.(2010). *Geochimica et Cosmochimica Acta* 75(17), pp. 5097–5100.

Révillon, S., Hallot, E., Arndt, N.T., Chauvel, C. and Duncan, R.A., 2000a. A complex history for the Caribbean Plateau: petrology, geochemistry, and geochronology of the Beata Ridge, South Hispaniola. *The Journal of Geology* 108(6), pp. 641–661.

Révillon, S., Arndt, N.T., Chauvel, C. and Hallot, E., 2000b. Geochemical Study of Ultramafic Volcanic and Plutonic Rocks from Gorgona Island, Colombia: the Plumbing System of an Oceanic Plateau. *Journal of Petrology* 41(7), pp. 1127–1153.

Rodriguez, G. and Arango, M.I., 2013. Barroso Formation: a Tholeiitic volcanic arc and San Jose de Urama diabases: a T-MORB Type accretionary prism in the northern segment of Western Cordillera of Colombia. *Boletín de Ciencias de la Tierra* (33), pp. 17–38.

Rudnick, R.L. and Gao, S., 2003. Composition of the continental crust. *The crust* 3, pp. 1–64.

Sak, P.B., Fisher, D.M., Gardner, T.W., Marshall, J.S. and LaFemina, P.C., 2009. Rough crust, forearc kinematics, and Quaternary uplfit rates, Costa Rican segment of the middle American Trench. *Geological Society of America Bulletin* 121(7–8), pp. 992–1012.

Serrano, L., Ferrari, L., Martínez, M.L., Petrone, C.M. and Jaramillo, C., 2011. An integrative geologic, geochronologic and geochemical study of Gorgona Island, Colombia: Implications for the formation of the Caribbean Large Igneous Province. *Earth and Planetary Science Letters* 309(3–4), pp. 324–336.

Shervais, J.W., Reagan, M., Haugen, E., Almeev, R.R., Pearce, J.A., Prytulak, J., Ryan, J.G., Whattam, S.A., Godard, M., Chapman, T. and Li, H., 2019. Magmatic Response to Subduction Initiation: Part 1. Fore-arc Basalts of the Izu-Bonin Arc From IODP Expedition 352. *Geochemistry, Geophysics, Geosystems* 20(1), pp. 314–338.

Sigurdsson, H., Leckie, R.M., Acton, G.D., Miller, C.M. and Maddox, E.M., 1997. Caribbean volcanism, Cretaceous/Tertiary impact, and ocean climate history: synthesis of Leg 165. In: *Proc. Ocean Drill. Program Initial Rep*., pp. 377–402.

Silver, E.A., Reed, D.L., Tagudin, J.E. and Heil, D.J.,1990. Implications of the North and South Panama Thrust Belts for the Origin of the Panama Orocline. *Tectonics* 9(2), pp. 261–281.

Sinton, C.W., Duncan, R.A. and Denyer, P., 1997. Nicoya Peninsula, Costa Rica: A single suite of Caribbean oceanic plateau magmas. *Journal of Geophysical Research: Solid Earth* 102(B7), pp. 15507–15520.

Sinton, C.W., Duncan, R., Storey, M., Lewis, J. and Estrada, J.J., 1998. An oceanic flood basalt province within the Caribbean plate. *Earth and Planetary Science Letters* 155(3), pp. 221–235.

Sinton, C.W., Sigurdsson, H. and Duncan, R.A., 2000. Geochronology and petrology of the igneous basement a the lower Nicaraguan Rise, Site 1001. In: *Proceedings of the Ocean Drilling Program: Scientific results*. The Program, p. 233.

Spikings, R., Cochrane, R., Villagomez, D., Van der Lelij, R., Vallejo, C., Winkler, W. and Beate, B., 2015. The geological history of northwestern South America: from Pangaea to the early collision of the Caribbean Large Igneous Province (290–75Ma). *Gondwana Research* 27(1), pp. 95–139.

Stern, R.J., 2004. Subduction initiation: spontaneous and induced. *Earth and Planetary Science Letters* 226(3–4), pp. 275–292.

Stern, R.J. and Bloomer, S.H., 1992. Subduction Zone Infancy - Examples from the Eocene Izu-Bonin-Mariana and Jurassic California Arcs. *Geological Society of America Bulletin* 104(12), pp. 1621–1636.

Su, Y., 2003. Global MORB chemistry compilation at the segment scale. *Ph. D. Thesis, Department of Earth and Environmental Sciences, Columbia University*

Tanaka, T., Shimizu, H., Kawata, Y. and Masuda, A., 1987. Combined La–Ce and Sm–Nd isotope systematics in petrogenetic studies. *Nature* 327(6118), pp. 113–117.

Tejada, M.L.G., Mahoney, J.J., Duncan, R.A. and Hawkins, M.P., 1996. Age and geochemistry of basement and alkalic rocks of Malaita and Santa Isabel, Solomon Islands, southern margin of Ontong Java Plateau. *Journal of Petrology* 37(2), pp. 361–394.

Tejada, M.L.G., Mahoney, J.J., Neal, C.R., Duncan, R.A. and Petterson, M.G., 2002. Basement geochemistry and geochronology of Central Malaita, Solomon Islands, with implications for the origin and evolution of the Ontong Java Plateau. *Journal of Petrology* 43(3), pp. 449–484.

Thompson, P.M.E., Kempton, P.D., White, R.V., Kerr, A.C., Tarney, J., Saunders, A.D., Fitton, J.G. and McBirney, A., 2004. Hf–Nd isotope constraints on the origin of the Cretaceous Caribbean plateau and its relationship to the Galapagos plume. *Earth and Planetary Science Letters* 217(1–2), pp. 59–75.

Toth, J. and Gurnis, M., 1998. Dynamics of subduction initiation at preexisting fault zones. *Journal of Geophysical Research: Solid Earth* 103(B8), pp. 18053–18067.

Tournon, J., Triboulet, C. and Azéma, J., 1989. Amphibolites from Panama: anticlockwise P-T paths from a Pre-upper Cretaceous metamorphic basement in Isthmian Central America. *Journal of Metamorphic Geology* 7, pp. 539–546.

Trela, J., Gazel, E., Sobolev, A.V., Moore, L., Bizimis, M., Jicha, B. and Batanova, V.G., 2017. The hottest lavas of the Phanerozoic and the survival of deep Archaean reservoirs. *Nature Geoscience* 10(6), pp. 451–456.

Ueda, K., Gerya, T. and Sobolev, S.V., 2008. Subduction initiation by thermal–chemical plumes: Numerical studies. *Physics of the Earth and Planetary Interiors* 171(1–4), pp. 296–312.

Verati, C. and Jourdan, F., 2014. Modelling effect of sericitization of plagioclase on the $^{40}K/^{40}Ar$ and $^{40}Ar/^{39}Ar$ chronometers: implication for dating basaltic rocks and mineral deposits. *Geological Society, London, Special Publications* 378(1), pp. 155 LP – 174.

Villagómez, D., Spikings, R., Magna, T., Kammer, A., Winkler, W. and Beltrán, A., 2011. Geochronology, geochemistry and tectonic evolution of the Western and Central cordilleras of Colombia. *Lithos* 125(3–4), pp. 875–896.

Villagómez, D. and Spikings, R., 2013. Thermochronology and tectonics of the Central and Western Cordilleras of Colombia: Early Cretaceous–Tertiary evolution of the northern Andes. *Lithos* 160, pp. 228–249.

Vlaar, N.J. and Wortel, M.J.R., 1976. Lithospheric aging, instability and subduction. *Tectonophysics* 32(3–4), pp. 331–351.

Walker, R.J., Echeverria, L.M., Shirey, S.B. and Horan, M.F., 1991. Re—Os isotopic constraints on the origin of volcanic rocks, Gorgona Island, Colombia: Os isotopic evidence for ancient heterogeneities in the mantle. *Contributions to Mineralogy and Petrology* 107(2), pp. 150–162.

Walker, R.J., Storey, M., Kerr, A.C., Tarney, J. and Arndt, N.T., 1999. Implications of 187Os isotopic heterogeneities in a mantle plume: evidence from Gorgona Island and Curaçao. *Geochimica et Cosmochimica Acta* 63(5), pp. 713–728.

Weber, M., Gómez-Tapias, J., Cardona, A., Duarte, E., Pardo-Trujillo, A. and Valencia, V.A., 2015. Geochemistry of the Santa Fé Batholith and Buriticá Tonalite in NW Colombia – Evidence of subduction initiation beneath the Colombian Caribbean Plateau. *Journal of South American Earth Sciences* 62, pp. 257–274.

Wegner, W., Wörner, G., Harmon, R.S. and Jicha, B.R., 2011. Magmatic history and evolution of the Central American Land Bridge in Panama since Cretaceous times. *Geological Society of America Bulletin* 123(3–4), pp. 703–724.

Whattam, S.A., Montes, C., McFadden, R.R., Cardona, A., Ramirez, D. and Valencia, V., 2012. Age and origin of earliest adakitic-like magmatism in Panama: Implications for the tectonic evolution of the Panamanian magmatic arc system. *Lithos* 142-143, pp. 226–244.

Whattam, S.A. and Stern, R.J., 2011. The ‘subduction initiation rule’: a key for linking ophiolites, intra-oceanic forearcs, and subduction initiation. *Contributions to Mineralogy and Petrology* 162(5), pp. 1031–1045.

Whattam, S.A. and Stern, R.J., 2015. Late Cretaceous plume-induced subduction initiation along the southern margin of the Caribbean and NW South America: The first documented example with implications for the onset of plate tectonics. *Gondwana Research* 27(1), pp. 38–63.

Whattam, S.A., Montes, C. and Stern, R.J., 2020. Early central American forearc follows the subduction initiation rule. *Gondwana Research* 79, pp. 283–300.

Workman, R.K. and Hart, S.R., 2005. Major and trace element composition of the depleted MORB mantle (DMM). *Earth and Planetary Science Letters* 231(1), pp. 53–72.

Wörner, G., Harmon, R.S., Wegner, W. and Kay, S.M., 2009. Geochemical Evolution of igneous rock and changing Magma Sources during the Evolution and Closure of the Central American Landbridge. In: Mahlburg Kay, S. and Ramos, V. eds. *Backbone of the Americas*., pp. 183–196.

Wright, J.E. and Wyld, S.J., 2011. Late Cretaceous subduction initiation on the eastern margin of the Caribbean-Colombian Oceanic Plateau: One Great Arc of the Caribbean (?). *Geosphere* 7(2), pp. 468–493.

Zimmer, M.M., Plank, T., Hauri, E.H., Yogodzinski, G.M., Stelling, P., Larsen, J., Singer, B., Jicha, B., Mandeville, C. and Nye, C.J., 2010. The role of water in generating the calc-alkaline trend: new volatile data for Aleutian magmas and a new tholeiitic index. *Journal of Petrology* 51(12), pp. 2411–2444.

APPENDIX A – LABORATORY METHODS

A.1 Major and trace element analysis

Whole rock samples in this study were analysed using three different methods in two different laboratories. Two of these methods were performed at Cardiff University and one at Stellenbosch University. All whole rock geochemical results are shown in Appendix E2, where the analytical laboratory is indicated for each sample. Here, all methods will be described.

A.1.1 Preparation of rock samples into powder

All rock samples in this study were prepared into powder using the rock preparation facilities at Cardiff University. Weathered surfaces, veins and alteration patches were removed from the rock samples using a diamond-bladed rock saw. Samples were then crushed to a coarse grit by an Mn-steel jaw crusher. Rock chips for each sample were then reduced to a fine powder in an agate ball mill or an agate ring-and-puck mill.

For samples analysed at Cardiff University, approximately 2 g of each powdered sample was ignited for two hours in a furnace at 900°C to drive off volatile substances and determine loss on ignition (LOI) values.

For samples analysed at the University of Stellenbosch, samples were ignited in a furnace at 1000°C to drive off volatile substances, until the mass remained stable.

The LOI of all samples were calculated using the following equation (Equation A.1):

$$LOI\ (wt.\%) = \frac{Mass\ of\ wet\ powder - mass\ of\ ignited\ powder}{Mass\ of\ wet\ powder} \times 100$$

A.1.2 Preparation of solutions from ICP-OES and ICP-MS (Cardiff, 2017)

Samples in this study were prepared for ICP analysis using the lithium metaborate fusion method. To prepare the samples, 0.1 ± 0.001 g of each ignited sample was mixed with 0.6 ± 0.004 g of lithium metaborate flux in a platinum crucible. A few drops of lithium iodide wetting agent were added to each mixture which was then fused using the Claisse Fluxy automated fusion system. After the mixture was then dissolved in a 50 ml solution of 20 ml of 10% HNO3 and 30 ml of 18.2 Ω deionised water obtained using a Milli-Q purification system. After the mixture had fully dissolved, 1 ml of 100 ppm Rh spike was added to the solution

347 which was then made up to 100 ml with 18.2 Ω deionised water. Approximately 20 ml of each solution was run on ICP-OES to obtain major element and some trace element abundances. An aliquot of 1 ml of each solution was added to 1 ml of In and Tl and 8 ml of 2% HNO3 and run on the ICP-MS to obtain trace element abundances. The instruments at Cardiff University used to analyse elemental abundances are a Jobin Yvon Horiba Ultima 2 ICP-OES and a Thermo Elemental X7 series ICP-MS. The samples were run on the mass spectrometers by Dr. Iain McDonald.

A.1.3 Preparation of solutions from ICP-OES and ICP-MS (Cardiff, 2018)

Samples in this study were prepared for ICP analysis using the lithium metaborate fusion method. To prepare the samples, 0.1 ± 0.001 g of each ignited sample was mixed with 1.0 ± 0.010 g of lithium tetraborate and lithium metaborate flux, with added lithium iodide flux, in a platinum crucible. Samples were then fused using the Claisse M4 Fluxy automated fusion system. After the mixture was then dissolved in a 50 ml solution of 20 ml of 10% HNO3 and 30 ml of 18.2 Ω deionised water obtained using a Milli-Q purification system. After the mixture had fully dissolved, 1 ml of 50 ppm Rh spike was added to the solution which was then made up to 100 ml with 18.2 Ω deionised water. Approximately 20 ml of each solution was run on ICP-OES to obtain major element and some trace element abundances. An aliquot of 1 ml of each solution was added to 1 ml of In and Tl and 8 ml of 2% HNO3 and run on the ICP-MS to obtain trace element abundances. The instruments at Cardiff University used to analyse elemental abundances are a Thermo iCAP 7000 ICP-OES and a Thermo iCAP RQ ICP-MS. The samples were run on the mass spectrometers by Dr. Iain McDonald.

A.1.4 Preparation of fusion disk for XRF and LA ICP-MS (Stellenbosch)

Glass disks were prepared for XRF analysis using 7 g of high purity trace element and Rare Earth Element-free flux (LiBO2 = 32.83%, Li2B4O7 = 66.67%, LiI = 0.50%) mixed with 0.7g of the powder sample. Mixture of sample and flux were fused in platinum crucibles with Claisse M4 gas fluxer at temp between 1100OC -1200OC. Whole-rock major element compositions were determined by XRF spectrometry on a PANalytical Axios Wavelength Dispersive spectrometer. The spectrometer is fitted with an Rh tube and with the following analysing crystals: LIF200, LIF220, PE 002, Ge 111 and PX1. The instrument is fitted with a gas-flow proportional counter and a scintillation detector. The gas-flow proportional counter uses a 90% Argon-10% methane mixture of gas. Major elements were analysed on a fused glass disk using a 2.4kW Rhodium tube. Matrix effects in the samples were corrected for by applying theoretical alpha factors and measured line overlap factors to the raw intensities measured with the SuperQ PANalytical software. The concentration of the control standards that were used in the calibration procedures for major element analyses fit the range of

concentration of the samples. Trace elements in bulk rock samples are analysed on polished mounts prepared from XRF fusions, and followed the methods of Eggins (2003). A Resolution 193nm Excimer laser ablation system is connected to an Agilent 7700 (for analysis in October 2018) or Agilent 8800 (for analysis after October 2018) ICP-MS for most of the trace element analysis, using spot sizes between 100 and 104µm.

A.1.5 Evaluation of the accuracy and precision of elemental data

A.1.5.1 Standards used

A series of internal and external standards were used to assess the accuracy and precision of the whole rock elemental data obtained by the above methods. Standards used in the Cardiff methods were MRG1, JA2, JB1A, W1, BIR-1 and JB2. At Stellenbosch, standards used were BE-N, JB1, BHVO-1, BHVO-2G, BCR-2, BCR-2G, NIST 614, GOR-132-G, GOR-128-G and K-2-G. Internal standards JB17-001 and DB15-030 were also run in each laboratory for both major and trace elements.

A.1.5.2 Accuracy

Results from different runs of standards are given in Appendix E2 along with percentage errors of the measured values compared to certified values. The % errors for all elements in the standards are calculated using the following equation (Equation A.2)

$$\%\ error = \frac{Differernce\ between\ meaured\ and\ certified\ concentrations\ of\ element}{Certified\ concentration\ of\ element} \times 100$$

A.1.5.3 Precision

The precision of elemental data can be determined by examining the multiple analyses of the external and internal standards. The precision of a standard samples with respect to each element is represented by the relative standard deviation (RSD). The RSD is a percentage value, calculated for each element using the equations below (Equations A.3 to A.5).

$$x_a = \frac{\sum x}{n}$$

Where x_a is the average element concentration, x is the element concentration and n is the number of measurements.

$$s = \frac{\sqrt{\sum (x - x_a)^2}}{n - 1}$$

Where s is the standard deviation.

$$RSD\ (\%) = \frac{100s}{x_a}$$

A.1.5.4 Discussion on consistency and use of major and trace element data from Cardiff (2017), Cardiff (2019) and Stellenbosch

This section will discuss the consistency and comparability of whole rock major and trace element data from the different laboratories and methods utilised in this study. Major elements and trace elements were analysed at Cardiff University in 2017 and 2019, and at the University of Stellenbosch between 2018 and 2020, using the methods outlined above. Appendix A. includes details of laboratory used for each sample, for both major and trace element analysis.

The major element percentage error values for certified standards analysed in Cardiff (2017, 2019) are generally below 3 %, while major element analysis from Stellenbosch gives percentage errors for certified standards that are generally below 2 %. Sample JB1a was analysed in Cardiff in both 2017 and 2019 and gives low RSD values, lying between 0.32 – 1.77 (with an outlier of 23.45 for P_2O_5). Major elements analysis of certified standards at Stellenbosch generally gave RSD values below 1.

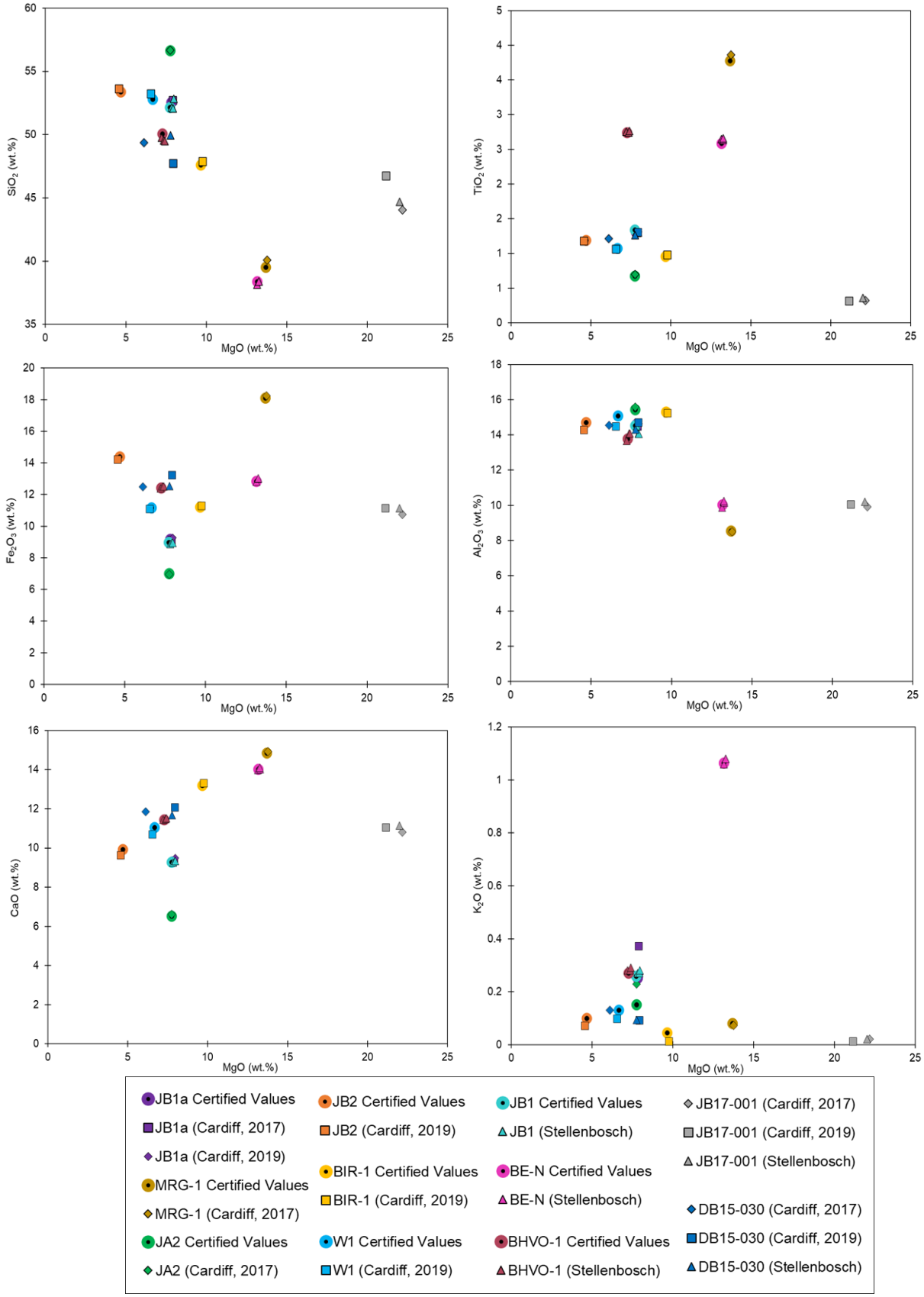

Figure A.1: Bivariate diagrams of selected major elements vs MgO for certified and internal standards used in major element analyses in Cardiff and Stellenbosch laboratories.

Samples DB15-030 and JB17-001 were analysed for major elements at both Cardiff (2017, 2019) and Stellenbosch. Using results from all laboratories, the RSD of DB15-030 ranges between 1.17 – 3.75 for most major elements, with a higher value of 13.98 for MgO, and values ranging from 12.53 – 21.13 for Na2O, K2O and P2O5. Using only results from Cardiff (2019) and Stellenbosch, the RSD values have a similar range from 1.30 – 3.737, including MgO. High RSD values remain for Na2O (30.05) and K2O (11.89).

Sample JB17-001 gives RSD values generally ranging from 1.35 – 3.21 for results from all laboratories, with outliers of 7.49 for TiO2, and a range of 21.63 – 126.52 for Na2O, K2O and P2O5. These RSD values remain relatively consistent when only considering analyses from Cardiff (2019) and Stellenbosch.

Low percentage errors and RSD values for the Certified standards, along with low RSD values for internal standards indicates that the major element analysis from Cardiff (utilising those methods used in 2017 and 2019) and Stellenbosch gives accurate and precise major element results. Major element results for any particular sample using any single laboratory utilised in this study are directly comparable to results of the other laboratories utilised in this study (Figure A.1).

Samples included in this study have relatively low concentrations of some trace elements, including the LREE, Nb and Th. This has made accurate trace element analysis particularly challenging, and is why is has been important to ascertain which laboratories could accurately detect low concentrations of these trace elements.

Percentage errors for trace element analysis of certified standards at Cardiff (2017, 2019) and Stellenbosch were generally below 10 %. Standard JB1a (analysed in Cardiff in both 2017 and 2019) gave RSD values between 0.04 – 7.79 for all trace elements, with the majority of elements having an RSD below 5. The trace element RSD values for certified standards analysed in Stellenbosch are generally below 5 (Figure A.2, A.3).

Again, samples DB15-030 and JB17-001 were analysed for trace elements at both Cardiff (2017, 2019) and Stellenbosch. Using results from all laboratories, the RSD of DB15-030 ranges between 1.62 – 49.44 for all trace elements, with many elements having RSD values above 15. Using only results from Cardiff (2019) and Stellenbosch, the RSD values have a narrower range from 0.57 – 30.35, with the majority of trace elements having RSD values under 10. Figure A.4 shows that on a primitive mantle-normalised multielementary diagram, results from Cardiff (2017),

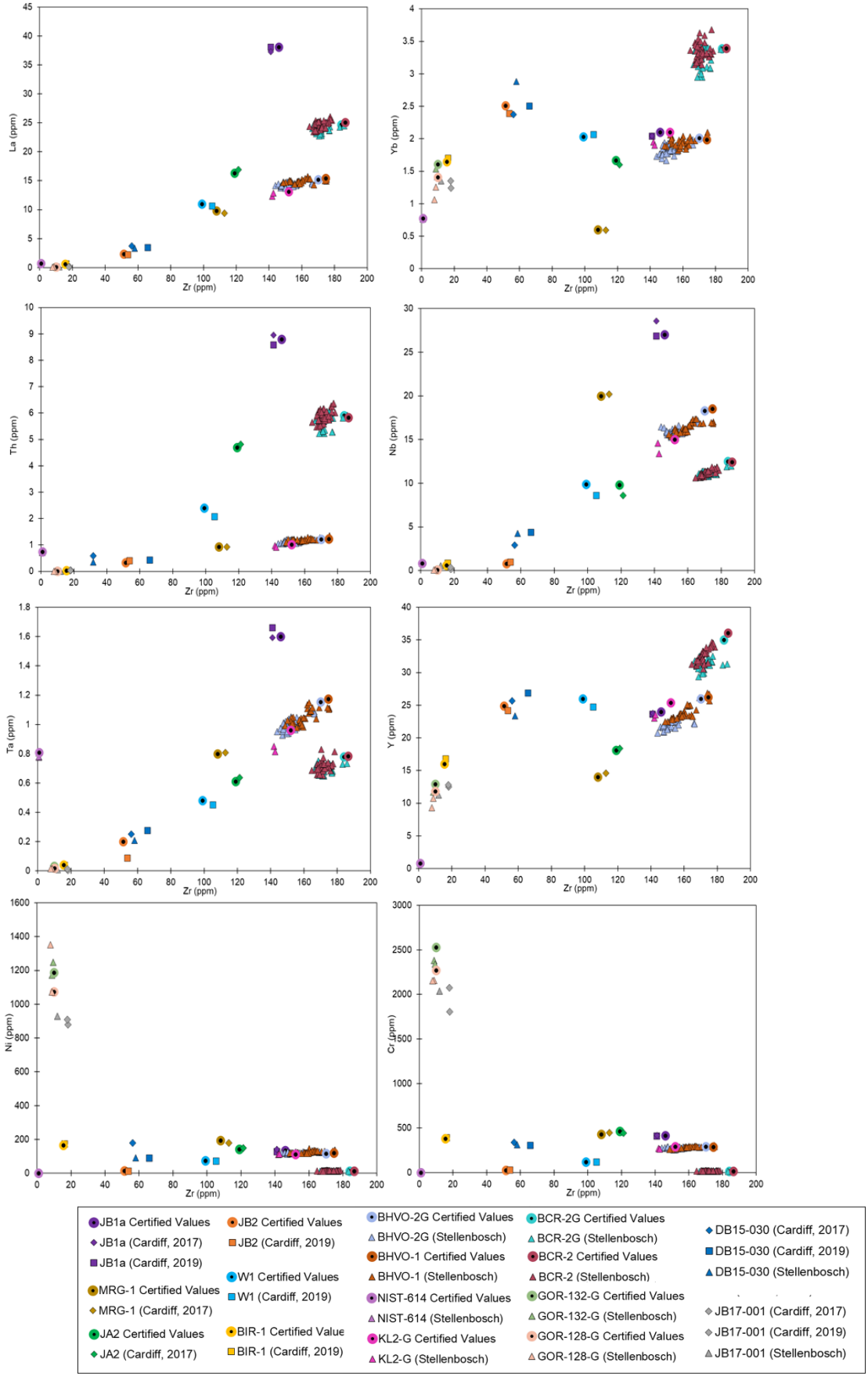

Figure A.2: Bivariate diagrams of selected major elements vs MgO for standards used in trace element analyses in Cardiff and Stellenbosch laboratories.

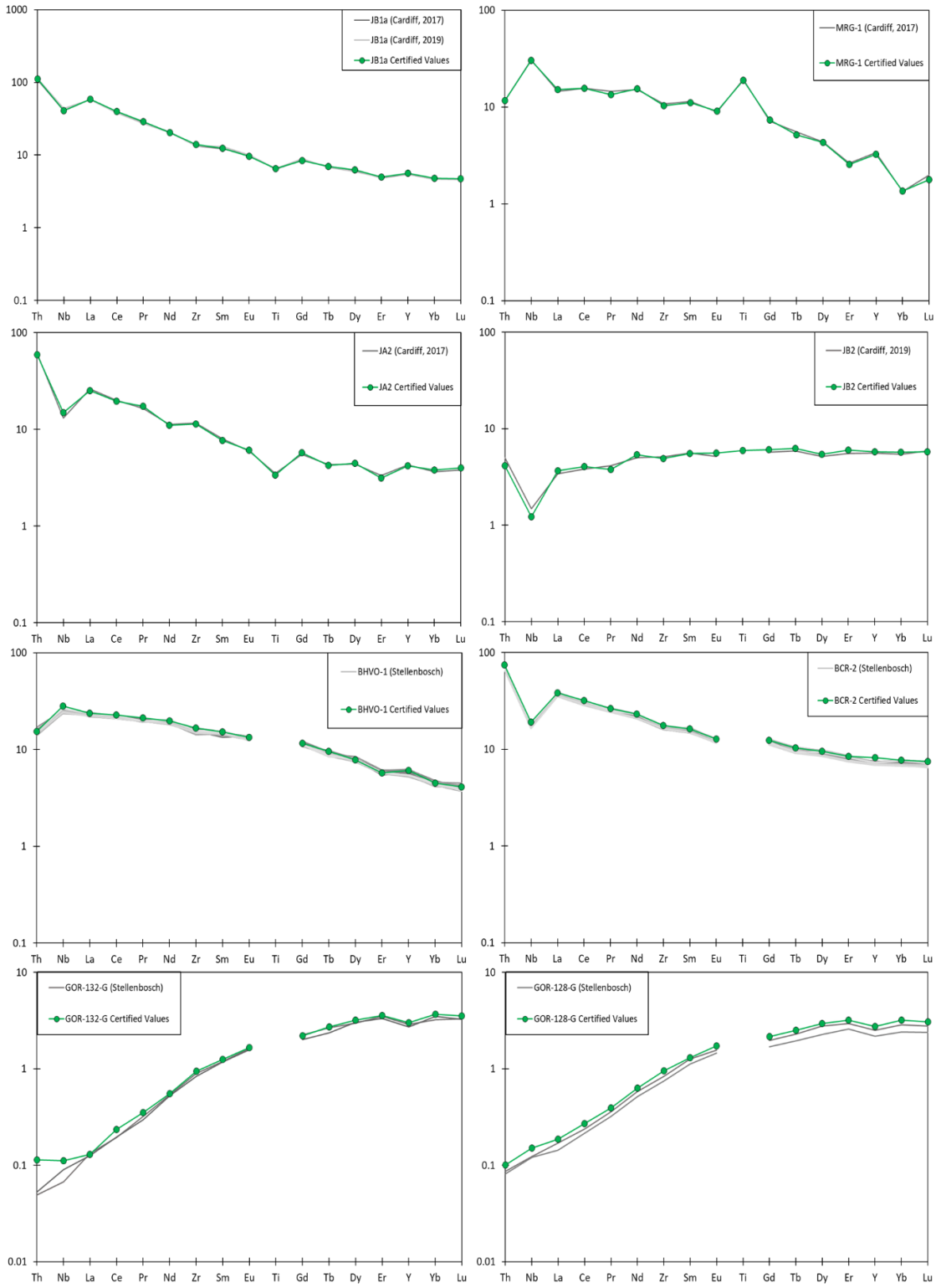

Figure A.3: Primitive mantle-normalised multi-element diagrams for standards used in trace element analyses in Cardiff and Stellenbosch laboratories.

Cardiff (2019) and Stellenbosch have similar values for the majority of trace elements, although the values of Cardiff (2019) and Stellenbosch plot closest together. The clear difference is shown in Th, and Nb, where the Cardiff (2017) analysis has higher Th values, and lower Nb.

Although the analysis of Cardiff (2017) gave accurate results for all certified standards, it is shown in Figure A.4 that the results for the analysis of DB15-030 are not comparable to the results which were consistently achieved for the same sample at Cardiff (2019) and Stellenbosch. Therefore, Cardiff (2017) trace element results were not utilised in this study, as they appear to be problematic in two key elements for this study, Nb and Th.

Using results from all laboratories, sample JB17-001 gave RSD values ranging from 2.27 – 112.98 for all trace elements, with most elements having values over 15. Using only the results of Cardiff (2019) and Stellenbosch, the RSD values largely range from 2.15 – 63.68, with higher values of 103.02 for Th, and 94.06 for Ta. Figure A.4 again shows that results from Cardiff (2017), Cardiff (2019) and Stellenbosch give similar values for the majority of trace elements. However, the results of Cardiff (2017) give lower Nb values in comparison to the results of Cardiff (2019) and Stelllenbosch, and that Stellenbosch gives lower values of Th than the results of Cardiff (2017) and Cardiff (2019).

Sample JB17-001 was analysed alongside certified standards GOR-128-G and GOR-132-G at Stellenbosch. These standards are depleted in the LREE, Th and Nb, with trace element contents similar to those of JB17-001. In Cardiff (2017) and Cardiff (2019), no such depleted certified standards were analysed. As these certified standards were analysed with both accuracy and precision at Stellenbosch, it is clear that this method can accurately measure the trace element contents of samples such at JB17-001, even when there are present in very low concentrations. Therefore, only trace element results from Stellenbosch are used for samples which are highly depleted.

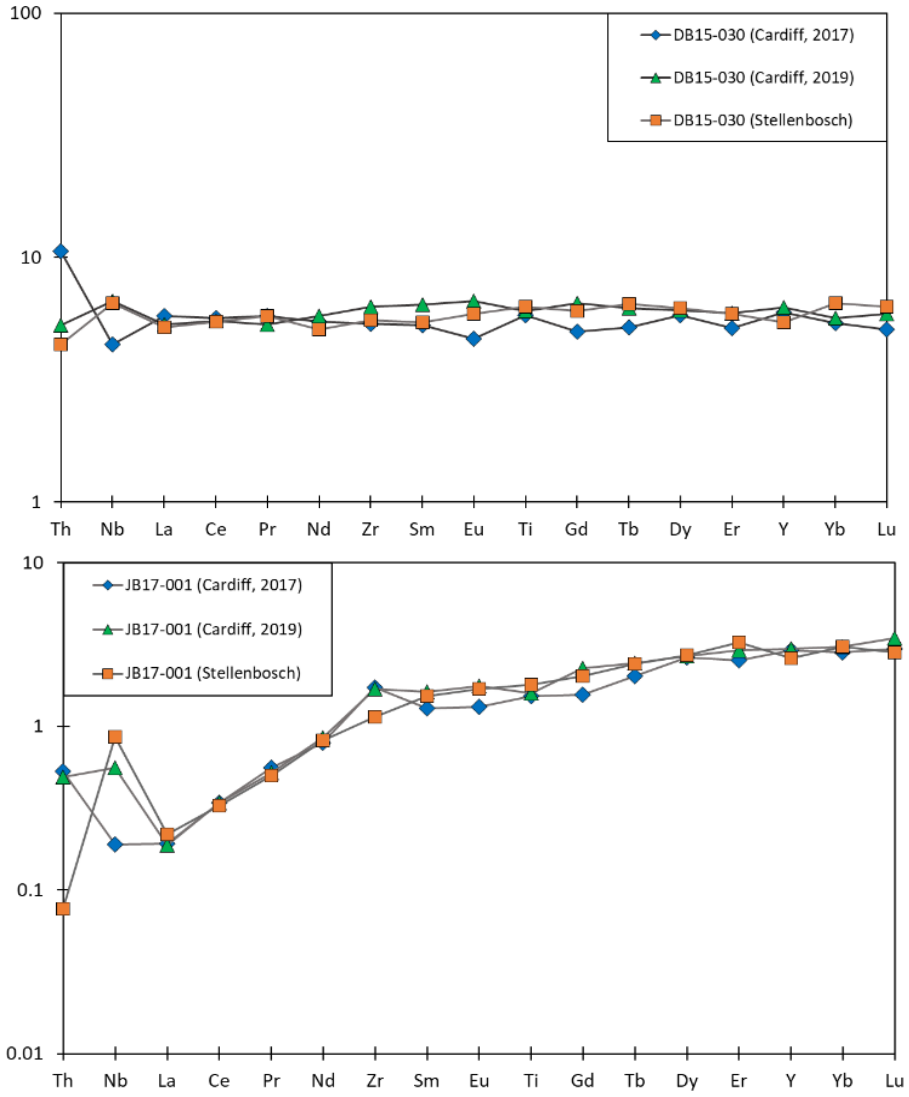

Figure A.4: Primitive mantle-normalised multi-element diagrams for standards used in trace element analyses in Cardiff and Stellenbosch laboratories. g

A.2 Nd isotope analysis

A.2.1 Sample selection and initial preparation

A total of 33 samples were selected for Nd isotope analysis. Samples were selected based on spatial distribution, geochemical grouping, freshness and availability of samples. Powders were initially prepared at Cardiff University using the method described above in Section A.1.1. Full Nd isotope results can be found in Appendix E3.

A.2.2 Nd preparation and analysis

Samples were prepared for Nd analysis following the procedure outlined by McCoy-West et al. (2017). The standard used was JB2 basalt. 150 mg of powdered sample was digested in PTFE beakers with 300 µl conc HNO_3 + 1 ml conc HF and fluxed on a hotplate at 120°C for at least 24 hours. Samples were dried down, before being fluxed in 0.5 ml conc HNO3 and dried down three times. Samples were then fluxed in 1 ml conc HCl and again dried down. Finally, samples were dissolved in 3 ml 1M HCl, in preparation for neodymium separation.

Neodymium was separated from other trace elements by two stages of column chemistry. In the first stage, polypropylene R1040 columns containing 2 ml of AG-50W-X8 resin were washed and equilibrated using 10 ml 6M HCl and 10ml 1M HCl respectively, before samples were loaded. Samples were then washed with a 10ml solution of 1M HCl and 1M HF, followed 12 ml 2.5M HCl, and finally 8 ml 2M HNO_3. Samples were then collected with 14 ml HCl, before being dried down and dissolved in 0.5 ml 0.2M HCl. In the second stage of column chemistry, 5ml Pasteur pipettes filled with Ln-spec resin were equilibrated with 0.2M HCl. Samples were loaded and washed with 6 ml 0.2M HCl, before being collected with 6 ml 0.2M HCl.

Nd isotopes were then measured at Cardiff University on a nu-Plasma II Multi Collector Inductively Coupled Plasma Mass Spectrometer (MC-ICP-MS). Synthetic standard JNd-i was used to calibrate the instrument and to correct for instrumental drift during the analyses. Procedural blanks were found to be in line with long-term laboratory measurements of ≤20pg Nd with a voltage too low to measure the Nd isotope ratio and therefore negligible effect on isotopic measurements of samples. Standard JB2 gave a $^{143}Nd/^{144}Ndi$ values of 0.513091 ± 0.000005 and 0.513091 ± 0.00001, which is within the published range of values (eg. Tanaka et al., 1987; Miyazaki and Shuto, 1998; Orihashi et al., 1998).

A.3 $^{40}Ar/^{39}Ar$ analysis

In total, 17 samples were selected for $^{40}Ar/^{39}Ar$ analysis. Samples were selected based on spatial distribution, whole rock geochemistry, grain size and freshness of samples. Samples were first checked in thin section to observe secondary alteration effects and confirm suitability for $^{40}Ar/^{39}Ar$ dating. K-rich mineral phases, such as feldspar and biotite, and rock groundmasses are used for the argon dating analysis. It is advantageous to use samples which lack secondary K-rich phases, such as sericite, because they could contain excess argon and give younger ages. Full $^{40}Ar/^{39}Ar$ results can be found in Appendix E4

Both feldspar and groundmass were used in the $^{40}Ar/^{39}Ar$ analysis. Initially, samples were prepared into a powder using the rock preparation facilities at Cardiff University. Weathered surfaces, veins and alteration patches were removed from the rock samples using a diamond-bladed rock saw. Samples were then crushed to a ~2000 µm grain size by an Mn-steel jaw crusher. Samples were then pulsed in a tungsten carbide ring and puck mill, and sieved to gain the 250-500 µm aliquot. Fines and dust <250 µm were removed, as after irradiation very fine-grained separates become a radioactive powder. A magnet was then passed over crushed samples, to remove any metal particles potentially introduced during the crushing process.

Samples were rinsed in deionized water (DI), and washed in DI in an ultrasonic bath for 60 minutes. Samples were then leached in 1N HCl for ~20 minutes in an ultrasonic bath, followed by a second leaching in 3N HNO_3 for another ~20 minutes in an ultrasonic bath. This secondary leaching was extended until alteration phases were visibly largely removed and the solution remained clear. Samples were then rinsed and washed in DI in an ultrasonic bath until the DI remained clear. Samples were then dried at 70°C.

Samples were magnetically separated using a Frantz Isodynamic Separator. For groundmass samples, this was to separate the groundmass from phenocrysts and alternation products, and for plagioclase samples, this was to extract the plagioclase crystals from the groundmass and alteration products. Finally, samples were hand-picked under a binocular microscope to remove altered grains. Due to the altered state of many of these samples, this was an extensive process which took over 3 months. For each sample, 250 mg was obtained for analysis.

Samples and neutron flux monitors were packaged in copper foil and stacked in quartz tubes with the relative positions of packets precisely measured for later reconstruction of neutron flux gradients. The sample package was irradiated in the Oregon State University reactor, Cd-shielded facility. Alder Creek sanidine (1.1891±0.0008 (1σ) Ma, (Niespolo et al., 2017)) was used to monitor ^{39}Ar production and establish neutron flux values (J) for the samples. Gas was extracted from samples via step-heating using a mid-infrared (10.6 µm) CO2 laser with a non-gaussian, uniform energy profile and a 3.5 mm beam diameter rastered over a sample well. The samples were housed in a doubly-pumped ZnS-window laser cell and loaded into a copper planchette containing four 1.6 cm x 1.6 cm square wells. Liberated argon was purified of active gases, e.g., CO_2, H_2O, H_2, N_2, CH_4, using three Zr-Al getters; one at 16°C and two at 400°C. Data were collected on a Mass Analyser Products MAP-215-50 single-collector mass spectrometer using an electron multiplier collector in dynamic collection (peak hopping) mode. Time-intensity data are regressed to inlet time with second-

order polynomial fits to the data. The average total system blank for laser extractions, measured between each sample run, was 5.9±2.5×10^{-15} mol ^{40}Ar, 2.2±1.8×10^{-16} mol ^{39}Ar, 3.5±1.6×10^{-17} mol ^{36}Ar. Mass discrimination was monitored on a daily basis, between and within sample runs by analysis of an air standard aliquot delivered by an automated pipette. All blank, interference and mass discrimination corrections and age calculations were performed with the MassSpec software package (MassSpec, version 8.058, authored by Al Deino, Berkeley Geochronology Center). Decay constants were sourced from Renne et al. (2011).

A.4 References

Eggins, S.M. 2003. Laser ablation ICP-MS analysis of geological materials prepared as lithium borate glasses. *Geostandards Newsletter* 27(2), pp. 147–162.

McCoy-West, A.J. et al. 2017. The neodymium stable isotope composition of the silicate Earth and chondrites. *Earth and Planetary Science Letters* 480, pp. 121–132.

Miyazaki, T. and Shuto, K. 1998. Sr and Nd isotope ratios of twelve GSJ rock reference samples. *Geochemical Journal* 32(5), pp. 345–350.

Niespolo, E.M. et al. 2017. Intercalibration and age of the Alder Creek sanidine 40Ar/39Ar standard. *Quaternary Geochronology* 39, pp. 205–213.

Orihashi, Y. et al. 1998. Sr and Nd isotopic data for the seven GSJ rock reference samples; JA-1, JB-1a, JB-2, JB-3, JG-1a, JGb-1 and JR-1. *Geochemical Journal* 32(3), pp. 205–211.

Renne, P.R. et al. 2011. Response to the comment by WH Schwarz et al. on “Joint determination of 40K decay constants and 40Ar∗/40K for the Fish Canyon sanidine standard, and improved accuracy for 40Ar/39Ar geochronology” by PR Renne et al.(2010). *Geochimica et Cosmochimica Acta* 75(17), pp. 5097–5100.

Tanaka, T. et al. 1987. Combined La–Ce and Sm–Nd isotope systematics in petrogenetic studies. *Nature* 327(6118), pp. 113–117.

APPENDIX B - LIST OF ELECTRONIC APPENDICES

APPENDIX E1

Excel spreadsheet listing all samples collected or used in this study, with grid references.

APPENDIX E2

Excel spreadsheet with all raw whole rock data collected in this study, with analytical tables for whole rock precision and accuracy.

APPENDIX E3

Excel spreadsheet containing the Nd isotope results from this study

APPENDIX E4

Excel spreadsheet with the $^{40}Ar/^{39}Ar$ results from this study.

APPENDIX E5

Biostratigraphic dating summary provided by Dr Jonathan Bryan